HURRICANES AND CLIMATE CHANGE

Edited by
James B. Elsner
and
Thomas H. Jagger

Aegean Conferences
Springer

Hurricanes and Climate Change

James B. Elsner • Thomas H. Jagger
Editors

Hurricanes and Climate Change

Springer

Editors
James B. Elsner
Florida State University
Tallahassee, FL, USA

Thomas H. Jagger
Florida State University
Tallahassee, FL, USA

ISBN 978-0-387-09409-0 e-ISBN 978-0-387-09410-6
DOI 10.1007/978-0-387-09410-6

Library of Congress Control Number: 2008926319

Printed on acid-free paper.

9 8 7 6 5 4 3 2 1

springer.com

Preface

Tropical cyclones are becoming more powerful with the most dramatic increase occurring over the North Atlantic. The increase is correlated with an increase in ocean temperature. A debate concerns the nature of this increase with some researchers attributing it to natural climate fluctuations while other researchers attributing it to anthropogenic increases in forcing from greenhouse gases. A Summit on Hurricanes and Climate Change held May 27–30, 2007 at the Aldemar Knossos Royal Village in Hersonissos, Crete brought together leading academics and researchers to discuss the issues and to address what research is needed to advance the science of hurricane climate.

The Summit was hosted by Aegean Conferences and supported by the Bermuda Institute for Ocean Sciences (BIOS) Risk Prediction Initiative and by the U.S. National Science Foundation. It was organized to provide a venue for encouraging a lively, spirited exchange of ideas. In this spirit, it was appropriate to convene at the birthplace of the Socratic method. This volume is a collection of research papers from participants of the Summit.

Tropical cyclones are typically analyzed as a passive response to climate forcing: the hurricane as a product of its environment. A warm ocean provides sustenance, a calm atmosphere nurturing, and a subtropical high-pressure cell forward direction. An increase in oceanic heat will raise a hurricane's potential intensity, yet an increase in shearing winds could counter by dispersing the heat in a fledgling storm. This perspective is useful for identifying the mechanisms responsible for making some seasons active while others inactive. A point of emphasis at the Summit was that statistical modeling is superior to data analysis (trend lines, etc) as it avoids cherry-picking the evidence and provides a framework for making use of older, less reliable data.

For example, a Poisson distribution is useful for modeling tropical storm counts over time. The benefit of a statistical approach is that it provides a context that is consistent with the nature of the underlying physical process, analogous to the way the laws of physics provide a context for studying meteorology. It was shown at the Summit that smoothing (filtering) the hurricane count data introduces low frequency patterns that may not be significant and that a statistical model of Atlantic hurricanes indicates a recent upswing in the number of strongest hurricanes with little or no multidecadal variation.

Although the question of whether we can ascribe a change in tropical cyclone intensity to anthropogenic climate change (attribution) is still open, it was argued based on statistical models for extreme winds that the difference in hurricane intensity for storms near the U.S. coast between globally warm and cool years is consistent in sign and magnitude with theory and simulations. In this regard it was noted that the discrepancy between numerical model results and observations is likely due to a reliance on data analysis rather than statistical models.

The collective role that hurricanes play in changing the climate was another point of emphasis at the Summit. Over the Atlantic Ocean, heat and moisture transport out of the tropics by an ensemble of hurricanes moving poleward in a given season was shown to have a detectable influence on the baroclinic activity at high latitudes the following winter, which in turn influences the preferred hurricane track type (recurving or straight-moving) during the subsequent hurricane season. Thus a communication between the tropics and the middle latitudes on the biennial time scale is accomplished through tropical cyclone track changes and middle latitude baroclinicity. This finding has important implications for financial markets because it provides a way to hedge risk through diversification.

Also, the relationship between global warming and ENSO was explained in terms of warming rather than warmth. A warming planet is associated with more El Nino events, which on the biennial time scale leads to cooling. These are intriguing hypotheses about climate change and tropical cyclones that merit further investigation. It was also shown that super typhoons in the western North Pacific need a deep ocean mixed layer for rapid intensification only in regions where the sub surface water temperatures are marginally supportive of tropical cyclone intensification. It was demonstrated that high aerosol concentrations lead to an invigoration of the convection in tropical cyclones through enhancement of the ice/water microphysical processes inside the clouds.

Another important theme of the Summit was paleotempestology—the study of prehistoric storms from geological and biological evidence. For instance, coastal wetlands and lakes are subject to overwash processes during hurricane strikes when barrier sand dunes are overtopped by storm surge. The assumption is that during landfall the waves and wind-driven storm surge reach high enough over the barrier to deposit sand in the lake. In a sediment core taken from the lake bottom, a sand layer will appear distinct from the fine organic mud that accumulates slowly under normal conditions. Sediment cores taken from the northeastern Caribbean show more sand layers during the second half of the Little Ice Age when sea temperatures near Puerto Rico were a few degrees C cooler than today providing some evidence that today's warmth is not needed for increased storminess. Not surprisingly intervals of more hurricanes correspond with periods of fewer El Nino events. It was shown that sedimentary ridges in Australia left behind by ancient tropical cyclones indicate activity from the last century under represents the continent's stormy past. It was argued that proxy techniques based on oxygen isotopes from tree rings and cave deposits show promise for studying prehistoric tropical cyclone events because of the signature left in the annual layers by the isotopically lighter tropical cyclone rainwater.

It was mentioned that a spatially limited set of proxies or historical records are not able to resolve changes in overall activity from changes in local activity due to shifts in tracks. While the northeastern Caribbean region is in the direct path of today's hurricanes, was it always? Network analysis of hurricane activity might be able to shed light on this question. The answer is important as more hurricanes locally could mean changes in steering rather than changes in abundance. Proxy data from the U.S. Gulf coast show a pattern of frequent hurricanes between 3800 and 1000 years ago followed by relatively few hurricanes during the most recent millennium which is explained in terms of the position of the subtropical North Atlantic High. Moreover it was shown that recent increases in typhoon intensities affecting Korea can be explained by an eastward shift in the subtropical North Pacific High allowing the storms to recurve over the warmer waters of the Kuroshio Current rather than over the colder subsurface waters of the Yellow Sea. In order to understand how climate influences local changes in tropical cyclone activity, it was remarked that more research is needed to identify factors influencing tropical cyclone tracks.

Results from high-resolution numerical models, including a 20 km-mesh model, were consistent in showing stronger tropical cyclones in a warmer future. Most models indicate an overall decrease in the number of storms, attributable in one study to greater atmospheric stability and a decrease in the vertical mass flux. Not all models agree on the change in individual basin numbers with some models showing an increase in the Atlantic and others a decrease. It was shown that models without tropical cyclones remove the oceanic heat in the tropics through stronger trade winds. It was noted that models may be better at identifying changes to the large-scale genesis fields and that models still do not have the resolution to be useful to society. Climate model projections can be downscaled to construct tropical cyclone climatologies using a method that combines rejection sampling by numerical models to determine genesis points with simple physical models for storm motion and winds. A few participants focused on the perception and politics of tropical cyclone risk in a changing climate.

This volume provides a cross-section of the topics that were covered during the Summit. It is broadly organized around study type with empirical analyses first followed by statistical models, then by numerical simulations.

We would like to extend our gratitude to the following individuals for helping with the review process: George Kallos. Kevin Hodges, Constantin Adronache. Anastasios Tsonis. Kyle Swanson. Fabrice Chauvin, Auguste Boissonnade, Bob Rohli, Claudia Mora, William Read, Kevin Walsh, Kerry Emanuel, Byron Daynes, and Greg Holland. Special thanks goes to Robert Hodges for his help with copy editing.

James B. Elsner

March 2008 *Thomas H. Jagger*

Contents

Contributors

Enrica Bellone
Risk Management Solutions, London, UK

Zafer Boybeyi
College of Science, George Mason University, Fairfax, VA 22030, USA

John A.T. Bye
The University of Melbourne, Melbourne, Victoria, Australia

Wenju Cai
CSIRO Marine and Atmospheric Research, Melbourne, Victoria, Australia

Fabrice Chauvin
GAME/CNRM (Météo-France/CNRS), 42 Avenue Coriolis, 31057 Toulouse Cedex 01, France

Shuyi Chen
RSMAS/University of Miami, 4600 Rickenbacker Causeway, Miami, FL 33149, USA

Themis G. Chronis
NASA Marshall Space Flight Center, Huntsville, AL, USA

N. Cohen
Department of Atmospheric Sciences, The Hebrew University of Jerusalem, Jerusalem, Israel

Katie Coughlin
Risk Management Solutions, London, UK

Tim Cowan
CSIRO Marine and Atmospheric Research, Melbourne, Victoria, Australia

Peter S. Dailey
AIR Worldwide Corporation, 131 Dartmouth Street, Boston, MA 02116, USA

Marta Domínguez
Environmental Sciences Institute, University of Castilla-La Mancha, Toledo, Spain

James B. Elsner
Department of Geography, Florida State University, Tallahassee, FL 32306, USA

Emily A. Fogarty
Department of Geography, Florida State University, Tallahassee, FL 32306, USA

Takeshi Furuhashi
Department of Computational Science and Engineering, Graduate School of Engineering, Nagoya University, Furo-cho, Chikusa-ku, Nagoya, Aichi 464-8601, Japan

Miguel Angel Gaertner
Environmental Sciences Faculty, University of Castilla-La Mancha, Toledo, Spain

Victoria Gil
Environmental Sciences Institute, University of Castilla-La Mancha, Toledo, Spain

Aslak Grinsted
Arctic Centre, University of Lapland, 96101 Rovaniemi, Finland
Department of Geophysics, P.O. Box 3000, University of Oulu, Oulu 90014, Finland

S. Gualdi
Centro Euro-Mediterraneo per i Cambiamenti Climatici (CMCC), Lecce, Italy

Jayanta Guin
AIR Worldwide Corporation, 131 Dartmouth Street, Boston, MA 02116, USA

Stéphane Hallegatte
Centre International de Recherche sur l'Environnement et le Développement (CIRED) and Ecole Nationale de la Météorologie, Météo-France

Satoshi Iizuka
National Research Institute for Earth Science and Disaster Prevention, Tsukuba, Japan

Thomas H. Jagger
Department of Geography, Florida State University, Tallahassee, FL 32306, USA

Svetlana Jevrejeva
Proudman Oceanographic Laboratory, Liverpool, UK

Stephen Jewson
Risk Management Solutions, London, UK

Menas Kafatos
College of Science, George Mason University, Fairfax, VA 22030, USA
Center for Earth Observing and Space Research, Fairfax, VA 22030, USA

David Karoly
School of Earth Sciences, University of Melbourne, Parkville, VIC, Australia

A. Khain
Department of Atmospheric Sciences, The Hebrew University of Jerusalem, Jerusalem, Israel

Shree Khare
Risk Management Solutions, London, UK

Jason T. Knowles
Department of Geography and Anthropology, Louisiana State University, Baton Rouge, LA, USA

Thomas Laepple
Risk Management Solutions, London, UK
Alfred-Wegener Institute, Bremerhaven, Germany

Andreas Langousis
Department of Civil and Environmental Engineering, MIT, Cambridge, MA 02139, USA

Greta Ljung
AIR Worldwide Corporation, 131 Dartmouth Street, Boston, MA 02116, USA

Manuel Lonfat
Risk Management Solutions, London, UK

Tomonori Matsuura
Tomonori Matsuura Faculty of Science / Graduate School of Science and Engineering, University of Toyama, Toyama, Japan

Terrence A. McCloskey
Department of Oceanography and Coastal Sciences, Louisiana State University, 1002Y Energy Coast and Environment Building, Baton Rouge, LA 70803, USA

Timothy L. Miller
NASA Marshall Space Flight Center, Huntsville, AL, USA

John Moore
Arctic Centre, University of Lapland, 96101 Rovaniemi, Finland

A. Navarra
Centro Euro-Mediterraneo per i Cambiamenti Climatici (CMCC), Lecce, Italy

Neville Nicholls
School of Earth Sciences, University of Melbourne, Parkville, VIC, Australia

Jonathan Nott
School of Earth and Environmental Sciences, James Cook University, Cairns, Australia

Kechi Nzerem
Risk Management Solutions, London, UK

Adam O'Shay
Risk Management Solutions, London, UK

Jeremy Penzer
Risk Management Solutions, London, UK
London School of Economics, London, UK

Minh Tuan Pham
Department of Computational Science and Engineering, Graduate School of Engineering, Nagoya University, Furo-cho, Chikusa-ku, Nagoya, Aichi 464-8601, Japan

Jasna V. Pittman
NASA Marshall Space Flight Center, Huntsville, AL, USA

Franklin R. Robertson
NASA Marshall Space Flight Center, Huntsville, AL, USA

Jean-François Royer
GAME/CNRM (Météo-France/CNRS), 42 Avenue Coriolis, 31057 Toulouse Cedex 01, France

Enrique Sánchez
Environmental Sciences Faculty, University of Castilla-La Mancha, Toledo, Spain

E. Scoccimarro
Istituto Nazionale di Geofisica e Vulcanologia (INGV), Bologna, Italy

Norihiko Sugimoto
Department of Computational Science and Engineering, Graduate School of Engineering, Nagoya University, Furo-cho, Chikusa-ku, Nagoya, Aichi 464-8601, Japan

Donglian Sun
College of Science, George Mason University, Fairfax, VA 22030, USA
Center for Earth Observing and Space Research, Fairfax, VA 22030, USA

Glen Sussman
Department of Political Science, Old Dominion University, Norfolk, VA, USA

Kanta Tachibana
Department of Computational Science and Engineering, Graduate School of Engineering, Nagoya University, Furo-cho, Chikusa-ku, Nagoya, Aichi 464-8601, Japan

Anastasios A. Tsonis
Department of Mathematical Sciences, University of Wisconsin-Milwaukee, Milwaukee, WI 53201, USA

Daniele Veneziano
Department of Civil and Environmental Engineering, MIT, Cambridge, MA 02139, USA

Kevin Walsh
School of Earth Sciences, University of Melbourne, Parkville, VIC, Australia
School of Geography and Environmental Science, Monash University, Clayton, VIC, Australia

Tomohiro Yoshikawa
Department of Computational Science and Engineering, Graduate School of Engineering, Nagoya University, Furo-cho, Chikusa-ku, Nagoya, Aichi 464-8601, Japan

Gerhard Zuba
AIR Worldwide Corporation, 131 Dartmouth Street, Boston, MA 02116, USA

Detection and Attribution of Climate Change Effects on Tropical Cyclones

Kevin Walsh, David Karoly, and Neville Nicholls

Abstract The status of attempts to detect climate trends in tropical cyclone data and the possible attribution of such trends to anthropogenic climate change are reviewed. A number of trends have been detected in tropical cyclone data but some of these are likely due to data inhomogeneities. Where the data is good, for instance in the Atlantic basin, detected trends are more likely to be real. Whether such trends can be attributed at this time to anthropogenic climate change relies not only upon good data but also upon the physical basis of the hypothesized links between global warming and variables related to tropical cyclone characteristics. These links may be made stronger through the use of numerical models and theoretically-based parameters. A process is outlined by which this might be achieved.

Introduction

The detection and attribution of the possible effects of anthropogenic climate change on tropical cyclones is one of the most controversial topics in present-day science. The increase in tropical cyclone numbers in the Atlantic since the mid 1990s, combined with the devastating impacts of individual hurricanes such as Katrina in 2005, has led to an urgent examination of trends in the available tropical cyclone data to see if these can be explained by man's effect on the climate.

To examine these issues, numerous recent studies have been performed to analyze the data record, to simulate future occurrence and intensity of tropical cyclones and to determine the influence of various environmental parameters on tropical cyclone characteristics. But no study has yet applied the standard, formal methodology to tropical cyclones that has been used previously to conclude, with high confidence, that a particular change in atmospheric or oceanic behavior is likely due to anthropogenic climate change. The formal process of detection and attribution is the most powerful tool available to climate scientists to build confidence in ascribing detected climate trends to man-made influences. This article discusses the relevance of this methodology for studies of tropical cyclones, outlines the current issues that limit its application to tropical cyclones and suggests

J.B. Elsner and T.H. Jagger (eds.), *Hurricanes and Climate Change,*
doi: 10.1007/978-0-387-09410-6,

ways in which these limitations can be addressed. The formal process of detection and attribution is first described and examples are given of its successful application in providing robust, high-confidence conclusions regarding the effects of anthropogenic climate change.

Detection and Attribution

Definition

Detection is the process of determining whether a climate signal has emerged from the background noise of the data. Typically this "noise" constitutes the natural climate variability of the atmosphere-ocean system., particularly variability on decadal time scales which can often be aliased onto longer-time scales trends such as those associated with global warming, thus making these trends difficult to detect unambiguously. A recent summary of the detection process is provided in Hegerl et al. (2007). Detection is largely a statistical issue and is usually determined by statistical techniques, ranging from simple trend analyses to multi-variate analysis.

For a signal to be detected unambiguously, good data for both the signal and the noise must exist. Like all good climate data, cyclone data must be free of inhomogeneities caused by changes in observing practices. The data must also be complete in that the data sample being analysed must be consistently collected at similar time intervals over the entire period of record. To estimate the magnitude of the climate noise in a particular climate parameter, it may not be possible to just use the available observational record, as this may be too short to fully characterize the long-term variability due to noise alone. In principle, data records much longer than the duration of the climate change signal are required to estimate the range of long-term variability that may occur due to climate noise alone (Santer et al., 1995). In practice, such lengthy observational records do not exist for any climate variables and so alternative approaches must be used to estimate the long term variability due to noise. Often, long control simulations from coupled ocean-atmosphere climate models performed with no changes in external forcing factors are used to estimate the long-term variability of climate variables due to climate noise alone, assuming that the models provide realistic simulations of the noise in such variables.

It is clear that the mere detection of a signal is not an indication of its cause. Further analysis needs to be undertaken to ascribe causes for any detected signals; this is known as the process of attribution. In the case of anthropogenic climate change, we are interested in whether the detected signal can be attributed to man-made global warming. As defined by the IPCC, in order for high confidence attribution conclusions to be reached, a signal needs to be detected that is not only of the expected pattern of change but also of the correct magnitude expected

from the response to anthropogenic climate forcing. This response is usually estimated using simulations with climate models forced by increases in atmospheric concentrations of greenhouse gases and aerosols, although theoretically-based approaches have also been used in some instances. Inherent in this process is the assumption that the simulations of climate models have reasonable skill, an assumption that is not justified at present for some small-scale, complex phenomena such as tropical cyclones (e.g. Randall et al. 2007; Walsh 2008).

Therefore, based on the formal Intergovernmental Panel on Climate Change (IPCC) definition of detection and attribution, the following conditions must be satisfied for successful detection and attribution:

- A signal must be detected;
- The signal must be consistent with the esimated response from modeling or theoretical techniques of a given combination of anthropogenic and natural forcings; and
- The detected signal must be inconsistent with alternative, plausible explanations that exclude important elements of the given combination of proposed forcings.

The last point is particularly important in that it provides a means of eliminating alternative explanations to a signal that might otherwise appear completely consistent with anthropogenic warming.

Attribution can also be achieved, but with considerably less confidence, by using statistical techniques to relate well-attributed variables to other climate phenomena. In this case, the confidence of the attribution would depend upon the plausibility of the hypothesized physical association between the variables. The current controversy regarding the influence to date of anthropogenic warming on tropical cyclones arises from this lower level of confidence.

Confident attribution of an anthropogenic effect depends on the likely magnitude of the anthropogenic effect as well as on the data and model simulations and theoretical understanding available for testing. Thus, if over the next few years a series of strong tropical cyclones were observed in the South Atlantic (a region where such events have been exceedingly rare in the past), we would be justified in concluding, with little formal studies, that this was likely the result of anthropogenic climate change. Similarly, if tropical cyclones off the east coast of Australia regularly started to retain their tropical characteristics as far away from the equator as, say, Sydney, we would again be justified in concluding that this was the result of anthropogenic changes. However, we do not expect such massive changes any time soon. So the question of attribution, given the expected degree of change from anthropogenic causes, is more difficult. This means that it is essential that we contrast the various formal and less-formal approaches to detection and attribution, so that we present balanced expressions of our confidence in any attribution statement. Quite simply, there are approaches than can yield strong statements about attribution, and others that can only yield weaker statements of confidence, given the tools and data available and the expected degree of change due to anthropogenic causes.

Examples of Detection and Attribution Studies

Before detailing the numerous obstacles facing detection and attribution studies of tropical cyclone behavior, we illustrate the process of detection and attribution through the use of a few examples. One of the easiest variables that can be used to demonstrate successful detection and attribution is global mean near-surface air temperature. Such a study is relatively straightforward for a number of reasons. The detected signal for global mean temperature increase in the past 100 years is highly statistically significant (e.g. Trenberth et al. 2007). The data used to estimate this trend have been extensively analyzed over many years and have small error bars. The main tool used for attributing this trend to man-made climate change, the global climate model, simulates global average temperature variability well (Randall et al. 2007). When global climate models are driven by the best available estimates of the radiative forcing of the 20th century, they reproduce well the observed temperature global average increase in the latter part of that century. Finally, when the key man-made elements of the forcing are removed, leaving only the naturally-varying components such as solar forcing, the models fail to reproduce the observed temperature increase. Thus the observed increase in global average temperature in the 20th century can be confidently ascribed to man-made global warming (Hegerl et al. 2007). Numerous earlier studies showed this (e.g Tett et al. 1999; Stott et al. 2001); more recently (Hegerl et al. 2007), this work has been extended to continental-average temperatures over most areas of the globe, demonstrating that these temperature increases can also be attributed to anthropogenic climate change.

Other observed climate trends have been formally ascribed to anthropogenic climate change. Barnett et al. (2005) and Pierce et al. (2006) analyzed trends in upper ocean temperatures in various ocean basins over the period 1960–2000, examining the observed change of temperature with depth and comparing it with the results of climate model simulations. They found that the oceanic warming over this period had been most pronounced in the upper part of the ocean and that this profile of temperature change was well simulated by numerical models using anthropogenic forcing, and could not be simulated when this forcing was removed. An increasing number of attribution studies have considered variables other than temperature. An anthropogenic influence has been formally identified in the increasing height of the tropopause over the last 3 decades (Santer et al. 2003), associated with stratospheric cooling due to ozone depletion and tropospheric warming due to increasing greenhouse gases. Observed multi-decadal changes in global patterns of mean sea level pressure have been attributed to anthropogenic forcing (Gillett 2005), as the observed changes cannot be explained by natural variability and are consistent with the response to anthropogenic forcing. However, the simulated pressure response to anthropogenic forcing is much weaker than the observed pressure trends, even though there is general agreement in the large scale spatial pattern of pressure changes.

These standard techniques have not been successfully applied to all climate variables, however. Problems have been encountered in detection and attribution

studies of variables such as precipitation, due to the generally poor ability of models to simulate precipitation trends, the expected strong regional variations in trends due to climate change and large interannual variability in current and future climates (e.g. Lambert et al. 2004). Similar problems would be encountered in any similar formal attribution studies for tropical cyclones, beginning with the effect of data quality on signal detection.

Detected Trends in Tropical Cyclone Characteristics

Tropical Cyclone Data

The data that are typically used in trend analyses of tropical cyclones are the so-called "best track" data (Neumann et al. 1993). The process of compiling the best track data involves a review of the available tropical cyclone data by tropical cyclone forecasters, usually at the end of the tropical cyclone season, using all data sources available at the time that the review is performed. Thus for climate analysis there are immediate issues regarding the homogeneity of such data, particularly for less well-estimated variables such as tropical cyclone intensity, as the best available techniques for estimating this have changed over time (Landsea et al. 2006).

There are really two questions that need to be addressed in a reanalysis of the best track data, depending on the ultimate use of the data. The data can be made as accurate as possible for each storm, using all data available at the time and our present-day improved knowledge of tropical cyclones to update earlier estimates of variables contained in the data sets. Nevertheless, a data set that was reanalyzed in this fashion would not be homogeneous, as observational data and techniques have improved over time, thus potentially introducing spurious trends into the data. An argument can therefore be made for the creation of a "degraded" but uniform data set, one in which only a base level of data is used, combined with present-day analysis techniques (e.g. Kossin et al. 2007).

There are good reasons to believe that inhomogeneities have been introduced into the tropical cyclone best track record (e.g. Harper 2006; Kepert 2006). A very obvious change was the introduction of weather satellites in the 1960s; before this, many storms would have gone unrecorded. By the 1970s, these polar-orbiting satellites were providing regular, twice-daily visible and infrared images. By the 1980s, geostationary satellites provided 3-hourly coverage. The introduction of passive microwave sensors, followed by scatterometer data and cloud drift winds in the 1990s, provided improved delineation of tropical cyclone structure. Finally, in recent years, 3-axis stabilized geostationary satellites have provided rapid interval scans of tropical cyclones.

Moreover, analysis techniques have themselves changed. The gradual introduction and evolution of the Dvorak (1975, 1984) technique (Velden et al. 2006) of

estimating tropical cyclone intensity from the appearance of the satellite image will have led to changes in estimated tropical cyclone intensities. This is particularly important in regions of the globe where there is no ground truthing of this technique as there is in the Atlantic ocean. More recently, objective techniques (Olander and Velden 2006) have further improved our ability to estimate tropical cyclone intensity.

It can be easily argued that even recent tropical cyclone records are not free from data inhomogeneities. The most telling example of this so far is the analysis of Kamahori et al. (2006) and Wu et al. (2006). Wu et al. (2006) examine trends in severe tropical cyclone numbers in different competing "best-track" data sets in the northwest Pacific region, those of the Joint Typhoon Warning Center, the Hong Kong Observatory and the Japanese Regional Specialized Meteorological Center (RSMC). The JTWC analyzed substantially greater numbers of intense cyclones than the other two forecast offices even in very recent times, when the data should be best. Wu et al. (2006) ascribe this result to the different analysis techniques used in the rival data sets; Kamahori et al. (2006) attribute these differences to modifications made by the Japan Meteorological Agency (JMA) to the original Dvorak technique so that it agreed better with surface observations. At present, it is not clear which data set best represents reality. Other best track data sets have similar issues. In the Australian best data set, three different versions of the Atkinson and Holliday (1977) wind-pressure relationship have been used at various times (Harper 2002; Kepert 2006).

In recognition of these problems, reanalyses of the tropical cylone record have been performed (Landsea et al. 2004; Harper 2006). Recent partial reanalyses of the tropical cyclone record have shown substantial corrections in trends compared with studies that have analysed existing best-track data. Kossin et al. (2007) use geostationary satellite images degraded to a consistent horizontal resolution over the period 1983 to 2005 to remove time-dependent biases, finding that detected changes in a measure of cyclone intensity in basins other than the Atlantic are smaller than in previous analyses. A recent reanalysis of the record in the western Australian region (Harper 2006) has also found that increases in severe tropical cyclone numbers are less than previously estimated using best track data. Landsea et al. (2006) use modern intensity estimation methods applied to satellite images of non-Atlantic tropical cyclones from the late 70s and early 80s to show that the intensities of the storms are likely significantly underestimated in the best track data that were compiled at that time.

There is a limit, however, to the ability of such studies to recreate completely the tropical cyclone record. Clearly, cyclones that have never been observed are lost forever and only estimates can be made of the numbers of storms that have been missed from the record. Landsea (2007) make such an estimate for the Atlantic basin, noting that although this region has been monitored by aircraft reconnaissance since 1944, such observations would not have covered the portion of the Atlantic east of 55W. Landsea (2007) estimates that about 2.2 storms per year would have been missed over the period 1900–1965, before the advent of routine satellite monitoring. In contrast, Holland and Webster (2007) estimate considerably

smaller numbers of missing storms. Moreover, Holland (2007) questions Landsea's (2007) assumption that the ratio of landfalling storms to oceanic storms has been constant over this period, showing that this ratio may have changed due to cyclical variations in the formation locations of tropical cyclones. This conclusion was reinforced by Chang and Guo (2007), who estimate about 1.2 missing storms per year over the same period. In any event, the magnitude of the detected trend in Atlantic tropical cyclone numbers appears only to be reduced, not eliminated entirely when missing storm numbers similar to those assumed by Landsea (2007) are included in the data record (Mann et al. 2007). Any trend analyses of best track data would need to consider this and other data issues.

Trend Analyses

Numerous studies have analyzed tropical cyclone best track data for trends in tropical cyclone numbers and various measures of tropical cyclone intntensity. All recent work suggests that there is no current detectable trend in global tropical cyclone numbers, with numbers typically 80–90 per year (Emanuel 2005; Webster et al. 2005). Regional trends are somewhat more difficult to analyze, given the lower signal to noise ratio due to the high interannual variability of tropical cyclone numbers in many formation basins (e.g. McBride 1995). Analyses that have been performed show different trends in different basins. Most work has been performed in the Atlantic, since this is the basin with the best data. Trends in tropical cyclone indicators in the Atlantic have shown substantial positive trends since 1980, and these trends appear to be real (e.g. Mann et al. 2007). Kossin et al. (2007) show that since 1980, the Atlantic has experienced very large upward trends in an intensity-related variable, the Power Dissipation Index (PDI), a measure of the total integrated power in the storm. According to Kossin et al. (2007), trends in the northwest Pacific have been modest, have been downwards in the northeast Pacific and approximately flat in the other regions.

In other basins, where the data are poorer, there is more dispute regarding trends, particularly of variables like intensity that are more difficult to estimate, leading to uncertainty in detected trends. Intensity trends in the Australian region differ by geographical location, with the northwest region showing some increases in intensity since 1980, but the eastern region exhibiting no trend (Harper 2006; Hassim and Walsh 2008).

In contrast, Webster et al. (2005) found large trends in global tropical cyclone intensities in the period from 1970 to 2004, noting a doubling in the global number of intense category 4 and 5 storms over this period. The value of this paper was that it identified that there *were* such unexplained trends in the best track cyclone data, a fact that was not previously generally appreciated. Nevertheless, subsequent worked showed that these detected trends were likely at least partly the result of artifacts of the data. Kossin et al. (2007) showed that there was no apparent trend in global tropical cyclone intensity over that period, a time during which there was a

substantial increase in category 4 and 5 storms numbers analysed by Webster et al. (2005). Instead, large decadal variations in global numbers of intense hurricanes were found. As already stated, there are a number of reasons to suspect that the best track data analysed by Webster et al. (2005) has artificial trends within it due to changes in observing practices. However, it is not clear to what extent correcting the existing data for inhomogeneities would alter the trends detected by Webster et al. (2005) and others: in other words, whether the trends would be eliminated, reversed or only modified.

In summary, the analysis of tropical cyclone trends is complicated by a lack of consensus regarding the state of the current tropical cyclone data used to determine such trends. The detected trends in the Atlantic ocean basin since 1980 appear to be real, however.

Attribution of Detected Trends in Tropical Cyclones

If a real trend is detected, attribution of such trends could be accomplished in a number of ways. A well-tested theory of tropical cyclone numbers or intensities could be compared with observed trends. Alternatively, a numerical simulation of tropical cyclones could be performed analogous to previously performed simulations of 20th century climate and the results with and without anthropogenic forcing compared with observations. Less confidently, statistical links could be made between well-attributed variables and tropical cyclone characteristics.

Studies that are largely statistical can give indications of associations that need to be investigated, but as tools for attribution they naturally provide less confident results. For example, Holland and Webster (2007) demonstrate a very plausible causal connection between the observed global warming, the warming of sea surface temperatures (SSTs) in the Atlantic and the subsequent changes in tropical cyclone behaviour in that region. A mechanism for this is proposed by Vimont and Kossin (2007), who show that there are apparent strong relationships between variations in tropical cyclone characteristics and the Atlantic Meridional Mode (AMM; see the review by Xie and Carton 2004). This is due to the circulation changes induced by the AMM, including changes to SST anomalies, whereby the main genesis regions of tropical cyclones tend to move equatorward to regions where the MPI is larger and where they are more likely to reach their MPI due to lower wind shear during positive phases of the AMM. One way to improve the confidence of the attribution to global warming in the analysis of Holland and Webster (2007) would be to employ physically-based modelling studies to show that a consequence of warming in the late 20th century is that changes in atmospheric circulation in models forced by changes in anthropogenic factors are consistent with a southward move in the main Atlantic tropical cyclone genesis regions, and that such circulation changes do not occur in unforced simulations. In this way, confidence would be improved in the Holland and Webster (2007)

conclusion that tropical cyclone trends in the Atlantic are due to global warming. Thus such attribution studies need not take the form of direct simulation of tropical cyclones in climate models – and, given the current state of the art, this would be difficult (Walsh 2008). But they should include, where possible, an assessment of how anthropogenic climate change is likely to affect the crucial variables used in detected statistical relationships, employing either simulations or theoretical techniques to do so.

Theoretical Techniques

Tropical Cyclone Numbers

One difficulty with applying theoretical concepts to predict tropical cyclone formation for this purpose is that there is no widely accepted quantitative theory of tropical cyclone formation (Emanuel 1986; Rotunno and Emanuel 1987; Bister and Emanuel 1997; Simpson et al. 1997; Ritchie and Holland 1997; Ritchie et al. 2003; Montgomery and Enagonio 1998; Reasor et al. 2005; Tory et al. 2006). In the absence of such a theory, tropical cyclone genesis parameters have been developed that statistically relate large-scale atmospheric and oceanic fields to formation of tropical cyclones. The earlier work of Gray (1975) and the more recent parameters of Royer et al. (1998), DeMaria et al (2001) and Emanuel and Nolan (2004) all show an ability to diagnose tropical cyclone formation when forced by large-scale fields, but since they are diagnostic parameters, none of them necessarily constitute a predictive theory of formation that would be valid in a changed climate. In particular, Gray's parameter is unrealistically sensitive to changes in SST (Ryan et al. 1992), which severely limits its application to climate change studies.

One way to build confidence that these parameters may be useful in a changed climate would be to compare their predictions with the number of tropical cyclones directly simulated by a climate model in current and enhanced greenhouse climates, applying the large-scale fields generated by the models to the genesis parameters. This approach was employed by McDonald et al. (2005), who found reasonable agreement between the predictions of the Royer et al. (1998) Convective Yearly Genesis Parameter (CYGP) and the model simulation of tropical cyclone formation. Chauvin et al. (2006) reached a similar conclusion, while Camargo et al. (2007) showed mixed results. Royer et al. (2008; this volume) apply the CYGP to the enhanced greenhouse predictions of fifteen general circulation models, finding a wide variation of responses of the CYGP, due to the considerable differences in the models' SST predictions in a warmer world. These conclusions are also subject to the criteria used to identify tropical cyclones in the output of climate models (Walsh et al. 2007); if different selection criteria are used, different numbers of tropical cyclones would be detected. One potential use of these cyclone genesis parameters in a detection and attribution study would be to apply them to a suite of forced

and unforced model simulations to determine whether there are any systematic differences in the genesis potential between the two and compare the differences to observed trends.

Tropical Cyclone Intensities

In contrast to tropical cyclone numbers, the theory of tropical cyclone intensities appears to be on a firmer foundation. The theory of tropical cyclone maximum potential intensity (MPI; Emanuel 1986, 1988) suggests that a tropical cyclone may be viewed as a Carnot cycle heat engine, with the warm reservoir being the sea surface temperature (or upper ocean heat content) and the cold reservoir being the upper tropospheric outflow temperature. The alternative, thermodynamic adjustment theory of Holland (1997) gives similar results. The application of earlier versions of these theories to the output of GCM simulations has suggested that increases in peak tropical cyclone intensities of 5–10% could occur some time after 2050 (Emanuel 1987; Henderson-Sellers et al. 1998; Walsh 2004).

Emanuel (2007) points out that the MPI predictions of Emanuel (1987) for the rate of change of intensity increase in the Atlantic since the 1970s, based upon the observed increase in SST, are considerably less than the observed changes in intensity in the Atlantic during that time. Emanuel (2007) has presented a new calculation based on the revised technique of Bister and Emanuel (2002). This version results in much better agreement with the observed intensity change in the Atlantic. Emanuel (2007) investigated the causes of the observed increase of tropical cyclone power dissipation index (PDI) over the period since 1950. He also created a diagnostic parameter that included the effects of changes in potential intensity, low-level vorticity and vertical wind shear. The results showed that the observed increase of PDI in the Atlantic since 1980 was consistent with changes in these three factors, including increases in low-level vorticity and potential intensity. The increases in potential intensity since 1980 were caused by increases in SST and decreases in upper troposphere temperature in the tropical Atlantic, thus increasing the thermodynamic efficiency of tropical cyclones. Note that the PDI is an integrated measure of cyclone characteristics and as such may not be the most sensitive variable for use in studies of detection and attribution.

Thus these results appear to indicate, with good skill, relationships between trends in large-scale variables and tropical cyclone PDI. Regarding attribution of these trends, it is clear that there is a relationship between the increases in Atlantic tropical SST and similar increases in global temperatures that have been well ascribed to global warming (Elsner 2006; Mann and Emanuel 2006; Trenberth and Shea 2006; Elsner 2007). In particular, Santer et al. (2006) showed this by using the standard formal attribution methodology in which a number of model simulations of 20th century climate were run with and without greenhouse gas forcings, so this is a conclusion with high confidence. It is also true that a number of studies have demonstrated a plausible statistical relationship between SST increases and intense tropical cyclone numbers in the Atlantic (Hoyos et al. 2006; Holland and

Webster 2007) and increases in SST are an expected consequence of global warming. Nevertheless, the decreases in tropical upper troposphere (100 hPa) temperature, which Emanuel (2007) found contributed to increased Atlantic tropical cyclone intensity, are not expected consequences of global warming. Meehl et al. (2007), among many others, show that tropical temperatures are expected to warm at this altitude in the 21st century, which is inconsistent with an anthropogenic cause for the observed cooling. It is also not clear why the low-level vorticity in the tropical Atlantic has been increasing. Nor is it clear what the relationship is between low-level vorticity and global warming. Thus the attribution of the increases in Atlantic tropical cyclone PDI to factors related to global warming is of less confidence as a result. For increased confidence, one would have to examine the simulation of Emanuel's (2007) diagnostic PDI in climate models forced with and without anthropogenic factors over the late 20th century. Additionally, the relationship between SST and PDI is much weaker in the northwest Pacific than in the Atlantic, where SSTs have also been increasing since 1980, but where the trend in PDI is not pronounced (Klotzbach 2006; Emanuel 2007). This is due to different trends in vertical wind shear and vorticity in this region. These different regional trends would also have to be seen in 20th-century climate simulations for confident attribution.

Simulation Techniques

Numerous studies have employed climate models to directly simulate the formation and intensification of tropical cyclones. Since the early work of Manabe et al. (1970), the ability of climate models to generate lows that resemble tropical cyclones has developed considerably. Currently, numerous groups worldwide are developing a capability to perform these types of simulations. A recent review is given in Walsh (2008).

Climate models have varying abilities to simulate tropical cyclone characteristics. In general, though, they usually do not simulate numbers that are very close to observed formation rates. One difficulty, as detailed in Walsh et al. (2007), is that the storm detection schemes used to determine the rate of formation within the models are often tuned to the observed formation rate, thus making it impossible to determine the actual ability of the model to generate tropical cyclones in the current amount.

The situation is even worse for intensities, with climate models having an inadequate simulation of the observed cyclone intensity distribution, mostly simulating tropical cyclones that are considerably weaker than observed. Thus simulating observed intensity trends as part of a model-based attribution study would be problematic.

Nevertheless, in general agreement with the earlier predictions of MPI theory, direct simulations of the effect of global warming on tropical cyclones suggest intensity increases of 5–10% by some time after 2050 (Knutson and Tuleya 1999; Walsh and Ryan 2000; Knutson et al. 2001; Knutson and Tuleya 2004).

Thus at present direct simulation as a tool for detection and attribution studies is in its infancy. Recently, though, Knutson et al. (2007) showed that a modeling system could reproduce the observed trend in Atlantic tropical cyclone numbers over the period 1980–2005. Emanuel et al. (2008) use a downscaling methodology employing a synthetic track generator to produce climatologies of tropical cyclones from climate model output. Similar modeling systems have the potential to elucidate the causes of the increase in numbers in the Atlantic by performing attribution experiments that change aspects of the simulation and examine their effects on simulated formation rates.

What is Required to Improve Detection and Attribution?

At present, the possibility that anthropogenic warming has affected tropical cyclone behavior in the Atlantic is a plausible hypothesis. Hegerl et al. (2007) indicate that it is more likely than not that anthropogenic warming has affected tropical cyclone behavior. This is a fairly weak conclusion but it is the best that we can obtain at present. It should be noted that the detection and attribution of a human influence on global climate has been an evolutionary process, with relatively weaker conclusions based on less formal approaches reached in the IPCC Second Assessment (Santer et al 1995). The Summary for Policymakers of that assessment concluded "The balance of evidence suggests a discernible human influence on global climate" (Houghton et al. 1995), which is much weaker than the conclusions of the IPCC Fourth Assessment: "Most of the observed increase in globally averaged temperatures since the mid-20th century is *very likely* due to the observed increase in anthropogenic greenhouse gas concentrations" (Hegerl et al. 2007).

The formal attribution process as clearly defined by the IPCC is the best way to make strong conclusions about climate change effects. Due to the current inadequacies of tropical cyclone models and theories, formal attribution following the IPCC approach is not possible at this time. Therefore we must also employ other methods, as has been done in the past for assessing the possible effects of global warming on the future behavior of tropical cyclones (e.g. Henderson–Sellers et al. 1998; Walsh 2004). It is inevitable that this will involve making hypotheses about the physical reality of statistical relationships between variations in variables that have already been formally attributed and variations in tropical cyclone characteristics. The level of confidence for attribution of these statistical relationships is directly related to the level of confidence that we have in the hypothesized physical relationship that explains them. If these physical relationships are well-established, either by theory, simulation or observation at shorter time scales, then this confidence can be reasonably high. Moreover, there must also be some reason to believe that this physical relationship will remain the same in a warmer world. These ideas could provide the basis for a more structured approach to attribution until such time as simulations and theory improve to the point when the much stronger formal attribution process becomes possible.

The first step in any attribution process, formal or otherwise, is detection of a trend. Improved tropical cyclone data records would increase our confidence that trends had actually been detected and were simply not due to data inhomogeneities. There are a number of approaches that could be undertaken: a consistent reanalysis of the polar-orbiting satellite record, for instance, could be performed similar to the method used Kossin et al. (2007) for the geostationary satellite data. Given the finer resolution or the polar-orbiting satellites, this may lead to a more accurate determination of intensity trends. There are a number of limitations of any reanalysis procedure, however. As mentioned previously, storms that were never observed by anyone are gone forever, and only estimates can be made of their effect on any detected trends. For a reanalysed tropical cyclone data set to most useful for climate analysis, there have to be no artificial trends in the data caused by changes in observing practices. The reanalysis of Kossin et al. (2007) attempts this but at the cost of a degraded resolution of recent satellite data. One possibility would be instead to create a best track dataset with all available data but include error estimates that are larger for earlier storms. In this way, climate trends could still be analysed with statistical techniques that take into account the change in the error distribution with time when statistical significance of trends is calculated. Additionally, change points in the observing systems should have created change points in the data, and these can be corrected using well-established methods (e.g. Lanzante et al. 2003).

Once a robust trend is detected, the attribution step would ideally utilize an excellent climate model that produces tropical cyclones of about the right intensity and numbers, run with and without anthropogenic forcing, that would reproduce with reasonable fidelity the observed intensity trends, particularly in the Atlantic. The work of Knutson et al. (2007) is an important step in this direction, as their results imply that the increase in tropical cyclone numbers in the Atlantic is related to the pattern of the observed SSTs that were used to force their model. Since the SST anomalies are likely related to global warming, at first glance this suggests a causal link between global warming and tropical cyclone numbers in the Atlantic. Similar models will be used to run coupled climate runs that could then help identify the anthropogenically-forced transient climate response of tropical cyclones in the Atlantic and elsewhere.

In the absence of excellent climate model simulations, studies such as those of Emanuel (2007) could be further analysed to strengthen their conclusions. Specifically, it is presently unclear whether all of the individual components of his PDI parameter (MPI, vorticity and vertical wind shear) are varying in a manner consistent with an anthropogenic cause. An anthropogenic influence on MPI is likely, based on its formulation and our theoretical understanding of influences on tropical cyclone intensity, but this is not clear for vorticity or vertical wind shear. For instance, Vecchi and Soden (2007) show that multi-model projections of vertical wind shear trends in the Atlantic over the 21st century are strongly positive in parts of the tropical Atlantic (i.e. more hostile to cyclone formation), although trends are neutral in the main development region. This issue can be addressed by examining changes in the large-scale atmospheric fields between two sets of GCM simulations,

with and without anthropogenic forcing, to determine whether the observed trends in vorticity and vertical wind shear are similar to those expected from anthropogenic forcing. Similar studies could be performed with other hypothesized combinations of variables. If a quantitative theory of tropical cyclone formation were to be developed, studies along these lines could also address the issue of the relative responses of formation and intensification to anthropogenic forcing. Important in all of these type of studies is whether there are good reasons to believe that relationships between parameters will remain the same in a warmer world. Such reasons would include a theory successfully tested at shorter time scales, such as the Emanuel MPI theory or a well-established observed relationship that is not expected to change in a warmer world, such as that between vertical wind shear and tropical cyclone intensification (e.g. Vecchi and Soden 2007).

Excellent climate model simulations have the potential to suggest where and when the detection of an anthropogenically-forced tropical cyclone signal might be achieved. Leslie and Karoly (2007) examine this issue using multi-member ensembles of simulations with a variable-resolution climate model, including both control and climate change simulations. They show that there is large natural decadal variability in the simulated number of strong tropical cyclones per decade in the northeast Australian region but that the simulated increase in strong tropical cyclones due to anthropogenic climate change should appear above the noise some time in the 2020s or later. The confidence of this prediction would be substantially increased if other independent models were to make similar predictions.

The formal detection and attribution methods described above and in Hegerl et al. (2007) use a null hypothesis of no expected change in the climate variable being considered, apart from that due to natural internal climate variations. Now that there is a substantial body of scientific research supporting the conclusion that most of the observed global average temperature increase since the mid-20th century is very likely (more than 90% certain) due to the increase in anthropogenic greenhouse gases in the atmosphere (Hegerl et al., 2007), it may be more appropriate to use a different null hypothesis. It is now appropriate to use a null hypothesis that global scale temperature increases, including sea surface temperature increases, over the past fifty years have a significant anthropogenic influence and then apply the same attribution methods to detect and attribute an anthropogenic climate change influence on tropical cyclones. The problem is substantially changed, now making use of the prior information that anthropogenic climate change is causing large scale warming and then seeking to quantify the specific changes expected to occur in the frequency and intensity of tropical cyclones. This is essentially a Bayesian statistical approach (e.g. Lee et al. 2005).

The use of Bayesian statistics has the potential to increase the sensitivity of detection and attribution studies and make it easier to increase the confidence that observed changes are due to anthropogenic influences. Bayesian techniques are being increasingly employed in atmospheric and oceanic statistical models (Wikle 2000; Berliner et al. 2002; Katz 2002). Elsner et al. (2004) apply Bayesian statistics to detect discontinuities ("change points") in hurricane data, while Elsner and Jagger (2004) show that the inclusion of 19th century data as priors improved the

significance of relationships between indices of ENSO and the NAO and 20th century North American coastal hurricane incidence. Jagger and Elsner (2006) used Bayesian extreme value statistics to show that warmer global temperatures were associated with larger numbers of intense hurricanes, although this result was not highly significant. Their results could also be interpreted to show that observed increases in global temperature and increases in maximum hurricane intensity are consistent with MPI theory.

Conclusion

Fundamentally, the main issue here is that the more sound, physically-based methods there are that make the same prediction, the more confidence that can be placed in that prediction. Formal detection and attribution of a climate change signal requires more than a plausible physical association between variables; it requires that predictive tools are employed to distinguish anthropogenic effects from natural variability. Current studies clearly show a detected signal of tropical cyclone changes in the Atlantic and there have been plausible arguments relating these changes to global warming. But formal attribution of these trends, quantifying the fraction of the observed change due to anthropogenic climate change and the fraction due to natural climate variations, has not taken place—yet. For this to occur, climate model simulations and theories of tropical cyclones need to improve. In the meantime, improved inferences can be made using a combination of large-scale numerical simulation and statistical methods. Such a process is vital in increasing the confidence of future projections of climate change.

References

Atkinson, G.D., and C.R. Holliday, 1977: Tropical cyclone minimum sea level pressure maximum sustained wind relationship for the western North Pacific. *Mon. Wea. Rev.,* **105**, 421–427.

Barnett, T.P., D.W. Pierce, K.M. AchutaRao, P.J. Gleckler, B.D. Santer, J.M. Gregory, and W.M. Washington, 2005: Penetration of a warming signal in the world's oceans: human impacts. *Science,* **309**, 284–287.

Berliner, L.M., C.K. Wikle, and N. Cressie, 2002: Long-lead prediction of Pacific SSTs via Bayesian dynamic modeling. *J. Climate,* **13**, 3953–3968.

Bister M, and K.A. Emanuel, 1997: The genesis of Hurricane Guillermo: TEXMEX analyses and a modeling study. *Mon. Wea. Rev.,* **125**, 2662–2682.

Bister M, and K.A. Emanuel, 2002: Low frequency variability of tropical cyclone potential intensity. 1: Interannual to interdecadal variability. *J. Geophys. Res.,* **107**, doi:10.1029/2001JD000776.

Camargo, S.J., A.H. Sobel, A.G. Barnston, and K.A. Emanuel, 2007: Tropical cyclone genesis potential in climate models. *Tellus A* **59**, 428–443.

Chang, E.K.M., and Y. Guo, 2007: Is the number of North Atlantic tropical cyclones significantly underestimated prior to the availability of satellite observations? *Geophys. Res. Letters*, **34**, L14801, doi:10.1029/2007GL030169.

Chauvin, F., J.-F. Royer, and M. Déqué, 2006: Response of hurricane-type vortices to global warming as simulated by ARPEGE-Climat high resolution. *Clim. Dyn.,* **27**, 377–399.

DeMaria, M., J.A. Knaff, and B.H. Connell, 2001: A tropical cyclone genesis parameter for the Tropical Atlantic. *Wea. Forecasting*, **16**, 219–233.

Dvorak, V.F., 1975: Tropical cyclone intensity analysis and forecasting from satellite imagery. *Mon. Wea. Rev.,* **103**, 420–430.

Dvorak, V.F., 1984: Tropical cyclone intensity analysis using satellite data. NOAA Tech. Rep. NESDIS 11, 47 pp. (Available from NOAA-NESDIS, World Weather Building, Washington, DC 20235).

Elsner, J.B., 2006: Evidence in support of the climate change-Atlantic hurricane hypothesis. *Geophys. Res. Letters,* **33**, doi:10.1029/2006GL026869.

Elsner, J.B., 2007: Granger causality and Atlantic hurricanes. *Tellus A*, **59**, 476–485.

Elsner, J.B., and T.H. Jagger, 2004: A hierarchical Bayesian approach to seasonal hurricane modeling. *J. Climate*, **17**, 2813–2827.

Elsner, J.B., X.-F. Niu, and T.H. Jagge, 2004: Detecting shifts in hurricane rates using a Markov chain Monte Carlo approach. *J. Climate*, **17**, 2652–2666.

Emanuel, K.A., 1986: An air-sea interaction theory for tropical cyclones. Part I: Steady-state maintenance. *J. Atmos. Sci*., **43**, 585–604.

Emanuel, K.A., 1987: The dependence of hurricane intensity on climate. *Nature,* **326**, 483–485.

Emanuel, K.A., 1988: The maximum intensity of hurricanes. *J. Atmos. Sci.,* **45**, 1143–1155.

Emanuel, K.A., 2005: Increasing destructiveness of tropical cyclones over the past 30 years. *Nature,* **436**, 686–688.

Emanuel, K., 2007: Environmental factors affecting tropical cyclone power dissipation. *J. Climate,* **22**, 5497–5509.

Emanuel, K., R. Sundararjan, and J. Williams, 2008: Hurricanes and global warming: results from downscaling IPCC AR4 simulations. *Bull. Amer. Meteorol. Soc*., submitted.

Emanuel, K.A., D.S. Nolan, 2004: Tropical cyclone activity and global climate. In:: Proceedings of 26th Conference on Hurricanes and Tropical Meteorology, American Meteorological Society, pp 240–241.

Franklin, J.L., M.L. Black, and K. Valde, 2003: GPS dropwindsonde wind profiles in hurricanes and their operational implications. *Wea. Forecast,* 18, 32–44.

Gillett, N.P., R.J. Allan, and T.J. Ansell, 2005: Detection of external influence on sea level pressure with a multi-model ensemble. *Geophys. Res. Letters,* **32**, L19714, doi:10.1029/2005GL023640.

Gray, W.M., 1975: Tropical Cyclone Genesis. Dept of Atm Sci Paper No. 234, Colorado State Univ., Ft. Collins, CO

Harper, B.A., 2002: Tropical cyclone parameter estimation for the Australian region: wind-pressure relationships and related issues for engineering planning and design. Discussion paper prepared by Systems Engineering Australia, 56 pp + appendices

Harper, B.A., 2006: Analysis of tropical cyclone climate change trends. Report prepared for Woodside Energy Ltd. by Systems Engineering Australia, 38 pp + appendices.

Hasssim, M., and K.J.E. Walsh, 2008: Tropical cyclone trends in the Australian region. *Geochem. Geophys. Geosyst*., **9**, Q07V07, doi:10.1029/2007GC001804.

Hegerl, G.C., F.W. Zwiers, P. Braconnot, N.P. Gillett, Y. Luo, J.A. Marengo Orsini, N. Nicholls, J. E. Penner, and P.A. Stott, 2007: Understanding and Attributing Climate Change. In: Solomon S, Qin D, Manning M, Chen Z, Marquis M, Averyt KB. Tignor M, Miller HL (eds.) Climate Change 2007: The Physical Science Basis. Contribution of Working Group I to the Fourth Assessment Report of the Intergovernmental Panel on Climate Change. Cambridge University Press, Cambridge, United Kingdom and New York, NY, USA, pp 663–745.

Henderson–Sellers, A., H. Zhang, G. Berz, K. Emanuel, W. Gray, C. Landsea, G. Holland, J. Lighthill, S.-L. Shieh, P. Webster, K. McGuffie, 1998: Tropical cyclones and global climate change: a post-IPCC assessment. *Bull. Amer. Met. Soc.,* **79**, 19–38.

Holland, G.J., 1997: The maximum potential intensity of tropical cyclones. *J. Atmos. Sci.,* **54**, 2519–2525.

Holland, G.J., and P.J. Webster, 2007: Heightened tropical cyclone activity in the North Atlantic: natural variability or climate trend? *Phil. Tran. Roy. Soc. A*, doi:10.1098/rsta.2007.2083.

Houghton, J.T., L.G. Meira Filho, B.A. Callander, N. Harris, A. Kattenberg, K. Maskell (eds.), 1995: Climate Change 1995: The Science of Climate Change. Contribution of WGI to the Second Assessment Report of the Intergovernmental Panel on Climate Change. Cambridge University Press, Cambridge, United Kingdom, 572 pp.

Hoyos, C.D., P.A. Agudelo, P.J. Webster, and J.A. Curry, 2006: Deconvolution of the factors contributing to the increase in global hurricane activity. *Science,* **312**, 94–97.

Jagger, T.H., and J.B. Elsner, 2006: Climatology models for extreme hurricane winds near the United States. *J. Climate,* **19**, 3220–3236.

Kamahori, H., N. Yamazaki, N. Mannoji, and K. Takahashi, 2006: Variability in intense tropical cyclone days in the western North Pacific. *SOLA,* **2**, 104–107.

Katz, R.W., 2002: Techniques for estimating uncertainty in climate change scenarios and impact studies. *Climate Res.,* **20**, 167–185.

Kepert, J., 2006: The Need For a Tropical Cyclone Reanalysis in the Australian Region. In: Proceedings of Bureau of Meteorology/ARC Network for Earth System Science workshop on the reanalysis of the Australian tropical cyclone record, August 16, 2006, Melbourne, Australia. Available at http://www.arcness.mq.edu.au/fileadmin/general/docs/58_-_Intro_ARCNESS_BoM_1.pdf.

Klotzbach, P.J., 2006: Trends in global tropical cyclone activity over the past twenty years (1986-2005). *Geophys Res Letters*, **33**, L10805, doi:10.1029/2006GL025881.

Knutson, T.R., and R.E. Tuleya, 1999: Increased hurricane intensities with CO2-induced warming as simulated using the GFDL hurricane prediction system. *Clim. Dyn.,* **15**, 503–519.

Knutson, T.R., R.E. Tuleya, W. Shen, and I. Ginis, 2001: Impact of CO2-induced warming on hurricane intensities as simulated in a hurricane model with ocean coupling. *J. Climate,* **14**, 2458–2468.

Knutson, T.R., R.E. Tuleya, 2004: Impact of CO2-induced warming on simulated hurricane intensity and precipitation: sensitivity to the choice of climate model and convective parameterization. *J. Climate,* **17**, 3477–3495.

Knutson, T.R., J.J. Sirutis, S.T. Garner, I.M. Held, R.E. Tuleya, 2007: Simulation of the recent multi-decadal increase of Atlantic hurricane activity using an 18-km grid regional model. *Bull. Amer. Meteorol. Soc.,* **88**, 1549–1565.

Kossin, J.P., K.R. Knapp, D.J. Vimont, R.J. Murnane, B.A. Harper, 2007: A globally consistent reanalysis of hurricane variability and trends. *Geophys. Res. Lett.*, **34**, L04815, doi:10.1029/2006GL028836.

Lambert, F.G., P.A. Stott, M.R. Allen, and M.A. Palmer, 2004: Detection and attribution of changes in 20th century land precipitation. *Geophys. Res. Lett.,* **31**: L10203, doi:10.1029/2004GL019545.

Landsea, C.W., 2007: Counting Atlantic tropical cyclones back to 1900. *EOS,* **88**, 197–208.

Landsea, C.W., C. Anderson, N. Charles, G. Clark, J. Dunion, J. Fernandez-Partagas, P. Hungerford, C. Neumann, and M. Zimmer, 2004: The Atlantic hurricane database re-analysis project: Documentation for the 1851–1910 alterations and additions to the HURDAT database. In: Murname RJ, Liu, K-B (eds), Hurricanes and Typhoons: Past, Present and Future, Eds., Columbia University Press, pp 177–221.

Landsea, C.W., B.A. Harper, K. Hoarau,and J.A. Knaff, 2006: Can we detect trends in extreme tropical cyclones? *Science*, **313**, 452–453.

Lanzante, J.R., S.A. Klein, and D.J. Seidel, 2003: Temporal homogenization of monthly radiosonde temperature data. Part I: Methodology. *J. Climate,* **16**, 224–240.

Lee, T.C.K., F.W. Zwiers, G.C. Hegerl, X. Zhang, M. Tsai, 2005: A Bayesian climate change detection and attribution assessment. *J. Climate,* **18**, 2429–2440.

Leslie, L.M., D. Karoly, M. Leplastrier, and B.W. Buckley, 2007: Variability of tropical cyclones over the South-West Pacific ocean using a high resolution climate model. *Meteorol. Atm. Phys.,* **97**, 171–180.

Manabe, S., J.L. Holloway, Jr., and H.M. Stone, 1970: Tropical circulation in a time-integration of a global model of the atmosphere. *J. Atmos. Sci.,* **27**, 580–613.

Mann, M.E., and K.A. Emanuel, 2006: Atlantic hurricane trends linked to climate change. *EOS,* **87**, 233–244.

Mann, M.E., G.J. Holland, and P.J. Webster, 2007: Atlantic tropical cyclones revisited. *EOS*, **88**, 349–350.

McBride, J.L., 1995: Tropical cyclone formation. In: Elsberry RL (ed) Global perspectives on tropical cyclones, WMO/TD-No. 693, pp 63–105.

McDonald, R.E., D.G. Bleaken, D.R. Cresswell, V.D. Pope, and C.A. Senior, 2005: Tropical storms: representation and diagnosis in climate models and the impacts of climate change. *Clim. Dyn.,* **25**, 19–36.

Meehl, G.A., T.F. Stocker, W.D. Collins, P. Friedlingstein, A.T. Gaye, J.M. Gregory, A. Kitoh, R. Knutti, J.M. Murphy, A. Noda, R.C.B. Raper, I.G. Watterson, A.J. Weaver, and Z.-C. Zhao, In: Solomon S, Qin D, Manning M, Chen Z, Marquis M, Averyt KB. Tignor M, Miller HL (eds.) Climate Change 2007: The Physical Science Basis. Contribution of Working Group I to the Fourth Assessment Report of the Intergovernmental Panel on Climate Change. Cambridge University Press, Cambridge, United Kingdom and New York, NY, USA, pp 747–845.

Montgomery, M.T., and J. Enagonio, 1998: Tropical cyclogenesis via convectively forced vortex Rossby waves in a three dimensional quasigeostrophic model. *J. Atmos. Sci*., **55**, 3176–3207.

Neumann, C.J., B.R. Jarvinen, C.J. McAdie, and J.D. Elms, 1993: Tropical cyclones of the North Atlantic Ocean, 1871–1992. NOAA National Climatic Data Center and National Hurricane Center, 193 pp.

Olander, T., and C.S. Velden, 2005: The Advanced Dvorak Technique (ADT) - Continued development of an objective scheme to estimate TC intensity using geostationary IR satellite imagery. *Wea. Forecasting,* **22**, 287–298.

Pierce, D.W., T.P. Barnett, K.M. AchutaRao, P.J. Gleckler, J.M. Gregory, and W.M. Washington, 2006: Anthropogenic warming of the oceans: observations and model results. *J. Clim*., **19**, 1873–1900.

Randall, D.A., R.A. Wood, S. Bony, R. Colman, T. Fichefet, J. Fyfe, V. Kattsov, A. Pitman, J. Shukla, J. Srinivasan, R.J. Stouffer, A. Sumi, and K.E. Taylor, 2007: Climate models and their evaluation. In: Solomon S, Qin D, Manning M, Chen Z, Marquis M, Averyt KB. Tignor M, Miller HL (eds.) Climate Change 2007: The Physical Science Basis. Contribution of Working Group I to the Fourth Assessment Report of the Intergovernmental Panel on Climate Change. Cambridge University Press, Cambridge, United Kingdom and New York, NY, USA, pp 590–662.

Reasor, P.D., M.T. Montgomery, and L.F. Bosart, 2005: Mesoscale observations of the genesis of Hurricane Dolly (1996). *J. Atmos. Sci.,* **62**, 3151–3171.

Ritchie, E.A., and G.J. Holland, 1997: Scale interactions during the formation of Typhoon Irving. *Mon. Wea. Rev*., **125**, 1377–1396.

Ritchie, E., J. Simpson, W.T. Liu, J. Halverson, C.S. Velden, K.F. Brueske, H. Pierce, 2003: Present day satellite technology for hurricane research. In: Simpson R (ed.) Hurricane: Coping with Disaster*, Amer Geophys Union,* pp 249–289.

Rotunno, R., and K.A. Emanuel, 1987: An air-sea interaction theory for tropical cyclones. Part II. *J. Atmos. Sci.,* **44**, 542–561.

Royer, J.-F., F. Chauvin, B. Timbal, P. Araspin, and D. Grimal, 1998: *Clim. Change,* **38**, 307–343.

Royer, J.-F., and F. Chauvin, 2008: Response of tropical cyclogenesis to global warming in IPCC AR-4 scenarios assessed by a modified yearly genesis parameter (this volume).

Ryan, B.F., I.G. Watterson, and J.L. Evans, 1992: Tropical cyclone frequencies inferred from Gray's yearly genesis parameter: Validation of GCM tropical climates. *Geophys. Res. Letters,* **19**, 1831–1834.

Santer, B.D., T.M.L. Wigley, T.P. Barnett, and E. Anyamba, 1995: Detection of Climate Change and Attribution of Causes. In: Houghton JT, Meira Filho LG, Callander BA, Harris N, Kattenberg A, Maskell K (eds.) Climate Change 1995: The Science of Climate Change. Contribution of WGI to the Second Assessment Report of the Intergovernmental Panel on Climate Change Cambridge University Press, Cambridge, United Kingdom, pp 407–443.

Santer, B.D., M.F. Wehner, T.M.L. Wigley, R. Sausen, G.A. Meehl, K.E. Taylor, C. Ammann, J. Arblaster, W.W. Washington, J.S. Boyle, and W. Brugemann, 2003: Contributions of natural and anthropogenic forcing to recent tropopause height changes. *Science* **301**: 479–483.

Santer, B.D., T.M.L. Wigley, P.J. Gleckler, C. Bonfils, M.F. Wehner, K. AchutaRao, T.P. Barnett, J.S. Boyle, W. Bruggemann, M. Fiorino, N. Gillett, J.E. Hansen, P.D. Jones, S.A. Klein, G.A. Meehl, S.C.B. Raper, R.W. Reynolds, K.E. Taylor, and W. M. Washington, 2006: Forced and unforced ocean temperature changes in Atlantic and Pacific tropical cyclone genesis regions. *Proc. Natl. Acad. Sci. USA,* **103**, 13,905–13,910.

Simpson, J., E.A. Ritchie, G.J. Holland, J. Halverson, and S. Stewart, 1997: Mesoscale interactions in tropical cyclone genesis. *Mon. Wea. Rev.,* **125**, 2643–2661.

Stott, P.A., S.F.B. Tett, G.S. Jones, M.R. Allen, W.J. Ingram, and J.F.B. Mitchell, 2001: Attribution of twentieth century temperature change to natural and anthropogenic causes. *Clim. Dyn.,* **17**, 1–21.

Tett, S.F.B., P.A. Stott, M.R. Allen, W.J. Ingram, and J.F.B. Mitchell, 1999: Causes of twentieth-century temperature change near the Earth's surface. *Nature*, **399**, 569–572.

Tory, K.J., M.T. Montgomery, and N.E. Davidson, 2006: Prediction and diagnosis of tropical cyclone formation in an NWP system. Part I: The critical role of vortex enhancement in deep convection. *J. Atmos. Sci.,* **63**, 3077–3090.

Trenberth, K.E., P.D. Jones, P. Ambenje, R. Bojariu, D. Easterling, A. Klein Tank, D. Parker, F. Rahimzadeh, J.A. Renwick, M. Rusticucci, B. Soden, and P. Zhai, 2007: Observations: Surface and atmospheric climate change. In: Solomon S, Qin D, Manning M, Chen Z, Marquis M, Averyt KB. Tignor M, Miller HL (eds.) Climate Change 2007: The Physical Science Basis. Contribution of Working Group I to the Fourth Assessment Report of the Intergovernmental Panel on Climate Change. Cambridge University Press, Cambridge, United Kingdom and New York, NY, USA, pp 235–336.

Trenberth, K.E., and D.J. Shea, 2006: Atlantic hurricanes and natural variability in 2005. *Geophys. Res. Lett.,* **33**, L12704, doi:10.1029/2006GL026894.

Velden, C., B. Harper, F. Wells, J. Beven, R. Zehr, T. Olander, M. Mayfield, C. Guard, M. Lander, R. Edson, L. Avila, A. Burton, M. Turk, A. Kikuchi, A. Christian, P. Caroff,and M. McCrone, 2006: The Dvorak tropical cyclone estimation technique. *Bull. Amer. Meteorol. Soc*., **87**, 1995–1210.

Vecchi, G.A., and B.J. Soden, 2007: Increased tropical Atlantic wind shear in model projections of global warming. *Geophys. Res. Letters,* **34**, doi:10.1029/2006GL028905.

Vimont, D.J., and J.P. Kossin, 2007: The Atlantic meridional mode and hurricane activity, *Geophys. Res. Lett*., L07709, doi:10.1029/2007GL029683.

Xie., S.–P., and J.A. Carton, 2004: Tropical Atlantic variability: Patterns, mechanisms, and impacts. In: Wang C, Xie S-P, Carton JA (eds) Earth's Climate: The Ocean-Atmosphere Interaction, AGU Press.

Walsh. K., 2004: Tropical cyclones and climate change: unresolved issues. *Climate Research*, **27**, 77–83.

Walsh, K., 2008: The ability of climate models to generate tropical cyclones: implications for prediction. In: Peretz L (ed.) Climate Change Research Progress, Nova Publishers, pp. 313–329

Walsh, K., M. Fiorino, C. Landsea, and K. McInnes, 2007: Objectively-determined resolution-dependent threshold criteria for the detection of tropical cyclones in climate models and reanalyses. *J. Climate,* **20**, 2307–2314.

Walsh, K.J.E., and B.F. Ryan, 2000: Tropical cyclone intensity increase near Australia as a result of climate change. *J. Climate,* **13**, 3029–3036.

Webster, P.J., G.J. Holland, J.A. Curry, and H.-R. Chang, 2005: Changes in tropical cyclone number, duration and intensity in a warming environment. *Science,* **309**, 1844–1846.
Wikle, C.K., 2000: Hierarchical space-time dynamic models. In: Berliner LM, Nychka D, Hoar T (eds) Lecture Notes in Statistics: Studies in the Atmospheric Sciences, Springer.
Wu., M.-C., K.-H. Yeung, and W.-L. Chang, 2006: Trends in western North Pacific tropical cyclone intensity. *EOS,* **87**, 537–548.

Electrification in Hurricanes: Implications for Water Vapor in the Tropical Tropopause Layer

Jasna V. Pittman, Themis G. Chronis, Franklin R. Robertson, and Timothy L. Miller

Abstract This study explores the relation between lightning frequency associated with hurricanes and water vapor in the Tropical Tropopause Layer (TTL) over the Tropical Americas (Caribbean and Gulf of Mexico) during the 2005 hurricane season. The hypothesis herein is that hurricanes that exhibit increases in lightning frequency are associated with stronger updrafts that can transport more moisture into the TTL. This added moisture can potentially be transported irreversibly into the stratosphere and alter the chemical and radiative properties of this layer of the atmosphere. Several studies predict increases in hurricane intensity, particularly in the Atlantic basin, as a result of increases in sea surface temperature due to global warming. Given that climate forecasts are very sensitive to water vapor concentrations in the TTL and in the stratosphere, it is essential to understand the effect that hurricanes have on TTL moisture.

In our analysis, we use a combination of ground-based and space-borne measurements. These measurements consist of cloud-to-ground lightning data from the Long Range Lightning Detection Network, GOES–12 infrared brightness temperatures, and water vapor from the Microwave Limb Sounder instrument aboard the Aura satellite obtained at 100, 147, and 215 hPa. In general, we find a negative correlation between lightning frequency and storm intensification (i.e., minimum central pressure) with a significant storm-to-storm variability. On hurricane days, we find hydration within 5° from the center of the storm at the 215 and 147 hPa levels, and practically no perturbation to the 100 hPa water vapor field by the storms. Statistical analysis show weak but statistically significant correlations between lightning frequency and 215 hPa MLS water vapor ($r = +0.2115$), 215 hPa and 147 hPa MLS water vapor ($r = +0.2689$), and 147 hPa and 100 hPa MLS water vapor ($r = -0.2936$) within the uncertainty of the measurements. These correlations suggest that increases in lightning frequency correspond to hydration of the upper troposphere and dehydration of the 100 hPa level within the hurricane.

J.B. Elsner and T.H. Jagger (eds.), *Hurricanes and Climate Change,*
doi: 10.1007/978-0-387-09410-6,

Introduction

The accurate forecast of changes in the climate system requires understanding of processes that control the chemical composition and the radiative balance of the atmosphere. One of such processes is troposphere-to-stratosphere transport (TST). Exchange between these two regions of the atmosphere occurs predominantly in the tropics and requires crossing of the cold-point tropopause. In the extratropics, the tropopause acts a material surface separating tropospheric from stratospheric air, whereas in the tropics this separation occurs gradually within a layer. This layer is referred to as the Tropical Tropopause Layer (TTL), where air transitions from the convectively-dominated troposphere into the radiatively-dominated stratosphere. This layer is physically bound from below by the level of neutral buoyancy or height of main convective outflow (located at ~350 K, or ~150 hPa, or ~14 km) and from above by the cold-point tropopause (located at ~380 K, ~100 hPa, ~17 km) (Gettelman and Forster 2002).

The most powerful and naturally encountered greenhouse gas in the atmosphere is water vapor. This gas plays a critical role in the radiative balance of the TTL, which contains the transition from the net radiative cooling region where air sinks to the net radiative heating region where air rises. The net radiative cooling is dominated by longwave cooling due to water vapor, while the net radiative heating is dominated by shortwave heating due to ozone (Gettelman et al. 2004). Water vapor, however, offsets both the longwave and the shortwave heating by ozone. In addition to locally impacting heating and cooling rates, model runs and observations have shown that water vapor at the bottom of the TTL has a positive climate feedback on surface temperatures (i.e., warmer surface temperatures drive deeper convective systems that increase the concentration of water vapor at the bottom of the TTL via deep convection, which in return serves to further increase surface warming) (Minschwaner et al. 2006; Minschwaner and Dessler 2004).

The thermodynamic and convective properties of the TTL regulate the amount of water vapor that eventually reaches into the tropical stratosphere. Mechanisms ranging from freeze-drying by the cold-point tropical tropopause (Brewer 1949) to freeze-drying by horizontal advection through cold pools during slow diabatic ascent in the TTL (Holton and Gettelman 2001) to overshooting convection (Danielsen 1993) to mixing of dry and moist air in the TTL (Sherwood and Dessler 2001) to cloud microphysics (Jensen et al. 2001; Jensen and Pfister 2004) have been proposed to control TTL water vapor. Once in the stratosphere, water vapor plays a critical role in stratospheric ozone chemistry by providing OH radicals that can directly destroy ozone molecules and by providing one of the ingredients needed in the formation of polar stratospheric clouds, where activation of ozone-destroying chlorine radicals is initialized. Besides stratospheric chemistry, the concentration of water vapor can affect stratospheric temperatures (Forster and Shine 1999) and changes in the stratosphere can be reflected in tropospheric circulation (Shindell et al. 1999). Given the broad and significant impact that water vapor has on the chemical composition and radiative balance of the lower atmosphere, and in

particular the TTL, it is essential to have an accurate understanding of the processes that regulate its concentration.

One of the mechanisms that affect water vapor concentrations in the TTL is deep convection. This relation has been confirmed using lightning activity, as a proxy for deep convection, and the NCEP/NCAR reanalysis water vapor product at 300 hPa (Price and Asfur 2006).

Within deep convective cloud systems, lightning activity is an electrical manifestation of thermodynamic and mechanical work performed by vertical air motion varying non-linearly with the updraft speed (Baker et al. 1999). The basis for this sensitivity lies in the supply of condensate to drive mixed phase cloud microphysics (Petersen and Rutledge 2001). Satellite observations have shown that lightning is more likely to occur over land where mixed phase microphysics and the strength of convective updrafts are typically more pronounced than over oceans (Christian et al. 2003). Conversely, updraft velocities in oceanic convection are often too small to support the production of robust mixed phase processes and lightning.

Hurricanes are a type of oceanic convection whose main driving force is horizontal advection. These storms are accompanied by fairly weak vertical updrafts, even in the eyewall region where updrafts are the strongest. This condition results in limited charge separation and hence lightning activity (Saunders 1993). Several studies have reported on the scarcity of lightning activity in hurricanes (Black and Hallett 1999; Molinari et al. 1994). Lightning activity, however, is not always absent or insignificant in hurricanes. An examination of different hurricanes using continuous ground-base observations of lightning revealed the presence of significant lightning outbreaks in the eyewall region coincident in time with storm intensification (Molinari et al. 1998). So far, many uncertainties still remain in our understanding of the driving mechanism(s) for lightning generation in hurricanes and the cause(s) for storm-to-storm variability.

The goal of this study is to investigate the effect that hurricanes, which are large-scale and longer-lived oceanic convective systems, have on TTL water vapor. A recent study by Ray and Rosenlof (2007) showed that hurricanes serve to moisten an area $\sim$1500 km^2 around the center of the storm at altitudes between 300 and 150 hPa. Our study seeks to explore the relation between lightning frequency, which is typically associated with strong updrafts and thus deeper convection, and TTL water vapor. We address the question; can we see an increase in TTL moisture when lightning frequency increases?

Hurricanes are not only of interest to our study because of their spatial and temporal scales. Theory, model, and observations predict an increase in hurricane intensity as a result of warmer sea surface temperatures due to global warming (Emanuel 1987; Knutson and Tuleya 2004; Kossin et al. 2007). Therefore, a forecast of warmer environmental conditions might make hurricanes a significant source of water vapor to the TTL in the years to come.

We focus our study on hurricanes that developed and/or evolved in the Tropical Americas region. In addition to being a hurricane-active region and a region predicted to see an increase in hurricane intensity based on trends observed over the last 23 years (Kossin et al. 2007), this region has the following additional

characteristics during the summertime: (i) it becomes the second most dominant source of air to the TTL as revealed by trajectory calculations (Fueglistaler et al. 2004), (ii) it exhibits the largest seasonal increase in percent contribution to stratospheric moisture (Fueglistaler et al. 2004), and (iii) it has the warmest tropical tropopause temperatures that can sustain saturation mixing ratios ranging from 7 to 13 parts per million by volume (ppmv) compared to a global average in the tropics of 6.6 ppmv and Western Tropical Pacific ranges of 3 to 5 ppmv (Pittman 2005).

This paper is structured as follows. We introduce the data and methodology in Section 2. We discuss our findings in Section 3. We present our conclusions in Section 4.

Data and Methodology

This study focuses on the hurricanes that developed and/or evolved in the Tropical Americas region, which encompasses the Gulf of Mexico and Caribbean, in 2005. These hurricanes are: Dennis (July 5–10), Emily (July 11–19), Katrina (August 24–28), Rita (September 18–23), and Wilma (October 16–23). We perform our analysis on days when the hurricanes were over water only, which is when they were the strongest and the most structured.

In this study, we use a combination of continuous ground-based measurements and cloud-penetrating space-borne observations. Ground-based observations comprise of cloud-to-ground (CG) lightning flashes collected by the Long Range Lightning Detection Network (LLDN), which includes sensors from the U.S. and Canadian Lightning Detection Networks. The LLDN uses time of arrival and direction finding technology to determine the location of each CG flash (Cummins et al. 1998). Accurate flash placement depends on distance and location of the CG flash with respect to the network. In order to identify significantly misplaced CG flashes, we use hourly observations of 4 km horizontal resolution infrared brightness temperatures (IR Tb) from GOES–12 as a filter. We compare the location of lightning flashes within a $+/-15$ minute observation of IR Tb from GOES–12. Any flashes associated with co-located IR Tb warmer than 260 K are consequently excluded from the analysis.

Space-borne observations consist of water vapor measurements obtained from the Microwave Limb Sounder (MLS) instrument aboard the Aura satellite (Waters et al. 2006). This satellite was launched on July 15, 2004 and started reporting measurements in August 2004. The advantage of using this dataset is the capability of measuring in regions where ice clouds and aerosols are present. This cloud-penetrating capability allows for vertical profiling within convective systems, which makes it ideal for our study of hurricanes. Each orbit of the satellite covers from 82°N to 82°S with 14 orbits per day ($\sim$25° sampling in longitude). Measurements are obtained every 1.5° along the orbit track and cover a few kilometers across track. In this study, we use MLS version 1.51, Level 2 data, which covers the upper troposphere and lower stratosphere with a $\sim$3 km vertical resolution.

We focus on measurements reported at 100, 147, and 215 hPa. At these altitudes, the single profile precision is less than 10%, and the averaging kernels are so sharply peaked that there is no instrument induced correlation among levels.

In order to elucidate the spatial and temporal evolution of the water vapor, lightning, and IR Tb fields over the Tropical Americas, we construct Hövmoller plots averaged over the 12°–30° North latitude band. For the cases of lightning and IR Tb, we calculate cumulative flashes and minimum IR Tb, respectively, in longitude increments of 2° on a daily basis. For the case of water vapor, we calculate averages in longitude increments of 8° every two days. The analysis focused on areas surrounding the center of the hurricane uses daily 2° × 2° grids of cumulative lightning flashes and co-located averaged water vapor.

Results and Discussion

In order to understand the effect that hurricanes have on TTL moisture, we first examine lightning activity and minimum IR Tb throughout the Tropical Americas as a function of time. Figure 1 shows a map of the geographical locations used in the Hövmoller plots. Figure 2 shows the Hövmoller plots of daily lightning activity and daily minimum IR Tb from July 1 to November 30, 2005. The white horizontal lines between 40° and 100° W correspond to the location of the five hurricanes analyzed in this study. First, we note the overall negative correlation between lightning frequency and IR Tb. Locations with higher lightning frequency are associated with colder cloud tops. Second, we note that both shorter-lived convection and the longer-lived hurricanes are associated with lightning activity. Furthermore, both types of convective systems have very cold cloud tops that reach deep into the upper troposphere. On average, the coldest IR Tb reached by the five hurricanes during their lifetimes was 214 +/− 16 K. Third, we note that the most intense lightning occurs mainly over water.

Lightning activity is typically associated with strong updrafts and deeper convection. This is evident in the relation with IR Tb shown in Fig. 2. Studies such as Molinari et al.'s (1998) suggested the use of lightning outbreaks in the core of hurricanes as a diagnostic for storm intensification. While our analysis is not performed on the hourly timescales and the eyewall regions used by Molinari et al. (1998), the proposed correlation is still evident on larger temporal and spatial

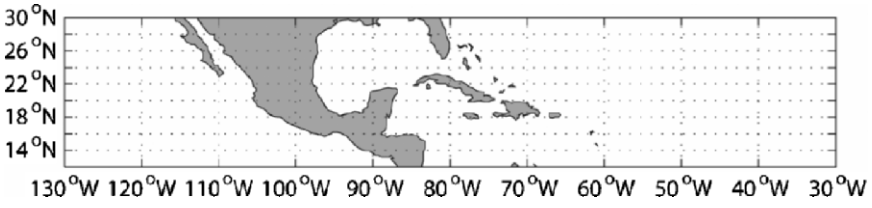

Fig. 1 Geographical locations used to construct the Hövmoller diagrams shown in Fig. 2

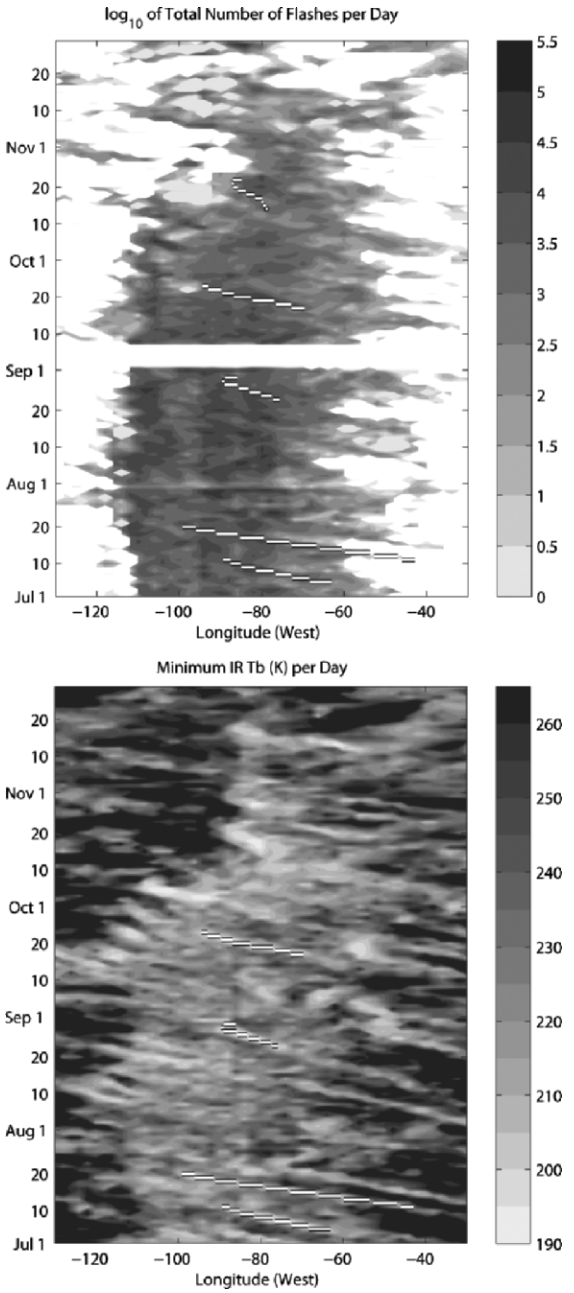

Fig. 2 Hövmoller diagrams of the number of CG lightning flashes (*top*) and minimum infrared brightness temperatures (*bottom*) averaged from 12° to 30° N over the Tropical Americas region every day. The horizontal white lines correspond to the location of the hurricanes in longitude and time. Due to the large range of values, the top panel is plotted as the exponent of $\log_{10}$(Lightning)

scales. Figure 3 shows time series of daily lightning activity during each of the five hurricanes analyzed in this study. The top panel shows total number of lightning flashes and minimum central pressure as a function of time as well as the number of

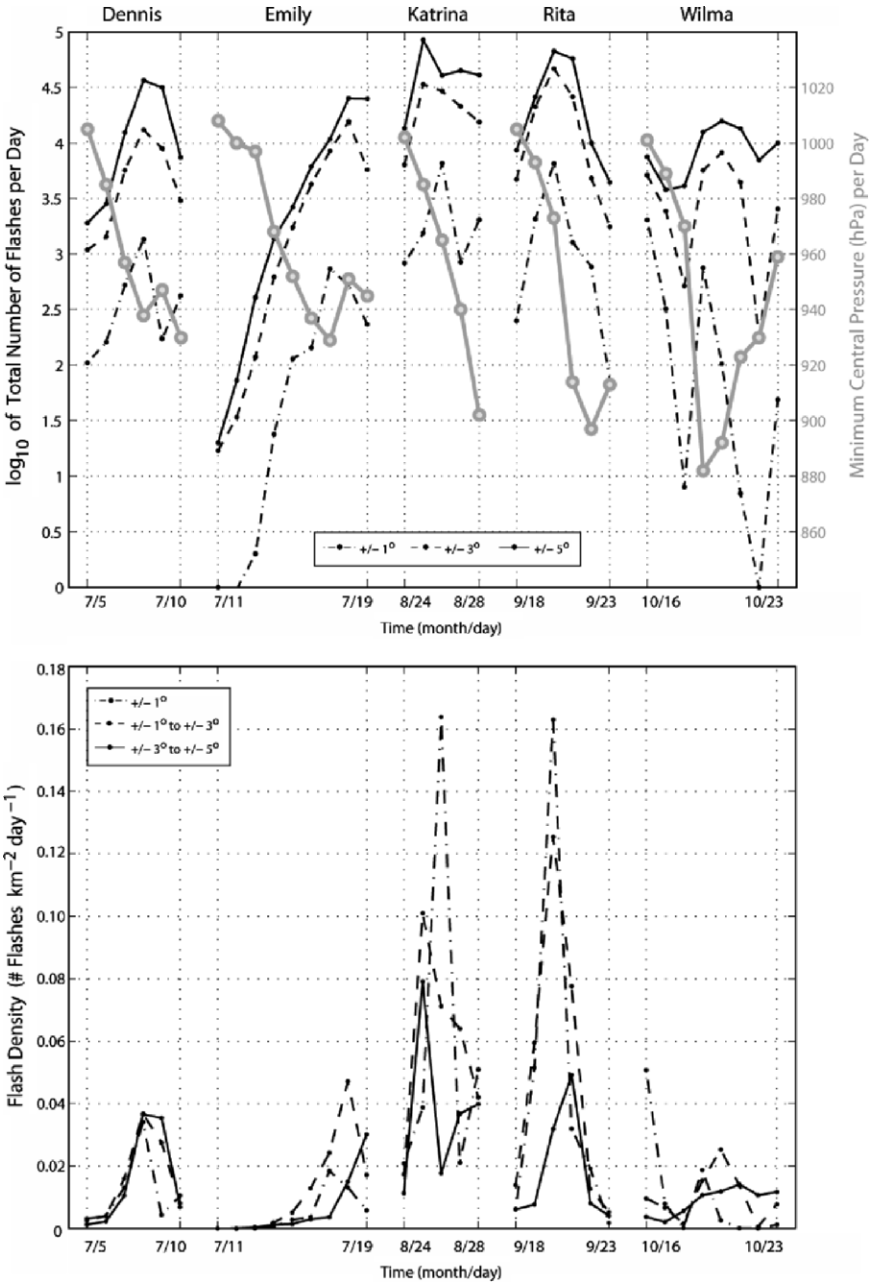

Fig. 3 (*Top*) Time series of daily total number of flashes (*black*) and daily minimum storm central pressure (*gray*). The three black curves are for different spatial coverage: dot-dash for flashes collected within +/−1° from the storm center, dash for flashes collected within +/−3° from the storm center, and solid for flashes collected within +/−5° from the storm center. Due to the large

lightning flashes over several centered at +/−1°, +/−3°, and +/−5° around the storm center. In general, this plot shows that lightning frequency increases as the storm intensifies (i.e., central pressure decreases). Hurricanes Katrina, Rita, and Wilma exhibited high lightning frequency even at their early stages. Hurricane Katrina, in particular, was unusual compared to the rest of the storms in that it maintained very high lightning frequency throughout its lifetime. Lightning frequency within +/−3° and +/−5° from the center of the storm had comparable temporal evolution and comparable magnitude at times for all hurricanes. Closer to the eye, within +/−1°, however, lightning frequency revealed a different temporal evolution. The bottom panel of Fig. 3 shows flash density at different radii from the center of the storm, namely within +/−1°, between +/−1° and +/−3°, and between +/−3° and +/−5°. During Hurricanes Dennis, Emily, and Wilma, the distribution of flash density in all three annuli is fairly comparable in temporal evolution and in magnitude. During Hurricanes Katrina and Rita, however, flash density closer to the eye of the storm increased significantly. These findings are consistent with the findings of Shao et al. (2005). Besides areas closer to the eye of the storm, this panel also shows a significant increase in flash density over locations as far out as +/−3° from the center of these two storms. Recall we are using 2° × 2° bins of daily lightning flashes, so locations at +/−3° physically extend out an additional degree, or ∼100 km.

After examining the spatial and temporal distribution of lightning activity in the Tropical Americas, we proceed to examine the water vapor field below and at the bottom of the TTL, namely at 215, 147, and 100 hPa. Similar to Fig. 2, we construct Hövmoller plots for MLS water vapor at the three pressure levels as shown in Fig. 4.

Some of the largest magnitudes for MLS water vapor at 147 hPa and 215 hPa are not observed exclusively over continental longitudes. Instead, both maritime and continental longitudes show significant enhancements and variability. When we examine the 100 hPa level, however, we notice that the largest magnitudes are found mostly west of Central America and without a corresponding hydration over the same longitudes at lower altitudes. This suggests easterly and upwards advection of moisture to the 100 hPa level. At the hurricane longitudes, these Hövmoller plots show hydration at the 147 and 215 hPa levels usually towards the later stages of the storms. From these plots, the effect of hurricanes at 100 hPa is not entirely clear.

Next, we focus on hurricane days only and examine the moisture field and lightning frequency around the center of the storms. We construct storm-centered plots using the methodology of Ray and Rosenlof (2007). These are Lagrangian

Fig. 3. (Continued) range of values, flashes per day are plotted as the exponent of $\log_{10}$(number of flashes per day). (*Bottom*) Times series of flash density at different radii from the storm center. The three black curves are for: density within +/−1° from the storm center in dot-dash, density between +/−1° and +/−3° from the storm center in dash, and density between +/−3° and +/−5° from the storm center in solid. Note highest density observed within +/−1° in Hurricanes Katrina and Rita (Reported degree distances from the center of the storm represent the value at the center of a 2° × 2° bin. For example, values at 3° are for measurements between 2° and 4°.)

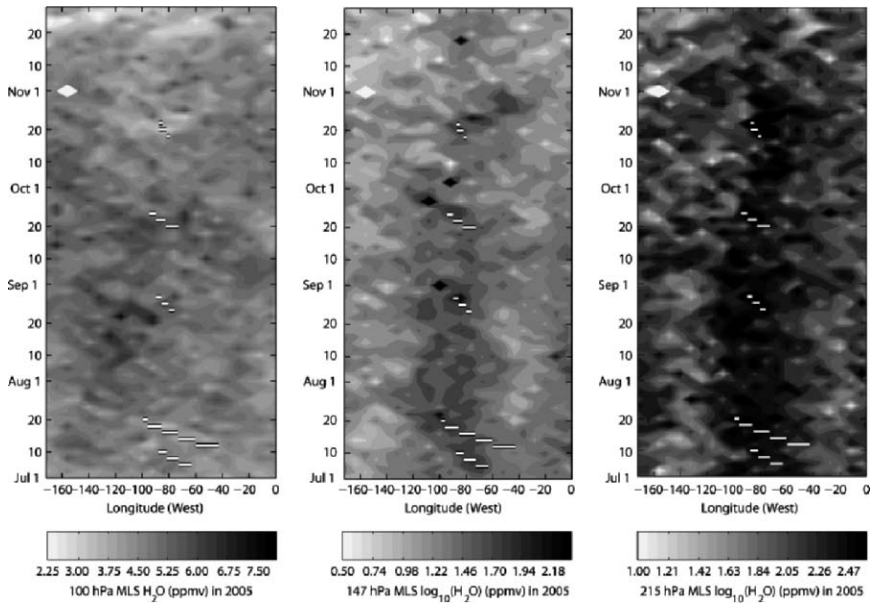

Fig. 4 Hövmoller diagrams of MLS-water vapor at 100 hPa (*left*), 147 hPa (*middle*), and 215 hPa (*right*) panels averaged from 12° to 30° N every two days. The horizontal white lines correspond to the location of the hurricanes in longitude and time. Due to the large ranges in water vapor magnitudes, values at 147 and 215 hPa are plotted as the exponents of $\log_{10}(H_2O)$

plots that follow each hurricane with the origin of both x and y axes being co-located with the center of the storm. The values reported in these plots are averages of $2^\circ \times 2^\circ$ bins within a given longitude and latitude range from the center of the storm for each hurricane day. Using infrared data from the Atmospheric Infrared Sounder (AIRS) instrument aboard the Aqua satellite, Ray and Rosenlof (2007) showed that tropical cyclones hydrate the 223 hPa level. Here we use microwave data at 100, 147, and 215 hPa instead. Figure 5 shows these storm-center plots for MLS water vapor and lightning frequency. These plots confirm the hydration by the hurricanes at the 147 and 215 hPa. At the 100 hPa, however, there is no evidence of direct hydration by the hurricanes. Lightning frequency, similar to 147 and 215 hPa MLS water vapor, shows increases around the center of the storm. Considering that the spatial distribution and the intensity of lightning activity varies from storm to storm, it is not surprising to find a lack of spatial correlation between lightning flashes and water vapor fields in this figure. Recall that these storm-center plots are averages over all five hurricanes.

Figure 5 also shows that the most significant hydration by the hurricanes occurs in an area that is $+/-5^\circ$ in both longitude and latitude from the center of the storm. Our next step consists of exploring correlations between MLS water vapor and lightning frequency over this focused area. Since we have limited spatial and temporal

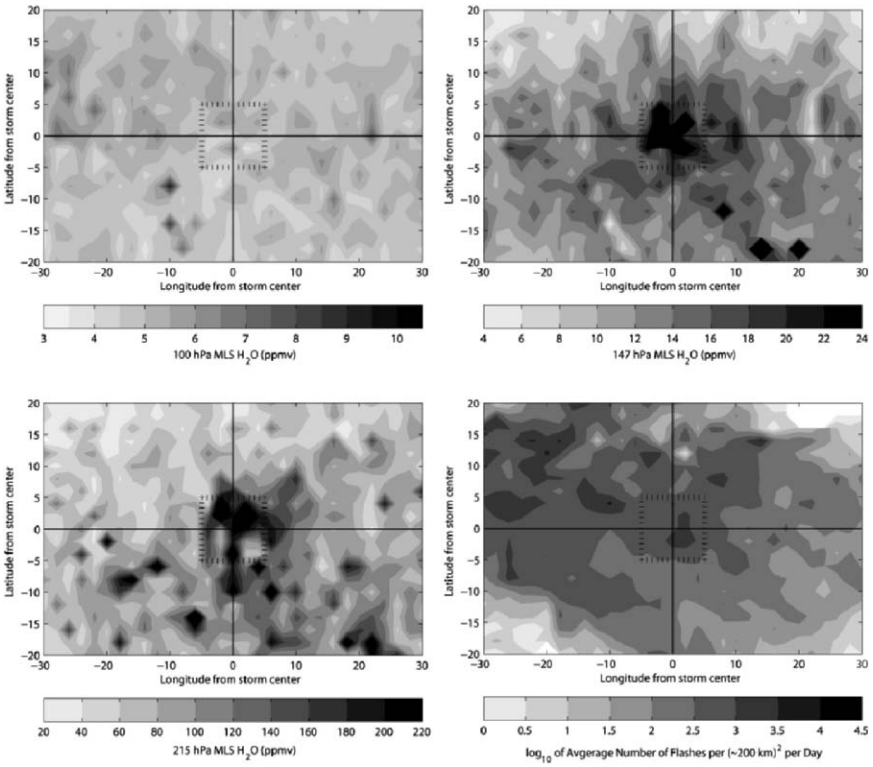

Fig. 5 Average fields of MLS-Aura water vapor and lightning frequency. The averages are calculated over daily $2^\circ \times 2^\circ$ bins during all days of Hurricane Dennis, Emily, Katrina, Rita, and Wilma. The dashed inner box corresponds to the area that is $+/-5^\circ$ from the center of the storm

coverage from the MLS instrument, we compare only daily $2^\circ \times 2^\circ$ bins within the $+/-5^\circ$ area from the storm center where MLS measurements were available.

Statistical analysis on correlations among 100 hPa, 147 hPa, 215 hPa MLS water vapor, and lightning frequency reveal the existence of weak, but nonetheless statistically significant correlations at the 95% confidence level. A total of 94 data points are used for each parameter. Recall this analysis is performed while storms remain over water only. We find lightning frequency and 215 hPa MLS water vapor to have a statistically significant correlation with a linear correlation coefficient of $+0.2115$ and lower and upper bounds of $+0.0070$ and $+0.3990$, respectively. We also find 215 hPa and 147 hPa MLS water vapor to have a statistically significant correlation with a linear correlation coefficient of $+0.2689$ and lower and upper bounds of $+0.0678$ and $+0.4490$, respectively. Lastly, we find 147 hPa and 100 hPa MLS water vapor to have a statistically significant correlation with a linear correlation coefficient of -0.2936 and lower and upper bounds of -0.4701 and -0.0944, respectively. Correlation plots for these three pairs of parameters are shown in Fig. 6.

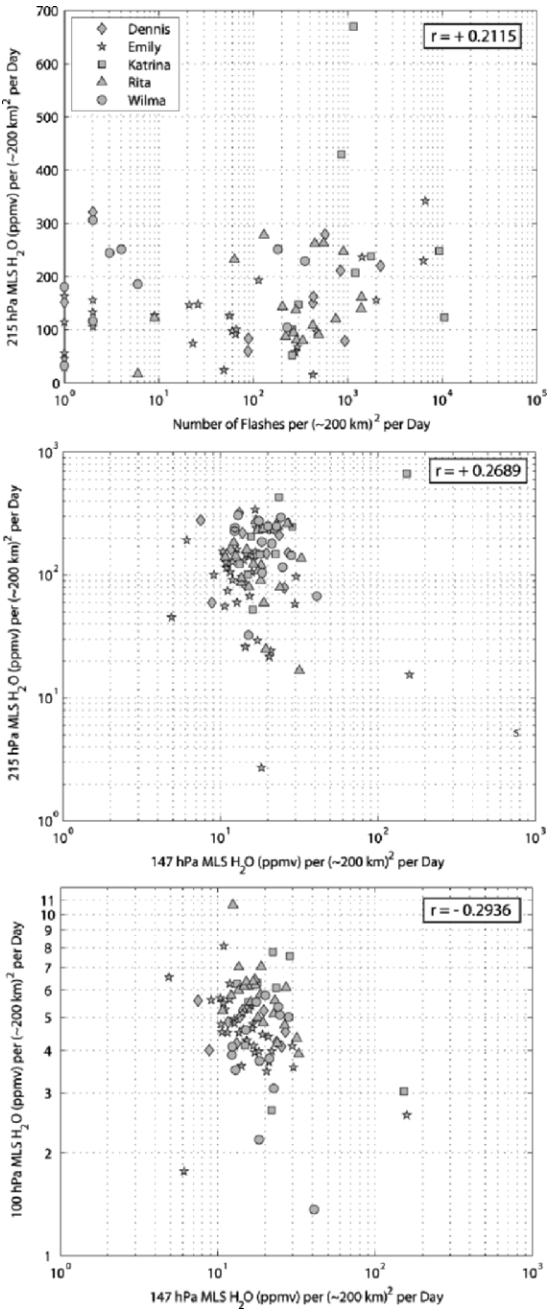

Fig. 6 Correlation plots between (*top*) lightning frequency and 215 hPa MLS-Aura water vapor, (*middle*) 147 and 215 hPa MLS-Aura water vapor, and (*bottom*) 147 and 100 hPa MLS-Aura water vapor. Each value is the average of water vapor or total number of lightning flashes collected in $2^\circ \times 2^\circ$ bins over a day. All bins are located within $+/-5^\circ$ from the storm center

Lightning frequency was only correlated with MLS water vapor at the 215 hPa level based on statistical results. Recall from Fig. 3 how Hurricane Katrina exhibited the highest lightning frequency of all hurricanes analyzed. As shown in Fig. 6, Hurricane Katrina also had the highest 215 hPa MLS water vapor of all hurricanes. At higher altitudes, Hurricane Katrina had some of the highest water vapor and some of the lowest water vapor measurements observed at 147 and 100 hPa, respectively. At the opposite end the lightning frequency spectrum, Hurricane Emily started out with the lowest lightning frequency. This same storm also had some of the lowest observations of MLS water vapor at both 215 and 147 hPa, and some of the highest observations of MLS water vapor at 100 hPa.

Conclusions

Many new satellite-based data sets are now available to allow us to explore tropical cyclones with unprecedented temporal and spatial scales. These tropical systems have very strong interactions with the surface, but in this study we focused on the effects of hurricanes at the higher altitudes of the TTL. With lightning activity being associated with strong updrafts and therefore deeper convection, we explored the impact that lightning frequency had on TTL water vapor within hurricanes.

Our analysis was limited to five hurricanes in the Tropical Americas region in 2005 when both lightning and MLS water vapor data were available. We found weak, but statistically significant correlations (within measurement uncertainty) between lightning and MLS water vapor. Hydration at the 215 hPa level was positively correlated with lightning frequency. At 215 hPa, water vapor was also positively correlated with water vapor at 147 hPa. At 147 hPa, however, water vapor was negatively correlated with water vapor at 100. In other words, an increase in lightning frequency favors hydration at the 215 hPa level, which in turn favors hydration aloft at the 147 hPa level. However, when this hydration occurs below, the 100 hPa level experiences dehydration instead. While physically plausible, the strength of this mechanism by which the upper troposphere is hydrated and the 100 hPa level is dehydrated as a result of increasing lightning frequency within a hurricane should be further explored with a larger data set.

From the climate perspective, it is necessary to investigate the fate of the added moisture to the TTL by hurricanes. Are these air masses returning to the troposphere or are they being transported irreversibly into the stratosphere? With a forecast of increasing sea surface temperatures and strengthening of hurricanes in the Atlantic basin in particular (Kossin et al. 2007), is lightning frequency going to increase and affect the chemical and radiative properties of the TTL via transport of boundary layer air and production of ozone and NO_x, for example? Many questions and many uncertainties remain. However, addition of new measurements such as space-borne radars and lidars flying on the CloudSat and Calipso satellites, and lightning instruments proposed to fly on geostationary satellites should give us more insights into the structure, evolution, and impact of these powerful tropical systems.

Acknowledgements This research was supported by an appointment to the NASA Postdoctoral Program at Marshall Space Flight Center, administered by Oak Ridge Associated Universities through a contract with NASA. LLDN data provided by the NASA Lightning Imaging Sensor (LIS) instrument team and the LIS data center via the Global Hydrology Resource Center (GHRC) located at the Global Hydrology and Climate Center (GHCC), Huntsville, Alabama through a license agreement with Global Atmospherics, Inc (GAI). The data available from the GHRC are restricted to LIS science team collaborators and to NASA EOS and TRMM investigators.

References

Baker, M. B., A. M. Blyth, H. J. Christian, J. Latham, K. L. Miller and A. M. Gadian, 1999: Relationships between lightning activity and various thundercloud parameters: Satellite and modeling studies, *Atmos. Res.*, **51**, 221–236.

Black, R.A., and J. Hallett, 1999: Electrification of the hurricane, *J. Atmos. Sci.*, **56**, 2004–2028.

Brewer, A. W., 1949: Evidence for a world circulation provided by measurements of helium and water vapor in the stratosphere, *Quart. J. Roy. Meteorol. Soc.*, **75**, 351–363.

Christian, H. J., R. J. Blakeslee, D. J. Boccippio, W. L. Boeck, D. E. Buechler, K. T. Driscoll, S. J. Goodman, J. M. Hall, W. J. Koshak, D. M. Mach, and M. F. Stewart, 2003: Global frequency and distribution of lightning as observed from space by the Optical Transient Detector, *J. Geophys. Res.*, **108**, D002347.

Cummins, K. L., M. J. Murphy, E. A. Bardo, W. L. Hiscox, R. B. Pyle, and A. E. Pifer, 1998: A combined TOA/MDF technology upgrade of the U. S. National Lightning Detection Network, *J. Geophys. Res.*, **103**, 9035–9044.

Danielsen, E. F., 1993: In situ evidence of rapid, vertical, irreversible transport of lower tropospheric air into the lower tropical stratosphere by convective cloud turrets and by large-scale upwelling in tropical cyclones, *J. Geophys. Res.*, **98**, 8665–8681.

Emanuel, K. A., 1987: The dependence of hurricane intensity on climate, *Nature*, **326**, 483-485.

Forster, P. M. D., and K. P. Shine, 1999: Stratospheric water vapour changes as a possible contributor to observed stratospheric cooling, *Geophys. Res. Lett.*, **26**, 3309–3312.

Fueglistaler, S., H. Wernli, and T. Peter, 2004: Tropical troposphere-to-stratosphere transport inferred from trajectory calculations, *J. Geophys. Res.*, **109**, D03108.

Gettelman, A., and P. M. D. Forster, 2002: A climatology of the tropical tropopause layer, *J. Meteorol. Soc. Jpn.*, **80**, 911–924.

Gettelman, A., *et al.*, 2004: Radiation balance of the tropical tropopause layer, *J. Geophys. Res.*, **109**, D07103.

Holton, J. R., and A. Gettelman, 2001: Horizontal transport and the dehydration of the stratosphere, *Geophys. Res. Lett.*, **28**, 2799–2802.

Jensen, E. J., and L. Pfister, 2004: Transport and freeze-drying in the tropical tropopause layer, *J. Geophys. Res.*, **109**, D02207.

Jensen, E. J., L. Pfister, A. S. Ackerman, A. Tabazadeh, and B. O. Toon, 2001: A conceptual model of the dehydration of air due to freeze-drying by optically thin, laminar cirrus rising slowly across the tropical tropopause, *J. Geophys. Res.*, **106**, 17252–17273.

Knutson, T. R. and R. E. Tuleya, 2004: Impact of CO2-induced warming on simulated hurricane intensity and precipitation: Sensitivity to the choice of climate model and convective parameterization, *J. Clim.*, **17**, 3477–3495.

Kossin, J. P., K. R. Knapp, D. J. Vimont, A. J. Murnane, and B. A. Harper, 2007: A globally consistent reanalysis of hurricane variability and trends, *Geophys. Res. Lett.*, **34**, L04815.

Minschwaner, K., and A. E. Dessler, 2004: Water vapor feedback in the tropical upper troposphere: Model results and observations, *J. Clim.*, **17**, 1272–1282.

Minschwaner, K., A. E. Dessler, and P. Sawaengphokhai, 2006: Multimodel analysis of the water vapor feedback in the tropical upper troposphere, *J. Clim.*, **19**, 5455–5464.

Molinari, J., P. K. Moore, V. P. Idone, R. W. Henderson, and A. B. Saljoughy, 1994: Cloud-to-ground lightning in Hurricane Andrew, *J. Geophys. Res.*, **99**, 1665–16676.

Molinari, J., P. Moore, and V. Idone, 1998: Convective structure of hurricanes as revealed by lightning locations, *Mon. Wea. Rev.*, **127**, 520–534.

Petersen, W. A., and S. A. Rutledge, 2001: Regional Variability in Tropical Convection: Observations from TRMM, *J. Climate*, **14**, 3566–3586.

Pittman, J. V., 2005: Transport in the tropical and subtropical lower stratosphere: Insights from in situ measurements of chemical tracers, *Ph.D. thesis*, Harvard University.

Price, C. and M. Asfur, 2006: Can lightning observations be used as an indicator of upper tropospheric water vapor variability?, *Bull. Amer. Meteor. Soc.*, **87**, 291–298.

Ray, E. A. and K. H. Rosenlof, 2007: Hydration of the upper troposphere by tropical cyclones, *J. Geophys. Res.*, **112**, D12311.

Saunders, C. P. R., 1993: A review of thunderstorm electrification processes, *J. Appl. Meteor.*, **32**, 642–655.

Shao, X. -M., J. Harlin, M. Stock, M. Stanley, A. Regan, K. Wiens, T. Hamlin, M. Pongratz, D. Suszcynsky, and T. Light 2005, Katrina and Rita Were Lit Up With Lightning, *Eos Trans. AGU*, **86**, 398.

Sherwood, S. C. and A. E. Dessler, 2001: A model for transport across the tropical tropopause, *J. Atmos. Sciences*, **58**, 765–779.

Shindell, D. T., R. L. Miller, G. A. Schmidt, and L. Pandolfo, 1999: Simulation of recent northern winter climate trends by greenhouse-gas forcing, *Nature*, **399**, 452–455.

Waters, J. W. et al., 2006 : The Earth Observing System Microwave Limb Sounder (EOS MLS) on the Aura satellite, *IEEE Trans. Geosci. Remote Sens.*, **44**, 1075–1092.

Long-Term Natural Variability of Tropical Cyclones in Australia

Jonathan Nott

Abstract Numerous late Holocene records of tropical cyclones have been collected from tropical northern Australia. They are in the form of multiple shore parallel sedimentary ridges deposited over the past 6,000 years and an 800 year long annual resolution oxygen isotope record from a calcium carbonate cave stalagmite. The sedimentary ridges are composed of coral fragments, or shell and sand or pure sand. Numerical models relating surge height and tropical cyclone central pressure were used to determine the intensity of the tropical cyclone responsible for deposition of the ridges at each site. The results suggest that in the majority of cases these features were deposited by very high magnitude events. The results suggest that extrapolation from short instrumental and historical records, which is the method commonly used to assess risk from this hazard, substantially underestimate the risk from this hazard. This is confirmed for the Cairns region by the 800 year long high resolution isotope record which suggests that tropical cyclone activity in northeast Queensland has been in a phase of quiescence since before European settlement of the region in approximately AD 1870. Comparisons between the short and long-term records suggest that non-stationarity may be an inherent feature of the long-term natural variability of tropical cyclones in this region.

Introduction

The past few years have seen considerable debate over whether anthropogenically induced global climate change has already influenced the behaviour of tropical cyclones. Much of the debate has focused on the veracity and length of the time series used. Emanuel (2005) and Webster et al., (2005) used time series a few decades in length and in the case of the Nth Atlantic since approximately AD 1930. Landsea (2005) challenged the interpretation of the earlier part of the Atlantic record and suggested that calculations by Emanuel to estimate the PDI were incorrect and re-assessment showed that the PDI over the past 70 or so years appears to have changed little for this basin. Suggestions were then made that fluctuations in the Atlantic PDI were in tune with the Atlantic Multidecadal

J.B. Elsner and T.H. Jagger (eds.), *Hurricanes and Climate Change,*
doi: 10.1007/978-0-387-09410-6,

Oscillation (AMO) although recent suggestions have been made that recent fluctuations in the AMO may be an artifact of aerosols emitted from the USA (Mann & Emanuel 2006).

Each of these debates, and those that continue (Landsea, 2007; Mann et al., 2007, Kossin et al., 2007), have been concerned with a relatively short historical record (100–150 yrs). As such it has been difficult to discern whether the apparent upswing in Atlantic tropical cyclone activity since the 1970s is abnormal in terms of the natural variability of events in this basin. Nyberg et al. (2007) have shown however, based upon the character of a 270 year luminescence line record in Caribbean corals, that the 1970s and 1980s experienced the quietest phase in tropical cyclone activity for nearly the past 300 years and the recent upswing is nothing unusual. This evidence, despite its significance has not figured prominently in the debate regarding anthropogenic change versus natural variability. The same is true for other century to millennial scale records of tropical cyclones such as the overwash deposits in the Gulf of Mexico (Liu and Fearn, 2000; Liu, 2004) and the US Atlantic coast (Donnelly and Webb, 2001; Donnelly et al. 2004), tree ring records for the US (Miller et al., 2006), sedimentary deposits in Australia (Nott and Hayne, 2001; Nott, 2003) and also an oxygen isotope record from a calcium carbonate stalagmite in NE Queensland (Nott et al. 2007). The reasons behind this are unclear but may be because these data are in a proxy form and hence do not deal with instrumented or historical data. However this is not true of Nyberg et al. (2007) record for there is a close correlation between the latter part of their time series and the instrumented record.

A similar debate concerning global climate change and tropical cyclone behaviour has not as yet occurred in the Australian region. Here the instrumented record extends back a little over 30 years and the historical record just over 100 years, and on the basis of these records there doesn't appear to have been a recent upswing in tropical cyclone activity as has occurred in the NW Pacific and Atlantic Basins. A considerable archive of paleo-proxy data on the long-term natural variability of tropical cyclones is being amassed from northeast Queensland to Western Australia (Nott, 2006). The results of this work will be useful to better ascertain when and if global warming begins to have an effect on tropical cyclone behaviour in this region.

This chapter outlines these various types of long-term natural records of tropical cyclones from across the Australian continent and discusses their trends in relation to the trends seen in the shorter historical and instrumental records.

Australian Paleocyclone Records

The Sedimentary Record

The sedimentary record of paleocyclones along the northeast, northern and western Australian coast typically occurs in the form of multiple shore parallel ridges standing up to 5–6 m above Australian Height Datum (AHD) or mean sea level

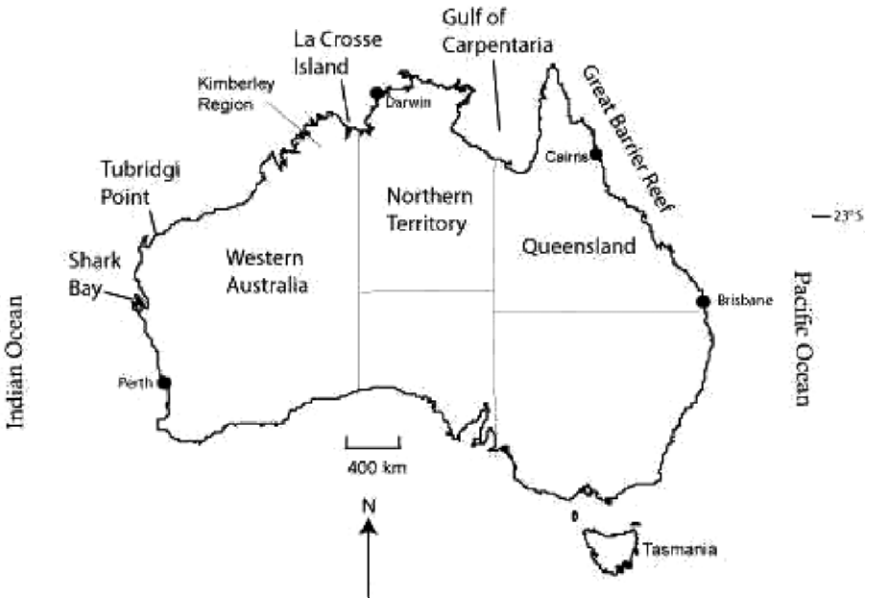

Fig. 1 Location sites across northern and Western Australia

(Fig. 1). The ridges at any one location are composed of either coral fragments, or sand with layers of marine shells, or pure sand, or lithic gravels and in one instance in Western Australia the ridges are entirely composed of one species of shell (*F. eragatum*). The composition of the ridges ay any one location is a function of the availability of source materials.

Tsunamis are unlikely to be a mechanism responsible for deposition of any of the ridge sequences along the northeast Queensland coast. Eye witness accounts reveal that ridges are commonly formed during tropical cyclone surge and wave events throughout the south Pacific and also along the Queensland coast (Nott, 2003). Post-event surveys of tsunamis over the past decade do not reveal deposition of coral shingle or sand/shell ridges even though these waves impact sections of coast where this sediment is available to be transported landward. Indeed, sediment is deposited onshore but usually as a sheet that tapers in thickness landwards and not as a distinct ridge (Nott, 2006).

Eolian activity is also unlikely to be responsible for deposition of the ridges discussed here. These ridges contain either coral fragments, marine shells or coarse-grained sands derived from the beach which, in the latter case, would have been submerged by storm surge during emplacement of the ridge. As is shown here, and in more detail by (Nott, 2003), only waves and surge generated by intense tropical cyclones can generate marine inundations sufficiently high to reach the crests of these ridges.

At every site examined the ridges get progressively older with distance inland. The most recently deposited ridges occur on the seaward side of the ridge plain. In some locations there can be two distinct sections to the beach ridge plain; an inner (Pleistocene) barrier plain sequence and an outer (more seaward) Holocene sequence. The inner barrier plain sequence was typically deposited during the last interglacial when sea-levels were last at or near their present position. The outer barrier sequence usually begins to form just after 6,000 yrs B.P when present sea-levels stabilized. Hence the oldest, most inland ridge of the outer barrier sequence typically has an age of between 5,500–6,000 yrs B.P. The outer and inner barrier ridge plain sequences are often, but not always, separated by a lagoon or swamp. Many of the sites examined so far throughout northern Australia only have the outer (Holocene) barrier ridge plain preserved.

Queesnland – Coral Rubble Ridges

Coral rubble/shingle ridges occur in locations where coral reefs occur close to shore. Most of the paleorecords derived from these ridges comes from sites along the Great Barrier Reef region offshore from Queensland's east coast. Coral rubble ridges also occur on the Abrolhos Islands off the southwest Western Australian coast but to date no detailed work has been published from this site. The ridges are formed when coral fragments are eroded from near-shore reefs by wave action during a tempest and transported either onshore or offshore (Hughes,1999; Davies, 1983; Baines et al., 1974; Rasser and Riegl, 2002). Fragments can also be transported from existing accumulations of coral rubble in the offshore zone. These offshore accumulations result from erosional processes such as biodegradation and wave action during both storms and fair weather conditions. (Rasser and Riegl, 2002; Hughes, 1999). It is thought that the angle of the offshore reef slope plays a role in whether the eroded fragments are transported predominantly offshore or onshore. Steep reef fore-slopes favour offshore transport of fragments, often to depths of greater than 50 m which is too deep to be reworked and transported by storm waves. Shallow sloping, and particularly wide, reef fronts favour transport onshore and the formation of coral rubble ridges. However, some sites, such as Curacoa Island in the central Great Barrier Reef, Australia (Figs. 2 and 3) that are fronted by narrow, steep reef slopes have extensive coral rubble ridge development on land (Hayne and Chappell, 2001; Nott and Hayne, 2001). These sites with presumably minimal accumulation of coral rubble in the shallow waters of the reef and maximum accumulation of rubble in the deeper offshore waters below wave base suggest that the onshore ridges could have formed from predominantly live coral fragments broken off during the storm. At other sites, however, there can be little doubt that onshore ridges were formed from the reworking of existing accumulations of rubble in the shallow waters offshore.

Along the east coast of Queensland coral rubble ridges often accumulate on the sheltered side of islands (Fig. 3), presumably because on the exposed sides they are constantly removed by the largest or most intense tropical cyclones affecting a

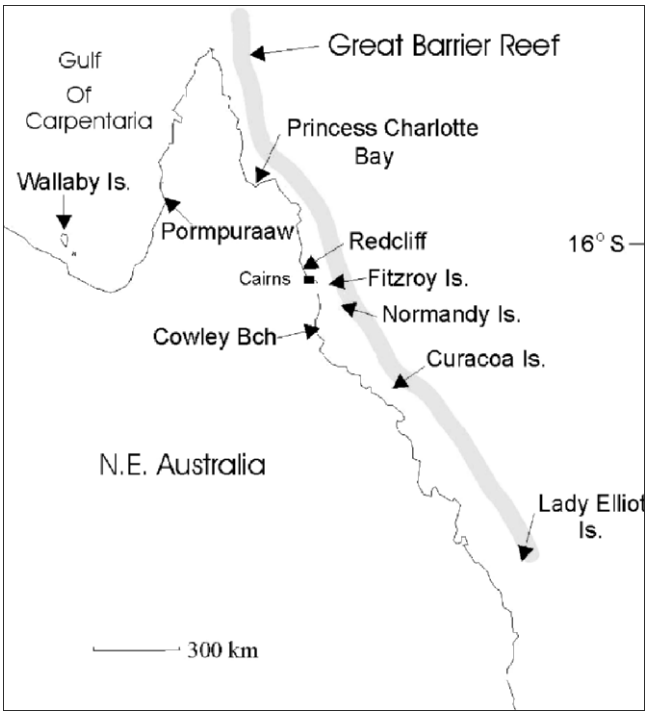

Fig. 2 Location of sites in northeast Queensland

region. The sheltered sides will experience diminished wave energy, but at the same time a substantial surge. Because the wave energy is reduced, the likelihood of the ridge being removed during subsequent cyclones is lessened. Where the preservation potential for ridges is high, such as on the lee side of islands, a number of ridges are sometimes able to accumulate over time. Curacoa Island on the Great Barrier Reef (GBR) has 22 consecutive coral rubble ridges paralleling the shore on its northwestern or sheltered side (Fig. 4). Individual ridges extend for over 100 m along shore and rise to over 5 m above the mid-tide level (the tidal range here is approximately 3 m) or Australian Height Datum (AHD). The ridges were deposited by successive cyclones so that new ridges are deposited seaward of the previously emplaced ridge. The radiocarbon age of the ridges increases progressively with distance inland. The average interval between ridge emplacement here is 280 years over the past 5,000 years.

Lady Elliot Island at the southern end of the GBR also has an extensive sequence of coral shingle ridges. About fifteen successive ridges are preserved here with an average interval between ridge emplacement of 253 years (dated using radiocarbon) over the past 3,200 years (Chivas et al., 1986; Nott and Hayne, 2001). Other ridge sequences have been radiocarbon dated at Normandy Island, Fitzroy Island and Double Island in the central north GBR region (Nott, 2003). These latter sites have

Fig. 3 Oblique aerial vie of Curacoa Island Central Great barrier Reef. Open ocean is toward background. Location of cross-section shown in Fig. 4 shown by white line (Photo D. Hopley)

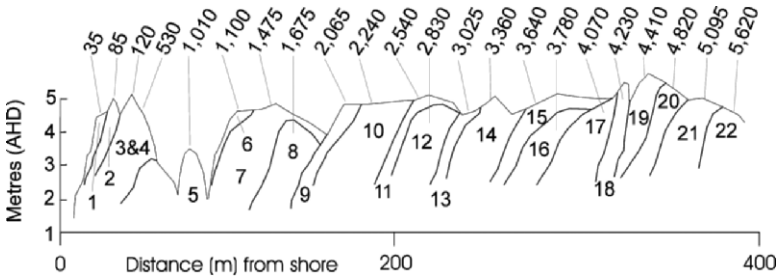

Fig. 4 Stratigraphy and chronology of shingle ridges at Curacoa Island

considerably fewer ridges in their sequences and do not provide the length of record found at Curacoa and Lady Elliot Islands. They do show though that the average interval between ridge emplacement is, like the other sites, between 200–300 years (Nott and Hayne, 2001; Nott, 2003). Wallaby Island in the southern Gulf of Carpentaria has a sequence of 14 coral shingle ridges spanning the past 4,100 years with an average interval between ridge emplacement of 180 years.

Shell and Sand Beach Ridges

Tropical cyclone storm tides and waves can deposit ridges composed of other materials besides coral shingle depending upon the source material availability.

Princess Charlotte Bay (PCB) in the northern GBR has a sequence of 12 ridges composed of sand and matrix supported marine shells. Here the sequence spans the past 2,500 years with an average interval between ridge emplacement of 177 years. Near Pormpuraaw on the western side of Cape York Peninsula over 30 ridges have been emplaced over the past 3,000 years giving an average interval between ridge emplacement of 100 years (Figs. 5 and 6). Here the ridges are composed of medium-grained sand with clast supported beds of marine shell (typically *Anadara sp*.) between 0.5 to 2m thick. The ridges rise in height to 5 m above AHD and the stratigraphy and chronology of the shell beds within the ridges suggests that each ridge represents a separate tropical cyclone event (Rhodes et al., 1980; Nott and Hayne in prep).

Sand Beach Ridges

South of Cairns on the east coast of Cape York Peninsula a sequence of 29 shore parallel coarse-grained sand ridges occurs at Cowley Beach. These ridges have been dated using optically stimulated luminescence (OSL) and they span the past 5,500 years with an average interval between ridge emplacement of 260 years (Fig. 7 and 8, Nott et al., in prep). These ridges also rise to approximately 5 m AHD and they extend alongshore for several kilometers. Like Pormpuraaw, there are no

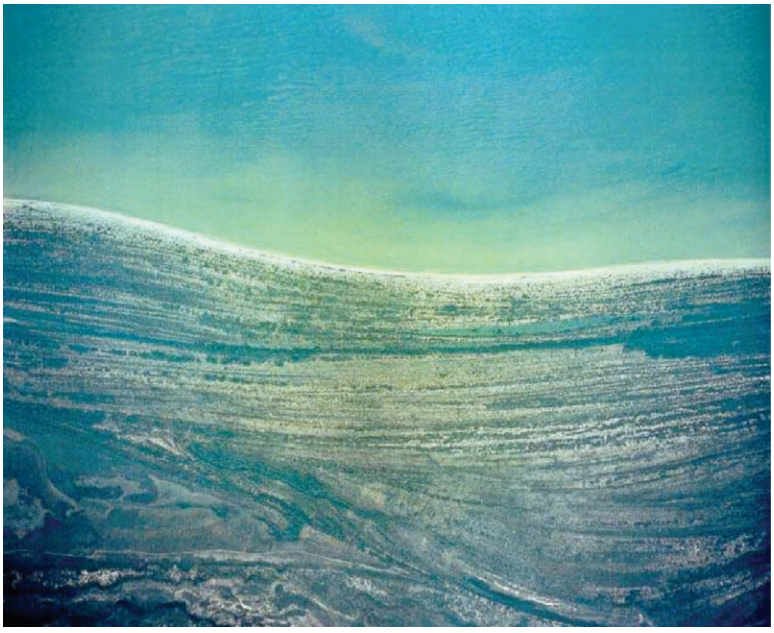

Fig. 5 Aerial photo of beach ridge sequence at Pormpuraaw. Distance from shore to inland extent in photo is approximately 3 km

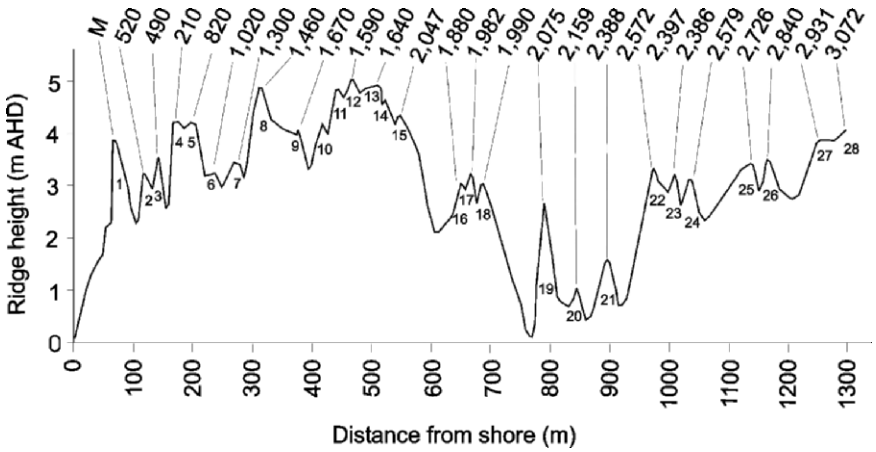

Fig. 6 Topography and chronology of sand/shell ridges at Pormpuraaw

Fig. 7 Oblique aerial view of sand ridges at Cowley Beach. Ridge crest are dominated by darker vegetation (Photo D. Hopley)

coral reefs close to shore at this location so coral fragments are absent within the ridges. Here, shell production is much lower in the inshore zone compared to Pormpuraaw and marine shells are sparse within these ridges. The local stream (Liverpool Creek) entering the sea near Cowley Beach drains a granite and metamorphic hinterland and has dissected a broad valley infilled with late Pleistocene

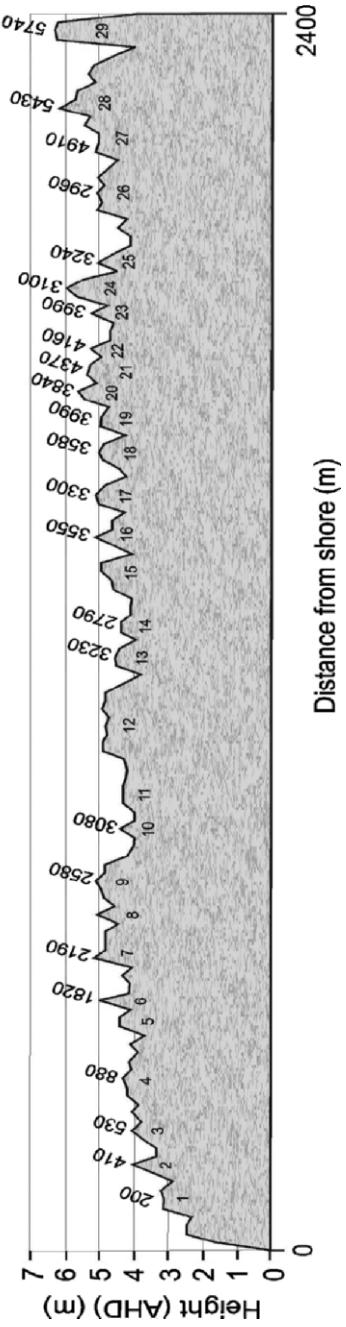

Fig. 8 Topography and chronology of pure sand beach ridges at Cowley Beach

fluvial terraces composed predominantly of coarse-grained sands. It is this material that has been the source of sediment to the nearshore coastal environment and which is exposed on the beach face at Cowley Beach following storms.

Several other sand beach ridge sequences also occur along the northeast coast of Australia where multiple beach ridges parallel the coast. Over 30 Holocene ridges rising to 4–5 m AHD occur near the Haughton River south of Townsville. Here the ridges are composed of fine to medium grained sands. Given that landforms composed of sands of this texture can be eolian in origin it is difficult to be as confident that these ridges were emplaced by tropical cyclone generated storm tides and waves. However, like Cowley Beach this is the only material available in the nearshore environment for transportation by waves.

Pumice Ridges

A ridge of pumice was deposited at North Mission beach, Queensland, during the marine inundation generated by an intense tropical cyclone on March 10, 1918 (Taylor, 1982). The inundation occurred at high tide and was reported to have reached at least 3.5 m above normal sea level. The inundation resulted in the deaths of many people and transported and deposited onto the mainland supplies from a shed on Dunk Island approximately 5 km offshore. Indeed, one large bag of flour was deposited over 3.5 m high in a tree and the flour in the center of the bag was still sufficiently dry to be able to make damper (a type of bread) the following day after the maelstrom (Taylor, 1982). The crest of the pumice ridge here reaches 5 m AHD and it extends alongshore for approximately 500 m. This is the only reported ridge of pumice deposited during a tropical cyclone so far, and it is not known whether sand was also deposited along with pumice to form this ridge at the time. No sand occurs in the ridge today, for it is composed entirely of well-rounded pumice particles; however, a sand beach ridge (up to 3–4-m-high AHD) at South Mission Beach was reported (Taylor, 1982) to have been deposited during this same event. The source of the pumice is likely to be the volcanic islands to the east of Queensland such as Vanuatu although no detailed petrographic analyses have been undertaken to confirm this.

Northern Territory/Western Australia – Lithic Gravel Ridges

Ridges composed entirely of lithic gravel and occasional coral fragments are common along the Kimberley Coast of northwest Western Australia, close to the border with the Northern Territory. These ridge sequences form gravel barriers and often impound back-barrier lagoons in embayments along sections of coast dominated by steep rock cliffs (Fig. 9). They are particularly common along the western side of Cambridge Gulf north of Wyndham in the east Kimberley region. The gravel ranges in size up to 1.6-m diameter (A-axis) and 1.4 m (B-axis) and have been deposited into sequences of up to 9 ridges paralleling the shore. At La Crosse Island

Fig. 9 Lithic gravel ridges at La Crosse Island, Cambridge Gulf, Western Australia

(Fig. 9) offshore from the mouth of the Ord River, gravel ridges have been deposited in every embayment and thereby form a discontinuous sequence that surrounds the island. The ridges at two surveyed sites each on opposite sides of the island extend up to 5 m AHD, and radiocarbon samples on coral fragments embedded with the core of ridges from each of seven ridges from these sites show that they were deposited between approximately 5,000 yrs B.P. until recently (Nott, 2000). The radiocarbon samples do not show a progressive increase in age with distance inland, suggesting that the ridges are regularly overtopped and reworked by marine inundations.

Pure Shell Ridges

Multiple shore parallel ridges composed of pure shells (*Fragan eragatum*) occur at the head of a long indented bay known as Hamlin Pool at Shark Bay, Western Australia (Figs. 10 and 11). This species of shell fish normally grows much larger in size in open ocean conditions but here at Hamlin Pool the hyper-saline conditions, which also promote stromatolite growth here, result in these shells only growing to a maximum of 1–1.5 cm across. Beaches are entirely composed of these shells in this immediate region and as a consequence so too are the beach ridges. The majority of the ridges rise to 4 m AHD but a few in the middle of the sequence rise to 5 and 6 m AHD. Figure 11 shows that the ridges date to before the Holocene transgression and ages on these pre-Holocene ridges exceed the radiocarbon limit. Hence they are presumably Pleistocene in age and likely last interglacial. These

Fig. 10 Location map of Hamlin Pool, Shark Bay, Western Australia

pre-Holocene ridges are composed of a variety of different species of shells and they are also present in a variety of sizes unlike the Holocene ridges with their mono-specific shells of the same size. Clearly environmental conditions have changed here since the Holocene transgression compared to the last interglacial and one assumption is that the present day hyper-saline conditions did not exist here during the last interglacial. The ridge stratigraphy also suggests that an period of aridity lasting approximately 1,500 years also occurred during the mid-Holocene between approximately 2,200 to 3,700 years B.P. The evidence for this suggestion comes from the eolian capping of very fine grained silt over the ridges dating from approximately 3,700 to 5,500 yrs BP and not before this time. There was a 1,500 year gap between deposition of the last (most recently deposited) ridge at 3,700 yrs BP and the next ridge which is not covered in a layer of fine silt at 2,300 yrs BP. Presumably here, which is part of the most arid section of Australia's coast, tropical cyclones of any substantial size (intensity) did not make landfall for this 1,500 yr period which also coincided with exceptionally dry conditions.

Erosional Records

The records of prehistoric tropical cyclones described thus far have all been depositional. At Red Cliff Point, 35 km north of Cairns, 4 terraces ranging from

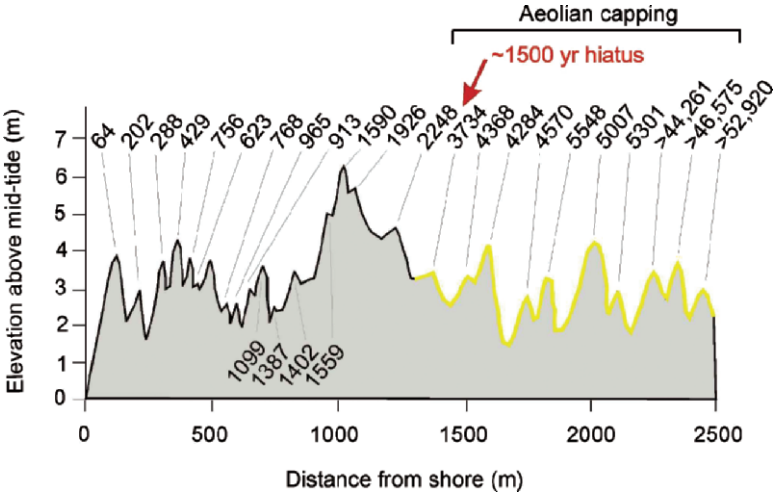

Fig. 11 Topography and chronology of shell ridges at Hamlin Pool

2.12 m to 6.1 m AHD are eroded into a raised lithic gravel beach deposit (Figs. 12 and 13). Nott (2003) concluded that these terraces were eroded by marine inundations most likely during tropical cyclones. These terraces are unlikely to have formed in response to falling sea-levels or recent tectonic uplift of the region. Mean sea-level has not varied by more than 1 m over the last 5,500 years along this section of coast, nor has the shoreline been uplifted by more than this amount over this time (Chappell et al., 1983). The gravel comprising the terraces was originally derived from the coarse-grained fluvial terraces and debris flows that extended farther seaward during a period of lower sea-level, most likely between 25,000–14,000 years B.P. (Thomas et al., 2001; Nott et al., 2001) and which was reworked by the Holocene marine transgression (Fig. 12). These sedimentary deposits now form sea cliffs between 5–10 m in height behind the gravel beaches. The gravel from these landforms have been re-deposited by waves to form the gravel beaches as evidenced by the presence of buried detrital corals. Sedimentological analyses of the gravels in the wave cut terraces show that they are generally well sorted and apart from the lower terrace show no sign of grain size variations from the toe to the crest of each terrace. This suggests that the upper three terraces have been eroded into the existing gravel deposit by waves rather than representing separate individual deposits.

As with the coral shingle ridges it is unlikely that tsunamis were responsible for erosion of the gravel terraces at Red Cliff Point. Nott (1997) proposed that tsunamis may have penetrated the Great Barrier Reef near Cairns and eroded and transported very large (>200 tonnes) lithic boulders along the coast once and possibly twice over the last millennium. Given that both tsunamis and tropical cyclone induced surges are possible in this environment, although the former are much less frequent, it is difficult to be absolutely sure that tsunamis were not responsible. However, if

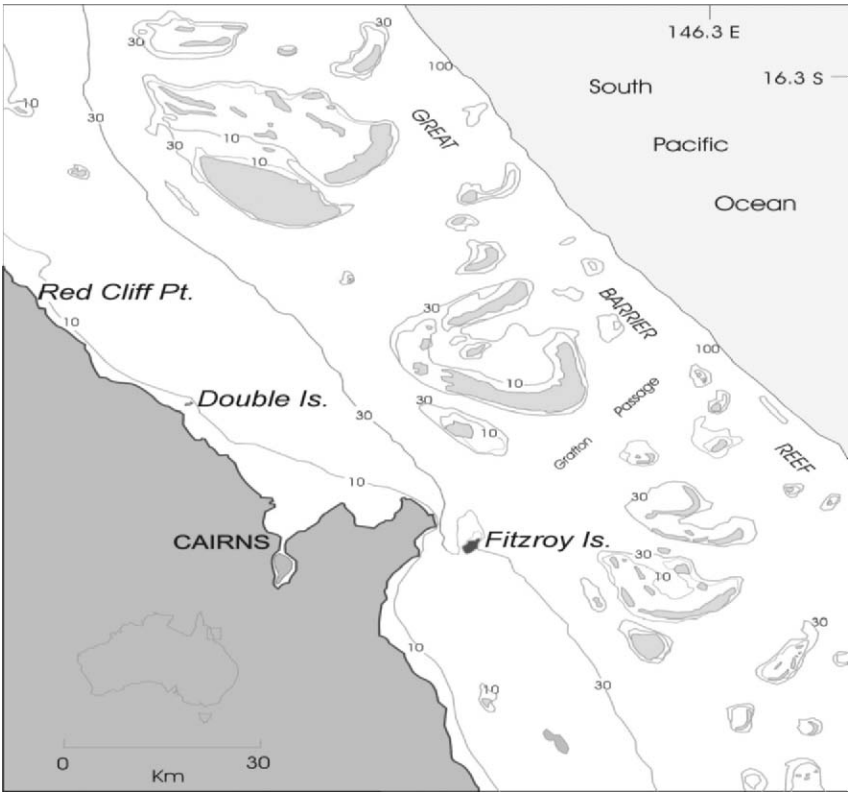

Fig. 12 Location map of sites displaying erosional terraces near Cairns, Queensland

tsunamis had impacted the terraces they would have likely destroyed the terrace morphology given their substantially greater velocity than surge or wind waves and ability to transport considerably larger clasts than those comprising the terraces. Hence it is suggested that tsunamis were unlikely to be responsible.

Radiocarbon ages from coral clasts buried amongst the gravels within the terraces at Red Cliff Point are presented in Table 1. They range in age from 4,200 yr B.P. to 340 yr B.P. (conventional radiocarbon ages) (Fig. 13). The older ages come from the lower terraces and the two youngest ages from the highest terrace (Terrace 4). It is suggested here that because these terraces are erosional, the lower terraces must have developed after Terrace 4 (the highest elevation terrace) and hence post-date the youngest age from this terrace; this age when calibrated at the 2σ uncertainty margin occurs between AD 1815 and 1870. This then represents the time when this section of coast experienced an inundation event reaching 6.1 m AHD (Table 2). The much older radiocarbon dated coral clasts have been reworked over the millennia and reincorporated into the terraces more recently.

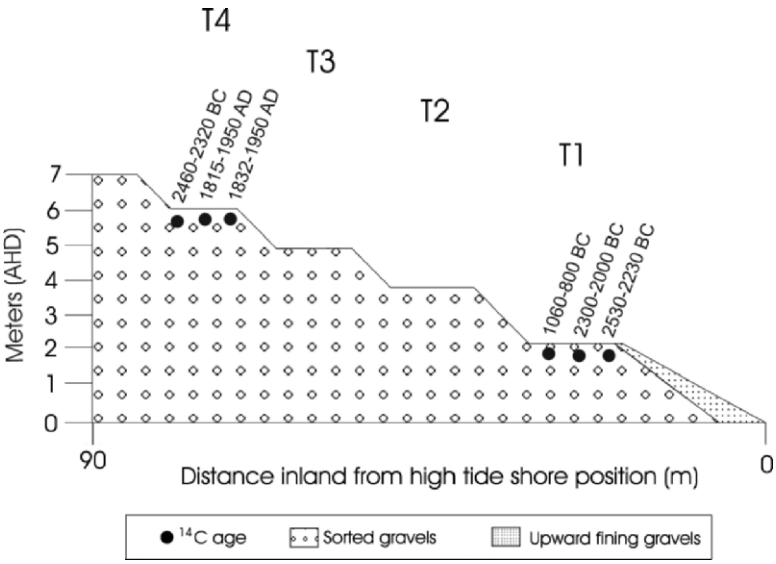

Fig. 13 Topography and chronology of erosional terraces at Red Cliff Point

Table 1 Radiocarbon chronology of coral clasts at Red Cliff Point

Location	Conv. Age, years B.P.	Cal. 1s, Age A.D.	Cal. 2s Age, A.D.
Terrace 1 A (2.97m)	3110 ± 70	990–860 BC	1060–800 BC
Terrace 1 B (2.97m)	4070 ± 50	2220–2050 BC	2300–2000 BC
Terrace 1 C (2.97m)	4240 ± 50	2460–2320 BC	2530–2230 BC
Terrace 4 A (6.1m)	4170 ± 50	2370–2200 BC	2440–2140 BC
Terrace 4 B (6.1m)	370 ± 50	1885–1950	832–1950
Terrace 4 C (6.1m)	400 ± 50	1880–1950	1815–1950

Conv. = Conventional radiocarbon age, Cal. = Calibrated radiocarbon age (at 1 sigma and 2 sigma uncertainty margins); heights in brackets are metres AHD.

Intensity of Tropical Cyclones from Sedimentary and Erosional Evidence

Apart from determining the frequency of tropical cyclone occurrence, the ridge and terrace records of these events in Queensland can also be used to reconstruct the intensity of the events responsible for emplacement of individual ridges. The technique involves an assumption that the height of these landforms represents the minimum height of the storm inundation during the event responsible. The elevation of the ridges and terraces is accurately surveyed to datum, and samples of coral and/or shell radiocarbon dated or sands dated using OSL to determine the minimum height and times of inundation, respectively. The height of this inundation is then related to the intensity of the paleocyclone which is determined through

Table 2 Calculated central pressure of tropical cyclones responsible for emplacing ridges and eroding terraces

Location	Inun.	H_s	Set-up	Run-up	Surge	hPa mean	±1σ	±2σ
Wallaby Is.	5.08	3.9	0.39	1.2	3.43	861	9	30
	4.1	3.6	0.36	1.1	2.58	896	8	29
	3.6	3.4	0.38	1.0	2.24	910	8	29
Pormpuraaw	5	3.3	0.2	0.9	3.9	942	7	15
	4	3	0.15	0.7	2.9	955	7	15
Princess Charlotte Bay	3.1	2.32	0.23	0.7	2.17	924	9	30
	2.9	2.26	0.22	0.67	1.99	931	9	29
Red Cliff Pt.	6.1	5.2	0.52	1.56	3.99	900	12	25
	4.9	4.7	0.47	1.4	3.0	926	12	24
	3.8	4.13	0.41	1.24	2.11	949	12	23
	2.12	3.1	0.31	0.92	0.86	982	10	17
Double Is	1.9	2.0	0.2	0.6	0.8	980	15	27
	3.5	3.8	0.38	1.0	2.2	941	15	27
Fitzroy Is	4.5	7.4	0.74	2.2	1.5	894	20	39
	3.9	6.7	0.67	2.0	1.2	912	19	36
Normanby Is	4.71	7.9	0.79	2.4	1.4	893	13	31
	3.8	6.7	0.67	2.0	1.0	924	12	29
Cowley Bch	5	9.5	0.9	1.2	3.7	910	12	24
	4	8.5	0.8	1.0	2.8	931	12	24
Curacoa Is	5.5	6.3	0.63	1.89	2.95	893	9	29
	4.8	5.8	0.58	1.73	2.47	912	8	28
Lady Elliot Is	5.1	11.2	1.12	3.4	0.52	896	15	35
	4.9	10.6	1.06	3.2	0.47	906	14	32
	4.5	9.9	0.99	3.0	0.43	916	14	30

Inun. = inundation or height of ridge or terrace, H_s = significant wave height. Mean central pressure in hPa represents cyclone intensity if storm crossed at mean tide level which occurs at majority of time over full nodal (~19 yrs) tidal cycle. Central pressures are regarded as minimum intensity values.

the use of numerical storm surge and shallow water wave models (Nott, 2003). The models are used to determine the relationship between surge height and central pressure for each location containing evidence of paleocyclones. Also, the relationship between surge height and translational velocity of the cyclone, the radius of maximum winds and the track angle of the cyclone as it approaches and crosses the coast are determined. Model results are compared to measured surge heights from

recent or historical cyclone events near the study sites. The central pressure of the cyclone responsible for formation of the ridge or terrace is determined by modeling the magnitude of the surge plus wave set-up, and run-up and tide required to inundate the ridge or terrace.

The tide height at the time of the prehistoric event is unknown but can be estimated (at the 95% confidence level) to have occurred within the 2σ probability tidal range of the frequency distribution nodal tide curve for each site (Table 2). Likewise, the tide height at the time can be estimated at the 1σ probability tidal range (68% confidence level). These tidal ranges effectively form the uncertainty margins associated with the mean central pressure of the cyclone responsible for producing an inundation equal in height to the elevation of the ridge or terrace (Nott, 2003).

Nott and Hayne (2001) and Nott (2003) applied this technique to seven sites along the Queensland coast. More recently, analyses for the ridge sequences at Pormpuraaw and Cowley Beach have also been undertaken. The results are presented in Table 2. They show that the ridges at virtually all of the locations studied were emplaced during category 5 cyclones (category 5 being the most intense and category 1 being the least intense), which probably had central pressures of less than 920 hPa (Table 2). Even at the 95% uncertainty margin, these cyclones were still category 5 or at least severe category 4 events. The storms responsible for construction of the ridges at Princes Charlotte Bay (PCB) appear to have been less intense (929 ± 31 hPa) than elsewhere; however, the lower elevation of these ridges may be due to limited sediment supply rather than less intense cyclones (Nott and Hayne, 2001).

In the immediate Cairns region the surge and wave numerical modeling revealed that a range of cyclones of varying intensities occurred between AD1800 and 1870. Table 2 presents the mean intensity and the 1σ and 2σ range of intensities for individual cyclone events at each site. The highest terrace at Red Cliff Point was eroded by a cyclone with a mean central pressure of 900 ± 25 hPa at the 2σ uncertainty margin. This suggests that there is only a 5% probability that this cyclone had a central pressure higher (weaker) than 925 hPa (Table 2). The mean central pressure of this storm (900 hPa) is close to the thermodynamic limit for tropical cyclones in this region [Holland, 1997]. The mean central pressures for the storms responsible for eroding each of the successively lower terraces were 926, 949 and 982 hPa, respectively. The latter figure accords closely with the central pressures (980, 975 hPa) of the two tropical cyclones to cross near Red Cliff Point in recent years (TC Justin and TC Steve) and which caused inundations close to the crest of Terrace 1. The mean central pressures for the storms responsible for depositing the shingle ridges at Fitzroy Island were 894 and 912 hPa (Table 2). The ridges at Double Island are lower in elevation compared to Fitzroy Island and were likely deposited by less intense cyclones. The numerical modeling and chronologies from the coral shingle ridges and eroded gravel terraces near Cairns suggest that one and possibly two intense (severe category 4 or category 5) tropical cyclones occurred here between AD 1815 and 1870.

High Resolution (Isotope) Records of Tropical Cyclones

The sedimentary evidence of past tropical cyclones tends to record the most extreme events. Smaller ridges will be built by weaker cyclones but these are either destroyed or overridden by more intense events and tend not to be as well preserved. As a consequence the frequency of events recorded is lower and only one spectrum of the climatology of these events remains. This together with the inherently moderate resolution of the dating techniques (radiocarbon and luminescence) limits the ability to identify trends at decadal to centennial scales. In order to overcome this problem high resolution records (annual) have been recently derived from isotopic analysis of annually layered carbonate stalagmites extending back nearly 800 years near Cairns.

Tropical cyclone rain, compared to normal tropical rain, is strongly depleted in ^{18}O because of extensive fractionation during condensation of uplifted air and the continuous and higher levels of rainfall (amount effect) (Lawrence and Gedzelman, 1996). Tropical cyclone rain typically contains ^{18}O levels between -5 and -15 ‰ (vSMOW) (Lawrence and Gedzelman, 1996; Lawrence, 1998). These isotope values have been measured as far as 400 km from the centre of the cyclone (Lawrence and Gedzelman, 1996). An isotope gradient occurs across the cyclone with the eye wall region generally experiencing lowest levels of ^{18}O and low values also occur within the zones of uplifted air around the cyclone known as spiral bands (Lawrence and Gedzelman, 1996). While the levels of ^{18}O appear to be inversely proportional to the altitude of uplifted air within the one cyclone there have not been any systematic studies to date that focus specifically on the relationship between isotope depletion and cyclone intensity. It is possible that this relationship does exist since more intense cyclones have cloud tops at greater altitude around the eye and in spiral bands. The longevity of the system and hence the amount of rain that has occurred prior to the system crossing the coast also plays a role in the extent of isotope depletion (amount effect) (Dansgaard, 1964; Hendy and Wilson, 1968; Hendy, 1971). Because of these factors, rain water falling in tropical coastal regions with $\delta^{18}O$ below -6 ‰ (vSMOW) can be regarded as a signature of its origin in a tropical cyclone (Lawrence and Gedzelman, 1996; Lawrence, 1998). Dilution of this rain water will occur when mixed with ground and surface waters and this would also be expected when such waters are utilized in the formation of terrestrial faunal carbonate shells and limestone speleothems in caves. These diluted water isotope values have been measured between -5 and -10 ‰ (vPDB) (Lawrence, 1998). To date however this isotopic signature has not been used as a measure of the long-term history of tropical cyclones in well preserved carbonates.

An annually layered stalagmite was sampled from Chillagoe approximately 130 km west of Cairns. Oxygen isotope ($\delta^{18}O$) analyses were undertaken on each of the 777 layers (AD 2004 to AD 1228) (Fig. 14). (Nott et al., 2007). Comparisons were made between the isotope and historical records of tropical cyclones (starting AD 1907) passing through the region (Fig. 15). Each of the peaks in the $\delta^{18}O$ depletion curve corresponds to the passage of a cyclone within 400 km of Chillagoe. Twenty

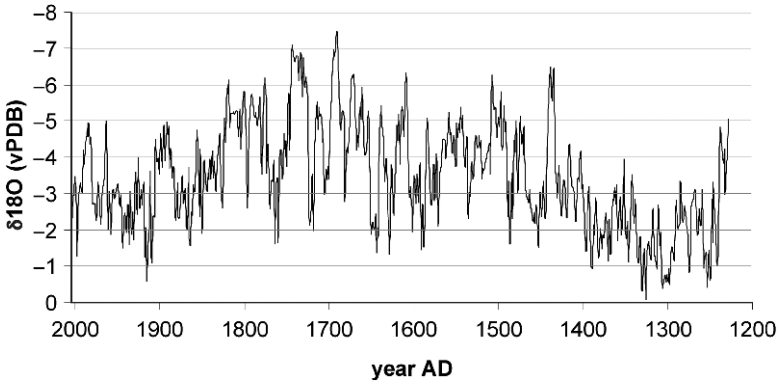

Fig. 14 Annual $\delta^{18}O$ ‰ (vPDB) AD 1226 to 2003

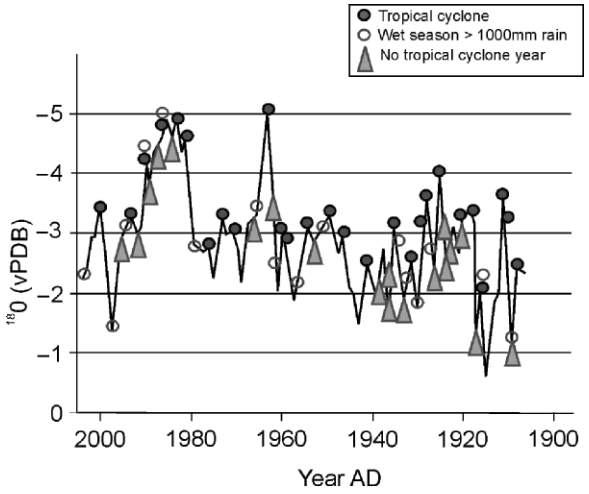

Fig. 15 Timing of tropical cyclone occurrences, high wet seasonal rainfalls and no cyclone years relative to $\delta^{18}O$ ‰ (vPDB) record for period AD 1907 to 2003

of these twenty seven cyclones passed within 200 km of Chillagoe, 22 within 230 km, 23 within 270 km and the other three within 400 km. The record accounts for 63% of all cyclones that passed within 200 km of Chillagoe since AD 1907. It is not reasonable to expect all cyclones to be registered in the stalagmite for a number of reasons including a) many cyclones in this region are ‘midgets’ (very small diameter) and even tracking within 200 km these cyclones will not produce ^{18}O

depleted rain at Chillagoe, b) the cyclones were short lived and hence had higher levels of ^{18}O because the amount effect (Dansgaard, 1964; Hendy and Wilson, 1968; Hendy, 1971) had not had time to develop, or c) the cyclones were of low intensity. Despite the absence of many cyclones it is important to note that every intense cyclone (i.e. AD 1911, 1918, 1925, 1934, 1986 as determined by barometer or damage to urban infrastructure and loss of life) (Callaghan, 2005) to make landfall in the region (400 km region) since AD 1907 is registered by a peak in the isotope depletion curve.

The magnitude of each of the depletion peaks is likely to be a function of the level of ^{18}O in the cyclone rain and the amount of ^{18}O in soil water from the previous wet season rainfall or previous rainfall events in the same season. The step function appearance of the raw isotope data plot seen in Fig. 14 is likely to be due to the relative increase in soil water $\delta^{18}O$ content, as seen following approximately AD 1400, and decrease following approximately AD 1800. Because of the ^{18}O soil water lag effect, Nott et al. (2007) suggested that a more appropriate measure of the level of isotope depletion for a cyclone event is the difference in ^{18}O between the depletion peak and the preceding curve trough. A curve of $\delta^{18}O$ differences is presented in Fig. 16.

Multiple regression analysis showed that isotope depletion levels have their closest relationship to the intensity of the cyclone divided by the distance (closest point on path) of the cyclone from Chillagoe ($R^2 = 0.6$, $p < 0.001$). A very low isotope value (high peak on Fig. 16) is therefore more likely to be a product of an intense event that tracks very close to the site which as a consequence experiences a

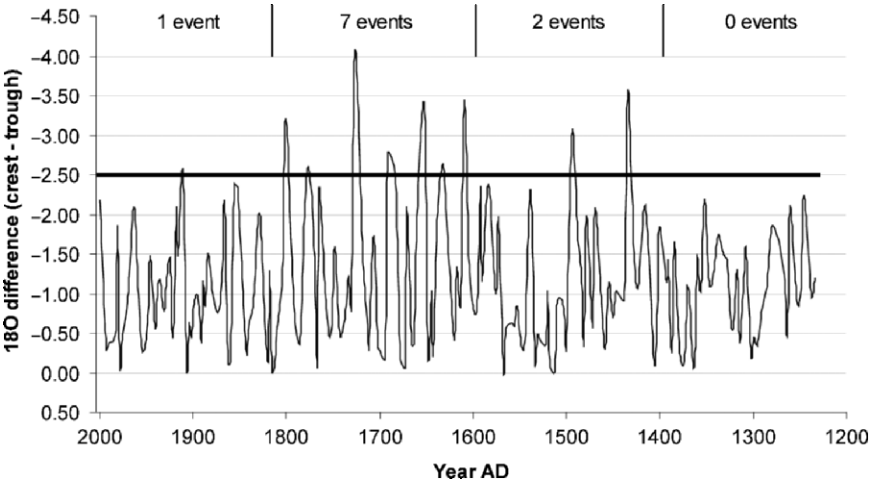

Fig. 16 Detrended $\delta^{18}O$ ‰ (vPDB) values (crest – preceding trough from Fig. 15) to account for $\delta^{18}O$ soil water dilution for landfalling tropical cyclones from AD 1228 to 2003. Critical value for moderate to severe hazard impact at-a-station is −2.50 ‰. Note no events above this value between AD 1200 to 1400 and AD 1500–1600, 2 events between AD 1400–1500, 7 events between AD 1600–1801 and 1 event (just above this value) since AD 1801

severe hazard. A higher isotope value could be due to an intense event at a greater distance or a low intensity event very close to the site. Either way the site experiences a lower severity hazard. The higher isotope values could also be due to some other environmental variable (i.e. slight variations in isotope values in evaporated source waters) and not necessarily be due to a distant or weaker tropical cyclone. However, as discussed it is unlikely that the lower isotope values are due to anything else besides tropical cyclone rainfall.

Only one cyclone event (AD 1911) during the historical period (post AD 1907) has an isotope difference less than −2.5 ‰ (*i.e.* a more negative value) (Fig. 15). A barometric pressure measurement of 959 hPa was made approximately 50 km from the estimated landfall point of this cyclone; the central pressure of this cyclone is not known but must have been considerably lower. This cyclone registers as the highest historical peak on Figure 16 because of its intensity and also because it passed within 30 km of Chillagoe. This cyclone also produced the highest peak during the period AD 1802–2004. In comparison, the period AD 1600–1801 registers 3 peaks with a lower than −2.5 ‰; isotope difference value, 3 more were below −3.0 ‰, and 1 was below −4.0 ‰ from AD 1500–1600 there were no peaks with an isotope difference value lower than −2.5 ‰; the period AD 1400–1600 had 1 event below −3.0 ‰ and one below −3.5 ‰.

Using the isotope difference value of 2.5 ‰ for the 1911 cyclone as a reference it is clear that the period between AD 1600 to 1800 had many more intense or hazardous cyclones impacting the site than the post AD 1800 period. Seven events that were more intense/hazardous than the 1911 event occurred during this 200 year period. Indeed the cyclone registering the lowest isotope difference value (<−4.0 ‰), hence the most intense or hazardous, of the entire record occurred during this time. There were no comparatively hazardous cyclones during the period AD 1500 –1600 yet the period from AD 1400 to 1500 had two events with considerably lower isotope difference values and hence were presumably more hazardous than the AD 1911 event. The two centuries from AD 1200 to 1400 had no events equal in intensity to the AD 1911 event.

These results suggest that there may be centennial scale regimes in landfalling tropical cyclone activity in this region. Comparisons with sea surface temperature (SST) data from geochemical proxies in corals from the GBR (Hendy et al., 2002) show that these centennial scale phases of heightened landfalling cyclone frequency occurred during both warmer (AD 1700–1800) and cooler (AD 1600–1700) than present SSTs in this region (Nott et al., 2007). This is the first time that centennial scale variations in landfalling cyclone activity have been recognised for any ocean basin and such information can be invaluable in decoupling human induced changes in cyclone behaviour from natural variability. Before such goals can be properly realised however it is imperative that further high resolution, long-term records of this hazard are investigated from both this region and other ocean basins globally. While this single station record is insufficient on its own to draw any conclusions about natural variability versus global climate change issues it is very useful for better assessing risk from this hazard for this region.

The Quaternary versus the Instrumental Record

The historical record of tropical cyclones in the Australian region shows some degree of decadal variability over the last 130 years especially in connection with variations in ENSO (e.g. Solow and Nicholls, 1990). The longest complete data set of land falling cyclones occur from northeast Queensland (Callaghan, 2005) and here the usual pattern of many more lower magnitude events occurring compared to higher magnitude ones exists. The record is interesting as it shows that during this time period only two category 5 and two category 4 cyclones struck the northeast Queensland coast. The rarity of these extreme events has led to a relatively blasé attitude towards the severity and consequences of such a hazard in some regional centres (Anderson-Berry, 2003).

Using only instrumental (last 30–40 years) and/or historical data sets (last approximately 100 yrs), several studies have determined the recurrence intervals of cyclones in this region. This has usually involved extrapolating centuries to millennia beyond the short record to determine the frequency of the most extreme events i.e. the 0.1% Annual Exceedence Probability event (AEP) (Harper, 1999; McInnes et al., 2000). The most recent magnitude frequency analysis of cyclones for the Queensland region used only the last 33 years (AD 2004–1970) of record, being the instrumental period (Queensland Government, 2001). Based on these analyses Cairns can expect a severe Category 5 cyclone (900 hPa) approximately every 1,000 yrs. Likewise, the Queensland Govt. (2004) showed that the probability of a category 5 cyclone crossing at Cairns and generating a storm tide equal to that needed to generate the sedimentary ridges discussed in this study was 0.001 (annual exceedence probability) or once every 1,000 years.

The Quaternary sedimentary record for the Queensland region suggests that over the past 5,000 years a category 5 cyclone occurs at any one location on average every 200–300 years (Nott and Hayne, 2001) which is approximately four times more frequent than that suggested by the instrumental period. In the Cairns region the sedimentary record suggests a category 5 cyclone made landfall here sometime between AD 1800–1870, the latter being the date of first European settlement. The isotope stalagmite record suggests that the last intense cyclone to occur near Cairns was AD 1801. This record also suggests that Cairns has experienced between 5 and 7 intense cyclones which were likely to be category 4 or 5 events over the past 800 years.

The clear message is that the Quaternary record demonstrates that the historical/instrumental record substantially underestimates the frequency of the most extreme tropical cyclone events. It also suggests that the size of the 1% annual exceedence probability (AEP) event is much more intense than had been previously estimated. Present policies and guidelines for hazard risk mitigation and urban planning, particularly for storm tides, are based upon the estimates from the historical/instrumental records despite the fact that the Quaternary records cast strong doubt upon the veracity of this approach. There is a reluctance to accept the Quaternary record as realistic because it is less precise than the instrumental record. Nott (2006)

has suggested that this may be because of the lack of familiarity with reconstructing long-term time series from natural records by those undertaking the risk assessments.

Conclusion

Considerable data on the frequency and magnitude of tropical cyclones in northern and Western Australia over the late Holocene has now been collected. From the earliest studies of Chappell et al. (1983) and Chivas et al. (1986) and then Hayne and Chappell (2001) and Nott and Hayne (2001) the regional record suggests that the more intense cyclone events occur on average every 200–300 years for most locations along the Queensland coast. The recent isotope studies of annually layered carbonate stalagmites also confirms that extreme tropical cyclones occur in the Cairns region considerably more frequently than previously estimated from the short instrumental record. Unfortunately, this disparity between the paleo and shorter records is often ignored in risk assessments of tropical cyclones in this region (cf Queenaland Government, 2001, 2004). To incorporate the Quaternary data when assessing risk from this hazard will lead to a more realistic assessment of the tropical cyclone magnitude and frequency relationship and a reduction in risk as a consequence.

References

Anderson-Berry, L., 2003: Community Vulnerability to Tropical Cyclones: Cairns, 1996–2000. *Natural Hazards,* **30**, 209–232.

Baines, G. B. K, and R. F. McLean, 1976: Sequential studies of hurricane deposit evolution at Funafuti Atoll. *Marine Geology*, **21**, M1–M8.

Callaghan, J., 2005: *Bureau of Meteorology record of Australian east coast tropical cyclones*, Australian Bureau of Meteorology, Brisbane.

Chappell, J., A.Chivas, E. Rhodes, and E. Wallensky, 1983: Holocene paleo-environmental changes, central to north Great Barrier Reef inner zone. *BMR Journ. Aust. Geol and Geophys*, **8**, 223–235.

Chivas A., J. Chappell, and E. Wallensky, 1986: Radiocarbon evidence for the timing and rate of island development, beach rock formation and phosphatization at Lady Elliot Island, Queensland, Australia. *Marine Geology*, **69**, 273–287.

Dansgaard, W., 1964: Stable isotopes in precipitation. *Tellus*, **16**, 436–468.

Davies, P. J. 1983: Reef Growth. *Perspectives on coral reefs*. D.J. Barnes, Ed., Aust. Inst. Mar. Sci. B. Clouston Publishing, Manuka, 69–106.

Donnelly, J. P., and T. Webb III, 2004: Backbarrier sedimentary records of intense hurricane landfalls in the northeastern United States. In: R. Murnane, and K. Liu, *Hurricanes and Typhoons:Past Present and Potential*, Eds., New York: Columbia Press, pp. 58–96.

Donnelly, J. P., S. S. Bryant, J. Butler, J. Dowling, L. Fan, N. Hausmann, P. Newby, B. Shuman, J. Stern, K. Westover, and T. Webb III, 2001: 700 yr sedimentary record of intense hurricane landfalls in southern New England. *Geo. Soc. Am. Bull.* **113**, 714–724.

Emanuel, K., 2005: Increasing destructiveness of tropical cyclones over the past 30 years. *Nature,* **436**, 686–688.

Harper, B., 1998: *Storm tide threat in Queensland: History, prediction and relative risks*. Qld. Dept. Env. & Her. Technical Report 10.

Hayne, M., and J. Chappell, 2001: Cyclone frequency during the last 5,000 yrs from Curacoa Island, Queensland. *Paleogeog., Paleoclim., Paleoecol*., **168**, 201–219.

Hendy, C., and A. Wilson, 1968: Paleoclimatic data from speleothems. *Nature*, **219**, 48–51.

Hendy, C., 1971: The isotope geochemistry of speleothems 1. The calculation of the effects of different modes of formation on the isotopic composition of speleothems and their applicability as paleoclimatic indicators. *Geochem et Cosm. Act*. **35**, 802–824.

Hendy, E. J., et al., 2002: Abrupt decrease in tropical Pacific sea surface salinity at end of Little Ice Age. *Science*, **295**, 1511–1514.

Holland, G., 1997: The maximum potential intensity of tropical cyclones. *Jour. Atmos. Sci*., **54**, 2519–2541.

Hughes, T. P., 1999 Off-reef transport of coral fragments at Lizard Island, Australia. *Marine Geology*, **157**, 1–6.

Kossin, J. P., K. R. Knapp, D. J. Vimont, R. J. Murnane, and B. A. Harper, 2007: A globally consistent reanalysis of hurricane variability and trends. *Geophys. Res. Lett.,* **34**, L04815, doi:10.1029/2006GL028836.

Landsea, C. W., 2007: Counting Atlantic tropical cyclones back to 1900. *Eos Trans. AGU,* **88**, 18, 197–202.

Lawrence J. R., and S. D. Gedzelman, 1996: Low stable isotope ratios of tropical cyclone rains, *Geophysical Research Letters*, **23**, 527–530.

Lawrence, J.R., 1998 Isotopic spikes from tropical cyclones in surface waters: opportunities in hydrology and paleoclimatology. *Chemical Geology,* **144**, 153–160.

Liu, K. B., and M. L. Fearn, 2000: Reconstruction of prehistoric landfall frequencies of catastrophichurricanes in northwestern Florida from lake sediment records. *Quat. Res*. **54**, 238–245.

Liu, K. B., 2004: Paleotempestology: Principles, methods, and examples from Gulf Coast lakesediments. *Hurricanes and Typhoons: Past, Present, and Future*. R. Murnane, and K.B. Liu, Eds. Columbia University Press, New York, 13–57.

Mann, M. E., and K. A. Emanuel, 2006: Atlantic hurricane trends linked to climate change. *Eos Trans. AGU,* **87**, 24, 238–241.

Mann, M. E., K. A, Emanuel, G. J. Holland, and P. J. Webster, 2007: Atlantic Tropical Cyclones Revisited. *Eos Trans. AGU*, **88**, 36, 249–350

McInnes, K. et al., 2000: *Impact of sea-level rise and storm surges on coastal resorts*. A report for CSIRO Tourism Research, CSIRO Atmospheric Research, Melbourne.

Miller, D. L., C. I. Mora, H. D. Grissino-Mayer, M. E. Uhle,. and Z. Sharp, 2006: Tree-ring isotope records of tropical cyclone activity. *Proc. Nat. Acad. Sci.* **103**, 14294–14297.

Nott, J., 2000: Records of prehistoric tsunamis from boulder deposits; evidence from Australia. *Science of Tsunami Hazards,* **18**, 3–14.

Nott, J., 2003: Intensity of prehistoric tropical cyclones. *Journal of Geophysical Research*, **108** (D7), 4212–4223.

Nott, J., 1997: Extremely high magnitude waves inside the Great Barrier Reef: determining the cause – tsunami or tropical cyclone. *Marine Geology*, **141**, 193–207.

Nott, J., and M. Hayne, 2001: High frequency of 'super-cyclones' along the Great Barrier Reef over the past 5,000 years. *Nature*, **413**, 508–512.

Nott, J., M. Thomas, and D. Price, 2001: Alluvial fans, landslides and late Quaternary climatic change in the wet tropics of northeast Queensland. *Australian Journal of Earth Sciences*, **48**, 875–882.

Nott, J. F., 2006. *Extreme Events; their physical reconstruction and risk assessment*. Cambridge University Press, Cambridge, U.K. 310pp.

Nott, J. F., J. Haig, H. Neil, and D. Gillieson, 2007: Greater frequency variability of landfalling tropical cyclones at centennial compared to seasonal and decadal scales. *Earth and Planetary Science Letters*. **255**, 367–372.

Nott, J. F., M. Hayne, Long-term tropical cyclone history from sand and shell beach ridges, Gulf of Carpentaria, Australia (in prep.).

Nott, J. F., S. Smithers, , K. Walsh, and E. Rhodes, 2008: Tropical sand beach ridges record 5,000 year history of tropical cyclones, Cowley Beach, Australia (in prep.).

Nyberg, J., A. M. Bjórn., A. Winter, M. R. Jury, H. Kilbourne, and. T. M. Quinn, 2007: Low Atlantic hurricane activity in the 1970s and 1980s compared to the past 270 years. *Nature*, **447**, 698–701.

Queensland Government, 2001: *Queensland climate change and community vulnerability to tropical cyclones ocean hazard assessment Stage 1*, Department of Natural Resources and Mines, Queensland Government, Brisbane.

Queensland Government, 2004. *Queensland climate change and community vulnerability to tropical cyclones ocean hazard assessment, Stage 4 Synthesis*, Department of Natural Resources and Mines, Queensland Government, Brisbane.

Rasser, M. W., and B. Riegl, 2002 : Holocene reef rubble and its binding agents. *Coral Reefs*, **21**, 57–72.

Rhodes, E. G., H. A. Polach, B.G. Thom, and S. R. Wilson, 1980: Age structure of Holocene coastal sediments, Gulf of Carpentaria, Australia. *Radiocarbon*, **22**, 718–727.

Solow, A., and N. Nicholls, 1990: On the relationship between the Southern Oscillation and tropical cyclone frequency in the Australian region. *Journal of Climate*, **3**, 1097–1101.

Thomas, M. F., J. F. Nott, and D. Price, 2001: The late Quaternary alluvial record in humid tropical environments. *Geomorphology*, **39**, 53–68.

Webster, P. J., G. J. Holland, J. A. Curry and H. R. Chang, 2005: Changes in tropical cyclone number, duration, and intensity, in warming environment. *Science*, **309**, 844–1846.

Western Australian Government, 2003: *WA State Planning Policy 2.6 (SPP 2.6)*, WA Planning Commission.

Statistical Link Between United States Tropical Cyclone Activity and the Solar Cycle

James B. Elsner and Thomas H. Jagger

Abstract The recent increase in the power of Atlantic tropical cyclones is attributable to greater oceanic warmth in part due to anthropogenic increases in radiation from greenhouse gases. However solar activity may directly influence a hurricane's power as well. In this chapter we report on a finding that Caribbean tropical cyclone activity and U.S. hurricane counts have a pronounced 10-year periodicity with tropical cyclone intensities inversely correlated with sunspot number on the interannual and daily time scales. The finding is in accord with the heat-engine theory of hurricanes that predicts a reduction in the maximum potential intensity with a warming in the layer above the hurricane. An active sun warms the lower stratosphere through ozone absorption of additional ultraviolet (UV) radiation. Since the dissipation of the hurricane's energy occurs through ocean mixing and atmospheric transport, tropical cyclones can act to amplify the effect of a relatively small change in the sun's output appreciably altering the climate. The finding has serious implications for life and property throughout the Caribbean, Mexico, and portions of the United States.

Introduction

On average Atlantic tropical cyclones are getting stronger with a trend that is related to an anthropogenic increase in oceanic heat content over the North Atlantic (Emanuel 2005; Webster et al. 2005; Trenberth 2005; Elsner 2007). Consistent with the "heat-engine theory", increases in tropical cyclone intensity over the past 25 years for the set of strongest storms are noted in other tropical cyclone basins as ocean temperatures rise (Elsner et al. 2008). However, a hurricane's maximum potential energy is inversely related to the temperature above the thunderstorm clouds in the central core (Emanuel 1991; Holland 1997). A warming of the lower stratosphere, near the tropopause (~16 km altitude), resulting from increased UV radiation absorbed by ozone will decrease the convective available potential energy limiting the intensity of the cyclone. Variation in radiation between extremes of the

J.B. Elsner and T.H. Jagger (eds.), *Hurricanes and Climate Change,*
doi: 10.1007/978-0-387-09410-6,

10–11-year sunspot cycle reaches 35% in portions of the UV range. Here we examine whether we can find a solar signal in the record of hurricanes, especially those affecting the United States. The focus on U.S. hurricanes and those over the Caribbean is motivated by the reliability of records back through the 20th century and by their social and economic importance. In fact, hurricane damage to the United States has averaged greater than $35 bn (U.S.) per year since 2002.

Model for Seasonal North Atlantic Hurricane Counts

To a first approximation on the annual time scale, high ocean heat content, low values of wind shear, and westerly steering currents increase the risk of hurricanes (Gray 1968; DeMaria et al. 2001; Elsner 2003). Indexes that track variations in these factors are used to construct skillful statistical models of coastal hurricane activity and potential financial losses (Saunders and Lea 2005; Jagger et al. 2008). Table 1 lists the coefficient estimates of a generalized linear regression model for Atlantic tropical cyclone counts (tropical storms and hurricanes) using data that starts at different years. The model covariates include sea-surface temperature

Table 1 Coefficients of a generalized linear model (Poisson) of tropical cyclone counts. The model uses the logarithm of the rate as the link function to a linear regression of the covariates. Model coefficients are determined from a maximum likelihood procedure. The covariates include the May through June averaged North Atlantic Oscillation (NAO) index in units of standard deviation, the August through October averaged Southern Oscillation Index in units of standard deviation, and the August through October averaged SSTs in the main development area of the central North Atlantic Ocean (see Fig. 2). For a one unit change in the covariate, the difference in the logarithms of expected tropical cyclone counts changes by the respective model coefficient given that the other covariates are held constant. The reduction in deviance from a model with no covariates is between 40 and 48% depending on start year. The intercept term is not included in the table

Term	Estimate	S.E.	z value	Pr($>z$)
		TS + H 1900–2006		
NAO	−0.086	0.036	−2.694	0.007
SOI	+0.138	0.035	+3.899	<0.001
SST	+0.859	0.105	+8.191	<0.001
		TS + H 1914–2006		
NAO	−0.096	0.034	−2.839	0.005
SOI	+0.150	0.038	+3.931	<0.001
SST	+0.981	0.121	+8.110	<0.001
		TS + H 1944–2006		
NAO	−0.084	0.042	−2.000	0.046
SOI	+0.146	0.044	+3.291	0.001
SST	+0.817	0.148	+5.502	<0.001

(SST) as an indicator of ocean heat content averaged over the main development area of the Atlantic Ocean (80W to 20W by 5N to 25N), the Southern Oscillation Index (SOI) as a remote indicator of shear, and the North Atlantic Oscillation index (NAO) as an indicator of steering currents.

Monthly values of the NAO and SOI are obtained from the *Climatic Research Unit* of the University of East Anglia. The May and June values of the NAO are averaged to produce the NAO covariate. The August through October values of the SOI are averaged to produce the SOI covariate. Both covariates have units of standard deviations. The monthly SST values were obtained from the U.S. National Oceanic and Atmospheric Administration (NOAA) in Boulder, Colorado, USA (http://www.cdc.noaa.gov/) and are from the Kaplan SST V2 data (Kaplan et al. 1998). The data are averaged over the main development area of the Atlantic Ocean (80W to 20W by 5N to 25N) from 2 degree by 2 degree latitude-longitude grids and have units of degrees Celsius.

The generalized linear model for tropical cyclone count data is the Poisson regression (Elsner and Schmertmann 1994; McDonnell and Holbrook 2004). It attributes to the response variable (annual tropical cyclone counts) a Poisson distribution whose expected value depends on a set of covariates in the following way

$$\log(\hat{\lambda}) = \alpha_0 + \alpha_1 \cdot NAO + \alpha_2 \cdot SOI + \alpha_3 \cdot SST$$

where lambda hat is the expected annual tropical cyclone rate, NAO, SOI, and SST are the covariates, and the alphas are the model parameters estimated using the method of maximum likelihoods. In the parlance of generalized linear models, the logarithm is the link function.

The reduction in deviance (analogous to the percentage of variance explained in an ordinary least-squares regression) from a model with no covariates ranges from 40% using data back to 1900 to 48% using data back only to 1944. It needs to be emphasized that a Poisson regression is not the same as a normal regression on the logarithm of counts. With Poisson regression you cannot explain all the variation in the data; there will be unexplainable variation due to the stochastic nature of the model. Thus, given that the counts follow a Poisson distribution (excellent assumption), even if the model precisely predicts the rate, the counts will have a degree of variability that cannot be reduced by the model (this is what is called aleatory uncertainty).

Signs on the coefficient estimates are consistent with the theory indicating more disturbances reaching tropical cyclone intensity with greater ocean heat content (positive on the SST coefficient estimate), more cyclone intensification with less shear (positive on the SOI estimate indicating La Nina conditions), and a greater number of cyclones reaching tropical cyclone intensity with a weaker pre-season NAO indicating a preference for storms to remain in the deep tropics (e.g., hurricanes Dean and Felix over the Caribbean Sea during 2007).

Model for Seasonal U.S. Hurricane Counts

The autocorrelation function of the seasonal tropical cyclone model residuals is plotted in Fig. 1. The plot shows a relatively high correlation at a 10-year lag, which is unrelated to the covariates in the model. We add a term to the model to account for this lag and find that it is indeed significant (Table 2). In fact, a 10-year lag term is significant in models for basin-wide tropical storms and hurricanes and hurricanes alone. The lag term reduces the model deviance by an additional 4 percentage points for the tropical storm-and-hurricane model and by an additional 7 points for the hurricane-only model. The coefficient value of 0.054 on the lag term in the hurricane-only model indicates an increase of 5.4% per hurricane so if there were 10 hurricanes a decade ago, the rate would be 32% higher than if there were only 4

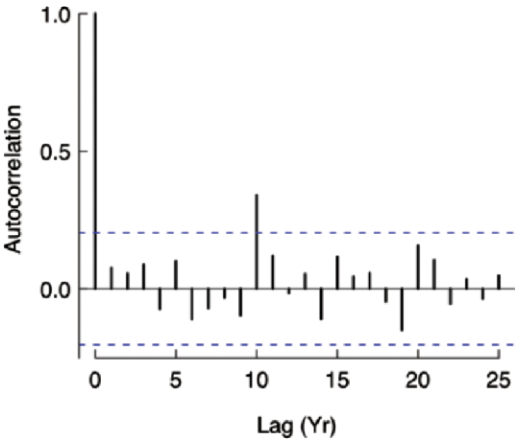

Fig. 1 Autocorrelation function of the residuals from a generalized linear model of Atlantic tropical cyclone counts. The model response variable is the count of tropical cyclones and hurricanes over the period 1914–2006. The dotted lines are the 95% confidence limits. A pronounced 10-year peak is noted

Table 2 Same a Table 1, except with a 10-year term (LAG) added. Also included is a hurricane-only model

Term	Estimate	S.E.	z value	Pr($>z$)
TS + H 1914–2006				
NAO	−0.108	0.037	−2.925	0.003
SOI	+0.139	0.041	+3.386	0.001
SST	+0.762	0.142	+5.376	<0.001
LAG	+0.031	0.010	+3.268	0.001
H only 1900–2006				
NAO	−0.144	0.045	−3.195	0.001
SOI	+0.161	0.049	+3.261	0.001
SST	+0.609	0.162	+3.745	<0.001
LAG	+0.054	0.018	+2.958	0.003

hurricanes a decade ago. The result suggests the possibility of an additional forcing mechanism for Atlantic hurricanes related to the solar cycle.

To examine this possibility we focus on U.S. hurricanes. Reliable records of U.S. hurricane counts extend back to solar cycle number 10 (1860s). Since the statistical model above includes SST, the missing thermodynamic variable in the heat-engine theory is near-tropospheric temperature. We speculate that an increase in solar UV radiation during periods of strong solar activity will have a negative influence on tropical cyclone intensity as the temperature near the tropopause will warm through absorption of the radiation by ozone possibly modulated by the transport of ozone (Labitzke and van Loon 1988; Rind and Balachandran 1995; Shindell et al. 1999; Crooks and Gray 2005; Salby and Callaghan 2007). This effect will be most pronounced in regions of sufficient oceanic heat content and for stronger tropical cyclones. In fact, an 8–11 year cycle in a 270-year proxy for major Atlantic hurricane activity from coral and marine sediments in the Caribbean has been noted (Nyberg et al. 2007). As upper tropospheric data are not available earlier than about 1940, solar activity serves as a proxy for upper tropospheric temperature.

For solar activity we use the August through October averaged sunspot number (SSN). The sunspot numbers produced by the *Solar Influences Data Analysis Center* (SIDC), World Data Center for the Sunspot Index, at the *Royal Observatory of Belgium* are obtained from NOAA.

The model for U.S. hurricane counts using data starting with 1866 shows that SSN is significant (p value = 0.048) after accounting for the NAO, SOI, and SST (Table 3). Average sunspot number, as a predictor is more significant using data beginning with 1878. The sign on the coefficient is negative indicating that the U.S.

Table 3 Same a Table 3, except a model for U.S. hurricanes that also includes a term for the solar cycle: sunspot number (SSN)

Term	Coefficient Estimate	S.E.	z value	Pr($>z$)
US H 1866–2006				
NAO	−0.207	0.066	−3.143	0.002
SOI	+0.238	0.068	+3.514	<0.001
SST	+0.508	0.235	+2.164	0.030
SSN	−0.003	0.001	−1.979	0.048
US H 1878–2006				
NAO	−0.202	0.069	−2.931	0.003
SOI	+0.272	0.071	+3.829	<0.001
SST	+0.499	0.236	+2.120	0.034
SSN	−0.003	0.002	−2.194	0.028
US H 1900–2006				
NAO	−0.214	0.076	−2.820	0.005
SOI	+0.285	0.081	+3.487	<0.001
SST	+0.545	0.252	+2.161	0.031
SSN	−0.003	0.002	−1.992	0.046

hurricane rate decreases with increasing solar activity. The coefficient magnitude indicates that for every additional 100 sunspots, the U.S. hurricane rate is reduced by a factor of 0.74. This is consistent with the heat engine theory and with the notion that increased UV radiation accompanying an active sun raises the temperature in the atmosphere above the hurricane. Correlation between the covariates range in absolute value from 0.05 to 0.19 with the highest occurring between SST and SOI and between SST and SSN.

With a generalized linear model, adequacy is checked by examining the Pearson residuals. Under the null hypothesis that the model provides an adequate fit to the data, the sum of the squared Pearson residuals has a chi square distribution with N-p degrees of freedom, where N is the record length and p is the number of model parameters. For all four seasonal models (data starting at different years) considered, the p-value on the chi square goodness-of-fit test is 0.2 or greater indicating no significant lack of fit.

Model for Daily Tropical Cyclone Intensity

To examine the hurricane-sun relationship in more detail we consider daily data. We first spline interpolate the 6-hr positions and maximum wind speeds to hourly values (Jagger and Elsner 2006) using the U.S. National Hurricane Center best-track data (Neumann et al. 1999) for all tropical storms and hurricanes over the 63-year period 1944–2006. Tropical cyclones over the Caribbean Sea and near the United States were routinely monitored with aircraft reconnaissance during this time period. We then compute daily average tropical cyclone wind speed intensity from the spline-interpolated values.

Tropical cyclone intensity depends on many factors including low-level spin and wind shear. These factors will confound attempts to identify a solar signal in the data. In order to provide some control, we correlate tropical cyclone intensity with solar activity using cyclones over a uniformly warm part of the western half of the basin and mainly within the deep tropics. The domain is bounded by 65 and 100 degrees W longitude and 10 and 30 degrees N latitude (Fig. 2a). This region is where oceanic heat content is the largest during the hurricane season so the limiting thermodynamic variable is upper atmosphere temperature rather than SST.

The rank correlation between daily SSN and daily averaged tropical cyclone intensity for all tropical storms and hurricanes in the domain over the period 1944–2006 is -0.11 (p value < 0.001, 413 dof). Although explaining only a small amount of the variability, the result is consistent with output from the seasonal models above showing an inverse relationship between hurricane intensity and solar activity. The daily correlation between SSN and storm intensity is based on the Spearman rank correlation since daily SSN and tropical cyclone intensity are not multivariate normal. The significance includes a reduction in the degrees of freedom since daily intensities and SSN are serially correlated. Each storm is given one degree of freedom regardless of the number of days it stays in the region.

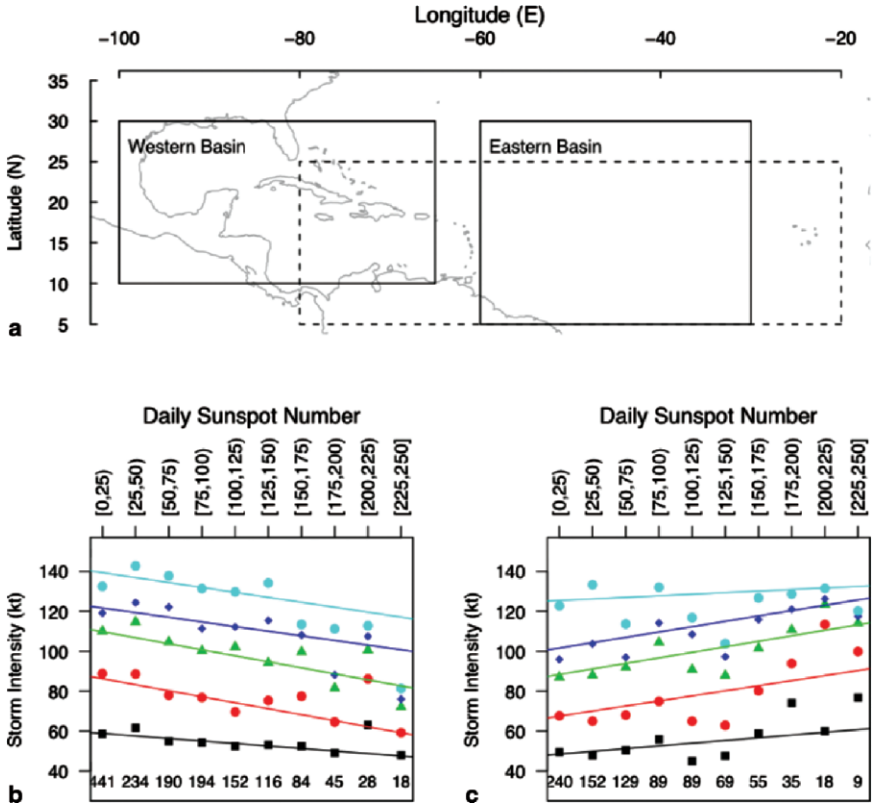

Fig. 2 Region map and upper quantiles of hurricane intensity grouped by daily sunspot numbers. **a.** Solid boxes delineate regions used to model daily tropical cyclone intensities. The dotted box delineates the averaging region for SST as an index of ocean heat content for the seasonal model of tropical cyclone activity. **b.** Quantile values and regression model lines using daily tropical cyclone intensity in the western basin as the response and daily SSN as the covariate. The symbols correspond to the 50th, 75th, 90th, 95th, and 99th percentiles starting at the bottom for each sunspot group. The lines correspond to the respective quantile regression lines. Numbers above the abscissa are the sample sizes (number of days with sunspot numbers in the interval). **c.** Same as b, except for the eastern Atlantic basin

Quantile regression is a model to estimate the conditional quantile of a response variable given a set of observed covariates. Here we consider the 50, 75, 90, 95 and 99 percentiles of daily mean maximum tropical cyclone wind speed as an affine transformation of the daily number of sunspots. Quantile regression is an extension of median regression based on estimating the value of the parameter vector from the set of allowable vectors that minimizes the mean loss function

$$L_\tau(\beta, y) = \frac{1}{n}\sum_{i=1}^{n} p_\tau(y_i - \mu(x_i, \beta))$$

where the y's are the response values, mu is the estimate of the tau quantile, and the x's and beta's are the covariate vector and parameter vector, respectively. The loss function is p sub tau, where

$$p_\tau(z) = |z|\{\tau \cdot I(z > 0) + (1 - \tau) \cdot I(z < 0)\}$$

and $I(x)$ is the indicator function, which is one when x is true and zero otherwise. The loss function is non-negative taking a minimum value of zero only when z is zero.

If one has a series of samples and mu is a constant, i.e. an intercept-only model, then the resulting value of beta that minimizes the total loss function occurs only when mu is equal to the tau quantile of the response. Then, if the model fits well, a plot of the fitted values versus the actual values will show that tau observed values are less than the fitted values, with 1-tau observed values greater than the fitted values (Yu et al. 2003). The total loss function is an unbiased sample estimate of the expected value of

$$p_\tau(Y - \mu(x \cdot \beta))$$

and the minimization over beta is a consistent estimate of the minimization of this expected value. For the fit we choose a linear model for the regression function of the form

$$\hat{\mu} = \beta_0 + \beta_1 \cdot \mathrm{SSN}_i$$

where SSN is the daily sunspot count.

Figure 2b shows the upper quantiles of hurricane intensity by categories of daily SSN. The slopes from a quantile regression are negative at the median and above (Q50, Q75, Q90, Q95, and Q99) indicating an inverse relationship between sunspots and storm intensity. The relationship is generally stronger for the more intense cyclones (Table 4).

Over the western Atlantic including the Carilbrean Sea and Gulf of Mexico where oceanic heat content is sufficiently large, the limiting thermodynamic factor for a tropical cyclone to reach its maximum potential intensity (MPI) is the near-

Table 4 Quantile regression coefficients from a model of storm intensity on daily sunspot number (SSN). The values are estimates of the slope over the western North Atlantic basin (see c). SSN is grouped in 25 count intervals. The slope has units of kt/SSN

Quantile	Estimate	S.E.	*t* value	Pr(>*t*)
Q50	0.050	0.012	4.017	<0.001
Q75	0.120	0.025	4.908	<0.001
Q90	0.121	0.028	4.368	<0.001
Q95	0.093	0.027	3.461	0.001
Q99	0.099	0.042	2.342	0.019

troposphere temperature. Since this factor is inversely related to MPI, we note that an active sun warms the lower stratosphere thereby decreasing potential intensity. Indeed, the correlation between seasonally averaged SSN and temperatures near the tropopause over the domain is consistently positive based on atmospheric data over the period 1948–2006. The seasonal averaged (August–October) near-tropospheric (200, 150, 100, and 70 mb) temperatures are obtained from the U.S. NCAR/NCEP re-analysis dataset (Kalnay et al. 1996). These results using a quantile regression model on daily cyclone intensity are in agreement with the results of our seasonal model and thus they add evidential support to the hypothesis of a solar hurricane link.

In marked contrast, the daily SSN is positively correlated with daily averaged tropical cyclone intensity for cyclones over the domain bounded by 30 and 60 degrees W longitude and 5 and 30 degrees N latitude. Figure 2c shows the upper quantiles of hurricane intensity by categories of daily SSN over this eastern part of the Atlantic basin. Here the slopes from a quantile regression are positive at the median and above (Q50, Q75, Q90, Q95, and Q99) indicating an direct relationship between sunspots and storm intensity over the central and eastern Atlantic.

Discussion and Summary

An explanation for this geographic difference in the SSN-hurricane intensity relationship centers on the difference in the limiting factors associated with tropical cyclone intensity. As mentioned over the western Atlantic cloud top temperature appears to be the limiting factor, whereas over the eastern and central tropical Atlantic, the limiting factor in the thermodynamic potential for intensity is oceanic heat content. Since there is a direct relationship between SST and MPI, an active sun increases the shortwave flux to the ocean raising the heat content and increasing the potential for tropical cyclone intensification. In fact, a time series model of Atlantic SST contains a component corresponding to the solar cycle (Elsner et al. 2008) with Aug-Oct SST values generally higher (lower) during years of high (low) sunspot numbers.

To better understand and predict how global warming affects hurricanes it is necessary to consider the full range of natural factors responsible for variations in tropical cyclone activity. Here we identify a 10-year cycle that explains a significant portion of the inter-annual variability in tropical cyclone frequency after accounting for SST, shear, and steering. The cycle is negatively correlated with solar activity. Daily SSN is significantly negatively correlated to tropical cyclone intensity over the Caribbean especially for storms near their MPI. The variation in tropical cyclone frequency related to the solar cycle is explained by the heat-engine theory of tropical cyclones that for a constant ocean heat content implies an inverse relationship between storm intensity and cloud top temperature and therefore the amount of UV radiation absorbed by ozone.

This natural co-variability between solar and tropical cyclone activity needs to be incorporated into forecasts of hurricanes that look decades ahead. Since the dissipation of the cyclone's energy occurs through ocean mixing and atmospheric transport, tropical cyclones act as an amplifying mechanism by which small changes in the sun's output can appreciably alter the climate. The discovery has critical implications for life and property throughout the Caribbean, Mexico, and portions of the United States.

Acknowledgments We acknowledge the SIDC for the sunspot data and the NHC for the tropical cyclone data. Partial support for this study was provided by the National Science Foundation (ATM-0435628) and the Risk Prediction Initiative (RPI-05001). The views expressed within are those of the authors and do not reflect those of the funding agencies. All statistical modeling was done using R (R Development Core Team 2006).

References

Crooks, S.A. and L.J. Gray, 2005: Characterization of the 11-year solar signal using a multiple regression analysis of the ERA-40 dataset. *J. Clim.*, **18**, 996–1015.

DeMaria, M., J.A. Knaff, and B. Connell, 2001: A tropical cyclone genesis parameter for the tropical Atlantic. *Wea. Forecasting*, **16**, 119–233.

Elsner, J.B., 2007: Granger causality and Atlantic hurricanes. *Tellus*, **59A**, 476–485.

Elsner, J.B., 2003: Tracking hurricanes. *Bull. Amer. Meteor. Soc.*, **84**, 353–356.

Elsner, J.B. and C.P. Schmertmann, 1994: Assessing forecast skill through cross validation. *Wea. Forecasting*, **9**, 619–624 (1994).

Elsner, J.B., T.H. Jagger, M. Dickinson, and D. Rowe, 2008: Improving multiseason forecasts of North Atlantic hurricane activity. *J. Appl. Meteor. Clim.*, **21**, 1209–1219.

Elsner, J.B., J.P. Kossin, and T.H. Jagger, 2008: The increasing intensity of the strongest tropical cyclones. *Nature*, **455**, 92–95.

Emanuel, K.A., 1991: The theory of hurricanes. *Annu. Rev. Fluid. Mech.*, **23**, 179–196.

Emanuel, K.A., 2005: Increasing destructiveness of tropical cyclones over the past 30 years. *Nature*, **436**, 686–688.

Gray, W.M., 1968: Global view of the origin of tropical disturbances and storms. *Mon. Weath. Rev.*, **96**, 669–700.

Holland, G.J., 1997: The maximum potential intensity of tropical cyclones. *J. Atmos. Sci.*, **54**, 2519–2541.

Jagger, T.H., and J.B. Elsner, 2006: Climatology models for extreme hurricane winds near the United States. *J. Climate*, **19**, 3220–3226.

Jagger, T.H., J.B. Elsner, and M.A. Saunders, 2008: Forecasting U.S. insured hurricane losses. In *Assessing, Modeling, and Monitoring the Impacts of Extreme Climate Events*, Eds, R. Murnane, and H. Diaz, Cambridge University Press.

Kalnay, E., *et al.*, 1996: The NCEP/NCAR 40-year reanalysis project. *Bull. Am. Meteorol. Soc.*, **77**, 437–471.

Kaplan, A., M. Cane, Y. Kushnir, A. Clement, M. Blumenthal, and B. Rajagopalan, 1998: Analyses of global sea surface temperature 1856–1991. *J. Geophys. Res.*, **103**, 18,567–18,589.

Labitzke, K. and H. van Loon, 1988: Associations between the 11-year solar cycle, the QBO (quasi-biennial-oscillation) and the atmosphere. Part I: the troposphere and stratosphere in the northern hemisphere in winter. *J. Atmos. Terr. Phys.*, **50**, 197–206.

McDonnell, K.A. and N.J. Holbrook, 2004: A Poisson regression model of tropical cyclogenesis for the Australian-Southwest Pacific Ocean region. *Wea. Forecasting*, **19**, 440–455.

Neumann, C.J., B.R. Jarvinen, C.J. McAdie, and G.R. Hammer, 1999: *Tropical Cyclones of the North Atlantic Ocean, 1871–1998*. National Oceanic and Atmospheric Administration, 206 pp.

Nyberg, J., B.A. Malmgren, A. Winter, M.R. Jury, K.H. Kibourne, and T.M. Quinn, 2007: Low Atlantic hurricane activity in the 1970s and 1980s compared to the past 270 years. *Nature*, **447**, 698–701.

R Development Core Team, 2006: *R: A Language and Environment for Statistical Computing*, R Foundation for Statistical Computing, Vienna, Austria, ISBN 3-900051-07-0, http://www.R-project.org.

Rind, D., and N.K. Balachandran, 1995: Modeling the effects of UV variability and the QBO on the troposphere-stratosphere system. Part II: The troposphere. *J. Clim.*, **8**, 2080–2095.

Salby, M.L. and P.F. Callaghan, 2007: Interaction between the QBO and the Hadley circulation: Evidence of solar influence? *J. Clim.*, **20**, 1583–1592.

Shindell, D.T., D. Rind, N. Balachandran, J. Lean, and P. Lonergan, 1999: Solar cycle variability, ozone, and climate. *Science*, **284**, 305–308.

Saunders, M.A., and A.S. Lea, 2005: Seasonal prediction of hurricane activity reaching the coast of the United States. *Nature*, **434**, 1005–1008.

Trenberth, K. 2005: Uncertainty in hurricanes and global warming. *Science*, **308**, 1753–1754.

Webster, P.J., G.J. Holland, J.A. Curry, and H.R. Chang, 2005: Changes in tropical cyclone number, duration, and intensity in a warming environment. *Science*, **309**, 1844–1846.

Yu, K., Z. Lu, and J. Stander, 2003: Quantile regression: applications and current research areas. *The Statistician* **52**, Part 3, 331–350, doi:10.1111/1467-9884.00363.

Five Year Prediction of the Number of Hurricanes that make United States Landfall

Stephen Jewson, Enrica Bellone, Thomas Laepple, Kechi Nzerem, Shree Khare, Manuel Lonfat, Adam O'Shay, Jeremy Penzer, and Katie Coughlin

Abstract The insurance industryis interested in five-year predictions of the number of Atlantic hurricanes which will make landfall in the United States. Here we describe a suite of models developed by Risk Management Solutions, Inc. to make such predictions. These models represent a broad spectrum of view-points to be used as a basis for an expert elicitation.

Introduction

The question of how to predict the number and intensity of Atlantic hurricanes that make landfall in the United States is of great interest to the insurance and reinsurance industry. There is interest in predictions on time-scales from as short as a few hours to as long as 50 years. The physical processes that determine predictability, and the methods that one might use to make predictions, vary greatly according to time-scale. Here we are concerned with predictions on time-scales of one to five years. For these time-scales both natural variability and anthropogenic influences contribute to the climatic conditions which impact hurricanes. As a result, one to five year hurricane predictability depends on the extent to which current climate, decadal fluctuations and trends can be estimated in the hurricane numbers and associated parts of the climate system. This leads to the use of prediction methodologies that first attempt to define the current state, and then try to capture the variability and/or trends that might determine changes from this current state.

Our approach to making predictions of hurricane numbers on these interannual time-scales has two steps. First, we build a large number of forecast models based on different ideas for how one might predict future hurricane numbers. We try and include all reasonable and obvious approaches. Our models are based on inputs such as historical numbers of landfalling Atlantic hurricanes, historical numbers of hurricanes in the Atlantic basin, historical sea surface temperatures (SSTs) and predictions from dynamical model simulations. The second step is to present these

J.B. Elsner and T.H. Jagger (eds.), *Hurricanes and Climate Change,*
doi: 10.1007/978-0-387-09410-6,

models to a panel of experts, who combine the various predictions by weighting the models using their best judgement. This paper focuses on the first step (the modelling), and presents the models that were used as input for expert elicitation processes in 2006 and 2007. The details of the elicitation process itself are described in another paper (Lonfat et al., 2007).

Background and Motivation

Insurance and reinsurance rates for property on the gulf and east coasts of the United States are strongly influenced by predictions of the possible number and intensity of future hurricanes making landfall in these regions. The insurance industry is interested in such predictions on a wide range of time-scales. In particular, there is interest in predictions of the number of hurricanes in the next one to five years. Such predictions are used for the pricing of insurance and reinsurance contracts, and for the allocation of capital to businesses and business units.

Following the high levels of Atlantic basin hurricane activity over the past decade, a considerable amount of research regarding the influences of natural and human-induced variability on hurricane behaviour has been published. Much of this work is relevant to our question of how to predict hurricane numbers and intensities on five year time-scales, although there is still some controversy regarding the mechanisms which have caused the recent increase in hurricane numbers as well as uncertainty regarding the likely nature of future changes. Work by Webster et al. (2005), Elsner (2006), Mann and Emanuel (2006) and Hoyos et al. (2006) suggests that, in the Atlantic, there is an increasing trend in frequency and intensity of hurricanes, in part due to the rise in SSTs brought on by global warming. Trenberth (2005), however, suggests that although increasing SSTs are likely to increase intensity and rainfall from hurricanes, the effect of increasing SSTs on hurricane numbers is unclear. Dynamical prediction models have been used to estimate the impact of global warming on hurricane intensity and precipitation (Knutson and Tuleya, 1999, 2004, Vecchi and Soden, 2007) and these models show a CO_2-induced increase in storm intensity and rainfall and a small *decrease* in storm frequency over the next century. Further studies by Klotzbach (2006) and Goldenberg et al. (2001) suggest that long-term Atlantic hurricane variability is more influenced by natural variability, such as the Atlantic Multidecadal Oscillation (AMO), than by anthropogenic changes. A number of other authors have also looked into aspects of natural and human-induced impacts of hurricane variability (for example: Kerr, 2005, and Bengtsson, 2001). In summary, there is agreement that we are currently in a period of increased hurricane activity, and there is perhaps a weak consensus forming that the intensity of hurricanes may increase in the future, but there is no consensus as to what will happen to the future frequency of hurricanes. Based on this range of evidence and opinions we develop a variety of prediction models that are consistent with different underlying physical mechanisms and interpretations of the data.

In addition to the internal variability of the Atlantic Multidecadal Oscillation and the global warmingtrend in SST, other climatic features such as the North Atlantic Oscillation (NAO) (Elsner et al., 2000) and the El Nino Southern Oscillation (ENSO) (Bove et al., 1998; Camargo and Sobel, 2005) are known to influence hurricane activity. Is this relevant for our one to five year time-scale? Lyons (2004) has shown that ENSO has predictability on up to annual time-scales but for five year time-scales there is at present no effective way to predict ENSO (and there very possibly never will be). Similarly, the NAO, is not currently predictable out to five years and therefore lacks skill for our prediction purposes. The lack of predictability of ENSO on one to five year time-scales means that the prediction methods we describe below are very different from those used in seasonal predictions (see for example Saunders and Lea, 2005 or Vitart and Anderson, 2001).

General Strategy

The first issue we consider in developing our five year hurricane number prediction schemes is how to estimate the current climate state. Recent historical data is likely to be more relevant to making such estimates than earlier historical data. We therefore address the question of exactly how much of the historical data one should use, and with what weight. The next issue we consider in our model development is how to model potential future changes over the next five years. We include some methods that assume that the future will not change from the current state, and others that model systematic future changes. Some of our methods, for example, attempt to model a trendand extrapolate it into the future, while other models estimate the probability of future climate shifts. We note, however, that *all* of our models incorporate any *past* effects of trends and variability when they attempt to capture the current level of activity.

To keep things simple, the goal we set for our predictions is to minimize the root mean square error (RMSE) between the predicted and actual numbers of hurricanes. We note that one might eventually want to move beyond RMSE as a metric because, among other reasons, RMSE gives equal weight to errors on both sides of the prediction, while the consequences of overpredicting and underpredicting may not have symmetric affects. Furthermore, we note that one might ultimately want to consider making probabilistic forecasts and evaluating them using a probabilistic metric. We have taken this approach in Hall and Jewson, 2006.

Most of our analysis uses simple classical statistical methods, with the addition of some use of model shrinkage (which is described in section 5). Given that the amount of data is rather small, the signals are weak, and the parameter uncertainty is high one might consider using more elements of Bayesian statistics (Litterman, 1979, 1986) to attack this problem. However, Bayesian methods tend to be both complex and controversial and we are not yet convinced that the potential benefits of using them, in terms of greater scientific accuracy, would outweigh the loss of transparency for the problem at hand. This is partly because one of our goals is to

introduce methods that can be widely understood by meteorologists, climate modelers, and insurance industry practitioners. We feel that at this early stage in the development of the ideas presented here it is more important to focus on the discussion of what methods fundamentally make sense, and what assumptions the different methods depend on, rather than taking the level of technical and statistical sophistication as far as it could be taken.

In the following sections, we present the methods developed for predicting the number of Atlantic hurricanes that will make U.S. landfall in the periods 2006–2010, 2007–2011 and 2008–2012. These predictions are made given data up to the end of the hurricane seasons in 2005 and 2006 and using an estimate for the 2007 season given information up to 15 Oct, 2007. The data used is described in section two. In section three we describe what we call 'long baseline methods'. In section four we discuss issues related to the non-stationarity of the hurricane number time-series. In this section we describe what we call 'short baseline methods', and introduce the idea of *direct* and *indirect* predictions of landfall numbers. In section five we describe what we call 'mixed baseline' methods that mix the historical levels of hurricane activity in an optimal way. Our climate-shift models are also introduced in this section. In section six we describe prediction methods based on sea-surface temperature (SST) and in section seven we describe a model which uses both SST and windshear to predict hurricane numbers. In all cases, predictions are made for the expected numbers of category 1–5 and category 3–5 hurricanes hitting the U.S. coastline for five years ahead. The estimated model skill for each of the models, determined by the root mean squared error, is shown in section 8. We present predictions for 2006–2010, 2007–2011 and 2008–2012. The 2006–2010 predictions are those that were used in the RMS 2006 expert elicitation. The 2007–2011 predictions are made from the same models but also include data from 2006. The 2008–2012 predictions are made from the slightly different (and hopefully improved) set of models that were used in the RMS 2007 expert elicitation. Tables of the predictions from all the models are shown, and discussed, in the summary section 9.

All the methods we present have been described in detail in Risk Management Solutions technical reports, and are available from the Arxiv preprint server at arxiv.org. They can also be accessed by following links from www.rms-research.com and are cited throughout this article. Relative to those reports, this article summarizes the methods used, explains the connections between them, and publishes the results from all the methods side by side for the first time.

Data

The hurricane numbers used in our analysis (see Fig. 1) come from the 2006 version of the HURDAT data-set (Jarvinen et al., 1984 and Jarrell et al., 1992). We use sea surface temperatures from HADISST (Rayner et al., 2002). A couple of our models also use Northern Hemisphere temperature anomalies relative to the base period

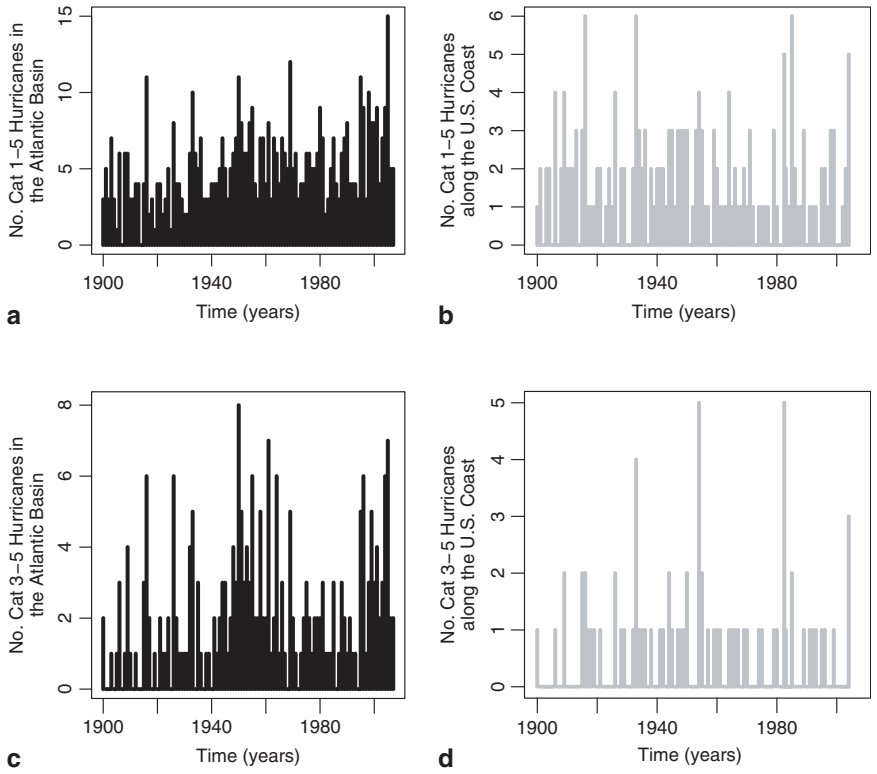

Fig. 1 Atlantic Hurricane Numbers since 1900. (**a**) Numbers of Category 1–5 Hurricanes in the Atlantic Basin. (**b**) Numbers of those hurricanes which hit the U.S. coastline. (**c**) Number of Category 3–5 Hurricanes in the Atlantic Basin. (**d**) Number of those hurricanes which hit the U.S. coastline

1951–1980, which can be found at http://www.giss.nasa.gov/gistemp (Hansen and Lebedeff, 1987).

The HURDAT data is considered to be reasonably accurate since 1950. Prior to 1950, the numbers of hurricanes in the basin may be less accurate, however, as there were fewer observational opportunities over the ocean at this time. Aircraft reconnaissance, for example, did not begin until 1944. Numbers of hurricanes hitting the US coastline are generally considered accurate since 1900, although the intensities of such landfalling storms may be poorly estimated due to the distances between proper meteorological measurements and the probability of missing measurements of the most intense windspeeds. Prior to 1900 even the landfall numbers are suspect because of the sparsity of population along the US coast line. Based on this, we never use data before 1900 and only use data from 1950 to build relationships between SSTs, hurricane numbers within the Atlantic basin and hurricane numbers at landfall. Any conclusions drawn from our analyses need to bear in mind these

Table 1 Estimates for Hurricane Numbers in 2007

	Historical Ratio	2007 season up to 15 Oct.	Likely 2007 season
Basin Cat 1–5	0.15	4	5
Basin Cat 3–5	0.06	2	2
Landfall Cat 1–5	0.035	1	1
Landfall Cat 3–5	0.029	0	0

issues of data quality, since our forecasts can only ever be as good as the data on which they are based.

Atlantic SSTs are used to help predict hurricane numbers in some of our models, and the strength of the relationship between SSTs and hurricane frequency is dependent on the region of the north Atlantic being considered (Shapiro and Goldenberg, 1989; Raper, 1993; Goldenberg et al., 2001). The SSTs which correlate most highly with hurricane activity are the SSTs within the main development region (MDR), 10-20N, 15-70W. MDR SSTs are also highly correlated with each other in space (see figure 10 in Meagher and Jewson, 2006). It therefore makes sense to construct a single index that captures the MDR SSTvariability. We tested various combinations and came up with an index based on July-September SST variability as having the highest correlation with hurricane activity.

Estimating 2007

For the 2008–2012 predictions, we include an estimate of the 2007 season in the data used by our models. Since the 2007 expert elicitation took place in October, and the 2007 season was not complete at that time, the numbers used for the 2007 prediction were calculated by taking the number of storms that had occurred up to October 15, 2007 and adding a correction factor for the rest of the season. The correction factor is based on the historical ratio of the number of storms after and before October 15. This ratio is shown in Table 1 along side the number of storms before October 15th, 2007, and the number of storms in each category for the year 2007 that were used for the 2008–2012 predictions.

We note that for the 2006–2010 and 2007–2011 predictions, the models used full seasons for the years preceding the predictions.

Long Baseline Methods

The simplest method we present for predicting landfalling hurricane numbers is based on taking an average of the number of hurricanes that made landfall in the historical data, using data as far back as is considered accurate. We call this method the ‘long baseline’ method. As mentioned in section 2, we consider landfalling

hurricane number data to be accurate back to 1900, and so our first prediction is based on the average number of hurricanes per year from 1900. In the insurance industry this is the traditional method used for estimating future hurricane numbers and, in some cases, is still used. The 2006–2010 predictions from this method are given in row 1 of Table 2 in the summary section. The 2007–2011 predictions are given in Table 3, and the 2008–2012 predictions are given in Table 4. Since there has been some discussion as to whether the intensities of storms prior to 1950 were really estimated correctly, as mentioned in section two, we also present results for an alternative baseline that extends from 1950 to the present in row 2 of the summary tables. We call this the 'medium baseline' model.

Non-Stationarity of Hurricane Number Time-Series

As a method for predicting future hurricane numbers, the long baseline method is only appropriate if the landfalling hurricane number record is stationary, or at least close to stationary. A large number of studies have looked at the stationary of hurricane number records. With respect to hurricane numbers in the *basin*, it has been clearly shown that the record is not stationary. For instance, Elsner et al. (2001) detected the presence of statistically significant change-points in the cat 3-5 basin hurricane number series in the years 1942/43, 1964/65 and 1994/95. Using a different methodology the same authors repeated their analysis (Elsner et al., 2004) and showed the presence of statistically significant change-points in the years 1905/06, 1942/43 and 1994/95. In our own change-point analysis, which uses a different methodology yet again, we detected the existence of statistically significant change-points in the cat 1-5 basin hurricane number series in the years 1931/32, 1947/48, 1969/70 and 1994/95 (Jewson and Penzer, 2006). In fact, some of these change-points can be seen rather clearly by eye in the data itself, especially those in the cat 3-5 series at the end of the 1960s and in the mid 1990s: see Fig. 2. By contrast, for *landfalling* numbers, it is much harder to detect change-points. Elsner et al. (2004) couldn't find any, and neither could we (Jewson and Penzer, 2006). In a different kind of analysis, we did find statistically significant evidence of autocorrelation in the landfall time-series (see Khare and Jewson, 2005a, b), although the signal was rather weak.

Why is it that the *basin* hurricane number time-series shows such significant change-points, while the *landfalling* time-series does not? There are two obvious limiting-case explanations: (a) the interannual probability[1] of hurricanes making landfall is constant from year to year. In this case, the landfalling number time-series would be expected to inherit properties of the basin hurricane number time-series, such as change-points. The apparent lack of change points in the landfalling

[1] By 'interannual probability of landfall' we mean the probability of landfall, estimated a year before the beginning of the hurricane season. Such an estimate is unconditional with respect to ENSO state, since ENSO is not predictable that far in advance.

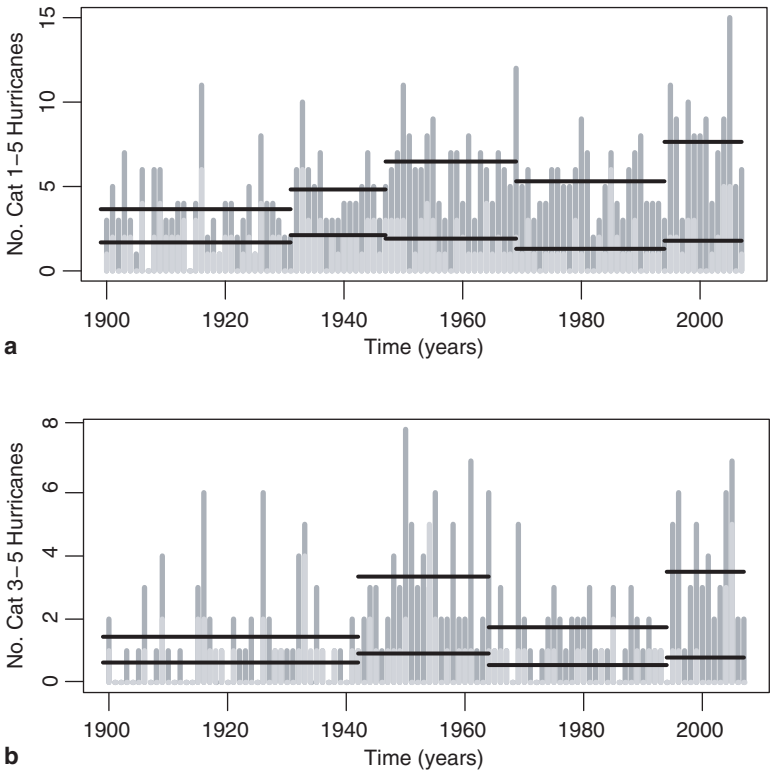

Fig. 2 Examples of Change-Points in Hurricane Numbers: (**a**) Levels between RMS change-points for category 1–5 hurricanes. (**b**) Levels between Elsner's 2004 change-points for category 3–5 hurricanes. The vertical dark grey bars indicate the number of storms in the Atlantic basin for each year and the overlaid light gray bars indicate the number of those storms which hit the U.S. coastline

time series must then be explained by the hypothesis that they are obscured by noise for statistical reasons, or (b) the interannual probability of hurricanes making landfall is *not* constant from year to year, and varies in such a way as to cancel the effect of the basin changes, meaning that the landfall numbers are actually stationary. Reality may be in-between these two limiting cases.

Given the importance of this question for the prediction of future numbers of landfalling hurricanes, we have investigated this in some detail. In Nzerem et al. (2006) we asked the question: if the basin series contains real change-points of the same size as the observed 1994/1995 change-point, what is the probability of detecting that change-point in the basin data and in the landfall data? Given an assumption of constant probability of landfall for each storm, it turns out that the change-point would usually be detectable in the basin data, but would usually *not* be detectable in the landfall data. The explanation is purely statistical: in going from basin to landfall, the number of storms reduces by a factor of four. This reduces the

signal-to-noise ratio by a factor of two, and makes it twice as hard to detect any change-point. The observed change-points are of a size that this reduction in signal-to-noise is just enough to hide them in the variability of the landfall data. This analysis shows that explanation (a) above is plausible, and that, based on this result, we should not necessarily be surprised that we can't detect change-points in the landfall series, and the fact that we cannot should not lead us to conclude that they are not there. Approaching the same question from a different perspective we looked at the proportion of basin hurricanes that make landfall during active and inactive historical periods (Bellone et al., 2007). The results are very clear. The proportion of storms making landfall prior to 1948 is different to the proportion making landfall after 1948. This is most likely explained by poor observations of basin storms before that time. However, after 1948, during the period of reliable observations, the proportion of storms making landfall cannot be shown to vary (i.e. we cannot reject the null hypothesis that the proportion is constant). Another way to interpret this result is that if the proportion of storms making landfall does vary (and it very likely does vary at some level) then the size of those variations are too small to detect, and would be too small to estimate effectively and use in predictions. In Bellone et al. it is also shown that this result holds even without consideration of the change-point locations. Finally, in Hall and Jewson (2008), we studied the historical behaviour of hurricanes in years with warm and cold tropical North Atlantic sea-surface temperatures (SSTs). We find that although the number of hurricanes, their genesis sites and the characteristics of their propagation all depend on SST in statistically significant ways, the overall proportion of Atlantic storms making landfall along the U.S. coast does not.

Based on these studies, we conclude that it is reasonable to build hurricane prediction models that use the assumption that the probability of storms making landfall over the next five years is well predicted using the proportion that have made landfall since 1950. We will call this the 'constant landfall probability' model (CLP), although the model does not, strictly speaking, assume landfall probabilities are constant, but just that the proportion varies sufficiently little that we cannot properly estimate the variations and we are better off modelling it as constant. The estimate of the proportion based on this assumption is shown in Fig. 3. Note that the long-baseline model is essentially based on the opposite set of assumptions: that the proportion of storms making landfall varies in such a way as to cancel out the non-stationarity in the basin so that the mean number making landfall is approximately constant. We include predictions from both sets of assumptions in our model set, for completeness, although we believe that the data slightly favour the CLP model, as discussed above. The CLP model has various interesting implications, as we discuss below.

Short Baseline Predictions

In the previous section, we justify the CLP model of basin and landfalling hurricane numbers that assumes (a) the mean number of basin storms varies in time and

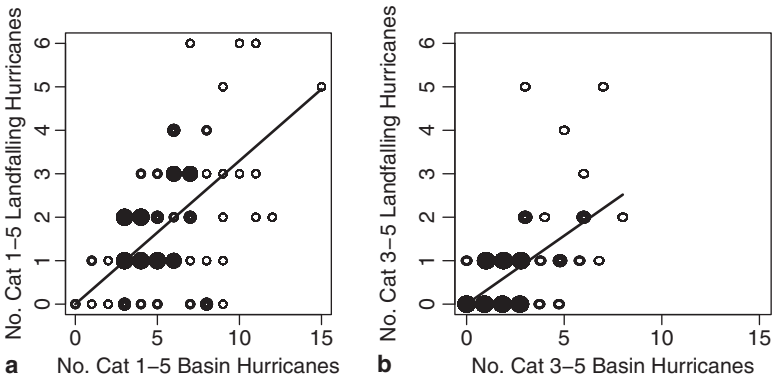

Fig. 3 Relationship between landfalling hurricanes and basin hurricanes for (**a**) Cat 1-5 and (**b**) Cat 3-5 intensities from 1948 to 2007. The larger circles indicate higher frequency. The largest filled circles indicate six or more years with the same landfall to basin ratio

(b) the probability of storms making landfall can be modeled as constant. A consequence of these assumptions is that the mean number of storms making landfall varies in time, following the mean number in the basin.

There are two important implications of this model for the prediction of numbers of landfalling hurricanes. The first is that we can take the change-points that have been identified in the basin hurricane number time-series, and assume that they apply to the landfalling series, even though they cannot be detected in the landfalling series. This leads to a method for predicting the landfalling series, which we call the 'short baseline' method, and which involves making a prediction for future landfalling hurricane numbers which consists of the average number of landfalling hurricanes since the most recent basin change-point. Based on the CLP model assumptions, this is then likely to be a better prediction method than the long baseline method, because of the underlying non-stationarity in the series.

Based on the estimated levels between the change-points, the CLP model implies that we would expect the long-baseline prediction to be biased. If we assume that the level of hurricane activity over the next five years will remain at the same level that it has been at since 1995, then the short baseline prediction will, on the other hand, be unbiased. The assumption that the number of hurricanes will remain at the same level clearly ignores decadal oscillations and trends, and the possible occurrence of further change-points in the next five years. These approximations may be good ones since our forecast horizon is fairly short and the trends are apparently rather weak. Nevertheless, we do try to model these effects in other models (see below). Conveniently, the various change-point analyses listed above all give the same point in time for the most recent change-point (1994/1995), and so all lead to the same short baseline prediction. This prediction is given in row 3 of the summary tables.

Indirect Method

The second implication of the CLP model is that there is a relationship between landfalling hurricane numbers and the number of hurricanes in the basin. Given this, it might make sense to predict landfalling hurricane numbers by first predicting basin hurricane numbers, and then converting the basin prediction to a prediction of landfalling numbers using the probability of landfall estimated from historical data since 1950. We will apply this idea to all subsequent models (thus doubling the number of predictions) and will call such predictions 'indirect' predictions, as opposed to 'direct' predictions which predict landfalls directly from landfall data. Should we expect such indirect predictions to be better than direct predictions? In Laepple et al. (2007b) we find that, if the probability of storms making landfall is constant, then there are situations in which we would expect the indirect methods to be better. For instance, if we make a short baseline prediction of the number of *basin* storms using data since 1995, and then convert that to a prediction of *landfalling* storms using a probability of landfall estimated from the number of basin and landfalling storm numbers since 1950, theoretically we expect the resulting prediction to be nearly twice as accurate as the direct short baseline prediction that uses landfalling data alone. The explanation for why indirect methods beat direct methods in this case is that there are more storms in the basin, and so the predictable signal can be estimated more accurately than when only using the landfall data. If the probability of landfall can also be estimated relatively accurately (as it can if we use data since 1950), then this increased accuracy propagates through to the prediction at landfall. In practice, our backtesting studies show that the indirect predictions *do* lead to better predictions, but are not usually twice as accurate as the direct predictions. Model skill is discussed in section 8 and Fig. 4 shows a comparison of model errors. Row 6 in Tables 2 and 3 shows the indirect short baseline predictions.

Mixed Baseline Predictions

Up to this point, we have presented averaged baseline prediction methods. The long and medium baseline prediction methods have the advantage that they use a large amount of historical data, but since, in the CLP model, we believe that the landfalling hurricane number time-series is non-stationary, we expect that the long-baseline and medium-baseline predictions are biased. The short-baseline scheme only uses the most recent data, which is likely to be more relevant to the current climate, and so is likely to reduce the bias, but possibly suffers from the fact that there are simply not many years of data since the last change-point to make an accurate estimate of the mean number of storms. Consideration of the pros and cons of the long and short baseline models motivates the idea that there may be a forecast methodology that lies 'in between' the two, and performs better than both. We have

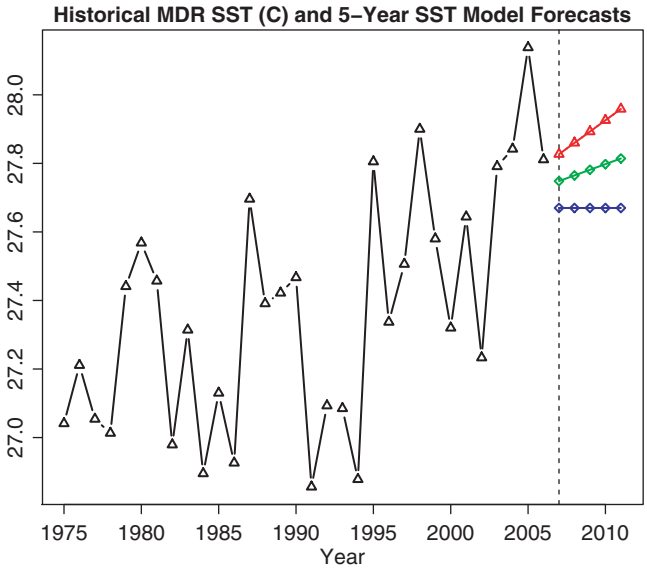

Fig. 4 **a**) The SSTs in the MDR region since 1880. **b**) Predictions of the 2006–2010 MDR SSTs using flat-line (*diamond*), damped trend (*middle prediction*) and linear trend (*triangle*) predictions

investigated this idea in a series of technical reports [Jewson et al., 2005; Jewson et al., 2006 and Binter et al., 2006]. The methodology we use is to formulate the question as a classical mathematical 'bias-variance trade-off' problem, and ask what weights we should put on the different parts of the historical hurricane data in order to minimize the RMSE of our predictions. We call predictions from the resulting method 'mixed-baseline predictions'. They are an example of a statistical modelling methodology known as 'shrinkage'. As with the short baseline predictions, we have two versions of each mixed baseline prediction: one direct (determined by applying weights directly to the historical landfall number data) and one indirect (determined by applying weights to the historical basin number data, and then converting the basin prediction to a landfall prediction using an estimated proportion).

To estimate the optimal weights on the mean levels of activity between change-points we use the weights which minimize the RMSE of hurricane number predictions (Binter et al., 2006). We find that the lowest RMSE prediction for the current level of category 3–5 storms comes from a set of weights corresponding to a straight average of the two most active periods in the historical record for both the Elsner and the RMS change-points. For the Elsner change-points these are 1943–1964 and 1995–2005 and for the RMSchange-points these are 1932–1947 and 1995–2005. The mixed baseline model analysis tells us that this gives a more accurate prediction than just using data from the recent active period because it makes use of more historical data, while only introducing a small bias. Interestingly, for the category 1–5 basin storms, the best prediction comes from a set of weights corresponding to

just using the historical data since the last change point, because there are enough cat 1–5 basin storms since 1995 that it is no longer beneficial to try and reduce the variance of the forecast using earlier data.

In order to address the question of how sensitive these predictions are to the change-points identified in the historical hurricane number time-series, we apply mixed baseline methods to the change-points from both Elsner et al. (2004) and from Jewson and Penzer (2006). The four combinations (two sets of change-points and both direct and indirect methods) lead to the predictions given in rows 4, 5, 7 and 8 of summary tables, 2 and 3 Note that the indirect predictions of the category 1-5 hurricane numbers for the Elsner and RMS change-points will be the same as the indirect predictions of the short baseline since the optimal mixed baseline for basin category 1–5 hurricane numbers *is* just the short baseline.

Climate Shift Models

Up to this point, the prediction methods that have been discussed assume that an estimate of current hurricane activity is a good estimate of future activity. This assumption, that the mean number of hurricanes will remain at the same level as it is now, clearly ignores the possible occurrence of further change-points in the next five years. This may be a reasonable approximation, considering that the last change-point was 10–13 years before our predictive period, which is only five years. Since hurricane change-points might well be related to the Atlantic Multi-decadal Oscillation (AMO), and according to Sutton and Hodson (2005), AMO phases currently last about 30 years, we might expect to wait another decade or so before worrying about future change- points. However, the possibility of a climate shift in the next five years may not be entirely negligible. Enfield and Cid-Serrano (2006) use Gray et al.'s (2004) tree ring reconstruction of the AMO to estimate the probability of regime shifts. The probabilities are derived using a Monte-Carlo re-sampling of the frequency space of the reconstructed paleo time-series and give us an approximation for the probability of a shift in the AMO over the next five years. There are a few issues with this analysis that need to be taken into consideration; namely (a) that the tree ring time-series is shown to be non-stationary, so the frequency distribution for the present and the future may be quite different from the past, and (b), although the tree ring time-series has been fitted to the recent AMO index, there is no certainty that the past part of the record also reflects only the AMO since tree rings can be influenced by other large-scale atmospheric features. Given these issues, in our climate shift prediction models, we let the hurricane experts determine both the probability of a shift by the next year and a probability of a shift within the next five years using their own best judgement (rather than taking these probabilities directly from the Enfield Cid-Serrano model). This model is restricted to downward shifts from the current activity rate. Using the probabilities that the experts provide we estimate the annual mean expected number of hurricanes for the next five years under the assumption that the probability of a

shift increases linearly through the five years. The estimate for the annual mean number of hurricanes is then

$$\hat{\mu}_{1-5} = \sum \hat{\mu}_i / 5$$

where $\hat{\mu}_i$ is the estimated number of hurricanes for year i, given by

$$\hat{\mu}_i = (1 - \hat{p}_i)\hat{\mu}_c + \hat{p}_i \hat{\mu}_1$$

μ_c and μ_l are the estimated annual hurricane numbers for the current state and for the low state of hurricane activity and $\hat{p}_i$ is the probability that the i-th year is in the low state. The low state estimate is made using the hurricane numbers between 1970 and 1994 and the current estimate of the annual number of hurricanes is derived using the mixed baseline model.

Predictions from the climate shift model vary according to the shift probabilities that the experts assign. If the probability of a shift is zero, then this model is just the mixed baseline model so, for the 2007 elicitation, this model was used in place of the mixed baseline model. For the 2008–2012 predictions in Table 4, the low state estimate of activity and the mixed baseline estimates are shown in rows 4a and 4b for the direct climate shift model and in rows 5a and 5b for the indirect climate shift model. These estimates give the possible range that experts could have chosen.

SST-Based Predictions

So far we have presented landfalling hurricane-number prediction methods that are based on historically observed hurricane numbers alone. These methods have the advantage that they depend on relatively few assumptions. On the other hand, they have the disadvantages that (a) there seems to be no very satisfactory way to represent possible climate-related changes in hurricane numbers in these methods, and (b) the signals that we are trying to predict tend to be obscured by noise due, in large part, to the scarcity of hurricanes. In this section we now present a different set of models for predicting future hurricane numbers, based on the idea of first predicting SSTs in the tropical North Atlantic, and then converting these SST predictions to predictions of hurricane numbers. The rationale for these methods is that (a) the effects of climate trends and climate variability may be more robust, and hence easier to predict, in the SSTs than they are in the hurricane number time-series, and (b) there is a clear historical relationship between SSTs in the subtropical North Atlantic and the number of hurricanes in the Atlantic basin. All of the SST prediction methods we use assume that this relationship between SST and hurricane numbers will continue into the future. This is an assumption that is needed in order to make these predictions: however, it is not necessarily the case that this assumption is true. For instance, it may be that the historic relationship between SSTs and hurricane numbers will not apply if patterns of SST in the future are different from patterns experienced in the past, and it may be inappropriate to extrapolate the relationship between SST and hurricane numbers to levels of SST that are higher than those experienced in the past.

The first part of the development of our SST-based hurricane number prediction schemes is to predict future SSTs. We consider four different classes of models for making such predictions: one-step models, two-step models, models based on numerical model output, and climate-shift models. The one-step models predict future MDR SST based on past MDR SSTs. The two-step models predict future MDR SSTs by first predicting future Northern Hemisphere temperatures, and then predicting MDR SSTs from the predicted Northern Hemisphere temperatures. The climate-shift models attempt to model changes in SST as a combination of gradual climate change and climate shifts. We describe each of these model classes in more detail below, followed by a description of how these SST predictions are then converted to hurricane number predictions.

The methods we use are described in detail in a series of technical reports (Meagher and Jewson, 2006; Laepple et al., 2007, Jewson, 2007, Binter et al., 2007a,b).

One-Step SST Predictions

The one-step statistical schemes we use for predicting SST are taken from methods developed for making short-time climate predictions of temperature in the weather derivatives industry. They consist of moving averages, fitted linear trends, and fitted damped linear trends. Damped linear trends are a compromise between moving averages, which don't capture trends, and fitted linear trends, which, by construction, suffer from being overfitted and are never optimal predictors, even for data with real linear trends (for a discussion of the surprisingly difficult question of how to predict noisy data with linear trends, see Jewson and Penzer, 2004, 2006). For moving averages and linear trends, we use backtesting (also known as hindcasting) to determine how many years of data over which to fit the average or the trend. The window length over which past predictions minimize the RMSE are the window lengths we use to make our predictions. For the damped linear trend, we take the ad-hoc decision to make a 50–50 combination of the prediction from the moving average and the prediction from the fitted linear trend. Due to the relatively large variance in the SSTs, this 50–50 combination is actually more accurate in hindcast experiments than the trend predictions. These three SST predictions for 2007–2011 are given in Fig. 6.

Two-Step SST Predictions

The weakness of the one-step SST prediction schemes that involve estimating a trend is that this trend is very hard to estimate accurately because of the noise in the data. In the 2007 elicitation, we tried to overcome this limitation by introducing two-step schemes that assume that the MDR SST trend is similar to the Northern Hemisphere temperature trend. The Northern Hemisphere temperature trend is

much easier to estimate because of the lower level of noise in the Northern Hemisphere time-series. The two-step method consists of making a statistical prediction of the Northern Hemisphere trend, and then converting that prediction to a prediction of MDR SST. This assumes that the relationship between Northern Hemisphere temperature and MDR SST that held in the past will also hold for the next five years. Whether the two-step method is likely to out-perform the one-step method depends on the degree of similarity between the trends in the Northern Hemisphere temperature and the MDR SST and the relative levels of noise in the two series. In practice, out of sample hindcasts show that the two-step method has worked better in the past (Laepple et al., 2007).

Numerical Ensemble Based SST Predictions

In our 2007 model suite, we also included another way to estimate future changes, based on output from global climate models. The multi-model ensemble mean of model runs assembled for the IPCC AR4 report (available at www.pcmdi.llnl.gov) were found to have skill in predicting past values of both MDR SST and Northern Hemisphere temperature in a paper by Laepple et al. (2007). These ensemble means provide a non-linear estimate of future changes that lies between the flat line estimates and the linear trend estimates described above. For this model, our predictions are based on an estimate of the current state and an estimate of the change from that state. The ensemble mean, which effectively averages out the natural variability of the model runs, predicts the future non-linear trend. This is then adjusted to the current state using a bias correction. The current state is estimated using the mean of the last 8 years, since 8 years is the optimal window length calculated by minimizing the out-of-sample RMSE of hindcasts.

Our simple technique of using the IPCC ensemble mean, bias-corrected to the current climate, as a prediction for future temperatures, compares favorably with both our purely statistical predictions and the predictions from a complex initial-condition driven forecast model by Smith et al. (2007).

SST Climate Shift Predictions

Up until now, we have discussed SST prediction in terms of extrapolating past estimates of either a trend or a current level into the future, and in terms of estimating future changes using the IPCC-based model ensemble. However, like hurricane numbers, SSTs may also experience multidecadal shifts, or oscillations. Note that these types of shifts can not be accounted for in the multi-model ensemble because the natural oscillations in these models are independent from the prescribed forcing and will average out in the ensemble mean. With the SST Climate Shift model we attempt to account for the possibility of a future shift in SSTs. There are

five steps to making the SST Climate-Shift predictions (this is our most complex model). The first step is to isolate the multidecadal oscillation in the SST time-series. This is not an easy task as there is a trend in the time-series which must first be removed. It is obvious that removing a linear trend is not the correct thing to do because we expect that at least part of the trend in SSTs is due to anthropogenic forcing which we know has had a non-linear effect on the past record. To deal with this we use the IPCC ensemble mean as an estimate of the historical trend. Although not a perfect estimate, this is certainly better than removing a linear trend and it captures at least some of the non-linearities in the anthropogenic trend. Once this non-linear trend has been removed from the time-series, the second step is to estimate the current state and the low state as we did in section 5.1. This is done using the estimated warm and cold AMO periods from Trenberth and Shea (2006). The third step is to ask the experts to estimate the probability of being in the cold state next year and the probability of an AMO shift in the next five years. Given these values we estimate the probability of a shift for each of the following years and we calculate the average level of this oscillation for the next 5 years. The fourth step is to then add back the non-linear trend that we originally removed. This then gives us a prediction for the SSTs over the next five years. These SST predictions will vary depending on the probabilities that are given by the experts.

SST-Hurricane Number Relationship

Having predicted SST using one of the four methods described above, the second part of the development of our SST-based hurricane number predictions is to model the relationship between SST and hurricane numbers. To do this, we consider only data from 1950 to the present, because of the data quality issues discussed in section 2. Using the framework of the Poisson Generalized Linear Model, SST was found to be a significant predictor for the number of hurricanes in the Atlantic basin. The relationship between SST and *landfalling* hurricane numbers, however, is only marginally significant. Why is there apparently such a large difference between the behaviour of basin and landfalling numbers? Is it that SST really doesn't affect landfalling hurricane numbers, or is the disappearance of the relationship at landfall just a statistical effect, similar to the disappearance of change-points when going from basin to landfall that was discussed in section 4? We considered this question in detail in Laepple et al., 2007, in which we showed that we would *expect* the correlation between SST and landfalling numbers to disappear, purely on statistical grounds. The argument is indeed very similar to the argument for why change-points disappear in the landfalling series: the signal-to-noise ratio decreases by a factor of two, which is just enough to hide the signal we might want to detect.

Based on this result, we believe that it is very possible that there is a dependency between the SST time-series and landfalling hurricane numbers, and that it makes sense to develop prediction models based on this assumption. We then have the possibility of using a direct prediction method (relate observed landfalling hurri-

cane numbers directly to SSTs) or an indirect prediction method (relate observed basin hurricane numbers to SSTs, and then predict landfalling hurricane numbers from basin hurricane numbers). Which is likely to be better? We investigated this question in some detail in Nzerem et al., 2007, and concluded that the indirect method is possibly slightly better, but that the two methods are likely to be very close (in terms of accuracy), so it is worth considering both.

The next question to address is which *link function* should we use to model the effects of SSTs on hurricane numbers. In the academic literature, it is common to use a log link i.e. to consider hurricane numbers as an exponentially increasing function of SST (see for example Elsner and Schmertmann, 1993 and Solow and Moore, 2000). This is mainly because it is common statistical practice to use a log link function when doing poisson regression, rather than for any more fundamental reason to do with hurricanes and SST. Fitting an exponential curve to the SST-hurricane number relation, is, however, rather dangerous, especially if we predict future SSTs to be as high, or higher, than have ever occurred in the past. This could potentially lead to predictions of very large numbers of hurricanes. We performed a laboriously detailed analysis of the observed relationships between SST and hurricane numbers (Binter et al., 2007a, b) and concluded that it is just as reasonable to model the SST hurricane number relationship using a piecewise linear function that is a straight line fit in the region of interest. This relationship is shown in Fig. 5.

In 2006, our SSTmodel range included three types of SST predictions; flat, linear and damped, direct and indirect predictions, and linear and log links for estimating the SST-hurricane number relationship. Combinations of these prediction types give a total of 12 SST-based predictions for landfalling hurricane numbers. These predictions are given in rows 9 to 20 of the summary Tables 2 and 3.

In 2007, we omitted the models based on the log link between hurricane number and SSTs partly because we ourselves felt this had little physical justification and partly because the 2006 experts indicated that they thought there was little physical justification for it (in the 2006 elicitation, these models were not given any weight by any of the experts). The damped predictions were also eliminated in the 2007 model suite because they are weighted combinations of the flat and linear predictions. Instead of an explicit damped model, the experts determined the damping for themselves by weighting the flat and linear models directly. The flat, linear, direct and indirect SST predictions for 2008–2012 are shown in rows 6–9 of Table 4 and similar predictions using the NH temperature are found in rows 10–13.

Predictions of landfalling numbers from the IPCC model predictions of SST, using both one and two-step methods, and direct or indirect predictions, are given in rows 14–17 of summary Table 4.

Since the climate shift predictions will vary depending on the probabilities that are given by the experts during the elicitation process, we do not show the actual predictions but we instead show the lowest and highest predictions of landfalling numbers that these models produce. These numbers are shown in rows 19a, b and 20a, b in summary Table 4.

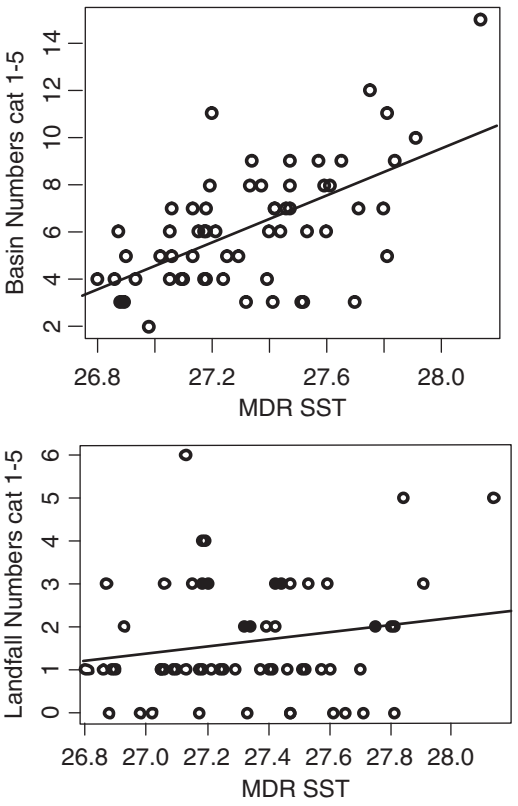

Fig. 5 Correlation between Numbers of (**a**) Basin Hurricanes, (**b**) Landfalling Hurricanes and the SSTs in the MDR region

Using Windshear and SSTs

Many general circulation climate models predict an increase of the vertical windshear in the Main Development Region in the future due to anthropogenic forcing (Vecchi and Soden, 2007). As the windshear has an important effect on hurricane formation, this could affect future hurricane rates. In the last few decades, we have seen that the windshear in the Atlantic MDR region is quite strongly correlated with the MDR SSTs, so that as the SSTs increase, the windshear decreases (see Fig. 6). However, some climate model integrations imply that this relationship may decouple in the future meaning that it will be difficult to predict future changes just from past data. To take this into consideration we include this final model which estimates future changes in windshear and SST from the IPCC ensemble means while the current state is estimated from the historical record. The windshear estimates are based on the climate predictions of Vecchi and Soden [2007] and the SST estimates are based on the predictions from Laepple et al. [2007]. The framework of the Poisson Generalized Linear Model provides a combined relationship with basin hurricane numbers so that the predictions of windshear and SST can

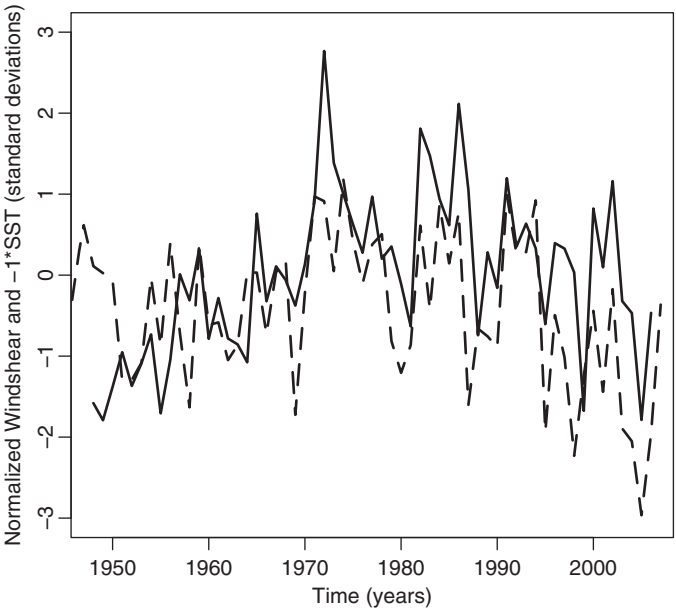

Fig. 6 Historically, there has been a strong correlation between Windshear and SSTs in the MDR region. The solid line shows the normalized 2D windshear between 800 and 250hPa, averaged from July to September and from 15-70W and 10-20N is shown. The dashed line shows the inverse of the normalized HadISSTs averaged over the same time and area from 1948–2006

be converted to basin numbers which are in turn converted to a prediction of landfalling numbers. The results are shown in row 18 of summary Table 4.

Model Comparison

The prediction models described represent a variety of ways to predict future hurricane numbers given different assumptions. The skill of the models is measured by comparing the root mean squared errorin out-of-sample hindcasting tests to the root mean squared error of the long term mean. The out of sample hindcasting was performed with a buffer around the years to be predicted in order to prevent correlated information leaking into the test set and artificially reducing error. Figure 7 shows the root mean squared errors for a number of the models with 5% to 95% confidence intervals. Except for the medium term baseline, the models historically (since the 60s) all produce more accurate forecasts than the long term baseline. This figure also shows that indirect methods tend to have less error than direct methods. For cat 1–5 hurricane predictions, none of the model errors are *significantly* lower than the RMSEfor the long term mean but, for the more intense

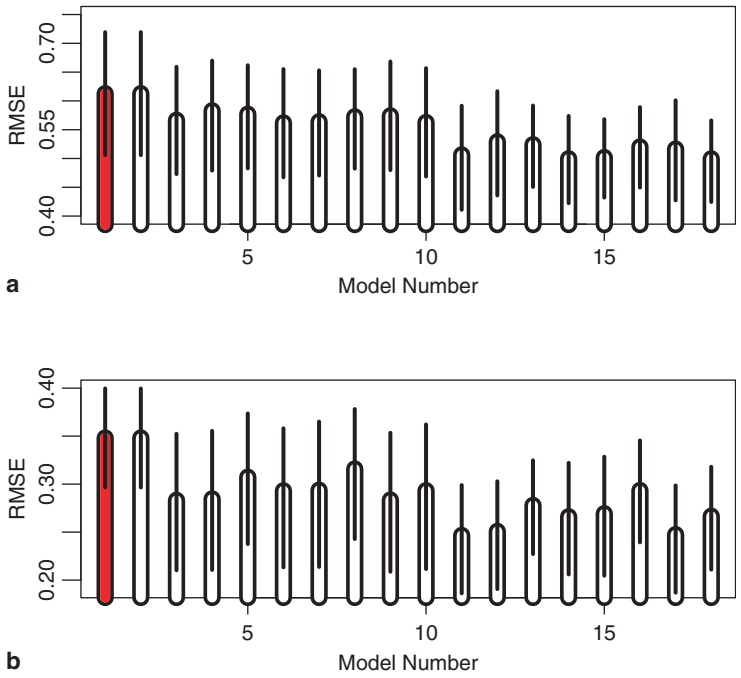

Fig. 7 Out-of-Sample Root Mean Squared Error of (**a**) Landfalling Cat 1–5 and (**b**) Landfalling Cat 3–5 model predictions hindcast from 1960-1964 to 2003–2007. Bars represent the 5% and 95% confidence intervals. Models listed are 1. Long Term Mean 2. Medium Term Mean 3. Flat Line SST 4. Linear Trend SST 5. IPCC SST 6. Flat Line NH-SST 7. Linear Trend NH-SST 8. IPCC NH-SST 9. 50/50 SST 10. 50/50 NH-SST 11. Indirect Flat Line SST 12. Indirect Linear Trend SST 13. Indirect IPCC SST 14. Indirect Flat Line NH-SST 15. Indirect Linear Trend NH-SST 16. Indirect IPCC NH-SST 17. Indirect 50/50 SST 18. Indirect 50/50 NH-SST

hurricanes, cat 3–5, three of the SST predictions do have significantly lower error than the long term mean.

Summary

We have presented a set of models that produce predictions for the number of US landfalling hurricanes likely to occur in the next five years. The models are based on a variety of plausible assumptions and methods. In this article we have emphasized the assumptions, the benefits and the shortcomings of each model.

In developing our prediction schemes we first address the problem of estimating the current state. We solve this problem in a variety of ways. Initially we make the assumption that the rate at which hurricanes are generated and subsequently hit land is a stationary random process. In this case, it makes sense to use all the available reliable historical data equally. However, since the time-series of basin hurricane

numbers is not stationary, we go beyond such straight historical averages to consider alternative methods to estimate the current state which involve giving more weight to the more recent years in the data. We also consider models that use related information, such as information from the basin hurricanes and from sea surface temperatures, to predict landfalling hurricane numbers. These variables are less noisy than the landfalling hurricane number time-series and there are good reasons to believe they may allow us to make more accurate predictions of landfall numbers. The next issue we consider in our model development is how to model potential changes from the current state over the next five years. We include models that account for both gradual trends and jumps in the climate.

To keep things simple, the goal we set for our predictions is to minimize the root mean square error (RMSE) between the predicted and actual numbers of hurricanes. This provides a useful metric of comparison for parameter choices (like window lengths for calibration and extrapolation) as well as for model comparison. We also note that most of our analysis uses simple classical statistical methods, which have the benefits of simplicity and transparency. This directly addresses one of our primary goals, which is to introduce methods for the 5 year prediction of hurricane numbers that can be widely understood by meteorologists, climate modelers, and insurance industrypractitioners. Our suite of models achieves this goal, as well as providing a broad range of predictions representing the various relevant scientific theories and ideas. We then rely on a panel of international hurricane experts to weight these models in an expert elicitation process to give us a prediction of future hurricane activity.

Looking to the future, we plan to continue to update our model set as new scientific ideas and understanding relevant to the question of how to predict landfalling hurricane numbers appear.

Summary Tables

Table 2 Predictions for the number of Hurricanes hitting US land for the 2007–2011 period

	Model	5-year Prediction of Cat 1–5 U.S. Landfall Number	5-year Prediction of Cat 3–5 U.S. Landfall Number
1	Baseline Mean 1900–2006	1.70	0.64
2	Baseline Mean 1950–2006	1.56	0.63
3	Short Baseline 1995–2006	2.08	0.83
4	Mixed Baseline Elsner's Change Points	2.00	0.82
5	Mixed Baseline RMS Change Points	2.11	0.86
6	Indirect Short Baseline 1995-2006	2.05	0.92
7	Indirect Mixed Baseline Elsner Change Points	2.05	0.85
8	Indirect Mixed Baseline RMS Change Points	2.05	0.84
9	Flat-line SST prediction, linear link	1.84	0.82
10	Damped SST prediction, linear link	1.94	0.88

Table 2 (continued)

	Model	5-year Prediction of Cat 1–5 U.S. Landfall Number	5-year Prediction of Cat 3–5 U.S. Landfall Number
11	Linear trend SST prediction, linear link	2.03	0.95
12	Flat-line SST prediction, log link	1.92	0.87
13	Damped SST prediction, log link	2.06	0.96
14	Linear Trend SST prediction, log link	2.21	1.08
15	Indirect prediction Flat-line SST linear link	1.96	0.89
16	Indirect prediction Damped SST linear link	2.09	0.98
17	Indirect prediction Linear Trend SST linear link	2.23	1.06
18	Indirect prediction Flat-line SST log link	2.03	0.92
19	Indirect prediction Damped SST log link	2.21	1.05
20	Indirect prediction Linear Trend SST log link	2.43	1.21

Table 3 Predictions for the number of Hurricanes hitting US land for the 2006–2010 period

	Model	5-year Prediction of Cat 1–5 U.S. Landfall Number	5-year Prediction of Cat 3–5 U.S. Landfall Number
1	Baseline Mean 1900–2005	1.72	0.65
2	Baseline Mean 1950–2005	1.59	0.64
3	Short Baseline 1995–2005	2.27	0.91
4	Mixed Baseline Elsner's Change Points	2.06	0.85
5	Mixed Baseline RMS Change Points	2.19	0.89
6	Indirect Short Baseline 1995–2005	2.12	0.96
7	Indirect Mixed Baseline Elsner Change Points	2.12	0.90
8	Indirect Mixed Baseline RMS Change Points	2.12	0.90
9	Flat-line SST prediction, linear link	1.94	0.87
10	Damped SST prediction, linear link	2.04	0.93
11	Linear trend SST prediction, linear link	2.14	0.99
12	Flat-line SST prediction, log link	2.05	0.93
13	Damped SST log link	2.20	1.04
14	Linear Trend SSTprediction, log link	2.37	1.16
15	Indirect prediction Flat-line SST linear link	2.04	0.94
16	Indirect prediction Damped SST linear link	2.17	1.02
17	Indirect prediction Linear Trend SST prediction, linear link	2.29	1.10
18	Indirect prediction Flat-line SST log link	2.13	0.99
19	Indirect prediction Damped SST prediction, log link	2.31	1.12
20	Indirect prediction Linear Trend SST prediction, log link	2.52	1.28

Table 4 2008–2012 predictions from the model suite developed for the 2007 elicitation

	Model	5-year Prediction of Cat 1–5 U.S. Landfall Number	5-year Prediction of Cat 3–5 U.S. Landfall Number
1	Baseline Mean 1900–2007	1.74	0.69
2	Baseline Mean 1948–2007	1.63	0.72
3	Short Baseline 1995–2007	1.92	0.85
4a	Direct Climate Shift (Low)	1.30	0.53
4b	Direct Climate Shift (Current)	2.00	0.89
5a	Indirect Climate Shift (Low)	1.40	0.42
5b	Indirect Climate Shift (Current)	2.08	0.95
6	Flat-line SST prediction, linear link	1.87	0.90
7	Linear-trend SST prediction, linear link	1.95	0.95
8	Indirect Flat-line SST prediction	2.02	1.02
9	Indirect Linear-Trend SST prediction	2.14	1.10
10	Flat-line NH prediction	1.97	0.96
11	Linear-Trend NH prediction	2.05	1.02
12	Indirect Flat-Line NH prediction	2.17	1.12
13	Indirect Linear-Trend NH prediction	2.29	1.21
14	IPCC ensemble SST prediction	1.90	0.92
15	Indirect IPCC ensemble SST prediction	2.07	1.05
16	IPCC ensemble NH prediction	2.04	1.02
17	Indirect IPCC ensemble NH prediction	2.29	1.21
18	Windshear/SST	2.05	0.97
19a	SST Climate Shift (Low)	1.30	0.42
19b	SST Climate Shift (Current)	1.85	0.83
20a	Indirect SST Climate Shift (Low)	1.46	0.60
20b	Indirect SST Climate Shift (Current)	2.04	0.99

References

Bellone, et al., 2007: Statistical testing of the proportion of hurricanes making landfall, in preparation.

Bengtsson, 2001: Weather - Hurricane threats, *Science*, **293**, 440–441.

Binter, et al., 2006: Year ahead prediction of US landfalling hurricane numbers: the optimal combination of multiple levels of activity since 1900, *http://www.arxiv.org/abs/physics/0611070,* **7** Nov. 2006.

Binter, et al., 2007a: Statistical modeling of the relationship between main development region sea surface temperature and Atlantic basin hurricane numbers, *http://www.arxiv.org/abs/physics/0701170,* **29** Jan. 2007.

Binter, et al., 2007b: Statistical modeling of the relationship between main development region sea surface temperature and landfalling Atlantic basin hurricane numbers, *http://www.arxiv.org/abs/physics/0701173,* **15** Jan. 2007.

Bove, M.C., et al., 1998: Effect of El Nino on U.S. Landfalling Hurricanes, *Bull. Am. Meteorol. Soc.,* **79**, 2477–2482.

Camargo, and Sobel, 2005: Western North Pacific Tropical Cyclone Intensity and ENSO, *J. Climate,* **18**, 2996–3006.

DeMaria, M., et al., 1993: Upper-level angular momentum fluxes and tropical cyclone intensity change, *J. Atmos. Sci.*, **50**, 1133–1147.

De Maria, 1996: The effect of vertical shear on tropical cyclone intensity change, *J. Atmos. Sci.*, **53**, 2076–2087.

Elsner, J.B., and C.P. Schmertmann, 1993: Improving Extended-Range Seasonal Predications of Intense Atlantic Hurricane Activity, *Weather and Forecasting,* **121**, 345–351.

Elsner, J.B., et al., 1999: Fluctuations in North Atlantic Hurricane Frequency, *J. Climate*, **12**, 427–437.

Elsner, J.B., et al., 2000: Spatial variations in major U.S. hurricane activity: Statistics and a physical mechanism*, J. Climate*, **13**, 2293–2305.

Elsner, J.B., et al., 2001: Changes in the rates of North Atlantic major hurricane activity during the 29th Century, *Geophysical Research Letters,* **27**, 1743–1746.

Elsner, J.B., et al., 2004: Detecting shifts in hurricane rates using a Markov Chain Monte Carlo approach, *J. Climate*, **17**, 2652–2666.

Elsner, J.B., 2006: Evidence in support of the climate change-Atlantic hurricane hypothesis, *Geophysical Research Letters,* v33, L16705, doi:10.1029/2006GL026869, August 2006.

Emanuel, K., 2005: Increasing destructiveness of tropical cyclones over the past 30 years, *Nature*, **436**, 686–688.

Enfield, D.B., and L. Cid-Serrano, 2006: Projecting the risk of future climate shifts. *Int'l J. Climatology,* **26**, 885–895.

Epstein, E.S., 1985: Statistical inference and prediction in climatology: a Bayesian approach, *Meteorol. Monographs,* **20**. Am. Meteorol. Soc., p.199.

George, E.I., et al., 2006: Improved minimax prediction under Kullback-Leibler loss, *Annals of Statistics,* **34**, 78–91.

Goldenberg, S.B., and L.J. Shapiro, 1996: Physical mechanisms for the association of El Nino and West African rainfall with Atlantic major hurricane activity, *J. Climate*, **9**, 1169–1187.

Goldenberg, S.B., et al., 2001: The recent increase in Atlantic hurricane activity: Causes and Implications, *Science*, **293**, 474–479.

Gray, W.M., 1968: Global view of the origin of tropical disturbances and storms, *Mon. Wea. Rev.,* **96**, 669–700.

Gray, S.T., et al., 2004: A tree-ring based reconstruction of the Atlantic Multidecadal Oscillation since 1567 A.D., *GRL*, **31**, No. 12, L1220510.1029/2004GL019932.

Hall, T., and S. Jewson, 2005: Statistical modeling of tropical cyclone tracks: a semi-parametric model for the mean trajectory, *http://www.arxiv.org/abs/physics/0503231,* 31 Mar. 2005.

Hall, T., and S. Jewson, 2006a: Comparing classical and Bayesian methods for predicting hurricane landfall rates, *http://arxiv.org/abs/physics/0611006,* 01 Nov. 2006.

Hall, T., and S. Jewson, 2006b: Predicting hurricane regional landfall rates: comparing local and basin-wide track model approaches, *http://arxiv.org/abs/physics/0611103*, 10 Nov. 2006.

Hall, T., and S. Jewson, 2007: SST and North American tropical cyclone landfall: a statistical modeling study, *http://arxiv.org/abs/0801.1013*

Hansen, J.E., and S. Lebedeff, 1987: Global trends of measured surface air temperature. *J. Geophys. Res.*, **92**, 13345–13372.

Hoyos, et al., 2006: Deconvolution of the factors contributing to the increase in global hurricane intensity, *Science,* **312**, 94–97.

Jarrell, J.D., et al., 1992: Hurricane Experience Levels of Coastal County Populations from Texas to Maine, *NOAA Technical Memorandum,* NWS TPC-1.

Jarvinen, et al., 1984: A tropical cyclone data tape for the North Atlantic Basin, 1886–1983: Contents, limitations, and uses. *NOAA Technical Memorandum NWS NHC 22,* Coral Gables, Florida, p.21.

Jewson, S., 2004: The Relative Importance of Trends, Distributions and the Number of Years of Data in the Pricing of Weather Options, *http://ssrn.com/abstract=516503*, 11 March 2004.

Jewson, S., 2004: Probabilistic forecasting of temperature: comments on the Bayesian model averaging approach, *http://www.arxiv.org/abs/physics/0409127,* 24 Sept. 2004.

Jewson, S., and J. Penzer, 2004: Weather derivative pricing and the detrending of meteorological data: an empirical evaluation of damped linear detrending, *http://ssrn.com/abstract=623381,* 26 Nov. 2004.

Jewson, S., and J. Penzer, 2005: Weather derivative pricing and the detrending of meteorological data: three alternative representations of damped linear detrending, *http://ssrn.com/abstract=653241*, 24 Jan. 2005.

Jewson, S., et al., 2005: Year ahead prediction of US landfalling hurricane numbers: the optimal combination of long and short baselines, *http://www.arxiv.org/abs/physics/0512113,* 13 Dec. 2005.

Jewson, S., and J. Penzer, 2006a: An objective change-point analysis of historical Atlantic hurricane numbers, *http://www.arxiv.org/abs/physics/0611071,* 7 Nov. 2006.

Jewson, S., and J. Penzer, 2006b: An objective change-point analysis of landfalling historical Atlantic hurricane numbers, *http://www.arxiv.org/abs/physics/0611071,* 7 Nov. 2006.

Jewson, S., and J. Penzer, 2006c: Estimating trends in weather series: consequences for pricing derivatives, *Studies in Non-linear Dynamics and Econometrics,* 10, No. 3, Article 9.

Jewson, S., et al., 2006: Year ahead prediction of US landfalling hurricane numbers: the optimal combination of long and short baselines for intense hurricanes, *http://www.arxiv.org/abs/physics/0606192,* 21 Jun. 2006.

Jewson, S., et al., 2007a: Predicting landfalling hurricane numbers from sea surface temperatures: theoretical comparisons of direct and indirect approaches, *http://arxiv.org/abs/physics/0701176,* 29 Jan 2007.

Jewson, S., et al., 2007b: Predicting hurricane numbers from sea surface temperature: closed-form expressions for the mean, variance and standard error of the number of hurricanes, *http://arxiv.org/abs/physics/0701167,* 15 Jan. 2007.

Jewson, S., et al., 2007c: Predicting landfalling hurricane numbers from basin hurricane numbers: basic statistical analysis, *http://arxiv.org/abs/physics/0701166*, 29 Jan. 2007.

Kerr, 2005: Is Katrina a Harbinger of Still More Powerful Hurricanes?, *Science,* **309**, 1807.

Khare, and Jewson, 2005a: Year ahead prediction of US landfalling hurricane numbers, *http://www.arxiv.org/abs/physics/0507165,* 21 July 2005.

Khare, and Jewson, 2005b: Year ahead prediction of US landfalling hurricane numbers: intense hurricanes, *http://www.arxiv.org/abs/physics/0512092,* 10 Dec. 2005.

Klotzbach, 2006: Trends in global tropical cyclone activity over the past twenty years, 1986–2005, *Geophys. Res. Letts.,* **35**, L10805, doi: 10.1029/2006GL025881.

Knutson, T.R., and R.E. Tuleya, 1999: Increased hurricane intensities with CO2-induced warming as simulated using the GFDL hurricane prediction system, *Climate Dynamics*, **15**, 503–519.

Knutson, T.R., and R.E. Tuleya, 2004:Impact of CO2-induced warming on simulated hurricane intensity and precipitation: Sensitivity to the choice of climate model and convective parameterization, *J.Climate,* **17**, 3477–3495.

Komaki, F., 2001: A shrinkage predictive distribution for multivariate normal observables, *Biometrika,* **88**, 859–864.

Laepple, T., et al., 2007a: Correlations between hurricane numbers and sea surface temperature: why does the correlation disappear at landfall?, *http://arxiv.org/abs/physics/0701175,* 15 Jan. 2007.

Laepple, T., et al., 2007b: Five year prediction of sea surface temperature in the tropical Atlantic: a comparison of simple statistical methods, *http://arxiv/org/abs/physics/0701162*, 15 Jan. 2007.

Laepple, T., and S. Jewson, 2007: Five year ahead prediction of sea surface temperature in tropical Atlantic: a comparison between IPCC climate models and simple statistical models, *http://arxiv.org/abs/physics/0701165*, 15 Jan. 2007.

Landsea, C.W., 1998: The extremely active 1995 Atlantic hurricane season: environmental conditions and verification of seasonal forecasts, *Mon. Wea. Rev.,* **126**, 1174–1193.

Landsea, C.W., et al., 1999: Atlantic basin hurricanes: Indices of climatic changes, *Climatic Change,* **42**, 89–129.

Lavielle, M., and M. Labarbier, 2001: An application of MCMC methods for the multiple change-points problem, *Signal Process*, **81**, 39–53.

Litterman, R.B., 1986: Forecasting with Bayesian vector autoregressions – 5 years of experience, *The Journal of Business and Economic Statistics*, **4**, 25–38.

Lonfat, M., A. Boissonnade, and R. Muir-Wood, 2007: Atlantic basin, U.S. and Caribbean landfall activity rates over the 2006–2010 period: an insurance industry perspective. *Tellus A*, **59**, 499–510.

Lyons, S.W., 2004: U.S. Tropical Cyclone Landfall Variability: 1950–2002, *Weather and Forecasting,* **19**, 473–480.

Mann, and Emanuel, 2006: Atlantic Hurricane Trends Linked to Climate Change, *EOS Transactions, AGU,* **87**, 233–244.

Meagher, J., and S. Jewson, 2006: Year-ahead prediction of hurricane season sea surface temperature, *http://www.arxiv.org/abs/physics/0606185*, 21 June 2006.

Nzerem, K., et al., 2006: Change-point detection in the historical hurricane number time-series: why can't we detect change-points at US landfall?, *http://arxiv.org/abs/physics/0611107,* 10 Nov. 2006.

Peixoto, J.P., and A.H. Oort, 1992: Physics of Climate, American Institute of Physics, p.520.

Raper, S.C.B., 1993: Observational data on the relationships between climatic change and the frequency and magnitude of severe tropical storms. Climate and Sea Level Change: Observations, Projections and Implications, R.A. Warrick, E.M. Barrow and T.M.L. Wigley, Eds., Cambridge University Press, Cambridge, UK, 192–212.

Rayner, et al., 2002: Global analysis of sea surface temperature, sea ice, and night marine air temperature since the late nineteenth century, *J. Geophys. Res.,* **108**, D14 4407, doi:10.1029/2002JD002670.

Saunders, M.A., and A.R. Harris, 1997: Statistical evidence links exceptional 1995 Atlantic hurricane season to record sea warming, *Geophys. Res. Letts.,* **24**, 1255–1258.

Saunders, M.A., and A.S. Lea, 2005: Seasonal prediction of hurricane activity reaching the coast of the United States, *Nature,* **434**, 1005–1008.

Schlesinger, M.E., and N. Ramankutty, 1994: An oscillation in the global climate system of period 65–70 years, *Nature*, **367**, 723–726.

Shapiro, L.J., 1982: Hurricane climate fluctuations. Part I: Patterns and cycles, *Mon. Wea. Rev*., **110**, 1014–1023.

Shapiro, L.J., and S.B. Goldenberg, 1989: Atlantic sea surface temperatures and tropical cyclone formation, *J. Climate*, **11**, 578–590.

Shephard, N., 1993: Distribution of the ML estimator of a MA(1) and a local level model, *Econometric Theory,* **9**, 377–401.

Smith, D. et al., 2007: Improved surface temperature prediction for the coming decade from a global climate model, *Science,* **317**, 796–799.

Solow, A.R., and L. Moore, 2000: Testing for a trend in a partially incomplete hurricane record, *J. Climate,* **13**, 2293–2305.

Sriver, R.L., and M. Huber, 2006: Low frequency variability in globally integrated tropical cyclone power dissipation, *Geophysical Res. Letts.,* **33**, L11705 doi:10.1029/2006GL026167.

Sutton, R.T., and D.L.R. Hodson, 2005: Atlantic Forcing of North American and European summer climate; *Science,* **309**, 115–118.

Trenberth, K., 2005: Uncertainty in Hurricanes and Global Warming; *Science,* **17**, 1753–1754, 2005.

Trendberth, K.E., and D.J. Shea, 2006: Atlantic hurricanes and natural variability in 2005, *GRL*, **33**, doi:10.1029/2006GL026894.

Vecchi, G.A., and B.J. Soden, 2007: Increased tropical Atlantic wind shear in model projections of global warming, *GRL,* **34**, doi:10.1029/2006GL028905.

Vitart, F., and J.L. Anderson, 2001: Sensitivity of Atlantic Tropical Storm Frequency to ENSO and Interdecadal Variability of SSTs in an Ensemble of AGCM Integrations, *J. Climate,* **14**, 533–545.

Webster, P.J., et al., 2005: Changes in Tropical Cyclone Number, Duration and Intensity in a Warming Environment, *Science,* **309**, 1844–1846.

Zehr, R.M., 1992: Tropical cyclogenesis in the Western Pacific, *NOAA Technical Report NESDIS*, **61**, NOAA; Washington D.C., USA.

A New Index for Tropical Cyclone Development from Sea Surface Temperature and Evaporation Fields

John A.T. Bye, Wenju Cai, and Tim Cowan

Abstract In this study, we present a new index (called the H-index) which is the spatial mean gradient of the logarithm of the surface wind speed with respect to sea surface temperature (SST), and can be easily computed from large scale fields of evaporation and SST Two independent physically based arguments indicate that tropical cyclones would tend to be spun-up in regions of negative H of large magnitude (<-1). In these regions which only occur in the tropics, significant releases of kinetic energy (KE) into the atmosphere from the ocean mixed layer due to convective instability give rise to warm core systems which may develop into intense TCs. The monthly mean histograms of H evaluated from reanalysis and SST data and averaged over the period 1979–2005 for three generation regions (the West Pacific, the Atlantic and the East Pacific) show a remarkable symmetrical pattern in which the standard deviation increases during the active season. This property is therefore ideally suited to being used as a predictor for TC development. The symmetry of the distributions indicates in addition that there are counter-balancing regions of large positive H within the generation regions where the KE is reabsorbed into the potential energy of the mixed layer, and the TCs would be spun-down. The inter-monthly variability of TC counts in the three generating regions during the period 1979–2005 was found to be well predicted by the variability of the standard deviation of H, giving confidence that the method may be used to simulate changes in the occurrence of TCs under global warming using the results of climate models that do not explicitly resolve TCs. The CSIRO Mk3 coupled climate model results predict increases in TC counts of 20%, 50% and 100% respectively in the West Pacific, the East Pacific and the Atlantic, and also a change in their seasonal distribution. In both the West Pacific and the Atlantic a secondary early seasonal maximum occurs in the period 2051–2080, which essentially advances the season in the West Pacific and lengthens the season in the Atlantic.

J.B. Elsner and T.H. Jagger (eds.), *Hurricanes and Climate Change,*
doi: 10.1007/978-0-387-09410-6,

Introduction

The occurrence of hurricanes is of great significance for many regions of the World. An important contemporary question is whether there are likely to be any changes in patterns due to global warming. In this paper we present a new, easily computed index for the development of hurricanes which is based on the spatial evaluation of the gradient of evaporation with respect to sea surface temperature over the ocean. The principle of the technique leading to the specification of the index (called the H-index), which was originally presented at the 8th International Conference on Southern Hemisphere Meteorology and Oceanography held at Foz do Iguacu, Brazil, April 24–28, 2006 (Bye and Keay 2006), is reviewed in The Global Relation Between Sea Surface Temperature and Evaporation, and is then applied spatially in Spatial Evaluation of the Temperature Gradient of Evaporation. The Physical Meaning of the Hurricane Index gives a detailed discussion of the physical meaning of the H-index in terms of the mixed layer dynamics and a simple cyclostrophic model of a hurricane, Results: (I) The Observed H Fields presents the results of the evaluation of the H-index, and Results: (II) Comparison Between Observed Tropical Cyclone Numbers and the Standard Deviation of the H-index applies the index to simulate TC occurrences in three generation regions (the West Pacific (WPAC), the Atlantic (ATL) and the East Pacific (EPAC)) using both reanalysis fields and climate model results. Discussion looks at the analysis in terms of the large scale dynamics and briefly compares the H-index with other hurricane indices, and also outlines possible future developments.

The Global Relation Between Sea Surface Temperature and Evaporation

The starting point for the analysis is the global relation between sea surface temperature and evaporation. Here, we use the monthly sea surface temperature data from the Hadley Centre (Rayner et al., 2003) and the monthly evaporation data computed from the NCEP reanalysis (Kalnay et al., 1996), from which the annual average fields have been computed. Each field is then zonally averaged over the ocean—on the T62 Gaussian grid of the NCEP data. The results for the period (1979-2001) for each hemisphere are plotted as lnE versus T, where E is the evaporation rate, and T is the sea surface temperature (SST), (Figs. 1 and 2). The data points correspond with the individual years of the 23 year record for each Gaussian grid. In the subtropics, especially in the southern hemisphere, the 23 years at each latitude are tightly clustered Similar results, obtained from the other two reanalysis products, ERA40 (Uppala et al., 2004) and NCEP2 (Kanamitsu et al., 2002) are given in Bye and Keay (2006). It is apparent that the evaporation has a maximum at about 26°C, which is the commonly stated threshold criterion for tropical cyclone (TC) development, and also that at higher temperatures E decreases. The physical processes operating in this tropical region will be considered in Discussion after the results of the analysis have been presented.

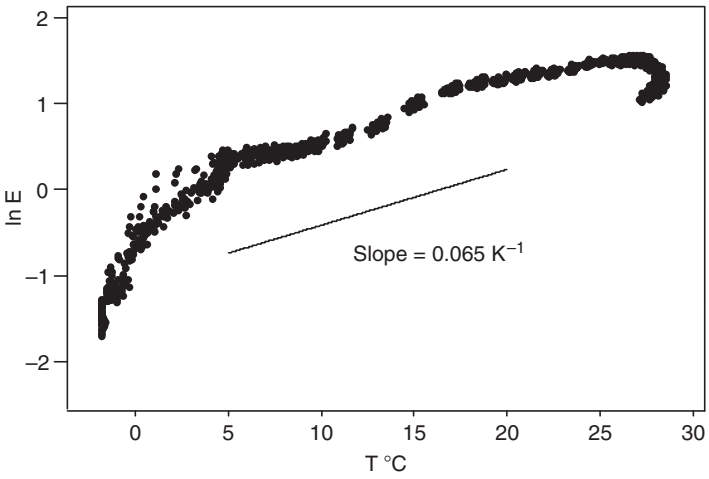

Fig. 1 ln E versus T Northern Hemisphere, from Bye and Keay (2006)

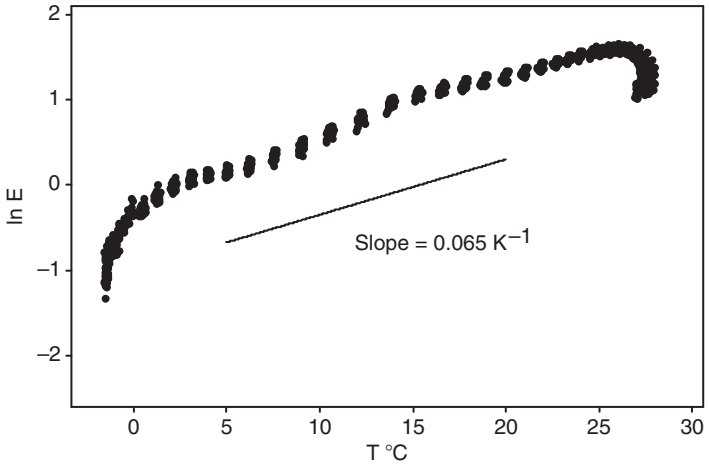

Fig. 2 ln E versus T Southern Hemisphere, from Bye and Keay (2006)

This global signal has prompted the investigation carried out below which is aimed at developing a method of estimating the likelihood of TC development using large scale fields of SST and E.

Theoretical Interpretation of the Global Fields

The interpretation of these observations can be made using the classical aerodynamic bulk relationship, which for the evaporative mass flux (Bye 1996), is,

$$F = \rho_a K_E u q_s (1 - r_s) \tag{1}$$

where $F = \rho E$, in which ρ and ρ_a are respectively the densities of freshwater and air, KE is the drag coefficient for water vapour, $q_s = q_s(T)$ is the saturated specific humidity at the sea surface where T is the sea surface temperature (SST), $r_s = q_{10}/q_s$ is the 10 m relative humidity with respect to T (which reduces to the relative humidity at 10 m for $T = T_{10}$), and $u = |u_{10}|$ is the surface wind speed at 10 m. On taking the (natural) logarithm of (1) we obtain the expression,

$$\ln E = \ln[\rho_a K_E/\rho] + \ln u + \ln q_s + \ln(1 - r_s) \tag{2}$$

in which

$$q_s = \varepsilon e_s/p \tag{3a}$$

where e_s is the saturated vapour pressure, p is the atmospheric pressure and $\varepsilon = 0.622$ is the ratio of the molecular weight of water to that of dry air. On using the Clausius-Clapeyron relation,

$$\ln e_s = -[\varepsilon L/(RT)] + \text{constant} \tag{3b}$$

where T(K), $L = 2.5\ 10^6$ J kg^{-1} is the latent heat of evaporation and R = 287 J kg^{-1} K^{-1} is the specific gas constant for dry air (Gordon et al. 1998), and differentiating (2) with respect to T, we obtain approximately,

$$d \ln u/dT \approx d \ln E/dT - \varepsilon L/(RT^2) \tag{4}$$

in which the variation of the first and fourth terms on the right hand side of (2), with respect to T, which is relatively insignificant, has been neglected, as discussed in Bye and Keay (2006).

Equation (4) is the central working relation for our study. Firstly, evaluating the second term on the right hand side for a sea surface temperature of 15°C (which is representative of the subtropics), yields, $\varepsilon L/(RT^2) = 0.065$ K^{-1}. Hence, since from Figs. 1 and 2, the mean slope (d ln E/dT) in the subtropics is approximately 0.065 K^{-1}, it is clear that the variation of wind speed with sea surface temperature is of relatively small account. Here the evaporation gradient is controlled almost completely by the Clausius-Clapyron relation. The match of the observed and theoretical slopes is particularly good in the maritime southern hemisphere In the subpolar regions (which are not considered here) and in the tropics other factors become important. Our focus turns now exclusively to the situation in the tropics.

Spatial Evaluation of the Temperature Gradient of Evaporation

In order to use the previous analysis to diagnose regions of likely tropical cyclone development, it is necessary to evaluate the gradient, d ln E/dT spatially. This is accomplished by evaluating the gradient of ln E with respect to T, and also the

gradient of T with respect to ln E along each direction, and then averaging each over all orientations to obtain the norm,

$$d\ln E/dT = \pm(<dlnE/dT>/<dT/dlnE>)^{1/2} \quad (5a)$$

where $< >$ denotes the integral around the circle. This yields the expression,

$$d\ln E/dT = \pm\left\{\left[(\partial lnE/\partial x)^2+(\partial \ln E/\partial y)^2\right]\Big/\left[(\partial T/\partial x)^2+(\partial T/\partial y)^2\right]\right\}^{1/2} \quad (5b)$$

in which d lnE/dT is positive if ∂lnE/∂x ∂T/∂x + ∂lnE/∂y ∂T/∂y > 0, and is negative if ∂lnE/∂x ∂T/∂x + ∂lnE/∂y ∂T/∂y < 0, and ox and oy are respectively towards the east and the north. This expression takes account of the full generality of the fields of lnE and T. On substituting (5b) in (4) we can evaluate,

$$H = d\ln u/dT \quad (6)$$

using the expression H = d lnE/ dT $-$ $\varepsilon L/(RT^2)$. The scalar quantity, H, which we will call the hurricane index is a practical index for potential TC development, as is evident from Figs. 1 and 2, which show that the zonal mean annual value of H is negative in the regions of TC development, equatorward of the maximum in lnE, which occurs at T $\sim$26°C.

The Physical Meaning of the Hurricane Index

The simple expression (6) conceals a great deal of physics, which we explore below for the two possibilities of $H > 0$ and $H < 0$, noting that in the subtropics $H \approx 0$.

Energy Exchange Processes for the Ocean Mixed Layer

Of great importance in tropical cyclone dynamics is the ocean mixed layer, which provides the energy required for development. The basic processes which maintain the mixed layer are (a) surface solar heating, (b) heat loss from the surface by evaporation and other processes, and (c) stirring by turbulence which entrains water from below which is then homogenized by vertical mixing. (a) decreases the potential energy (PE) of the mixed layer, and (b) and (c) increase the PE. Over the time scale of the development of a TC, it is likely that (b) is the most important of these three processes. Let us consider the energy changes which occur.

The change in potential energy of the mixed layer,

$$\mathrm{d\,PE} = \mathrm{d}\rho_w \mathrm{g D} \tag{7a}$$

where $\mathrm{d}\rho_w = -\alpha \mathrm{dT}$ is the change in seawater density, D is the mixed layer depth (assumed to be constant), g is the acceleration of gravity, and α is the coefficient of expansion of seawater. The corresponding change of kinetic energy of the wind,

$$\mathrm{d\,KE} = \rho_a \mathrm{u du} \tag{7b}$$

where u is the surface wind speed. On substituting the relations (7a) and (7b), which connect the two variables in the definition of H, into (6), we obtain,

$$\mathrm{H} = 1/\mathrm{u}\,\mathrm{du}/\mathrm{dT} = -\mathrm{A}\,\mathrm{d\,KE}/\mathrm{d\,PE} \tag{8}$$

in which $\mathrm{A} = (\alpha\ \mathrm{g}\ \mathrm{D})/(\rho_a\ \mathrm{u}^2)$. Hence H is proportional to the ratio of the change of kinetic energy and potential energy. Furthermore, for typical values of the parameters applicable in the tropics ($\alpha = 0.3\ \mathrm{K}^{-1}$, D = 20m, $\mathrm{u} = 5\ \mathrm{ms}^{-1}$ and $\mathrm{g} = 10\ \mathrm{ms}^{-2}$, $\rho_a = 1\ \mathrm{kgm}^{-3}$) we find that $\mathrm{A} \approx 4\ \mathrm{K}^{-1}$, although there is obviously a considerable variability in this estimate. This result indicates that H is a measure of the efficiency of the conversion between kinetic energy and potential energy. For small values of H the efficiency is low, whereas as H becomes large the efficiency also becomes significant, and for $\mathrm{A} \approx 4\ \mathrm{K}^{-1}$, an efficiency of 25% would be obtained for $|\mathrm{H}| = 1$. Two distinct processes are involved, depending on the sign of H.

(a) For $\mathrm{H} > 0$, a decrease in atmospheric KE gives rise to an increase in the PE of the mixed layer. However, due to surface friction (energy dissipation) only a proportion of the KE is available to the mixed layer.
(b) For $\mathrm{H} < 0$, on the other hand, an increase in the PE of the mixed layer gives rise to an increase in atmospheric KE. Here the surface heat transfer from the ocean to the atmosphere causes a convective instability, which is essentially the mechanism through which TCs are initiated.

Phase (b) is the spin-up phase, and phase (a) is the spin-down phase of a loop which characterizes the thermodynamical equilibrium of the coupled air-sea boundary layer, and since the occurrences of the two phases are separated in time and space, also the consequential atmospheric dynamics. Many studies have been reported in the literature of the spin-up phase (b), however, phase (a), has only recently received much attention, stimulated by observations of the reduction in drag coefficient in wind profiles at very high wind speeds (Powell et al. 2003).

As pointed out above, this loop only becomes important as $|\mathrm{H}|$ becomes large. This can be established in an alternative manner by considering the rate of change of KE with time, which from (8), is,

$$\mathrm{dKE}/\mathrm{dt} = -\mathrm{H}/\mathrm{A}\,\mathrm{dPE}/\mathrm{dt} \tag{9a}$$

and eliminating the rate of change of PE with time using (7a) and substituting for A, which yields the development equation,

$$dKE/dt = KE/\tau \tag{9b}$$

where $\tau = 1/[2HdT/dt]$ is a time constant for the growth or decay of the atmospheric KE. In phase (b) $\tau > 0$, and in phase (a) $\tau < 0$. Thus the time constant for development and decay is inversely proportional to H.

For example, in a region where the rate of change of temperature during the growth phase is –0.2°C/day (which on assuming that $\rho_w = 10^3$ kgm^{-3}, D = 20 m and the specific heat of water at constant pressure, Cp = 4 10^3 J kg^{-1}K^{-1} corresponds with a heat loss per unit area of 200 Wm^{-2}) and H = −2.5 K^{-1}, we find that τ = 1 day indicating an explosive growth process.

In summary, the two phases (a) and (b) are necessary to maintain the statistical equilibrium in the coupled air-sea boundary layer. They are only significant however when |H| is large, which occurs in the tropics. Here, rapid growth rates can occur in regions of positive SST anomaly, where the heat loss from the mixed layer is also large. In the subtropics $H \approx 0$, and the efficiency of the energy conversion between the PE of the mixed layer and the atmospheric KE is low, and hence the atmospheric dynamics are mainly controlled by other processes which are essentially independent of the mixed layer, i.e. baroclinic instability.

A Simple Hurricane Model

We now look at the significance of H from another point of view, using a simple cyclostrophic model of a tropical cyclone applied in a region where $H < 0$. For H locally constant, (6) can be integrated to yield,

$$\ln u/u_0 = H(T - T_0) \tag{10}$$

where $u = u_0$ at $T = T_0$. Hence if $H < 0$, u increases as T decreases. This is precisely the situation in a hurricane, which is characterised by a warm core. Conversely in the tropics in regions in which $H > 0$, there is a tendency for hurricane development to be suppressed.

In order to gain a greater insight into the significance of H, we may incorporate (10) into a standard model of hurricane dynamics. A suitable expression is the cyclostrophic 'thermal' wind relation (18.17) in Gordon et al. (1998),

$$\partial u^2/\partial z = r\,g/T\,\partial T/\partial r \tag{11a}$$

where r is the radial co-ordinate, and oz is vertically upward, which may be integrated with respect to height assuming the radial temperature gradient is a constant, to yield,

$$u^2 = -g\,h/T\,\partial T/\partial \ln r \tag{11b}$$

in which h is the height at which the (azimuthal) wind speed becomes zero. On substituting for u in (11b) from (10) and integrating with respect to lnr, assuming that (gh/T) is a constant, we obtain,

$$\ln r/r_0 = B(1 - \exp(-2H(T - T_0))) \tag{12}$$

in which $T = T_0$ and $u = u_0$ at $r = r_0$, and $B = -(gh/T)/(2H\,u_0{}^2)$.

Equations (10) and (12) are a model for a developing hurricane in which r_0, u_0 and T_0 are the conditions at the outer radius of the hurricane. On evaluating (10) and (12) at the outer radius of the warm core (r_1), assuming that (gh/T) is constant, we can determine u_0 as a function of H for a series of values of warm core temperature increment, $T = T_1 - T_0$, where $T_1 = T(r_1)$ is the temperature of the warm core. For the hurricane parameters h = 10 km, T = 300 K and g = 9.8 ms^{-2}, and a warm core of radius 1/10 that of the radius of the hurricane ($r_1/r_0 = 0.1$), we obtain the results shown in Table 1.

It is apparent that at small values of H, intense tropical storms (u_0) cannot be supported for any realistic warm core temperature increment (ΔT). As the magnitude of H increases, however, intense systems can occur for realistic warm core increments. Table 1 indicates that $H \approx -1\ K^{-1}$ marks an approximate upper limit for their development. The existence of regions of H of large magnitude, therefore, is a necessary condition for hurricane development, however it is not a sufficient condition since systems with small ΔT can also be supported, in which u_0 only attains a modest value.

Table 1 The wind speed (u_0) at the outer radius of the hurricane (r_0) as a function of the hurricane index (H) for a series of warm core temperature increments (ΔT)

H (K^{-1})	ΔT (K)	u_0 (ms^{-1})
−0.3	0.5	9
−0.3	1	14
−0.3	2	23
−0.3	3	35
−0.3	4	49
−1	0.5	11
−1	1	21
−1	2	62
−3	0.5	21
−3	1	98

Results: (I) The Observed H Fields

We have evaluated E from the NCEP reanalysis data (Kalnay et al. 1996) and T from the Hadley Centre monthly sea surface temperature data (Rayner et al. 2003) by averaging both sets of data over each month. The spatial resolution of the Hadley Centre data is 1^0, and the NCEP data, which are on a T62 Gaussian grid were interpolated on to the Hadley Centre grid. The gradient, dlnE/dT, was then computed at all sea points for which the first order finite-difference approximations of the spatial derivatives could be evaluated. Thus gaps in the field of H occur around islands and along the continental coastlines. 27 years (1979–2005) of data were available for analysis.

Results were obtained for three northern hemisphere regions in which tropical cyclones are known to be generated and one reference region in the southern subtropics (Table 2). The number of grid point—months in each region was approximately 20,000, giving a large sample for statistical analysis, from which the mean and standard deviation of H values were obtained by averaging over all grid points and all years for each month. Histograms of the distribution of H by 0.1 K^{-1} class interval, and the mean and standard deviation of H over the range, $-3 < H < 3\ K^{-1}$ were also computed. This was done because the evaluation of H from proposal next may contain 'outliers' of large magnitude due to the interpolation procedure, which were not representative of the physics.

The Distributions of H

Figure 3 shows that each of the three generation regions (WP, ATL and EP) demonstrate a clear annual cycle in the fields of H in which the standard deviation is relatively large in the active months and relatively small during the rest of the year. Each of the distributions is almost symmetrical and appears to be confined within the $-3 < H < 3\ K^{-1}$ range. The histograms for the SUBTROPICS (Fig. 3) are also almost symmetrical, but confined within the much smaller range, $-0.5 < H < 0.5\ K^{-1}$, with only a modest seasonal cycle which, as to be expected, is of opposite phase to that in the northern hemisphere generating regions. On the basis of the arguments presented in The Physical Meaning of the Hurricane Index, this is the basic reason for the absence of TCs in the subtropical latitudes. An inspection of the distributions indicates that they all have a steeper taper than the corresponding normal distributions, and more importantly that their standard deviations are all much

Table 2 The tropical cyclone generation regions and the subtropical reference region

Western Pacific (WF)	10−25°N	100−180°E
Eastern Pacific (EP)	10–25°N	140–90°W
Atlantic (ATL)	10–25°N	90–30°W
Subtropics (SUBTROPICS)	25–40°S	180–150°W

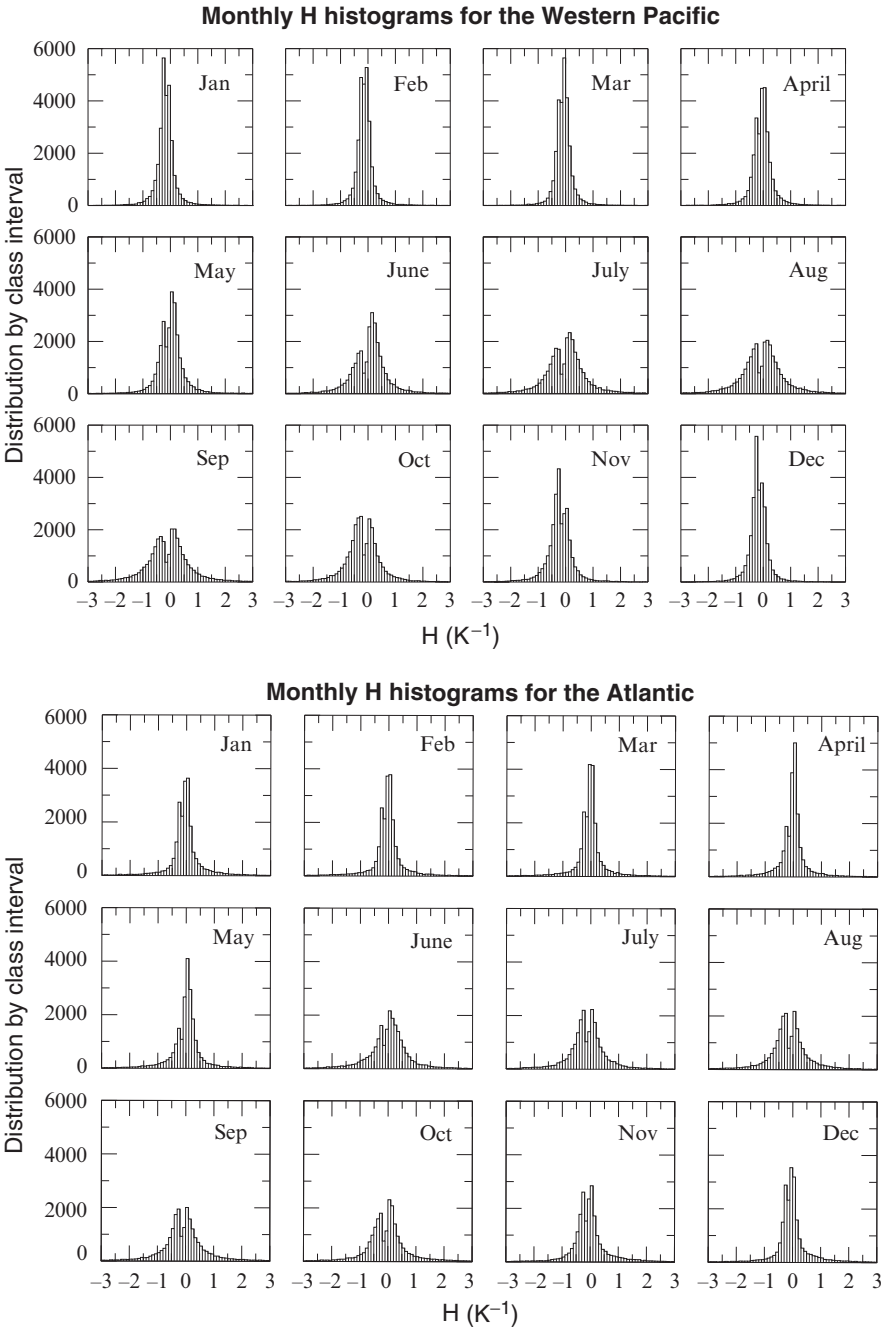

Fig. 3 Histograms of the monthly mean H for WP, ATL, EP and SUBTROPICS for the period 1979–2005

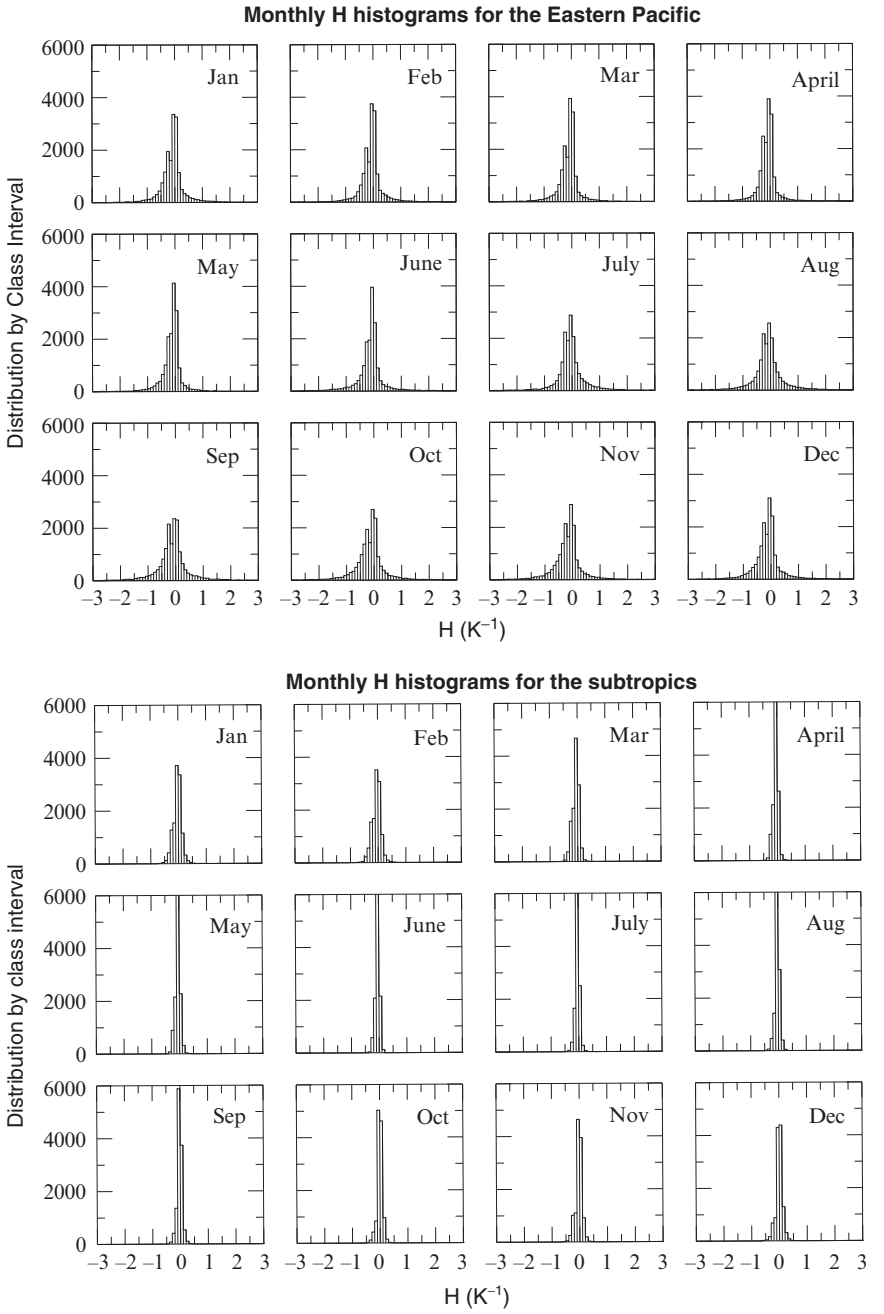

Fig. 3 (continued)

greater than their mean values. In addition, the approximate symmetry of the distributions of H points out that the spin-up and spin-down phases of the loop discussed in The Physical Meaning of the Hurricane Index, which characterizes the thermodynamic equilibrium, are complementary.

The hodographs of the standard deviation of H versus the mean of H show a negative annual mean H for each of the generation regions (WP, ATL and EP) and a positive annual mean H in the SUBTROPICS region, where $H \approx 0$ (Fig. 4). The negative annual mean H values in the three generation regions, and the near zero mean value in the subtropics are consistent with the zonal mean graphs of lnE versus T (Figs. 1 and 2). The standard deviations of H in each generation region have a maximum in September, whereas the minimum of H occurs in November in the WP and EP, and in August in the ATL. It is important to point out, however, that the mean and standard deviation values of H cannot be meaningfully compared between the three generation regions as they depend on the spatial specification adopted (Table 2), however, it would be expected that the structure of the hodograph would not be too sensitive to this choice.

These results suggest that the standard deviation of the H-index, rather than its mean value, should be used as a suitable index for the inter-monthly variability of the potential for TC development. We explore this proposal in Section 6.

The seasonal cycle of the standard deviation of the H index is compared with the SST cycle for each region in Fig. 5. The H-index signal tends to show two plateaux, which correspond respectively with the active and the inactive hurricane seasons, whereas the SST signal is sinusoidal in character.

Results: (II) Comparison Between Observed Tropical Cyclone Numbers and the Standard Deviation of the H-index

In order to compare the predictions of the standard deviation of the H-index with observations, we construct the integrated tropical cyclone index,

$$C = \sum n_i S_i \quad i = 1, 5 \tag{13}$$

where n_i is the number of TCs with the Saffir-Simpson scale (S_i). The count, C, which is computed from data in the website, http://weather.unisys.com/hurricane/, weights the tropical cyclones according to their intensity. The monthly average (V_m) of the standard deviation of the H-index (V), versus the corresponding monthly average (C_m) of the count (C) for each region (Fig. 6) has a linear trend with a high regression coefficient (r). The statistics of the regressions (Table 3), where s is the slope of C_m versus V_m, and V_0 is the intercept of V_m, at which no tropical cyclones occur ($C_m = 0$) have been used to simulate the inter-monthly variability of tropical cyclone occurrence (C) over the record period (1979–2005), from V in each region using the relation,

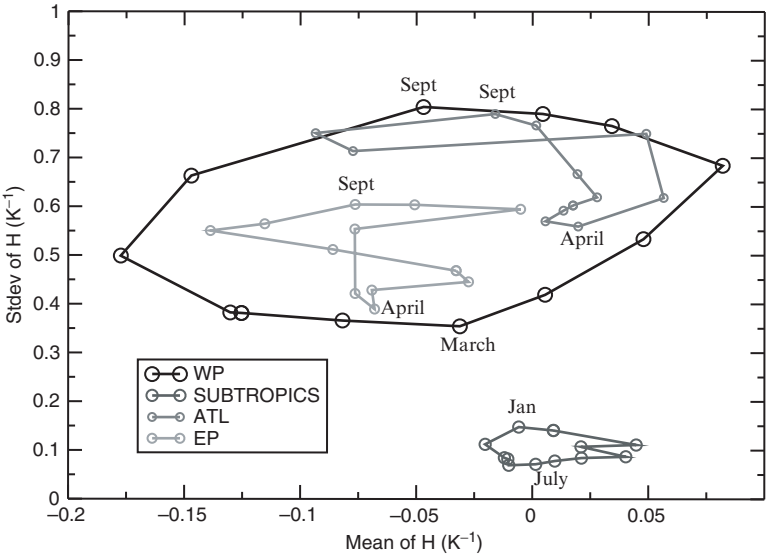

Fig. 4 Hodographs of the average (over the period 1979–2005) mean monthly standard deviation versus the mean of H for WP, ATL, EP and SUBTROPICS

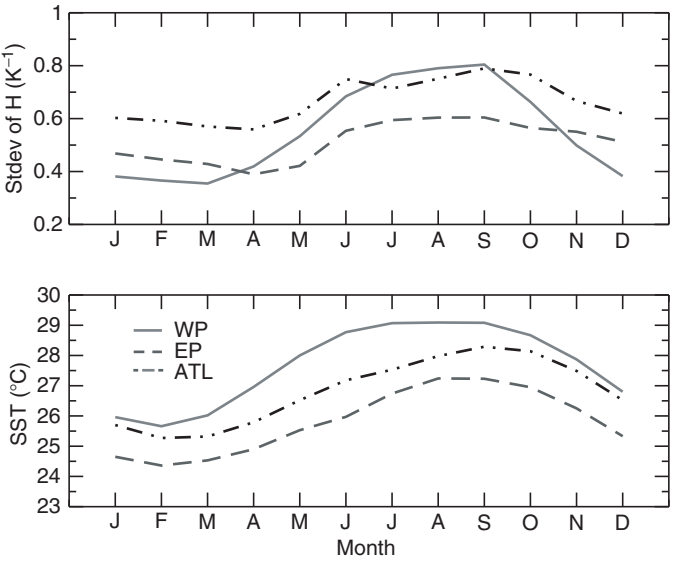

Fig. 5 Annual cycle of the average mean monthly standard deviation of H and the SST for WP, ATL, and EP

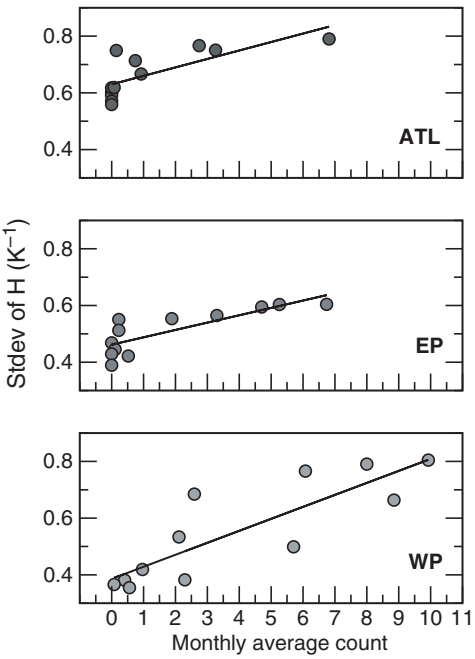

Fig. 6 Regressions of the average mean monthly standard deviation of H versus the monthly averaged count for WP, ATL, and EP

Table 3 Regression coefficients for the monthly average count versus the monthly average standard deviation of H

	V_0 (K^{-1})	s (K)	r
WP	0.39	23.65	0.85
EP	0.46	38.60	0.82
ATL	0.63	33.49	0.75

$$\begin{aligned} C &= s(V - V_0), \quad V > V_0 \\ C &= 0, \qquad\quad V < V_0 \end{aligned} \tag{14}$$

It is apparent from Fig. 7, that the simulated variability of C has a high skill. The correlation coefficients between the observed and simulated (modeled) monthly time series of C for the WP, ATL and EP are respectively, 0.62, 0.53 and 0.42. An inspection of Fig. 7 reveals some interesting features. In the WP, the relatively small TC activity in 1998 and 1999 followed by a subsequent increase in activity is very well represented as also is most of the inter-monthly variability in the early years, except for some high activity years which are under-simulated. In the ATL, the minimum in TC activity between 1990 and 1995 is well represented, as also is the inter-monthly signal in later years, except for 2004. In the EP, which has the poorest correlation, the variability prior to 1993 is very well simulated as also is that after 1998. Discrepancies, however, occur during the years 1992–1994, which are under-simulated.

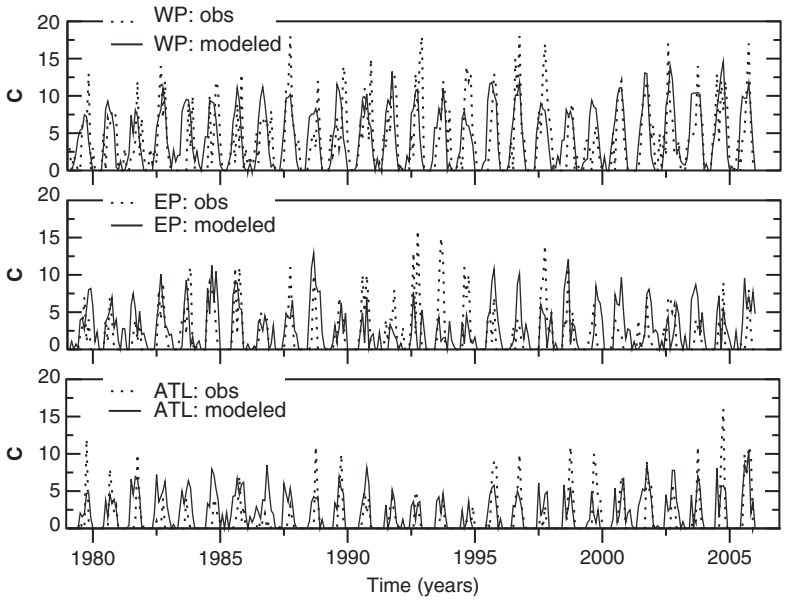

Fig. 7 Time series of C for the period 1979–2005 from observations and from the H-index model for WP, ATL, and EP

The field of H during each month can of course be displayed to show the structures which give rise to its standard deviation. This was done for the ATL in Bye and Keay (2008) to illustrate why 2005 was a prodigious hurricane season whereas during 1983 no major hurricanes were recorded. It was apparent that the spatial structure of both the SST and the evaporation fields contributed to the field of H, from which the standard deviation that is used as an index for TC initiation was computed. The patterns of H incorporated regions of more or less permanent sign, either positive or negative, which were interpreted in terms of the local climatology, and other regions in which the sign of H changed from month to month. In general terms, these two scenarios are analogous to stationary and transient eddies in a turbulent fluid. These conclusions are consistent with the results from global simulations with very high resolution in the Atlantic Ocean (Chauvin et al. 2006) which emphasized the importance of the SST anomaly distribution on hurricane activity.

Climate Model Downscaling of Tropical Cyclone Occurrences

Climate models are run with various resolutions, and many are unable to resolve the tropical cyclones, although a few with resolutions of <25 km can. This gives the opportunity to use the techniques of this paper in a predictive manner to downscale

the results of the coarse resolution models to provide information on tropical cyclone occurrence, and to use the results of the fine resolution models to make an explicit comparison with the resolved tropical cyclone occurrences. In general it would be expected that the standard deviation of the H-index would differ from that derived from the reanalysis data owing to differences in the resolution scale, however, a comparison between epochs should show whether the likelihood of tropical cyclone initiation would be less or greater under global warming.

Here, we present the results from the CSIRO Mk3 coupled climate model (Gordon et al. 2002) for two epochs, 1961–1990 and 2051–2080, and consider the mean monthly signals over these two periods. Figure 8 shows that the standard deviation of H, obtained from the model for the period, 1961–1990, is about one-half that from the reanalysis data (Fig. 5). In the WP, its seasonal signal is very similar to that of the reanalysis data, but in the ATL and EP it differs substantially. The seasonal SST signals from the model results (Fig. 8) are similar to those from the reanalysis data (Fig. 5) for each region, but the annual mean SSTs differ; the model being about 2°C less than the reanalysis, except for summer in the EP in which they are in agreement.

These discrepancies, although significant, will not deter us from making a comparison between the two epochs from the model in order to gain some insight into likely changes in tropical cyclone activity under global warming. It is emphasized however that the methodology to be used in this comparison can also be

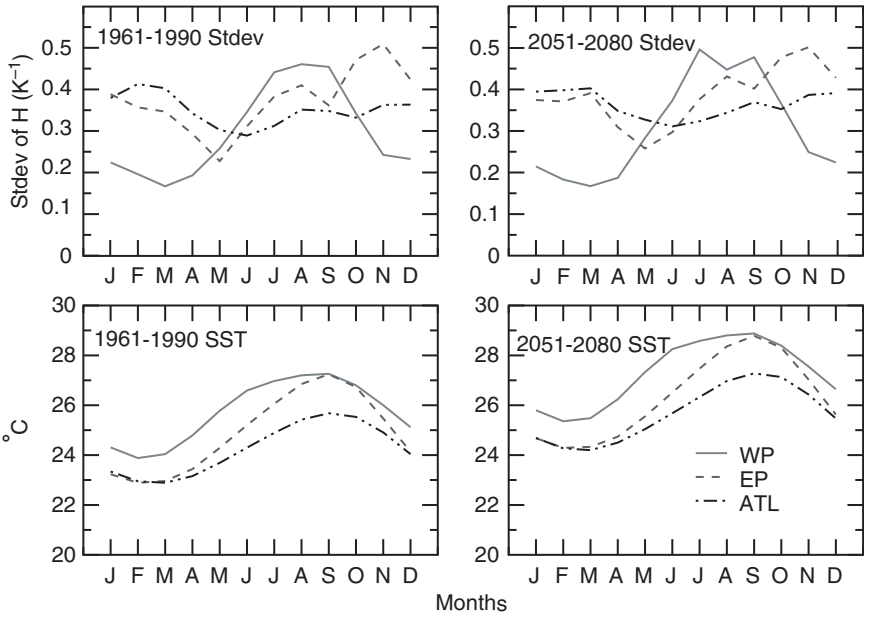

Fig. 8 Annual cycle of the average mean monthly standard deviation of H and SST obtained from the climate model for the periods 1961–1990 and 2051–2080 for the WP, ATL, and EP

applied to the results from other climate models which may represent the present day monthly climatology better.

The SST signal shows a very similar mean annual increase in the WP, ATL and EP of 1.54, 1.43 and 1.44°C respectively, which is almost uniform across the seasons in each basin (Fig. 8). The mean annual standard deviation of H, however, shows only a very modest increase in each basin of 3%, but with a significant change in the seasonal signal. These results indicate that the most important agent of change which determines H is the large scale adjustment of the evaporation and SST fields, rather than simply an increase in SST.

In order to see the predicted change in TC climatology more clearly, we have normalized the seasonal signal of the standard deviation of H in the model for the period, 1961–1990 by computing the factor,

$$F = (V_m)_{\text{reanalysis}} \Big/ (V_m)_{\text{model}(1961-1990)} \tag{15}$$

and then evaluating, $V_m' = F\,(V_m)_{\text{model}(2051-2080)}$. V_m' is the mean monthly standard deviation of H that would be obtained during the period 2051–2080 if the monthly signal of the model for the period 1961–1990 and the reanalysis signal for 1979–2005 were identical, on the assumption that the proportional changes in monthly standard deviation of H between the two model periods are correct. Fig. 9 shows the monthly averaged counts obtained by substituting for (V_m) reanalysis and V_m' in (13); the increases in the mean annual counts in the WP, EP and ATL are 20%, 50% and 100% respectively. This surprising result, that the mean annual counts have increased much more than the increases in the mean annual standard deviation of H of 3%, is due to the ratio of the standard deviations between the two model periods (1961–1990 and 2051–2080) tending to be larger in summer than in winter. In both the WP and ATL the monthly average count in the period 2051–2080 has an early season maximum which is absent in the contemporary climatology. The TC season is essentially advanced in the WP and lengthened in the ATL. The EC TC season is also lengthened with a small increase in the maximum count. We emphasize that as the count (C) depends on the intensity, any increase may be due to an increase in intensity rather than an increase in numbers.

Discussion

We have presented a physically based model of the ocean environment which has been used to predict the occurrence of tropical cyclones. The analysis leads to realistic predictions not only of the initiation of TCs, but also of their growth rate. The model is simple to apply both to reanalysis data and also to the results of climate models. The essential physical process is the interplay between evaporation and SST fields which are controlled by the large scale dynamics. In the tropics rising air occurs in the relatively cloudy regions of lower E and of higher SST

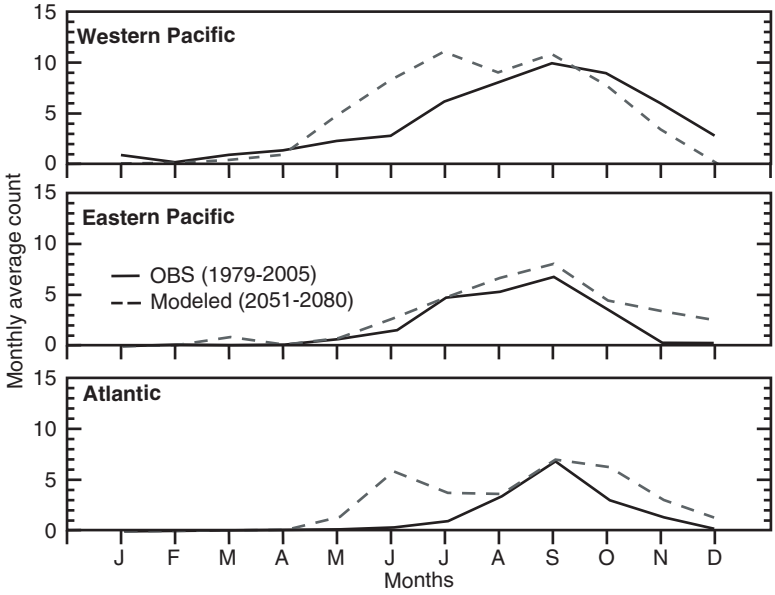

Fig. 9 Annual cycle of monthly average count for the observational period (1979–2005) and for the climate model predictions for 2051–2080

nearer the equator, and sinks over the relatively cloud free regions of higher E and lower SST further from the equator. This convective regime gives rise to a meridional region which extends from about 5°N (or 5°S) to the latitudes at which T ∼26°C, which correspond approximately with the peak in evaporation shown in Figs. 1 and 2. Note that the data points with lnE less than its maximum value with respect to T, occur in the range, 5°N–5°S (Bye and Keay, 2006).

The results of our analysis show however that the standard deviation of H is much greater than the magnitude of the mean of H. The enhanced negative regions of H are due to localized intense convection and the enhanced positive regions are due to localized subsidence; the two processes being on average in balance.

We emphasize that the H-index predicts the regions of *potential* TC development in each generation region, which during any month are many. Other conditions such as vertical wind shear and the instability of the lower atmosphere would then select the locations at which the TC actually develops. The comparison between observations and predictions from the H-index model (Fig. 7), however, suggests that on a monthly time scale at least, the proportion of favorable sites (as predicted by the H-index), which realize TCs does not vary greatly over the TC season or between TC generation regions.

This is the link between the H-index and other indices such as the seasonal genesis parameter (SGP) originally proposed by Gray (1975), and often applied to make seasonal predictions of TC occurrence, see for example Watterson et al (1995). The SGP consists of a product of a thermal potential and a dynamic

potential, in which the variability of the former is largely controlled by the ocean, and of the latter by the atmosphere. The modeling study of Royer et al. (1998) in which the results of a control run ($1 \times CO2$) were compared with those of a doubled CO2 environment ($2 \times CO2$) clearly showed that the increases in TC numbers were mainly brought about by changes in the thermal potential, i.e. the ocean. Royer et al. (1998) also replaced the thermal potential (which relies on the ocean temperature) by a convective potential (which relies ultimately on the ocean evaporation) to give a modified seasonal genesis parameter and found that the increases in TC numbers, although much more modest, were also mainly due to changes in the convective potential brought about by the ocean.

The success of the H-index supports the view that the major player in the TC variability is the ocean; in our case through the interaction of the ocean temperature and evaporation fields. This dual importance has also been recently recognized by Camargo et al. (2007) in a new generation potential, in which the ocean component (the potential intensity) depends on the sea surface temperature and pressure and vertical profiles of temperature and specific humidity, i.e. essentially on SST and E. The two prediction models, however, differ very significantly as the H-index is evaluated from the horizontal structure of the environment whereas the potential intensity is evaluated from its vertical structure.

In concluding this discussion, we suggest that the H-index may have the advantage over the oceanic component of GP and SGP and its convective modification, as it is based on robust elementary physical reasoning and is simple to calculate. We also note that the differences between the observations and the predictions from the H-index highlighted in the discussion in Results: (II) Comparison Between Observed Tropical Cyclone Numbers and the Standard Deviation of the H-index may be attributed to the variability of the dynamic potential, i.e. the atmosphere, rather than data inadequacies in the TC archives and the SST and reanalysis fields. This possibility, however, remains to be investigated.

We have used monthly mean data averaged over the generation region throughout. This gave rise, when further averaged over the record period (1979–2005) to almost symmetrical histograms of H (Fig. 3). The symmetry of the histograms, which was possibly the most unexpected finding of the study, signifies that the H-index captures the two-way energy exchange, characterized by the release of KE to the atmosphere from the mixed layer and its subsequent re-absorption, which lies at the centre of the tropical dynamics. This is an analogous process to the release of KE and its subsequent dissipation, which underlies the baroclinic instability mechanism in the subtropics.

The histograms for individual months, from which the inter-monthly time series (Fig. 7) were constructed, however, each showed an individual structure due to the synoptic evolution or suppression of the tropical cyclones It is anticipated that this structure would be even more marked over shorter averaging periods. This however remains to be checked.

With regard to climate models that do not explicitly resolve TCs, it was found that the standard deviation of H was smaller than for the reanalysis data, due to the poorer resolution. It is planned in a future study to obtain similar statistics using a

climate model that does resolve TCs., which will enable the spatial structure of H to be modeled on a finer scale, and compared with that derived from synoptic analyses supported by high resolution SST fields.

Acknowledgments J.A.T.B. would like to express his thanks to colleagues at the 1st International Summit on Hurricanes and Climate Change for many useful discussions. The authors also thank a reviewer for many useful and instructive comments, and Kevin Keay of the University of Melbourne for assistance with the processing of the text.

References

Bye, J.A.T., 1996: Coupling Ocean-Atmosphere Models. Earth-*Science Reviews*, **40**, 149–162.

Bye, J.A.T., Keay, K., 2006: A Global Relation for Tropical Cyclone Development. *Proceeedings of the 8th Intl. Conf. On Southern Hemisphere Meteorology and Oceanography,* Foz do Iguasu, Brazil, Amer. Meteorol. Soc.

Bye, J.A.T., Keay, K., 2008: A New Hurricane Index for the Caribbean. *Interciencia,* **33**(8), 556–560.

Camargo, S., K. A. Emanuel, et al., 2007: Use of a Genesis Potential Index to Diagnose ENSO Effects on Tropical Cyclone Genesis. *J. Climate*, **20**, 4819–4834 doi: 10.1175/JCLI4282.1.

Chauvin F., J. F. Royer, et al., 2006: Response of Hurricane-type Vorticies to Global Warming as Simulated by ARPEGE-Climat at High Resolution. *Climate Dynamics*, **27**, 377–399.

Gordon A., W. Grace, P. Schwerdtfeger, R. Byron-Scott, 1998: *Dynamic Meteorology: A Basic Course*. Arnold, London

Gordon H. B., L. D. Rotstayn, et al., 2002: The CSIRO Mk3 Climate System Model [Electronic publication], CSIRO Atmospheric Research (CSIRO Atmospheric research Tech Pap no 60).

Gray, W. M., 1975: Tropical Cyclone Genesis, Dept. of Atmospheric Science Paper 234, Colorado State University, Fort Collins, CO.

Kalnay, E., M. Kanamitsu, et al., 1996: The NCEP/NCAR 40-year Reanalysis Project. *Bull. Amer. Meteorol. Soc.*, **77**, 437–471.

Kanamitsu, M., W. Ebisuzaki, et al., 2002: NCEP-DOE AMIP-II Reanalysis (R-2) *Bull. Amer. Meteorol. Soc.*, **83**, 1631–1643.

Powell, M. D., P. J. Vickery, et al., 2003: Reduced Drag Coefficients for High Wind Speeds in Tropical Cyclones, *Nature*, **422**, 279–283.

Rayner, N. A., D. E. Parker, et al., 2003: Global Analyses of Sea Surface Temperature, Sea Ice, and Night Marine Air Temperature since the late Nineteenth Century. *J. Geophys. Res.*, **108**, doi 10.1029/2002JD002670.

Royer, J. F., F. Chauvin, et al., 1998: A GCM Study of the Impact of Greenhouse Gas Increase on the Frequency of Occurrence of Tropical Cyclones, *Climatic Change*, **38**, 307–343.

Uppala, S., P. Kallberg, et al., 2004: ERA-40: ECMWF 45-year Reanalysis of the Global Atmosphere and Surface Conditions, 1957–2002 ECMWF Newsletter No 101 – Summer-Autumn 2004, 2–21.

Watterson, I.G., J. L. Evans, et al., 1995: Seasonal and Interannual Variability of Tropical Cyclogenesis: Diagnostics from Large-scale Fields. *J. Climate*, **8**, 3052–3066.

Probability of Hurricane Intensification and United States Hurricane Landfall under Conditions of Elevated Atlantic Sea Surface Temperatures

Peter S. Dailey, Greta Ljung, Gerhard Zuba, and Jayanta Guin

Introduction

The genesis, intensification, and eventual demise of tropical cyclones (TCs) involve complex and dynamic interactions between the ocean, the atmosphere, and sometimes the land surface. Two key interactions are the favorable effects of sensible and latent heat transferred from the ocean's surface layer to the atmosphere [e.g., Emanuel, 2005], and the detrimental effects of vertical wind shear in the troposphere [e.g., Elsberry and Jeffries, 1996; Emanuel et al., 2004; Emanuel, 2005] on TC development. The competition amongst these factors can be viewed at a high level to determine seasonal activity levels. Most discussions surrounding tropical cyclogenesis, however, focus on the need for sufficiently warm sea surface temperatures (SSTs) [e.g. Chan et al., 2001]. Some of the latest research has shown that Tropical Cyclone Heat Potential (TCHP), which is a measure of upper layer ocean temperature, rather than that of the ocean's surface, is more highly correlated with TC intensification than SSTs alone, especially episodic and rapid intensification [Shay et al., 2000; Scharroo et al., 2005]. Unfortunately, this type of oceanographic data has only become available over the last ten years. Clearly, the enormous quantity of heat stored within the ocean serves as a reservoir of energy from which cyclones can develop and intensify. Other climate factors, such as the El Nino-Southern Oscillation (ENSO) cycle and its impact on Atlantic wind shear, tend to modulate the underlying capacity of the ocean-atmosphere system to support tropical activity, with ocean heat being the primary driver of activity.

Tropical latitudes within the North Atlantic Ocean have historically served as a fertile breeding ground for TCs, especially during the late summer and early autumn months, when SSTs are most elevated. The historical record indicates SSTs in the North Atlantic undergo fluctuations about a long-term average in phases that can last several decades. The physical cause of such multi-decadal fluctuations is a matter of debate [e.g., Mehta, 1998; Xue et al., 2003; Dima and Lohmann, 2007]. It is generally recognized, however, that fluctuations in SSTs are

J.B. Elsner and T.H. Jagger (eds.), *Hurricanes and Climate Change,*
doi: 10.1007/978-0-387-09410-6,

related to long-term fluctuations in tropical cyclone activity [Shapiro and Goldenberg, 1998].

Because the U.S. coastline lies in the path of many Atlantic TCs, and because population density has been trending upwards along the US coastline, it is important to study not only tropical activity as it occurs over the open ocean, but also the risk to life and property for those storms that make their way to the coastline. Historically, only about 12% of TCs reaching tropical storm strength (winds $\geq$ 35 knots) have struck the U.S. coastline as hurricanes, with an average annual frequency of about 1.5 landfalling hurricanes per year. Despite these relatively low numbers, it is well understood that a single intense landfalling event like Hurricane Andrew (1992) or Hurricane Katrina (2005) can cause catastrophic loss. The human impact of even one intense landfalling hurricane is often far greater than an entire season of TCs that remain at sea.

Thus, this paper will focus on the relationship between sea-surface temperatures (SST) in the North Atlantic basin and the propensity of TCs to make landfall along the US coastline. In order for a tropical cyclone to make landfall as a hurricane, two conditions are required. First, the TC must intensify to hurricane strength (winds $\geq$ 64 knots), and second, the hurricane must reach the U.S. coastline having maintained that strength. The paper will therefore focus on these two aspects of the TC evolution. Based on the historical record, we will examine the probability of a TC reaching hurricane strength, and the probability of the storm maintaining that strength through to the US coastline. By estimating these probabilities conditioned on regions where storms develop, one can assess how hurricane and landfall probabilities are modulated for individual seasons or individual events. In the end the comparison of warm SST years to climatology shows significant regional shifts conditioned on genesis for storms reaching the U.S. mainland as hurricanes.

Section 2 describes the data used in the study and the general approach to the analysis. The relationship between activity levels in the North Atlantic basin and the proportion of storms making U.S. landfall is analyzed in Section 3. Section 4 describes the balance between storms' probability to intensify and their probability to make landfall, based on the formation region.

Data

The analysis m+akes use of tropical cyclone track and intensity characteristics from the North Atlantic hurricane database (HURDAT) available from the National Hurricane Center [Jarvinen et al., 1984; http://www.aoml.noaa.gov/hrd/hurdat]. The analysis is limited to the period from 1948 to 2006 to eliminate uncertainty in storm counts and tracks in the North Atlantic basin in the early 1900s. Genesis locations for storms of at least tropical storm strength (named storms) are considered for the North Atlantic basin and are derived using the first track location in the

data set. A small number of storms that cross into the Atlantic from the Pacific are excluded. In the end, we use a total of 626 genesis locations over 59 North Atlantic seasons capturing an average annual frequency of 10.6 named storms per year.

For purposes of determining the point at which basin storms reach hurricane strength, maximum wind speed from HURDAT is considered for each event. We also make use of the HURDAT landfall point, if any, along the U.S. coastline by interpolating the intersection of HURDAT six hourly track points with the U.S. coastline. For purposes of this paper, we only considered storms that explicitly cross the U.S. mainland. For example, storms that only cross the Florida Keys and the outer banks of North Carolina were not counted as landfalls (such storms are fairly uncommon, occurring one about every 10 years).

For sea surface temperatures, the analysis is based on the Hadley Center HadSST2 [Rayner, 2006] supplemented with National Oceanic and Atmospheric Administration's (NOAA) optimum interpolated (OI) SSTs for the most recent years [Reynolds, 2002]. We also make use of the SST spatial distributions available from the National Center for Atmospheric Research/National Center for Environmental Prediction (NCAR/NCEP) Reanalysis Project, available for the period from 1948 to 2006 [Kalnay et al., 1996]. The average of the SST anomalies during the months of August, September, and October (ASO) are used to quantify variability for the analysis period. The Hadley SST anomaly data series is shown in Fig. 1 since 1900. It shows multi-decadal periods in which anomalies are persistently colder or warmer than average. For purposes of this analysis, years in which North Atlantic SST anomalies are greater than or equal to zero are considered *warm years* and all other years are considered *cold years*. Only in one year (1954) was the anomaly equal to zero. Over the 58 remaining seasons from 1948 to 2006, there are 31 years classified as warm and 27 years classified as cold.

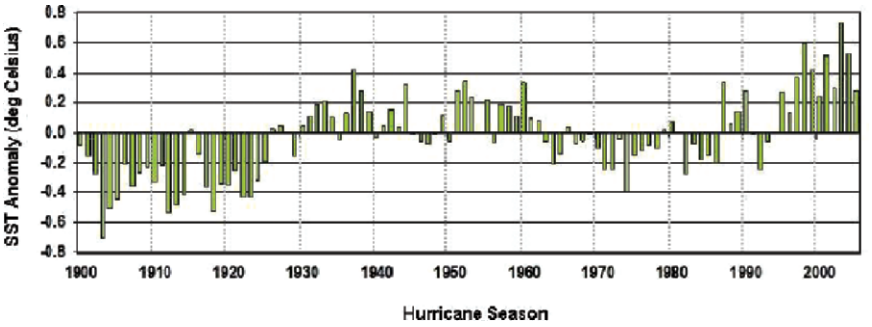

Fig. 1 Hadley Centre Sea Surface Temperature Anomalies Data Set (HadSST2-ASO). The figure shows by year the mean Atlantic Ocean anomaly (degrees ^{o}C) for the months of August, September and October (ASO), the core of the Atlantic hurricane season, from 1900 to 2006. There are multi-decadal episodes in which anomalies are consistently colder or warmer than average, including the current warm period which began in the mid-1990s

Relationship between Basin and Landfall Activity

To examine the physical relationship between basin and landfall activity, we begin by estimating the probability of a storm making U.S. landfall – climatologically and under anomalous SST conditions. The landfall *probability* is estimated by the *proportion* of basin TCs that have historically made landfall. To illustrate, consider a TC forming in the basin. Once it becomes a named (tropical) storm, it has some climatological probability of making a U.S. hurricane landfall, and that probability is estimated by the long-term ratio of hurricane landfalls to the number of named storms that developed in the basin over the same period.

Landfall Probability

Table 1 shows the estimated landfall probability for storms of various intensities. Column A shows that the historical proportion of storms making landfall at tropical storm strength or greater is 31.0% in warm SST years and slightly higher (31.7%) in cold years. Column B shows that landfall proportion at hurricane strength or higher is about 12.2% in warm years and the cold year proportion is slightly higher (12.6%). For stronger hurricanes, shown in columns C (winds $\geq$ 89 knots; strong hurricanes) and D (winds $\geq$ 96 knots; major hurricanes), the cold year proportion is again higher than the warm year proportion, and the marginal difference grows with increasing intensity. For storms with a landfall intensity of at least 89 knots, the landfall proportion in warm years is notably smaller than in cold years, and it can be shown that this difference is statistically significant for certain genesis sub-regions within the North Atlantic basin [Dailey et al., 2007]. For the proportions computed in columns (B) to (D), it should be noted that the sample size is small. For example,

Table 1 Landfall proportion based on landfall counts for storms of different intensities. The table shows the proportion of named historical storms that make U.S. landfall over the period from 1948 to 2006. Numerator in each ratio is the number of landfalls at a given wind speed or higher; denominator is the total number of basin storms under the cold or warm SST condition. The landfall proportion is the ratio of the landfall count to the basin storm count for a given landfall wind speed, using (A) tropical storm strength (B) hurricane strength, (C) 89 knots (referred to in the text as *strong* hurricane strength), and (D) major hurricane strength (Saffir Simpson category 3 to 5). The third column, using a threshold of 89 knots, is consistent with later analyses and takes advantage of a larger number of hurricanes than is available in column (D)

	(A) Landfalls $\geq$ 35 kt	(B) Landfalls $\geq$ 64 kt	(C) Landfalls $\geq$ 89 kt	(D) Landfalls $\geq$ 96 kt
Warm SST Years	31.0% (117/378)	12.2% (46/378)	5.8% (22/378)	4.8% (18/378)
Cold SST Years	31.7% (78/246)	12.6% (31/246)	6.5% (16/246)	5.3% (13/246)

there have only been 31 landfalling hurricanes since 1948, and only 13 of them have achieved major hurricane status.

These results, which are based on data for the entire U.S., raise several questions. First, would a lower landfall proportion in warm SST seasons versus cold SST seasons have some physical explanation, and second, would physical factors account for regional differences in the landfall probability? If there are locally strong signals in the historical data, this might shed light on the suppression of overall proportions as noted in Table 1.

Physical Factors Influencing Landfall Probability

To address these questions from a physical perspective, one must examine the complete life cycle of TCs as it relates to landfall probability. Given that a TC forms in the North Atlantic basin, its probability of making landfall as a hurricane is dependent on three fundamental factors, namely (a) *genesis* (where the storm is born), (b) *intensification and lyses* (the intensification life cycle), and (c) *tracking or steering* (the storm's ability to approach and potentially cross the coastline). Modulation of any one of these can bring about significant changes in landfall probability and the resulting proportion of storms making landfall. Genesis determines a TC's initial proximity to land, but increasing proximity also limits the time it has to grow and intensify. Thus, genesis and intensification are intimately related. Steering currents, which relate to the atmospheric circulation, determine how far a TC deviates from its expected or "climatological track", and hence the uncertainty in estimating landfall probability based solely on the climatological record. By closely examining each of these characteristics—genesis, intensification, and tracking—one can better understand which aspects of the TC life cycle are most sensitive to climate and most critical to landfall risk.

With regard to genesis, warm SSTs should have an enhancing effect since one of the necessary conditions for TC formation is the presence of sufficiently warm ocean temperatures. One expects warm SSTs to bring about increased intensification as well. This is not very clear from the historical data, however, since on average the probability of a TC intensifying to hurricane strength when the North Atlantic is anomalously warm is less than 2% higher than the long-term average. The explanation may lie in the fact that intensification is more sensitive to SST gradients than to SSTs themselves [Hennon, 2006; Chan et al., 2001], thus a uniform increase in ocean temperatures may not substantially modify intensification patterns. Finally, the degree to which TC steering responds to a warm ocean environment is difficult to quantify. Theoretically, a warmer than average ocean will translate into a warmer than average atmosphere, which in turn should induce a negative pressure perturbation on the semi-permanent high pressure situated over the North Atlantic. In fact, in an analysis using data from 1948 to 2005, we found a weak though statistically significant negative correlation between North Atlantic SST anomalies and sea-level pressure over the North Atlantic Ocean (not shown).

To quantify the impact of warm SSTs on storm tracks, one can apply stochastic or numerical modeling techniques to determine how historical storms would be steered differently under such SST conditions. A combination of long time scale fluctuations in ocean heat content and shorter time scale factors influencing TC steering, this complex subject will be considered in future work. In this study, we will limit the analysis to estimating hurricane probability and landfall probability conditioned on genesis alone.

Of course, if ocean anomalies were randomly distributed across the North Atlantic, or if they tended to concentrate outside the Main Development Region [MDR, see Emanuel, 2005], there might be little hope in tying SST anomalies to anomalies in genesis. But there are several plausible physical explanations for the spatial structure of ocean anomalies being systematic and non-random. First, the intensity of currents within the North Atlantic may limit the ability of anomalies to accumulate and stabilize. Modeling studies have shown that inter-annual variation in the upper ocean's heat content is linked to the advection of anomalous temperatures via the Gulf Stream [Dong and Kelly, 2003]. Within the Gulf Stream, ocean currents tend to be strong, thus, local anomalies may be short-lived. There is evidence, for example, that the strength of the Gulf Stream can reduce the persistence timescale of SST anomalies to just a few days [Gilman and Rothstein, 1994]. Shallow layers of ocean warmth may be transient not only because of swift currents, but also because passing disturbances tend to replace that warmth with cooler waters from below through the upwelling process. More stagnant regions of the North Atlantic, for example within parts of the Gulf of Mexico and along concave portions of the South American coastline, tend to accumulate warmth more readily than more dynamic regions of the open ocean. At the same time, during active periods of the "loop current" (the clockwise flow that extends northward into the Gulf of Mexico and joins the Yucatan Current and the Florida Current), North Atlantic anomalies are much less relevant to TCs within the Gulf of Mexico. The relationship between the distribution of North Atlantic anomalies and their impact on TC development and intensification is clearly complex, but it is expected that SST anomaly patterns can be coherent and associated with the dynamics of the large scale ocean system. Principal Components Analysis (PCA) of the SST anomaly structure and its association with hurricane tracks has been the subject of limited research [e.g., Xie, et al., 2005] and certainly merits additional investigation. While anomaly patterns may not be predictable on inter-annual timescales, for purposes of this study it will be assumed that tropical SST anomalies are coherent within a season.

Figure 2 shows the spatial distribution of tropical storm genesis location, along with corresponding contours of genesis density, for all tropical cyclones in the North Atlantic. Genesis for all tropical storms and hurricanes is considered since subsequent intensification occurs somewhat independently of genesis location. The genesis density was estimated using a spatial kernel smoothing procedure described by Hall and Jewson [2005]. The optimal radius of influence (ROI), defining the circle of points used to estimate genesis density locally, (usually about 200 km) was roughly doubled in Fig. 2 to draw attention to larger-scale features in the genesis

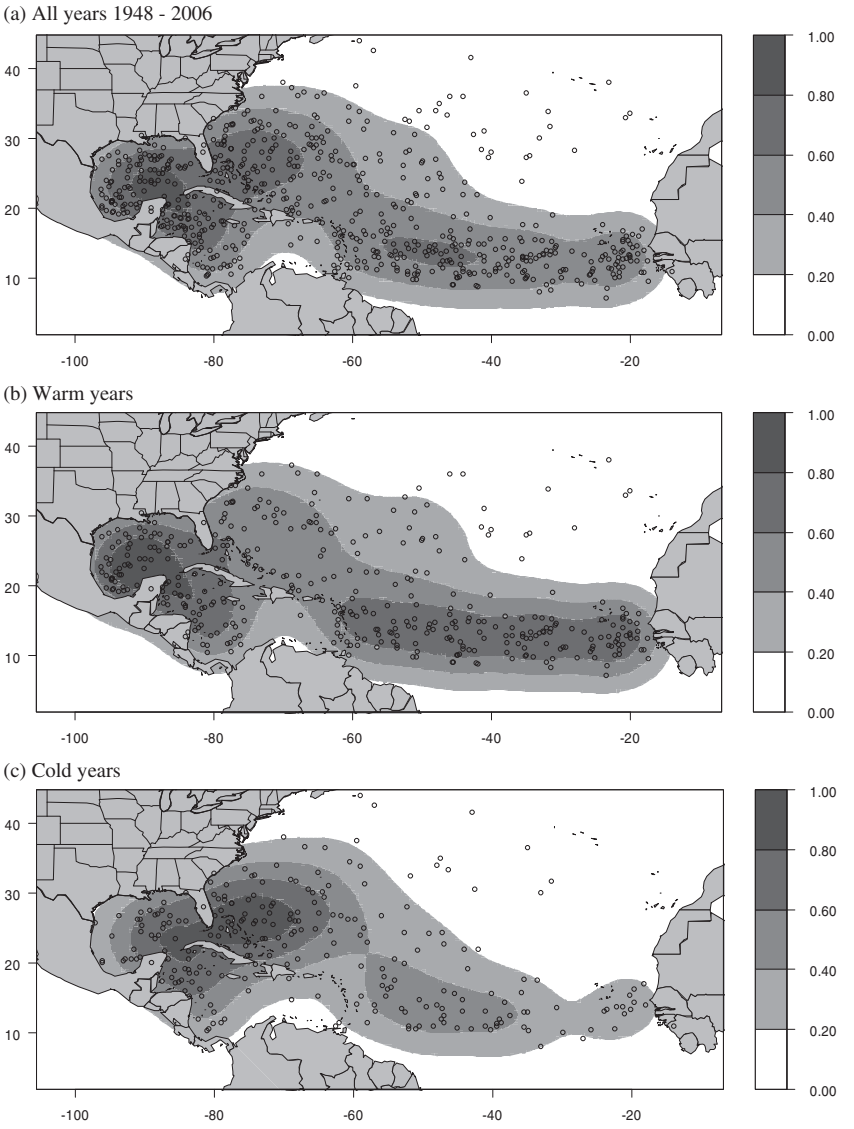

Fig. 2 Spatial Distribution and Density of Genesis for All Tropical Cyclones (1948–2006). Each dot represents a historical starting point for a TC that eventually reaches at least tropical storm strength. Grey scale contours show the mean genesis density in storms per square kilometer per year. In the top panel, the mean climatological genesis density is characterized by two hot spots, one within the Gulf and western Caribbean, and another along the Main Development Region (MDR). The center panel shows genesis distribution in warm years. Here, the pattern shifts with more focused genesis within the Gulf of Mexico and an eastward expansion of genesis along the MDR. The cold year counterpart is shown in the bottom panel

pattern. The top panel shows the climatological genesis pattern with two known "hot spots" within the Gulf of Mexico and along the MDR. The relative scarcity of genesis in the vicinity of the Caribbean Islands can be explained by this region's high vertical wind shear and strong teleconnection to ENSO [Aiyyer and Thorncroft, 2006]. The lower panel shows that, under warm SST conditions, genesis in the Gulf of Mexico shifts south and contracts while genesis in the North Atlantic shifts significantly eastward across the MDR and away from the U.S. coastline. This finding has several implications. First, storms that form in the Gulf are already close to the coastline; thus there is little time for a storm to intensify before landfall. If genesis density here tends to concentrate under warm SSTs, one expects increased probability of weaker hurricanes making landfall in the Gulf. Note that this does not account for less frequent Gulf landfalls with genesis outside the Gulf of Mexico. Though these are less frequent, they can be more intense. Second, storms that form in the MDR, especially off the coast of Africa, have a longer period to intensify, but are also much further from the U.S. coastline. This balance between opportunity to intensify and opportunity to make landfall naturally leads to the analysis carried out in Section 4.

Hurricane Intensification and Landfall Probability

Estimation Method

In this section we describe the method used to evaluate the likelihood of a storm making landfall given its genesis location. The same procedure is then used to evaluate the proportion of storms which later become hurricanes, and the proportion of storms which later make landfall as hurricanes.

One way to estimate the likelihood of storms originating from a specific region making landfall would be to subdivide the North Atlantic basin into sub-regions and compute the ratio of landfalling storms to the total number of storms that form in this region. However, a disadvantage of this method is that the result for a given location may be very sensitive to the size of the sub-region chosen. If the box is too small, it may not capture sufficient historical genesis, and accurate quantification of the proportion is not possible. We therefore prefer a smoothing based approach that allows for estimation of landfall probabilities without the use of grid boxes. The smoothing method used is a variant of a kernel smoothing method used to determine the density contours in Fig. 2.

The first step is to mark genesis locations with an indicator variable I_{LF} that depends on the landfall information for the corresponding storm track. The indicator variable is set to 1 if the storm later makes a U.S. landfall and to 0 if it does not. To estimate landfall probability for a given genesis location, we use a weighted averaging technique that incorporates genesis information from neighboring sites within the radius of influence (ROI). Gaussian weights are applied when averaging

within the ROI neighborhood. The length scale used for determining the neighborhood is calculated as follows.

1. ROI or length scale λ is chosen, e.g. 300 km, based on Hall and Jewson [2005]
2. Gaussian weights are calculated for all other genesis locations according to the distance d_i from the current location to a neighboring location according to $w_i = e^{-d_i^2/\lambda^2}$
3. Effective landfall proportion p_{LF} is computed as a weighted average of the indicator variable I_{LF} for all locations within the chosen ROI according to

$$p_{LF} = \sum_i I_{LF_i} w_i \Big/ \sum_i w_i$$

4. Steps 1–3 are repeated for all genesis locations

To estimate the optimum value for the length scale λ, a cross validation is performed by looping through all years between 1948 and 2006. For each year, the probability surface is calculated using data from all other years. Landfall probabilities for a given year are the values of the probability surface at the genesis locations of that year. These values are compared to the historical values and the differences in probabilities are accumulated for all locations and over all years. The total accumulation of all differences is minimized by varying the length scale λ. After the optimization is complete, the final probability surface is calculated using the optimal λ along with the historical data for 1948–2006.[1]

The optimal value of λ depends on the parameter of interest and the value increases with increasing sparseness of the data. In the current analysis, the length scale is about 400 km for genesis locations that produce landfalling TCs and about 800 km for genesis locations that produce strong hurricanes or strong landfalling hurricanes.

Hurricane Intensification Probability

The procedure described above will now be used to analyze the probability of tropical cyclones becoming a hurricane. However, instead of flagging a genesis

[1] The outlined procedure can be applied to various tropical cyclones parameters. Parameters analyzed here and their definitions include: *Landfalling Tropical Storms*: wind speed at landfall ≥35 knots; *Landfalling Hurricanes*: wind speed at landfall ≥64 knots; *Landfalling Strong Hurricanes*: wind speed at landfall ≥89 knots; *Storms Becoming Hurricanes*: maximum wind speed along track ≥64 knots; *Storms Becoming Strong Hurricanes*: maximum wind speed along track ≥ 89 knots. Note that strong hurricanes counts have been chosen for analysis (versus major hurricanes) in order to increase the sample size for the more intense events.

point according to subsequent landfall, each genesis point is now flagged 1 if the storm reaches hurricane strength at any point along the track, and 0 otherwise. After computing the probability surface, the average value at all historical genesis locations for the period 1948–2006 as well as the average value for individual years 2001–2006 are also computed.

The results of this analysis are shown in Table 2. Included in this table are also the historical proportions of storms that reach hurricane status over the period 1948–2006 as well as for the individual years 2001–2006. The table shows that historically 58% of storms have become hurricanes and 32% have become strong hurricanes (wind threshold of 89 knots) in the time frame of 1948–2006. The historical values are close to the predicted value of 59% and 33%, respectively, obtained through smoothing.

The advantage of having a probability surface is that the probability can be evaluated at any location, not just at the historically observed genesis locations. In addition, one can evaluate the average probability of storms becoming hurricanes given the genesis locations for a particular season. The value is then compared to climatology (long-term mean 1948–2006) and to the actual value realized in that season. This is illustrated by the modeled values for 2001–2006 given in Table 2. These values show that the probability of TCs becoming hurricanes is very close to the climatological value. The differences are larger for strong hurricanes. For example, the modeled value of 21% for 2002 is smaller than the climatological value of 33%, suggesting that the TC genesis in 2002 occurred in places where the chance of TC intensification was below average. The observed proportion of 17% is also smaller than the long term average of 32%. For 2004, on the other hand, the intensification probability of 37% for strong hurricanes exceeds the climatological value indicating that the genesis locations of 2004 were in regions with higher than average probability to intensify. The observed value for 2004 is also higher than the long term average indicating that favorable intensification conditions existed along the storm tracks. In contrast, the 2006 storms had a larger than average potential

Table 2 Probability of storms becoming hurricanes and strong hurricanes for the 1948-2006 analysis period and for select years. The values for individual years are calculated by averaging the estimated climatological values at the genesis locations of that year

	Hurricane (≥64 knots)		Strong Hurricane (≥89 knots)	
	modeled	actual	modeled	actual
Climatology (1948–2006)	0.59	0.58	0.33	0.32
2001	0.60	0.60	0.31	0.33
2002	0.54	0.33	0.21	0.17
2003	0.58	0.44	0.30	0.25
2004	0.61	0.60	0.37	0.47
2005	0.58	0.54	0.30	0.29
2006	0.63	0.50	0.39	0.20

(39%) of becoming strong hurricanes, while only a 20% proportion was observed. This points to unfavorable conditions along the storm tracks in 2006.

In Section 3 we established that the density pattern of genesis locations is different in warm versus cold SST years. To analyze if this has an influence on the probabilities presented in Table 2, we repeated the analysis and selected only genesis location of warm years. Fortunately, all years from 2001 through 2006 shown in Table 2 are all warm years, therefore one can make a direct comparison between conditioned (on warm SSTs) and unconditioned estimates. Table 3 shows the results of this analysis. Observed values for individual years are included for reference. Although there was an apparent regional shift in the genesis location for warm SST years compared to climatology (Fig. 2), the long term average probability of a tropical storm becoming a hurricane or a strong hurricane is essentially the same in Tables 2 and 3). Similarly, differences are small for individual years.

These results, which are based on data for the entire basin, suggest that warm SSTs do not have a significant impact on the basinwide probability of tropical storms becoming hurricanes. However, regional differences may still exist. This is illustrated in Fig. 3, which shows the probability distribution of storms becoming strong hurricanes given the genesis location. Regional differences tend to correspond to shifting genesis within the MDR. During warm SST years more TCs form in the eastern North Atlantic and these storms have a higher likelihood of becoming strong hurricanes contrasted with storms that form in the same region during cold years.

To summarize, the results so far show no basinwide difference in the likelihood of storms to become hurricanes or strong hurricanes during warm SST years. Regional differences presented in Fig. 3, however, imply that there might be larger impacts on landfalls. We will further explore this hypothesis.

Table 3 Probability of storms becoming hurricanes and strong hurricanes in warm SST years for the 1948–2006 analysis period and for select years. The values for individual years are calculated by averaging the estimated climatological values at the genesis locations of that year

	Hurricane (≥64 knots)		Strong Hurricane (≥89 knots)	
	modeled	actual	modeled	actual
Warm Year Climatology (1948–2006)	0.60	0.59	0.34	0.34
2001	0.59	0.60	0.30	0.33
2002	0.53	0.33	0.19	0.17
2003	0.57	0.44	0.29	0.25
2004	0.62	0.60	0.38	0.47
2005	0.58	0.54	0.29	0.29
2006	0.64	0.50	0.38	0.20

(a) All years 1948 - 2006

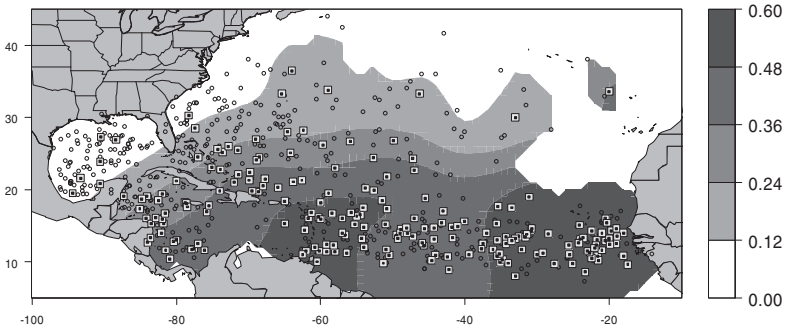

(b) Warm years

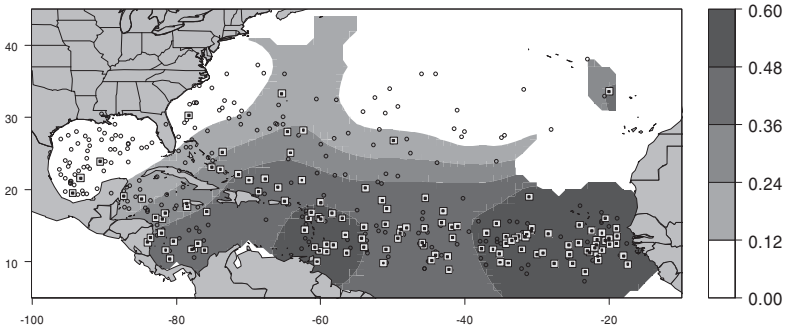

(c) Cold years

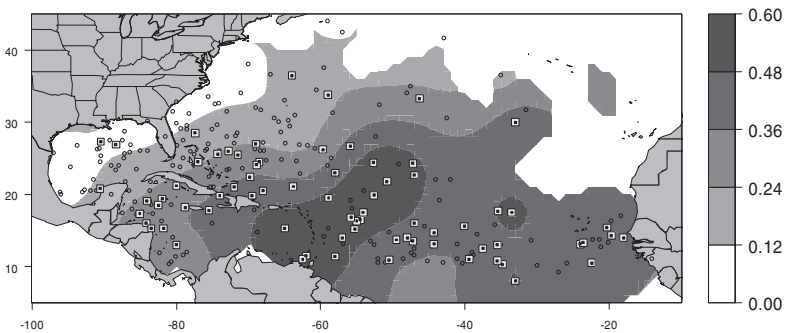

Fig. 3 Probability pattern for genesis locations of storms becoming strong hurricanes for (**a**) all years 1948–2006, (**b**) warm and (**c**) cold years within this period. All genesis locations for the selected years are drawn. Genesis locations that originate strong hurricanes are drawn as squares with a center dot. The darkest shade indicates that 48 to 60 percent of the storms forming in that region became strong hurricanes

Hurricane Landfall Probability

Table 4 shows the climatological probability of landfall as tropical cyclones (TC), hurricanes, and strong hurricanes, given all genesis locations. As in the previous analysis, estimates are also made for individual years from 2001 to 2006. The results show that genesis in 2002 produced storms with a higher than average likelihood (40% compared to 31%) of producing landfalling TCs and the observed landfall proportion was also above average (58%) in this year. For landfalling *strong* hurricanes in 2004 and 2005, the modeled probabilities were close to average (6%) but the actual values were well above average (27% and 14%, respectively). This implies "favorable" tracking conditions in these two years.

The information in Table 4 is based on data for the entire period 1948–2006. A similar analysis is presented in Table 5, using data from warm SST years only. The differences between the results in the two tables are generally small. The most notable differences in Table 4 can be found for storms that later become strong landfalling hurricanes. For example, for 2003, the potential for strong hurricane landfalls is 5.2% based on data for the entire period. This is 86% of the corresponding climatological value of 6.1%. The percentage drops to 4.4%, which is 79% of the climatological value (5.6%), when the analysis is based on warm SST years in Table 5.

In a separate analysis (Dailey et al., 2007), landfall counts in warm SST years were analyzed revealing marginal significance when considering the entire U.S. coastline. Significant differences in landfall rates were found regionally, however, especially for the Southeast coast of the U.S. from the tip of Florida to Cape Hatteras, where the landfall rates increased during warm SST years. This raises a logical question whether warm ocean conditions can translate to significant shifts in landfall probability. The estimated probability of a storm—having formed

Table 4 Probability of storms making landfall as tropical cyclones, hurricanes, or strong hurricanes for the 1948-2006 analysis period and for select years. The values for individual years are calculated by averaging the estimated climatological values at the genesis locations of that year

	All Tropical Cyclones (TC)		Hurricane (≥64 knots)		Strong Hurricane (≥89 knots)	
	modeled	actual	modeled	actual	modeled	actual
Climatology (1948–2006)	0.31	0.31	0.12	0.12	0.061	0.059
2001	0.28	0.20	0.11	0.00	0.049	0.000
2002	0.40	0.58	0.10	0.08	0.037	0.000
2003	0.32	0.31	0.12	0.13	0.052	0.000
2004	0.23	0.53	0.11	0.27	0.056	0.267
2005	0.30	0.25	0.12	0.14	0.060	0.143
2006	0.21	0.20	0.11	0.00	0.065	0.000

Table 5 Probability of storms making landfall as tropical cyclones, hurricanes, or strong hurricanes for warm SST years within the 1948–2006 analysis period and for select years. The values for individual years are calculated by averaging the estimated climatological values at the genesis locations of that year

	All Tropical Cyclones (TC)		Hurricane (≥64 knots)		Strong Hurricane (≥89 knots)	
	modeled	actual	modeled	actual	modeled	actual
Warm Year Climatology (1948–2006)	0.30	0.30	0.12	0.12	0.056	0.055
2001	0.30	0.20	0.10	0.00	0.044	0.000
2002	0.38	0.58	0.09	0.08	0.033	0.000
2003	0.34	0.31	0.11	0.13	0.044	0.000
2004	0.23	0.53	0.11	0.27	0.059	0.267
2005	0.29	0.25	0.12	0.14	0.052	0.143
2006	0.20	0.20	0.10	0.00	0.065	0.000

somewhere in the North Atlantic basin—making a hurricane landfall along the Southeast coast of the U.S. is 4.5%. The estimate increases to 5.5% when the analysis is based on warm SST years. The sample sizes are small, however, and the difference between cool and warm years is not statistically significant at the 10% level. This was established using bootstrapping as opposed to a traditional test on proportions because of the small sample sizes. Though some shifts in landfall risk cannot be firmly demonstrated as significant based on the limited historical record, there are plausible physical explanations for why such shifts may occur under the influence of a non-stationary climate. This is a subject of continuing research. Even a small increase in the underlying probability may be of practical significance to those interested in subtle frequency modulations brought about by climate (e.g., catastrophe risk managers).

The regional pattern of strong hurricane landfall probability is shown in Fig. 4. The figure is based on data for the entire U.S. coastline. Again regional shifts, away from the U.S. coast and towards the eastern part of the North Atlantic, are noticeable. In addition, Gulf coast probabilities decrease when only warm years are considered. It can be seen that strong hurricane landfalls originating from the eastern Atlantic occur almost exclusively during warm years. Not surprisingly, the cold year pattern is a mirror image of the warm with noticeable probability shifts in the Gulf of Mexico and along the MDR.

Summary

This study has examined a very specific aspect of tropical cyclone risk, namely the risk that storms forming in the North Atlantic basin will become hurricanes and subsequently make landfall as hurricanes along the U.S. coastline. Though much

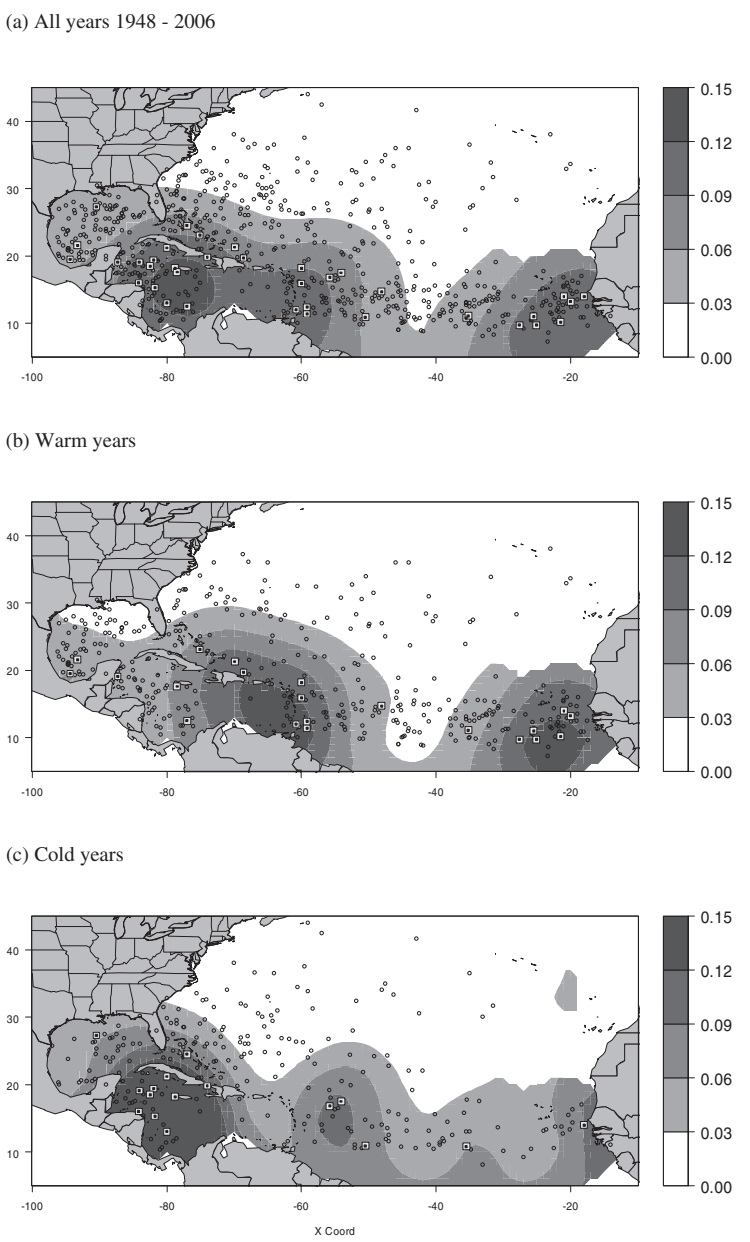

Fig. 4 Probability pattern for genesis locations of storms leading to a strong hurricane landfall for (**a**) all years 1948–2006, (**b**) warm and (**c**) cold years within this period. All genesis locations for the selected years are drawn. Genesis locations that originate strong hurricane landfalls are drawn as squares with a center dot. The darkest shade indicates that 12 to 15 percent of the storms forming in that region made landfall as a strong hurricane

attention has been paid to the influence of climate on the frequency of basin storms, less emphasis has been placed on the relationship between basin activity and landfall activity. Three key reasons are (a) the low level of long-term U.S. hurricane landfall frequency and the corresponding difficulty in detecting low level trends, (b) the general lack of fully reliable historical data, especially in the early 1900s, and (c) the complexity of the interaction and feedback amongst various climate signals. Despite these challenges, creative use of analytical tools can foster progress in this developing field. In this paper, we have examined from multiple perspectives the modulation of the regional risk of landfall in the North Atlantic basin. The analysis centers on the impact of warm SSTs on the probability of hurricane intensification (long-term average 58%) and the probability of US hurricane landfall (long-term average 12%). Though tracking mechanisms are very likely modulated by warm SSTs, such relationships are difficult to quantify since steering currents vary on a shorter timescale than the typical hurricane season. The data does, however, indicate that steering may be influenced by climate conditions, and this is a subject of continuing research.

The overall probability of tropical storms becoming hurricanes within the Atlantic basin appears to be stable under both warm and cold SST conditions. In fact, even within the current active period since 1995, data shows that the estimated probability of hurricane intensification lies relatively close to the long-term average despite large variations in seasonal genesis locations. The warm year spatial pattern is not very different than the climatological pattern.

When conditioned on genesis, the findings with regard to regional landfall proportion are noteworthy. Within the Gulf of Mexico, warm SSTs appear to reduce the probability of hurricane landfalls below the U.S. average. A physical explanation for this result is that increased genesis occurring with the Gulf should result in more storms that have a limited ability to intensify to hurricane strength. Thus, one expects a significant increase in the probability of tropical storm landfalls along the Gulf coast, but less so for hurricanes and especially major hurricane landfalls. Of course, not all Gulf landfalls originate within the Gulf of Mexico, but storms that spend their entire life cycle within the Gulf appear to dominate the landfall statistics for the region.

Genesis expansion and increased frequency within the MDR is indicated by the genesis data, but also by the regional warming of the ocean in this part of the North Atlantic during warm SST years. This is important for two reasons. First, this area has historically been a fertile source of major hurricanes, largely due to the longer period of intensification available from this source region. Second, when storms from the MDR become hurricanes and make landfall, they tend to do so along the Southeast U.S. coast. This is not to say that these storms never make their way into the Gulf, and in fact most storms from this region do not make landfall at all. Climatologically, when they do make landfall, they are more likely to land somewhere between Key West, Florida and Cape Hatteras, North Carolina than along any other part of the U.S. coastline. We conclude that there is an increased probability of storms making hurricane landfall along the Southeast coast from

this genesis region. Because some of these storms can make their way into the Gulf, however, there is likely a marginal impact on Gulf landfall risk as well.

Because the results are built on climatology, they apply more to a large number of seasons than to single one. Since many scientists expect the current warm phase of North Atlantic SST to continue for many years to come, the results of this study provide a basis for estimating landfall risk conditioned on a warm SST climate. This discussion can also serve to motivate further study of other climate signals, such as ENSO, and their influence on landfall risk. Though this study has focused on risk to the U.S. mainland, its techniques and analyses can be used to study similar aspects of risk in other areas prone to tropical cyclones.

Acknowledgements The authors would like to thank colleagues who contributed to this study. We are particularly grateful to Ioana Dima and Jason Butke for their significant contributions to this work.

References

Aiyyer, A. R., and C. Thorncroft, 2006: Climatology of Vertical Wind Shear over the Tropical Atlantic. *J. Clim.*, **19**, 2969–2983.

Chan, J. C. L., Y. Duan, and L. K. Shay, 2001: Tropical Cyclone Intensity Change from a Simple Ocean–Atmosphere Coupled Model, *J. Atmos. Sci.*, **58**, 154–172.

Dailey, P. S., G. Ljung, G. Zuba, and J. Guin, 2007: On the relationship between North Atlantic Sea Surface Temperatures and US Hurricane Landfall Risk. (In review, *J. Appl. Met. Clim.*, Sept. 2007).

Dima, M., and G. Lohmann, 2007: A Hemispheric Mechanism for the Atlantic Multidecadal Oscillation, *J. Clim.*, **20**, 2706–2719.

Dong, S., and K. A. Kelly, 2003: Heat Budget in the Gulf Stream Region: The Importance of Heat Storage and Advection, *J. Phys. Oceanography*, **34**, 1214–1231.

Elsberry, R. L., and R. A. Jeffries, 1996: Vertical Wind Shear Influences on Tropical Cyclone Formation and Intensification during TCM-92 and TCM-93, *Mon. Wea. Rev.*, **124**, 1374–1387.

Emanuel, K., C. DesAutels, C. Holloway, and R. Korty, 2004: Environmental control of tropical cyclone intensity. *J. Atmos. Sci.*, **61**, 843–858.

Emanuel, K., 2005: *Divine Wind: The History and Science of Hurricanes*, New York, Oxford University Press, 285 pp.

Gilman, C., and L. Rothstein, 1994: Gulf Stream warm surges: Thermal anomalies resulting from cold core ring interactions, *J. Geophys. Res.*, **99**, 15991–16000.

Hall, T., and Jewson, S., 2005: Statistical modeling of tropical cyclone genesis: a non-parametric model for the annual distribution. arXiv:physics/0510203.

Hennon, P., 2006: The role of the ocean in convective burst initiation: implications for tropical cyclone intensification. PhD Thesis, Ohio State University Libraries.

Jarvinen, B. R., C. J. Neumann, and M. A. S. Davis, 1984: A tropical cyclone data tape for the North Atlantic Basin, 1883–1983, contents, limitations, and uses. *NOAA Tech. Memo.*, NWS NHC 22, Miami, Florida.

Kalnay, E., M. Kanamitsu, R. Kistler, W. Collins, D. Deaven, L. Gandin, M. Iredell, S. Saha, G. White, J. Woollen, Y. Zhu, A. Leetmaa, R. Reynolds, M. Chelliah, W. Ebisuzaki, W.Higgins, J. Janowiak, K. C. Mo, C. Ropelewski, J. Wang, R. Jenne, and D. Joseph, 1996: The NCEP/NCAR 40-Year Reanalysis Project. *Bull. Amer. Met. Soc.*, **77**, 437–471.

Mehta, V.M., 1998: Variability of the Tropical Ocean Surface Temperatures at Decadal–Multidecadal Timescales. Part I: The Atlantic Ocean. *J. Clim.*, **11**, 2351–2375.

R Development Core Team, 2006: A language and environment for statistical computing. R Foundation for Statistical Computing, Vienna, Austria. ISBN 3-900051-07-0. URL http://www.R-project.org.

Ribeiro Jr., P.J., and P.J. Diggle, 2001: A package for geostatistical analysis. *R-News*, Vol **1**, No 2. ISSN 1609–3631

Rayner, N. A., P. Brohan, D. E. Parker, C. F. Folland, J. J. Kennedy, M. Vanicek, T. Ansell, and S. F. B. Tett, 2006: Improved analyses of changes and uncertainties in sea surface temperature measured in situ since the mid-nineteenth century: the HadSST2 data set. *J. Clim.*, **19**, 446–469.

Reynolds, R. W., N. A. Rayner, T. M. Smith, D. C. Stokes, and W. Wang, 2002: An improved in situ and satellite SST analysis for climate. *J. Clim.*. **15**, 1609–1625.

Scharroo, R., W. H. F. Smith, and J. L. Lillibridge, 2005: Satellite Altimetry and the Intensification of Hurricane Katrina, *EOS Trans. AGU*, **86**, 366.

Shapiro, L. J., and S.B. Goldenberg, 1998: Atlantic Sea Surface Temperatures and Tropical Cyclone Formation. *J. Clim.*, **11**, 578–590.

Shay L. K., G. J. Goni, and P. G. Black, 2000: Effect of a warm ocean ring on hurricane Opal. *Mon. Wea. Rev.*, **128**, 1366–1383.

Xie, L., T. Yan, L. J. Pietrafesa, J. M. Morrison, and T. Karl, 2005: Climatology and Interannual Variability of North Atlantic Hurricane Tracks. *J. Clim.*, **18**, 5370–5381.

Xue, Y., T. M. Smith, and R. W. Reynolds, 2003: Interdecadal Changes of 30-Yr SST Normals during 1871–2000, *J. Clim.,* **16**, 1601–1612.

Wavelet-Lag Regression Analysis of Atlantic Tropical Cyclones

John Moore, Aslak Grinsted, and Svetlana Jevrejeva

Abstract We discuss a novel wavelet-lag coherence method to study of cause-and-effect relations over a large space of timescales, phase lags and periods. We use 135 years of observational records to demonstrate how sea-surface temperature, sea-level pressure and cyclone numbers are linked. We examine the statistical properties of the time series and test how departure from Normality affects results found using the method. We also examine how historical inaccuracy in counting tropical cyclone numbers could influence the findings. Robustly we find that SST and cyclones in a negative feedback loop, where rising SST causes increased numbers of cyclones, which reduce SST. This is statistically most significant at decadal and not at longer periods. Only at periods of about 30 years do significant differences arise in using recently proposed corrections to cyclone numbers, and forcing the empirical distribution of cyclone numbers to be Normal. This could be incorrectly interpreted as support for a long period Atlantic Multidecadal Oscillation, whereas it actually reflects the time-varying bias functions applied to the observations. There is evidence of some linkage between Northern hemisphere snow cover and cyclone numbers, however this seems to be due to a common causative relationship between the known tropical cyclone drivers of ENSO and decadal scale North Atlantic ocean-atmospheric circulation systems.

Introduction

Increases in Atlantic tropical cyclone intensity have been related to increases in Atlantic sea surface temperature (SST), and Elsner (2007) has shown that it is likely to be rising global temperatures that drive the increases in both cyclone intensity and Atlantic SST. However, the nature of the climate relationships to tropical cyclones is likely to be complex, and certainly includes oceanic and atmospheric circulation patterns that operate on ocean basic scales. Significant but weak

J.B. Elsner and T.H. Jagger (eds.), *Hurricanes and Climate Change,*
doi: 10.1007/978-0-387-09410-6,

statistical correlations exist between the Atlantic hurricane source region and the northern Atlantic (Goldenberg et al., 2001) and tropical Pacific warm pools (Wang et al., 2006). Several authors have used these statistical relationships to produce predictive models of Atlantic hurricane season intensity and tropical storm numbers (e.g. Elsner and Jagger, 2006; Sabbatelli and Mann, 2007). In contrast with this kind of approach, here we attempt to understand relationships between the large scale driving mechanisms and Atlantic tropical storm activity by examining the behaviour of the various multi-year cycles that exist in the time series. Decadal cycles are fairly ubiquitous across the planet, and are therefore persuasive of a global-scale climate mechanism (Jevrejeva, Moore and Grinsted, 2004; Moron, Vautard and Ghil, 1998; Dijkstra and Ghil, 2005). The main features of the planet's climate are the ENSO and the polar annular modes, which is determined by the strength of the polar stratospheric vortex (Thompson and Wallace, 1998). An index of Atlantic climate variability that is often (but not always – Jevrejeva and Moore, 2001) closely related to the arctic annual mode (the Arctic Oscillation) is the North Atlantic Oscillation (NAO). Unlike the purely polar defined annular modes, the NAO is linked to the tropics via its interaction with the Atlantic thermohaline circulation, most particularly through the modulation of the Gulf Stream meanderings at 7.8 year periods (Dijkstra and Ghil, 2005). This is significant as Elsner, Kara and Owens (1999), noticed a 7.8 year periodicity in hurricane frequency.

Moore, Grinsted and Jevrejeva (2008) showed that robust linkages that may imply causal relationships between global sea-surface temperature (SST), pressure fields and cyclones exist. However, challenging the identification of such linkages are both the uncertainties in long-term observational records and the robustness of the advanced statistical methods designed specifically to extract possibly causal relationships that may be non-stationary and develop over many years. Here we examine how the results from wavelet lag regression are to perturbation of 135-year observational record and demonstrate cyclone numbers are linked on different time scales with high latitude processes that also determine snow cover in the Northern Hemisphere.

Data

In contrast with modern satellite-era observations of hurricane wind speeds and atmospheric physical variables, numbers of Atlantic tropical cyclones per year (TC), has been collected since at least 1851. They are defined simply as non-frontal, synoptic-scale cyclones over tropical or sub-tropical waters (Jarvinen, Neumann, and Davis, 2005). TC representing cyclone count and Power Dissipation Index (PDI) (Emanuel, 2005; Landsea, 2005), an index of hurricane destructive power available from 1944–2004 are correlated at 0.68. Recent modifications to TC have been suggested (Landsea, 2007; Mann et al., 2007), however testing our results with the proposed time-varying bias added to TC makes only very slight differences to our results. For example the correlation coefficient between PDI and TC changes

from 0.68 to 0.69. While Landsea (2007) makes good arguments for the systematic undercounting of tropical cyclones in the past due to the their existence being unnoticed, Mann et al., (2007) suggest various difficulties with a simple correction under the assumption of stationary climate forcing, and point out that sparse observations can also lead to over-counting when a single event is counted as two or more events. Moore, Grinsted and Jevrejeva (2008) showed the correlation between PDI and TC has varied over time, but for much of the common period of data the correlation is significant at the 95% level; with only the period prior to 1955 showing consistently lower significance. Moore, Grinsted and Jevrejeva (2008) concluded that as the moving correlation between TC and PDI (Fig. 1) was generally high, that TC could be used as a surrogate with reasonable confidence. Here, however we will examine the revised TC in some detail. The long TC record allows more rigorous significance testing for long period variability than analyses that have focused on the instrumental records available only from 1940s or later (Emanuel, 2005; Michaels, Knappenberger and Davis, 2006).

We consider the set of SSTs for the Atlantic averaged over the area 6–18°N, 20–60°W, defined as the cyclone main development region (MDR), during the months of August, September, and October, (SST_C). We use the HadISST2 data (Rayner et al., 2003) which extends from 1870 to 2004. There is no theory that predicts the number of Atlantic tropical storms directly as a function of SST (or potential intensity). GCM simulations suggest that there is a link between rising SST and strength of hurricane maximum wind speed, such that a 1°C rise in SST_C leads to a 5% increase in maximum wind speed (Knutson and Tuleya, 2004).

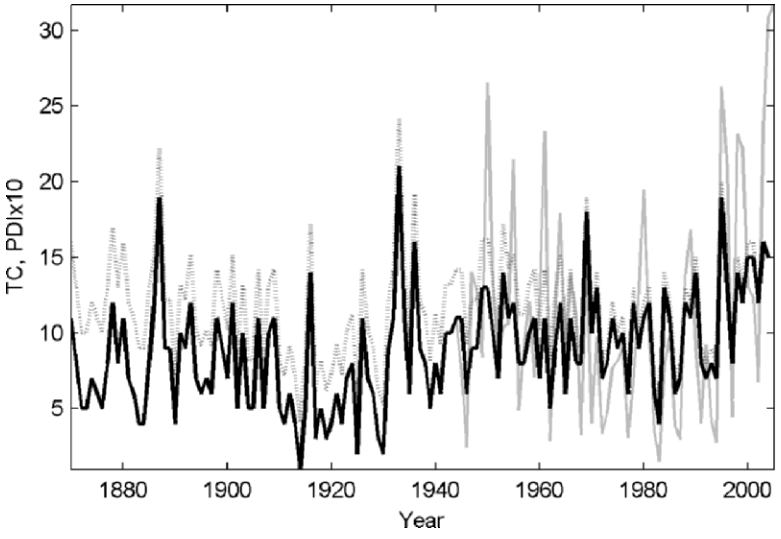

Fig. 1 Time series of TC (*black*), modified TC (*grey dotted*) and PDI (grey, multiplied by 10)

However observations in the Atlantic region suggest that the PDI, which is dominated by the largest storms, has increased by about 20% per °C since 1980, and perhaps by 10% per °C over the Twentieth Century (Emanuel, 2005; Landsea, 2005).

We used the historical variation in Northern Hemisphere and Eurasian snow cover extent derived from reconstructed daily snow depth (1922–1971) and NOAA satellite data (1972–1997). The method for reconstructing snow cover extent is described in Brown (2000). The spatial distribution of historical *in situ* data meant that reconstruction of continental-scale snow cover extent was only possible in three months: October, March and April for Eurasia, while for the whole Northern Hemisphere it was only possible for March and April. We constructed 2 indices: one of spring Northern hemisphere snow cover as the mean of march and April coverage, and one Autumn coverage for Eurasia based on the October extent in Eurasia. It is worth pointing out that these records are far longer than the purely satellite derived snow over extent data which begins only in 1972, and hence is of virtually no utility in examining decadal or longer relationships with other times series.

Methods

Elsner (2007) uses the method of Granger causality to determine phase relationships between time series, and finds convincing evidence for mechanistic relationships between Atlantic SSTs and global temperatures. In contrast with Granger causality methods that work in the time-domain, here we use wavelet methods. The method we use (Moore, Grinsted and Jevrejeva, 2007; Moore, Grinsted and Jevrejeva, 2008) determines the non-linear interactions between the two time series that may be chaotic. Briefly we extract the phase expression of the time series derived from the Continuous Wavelet Transform (CWT) of a time series (e.g. Grinsted, Moore and Jevrejeva, 2004; Torrence and Compo, 1998). Here we apply broad band pass wavelet (the Paul wavelet of order 4) to filter the time series. The centre frequency of the Paul wavelet, λ, is an important parameter in the analysis.

The wavelet is stretched in time by varying its scale (s), so that $\eta = s \cdot t$, and normalizing it to have unit energy. The CWT of a time series X, $\{xn, n = 1,\ldots,N\}$ with uniform time steps δt, is defined as the convolution of xn with the scaled and normalized wavelet.

$$W_X(s,t)|_{t=n} = \sqrt{\frac{\delta t}{s}} \sum_{n'=1}^{N} x_{n'} \psi_0 \left[(n' - n) \frac{\delta t}{s} \right].$$

The complex argument of WX(s,t) can be interpreted as the instantaneous phases of $X\{\phi 1\ldots, \phi N\}$ at the scale s. We utilize the strength of the instantaneous phase angle difference between two series (X and Y), also known as the mean phase

coherence, ρ(X,Y) (Mokhov and Smirnov, 2006). We are interested in causative relations, so it is appropriate to measure ρ between the instantaneous phases ϕ and θ of the two time series

$$\rho = \frac{1}{N}\sqrt{\left(\sum_{t=1}^{N}\cos(\phi_t - \theta_t)\right)^2 + \left(\sum_{t=1}^{N}\sin(\phi_t - \theta_t)\right)^2}$$

We vary the relative phase delay between the two series by lagging ϕ relative to θ by a phase lag, Δ. Significance testing of ρ is done by Monte Carlo methods against 1000 realizations of a red noise background (Grinsted, Moore and Jevrejeva, 2004), and the results can be visualized in a two-dimensional plot of ρ in λ-Δ space analogous to the wavelet frequency-time space plot. As a further refinement in the utility of such a plot we find it useful to contour the strength of linear regression of the wavelet filtered time series as a function of λ and Δ, so that the color scale bar corresponds to the value of m in the equation of WY(λ,t+Δ) = m WX (λ,t). The phase relationship over the range multi-year to decadal periods was examined by filtering both time series with a Paul wavelet with λ between the Nyquist frequency and 40 years with six λ per octave of scale.

Results

TC Corrections and Normality

It is well known that the TC time series is not Normally distributed but follows a Poisson distribution (Solow and Moore, 2000). However here we are interested to see how the non-Normality affects the novel statistical techniques we use. There is also a question as to how discrete data such as TC can be used in methods that were developed for continuously distributed data. One approach to providing a more continuous time series could be smoothing by running averaging the TC rate over a variety of scales, though any particular length of the running average would create data that would still be rational numbers. The smoothing window would naturally tend to produce a more Normal distribution via the Central Limit Theory. The CWT method is superior to running means as it effectively smoothes the data by the particular wavelet filter used, and this creates a much less discreet set of data. For both the modified and raw TC time series a Bera-Jarque test of Normality is rejected ($p = 0.02$) (Fig. 2), however, the data are acceptably Lognormal ($p = 0.15$). Clearly this is due to the TC being non-negative with a long tail.

We can remove the lack of Normality from the TC distribution completely by making use of a Normalization procedure (Jevrejeva, Moore and Grinsted, 2003). We transform the original data using a data adaptive transformation function. The transformation operator is optimally chosen so that the new probability density function is Normal, has zero mean and unit variance. This is calculated by making

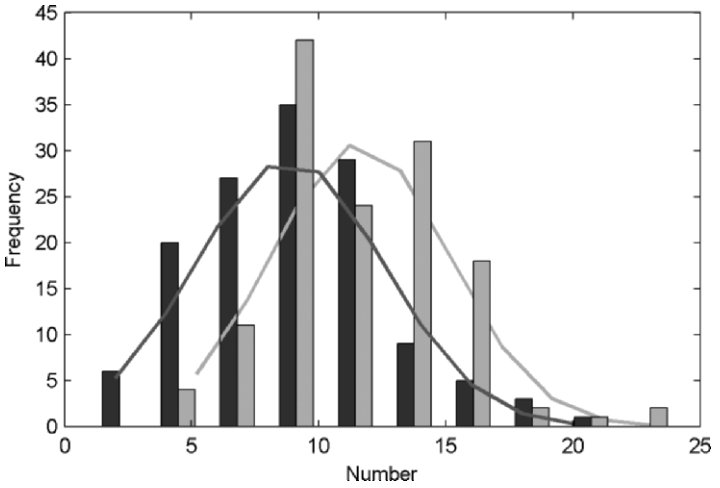

Fig. 2 Distribution of TC (*black*) and modified TC (*grey*), and their best fit Normal distributions

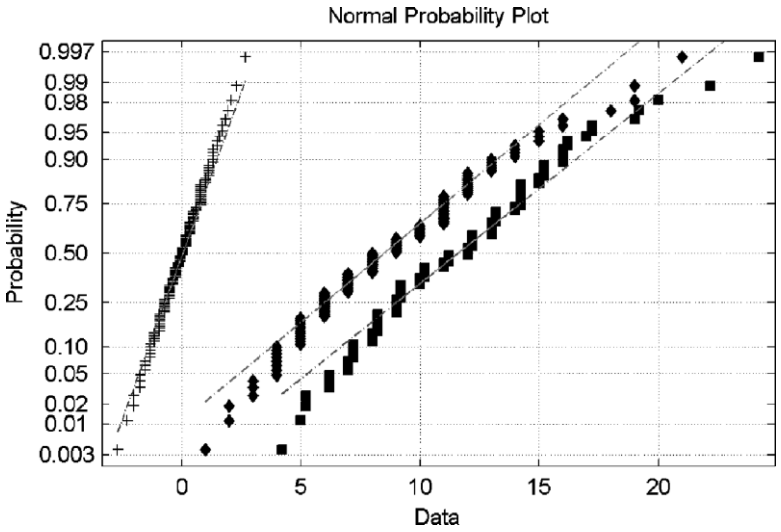

Fig. 3. The raw TC data (*diamonds*), (from Mann et al., 2007) modified TC (*squares*), (from Landsea, 2007) and Normalized modified TC (TC") (*marked by* +) created as described in the text, plotted on normal probability scaling so that straight lines represent a Normal probability distribution

the inverse normal cumulative distribution function of the percentile distribution of the original distribution (Fig. 3). We refer to this procedure as Normalization and it can be a rather drastic operation to use on a time series. However, Jevrejeva, Moore

and Grinsted, 2003 have shown that the results from even grossly non-Normal distributions, that would not produce reliable results with the wavelet method, do give results after Normalization that are consistent with alternative methods of signal extraction such as Singular Spectrum Analysis. Henceforth we denote the Normalized modified TC series as TC.

Figure 4 shows at first glance, quite large differences in significant regions. However, the differences in the actual values of coherence are rather slight, the coherence being quite close to the 95% value that marks the border. There are quite small differences in the time derivative dSSTC plots. The differences become smaller if the simple normalized times series or the simple modified time series are compared with the original TC. The largest differences are in the 25–30 year band, with no significant region in the raw TC curve but a quite large region in the normalized modified TC data. Again at first glance this may seem to offer support for the low frequency AMO oscillation, but there should be a number of cautions. The largest region of significance is in the rather dubious physical region of the graph whereby TC determines SSTC at rather long lead times of a decade or more.

An alternative complimentary method of examining the data is using wavelet coherence. Figure 5 shows that there are very slight differences between the TC" Normalized modified TC time series and the raw TC series.

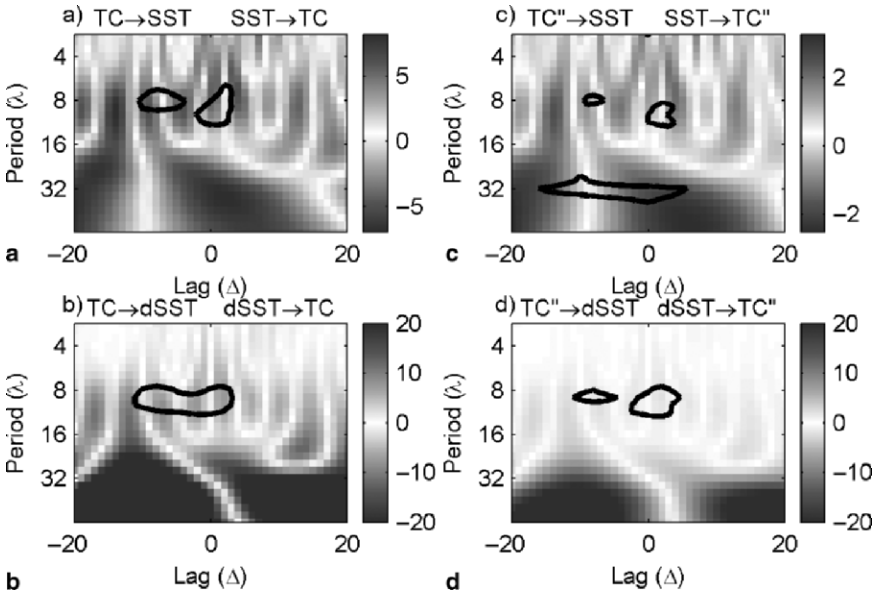

Fig. 4. Wavelet lag coherence plots showing: (**a**) TC sensitivity on SST_C ($W_Y(\rho,t+\Delta) = m\, W_X(\rho,t)$, *m* in number per °C is shown on the colour bar, as a function of Paul wavelet filtered period (ρ) and phase lag (Δ), solid black contour is 95% confidence interval of mean phase coherence (ρ) contours The arrow notation in Y→X etc. denotes that Y leads X in lag space. (**b**) TC and the d SST_C. (**c**) Normalized modified TC (TC") and SST_C and (**d**) TC" and the $dSST_C$

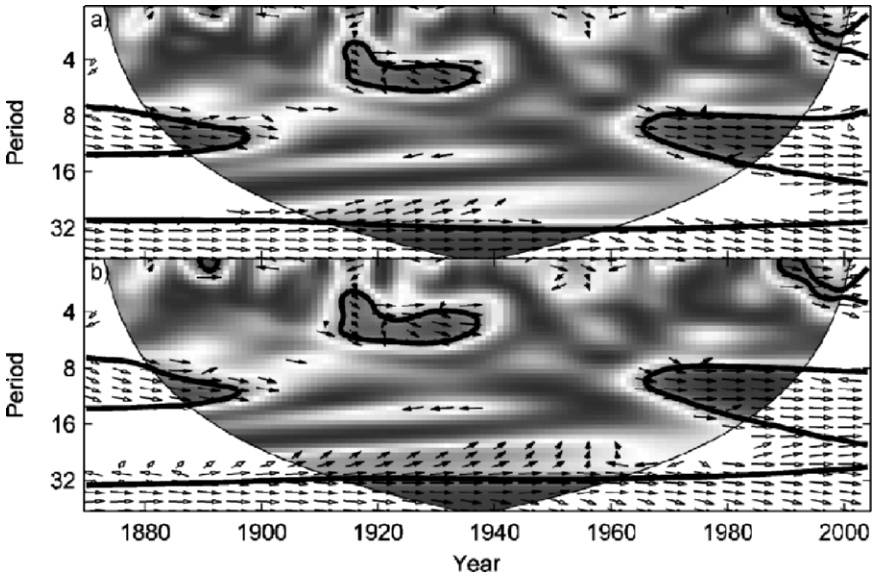

Fig. 5 (**a**) Squared wavelet coherence between SST_C and TC (dark high values, light low values). The 5% significance level against red noise is shown as a thick contour. The relative phase relationship is shown as arrows (with in-phase pointing right, anti-phase pointing left, and SST_C leading TC by 90° pointing straight down), the curved lines with no colouring delineate the region affected by data boundaries (Grinsted, Moore and Jevejeva, 2004); (**b**) As for (a) but with the Normalized modified TC and SST_C.

Snow Cover and Cyclones

It has been suggested that the large scale atmosphere is impacted by cyclone activity for some considerable period after the cyclone has dies away. This memory may be expected to manifest itself on seasonal snow cover in the Northern Hemisphere. We investigate this using the long series of snow cover estimates from Brown (2000). Figs. 6 and 7 show the behaviour of Northern Hemisphere spring snow coherence and sensitivity with TC and TC". Perhaps most surprising is that Fig. 6 shows that the relationship is basically in-phase, so that more spring snow implies greater numbers of TC. However, Fig. 7 shows that the relationship is not significant except at rather long positive and negative lags of about a decade. Particular mechanisms for interactions with snow cover have been proposed by Hart, Maue and Watson (2007). In particular they suggest that autumnal snow cover may be influenced by TC. Figs. 8 and 9 examine October snow cover extent 1922–1997 in Eurasia—time series for the whole Northern Hemisphere not being available. In contrast with Figs. 6 and 7, we see that the relationship is consistently anti-phase, with zero or small lag times, but significant only at decadal periods. Thus we see that the spring and autumn snow covers react in quite different ways. We also

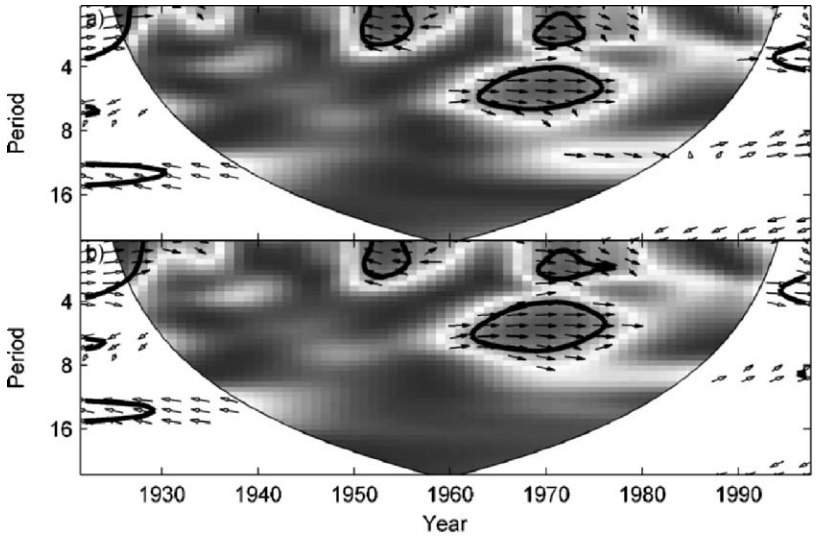

Fig. 6 (**a**) Squared wavelet coherence between Northern Hemisphere spring snow cover and TC. Contours and arrows as for Fig. 5. (**b**) coherence between Northern Hemisphere spring snow and TC"

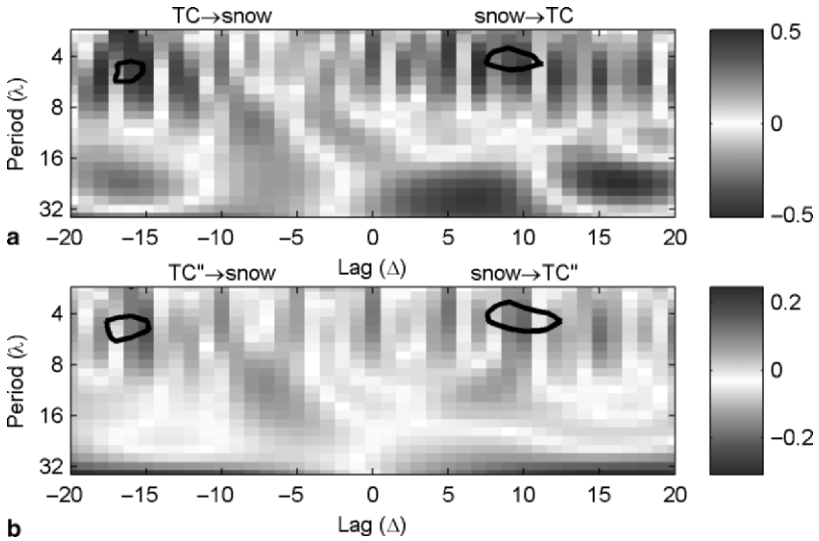

Fig. 7 (**a**) sensitivity of TC on Northern Hemisphere spring snow and (**b**) sensitivity of TC" on Northern Hemisphere spring snow. Contours and color bars as Fig. 4

tested the Eurasian spring snow cover relationship with TC (not shown here) and found the wavelet coherence to be very similar as for the Northern Hemisphere as a whole (see Fig. 6), but the lag coherence had no areas of significance.

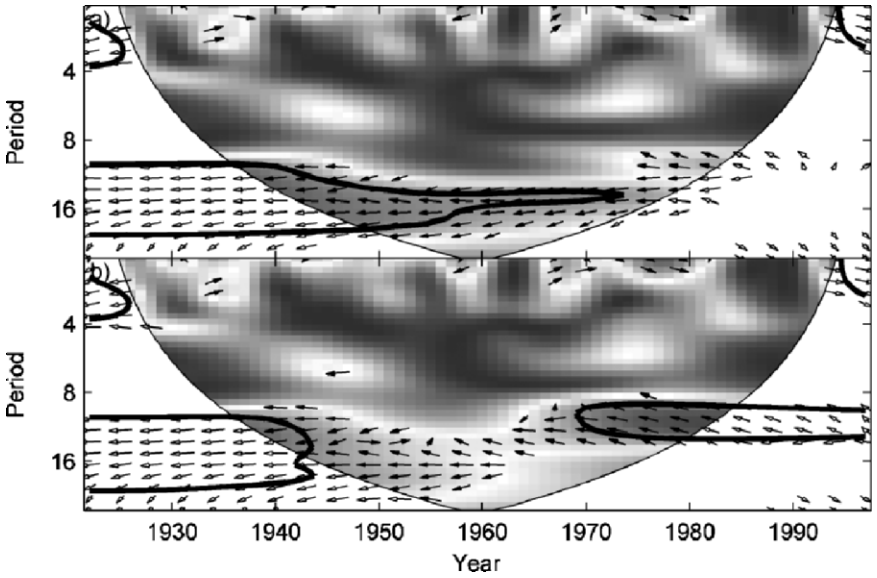

Fig. 8 As for fig. 5 but (**a**) TC and Eurasian autumn snow and (**b**) TC" and Eurasian autumn snow

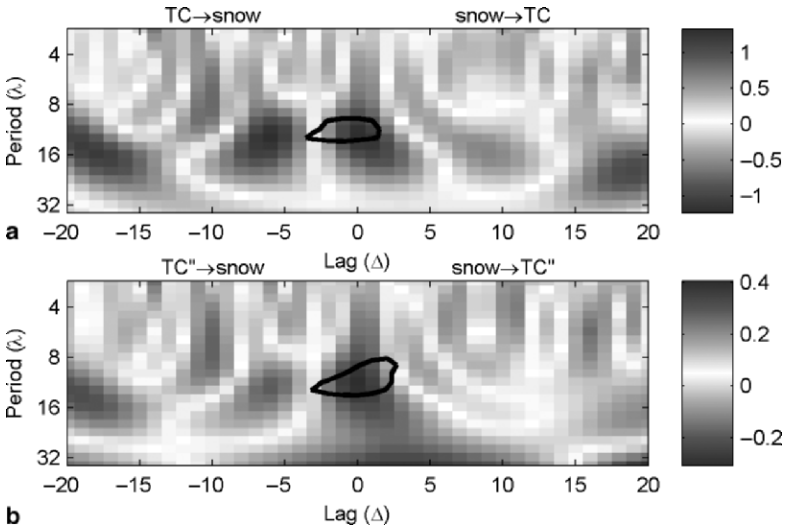

Fig. 9 As for Fig. 4 but (**a**) TC and Eurasian autumn snow and (**b**) TC" and Eurasian autumn snow

Discussion and Conclusions

TC Time Series and Statistical Testing

It has already been argued (Mann et al., 2007) that the modifications suggested by Landsea (2007) and others, do not affect the main results of trend and correlation analysis between SSTC and TC. We show quite clearly that this is also true of

analysis of the coherence and lag regressions of the modified time series, which even largely survive the gross manipulation of the time series to ensure complete Normality. One reason why the wavelet methods we use are not particular sensitive to the actual distribution of the data is that the Paul—and indeed most if not all wavelets, use more data points in their filter than required by simple Nyqust frequency considerations. This means that we smooth the data by a series of filters of different lengths. While the wavelet filters are infinitely long, the minimum scale used here is 2 which for the Paul wavelet of order 4 corresponds to a shortest period of about 2.8 years for annual data. The longer the filter, the more smoothed the data and the closer the distribution of data within that sample length will be to Normally distributed by the Central Limit Theory.

It has been suggested that our significance tests done on the wavelet data may be misinterpreted. That is small areas of significance at the 95% level could occur purely randomly some of the time, and so if the significant region is a small part of the whole figure, it may be there purely by chance. However this does not take into account that the tests are on phase relationships not measures of common power. Hence the significance will not be inflated simply by a few common bits of high power in the two series. This is borne out by testing of many series where we find absolutely no region of significant coherence regardless of how large the plot is made in lag-period space. The significance test uses the most conservative red noise model available, i.e. matching the original series mean, standard deviation and lag-1 autocorrelation, so the Monte Carlo common coherence thresholds found will be more conservative than simply random noise would give. This follows as red-noise that does not possess the same characteristics as the data would be less correlated with the data and hence provide a lower significance threshold in Monte Carlo testing than given by noise matching the data characteristics. However, since the procedure is essentially band pass filtering, the type of noise distribution is not very critical for significance testing. Similarly as the coherence is a phase matching rather than common power finding method, the relative power distribution is not important in frequency space. Therefore the actual noise model e.g. red noise auto regressive (AR1) or fractional Gaussian (self-similar scaling), is less important for significance testing than would be case for many other statistical methods.

TC Interaction with Snow Cover

The results presented in Figs. 6–9 are rather curious. The differences between spring and autumn snow cover are somewhat suggestive of the differences seen at 5 year and decadal periods in TC and SSTc which Moore, Grinsted and Jevrejeva (2008) interpreted by ENSO and Gulf Stream/NAO variability. The decadal power seen in autumn snow is consistent with the ideas suggested by Hart, Maue and Watson, 2007 regarding the extra-tropical impact of tropical cyclones. The larger the number of tropical cyclones, the less autumn snow cover appears to be logical

given the energy transport from tropics mediated by the cyclones. The surprising feature is that this effect is only apparent at decadal periods. This suggests a common causal factor with SSTc decadal variability (Figs. 4 and 5) ascribed to NAO/Gulf Stream variability at 7.8 years. NAO phase is known to strongly impact precipitation in Europe and the Middle East, so this observation is consistent with ideas that NAO plays a useful role in predicting TC. Positive NAO phase has been related to decreased sea level pressures (SLP) over the Arctic region - with a minimum over Iceland- and a northeastward extension of the Atlantic storm track to Greenland, Iceland, Norway and Barents Seas, causing major increases in cyclone activity in the area and thus increased heat flux over the region (Serreze et al., 1997; Alexandersson et al., 1998). Such situations enhance southerly warm winds over the western Nordic Seas, causing 1) compaction and reduced freezing in the ice margin (Vinje 2001), 2) warm air advection (Deser, Walsh and Timlin, 2000), and 3) enhanced flow of warm and saline Atlantic water (Grotefendt et al., 1998; Morison, Aagaard and Steele, 2000; Polyakov et al., 2004). Persistent positive NAO phase is predicted by climate models as a consequence of global warming (e.g. Gillett, Graf, and Osborn, 2003). Regardless of this, NAO relationships with Arctic environment are far from stationary. Surface air temperatures (SAT), SST, and SLP over the North Atlantic during the period 1873–2000 have alternated decades of strong negative with decades of strong positive correlations with NAO (Polyakova et al., 2006). Likewise, NAO and SAT records from Europe showed significant non-stationarities on decadal time-scales (Slonosky, Jones and Davies 2001). Suggested mechanisms for such non-stationarities are the co-occurrence or otherwise of several NAO-related SLP patterns (Maslanik et al., 200), or the planetary-scale SLP wave (Cavalieri, 2002).

The spring snow cover—in the northern hemisphere, but not in Eurasia, has significant common coherence with TC in the 5 year band. If this is an ENSO feature then it is entirely plausible given the impact of ENSO on the Pacific Decadal Oscillation (PDO) and the observed large impact that the PDO has on North American climate (Biondi, Gershunov, and Cayan, 2001). The long lags seen (Fig.7) may in fact be a reflection of the dominant bi-decadal periodicity of the PDO (Minobe, 1999) on the fundamental ENSO impact on TC that has been observed for many years (Gray, 1984; Moore Grinsted and Jevrejeva 2008.

Acknowledgments We thank the Finnish Academy, the Thule Institute and the Natural Environmental Research Council for financial support. An anonymous referee gave many valuable comments.

References

Alexandersson, H., T. Schmith, K. Iden, and H. Tuomenvirta, 1998: Long-term variations of the storm climate over NW Europe. *Global Ocean Atmos. Syst*., **6**, 97–120.

Biondi, F., A. Gershunov, and D.R. Cayan, 2001: North Pacific Decadal Climate Variability since 1661. *J. Clim.,* **14**, 5–10.

Brown, R.D., 2000: Northern Hemisphere snow cover variability and change, 1915–1997. *J. Clim.*, **13**, 2339–2355.

Cavalieri, D.J., 2002: A link between Fram Strait sea ice export and atmospheric planetary wave phase. *Geophysical Research Letters*, **29**(12), 1614, doi: 10.1029/2002GL014684.

Deser, C., J.E. Walsh, and M.S. Timlin, 2000: Arctic sea ice variability in the context of recent atmospheric circulation trends. *J. Clim.*, **13**, 617–633.

Dijkstra, H.A. and Ghil, M., 2005: Low-frequency variability of the large-scale ocean circulation: A dynamical systems approach. *Rev. Geophys.*, **43**, RG3002, doi:10.1029/2002RG000122.

Elsner, J.B., 2007: Granger causality and Atlantic hurricanes. *Tellus A,* **59**, 476, doi: 10.1111/j.1600-0870.2007.00244.x.

Elsner, T. H., and J. B. Jagger, 2006: Prediction models for annual U.S. hurricane counts. *J. Climate*, **19**, 2935–2952.

Elsner, J. B., A. B. Kara, and M. A. Owens, 1999: Fluctuations in North Atlantic hurricane frequency. *J. Climate*, **12**, 427–437.

Emanuel, K. A., 2005: Increasing destructiveness of tropical cyclones over the past 30 years. *Nature*, **436**, 686–688.

Gillett, N.P., H.F. Graf, and T. J. Osborn, 2003: Climate change and the North Atlantic Oscillation. *The North Atlantic Oscillation: Climatic Significance and Environmental Impact*, J.W. Hurrell, Y. Kushnir, G. Ottersen, and M. Visbeck, Eds., *Geophysical Monograph*, **134**, pp. 193–09.

Goldenberg, S. B., C. W. Landsea, A. M. Mestas-Nuñez and W. M. Gray, 2001: The Recent Increase in Atlantic Hurricane Activity: Causes and Implications. *Science*, **293**, 474–479.

Gray, W.M., 1984: Atlantic seasonal hurricane frequency. Part I: El Niño and 30 mb quasi-biennial oscillation influences. *Mon. Wea.Rev.*, **112**, 1649–1668.

Grinsted, A., J.C. Moore and S. Jevrejeva, 2004: Application of the cross wavelet transform and wavelet coherence to geophysical time series. *Nonlin. Proc. Geophys.,* **1**, 561–566.

Grotefendt, K., K. Logemann, D. Quadfasel, and S. Ronski, 1998: Is the Arctic Ocean warming? *J. Geophys. Res.*, **103**, 27679–27687.

Hart, R., R. Maue, and M. Watson, 2007: Estimating the atmospheric and SST memory of tropical cyclones through MPI anomaly evolution. *Mon. Wea. Rev.*, accepted April 2007, in press

Jarvinen, B.R., C. J. Neumann, and M.A.D. Davis 1984: A tropical cyclone data tape for the North Atlantic Basin, 1886–1983: Contents, limitations, and uses. *NOAA Tech. Memo., NWS NHC 22*. (Available at http://www.nhc.noaa.gov/tracks1851to2004_atl.txt.)

Jevrejeva, S., and J.C. Moore 2001: Singular Spectrum Analysis of Baltic Sea ice conditions and large- scale atmospheric patterns since 1708. *Geophys. Res. Lett*, **28**, 4503–4506.

Jevrejeva, S., J.C. Moore and A. Grinsted, 2003 Influence of the Arctic Oscillation and ENSO on Ice Conditions in the Baltic Sea: the Wavelet Approach. *J. Geophys. Res.,* 10.1029/2003JD003417.

Jevrejeva, S., J.C. Moore, and A. Grinsted, 2004: Oceanic and atmospheric transport of multi-year ENSO signatures to the polar regions. *Geophys. Res. Lett.*, **31**, L24210, doi:10.1029/2004GL020871.

Knutson, T.R., and R.E. Tuleya, 2004: Impact of CO2– induced warming on simulated hurricane intensity and precipitation: sensitivity to the choice of climate model and convective parameterization. *J. Clim.*, **17**, 3477–3495.

Landsea, C.W., 2005: Hurricanes and global warming. *Nature*, **438**, E11-13, doi:10.1038/nature04477.

Landsea, C.W., 2007: Counting Atlantic tropical cyclones back to 1900. *EOS,* **88**, 197–202.

Mann, M.E., K.A. Emanuel, G.J. Holland, and P.J. Webster, 2007: Atlantic tropical cyclones revisited. *EOS*, **88**, 349–350.

Maslanik, J., S. Drobot, C. Fowler, W. Emery, and R. Barry, 2007: On the Arctic climate paradox and the continuing role of atmospheric circulation in affecting sea ice conditions. *Geophys. Res. Lett.*, **34**, L03711, doi: 10.1029/2006GL028269.

Michaels, P.J., P.C. Knappenberger and R.E. Davis, 2006: Sea-surface temperatures and tropical cyclones in the Atlantic basin. *Geophys. Res. Lett.*, **33**, L09708, doi:10.1029/2006GL025757.

Minobe, S., 1999: Resonance in bidecadal and pentadecadal climate oscillations over the North Pacific: Role in climatic regime shifts. *Geophys. Res. Lett.,* **26**, 855–858.

Mokhov, I.I. and D.A. Smirnov, 2006: El Niño–Southern Oscillation drives North Atlantic Oscillation as revealed with nonlinear techniques from climatic indices. *Geophys. Res. Lett.*, **33**, L03708 10.1029/2005GL024557.

Moore, J.C., A. Grinsted, A., and S. Jevrejeva, 2007: Evidence from Wavelet Lag Coherence for Negligible Solar Forcing of Climate at Multi-year and Decadal Periods. *20 Years of Nonlinear Dynamics in Geosciences*, A. Tsonis & J.B. Elsner (Eds.), Springer.

Moore, J.C., A. Grinsted, A., and S. Jevrejeva, 2008: Gulf Stream and ENSO increasing the temperature sensitivity of Atlantic tropical cyclones. *J. Clim.* In press

Morison, J., K. Aagaard, and M. Steele, 2000: Recent Environmental Changes in the Arctic: A Review. *Arctic*, **53**, 359–371.

Moron, V., Vautard, R. and Ghil, M., 1998: Trends, interdecadal and interannual oscillations in global sea-surface temperatures. *Clim. Dyn.,* **14**, 545–569.

Polyakov, I.V., G.V. Alekseev, L.A. Timokhov, U. Bhatt, R.L. Colony, H.L. Simmons, D. Walsh, J.E. Walsh, and V.F. Zakharov, 2004: Variability of the intermediate Atlantic water of the Arctic Ocean over the last 100 years. *J. Clim.*, **17**, 4485–4497.

Polyakova, E.I., A.G. Journel, I.V. Polyakov, and U.S. Bhatt, 2006: Changing relationship between the North Atlantic Oscillation and key North Atlantic climate parameters. *Geophys. Res. Lett*., **33**, L03711, doi: 10.1029/2005GL024573.

Rayner, N.A., D.E. Parker, E.B. Horton, C.K. Folland, L., V. Alexander, D.P. Rowell, E.C. Kent, and A. Kaplan, 2003: Global analyses of sea surface temperature, sea ice, and night marine air temperature since the late nineteenth century. *J. Geophys. Res.,* **108**, 4407, doi:10.1029/2002JD002670.

Sabbatelli, T.A., and M.E. Mann, 2007: The influence of climate state variables on Atlantic Tropical Cyclone occurrence rates. *J. Geophys. Res*., **112**, doi:10.1029/2007JD008385.

Serreze, M.C., F. Carse, R. Barry, and J.C. Rogers, 1997: Icelandic Low cyclone activity: climatological features, linkages with the NAO, and relationships with recent changes in the Northern Hemisphere circulation. *J. Climate*, **10**, 453–464.

Slonosky, V.C., P.D. Jones, and T.D. Davies, 2001: Atmospheric circulation and surface temperature in Europe from the 18th century to 1995. *Int. J. Climatol*., **21**, 63–75.

Solow A. R., Moore L., 2000: Testing for a trend in a partially incomplete hurricane record. *J. Clim.*, **13**, 3696–3699.

Thompson, D.W.J. and J.M. Wallace, 1998:. The Arctic Oscillation signature in the winter geopotential height and temperature fields. *Geophys. Res. Lett*. **25**, 1297–1300.

Torrence, C. and G. P. Compo, 1998: A practical guide to wavelet analysis. *Bull. Am. Meteorol. Soc*., **79**, 61–78.

Vinje, T., 2001: Anomalies and trends of sea-ice extent and atmospheric circulation in the Nordic Seas during the period 1864–1998. *J. Clim.*, **14**, 255–267.

Wang, C., D.B. Enfield, S. Lee and C.W. Landsea, 2006: Influences of the Atlantic Warm Pool on Western Hemisphere Summer Rainfall and Atlantic Hurricanes. *J. Clim.* **19**, 3011–3028.

Network Analysis of U.S. Hurricanes

Emily A. Fogarty, James B. Elsner, Thomas H. Jagger, and Anastasios A. Tsonis

Abstract Hurricanes affecting the United States are examined with methods of network analysis. Network analysis is used in a variety of fields to study relational data, but has yet to be employed to study hurricane climatology. The present work is expository introducing network analysis and showing one way it can be applied to understand regional hurricane activity. The network links coastal locations (termed "nodes") with particular hurricanes (termed "links"). The topology of the network is examined using local and global measures. Results show that certain regions of the coast (like the state of Louisiana) have high occurrence rates, but not necessarily high values of connectivity. Regions with the highest values of connectivity include southwest Florida, northwest Florida, and North Carolina. Virginia, which has a relatively low occurrence rate, is centrally located in the network having a relatively high value of betweenness. Six conditional networks are constructed based on years of below and above average values of important climate variables. Significant differences in the connectivity of the network are noted between phases of the El Nino-Southern Oscillation.

Introduction

Hurricanes that make landfall in the United States pose a significant threat to life and property. The frequency and intensity of hurricanes at the coast has been studied extensively (Elsner and Kara 1999; Lyons 2004; Keim et al. 2007). In fact, over the long term the United States gets hit on average by one or two hurricanes per year. The strongest hurricanes (category three or higher on the Saffir-Simpson hurricane damage potentsial scale) occur less frequently, with the United States getting hit on average by three every five years. Studies have focused on how the frequency and intensity of coastal hurricanes fluctuate with climate variations (Gray et al. 1993; Lehmiller et al. 1997; Elsner and Jagger 2004; 2006).

J.B. Elsner and T.H. Jagger (eds.), *Hurricanes and Climate Change,*
doi: 10.1007/978-0-387-09410-6,

For instance, it is well known that pre-season values of the North Atlantic oscillation (NAO) portend the risk of hurricanes reaching the United States (Elsner and Jagger 2004). Results from these studies are important for quantifying the risk of a catastrophic hurricane.

While these studies are important for assessing the regional or local risk of a hurricane strike and how it varies with climate, they say nothing about the relationships of risk between regions or how such relationships change with climate variations. For instance, a hurricane moving out of the Caribbean Sea may affect more than one coastal region. Over the long run this introduces correlation between the frequencies of hurricanes at different locations. Knowing which regions tend to get hit in unison can help with risk assessment especially for those in the business of hurricane-related insurance.

Network analysis allows us to examine hurricane landfalls in a relational way. For instance how are Florida hurricanes related to Texas hurricanes, if at all? If every hurricane that strikes Florida goes on to strike Texas or North Carolina, then the risk of losses between Florida and elsewhere is correlated. This is important to know since insurance companies need to diversify their exposure over uncorrelated regions so as to minimize the impact of a single event on their book of business. It is our contention that interesting connections between coastal hurricane paths and climate analysis that have yet to be seen by more conventional approaches might be available through a network analysis.

Some previous studies have considered coastal hurricanes in a relational way. Elsner and Kara (1999) examined the occurrence of hurricanes that hit both Texas and Florida in a single season. They also looked at the occurrence of hurricanes hitting both Florida and North Carolina. They found that while the frequency of Florida to North Carolina hurricanes has remained rather constant, the frequency of Florida to Texas hurricanes decreased during the second half of the 20th century. However, there was no attempt to analyze the complete network of multiple landfalls. In studying typhoons affecting China, Fogarty et al. (2006) used a factor analysis model to understand the correlated risk between coastal provinces. They found that when hurricane activity is high in the southern provinces it tends to be low in the northern provinces and this seesaw in activity is related to the El Nino-Southern Oscillation (ENSO) phenomenon.

Network analysis offers a way to look at the correlated risk of hurricanes in a more direct and systematic way than these previous studies. Here we demonstrate one way network analysis can be applied to understand regional hurricane activity. This is the first such study of its kind so in section 2 we begin with an introduction to the basic ideas behind networks. Following this, in section 3, we examine the data on U.S. landfalls providing summary statistics and plots of frequency. In section 4 we show how to construct an adjacency matrix from an incidence matrix and show how the adjacency matrix leads to a network of landfalls. In section 5 we show how to compute local and global metrics associated with the topology of the network including the diameter and the prestige of individual nodes. In section 6 we examine how these metrics change with climate covariates including the NAO.

A Brief Introduction to Networks

Network analysis is the practical application of graph theory. Graph theory is the study of mathematical structures used to model pair-wise relations between objects. Networks (or graphs) have been constructed and studied for individuals, groups, transportation, or occurrences from a wide range of disciplines including computer science, biology, economics, political science, and sociology. In fact, an early application of network analysis was in the area of social interaction. Network analysis has recently been introduced into the study of climate by Tsonis et al. (2006; 2007). Because it is rather new to climatology and has not yet, to our knowledge, been applied to hurricanes, we begin with an introduction using concepts from social network analysis (Scott 1991; Wasserman and Faust 1994).

Consider authors publishing in the field of hurricane climatology. Authors can be represented as nodes with links to other authors established through a scientific citation. If author A is cited by authors B and C then a network is established between the authors. The connections between authors are called vertexes or nodes and the links connecting them are called edges. Figure 1 is a hypothetical example of a social network of authors linked by citation. If author B cites author A at least once then an arrow from B to A is drawn. If two authors cite each other a double arrow is used.

First note that the network is aspatial meaning that the absolute and relative positions of the nodes and links in the graph on the page are arbitrary. Instead what is important are the number of nodes and their linkages. Here our hypothetical network consists of 4 nodes and 5 links. The network is a concise way to examine relations. For instance the network shows that author A is cited by the three other authors so its node has the highest in-node value. While author A generates citations, he tends not to give them out. In contrast, author D is the only one that cites the other three authors so its node has the highest out-node value. Also author B does not cite author C and vice versa. But authors B and C are connected through authors A and D since B cites D who cites C and since B cites A who is cited by and cites C. This is an example of a directed graph since the links have arrows. In an undirected graph all links point both ways so no arrows are used. This is the case when the relationship between nodes is transitive. For example, if the network

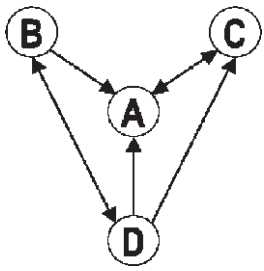

Fig. 1 Hypothetical social network of authors publishing in the field of hurricane climate. The authors (A, B, C, and D) are represented with circles (nodes) and the links indicating at least one citation are indicated with arrows

represents scientists who author papers and the links are co-authorships then all relations are transitive and the links do not have arrow heads.

The configuration of links among the network nodes reveals the network structure. A path connecting two nodes is a sequence of distinct nodes and links beginning with the first node and terminating with the last. For the example, above node B is connected to node C through A or through D, so that the path is BAC or BDC. If there is a path between two nodes then the nodes are said to be reachable. The length of the path is the number of links. So the length of the path from A to C is one and from B to C is two. However, another path from B to C is through A and D in which case the length between B and C is three. A shortest path between two nodes is called a geodesic. The diameter of the network is the length of the longest geodesic between all pairs of nodes in the graph. Therefore the maximum geodesic distance between any pair of nodes is the diameter. Interestingly, although the network is aspatial, many of the terms used in network analysis suggest spatial or geometric representations, including centrality, distance, isolation, and diameter.

U.S. Hurricanes

Our interest here is a network of hurricanes affecting the United States. First we take an exploratory look at the data that will be used in creating the network. A chronological list of all hurricanes that have affected the continental United States in the period 1851–2005, updated from Jarrell et al. (1992) is available from the U. S. National Oceanic and Atmospheric Administration (NOAA) at http://www.aoml.noaa.gov/hrd/hurdat/ushurrlist.htm. We use the May 2006 version of the data.

A hurricane is a tropical cyclone with maximum sustained (one-minute) 10 m winds of 65 kt (33 m/s) or greater. Hurricane landfall occurs when all or part of the storm's eye wall passes directly over the coast or adjacent barrier islands. Since the eye wall extends outward a radial distance of 50 km or more from the hurricane center, landfall may occur even in the case where the exact center of lowest pressure remains offshore. We also include hurricanes that do not make direct landfall, but produce hurricane-force winds at the coast. A hurricane can affect more than one region as hurricanes Andrew (1992) and Katrina (2005) did in striking southeast Florida and Louisiana.

Here it is assumed that the data on hurricanes affecting the United States are complete back to 1899, but less so in the interval 1851–1898. Since we are interested in multiple strikes rather than trends over time the fact that a few hurricanes may have been missed or that a few multiple hit storms are counted only as single hits will not materially influence the network.

The record contains 275 hurricanes affecting the United States in the period 1851–2005. Regions are divided along state lines from Texas to Maine, but Texas is further divided into south, central, and north Texas and Florida is further divided into four regions including northwest, southwest, southeast, and northeast Florida.

This gives a total of 23 non-overlapping regions. The state two-letter abbreviation is used. South, central, and north Texas are denoted ATX, BTX, and CTX, respectively. Northwest, southwest, southeast, and northeast Florida are denoted AFL, BFL, CFL, and DFL, respectively.

Figure 2 shows the frequency of hurricanes by region. The Gulf and Southeast coasts from Texas to North Carolina are affected most often by hurricanes. Within this high frequency zone, Louisiana, northwest Florida, and North Carolina have the most frequent hurricanes. Within the low frequency zone, the region from New York to Massachusetts has the largest frequency. We note that within Florida, the northeast coast has the fewest hurricanes and the northwest coast has most. It should be kept in mind that the regions used in this study do not have the same area or the same coastal exposure to hurricanes so it is not advisable to make anything more than broad generalizations of hurricane frequency. The frequency of major hurricanes (category three or higher) shows similar results (not shown) with most activity occurring in the region from Texas to North Carolina.

It is also interesting to consider the time variation in hurricane frequency. Figure 3 shows the cumulative sum of hurricanes by year for selected regions. Hurricane rates and how they fluctuate over time can be inferred directly by examining changes in slope on the cumulative sums. We see that the rate of hurricanes affecting Louisiana is rather constant over time as indicated by a nearly straight line cumulative sum, whereas the rate of hurricanes affecting southeast Florida is variable with activity appearing in clusters.

More relevant to the present work is the occurrence of years in which two different regions are affected by hurricanes. For example, Fig. 4 shows the cumulative sum of years in which both southeastern Florida and Louisiana were affect by hurricanes. Note that here the requirement is the both regions were affected in the same year, not necessarily by the same hurricane.

Again we see variations depending on regions. The overall rate of multiple hit years for Louisiana and southeast Florida is relative steady, whereas for northwest Florida and North Carolina the period from about 1875 through 1910 was quite active. Next we consider the relationship between regions affected by the same hurricane using the methods of network analysis.

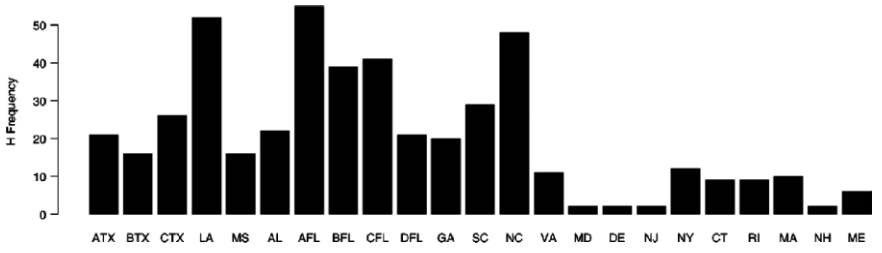

Fig. 2 Frequency of hurricanes affecting states from Texas to Maine. Texas is divided into 3 regions (south, central, and north) and Florida into four regions (northwest, southwest, southeast, and northeast)

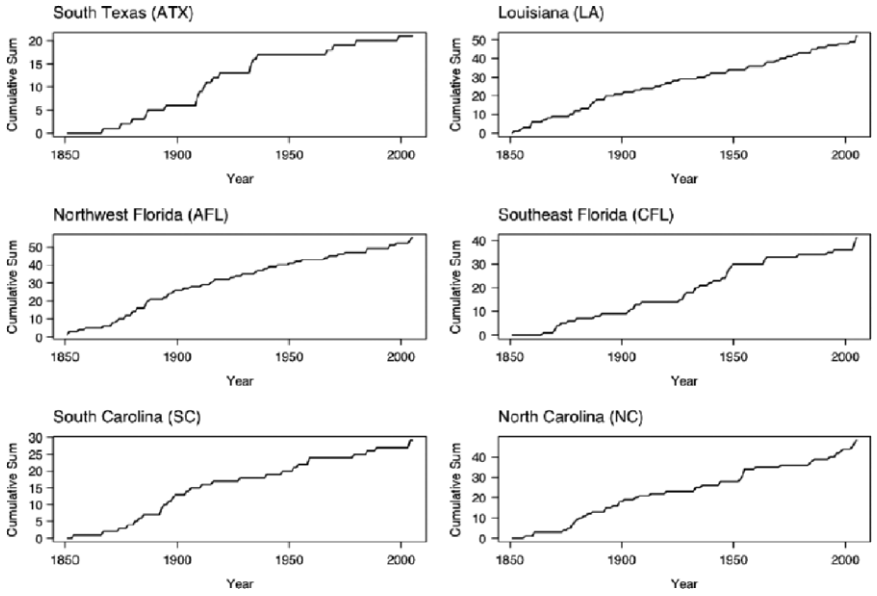

Fig. 3 Cumulative sum of hurricanes affecting selected regions along the U.S. coast

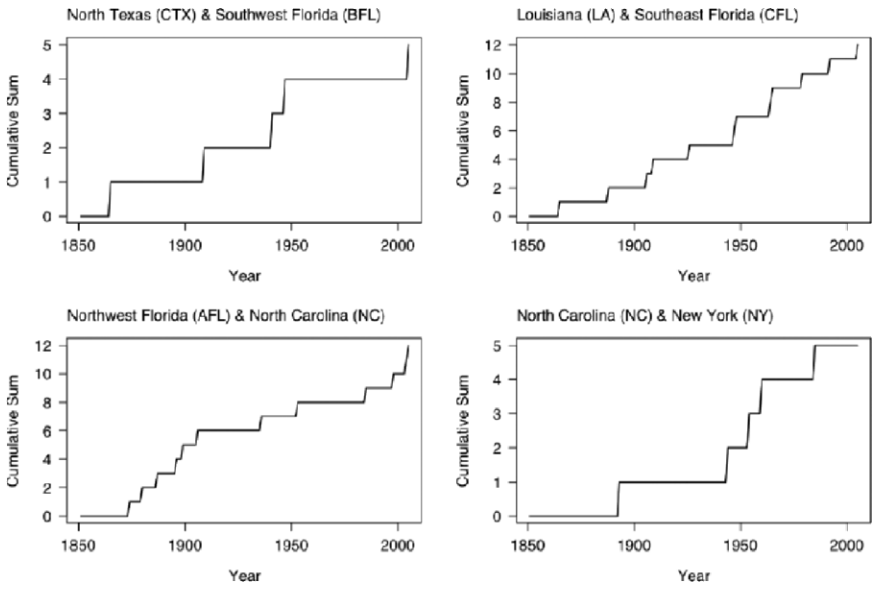

Fig. 4 Cumulative sum of years in which both regions where affected by a hurricane

A Network of U.S. Hurricanes

While the frequency of coastal hurricane activity is well documented, a systematic study of the relations of hurricanes affecting different regions has yet to be performed. Here we use network analysis to perform a systematic study of regional hurricane relations. As described in section 2, a network is graph connecting nodes. Here we consider a hurricane affecting a region as a node. If the hurricane affects more than one region then a link is drawn between nodes. The graph is undirected as the link between regions does not differentiate the time order of the regions affected.

Example

The network is constructed in three steps. In step 1, an incidence matrix is obtained that shows the occurrence of hurricanes by regions. In step 2 an adjacency matrix is computed from the incidence matrix using matrix algebra. In step 3, the network graph is drawn from the symmetry of the adjacency matrix. To see how this works, consider the following hypothetical table of hurricane occurrences. Hurricane 1 (H1) affected regions 1 (R1) and 3 (R3). Hurricane 2 (H2) affected regions 1 and 2, and so on. We therefore have a 4×5 (hurricanes $\times$ region) incidence matrix called X. Then a 5×5 adjacency matrix A (Table 2) is computed by pre-multiplying the incidence matrix by its transpose.

Table 1 A hypothetical incidence matrix consisting of 4 hurricanes and 5 regions. Hurricane 1 affected region 1 and 3, while hurricane 4 affected only region 1

	R1	R2	R3	R4	R5
H1	1	0	1	0	0
H2	1	1	0	0	1
H3	0	1	0	1	0
H4	1	0	0	0	0

Table 2 The adjacency matrix constructed from the hypothetical incidence matrix shown in Table 1. Here we see that region 1 is connected to regions 2, 3, and 5 since there was at least one hurricane to hit region 1 that went on to, or came from, these other regions. The diagonal elements of the matrix which consist of the frequency of hurricanes in each region are not used to construct the network

	R1	R2	R3	R4	R5
R1	–	1	1	0	1
R2	1	–	0	1	1
R3	1	0	–	0	0
R4	0	1	0	–	–
R5	1	1	0	0	–

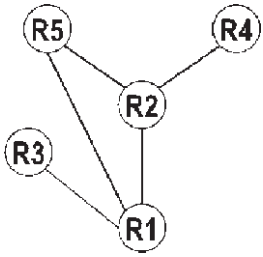

Fig. 5 Network graph based on the hypothetical set of hurricanes listed in Table 1. The network is constructed from the adjacency matrix shown in Table 2. Region 2 (R2) is connected to regions 1, 4, and 5

Note that the adjacency matrix is symmetric with the value in row R1 and column R2 matching the value in column R1 and row R2 and so on. The network is constructed directly from the adjacency matrix where values of 1 indicate a link between the regions. The diagonal values are ignored. Figure 5 shows a graph of the network. Regions 1 and 2 each have three links; region 5 has two links and regions 3 and 4 each have one link. As mentioned, since we do not distinguish the time order of hits, the links are undirected.

Full Network

The above example explains the steps we use to construct our U.S. hurricane network. Note that it is certainly possible to construct other networks with the same data, but here we limit ourselves to this straightforward approach. Figure 6 shows the incidence matrix, adjacency matrix, and network graph for the 275 hurricanes affecting the United States during the period 1851 through 2005. The incidence matrix has 275 rows and 23 columns while the adjacency matrix has dimensions 23 by 23. The network graph is plotted directly from the adjacency matrix. All the algebra, plots, and network analysis are done using the R language (R Development Core Team 2006).

The U.S. hurricane network shows the linkages between regions affected by the same hurricane. In small coastal states or regions a single hurricane can affect more than one region as is the case in the northeast. However, hurricanes affecting Florida frequently travel on to affect other non contiguous coastal regions.

As noted above, the network can be mapped in different ways. Figure 7 shows the U.S. hurricane network mapped onto a circle and onto the coastline. The circle map makes it easier to see the linkages resulting from traveling hurricanes. In particular we note relatively high number of links between northeastern Florida and the regions of New England.

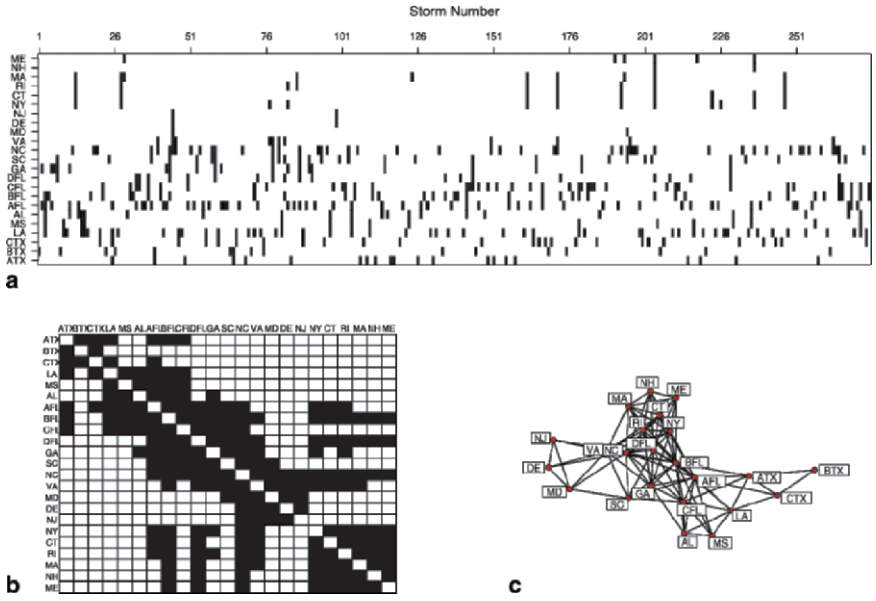

Fig. 6 Incidence matrix (**a**), adjacency matrix (**b**), and network (**c**) of U.S. hurricanes. The storm number in the incidence matrix refers to the consecutive list of hurricanes since 1851. The black squares in the adjacency matrix indicate regions connected by at least one hurricane

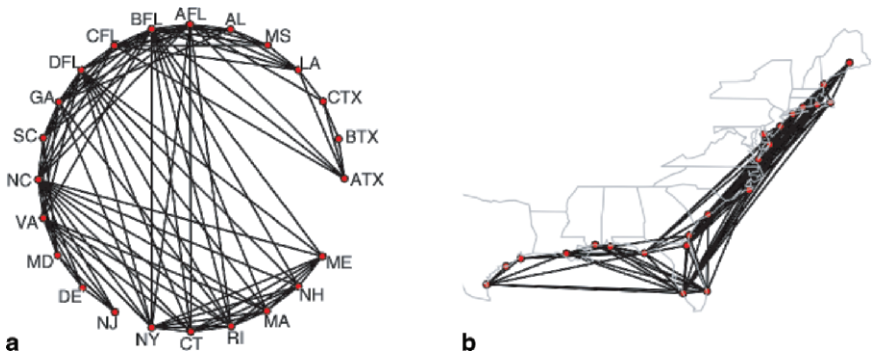

Fig. 7 The U.S. hurricane network mapped onto a circle (**a**) and onto the coastal geography (**b**)

Global and Local Metrics of the Network

Next we examine various structural properties (local and global) of the network. We use the R routines developed by Butts (2006) under the *sna* package and by Csardi (2007) under the *igraph* package. We consider three measures of nodal

centrality. Where centrality is loosely defined as being in the "middle" of the network. Middle nodes are nodes that are connected to many other nodes in the network. They are considered structurally important to the network. The three measures we consider are degree, closeness, and betweenness.

The "degree" (prestige) of a node (vertex) is its most basic structural property, the number of links (edges) connected to it. In the hurricane network the degree of the node is the number of regions that have been affected by a hurricane affecting the particular location. Figure 8 shows a bar plot of the nodal degree. Here we see that the south Texas node has degree of 6 since it is linked to 6 other regions including central Texas, north Texas, Louisiana, northwest Florida, southwest Florida, and southeast Florida. In comparison, the central Texas node has degree 2 being linked only to south and north Texas. Nodes with the largest degree include southwest Florida and North Carolina.

Paths through the network are the successive links between the nodes. One path from south Texas to Maine is constructed by starting in south Texas and following the link to northwest Florida. Since northwest Florida is linked to North Carolina, which is linked to Maine a path of length 3 links south Texas with Maine. The shortest path between any two nodes is called the geodesic. The shortest path between south Texas and Maine is 2 (through southwest Florida). A node's "closeness" provides an index for the extent to which it has short paths to all other nodes in the graph. Mathematically it is defined as

$$C_c(v) = \frac{|V(G)| - 1}{\Sigma_{i:i \neq v}\, d(v,i)}$$

where $d(i,j)$ is the geodesic distance between nodes i and j and $|V(G)|$ is the number of nodes in the network. Figure 9 shows the closeness by region.

Another important property of network nodes is called "betweenness." Betweenness is defined as the number of geodesic paths that pass through a node.

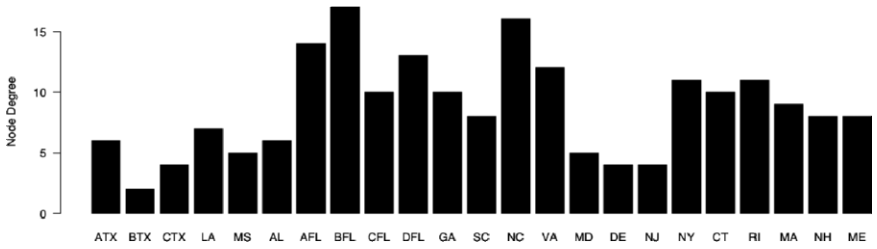

Fig. 8 Node degree. The node degree is the number of links connected to the node. Here the node degree represents the number of regions affected by hurricanes that have affected the particular region. For instance, south Texas (ATX) has degree 6 meaning that 6 other regions have been affected by hurricanes affecting south Texas

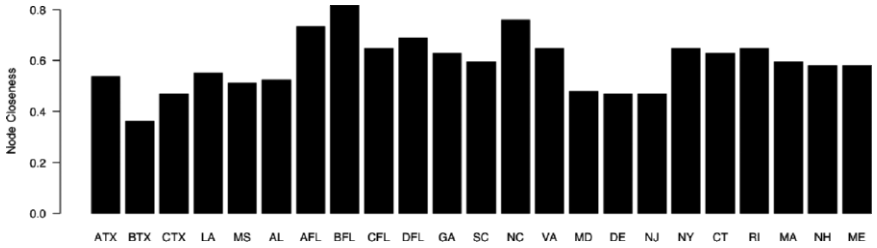

Fig. 9 Node closeness. The node closeness is an index that quantifies the number of paths through the node that are geodesics

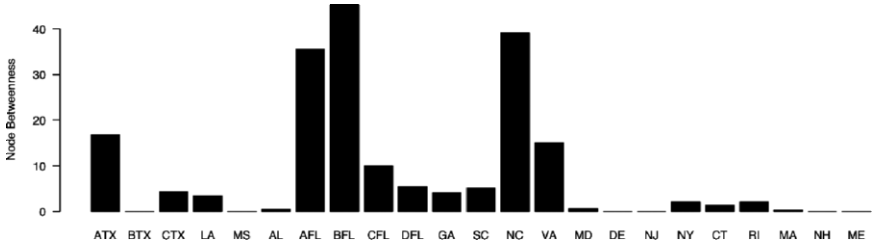

Fig. 10 Node betweenness. Node betweenness is defined as the number of geodesic paths that pass through a node

It is the number of "times" that any node needs to go through a given node to reach any other node by the shortest path. Conceptually, nodes with high betweenness lie on a large number of non-redundant shortest paths between other nodes; thus these nodes can thus be thought of as "bridges." A redundant path is one in which the path is traversed by more than one hurricane. Figure 10 shows betweenness values for each of the nodes in the hurricane network.

Global properties of the network may also be of interest. For instance, the diameter of the network can be defined as the maximum geodesic distance over the network. Here we find that this distance is 5 for the U.S. landfall network. Thus the maximum shortest path between any two nodes is 5 links. This path connects south Texas with New Hampshire and runs through central Texas, Alabama, New York, and Rhode Island. Note that these intermediate nodes tend to have small values of betweenness.

Another global property is the clustering coefficient. Returning to our example from section 2 where we considered the citation network of hurricane researchers, two authors are adjacent in the network if they site each other's work. Consider an author having two adjacent authors if these adjacent authors cite each other then we have a cluster or clique. The clustering coefficient of the entire network can be

defined as the probability that adjacent nodes of a node are connected. The clustering coefficient for the U.S. hurricane network is 0.46 indicating that slightly less than half of all regions that are linked to a specific region are also linked together.

Climate Conditioned Networks

It is interesting to consider how the hurricane network properties change with climate factors. Here we consider three variables that have been related to the frequency of U.S. hurricanes. The variables include an index of the North Atlantic Oscillation (NAO), an index of the El Nino-Southern Oscillation (ENSO), and North Atlantic ocean temperatures (SST). Ordered factors are created by consider whether a year is above or below the long term average based on seasonal averages of the variables. Six separate networks are constructed using only hurricanes from years that fall into the six factor groups.

NAO index values are calculated from sea level pressures at Gibraltar and at a station over southwest Iceland (Jones et al. 1997), and are obtained from the Climatic Research Unit. The values used here are an average over the pre- and early-hurricane season months of May and June and are available back to 1851. Units are standard deviations. These months are chosen as a compromise between signal strength and timing relative to the hurricane season. The signal-to-noise ratio in the NAO is largest during the boreal winter and spring (see Elsner et al. 2001), whereas the Atlantic hurricane season begins in June.

Values of the Southern Oscillation Index (SOI) are used as an indicator of ENSO. Although noisier than equatorial Pacific SSTs, values are available back to 1866. The SOI is defined as the normalized sea-level pressure difference between Tahiti and Darwin. The SOI is strongly anti-correlated with equatorial SSTs so that an El Nino warming event is associated with a negative SOI. Units are standard deviations. The relationship between ENSO and hurricane activity is strongest during the hurricane season, so we use an August through October average of the SOI for our covariate. The monthly SOI values are obtained from the Climatic Research Unit where they are calculated based on a method given in Ropelewski and Jones (1987).

The SST values are based on a blend of model values and interpolated observations, which are used to compute Atlantic SST anomalies north of the equator (Enfield et al. 2001). As with the SOI, we use August through October average of the SST anomalies as our covariate. The anomalies are computed by month using the climatological time period 1951–2000 and are available back to 1871. Units are degrees C. Values are obtained online from NOAA-CIRES Climate Diagnostics Center (CDC).

Table 3 summarizes the network properties conditional on each of the factors. We see that the hurricane network changes substantially between above and below phases of the ENSO. With below average values of the SOI characteristic of an El

Table 3 Network properties conditional on climate factors. The plus and minus indicate 1 standard error

	NAO		SOI		SST	
	Above	Below	Above	Below	Above	Below
Max Degree	16	16	16	11	16	14
Mean Degree	6.5 ± 0.95	6.4 ± 0.63	7.2 ± 0.98	4.8 ± 0.79	7.1 ± 0.86	5.6 ± 0.67
Max Betweenness	141 (BFL)	251 (NC)	94 (BFL)	73 (LA)	110 (NC)	134 (AFL)
Mean Betweenness	12.8 ± 6.4	22.3 ± 11.7	10.9 ± 4.4	13.3 ± 4.6	16.5 ± 6.6	14.5 ± 6.0
Connectedness	0.75	1.00	0.75	0.60	0.91	0.75

Nino event in the tropical Pacific, the mean nodal connectivity is 4.8 ± 0.79. This value is significantly less than the value of 7.2 ± 0.98 for the La Nina network of U.S. hurricanes. We also see more connectivity during warm SST years compared with cool SST years. The mean betweenness value during below average NAO years is higher largely due to the fact that North Carolina has a betweenness value of 251 compared with 9 during above average NAO years. The largest betweenness value during above average NAO years is 141 for southwest Florida. The connectedness which measures the fraction of all possible links over all nodes is highest for the below normal NAO and above normal SST and smallest for the below normal SOI.

Summary

Hurricane activity can have profound affects on lives and property along the coast. The frequency and intensity of hurricanes is the topic of much of the current research. Much less work has been done to understand the relationship of hurricanes across different regions. Here we examine the data on hurricanes that have affected the U.S. coast from a relational perspective using network theory. The tone of the chapter is expository since the analysis of climate data using networks is relatively new. In fact, the basics of networks are introduced using a hypothetical network of citations in the hurricane climate literature.

The primary analysis centers on the network of U.S. hurricanes. The network is created by considering hurricanes that have affected more than one coastal region. The regions are based on individual States, but Texas and Florida are further subdivided. The chapter describes how the adjacency matrix is derived from the incidence matrix and how a network is a graphical representation of the adjacency matrix. Graphical representations show ways to highlight different characteristics of the network.

The topology of the network is examined using various local and global metrics including degree, closeness, betweenness, diameter, and clustering coefficient. The degree quantifies the number of links between each node where a link between two

nodes is established if at least one hurricane affected both regions. Areas that are affected by hurricanes making multiple landfalls have high degree. Paths through the network are routes between nodes via the links. Closeness and betweenness quantify how many shortest paths go through each node. The diameter and clustering coefficient are global metrics and measure the maximum shortest path in the network and the probability that adjacent nodes are linked, respectively.

The question of how the topology changes with changing climate is considered by reconstructing networks based on three independent climate factors. It is found that the ENSO phenomenon in the equatorial Pacific has the most significant influence on the network. The present work represents a first step toward understanding relational aspects of hurricane activity using networks and how those relationships change under different climate scenarios. A next step might be to build prediction models of network structure based on pre-season climate conditions.

Acknowledgments Partial support for this study was provided by the National Science Foundation (ATM-0435628) and the Risk Prediction Initiative (RPI-05001). The views expressed within are those of the authors and do not reflect those of the funding agencies.

References

Butts, C.T., 2006: *The sna Package: Tools for Social Network Analysis*. R package version 1.4. http://erzuli.ss.uci.edu/R.stuff.

Csardi, G., 2007: *igraph: Routines for simple graphs, network analysis*. R package version 0.4.5. http://cneurocvs.rmki.kfki.hu/igraph.

Elsner, J.B., and A.B. Kara, 1999: *Hurricanes of the North Atlantic: Climate and Society*. Oxford University Press, 488 pp.

Elsner, J.B., and T.H. Jagger, 2004: A hierarchical Bayesian approach to seasonal hurricane modeling. *Journal of Climate*, **17**, 2813–2827.

Elsner, J.B., and T.H. Jagger, 2006: Prediction models for annual U.S. hurricane counts. *Journal of Climate*, **19**, 2935–2952.

Elsner, J.B., B.H. Bossak, and X.-F. Niu, 2001: Secular changes to the ENSO-U.S. hurricane relationship. *Geophysical Research Letters*, **28**, 4123–4126.

Enfield, D.B., A.M. Mestas-Nunez, and P.J. Trimble, 2001: The Atlantic multidecadal oscillation and it's relation to rainfall and river flows in the continental U.S. *Geophysical Research Letters*, **28**, 2077–2080.

Fogarty, E.A., J.B. Elsner, T.H. Jagger, K.-b. Liu, and K.-s. Louie, 2006: Variations in typhoon landfalls over China. *Advances in Atmospheric Sciences*, **23**, 665–677.

Gray, W.M., C.W. Landsea, P.W. Mielke Jr., and K.J. Berry, 1993: Predicting Atlantic basin seasonal tropical cyclone activity by 1 August. *Weather and Forecasting*, **8**, 73–86.

Jones, P.D., T. Jonsson, and D. Wheeler, 1997: Extension to the North Atlantic Oscillation using early instrumental pressure observations from Gibraltar and South-West Iceland. *International Journal of Climatology*, **17**, 1433–1450.

Keim, B.D., R.A. Muller, and G.W. Stone, 2007: Spatiotemporal patterns and return periods of tropical storm and hurricane strikes from Texas to Maine. *Journal of Climate*, **20**, 3498–3509.

Lehmiller, G.S., T.B. Kimberlain, and J.B. Elsner, 1997: Seasonal prediction models for North Atlantic basin hurricane location. *Monthly Weather Review*, **125**, 1780–1791.

Lyons, S.W., 2004: U.S. tropical cyclone landfall variability: 1950–2002: *Weather and Forecasting*, **19**, 473–480.

R Development Core Team, 2006: *R: A Language and Environment for Statistical Computing*, R Foundation for Statistical Computing, Vienna, Austria, ISBN 3–900051-07–0, http://www.R-project.org.

Ropelewski, C.F., and P.D. Jones, 1987: An extension of the Tahiti-Darwin Southern Oscillation Index. *Monthly Weather Review*, **115**, 2161–2165.

Scott, J., 1991: *Social Network Analysis*. SAGE Publications, 224 pp.

Simpson, R.H., and M. Lawrence, 1971: Atlantic hurricane frequencies along the United States Coastline. NOAA Tech. Memo. NWS-SR-58, 14 pp.

Tsonis, A.A., K.L. Swanson, and P.J. Roebber, 2006: What do networks have to do with climate? *Bulletin of the American Meteorological Society*, **87**, 585–595.

Tsonis, A.A., K.L. Swanson, and S. Kravtsov, 2007: A new dynamical mechanism for major climate shifts. *Geophysical Research Letters*, **34**, L13705, doi:10.1029/2007GL030288.

Wasserman, S., and K. Faust, 1994: *Social Network Analysis: Methods and Applications*. Cambridge University Press, 857 pp.

Migration of the Tropical Cyclone Zone Throughout the Holocene

Terrence A. McCloskey and Jason T. Knowles

Abstract This paper proposes that a combination of short and long term atmospheric oscillations have resulted in latitudinal movement of the tropical cyclone (TC) zone and location of landfall through the Holocene. A GIS-based approach demonstrates that currently intensity changes of the Bermuda High (BH) result in a large latitudinal spread of TC track and landfall location across the western North Atlantic (NA), while a literature-based examination of paleoclimatic evidence supports the view that long-term changes in the pole-equator temperature gradient has resulted in significant latitudinal migration of the general NA atmospheric system throughout the Holocene, with a heightened (reduced) gradient moving the entire system southward (northward).

Our model suggests that the location of hurricane landfall since the mid Holocene is controlled by a millennial scale migration of the hurricane **zone** (paralleling latitudinal movement of the entire system), complicated by the superimposition of a higher frequency variation in **track** location, (controlled by intensity oscillations). The resulting millennial scale shifts in landfall location of major hurricanes are hindcast, and methods for testing this hypothesis are described.

Introduction

The damage hurricanes inflicted upon the Caribbean and the United States during the 2004 and 2005 seasons dramatically demonstrate the societal importance of changes in tropical cyclone (TC) tracks and frequencies. The increase in coastal development that occurred during the relatively inactive TC regime that existed during the 1970s, 80s and early 90s has contributed to the mounting property losses and death toll that ensued following the return to a more active TC regime, beginning in 1995 (Pielke and Landsea 1998). Clearly, an increased understanding of the causes of these spatial/temporal oscillations is critical to achieving an effective response to this natural hazard. The proximate cause(s) of these shifts, which occur across a variety of scales, from interannual to millennial (Reading 1990; Walsh and Reading 1991; Liu and Fearn 2000; Elsner et al. 2000), are not

J.B. Elsner and T.H. Jagger (eds.), *Hurricanes and Climate Change,*
doi: 10.1007/978-0-387-09410-6,

well understood. This paper attempts to identify the average latitudinal position of the Intertropical Convergence Zone (ITCZ) as an important primary control over the location of the TC zone.

It should be noted that the correlation between the ITCZ and the TC zone is expected to manifest itself more clearly over longer (millennial) time scales, with the shorter term correspondence masked by "noisy" higher frequency atmospheric oscillations. Connecting the frequency/track pattern shifts to larger, better understood, and more easily tracked features of the general circulation system may lead not only to an improved understanding of the relationship between TC and climate, but also to improved coastal management.

In this paper we first explore the present relationship between various components of the North Atlantic (NA) atmospheric circulation system and NA TCs. We use a GIS-based approach to demonstrate a consistent relationship between circulation features and TCs, identifying TCs as a integrated feature of the larger system. We then use a literature-based approach to examine the structural stability of the NA circulation system over millennial timescales, focusing on the spatial relationship between the Bermuda High (BH) and the ITCZ, and examine evidence for long-term movement of this system. The effects of such movement on major hurricane landfall since the mid Holocene are explored.

Data

Storm track data were downloaded from the National Oceanic and Atmospheric and Administration (NOAA) best-track dataset (HURDAT) (http://hurricane.csc.noaa.gov/hurricanes/index.html) and imported into a geographic information system (GIS). In order to minimize the use of less reliable (pre-aircraft reconnaissance) data, our investigation covers the period 1948–2003. Two North Atlantic Oscillation (NAO) indices were used. The standard index (http://www.cru.uea.ac.uk/cru/data/nao.htm), which we refer to as NAO, is based on the normalized sea level pressures (SLP) between two fixed locations (normally southwest Iceland and the subtropical eastern NA). A second index, referred to here as NAO-mobile, calculates the NAO index values as the difference in normalized SLP anomalies at the locations of maximum negative correlation between the subtropical and subpolar North Atlantic (Portis et al. 2001). By being normalized both indices are dimensionless. Monthly and annual values from both NAO indices were added to the storm vectors database.

Three data sets were then created, 1. "Tropical Cyclones", including all vectors of all storms; 2. "Hurricanes", which included all vectors of all storms whose wind speed exceeded 74 mph at any point during the storm's lifetime, and 3. "Major Hurricanes", which included all vectors of all storms whose wind speed exceeded 111 mph at any point, corresponding to category 3 storms or greater on the Saffir-Simpson scale.

Using geoprocessing techniques the center of each 6 hr storm vector was converted to a point coverage in order to apply kernel density surface interpolation, which is a technique that generalizes individual point locations or events, *si*, to an entire area and provides density estimates, *ë^ (s)*, at any location within the study region (Bailey and Gatrell, 1995). For a more detailed description of the methodology and different visualization results, see Knowles and Leitner (2007).

Current Seasonal Variations in the NA Circulation System

As is well known, the NA circulation system basically consists of a series of latitudinally adjacent belts, starting near the equator with the ITCZ, and proceeding poleward through the trade wind belt, the Subtropical High Pressure Ridge, characterized by the Bermuda High (BH), the zone of midlatitude westerlies, the high latitude low pressure belt characterized by the Icelandic Low (IL), and the Polar High. These components exhibit an annual latitudinal migration, following the apparent annual solar movement. In the boreal winter these components drift southward, moving the BH and its zone of subsiding air equatorward (Hastenrath 1966; Sahsamanoglou 1990; Davis et al. 1997; Machel et al. 1998; Portis et al. 2001). In the Caribbean and Central America this results in frequent atmospheric inversions, increased trade wind strength and generally dry conditions, (i.e. the annual December to May dry season) (Hastenrath 1966; Trewartha 1981). Around June, when the ITCZ approaches from the south, the BH and the associated zone of subsiding air moves north out of the Caribbean, resulting in uplift, condensation, precipitation, and the region's annual wet season (Hastenrath 1966; Trewartha 1981; Sahsamanoglou 1990; Davis et al. 1997; Portis et al. 2001).

From May to November TCs form between the ITCZ and the BH, with cyclogenesis being dependent upon the same general conditions as regular rainfall, in addition to certain additional requirements, such as a threshold sea surface temperatures (SST), low vertical shear, an existing disturbance and high relative humidity in middle troposphere. TCs typically form in a narrow band off the west coast of Africa, with the Main Development Region (MDR), between 10 and 20°N, accounting for 60% of all TC and 85% of major hurricanes (Goldenberg and Shapiro 1996, Goldenberg et al. 2001). TCs then drift westward, spreading latitudinally, their track and eventual location of landfall (if any) controlled by a variety of transient meteorological factors. A spatially separate set of TCs forms in the western Caribbean and the Gulf of Mexico. The southern limit of TC activity is determined by a threshold level of vorticity generated by the Coriolis effect. This limit occurs around 8°N (Elsner and Kara 1999), meaning that the zone of TC formation consists of the area lying between 8°N and the subtropical high pressure ridge, although the latitude of track movement and landfall covers a much larger range.

Spatial Relationships Between Circulation Features

Short Term

The central node of the NA subtropical high-pressure ridge is referred to as either the BH or the Azores High, which, though displaying some differences in the winter are basically interchangeable during the summer months (Davis et al., 1997). Here we use the term BH. Being a high pressure system the BH rotates clockwise, spinning the northeasterly trade winds off its southern flank and the midlatitude westerlies to the north. Although the BH is a well-recognized atmospheric phenomenon, it remains a rather nebulous entity, defined in a number of ways (Shasamangolou 1990; Davis et al. 1997; Portis et al. 2001). The effect of the BH is most readily quantified by the NAO Index, which is the normalized difference, measured at a number of different locations, between the SLP below the BH and the IL (Hurrell 1995; Jones et al. 1997; Portis et al. 2001). The BH and IL generally behave in a "see-saw" manner, with high BH pressure intensity values correlating with low IL values, which coincides with large/positive NAO Index values and is referred to as a "strong" NAO; while low BH values generally correlate with high IL pressure intensity values, resulting in a "weak" NAO, with small/negative NAO Index values (Elsner et al. 2000). Because a more intense BH generally correlates to a northeastern position and a weaker BH to a southwestern position (Shasmangolou 1990; Machel et al. 1998), a "strong" NAO generally means a northeastern position of the BH, and a "weak" NAO a southwestern one.

Stronger NAO values, driven by the intensification of the BH, and the increased pressure gradient between the BH and IL, generally increase the intensity of the trade winds to the south and the midlatitude westerlies to the north, significantly impacting weather in the circum-NA region (Hurrell 1995; Kapala et al. 1998; Machel et al. 1998; Nyberg et al. 2001; Visbeck et al. 2001). Wind strength exerts an important control over SST, as increased surface winds increase heat transfer from the ocean to the atmosphere, lowering SST in the affected area (Hasanean 2004; Chiang and Bitz, 2005; Chiang, 2006). The strength of the trade winds also affects TC, by the effects on both SST and vertical shear.

Because NAO intensity is such a key feature of the NA circulation system the NAO index is more useful than the record of the central intensity of the BH in understanding the relationships between different components of the system.

That a close positive geographical relationship exists between the BH and TCs is demonstrated by a roughly tandem movement of TC tracks and the BH throughout the hurricane season, as they move first northeastward, before returning to the southwest in the fall.

The BH also operates as an important control over the steering of TC tracks, and consequently, for location of landfall. Elsner et al. (2000) show a direct relationship between NAO values and latitudinal position of landfalls for major hurricanes making landfall along the US coastline since 1865. Using bootstrap analysis they show statistically significant differences between the July NAO values for years with

at least one major hurricane strike along the Gulf Coast (south) and Atlantic Coast (north), with lower NAO values for the Gulf Coast strike years (Elsner et al. 2000).

Using the NOAA dataset (Neumann et al. 1999) for the period 1948–2003, we visually selected the 9 extreme years each for the most eastern and western group of TC tracks, and applied a kernel density surface interpolation to display their geographical distribution (Fig. 1). A calculation of the average annual NAO index values shows negative values for the extreme western track years and positive values for the extreme eastern years, for both the NAO and NAO-mobile indices. Annual NAO values were used due to the influence that a strong winter NAO can have on SST during the following TC season.

Using a data set consisting of all 6 hour segments for all TC for the period, we queried out all TC segments by monthly NAO value, forming two groups

1. All segments which occurred during periods of "Extreme High" NAO ($>2.5\ \sigma$)
2. All segments which occurred during periods of "Extreme Low" NAO ($<-2.5\ \sigma$)

Kernel density surface interpolations were applied to each group, after which the "Extreme Low" kernel density values were subtracted from the "Extreme High" kernel density values and the resulting differences plotted (Fig. 2). In this figure light gray shading represents negative values, indicating areas experiencing more

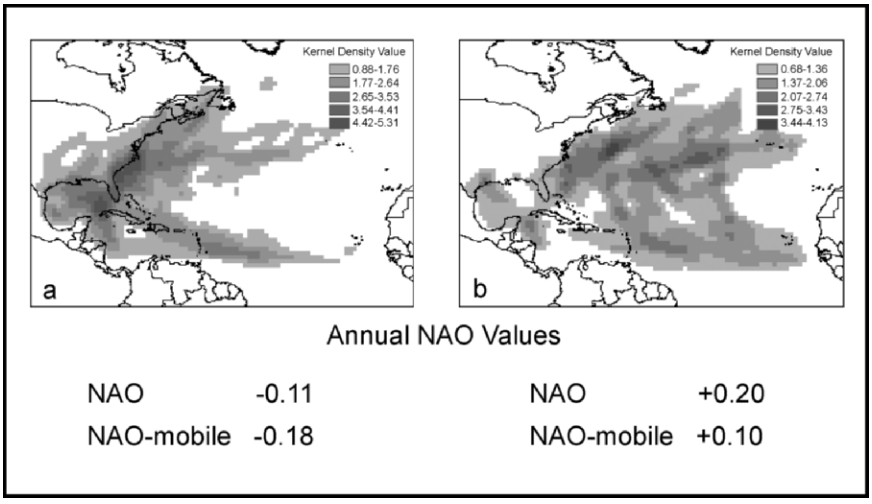

Fig. 1 Interannual variability in TC track location displayed as kernel density surface interpolation, a technique that generalizes individual point locations or events to an entire area and provides density estimates at any location within the study region. Density estimates were derived by placing a symmetrical surface (195 miles bandwidth), over each event and are displayed according to the resulting kernel density value. (**a**) all TC tracks for the 9 years visually selected as having the westernmost track location for the period 1948–2003, (**b**) the same for the 9 easternmost years. The average annual NAO Index value for the 9 westernmost years are –0.11 (data from http://www.cru.uea.ac.uk/cru/data/nao.htm), and –0.18 (data from Portis et al., 2001); for the 9 easternmost years the corresponding values are 0.20 and 0.10

TCs during periods of extreme low than extreme high NAO values, while dark gray areas indicate the reverse. Perhaps the most noticeable feature of this figure is the semicircular dark gray pattern over the western Atlantic, indicating the severe recurvature of TC paths connected with high NAO values. In contrast, the light gray areas form a more horizontal band, indicating a reduced tendency to curve northeastward during periods of low NAO values. A slight northward shift of TC tracks during high NAO values is also noticeable, with the horizontal light gray band covering extreme northern South America and southern Central America indicating that the most southern tracks occur mainly during periods of low NAO values.

Figure 3 maps the geographical distribution of the TC segments occurring during extreme NAO conditions. This figure, a three dimensional surface representation based on the kernel density values of TC incidence, facilitates the visualization of the transformation of the BH from a weak horizontal trough during periods of extreme low NAO ($<-2.5\ \sigma$) (Fig. 3a) to a strong circular depression translated to the northeast during periods of extreme high NAO ($>2.5\ \sigma$) (Fig. 3b). Note the similarity in shape and spatial placement between the extreme low/extreme high surface figures here and the extreme west/extreme east tracks in Fig. 1.

Kernel density analysis on all three storm groupings (TC, hurricanes, and major hurricanes) for the period 1948–2003 (Fig. 4) records a similar pattern in all three cases; namely a westward path occurs across the Atlantic from approximately the Cape Verde islands. Northeast of the Greater Antilles the pathway bifurcates, resulting in two distinct track paths recurving to the northeast. A separate cluster

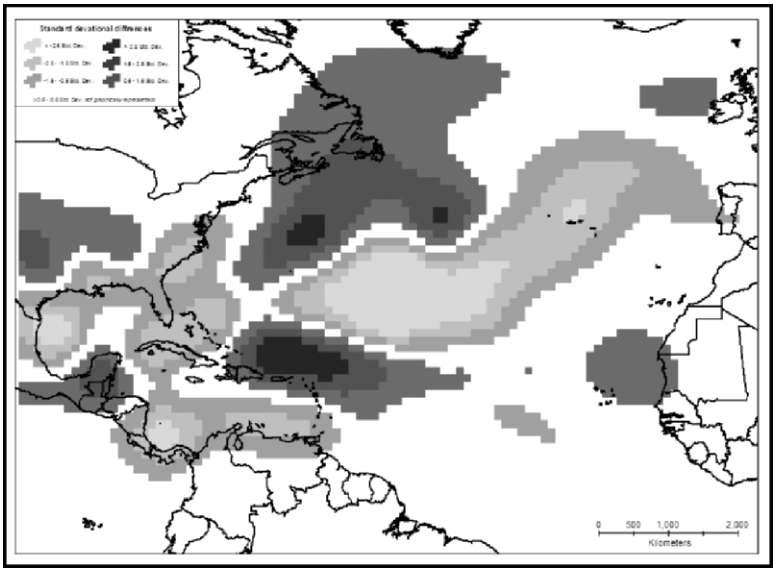

Fig. 2 Plot of kernel density values of TC tracks occurring during extreme low ($<-2.5\ \sigma$) NAO months subtracted from kernel density values of TC tracks occurring during extreme high ($>2.5\ \sigma$) NAO months for the period 1948–2003. Interpolation is by a 100 km bandwidth kernel density. Light gray shadings represent negative values, dark gray shadings represent positive values

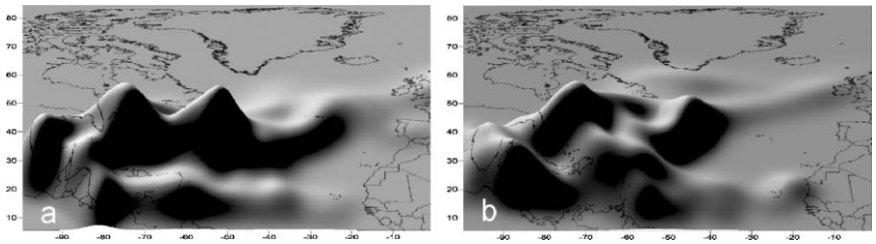

Fig. 3 Three dimensional surface representation based on the kernel density values of occurrence incidence of all six hour storm tracks for the period 1948–2000 that occurred during periods of (**a**) extreme low (<−2.5 σ), (**b**) extreme high (>+2.5 σ) NAO. Note that the center hollow, presumably representing the BH which the TC travel around, and not through, changes from a weak horizontal trough during extreme low NAO Index values to a strong circular depression during extreme high value, while moving to the northeast

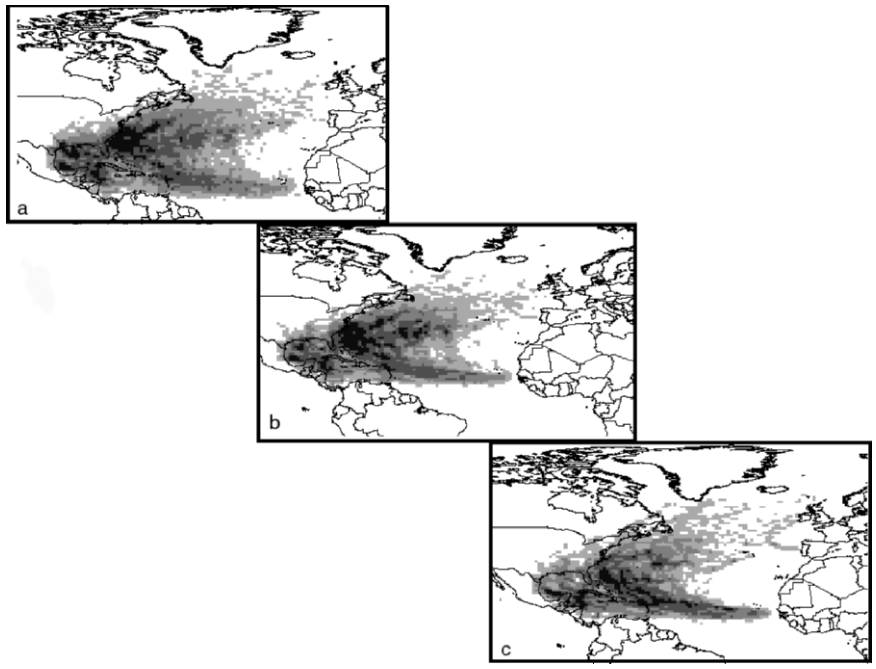

Fig. 4 Kernel density surface interpolation of all (**a**) TC, (**b**) Hurricanes, (**c**) Major Hurricane track sections for the period 1948–2003

of tracks is found in the Western Caribbean and Gulf of Mexico. The bifurcation of the Cape Verde hurricane tracks supports the idea of the bimodal influence the BH exerts over TC paths, related to NAO values. Presumably the distinct western cluster records the Western Caribbean hurricanes.

This preliminary analysis indicates that on an inter-annual basis the strength/position of the BH (as proxied by NAO values) exerts significant control over the

location of TC tracks as well as the location of hurricane landfall, as suggested by Elsner et al. (2000). Low NAO values (southwestern BH positions) correspond to less recurved, southern tracks, and high NAO values (northeastern BH positions) correspond to increased recurvature and more northern tracks.

The relationship between TCs and the NA circulation system extends beyond interactions with the BH. Bell and Chelliah (2006) show that for the period 1950–2004, hurricane activity is tightly linked to the general NA circulation system through a coherent set of interrelated atmospheric and oceanic features, including SST, West African rainfall, and overall climate variability in the tropics. An enhanced NAO results in strengthened trade winds (Nyberg et al. 2001), which correlates to reduced NA SST between 45-65°N (Black et al. 1999) and enhanced vertical wind shear in the MDR (Nyberg et al. 2007). In turn, a statistically significant correlation exists between these features and hurricane activity (Nyberg et al. 2007). This indicates that TCs are an integral and interconnected component of the larger NA circulation system.

Long Term

BH/TC

Sedimentary evidence indicates that the control the BH currently exerts over TCs operates over longer scales as well. Liu and Fearn (2000) have identified a period of hyperactivity on the northern Gulf coast (Louisiana-Florida), for the period 3400–1000 ^{14}C yr BP., with periods of reduced activity before and after. They suggest millennial-scale positional movement of the BH as the proximate cause of this oscillation in frequency of landfall, with positions to the southwest funneling storms into the Gulf of Mexico and positions to the northeast pushing the tracks along the Atlantic Coast. This implies an anti-phase relationship between the frequency of strike activity between the Gulf and Atlantic Coasts, supported by results from an Atlantic Coast paleotempestology study (Scott et al. 2003). The timing of the posited movements of the BH is supported by proxy paleoenvironmental data (Hodell et al. 1991), based on the premise that long-term residency of the BH over an area results in increased aridity.

ITCZ-BH

The long-term (centennial to millennial-scale) relationship between these two features may be more direct than the short-term, with the longer-term average annual latitude of both less affected by “noisy” short-term conditions. For both features the principal latitudinal control seems to be the pole-equator temperature gradient, with a steeper gradient resulting in a southern movement. For the BH this relationship is demonstrated by Fig. 5 (modified from Flohn 1984), based on the

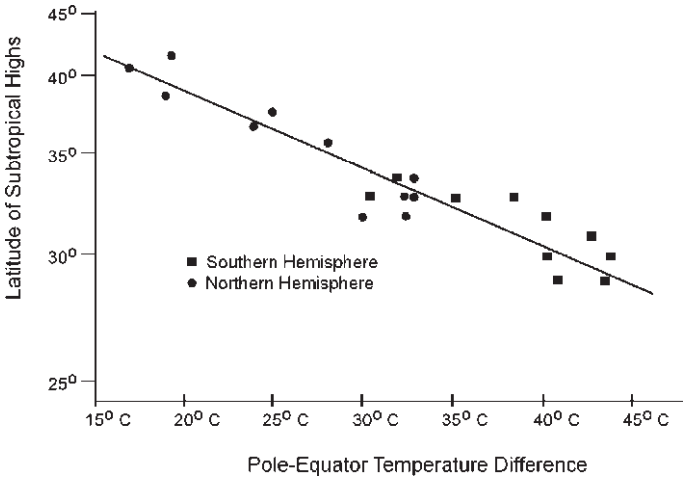

Fig. 5 Latitude of subtropical high pressure ridge versus Pole-Equator temperature difference, by month (modified from Flohn, 1984)

monthly average positions of the subtropical highs and the pole-equator temperature difference at the 300/700 mb layer. Since this gradient is primarily dependent upon polar temperatures (there being less variation in equatorial temperatures), warm (cold) periods tend to move the BH to the north (south). Flohn (1984) estimates that an increase in the average annual Arctic temperature of 7°C moves the average BH latitude 100–200 km northward in summer and 800 km northward in winter. Empirical evidence for this relationship also exists; as early as Lamb's (1977) estimation of a paleolatitudinal record for the BH based on palynological and vegetational boundary displacement and marine microfaunal analysis evidence found significant northward (southward) shifts paralleling overall hemispheric heating (cooling).

Much evidence, on a variety of time scales, supports temperature-driven movement of the ITCZ. Modeling studies simulating polar ice cover at the Last Glacial Maximum (LGM) support a southern movement of the ITCZ (Chiang et al. 2003; Chiang and Bitz 2005), with the increased pole-equator temperature gradient resulting in a 6° southern displacement of the ITCZ (Broccoli et al. 2006). Similar long-term temperature-driven movement of the ITCZ has occurred in both the equatorial Indian Ocean (Tiwari et al. 2006 and the eastern Pacific (Koutavasa and Lynch-Stieglitz 2004). Paleoclimatic evidence includes shifts in South American precipitation paralleling ITCZ movement, as recorded by Andean ice cores (Thompson et al. 2000), speleothems and travertine deposits in northeastern Brazil (Wang et al. 2004), and riverine discharge (Peterson et al. 2000; Haug et al. 2001). Drought records from the western United States support northward migration of the BH during the Medieval Warm Period (Seager et al., 2007).

In addition to the average long-term latitude of the two features being controlled by a single primary factor, Flohn (1984) suggests a more direct physical connection,

arguing that the northern displacement of the BH resulting from a 7°C increase of average annual north polar temperature alone is enough to move the ITCZ 3–4° northward. Theoretically, therefore, coordination of the low frequency movements of the two features seems likely.

Coordinated movement between the ITCZ and the subtropical highs implies anti-phase rainfall anomalies across the ITCZ; i.e. if the subtropical high moves in parallel with the ITCZ, southerly migration of the ITCZ resulting in positive Amazonian rainfall anomalies should correlate with negative rainfall anomalies for the Caribbean, which would be increasingly influenced by the dry subsiding air associated with the BH. Numerous studies support this relationship during the instrumental record for the tropical Atlantic for both the Caribbean-Central American region and the Sahel to the north and northeastern Brazil to the south of the ITCZ (Hastenrath 1976, 1985, 2000a, b; Lamb 1978; Kapala et al. 1998; Curtis and Hastenrath 1999). On both sides of the ITCZ, movement of the ITCZ toward (away from) the location tends to result in positive (negative) rainfall anomalies on an interannual basis, indicating coordinated movement between the subtropical highs and the ITCZ. Paleoenvironmental evidence (Baker et al. 2001; Mayle et al. 2000, Maslin and Burns 2000, Poore et al. 2003; Tedesco and Thunell 2003) for such coupling has also been demonstrated. Koutavasa and Lynch-Stieglitz (2004) include a review of a large number of studies, based on several different proxies supporting anti-phase precipitation anomalies across the ITCZ. Since trade wind-driven upwelling provides direct evidence for the proximity of the subtropical high, anti-phase rainfall and upwelling records from the Caricao basin provides strong support for parallel movement between the ITCZ and the BH (Haug et al. 2001).

ITCZ-BH-TC

Marine cores from the coast of Venezuela (Haug et al. 2001) indicate that, driven by latitudinal movement of the ITCZ, the region has been alternately subject to either ITCZ-induced rainfall or BH-driven trade winds for the last 14,000 years. This suggests that the TC zone, locked in at the northern edge of the ITCZ, south of the zone of intense trade winds and upwelling, has experienced a parallel migration. Based on sedimentary evidence from Saint-Martin in the French West Indies, Bertran et al. (2004) have suggested a millennial-scale ITCZ-driven latitudinal movement in the zone of TC activity.

ENSO and QBO

The influence of El Nino-Southern Oscillation (ENSO) on NA TC activity is well known, with El Nino (La Nina) periods reducing (increasing) overall activity, with some regional variation (Gray 1984; Richards and O'Brien 1996; Bove et al. 1998; Elsner and Kara 1999: Pielke and Landsea 1998; Bengtsson 2001; Tartaglione et al. 2003). The Quasi-Biennial Oscillation (QBO) also influences NA TC, with the

westerly phase corresponding to increases in frequency of both TCs and major hurricanes (Gray and Shaeffer 1991; Elsner et al. 1999; Elsner and Kara 1999; Landsea et al. 1999; Goldenberg et al. 2001). In this paper, however, we ignore both cycles, as in effect, both of these high-frequency oscillations become noise superimposed on the underlying system at the time scales (centennial to millennial) under consideration. The only exception is the possibility of significant long-term changes in ENSO frequency (Haug et al. 2001; Koutavas and Olive 2006), which potentially could affect TC frequency on the time scales of interest.

Paleo Conditions

ITCZ

Boundary conditions have not remained constant throughout the Holocene. Evidence from varved sediments obtained from the anoxic Cariaco Basin off the coast of Venezuela indicates significant migration of the mean latitude of the ITCZ over the last 14,000 years (Haug et al. 2001). This interpretation is based on the fluctuations in the seasonal hydrological cycle displayed in the high-resolution (subdecadal) bulk sedimentary metals record, resulting from the changing length/intensity of the annual dry and wet seasons. Intensified/lengthened wet seasons result in increased river discharge, rich in metals, while intensified/lengthened dry seasons result in increased biogenic silica, a result of increased trade wind-driven upwelling on the basin.

BH

The chronology of the latitudinal position of the BH can be estimated from paleoenvironmental records as areas directly under its influence are dominated by subsiding dry air. Arrival of the BH over an area not previously under its influence should result in increased aridity, detectable by a variety of vegetational and isotopic proxies. Palynological studies are especially useful for recording long-term shifts as their relatively low temporal resolution reduces the noise of higher-frequency oscillations and are less dependent upon confounding external factors such as local salinity and hydrological changes.

A large number of studies from the Central American-Caribbean region (Bradbury et al. 1981; Leyden 1985; Hodell et al. 1991; Peterson et al. 1991; Curtis and Hodell 1996; Islebe et al. 1996; Leyden et al. 1996; Curtis et al. 1998, 1999; Higuera-Gundy et al. 1999; Islebe and Sanchez 2002; Nyberg et al. 2001; Rosenmeier et al. 2002) have shown low-frequency environmental changes generally in temporal agreement with the ITCZ movement proposed by Haug et al. (2001). The northwestern edge of the region (in particular the northern Yucatan peninsula) seems to demonstrate a greater variability. This can perhaps be

attributed to its location on the edge of the zone of influence, which increases the site's ability to record small latitudinal movements, which leave no detectable signals in locations farther south and east. Complicating these estimations however, are more general hemispheric changes resulting from variability in solar insolation due to orbital influences, especially the processional aspects of the Milankovich cycles (Berger and Loute 1991; Leyden et al. 1994). Additionally, after the mid Holocene the difficulty in separating natural and anthropogenic effects becomes increasingly difficult regionally (Leyden 1987; Leyden et al. 1998). It should be noted that only areas located directly under shifts in BH location are expected to show evidence of such shifts; far southern areas, for example, are not expected to display palynological responses to shifts that occur to the north, as such shifts should not result in aridity changes at their location.

TC

Paleotempestology uses sedimentary evidence to establish long-term proxy hurricane strike records. In such studies, sediment cores are extracted from coastal wetlands and storm-generated layers, identified by a variety of geologic methods, are dated, permitting a chronology of site-specific landfalls (Liu and Fearn 1993, 2000; Liu 2004: Donnelly et al. 2001a,b, 2004; Donnelly 2005; Donnelly and Woodruffe 2007; Scott et al. 2003). Records from several sites can be correlated to develop regional hurricane histories (Liu 2004). Calibrations based on modern analogs indicate that the threshold storm intensity required for depositing recognizable sedimentary signatures is roughly that of major hurricanes (category 3 or greater) (Liu 2004; Donnelly and Webb 2004).

Significantly, the majority of millennial-scale proxy hurricane landfall records display evidence of the temporal clustering of events, often cyclic, indicating periods of hyperactivity. That these intervals are non-synchronous suggests a movement in the zone of maximum TC activity, as opposed to a basin-wide frequency increase. In the United States Liu and Fearn (1993, 2000) found evidence for a hyperactive period from 3400-1000 ^{14}C yr BP for the northern Gulf of Mexico, while Scott et al. (2003) emphasize the anti-phase timing of Atlantic and Gulf Coast hyperactivity, based on a site in South Carolina. In the Caribbean, Bertran et al. (2004) found cyclical periods of TC activity on Saint Martin in the French West Indies, with the hyperactivity dating from ~4900-2600 BP; McCloskey et al. (2004) found two periods of hyperactivity between 5500-2500 BP for the central coast of Belize, while Donnelly has found evidence for hyperactivity in Puerto Rico for the periods 5400-3600 BP, 2500-1000 BP and 250 BP to the present (Donnelly 2005; Donnelley and Woodruff 2007). If correct, these records indicate increased hurricane landfall from ~5500-2500 BP for the northern Caribbean and from ~ 3500-1000 BP for the northern Gulf Coast, with activity increased for both during the period ~3500-2500 BP. The timing of this slow south-to-north migration of hyperactivity roughly parallels that of the ITCZ movement postulated by Haug et al. (2001).

It should be noted that these proxy records, based only on landfall of major hurricanes, represent a minimum record of TC activity. Given the relative scarcity of major hurricanes, which currently comprise ~20% of US landfalling TCs, (Landsea 1993) it seems reasonable to assume that stratigraphic intervals providing sedimentary evidence for the increased frequency of landfalling major hurricanes do, in fact, represent extended periods of overall increase in TC activity, once geomorphological and sea level changes are controlled for. We suggest that the spatial/temporal shifts in these intervals result from the migration of the zone of maximum TC frequency.

Hindcast

By positing that the spatial relationships between the ITCZ, BH, and TC zone have remained relatively constant over the long-term, we are able to hindcast paleopositions of the BH and the TC zone based on ITCZ position. We base our hindcast on the Cariaco record of Haug et al. (2001) due to its large amplitude, high (subdecadal) resolution and inclusion of both rainfall and trade wind data. Although the latitudinal shifts represented by the changes in metal concentrations have not been quantified, the difference in sign and magnitude permit rough estimations.

Based on the Cariaco record, the chronology of significant changes in mean annual latitude of the ITCZ (and, by extension, location of the TC zone) is:

Northern residency: ~11,000-4000 BP, ~1100-600 BP (Medieval Warm Period)
Present position: ~2400-1100 BP
Southern residency: ~4000-2400 BP, ~400-200 BP (Little Ice Age)

A potential complication is the possibility of major change in the strength/variability of ENSO frequency, which has been argued to have become more prevalent in the late Holocene (Haug et al. 2001; Koutavas and Lynch-Stieglitz, 2004). Although this should not affect the average latitude of the BH or TC zone, it might affect landfall frequency. However, it is possible that the apparent increased variability of ENSO suggested by Haug et al. (2001) for the interval between ~4000-2400 BP actually results from increased instability in the general atmospheric circulation system, perhaps resulting from the establishment of a new atmospheric equilibrium.

Hypothesis Testing

Evidence for/against our proposed low-frequency latitudinal oscillation of the NA circulation system requires the long-term correlation of the various components.

In order to correlate low-frequency ITCZ and BH movements, it is necessary to establish an accurate proxy for BH location. One possibility is determining the zone

of aridity resulting from the subsiding air issuing from the BH, recognizable palynologically by increasingly xeric taxa, or isotopically by the changing $\delta^{18}O$ ratios of closed basin lakes. However, both vegetational and isotopic proxy records are subject to a variety of local controls; additionally, they are constrained geographically as only fringe areas are directly affected by BH movements.

The correlation of ITCZ and TC zone could be more direct, based upon a basin-wide paleo-strike record developed from paleotempestological studies extending to the mid Holocene. With recognizable sedimentary signatures posited to be deposited only for major hurricanes, longer paleo-strike records seem unlikely, since major hurricanes probably did not occur during the early Holocene due to the lowered surface sea temperatures resulting from the large volume of glacial meltwater entering the NA basin.

However, comprehensive paleo-strike records do not currently exist. For the NA basin multi-millennial scale proxy records are spotty at best, particularly for the Caribbean and the US Atlantic Coast. However, new research may prove fruitful; if the frequency of TC-inhibiting El Nino events has increased throughout the late Holocene as posited (Clement et al. 2000; Trudhope et al. 2001; Haug et al. 2001; Moy et al. 2002; Koutavas and Lynch-Stieglitz 2004), one result could be an overall increase in annual frequency for mid Holocene TCs. If so, such an increase improves the possibility that landfall patterns may be preserved in the sedimentary record.

Based on our model, increased hurricane landfall frequencies can be expected to have occurred along the northern area (US Atlantic Coast) from ~8-4000 BP, and during the Medieval Warm Period, ~1100-600 BP, while decreased landfall frequencies should have occurred ~4000-2400 BP and during the Little Ice Age, (~ 400-200 BP). The southern area (Gulf Coast and the Caribbean) should exhibit the reverse pattern.

Obtaining evidence for/against such temporal/spatial shifts in maximum strike frequency therefore presents a means of testing this model. During periods of extreme northern/southern movement, the fringe areas, which currently experience very low levels of TC activity, may have experienced increased activity, thereby producing relatively easily recognizable sedimentary evidence for frequency changes. Due to the latitudinal smearing of TC landfall resulting from the high-frequency oscillation in BH intensity, the record in central areas will quite possibly exhibit a less distinct signal. The long return intervals of major hurricanes, generally >100 years (Elsner and Kara 1999; Liu and Fearn 1993, 2000; Donnelly et al. 2001a,b, 2004) makes the existence of a clear sedimentary record over short time spans somewhat problematic, thereby reducing the utility of the recent oscillations connected to the Little Ice Age and the Medieval Warm Period. It is therefore suggested that studies focusing on the period from 8000-4000 BP in the extreme north and 4000-2400 BP in the south are the most likely to produce useful information.

Obviously, there are very significant practical difficulties in obtaining proxy strike records for the suggested periods, given the magnitude of sea level raise and geomorphological changes in dynamic coastal areas. Coring submerged kettle holes

in the northern area is one possibility (J. P. Donnelly, personal communication), as are study sites in areas of uplift and steep bathymetry, or areas where "keep-up" reefs/mangroves have minimized relative sea level rise.

Summary

Using both a GIS and literature-based analyses of current conditions we developed a model of current TC activity for the NA basin, in which TCs are latitudinally "fixed" between the ITCZ to the south and the BH to the north, with changes in the general atmospheric circulation, as proxied by the NAO Index values, resulting in the smearing of track location and landfall across the NA.

Evidence suggests that the coordinated movement of the ITCZ and the BH has existed through the Holocene, controlled primarily by the pole-equator temperature gradient. Changes in that gradient, ultimately driven by orbital factors, have resulted in latitudinal movement of this integrated atmospheric structure on a number of time scales. As part of this structure the TC zone has migrated north and south over the Holocene in rough parallel with the ITCZ. From $\sim$ 8000 BP on, sedimentary evidence for the migration of the zone of maximum hurricane landfall has potentially been preserved. Hindcasts, based on the proxy migration record of the ITCZ, the southern edge of the structure, suggest that the zone of maximum TC activity moved significantly to the

1. north from $\sim$8000-4000 BP and 1100-600 BP
2. south from $\sim$4000-2400 and 400-200 BP.

By providing proxy paleo-strike records, paleotempestology studies in the northern and southern edges of the TC zone provide a method of evaluating the validity of the model.

Acknowledgments This research was funded by National Science Foundation Graduate Research Fellowship, LSU Board of Regents Fellowship, (TAM), and National Science Foundation Doctoral Dissertation Research Improvement Grant (TAM and JTK). We thank Kam-biu Liu for his guidance and advice. The work was improved due to the comments of an anonymous reviewer.

References

Bailey, T.C., and A.C. Gatrell,1995: Interactive Spatial Data Analysis. Longman, Essex.

Baker, P.A., G.O. Seltzer, S.C. Fritz, et al, 2001: The history of South American tropical precipitation for the past 25,000 years. *Science*, **291**, 640–643.

Bell, G.D., and M. Chelliah, 2006: Leading tropical modes associated with interannual and multidecadal fluctuations in North Atlantic hurricane activity. *J Climate*, **19**, 590–612.

Bengtsson, L., 2001: Enhanced: Hurricane threats. *Science*, **293**, 440–442.

Berger, A., and M.F. Loute, 1991: Insolation values for the climate for the last 10 million years. *Quat Sci Rev*, **10**, 297–317.

Bertran, P.D., D. Bonnissent, P. Imbert, et al, 2004: Paleoclimat des Petites Antilles depuis 4000 BP: l'enregistrement de la lagune de Grand-Case a Saint-Martin. *CRGeoscience*, **336**, 1501–1510.

Black, D.E., L.C. Peterson, J.T. Overpeck, et al, 1999: Eight centuries of North Atlantic ocean atmosphere variability. *Science*, **286**, 1709–1713.

Bove, M.C., J.B. Elsner, C.W. Landsea, et al, 1998: Effects of El Nino on U.S. landfalling hurricanes, revisited. *Bull Amer Meteor Soc*, **76**, 2477–2482.

Bradbury, J.P., B.W. Leyden, M. Salgado-Labouriau et al, 1981: Late Quaternary environmental history of Lake Valencia, Venezuela. *Science*, **214**, 1299–1305.

Broccoli, A.J., K.A. Dahl, and R.J. Stouffer, 2006: Response of the ITCZ to northern hemisphere cooling. *Geophys Res Lett*, **33,** Art. No. L01702.

Chiang, J.C.H, 2006: Tropical Atlantic climate variability as a model for marine ITCZ displacements. Joint Assembly of the American Geophysical Union; Baltimore, Maryland from 23–26 May 2006.

Chiang, J.C.H., and C.M. Bitz, 2005: Influence of high latitude ice cover on the marine Intertropical Convergence Zone. *Climate Dyn*, **25**, 477–496, doi:10.1007/s00382-005-0040-5.

Chiang, J.C.H., M. Biasutti, and D.S. Battisti, 2003: Sensitivity of the Atlantic Intertropical Convergence Zone to last glacial maximum boundary conditions. *Paleoceanography*, **18**, 1094, doi:10.1029/2003PA000916.

Climate Research Unit University of East Anglia, (http://www.cru.uea.ac.uk/cru/data/nao.htm)

Clement, A.C., R. Seager, and M.A. Cane, 2000: Suppression of El Nino during the mid Holocene by changes in the earth's orbit. *Paleoceanography*, **15**, 717–737.

Curtis, S., and S. Hastenrath, 1999: Trends of upper-air circulation and water vapour over equatorial South America and adjacent oceans. *Int J Climatol*, **19**, 863–876.

Curtis, J.H., and D.A. Hodell, 1996: Climate variability on the Yucatan peninsula (Mexico) during the past 3500 years, and the implications for Maya cultural evolution. *Quat Res*, **46**, 37–47.

Curtis, J.H., M. Brenner, and D.A. Hodell, et al, 1998: A multi-proxy study of Holocene environmental change in the Maya lowlands of Peten, Guatemala. *J Paleolimnol*, **19**, 139–159.

Curtis, J.H., M. Brenner, and D.A. Hodell, 1999: Climate change in the Lake Valencia basin, Venezuela, ~12600 yr BP to present. *Holocene*, **9**, 609–619.

Davis, R.E., B.P. Hayden, and D.A. Gay, et al, 1997: The North Atlantic subtropical anticyclone. *J Climate*, **10**, 728–744.

Donnelly, J.P., 2005: Evidence of past intense tropical cyclones from backbarrier salt pond sediments: a case study from Isla de Culebrita, Puerto Rico, USA. *J Coastal Res*, **42**, 201–210.

Donnelly, J.P., and T. Web, III, 2004: Back-barrier sedimentary records of intense hurricane landfall in the northeastern United States. In: Murnane RJ, Liu K-B (eds) Hurricanes and typhoons: past, present and future, Columbia University Press, New York.

Donnelly, J.P., and J. Woodruff, 2007: Intense hurricane activity over the past 5000 years controlled by El Nino and the West African Monsoon. *Nature*, **447**, 465–468.

Donnelly, J.P., S.S. Bryant, and J. Butler, et al, 2001a: A 700 year sedimentary record of intense hurricane landfalls in southern New England. *Geol Soc Am Bull*, **113**, 714–727.

Donnelly, J.P., S. Roll, M. Wengren, et al, 2001b: Sedimentary evidence of intense hurricane strikes from New Jersey. *Geology*, **29**, 615–618.

Donnelly, J.P., J. Butler, S. Roll, et al, 2004: A backbarrier overwash record of intense storms from Brigantine, New Jersey. *Mar Geol* **210**, 107–121.

Elsner, J.B., and A.B Kara, 1999: Hurricanes of the North Atlantic: climate and society. Oxford University Press, Oxford

Elsner, J.B., A.B. Kara, and M.A. Owen, 1999: Fluctuations in North Atlantic Hurricane frequency. *J Climate*, **12**, 427–437.

Elsner, J.B., K.-B. Liu, and B. Kocher, 2000: Spatial variations in major U.S. hurricane activity: Statistics and a physical mechanism. *J Climate*, **13**, 2293–2305.

Flohn, H., 1984: Ice-free Arctic and glaciated Antarctic. In: Flohn H, Fantechi R (eds) The Climate of Europe: past, present and future. D. Reidel Publishing Company, Dordrecht.

Goldenberg, S.B., and L.J. Shapiro, 1996: Physical mechanisms for the association of El Nino and West African rainfall. *J Climate*, **9**, 1169–1187.
Goldenberg, S.B., C.W. Landsea, M.A. Mestas-Nunez, et al, 2001: The recent increase in Atlantic hurricane activity: causes and implications. *Science*, **293**, 474–479.
Gray, W.M., 1984: Atlantic seasonal hurricane frequency Part I-El Nino and 30 mb quasi-biennial oscillation influences. *Mon Wea Rev*, **112**, 1649–1668.
Gray, W.M., and J.D. Shaeffer, 1991: El Nino and QBO influences on tropical cyclone activity. In: Glantz MH, Katz RW, Nichols N (eds) Teleconnections linking worldwide climate anomalies. Cambridge University Press, New York.
Hasanean, H.M., 2004: Variability of the North Atlantic subtropical high and association with tropical sea-surface temperature. *Int J Climatol*, **24**, 945–957.
Hastenrath, S., 1966: On general circulation and energy budget in the area of the Central American seas. *J Atmos Sci*, **23**, 694–711.
Hastenrath, S., 1976: Variations in low-latitude circulation and extreme climatic events in the tropical Americas. *J Atmos Sci*, **33**, 202–215.
Hastenrath, S., 1985: Climate and circulation in the tropics. D Reidel Publishing Company, Dordrecht.
Hastenrath, S., 2000a: Interannual and longer-term variability of upper air circulation in the Northeast Brazil-tropical Atlantic sector. *J Geophys Res*, **105**, 7327–7335.
Hastenrath, S., 2000b: Interannual and longer term variability of upper-air circulation over the tropical Atlantic and West Africa in boreal summer. *Int J Climatol*, **20**, 1415–1430.
Haug, G.H., K.A. Hughen, D.M. Sigman, et al, 2001: Southward migration of the Intertropical Convergence Zone through the Holocene. *Science*, **292**, 1304–1314.
Higuera-Gundy, A.M., M. Brenner, D.A. Hodell, et al, 1999: A 10,300 ^{14}C yr record of Climate and Vegetation change from Haiti. *Qua Rev*, **52**, 159–170.
Hodell, D.A., J.H. Curtis, G.A. Jones, et al, 1991: Reconstruction of Caribbean climate change over the past 10,500 years. *Nature*, **352**, 790–793.
Hurrell, J.W., 1995: Decadal trends in the North Atlantic Oscillation and relationships to regional temperature and precipitation. *Science*, **269**, 676–679.
Islebe GA, Sanchez O, 2002: History of Late Holocene vegetation at Quintana Roo, Caribbean coast of Mexico. *Plant Ecol*, **160**, 187–192.
Islebe GA, Hooghiemstra H, Brenner M et al, 1996: A Holocene vegetation history from lowland Guatemala. *Holocene*, **6**, 265–271.
Jones PD, Jonsson T, Wheeler D, 1997: Extension to the North Atlantic Oscillation using early instrumental pressure observations from Gibraltar and south-west Iceland *Int J Climatol*, **17**, 433–1450.
Kapala A, Machel H, Flohn H, 1998: Behaviour of the centres of action above the Atlantic since 1881. Part II: associations with the regional climate anomalies. *Int J Climatol*, **18**, 23–36.
Knowles JT, Leitner M, 2007: Visual representations of the spatial relationship between Bermuda High strength and Hurricane tracks. *Cartogr Perspect*, **56**, 16–30.
Koutavas A, Lynch-Stieglitz J, 2004: Variability of the marine ITCZ over the eastern Pacific during the past 30,000 years. In: Diaz HF, Bradley RS (eds*)* The Hadley Circulation: present, past and future. Springer-Verlag, New York.
Koutavas A, Olive GC, 2006: Holocene modulation of ENSO by the Intertropical Convergence Zone. Joint Assembly of the American Geophysical Union; Baltimore, Maryland from 23–26 May 2006.
Lamb HH, 1977: Climate, present, past and future. Volume 2 climatic history and the future. Methuen and Co. Ltd, London.
Lamb PJ, 1978: Case studies of tropical Atlantic surface circulation patterns during recent sub-Saharan weather anomalies: 1967 and 1968. *Mon Wea Rev*, **106**, 482–491.
Landsea CW, 1993: A climatology of intense (or major) Atlantic hurricanes. *Mon Wea Rev*, **21**, 1703–1713.

Landsea CW, Pielke RA Jr, Mestas-Nunez AM et al, 1999: Atlantic Basin hurricanes: indices of climate change. *Climate Change*, **42**, 89–129.
Leyden BW, 1985: Late Quaternary aridity and Holocene moisture fluctuations in the Lake Valencia basin, Venezuela. *Ecology*, **66**, 1279–1295.
Leyden BW, 1987: Man and climate in the Maya lowlands. *Quat Res*, **28**, 407–417.
Leyden BW, Brenner M, Hodell DA et al, 1994: Orbital and internal forcing of climate on the Yucatan Peninsula for the past ca. 36 ka. *Palaeogeo P*, **109**, 193–210.
Leyden BW, Brenner M, Whitmore T et al , 1996: A record of long- and short-term climatic variation from northwest Yucatan: cenote San Jose Chulchaca. In: Fedick L (ed*)* The managed mosaic; ancient Maya agriculture and resource use. University of Utah Press, Salt Lake City.
Leyden BW, Brenner M, Dahlin B, 1998: Cultural and climatic history of Coba', a lowland Maya city in Quintana Roo, Mexico. *Quat Res*, **49**, 111–122.
Liu K-B, 2004: Paleotempestology: principles, methods, and examples from Gulf Coast lake sediments. In: Murnane RJ, Liu K-B (eds) Hurricanes and typhoons: past, present and future. Columbia University Press, New York.
Liu K-B, Fearn ML, 1993: Lake-sediment record of late Holocene hurricane activities from coastal Alabama. *Geology*, **21**, 793–796.
Liu K-B, Fearn ML, 2000: Reconstruction of prehistoric landfall frequencies of catastrophic hurricanes in northwestern Florida from lake sediment records. *Quat Res*, **54**, 238–245.
Machel HA, Kapala A, Flohn H , 1998: Behaviour of the centres of action above the Atlantic since 1881. Part I: characteristics of seasonal and interannual variability. *Int J Climatol*, **18**, 1–22.
Maslin MA, Burns SJ, 2000: Reconstruction of the Amazon Basin: Effective moisture availability over the past 14,000 Years. *Science*, **290**, 2285–2287.
Mayle FE, Burbridge R, Killeen TJ , 2000: Millennial-Scale dynamics of southern Amazonian rain forests. *Science*, **290**, 2291–2294.
McCloskey TA, Keller G, Cho A, 2004: 5000 Year Record of Hurricane Strikes for the Central Coast of Belize, AAG annual meeting, Philadelphia.
Moy CM, Seltzer GO, Rodbell DT et al, 2002: Variability in El Nino/Southern Oscillation at millennial timescales during the Holocene epoch. *Nature*, **420**, 162–165.
Neumann CJ, Jarvinen BR, McAdie CJ et al, 1999: Tropical Cyclones of the North Atlantic Ocean, 1871–1998. NOAA, Asheville, North Carolina.
NOAA website (http://hurricane.csc.noaa.gov/hurricanes/viewer.htm)
Nyberg JB, Malmgren BA, Kuijpers A et al, 2001: A centennial-scale variability of tropical North Atlantic surface hydrography during the late Holocene. *Palaeogeo P*, **183**, 25–41.
Nyberg JB, Malmgren BA, Winter A et al, 2007: Low Atlantic hurricane activity in the 1970s and 1980s compared to the last 270 years. *Nature*, **447**, 698–701.
Peterson LC, Overpeck JT, Kipp NG et al, 1991: A high-resolution Late Quaternary upwelling record from the Caricaco Basin, Venezuela. *Paleoceanography*, **6**, 99–119.
Peterson LC, Haug GH, Hughens KA et al, 2000: Rapid changes in the hydrological cycle of the tropical Atlantic during the last glacial. *Science*, **290**, 1947–1951.
Pielke RA Jr, Landsea CW, 1998: Normalized U.S. hurricane damages, 1925–1995. *Wea Forecasting, **13**, 621–631*.
Portis DH, Walsh JE, Hanley ME et al, 2001: Seasonality of the North Atlantic Oscillation. *J Climate, **14**, 2069–2078*.
Poore RZ, Dowsett HJ, Verardo S et al, 2003: Millennial-to century scale variability in Gulf of Mexico Holocene climate records. *Paleoceanography*, **18**, 1048 doi:10.1029/2002PA000868, 2003.
Reading AJ, 1990: Caribbean tropical storm activity over the past four centuries. *Int J Climatol*, **10**, 365–376.
Richards TS, O'Brien JJ, 1996: The effect of El Nino on U.S. landfalling hurricanes. *Bull Amer Meteo. Soc*, **77**, 773–774.
Rosenmeier MF, Hodell DA, Brenner M et al , 2002: A 4000-year lacustrine record of environmental change in the southern Maya lowlands, Peten, Guatemala. *Quat Res*, **57**, 183–190.

Sahsamanoglou HS, 1990: A contribution to the study of action centres in the North Atlantic. *Int J Climatol,* **10**, 247–261.

Scott DB, Collins ES, Gayes PT et al, 2003: Records of prehistoric hurricanes on the South Carolina coast based on micropaleontological and sedimentological evidence, with comparison to other Atlantic Coast record. *Geol Soc Am Bull*, **115**, 1027–1039.

Seager R, Graham N, Herweijer C et al, 2007: Blueprints for Medieval hydroclime. *Quat Sci Rev,* doi:10.1016/j.quascirev.2007.04.020.

Tartaglione CA, Smith SR, O'Brien JJ, 2003: ENSO impacts on hurricane landfall probabilities for the Caribbean. *J Climate*, **16**, 2925–2931.

Tedesco K, Thunell R, 2003: High resolution tropical climate record for the last 6,000 years. *Geophys Res Lett,* **30**, Art No 1891.

Thompson LG, Mosley-Thompson E, Henderson KA, 2000: Ice-core paleoclimate records in tropical South America since the Last Glacial Maximum. *J Quat Sci*, **15**, 377–394.

Tiwari MR, Ramesh R, Somayajulu B et al, 2006: Correlation between the equatorial and the high-latitude climatic variations and its implications. Joint Assembly of the American Geophysical Union; Baltimore, Maryland from 23–26 May 2006.

Trewartha GT, 1981: The Earth's problem climates, 2nd edn. The University of Wisconsin Press, Madison.

Trudhope AW, Chilcott CP, McCulloch MT et al, 2001: Variability in the El Nino-Southern Oscillation through the glacial-interglacial cycle. *Science*, **291**, 1511–1517.

Visbeck MH, Hurrell JW, Polvani L et al, 2001: The North Atlantic Oscillation: past, present and future. *PNAS*, **98**, 12876–12877.

Walsh JP, Reading AJ, 1991: Historical changes in tropical frequency within the Caribbean since 1500. *Wurz Geogr Arz*, **80**, 199–240.

Wang X, Auler AS, Edwards RL et al, 2004: Wet periods in northeastern Brazil over the past 210 kyr linked to distant climate anomalies. *Nature*, **432**, 740–743.

Aerosol Effects on Lightning and Intensity of Landfalling Hurricanes

N. Cohen and A. Khain

Abstract Intense and persistent lightning in landfalling hurricanes takes place within the 250–300 km-radius ring around the hurricane center. At the same time the lightning activity in the eye wall takes place only during comparatively short periods of tropical cyclone (TC) intensification related to the replacement of old eyewall by the new one. As soon as the hurricane weakens, the lightning in the eye wall disappears. The mechanisms responsible for most of the phenomena are unknown. In this study we provide some observational evidence and numerical estimations to show that lightning in hurricanes approaching or penetrating the land, especially at their periphery, arises under the influence of continental aerosols, which affect the microphysics and dynamics of clouds in TCs. Numerical simulations using a 2-D mixed phase cloud model with spectral microphysics show that aerosols that penetrate cloud base of maritime clouds dramatically increase the amount of supercooled water as well as ice content and vertical velocities. As a result, in clouds developing in dirty air ice crystals, graupel, frozen drop/hail and supercooled water can coexist within the same cloud zone which allows for collisions and charge separation. Simulation of the possible effects of aerosols on landfalling tropical cyclone has been carried out using a 3-km resolution Weather Research and Forecasting (WRF) mesoscale model. It is shown that aerosols change cloud microstructure in a way that allows one to attribute observed lightning structure to effects of continental aerosols. It is shown also that aerosols, invigorating clouds at 250–300 km from TC center decrease the convection intensity in the TC center leading to some TC weakening. The results suggest that aerosols change the intensity and spatial distribution of precipitation in landfalling TCs. These results can serve as a justification of the observed weekly cycle of intensity and precipitation of landfalling TCs caused, supposedly, by the weekly variation of anthropogenic aerosol concentration.

Keywords: Tropical cyclones, lightning, cloud-aerosol interaction, numerical modeling.

Introduction: Potential Mechanisms of Lightning in Hurricanes

Tropical cyclones (TCs) are known for their destructive power, particularly as they make landfall. TCs often are accompanied by extreme winds, storm surges and

J.B. Elsner and T.H. Jagger (eds.), *Hurricanes and Climate Change,*
doi: 10.1007/978-0-387-09410-6,

torrential rainfall. The TCs wind fields, area of heavy rain, and rain rate are determined by cloud microphysical processes and accompanying latent heat release. At the same time both experimental and numerical investigations of cloud microphysics in TCs are quite limited. Microphysical observations are usually limited by zones near the melting level (McFarquhar and Black, 2004). Numerical simulations of TCs are often carried out using mesoscale models, when clouds are not resolved. Lightning is one factor, which can shed light on the microphysical cloud structure and TC evolution. For instance, increasing lightning rates indicates invigoration of convection, accompanying increasingly larger volume of graupel or small hail aloft, strengthening updrafts and increased probability of heavier rainfall (e.g. Lhermitte and Krehbiel, 1979; Wiens et al., 2005; Fierro et al., 2007). Appearance and intensification of lightning in the eyewall can be a predictor of TC intensification (Orville and Coyne, 1999, Shao et al., 2005). Rodgers et al. (2000) found that the closer the lightning is to the storm center, the more likely the TC is to intensify. The latter makes lightning and its distribution in TCs to be an important characteristic that can be served as a predictor of change in TCs intensity and precipitation.

Lightning is a much more widespread phenomenon over the land than over the sea (Williams et al., 2005). It is important that lightning over the sea takes place manly nearly the continents or in regions located downwind of the continents (like in the Intertropical convergence zone to the west from Africa). Hurricanes are not an exception: a strong rise of the flash rate takes place in the hours prior to and after the landfall. An example of lightning activity in hurricane Katrina (2005) at several successive time instances is presented in Fig. 1.

One can see that intense and persistent lightning takes place within the 250–300 km-radius ring around the hurricane center, which is a typical feature of landfalling hurricanes (Molinari et al. 1999, Cecil et al., 2002a, b). Besides, the lightning activity within the eye wall takes place during a comparatively short period of the tropical cyclone (TC) intensification. According to Black and Hallet (1999) the updraft velocity W_{max} exceeding 10 ms^{-1} and the existence of supercooled cloud droplets above the $-13°C$ level are necessary conditions for the lightning in a hurricane eye wall. As soon as the hurricane stops intensify, the lightning in the eye

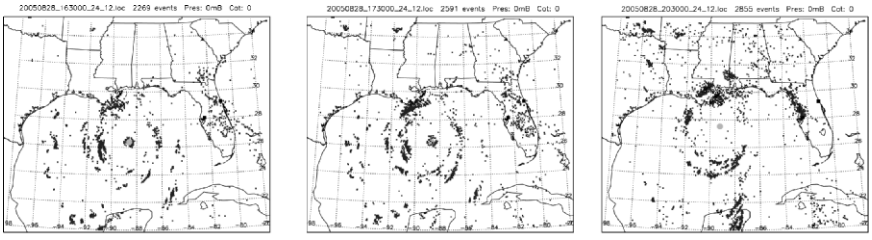

Fig. 1 Lightning in Katrina (2005) at different time instances (after Shao et al., 2005). Zones of lightning are marked by black dots; the TC eye is marked by gray. Specific shape and the locations of lightning allow one to assume the effects of aerosols penetrating from the land

wall disappears. Figure 1 also shows that the high flash rate over the sea takes place in the regions downwind from the land. Similar features were observed in hurricane Rita as well (Shao et al., 2005). Analysis of TRMM's Tropical Microwave Imager (TMI) images of TC Katrina and Rita indicates that precipitation in clouds at the TC periphery starts at higher levels than in the TC eye wall. The zones of intense reflectivity at higher levels coincide with those of enhanced lightning activity.

The mechanisms responsible for most of the characteristics of lightning in landfalling TCs are not well understood (Molinari et al., 1999). Molinari et al. (1999) assumed that one of the factors fostering the lightning activity at the TC periphery is the higher instability of the atmosphere at the periphery as compared to the TC eyewall. At the same time, the instability at the TC periphery is typical of the entire tropical zone over the oceans during the hurricane seasons (Jordan 1958), but it does not lead to the formation of dense lightning over the oceans. Besides, numerical simulations of evolution of an idealized hurricane-like vortex (Fierro et al., 2007) using a mesoscale 2-km resolution model with a bulk parameterization microphysical scheme describing 12 distinct hydrometeor habits (Straka and Mansell, 2005) and a lightning scheme (Mansell et al., 2002) showed much more intense convection and lightning within a TC central convective zone of ~50-km radius rather within outer rain bands.

It is known that the charging of hydrometeors in clouds takes place at temperatures below -13°C, when collisions of ice crystals and graupel take place in the presence of supercooled drops (e.g., Takahashi, 1978; Saunders, 1993; Cecil et al., 2002b; Sherwood et al., 2006). It means that supercooled drops have to ascend in clouds above ~5–6 km to trigger flash formation. One can suppose two main physical reasons retarding lightning formation in tropical maritime clouds. The first one is the low vertical velocity in marine clouds including that in hurricanes, which typically does not exceed 5–6 ms^{-1} (Jorgensen et al., 1985). The second reason is that the concentration of aerosol particles (AP) over the open oceans is very low. Hence, the concentration of cloud droplets growing on these AP is also small, and cloud droplets grow rapidly by condensation and collisions into raindrops that efficiently collect the remaining cloud droplets. Since the fall velocity of raindrops (about 10 ms^{-1}) exceeds the updraft velocities, raindrops start falling at low levels (3–5 km), and no liquid droplets reach the levels required for lightning formation. A classical illustration is that of Hawaiian clouds, where lightning is extremely rare phenomena.

The lightning onset indicates significant changes in cloud dynamics and/or in the cloud microphysics of maritime clouds. Correspondingly, there are two main plausible mechanisms (dynamical and microphysical) that could lead to the cloud structure suitable for lightning formation. The dynamical mechanism (e.g., increase in CAPE) may increase cloud updrafts decreasing the time for droplet collisions and elevating the level of raindrop formation. If these velocities exceed 10 ms^{-1} even raindrops will ascend leading to formation of graupel and hail by freezing aloft. The importance of the dynamical mechanism of lightning was stressed in several studies (Sherwood, 2002; Melani et al., 2003; Williams et al., 2002, 2005; Williams and Satori, 2004; Heymsfield et al., 2005; Khain et al., 2008). We suppose, however,

that in case of lightning in hurricanes, the changes in the atmospheric instability (CAPE) hardly can be the sufficient factor that is fully responsible for the increase in lightning activity. It is difficult to suggest a mechanism which is able to increase CAPE within a narrow concentric ring of 250–300 km radius around the center of TC located relatively far from the land. Characteristic scales of spatial SST variations in the zone of hurricane Katrina 2005, which could be the reason of variation of the atmospheric instability, are much larger than the scale of a few tens of kilometers representing the width of the ring of the intense TC lightning. Other factors, such as variation of surface properties, the boundary layer moisture and the surface friction take place when TC already penetrates the land (at least, partially), but these inhomogeneities affect usually the convergence in the central zone of TC and TC intensity (see e.g., Khain, 1984), and do not increase the CAPE at TC periphery, at least in the manner that could lead to the lightning structure seen in Fig. 1. Increase in instability of the atmosphere at the TC periphery could be caused by penetration of continental air in case it is colder than that over the sea. This opportunity will be tested in a separate study.

Here we will check other hypothesis, namely that the increase in lightning activity in hurricanes approaching the land is caused by continental aerosols involved into the circulation of the hurricane approaching the land.

To the best of our knowledge, the first attempt to study aerosol effects on TC was made by Khain and Agrenich (1987), who studied a possible effects of the Saharan dust on the TC development related to heating of air mass through the interaction of suspended dust and solar radiation. The relationship between weekly changes of anthropogenic particle pollutants and the TC-induced precipitation was reported first by Cerveny and Balling (1998). Here we discuss possible aerosol effects on lightning in hurricanes (and, on their intensity) in the context of cloud-aerosol interaction.

The "aerosol" hypothesis of lightning formation in deep convective clouds has been discussed by Williams et al. (2002), Sherwood et al. (2006), and Rosenfeld et al. (2007a). Sherwood et al. (2006) concluded that aerosols are a particular contributor to climatological land-ocean lightning contrasts.

How might continental aerosol particles (AP) foster lightning formation in hurricanes approaching the land? The concentration of submicron AP over the land is higher than that over the sea by one to two orders of magnitude. When aerosols penetrate oceanic clouds, they dramatically increase the concentration and decrease the size of cloud droplets. Since collisions of such droplets are inefficient, these droplets remain small for a longer time period and ascend in even moderate cloud updraft to higher levels than in clouds with low aerosol concentration (Khain et al. 2004, 2005, 2008; Wang 2005). As a result, in clouds developing in the dirty air supercooled cloud droplets can coexist with graupel and crystals, which is necessary condition for charge separation. Khain et al. (2005) found an invigoration of maritime tropical convection (an increase in updraft) in case of continental aerosol intrusion into the bases of maritime clouds. This increase also helps to transfer supercooled water to upper levels fostering lightning formation.

The formation of lightning at TC periphery indicates an invigoration of the convection there. The latter can affect structure and intensity of TCs. Significant effects of idealized seeding with small aerosol particles of clouds at TC periphery

on the intensity of hurricanes located over open sea was recently found by Rosenfeld et al. (2007b) in simulations using a two nested grid Weather Research and Forecasting (WRF) Model. A decrease in hurricane intensity in dirty air was also reported recently by Cotton et al. (2007) in simulations of an idealized TC using RAMS.

In this study we investigate the effect of aerosols both on individual deep maritime clouds (as an element of TC convection) and on the TC structure as a whole. The main purposes of these simulations are a) to justify that continental aerosols penetrating into TC clouds are able to create conditions favorable for lightning formation, b) to check whether aerosols can lead to the fine "coherent" spatial structure of the lightning rate, and c) to investigate the possible role of continental aerosols on the intensity of TC, structure of cloudiness and precipitation of landfalling TC.

The effects of aerosols on individual convective clouds under conditions typical of TC periphery is investigated using a very high resolution 2-D mixed phase Hebrew University cloud model (HUCM) with spectral bin microphysics (Khain et al. 2004, 2005, 2008). The aerosol effects on the cloudiness structure of TC approaching and penetrating the land is investigated using a two nested grid WRF model (Skamarock et al., 2005).

The combination of the two models for the investigation is natural: the high resolution HUCM can describe realistically vertical velocities, as well as all microphysical processes to evaluate the aerosol effects on the vertical profiles of liquid water content and that of different ice particles in individual clouds. These simulations will represent the main justification to the fact that an increase in the aerosol concentration can create conditions favorable for lightning formation in maritime clouds. At present the 3-D simulations of TCs cannot be carried out with so high resolution and with the microphysical scheme used in the HUCM due to computer limitations. These simulations do not resolve small clouds and underestimate vertical velocities. Correspondingly, the TC simulations provide less exact (but still useful) estimations of aerosol effects on individual clouds. At the same time the 3D model is able to reproduce effects of aerosols on the structure of TC cloudiness and precipitation over large areas.

Taking into account the factors affecting the lightning rate (Fierro et al., 2007), the lightning probability will be characterized by the magnitude of the product of total ice content, supercooled content and the vertical velocity above the 5-km level.

Aerosol Effects on Microstructure of Individual Tropical Maritime Clouds

Description of the Cloud Model

A 2-D mixed phase Hebrew University cloud model (HUCM) with spectral bin microphysics (Khain et al., 2004, 2005, 2008) has been used to investigate whether an increase in aerosol concentration in the zone of maritime tropical convection can

change the cloud microphysical structure of individual clouds to make it suitable for lightning formation. The HUCM model microphysics is based on solving a kinetic equations system for size distribution functions for water drops, ice crystals (plate-, columnar- and branch types), aggregates, graupel and hail/frozen drops, as well as atmospheric APs. Each size distribution is described using 43 doubling mass bins, allowing simulation of graupel and hail with sizes up to 4 cm in diameter. The model is specially designed to take into account the effects of AP on the cloud microphysics, dynamics, and precipitation. *The initial* (at t = 0) CCN size distribution is calculated using the empirical dependence

$$N = N_o S_1^k, \tag{1}$$

using the procedure described by Khain et al. (2000). In (1) N is the concentration of activated AP (nucleated droplets) at supersaturation S_1 (in %) is with respect to water, N_o and k are the measured constants. At t > 0 the prognostic equation for the size distribution of non-activated AP is solved. Using the value of S_1 calculated at each time step, the critical AP radius is calculated according to the Kohler theory. The APs with radii exceeding the critical value are activated and new droplets are nucleated. The corresponding bins of the CCN size distributions become empty.

Primary nucleation of each type of ice crystals is performed within its own temperature range following Takahashi et al. (1991). The dependence of the ice nuclei concentration on supersaturation with respect to ice is described using an empirical expression suggested by Meyers et al. (1992) and applied using a semi-lagrangian approach (Khain et al. 2000) allowing the utilization of the diagnostic relationship in the time dependent framework. The diffusional growth/evaporation of droplets and the deposition/sublimation of ice particles are calculated using analytical solutions for supersaturation with respect to water and ice. An efficient and accurate method of solving the stochastic kinetic equation for collisions (Bott, 1998) was extended to a system of stochastic kinetic equations calculating water-ice and ice-ice collisions. The model uses height dependent drop-drop and drop-graupel collision kernels following Khain et al. (2001) and Pinsky et al. (2001). Ice-ice collection rates are assumed to be temperature dependent (Pruppacher and Klett, 1997). An increase in the water-water and water-ice collision kernels caused by the turbulent/inertia mechanism was taken into account according to Pinsky and Khain (1998) and Pinsky et al. (2007). Advection of scalar values is performed using the positively defined conservative scheme proposed by Bott (1989). The computational domain is 178 km × 16 km with the resolution of 250 m and 125 m in the horizontal and vertical directions, respectively.

Design of Simulations with the Cloud Model

Simulations of development of individual maritime deep convective clouds under conditions typical of tropical oceans during hurricane season (Jordan 1958) have been performed. The sounding used indicates high humidity near the surface of about 90%, and relatively stable maritime conditions. The zero temperature level is at 4.2 km.

We assume that the AP size distributions over the sea at the periphery of landfalling TC can be represented as a sum of two distributions: one typical of maritime and, another, typical of continental conditions. Aerosol particles giving rise droplet formation in all simulations were assumed soluble. Under high winds, aerosol size distribution can contain a significant amount of large cloud condensational nuclei (CCN) arising because of the sea spray formation. Correspondingly, penetration of continental aerosol should create aerosol size distributions containing a significant concentration of both small continental aerosols and tails of large aerosols. To investigate the effects of a large concentration of small continental aerosols on cloud microphysics and dynamics under the existence of a significant amount of large maritime CCN, the following simulations have been performed (see Table 1): a) the "M-case" corresponding to typical maritime distribution outside of the area of strong winds. In this case the maximum radius of AP was set equal to 2-μm. The CCN number (at S = 1%) was set equal to 60 cm^{-3}. Activation of the largest APs leads to formation of 10 μm-radius droplets. b) the "M_c case", in which the AP distribution represents sum of a continental AP distribution (with maximum of dry AP radius of 0.6 μm) and a maritime distribution as in the previously described M-case. We suppose that this case represents the AP size distribution over the sea in case of continental aerosol intrusion under weak and moderate winds. c) The "M_tail-case", which has the same AP distribution as in the M-case until a dry CCN radius of 0.6 μm, but with 100 times higher AP concentration with radii exceeding 0.6 μm. As a result, the concentration of dry CCN (at S = 1%) with radii exceeding 0.6 μm is 60 cm^{-3}, which includes a concentration of 2 μm-radius CCN of 3.5 cm^{-3}. We suppose that this case may represent the AP distribution under hurricane winds in the central TC zone. d) In the "M_c_tail case" the AP is the same as in M_c, but with the tail of large CCN as in M-tail. We suppose that this case represents AP size distribution under intrusion of continental aerosols and strong wind conditions.

Parameters N_o and k were assumed in these simulations and corresponding references are presented in Table 1. We do not include CCN with dry radius above 2 μm into the simulations. In all simulations clouds were triggered by the initial heating within the zone centered at x = 54 km, to allow the cloud hydrometeors to be located longer in the computational zone. The maximum value of the dynamical time step was 5 s. Most simulations were conducted for time periods of 3 to 4 hours.

Results of 2-D Simulations

The first important result was that the tail of large CCN (within the radii range 0.6 μm to 2 μm) actually does not influence cloud microstructure structure and precipitation in the presence of high concentration of small CCN. For instance, accumulated rain amounts in the simulations M_c and M_c_tail are just similar (Fig. 2). This result can be explained as follows: the rate of diffusion growth is determined by supersaturation. In case when about 800–1000 cm^{-3} droplets are nucleated (as in the M_c and the M_c_tail cases), the supersaturated water vapor is sheared between a great number of droplets and the supersaturation is small. Note that droplets

Table 1 List of simulations and parameters characterizing aerosol distributions

Type of cloud	Short title	N_o (cm^{-3})	k	references
Maritime cloud	M	60	0.308	Khain et al. 2005
Sum of maritime and continental	M-c	2500 60	0.921 0.308	Khain et al. 2001b, 2004, 2005; Khain and Pokrovsky, 2004
Maritime cloud with increased fraction of large CCN	M_tail cloud	60 tail: 60 CCN with radii exceeding 0.6 μm	0.308	Sensitivity study
Sum of maritime and continental but with the increased fraction of large CCN	M_c_tail	2500 cm^{-3} 60 cm^{-3} tail: 60 particles with radii exceeding 0.6 μm	0.92 0.308	Sensitivity study

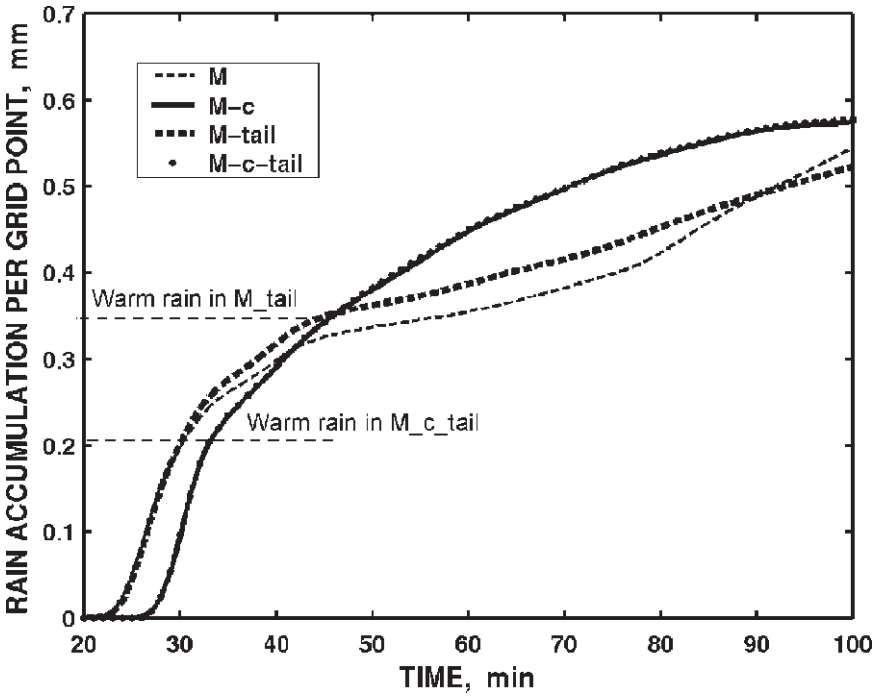

Fig. 2 Time dependence of accumulated precipitation at the surface in simulations with different concentrations of small (continental) and large aerosols (see Table 1). The increase in slope of curves indicates decrease in warm rain precipitation and beginning cold (melted) rain. Horizontal dashed lines denote the approximate amount of warm rain in the simulations. Remaining accumulated rain is mostly cold (melted) precipitation. The warm rain in clouds developing in dirty air is smaller than that in cloud developing in clean air. At the same time, total accumulated rain is larger in clouds developing in dirty air

growing on large CCN also contribute to the decrease in the supersaturation. As a result, the largest nucleated droplets with initial radius of about 10 μm grow relatively slow and reach the size necessary to collect smaller droplets at heights of about 5.5–6 km. It is necessary to recall that smaller droplets increase their size by diffusional growth faster than the largest ones (Rogers and Yau 1989), so that at the 6 km level the contribution of large CCN to the concentration of raindrops is not substantial. Stronger effect of large tail takes place in case of low droplet concentration, when supersaturation is higher than in case of high droplet concentration. Hence, raindrops in the M_tail form at about 3 km instead of 4 km in the M-case. The accumulated rain amount in the M_tail run is larger than in the M during the first 1.5 h. However, the difference in the rain amounts is not substantial in this case too. Low sensitivity of clouds developing under tropical maritime environmental conditions to amount of large CCN allows us to discuss effects of continental aerosols on TC clouds under a large uncertainty in the concentration of large CCN. Since, we expect the existence of the tail of large CCN in the TC clouds, we will discuss below the effects of continental aerosols on the cloud structure in the M_tail and the M_c_tail simulations. Note that no giant CCN with radii above 25–30 μm capable to trigger drop collisions in a short time after their penetration into a cloud, were assumed in the simulations.

Figure 3 shows the fields of cloud water content CWC (droplets with radii below 50 μm) in the M_tail and M_c_tail simulations at t = 25 min. One can see that while CWC in clouds with the low AP concentration decreases dramatically above 3.5–4 km because of rapid raindrop formation, the CWC in clouds with the high AP concentration remains significant to the upper atmosphere. This is a typical feature of clouds developing in dirty air (e.g., Andreae et al. 2004; Ramanathan et al. 2001; Khain et al. 2004, 2005). Specific feature of the present results is that large CWC takes place in dirty air in the presence of a high concentration of large CCN. Figure 4 shows the fields of crystal (upper panels), graupel (middle) and hail content in the M_tail (left) and M_c_tail (right) simulations. One can see that these contents are higher in clouds developing in polluted air, which can be attributed to a larger amount of CWC penetrating above the freezing level in this case. The vertical

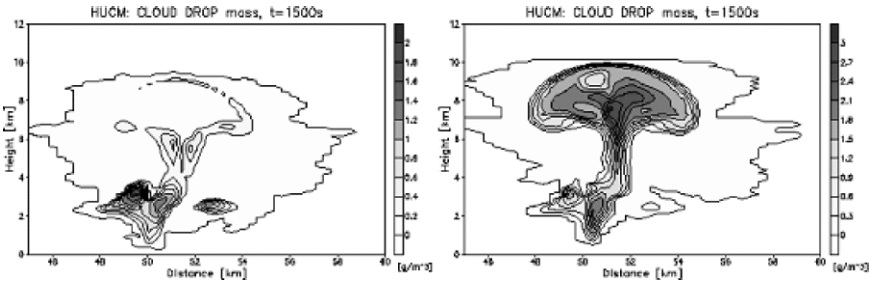

Fig. 3 Fields of cloud water content CWC (droplets with radii below 50 μm) in the M_tail and M_c_tail simulations at t = 25 min. CWC is significantly higher and reach higher levels in clouds developing in dirty air

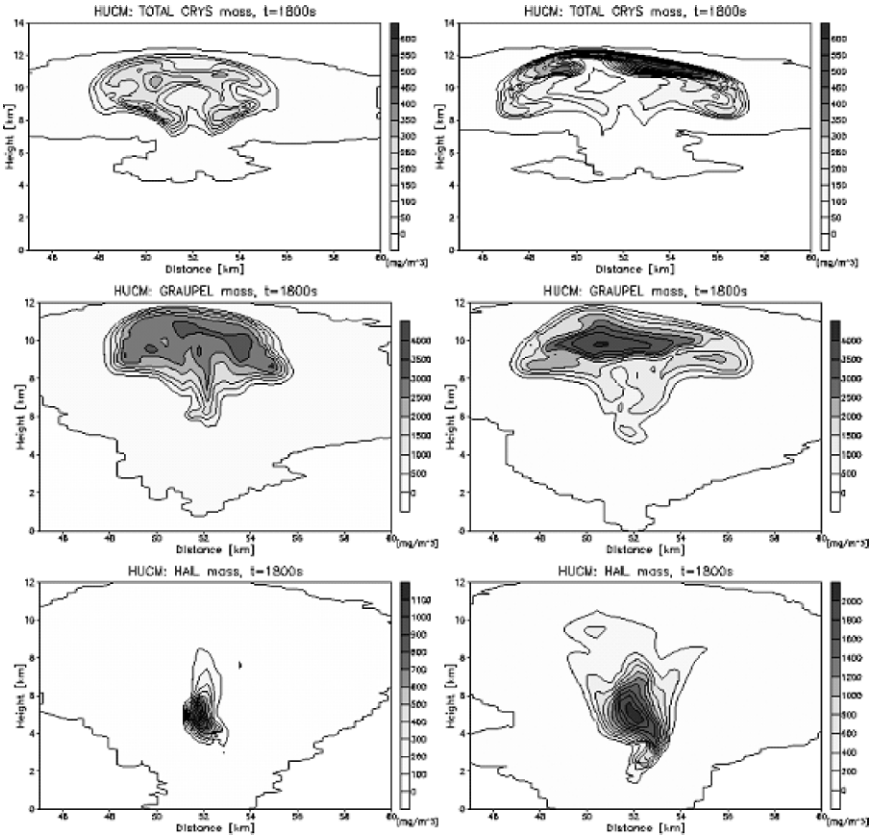

Fig. 4 The fields of crystal (*upper panels*), graupel (*middle*) and hail content in the M_tail (*left*) and M_c_tail (*right*) simulations. One can see that these contents are higher in clouds developing in the high aerosol concentration

velocities in clouds developing within the high AP concentration air are higher by a few m/s than in clouds developing under the low aerosol concentration cases. This aerosol effect on cloud dynamics was simulated and discussed in detail by Khain et al. (2005) and then simulated in many studies (e.g. Lynn et al., 2005a, b). The increase in the vertical updrafts in tropical clouds developing in dirty air can be attributed to extra latent heat release caused by extra condensational droplet growth (larger CWC) and extra freezing (larger ice contents) (see Figs. 4 and 5). The calculated radar reflectivity fields (not shown) indicate that high values of radar reflectivity in clouds forming in the dirty air reach (better to say, start) at higher levels as compared with the clouds developing in clean air, which agrees with the TRMM's Tropical Microwave images mentioned above.

All these results indicate that

a) *High vertical velocity which is possible in clouds at TC periphery is necessary, but not sufficient condition for the lightning formation.*

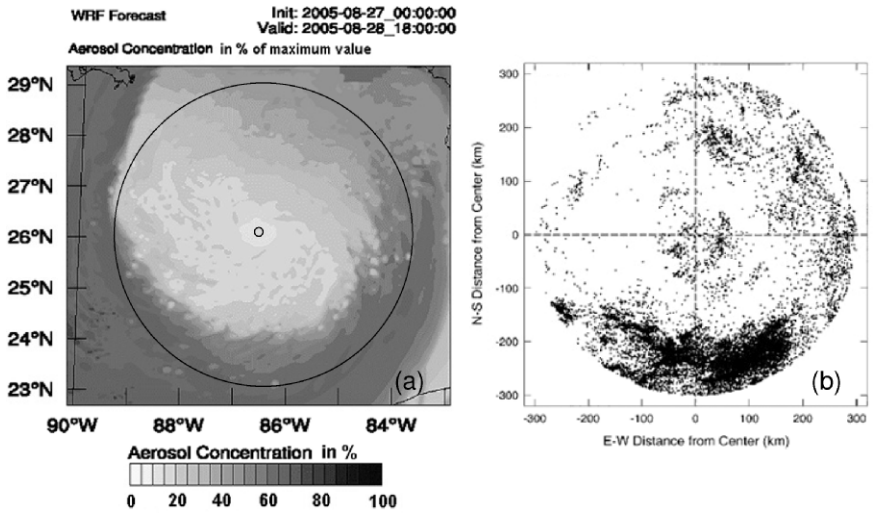

Fig. 5 The field of the aerosol concentration simulated in the lower troposphere in the TC zone on 28 August, 12 Z in % to the maximum value assumed to be over the continent (*left*). The locations of negative ground flashes observed during hurricane stage in the nine storms in the Western Atlantic, composited with respect to the hourly center position of each hurricane (adopted from Molinari et al. 1999) (*right*)

b) *Continental aerosols penetrating into the convective clouds via their cloud base can change dramatically the cloud microphysics and dynamics, making it possible the coexistence of cloud ice and supercooled water at high levels with temperatures below-13°C, i.e. transferring maritime convection into thunderstorms.*

Figure 3 shows time dependence of accumulated precipitation at the surface in the simulations with different concentrations of small and large CCN (see Table 1). One can see that a) accumulated precipitation from clouds developing in dirty air is higher than in clean air; b) warm rain amount decreases in clouds developing in dirty air, so that most precipitation in dirty clouds is cold rain formed by melting graupel and hail. On contrary, precipitation from clouds developing in clean air consists mainly of warm rain.

The results agree with observed data (e.g. Shepherd and Burian, 2003) and numerical results by Wang (2005), Lynn et al. (2005a) about aerosol effects on deep tropical convection under wet conditions. As it was discussed by Khain et al. (2004, 2005) and in more details by Khain et al. (2008), the increase in precipitation in dirty air under wet tropical conditions is related to the generation of larger condensate mass due to extra condensational growth of droplets and extra depositional growth of ice and comparatively low loss of precipitating mass in wet air.

The conclusions reached in this section allow us to carry out the simulations using a 3-D mesoscale model.

Aerosol Effects on TC Approaching the Land

Design of Numerical Simulations

A two nested grid WRF model was used to simulate landfall of hurricane Katrina. The resolution of the finest and the outer grid was 3 km and 9 km, respectively. A modified version of the bulk-parameterization by Thompson et al. (2006) was applied. The WRF lateral boundary conditions were updated every six hours using Global Forecast System Reanalysis data. The Gulf of Mexico's surface water temperatures were initialized at 28 August 12 Z, and were not updated during the experiments described below. The number of vertical levels was 31 with the distances between the levels increasing with height.

Because of computer limitations, the simulations were performed in two stages. At first stage the transport of continental aerosols by the TC circulation was calculated. Aerosols were considered as a passive scalar in the run. The TC was simulated beginning with 27 August 6 Z (when it was located to the south of Florida) till 28 August 12 Z. The purpose of the simulation was to check whether continental aerosols located initially over the land can be involved into the TC circulation and penetrate to the distances of about 300 km to the TC center toward the beginning of lightning in the Mexican Gulf (Fig. 1). The simulation showed that aerosols indeed penetrate in the lower troposphere of the TC "in time" (Fig. 5). Toward 28 August 12 Z aerosols form a concentric front of radius of about 250–300 km with a quite sharp gradient of aerosol concentration: while at the radii $r \geq 250$ km concentration in the lower atmosphere was actually similar to that over the land, the central TC zone with radius below 250 km was free from the continental aerosols. Figure 5 (left) shows that the aerosols penetrate closer toward the TC center on the south side. This effect can be attributed to the fact that aerosols are advected along spirals by the TC wind. Aerosols starting their motion at the continent (to the north of the TC) should approach the TC center during their motion along the spirals because of the radial wind directed inward. Thus, aerosols should be closer to the TC center on the southern and the eastern sides of TCs then in the west side. However, the AP concentration decreases along the stream limes. Hence, the concentration on the south side turns out to be higher than on the east side. It is interesting to note that the spatial distribution of the AP concentration obtained in the simulation resembles the locations of negative ground flashes observed during hurricane stage in the nine storms in the Western Atlantic (see Fig. 5 (right) adopted from Molinari et al. 1999), composited with respect to the hourly center position of each hurricane. One can see a good correlation between the distribution of aerosols and the lightning density. The similarity of the fields may be interpreted as some evidence of the validity of the aerosol hypothesis (at least, it does not contradict the hypothesis). These results indicate that while lightning at the distances of a few hundred km from the TC center may be related to aerosols as it is hypothesized here, lightning in the TC eye wall seen in Fig. 1 is not related to effects of continental aerosols. Note that developed rain bands form in

the TC within zone of about 300 km radius. Thus, we suppose that one the concentric lightning ring seen in Fig. 1 is that this ring forms in zone of the aerosol "front", which invigorates the convection transferring the maritime clouds into thunderstorms.

In the simulation, in which aerosols are treated as a passive scalar (tracer) the aerosol front approaches TC center in the inflow layer quite slowly, with the velocity close to the radial velocity of the flow. Passive aerosols reach the central TC toward the time, when Katrina was quite close to the land and lightning in its eye wall has already terminated (Fig. 1, right panel) In case cloud-aerosol interaction is taken into account, the concentration of continental aerosols must decrease from the TC periphery toward the TC center even much stronger because of the wash out of aerosols in TC rain bands. The results indicate that:

a) The lightning in the TC eye wall is not related to aerosols and caused by dynamical reasons. To reach a significant concentration of supercooled droplets above the $-13°C$ level in the TC eye wall (where concentration of continental CCN is small) vertical velocities must be especially high. At the same time the conditions at the TC periphery where concentration of continental CCN is high remain favorable for flash formation during the whole time period when the TC approaches or penetrates the land. This result allows one to explain why lightning in TC eye wall takes place only during TC deepening, while the lightning is permanent at the TC periphery (see e.g., Fig. 1).
b) The problem whether giant CCN arise in zone of maximum winds or not is not very important for our purposes, because continental aerosols do not reach TC center (at least, in TC simulated in the study).

At the second stage, the calculations of the TC were performed for cases when the aerosol effects on TC clouds were taken into account. The calculation was performed for the period from 28 Aug. 12 Z to 30 Aug. 6 Z. The way how the aerosol effects were accounted for requires some preliminary comments. The 3-km resolution and relatively crude vertical resolution does not allow one to reproduce the fine features discussed in the Section 2.3. It is well known that crude resolution decreases vertical velocities, which values are of crucial importance for simulation of cloud dynamics, microphysics and precipitation. As discussed by Khain et al. (2004), the utilization of crude resolution in cloud resolving models leads to the simulation of clouds with characteristics similar to those of maritime clouds, even if the concentration of droplets (either calculated with a model like HUCM or prescribed in a bulk scheme) is high.

Khain and Lynn (2008) describe another problem related to the utilization of the bulk parameterizations (including the Thompson bulk scheme 2006) for the simulation of the aerosol effects on precipitation. They used WRF to simulate super-cell storms with the scheme as well as with the spectral microphysics. They found that the microphysical structure of super-cell storms simulated by the bulk scheme was not very sensitive to large changes in initial cloud drop concentration, at least when compared to results of corresponding simulations with the spectral (bin) microphysics. Thus, the direct simulation of clouds with the bulk parameterization

scheme, just by presetting different droplet concentrations at cloud base would most likely misrepresent fine aerosol effects in cloud microphysics in the 3-km resolution model. To "sidestep" this problem, we simulated effects of continental aerosols in the simulations by preventing warm rain altogether in the Thomson scheme. As seen in Fig. 3, it is hardly possible to prevent warm rain in maritime deep clouds by an increase in aerosol concentration to the magnitudes typical of continental conditions. However, small aerosols significantly decrease the warm rain amount, and even more relevantly, the prevention of warm rain in the 3-D model allows reproduction of the aerosol effects qualitatively similar to those obtained in the 2-D 250 m resolution cloud model, namely, a substantial transport of large CWC upward and increase in the ice content.

The following simulations have been performed with the 3-D WRF model. The control run allowed for warm rain (WR) formation by drop-drop collisions (the WR run). In this run droplet concentration at cloud base N_d was set equal 30 cm^{-3}. This case corresponds to the M-run with the 2D model, where CCN concentration (at S = 1%) was assumed to be 60 cm^{-3} (usually about half of the available CCN are activated). In the second run referred to as No Warm Rain at the Periphery (NWRP-30), aerosol effects were parameterized by shutting off the drop-drop collisions only on the hurricane periphery, where the surface wind was smaller than 35 ms^{-1}. This threshold was chosen because the continental aerosol concentration in the TC central zone where wind speed exceeds 35 ms^{-1} should be negligibly small, as it was discussed above. Besides, very high wind speed supposedly is able to produce a significant amount of giant CCN in the eye wall which most likely render ineffective any effects of small aerosols. Hence, warm rain is shut off only in that part of the hurricane that has winds speeds less than the threshold value. Similar approach has been used by Rosenfeld et al. (2008).

The third simulation, referred to as NWRP-1000, is similar to NWRP-30, but the droplet concentration at cloud base was set to 1000 cm^{-3}. This is a supplemental run, which purpose is the illustration of difficulties to simulate properly the continental aerosol effects on maritime convection using the model with the crude horizontal and vertical resolution and changing only the droplet concentration.

Results of Simulations

In all runs the tracks of the simulated storms were actually similar and close to that of Katrina. The observed and simulated minimum pressures of the storm with time are shown in Fig. 6. The WRF model used does not allow exact assimilation of the initial TC intensity, so that the modelled hurricane was initially weaker than the real one. Nevertheless, the model was able to reproduce the main features of the hurricanes evolution, including the formation of the super hurricane with the minimum pressure of about 915–920 hPa. The main result that follows from Fig. 6 is that aerosols, affecting the hurricane clouds, affect both its structure and intensity. One can see that TC moving within a dirty air has smaller intensity that in that moving in clean air during the entire simulation. This effect (see below) can be attributed to the convection invigoration at TC periphery, which was caused

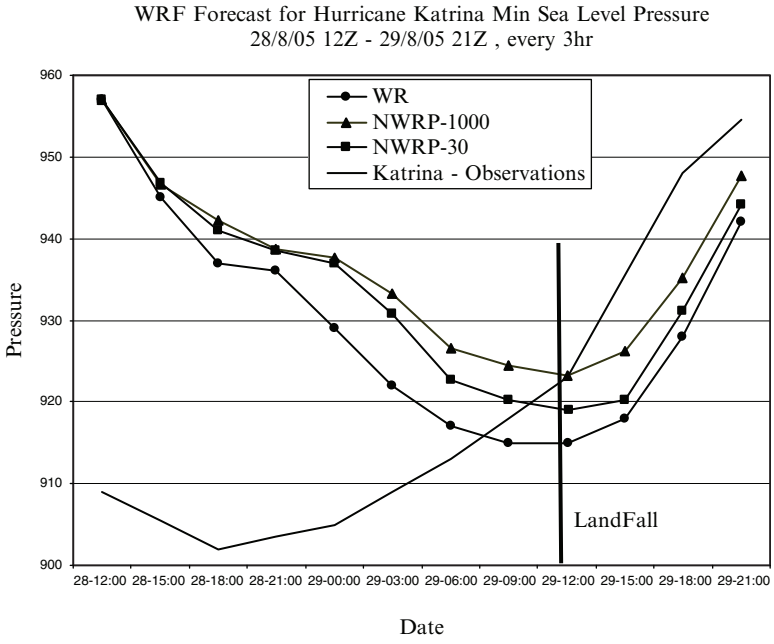

Fig. 6 The observed and simulated minimum pressures of the storm with time The WRF model used does not allow exact assimilation of the initial TC intensity, and the modelled hurricane was initially weaker than the real one. Nevertheless, the model was able to reproduce the main features of the hurricanes evolution, including the formation of the super hurricane with the minimum pressure of about 915–920 hPa. The warm rain prevention at the TC periphery decreased minimum pressure by 7–10 mb

by turning off the warm rain (representative of the potential impacts of high concentrations of aerosols on formation of droplets). As a result, some fraction of air moving within the inflow layer ascends at the periphery instead reaching the TC eye wall. Hence, the rate of latent heat release decreases within the eye wall, which results in some increase in the central pressure and increase in the maximum wind (and eyewall) radius.

Figure 7 illustrates the aerosol effects (as it was simulated by in the study) on microphysical and dynamical structure of the TC. One can see a good qualitative correspondence of obtained values of super cooled CWC and those found in the 2-D cloud simulations: the CWC maximum in dirty air is about 5 gkg^{-1}, while in the clean air it does not exceed 2 gkg^{-1}. One can see an aerosol-induced increase in the total ice content at the TC periphery in agreement with the results of the 2D model with the spectral microphysics. The maximum values of total ice content are also in good agreement with the 2-D results. The difference in the condensate mass contents in simulations WR and NWRP-30 indicates the differences in the latent heat release and the vertical updrafts (the third row panels). The maximum vertical velocity in many small clouds arising in dirty air exceeds 10 ms^{-1}, while in the TC central zone the typical maximum vertical velocity ranges mainly from 4 to 10 ms^{-1}. One can see that aerosols increase the intensity of convection within cloud bands

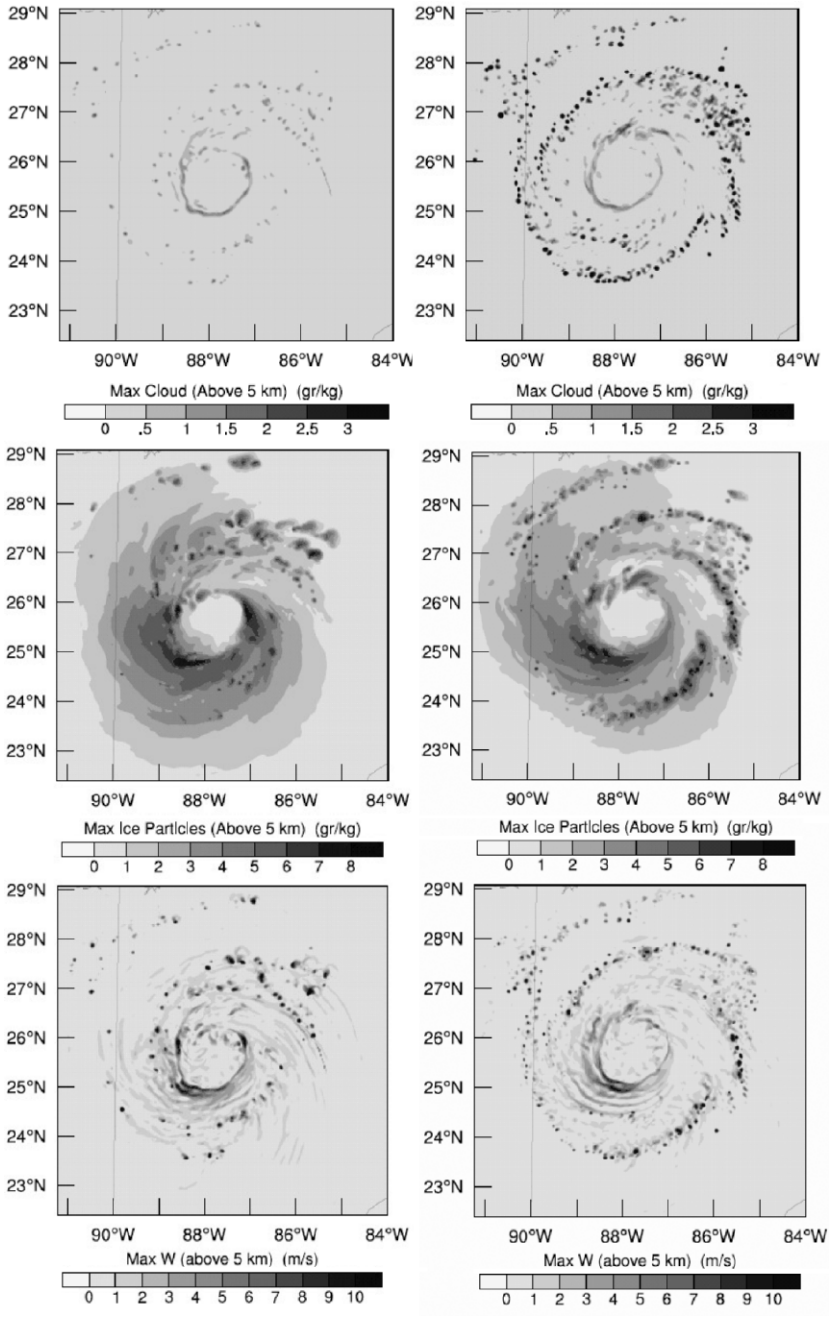

Fig. 7 Maximum values of super cooled CWC above the 5 km-level (*upper row*), total ice content (*middle*) and vertical velocities at t = 6 h in simulations with warm rain permitted (*left*) and no warm rain (*right*)

located at the distance of 250–300 km from the TC center. This radius corresponds to the TC remote cloud bands. Analysis of the vertical cross-sections of the differences of azimuthally averaged fields of total ice content (Qice), cloud water content (Qc), rain content (Qr), and vertical velocity between NWRP30 and WR runs (Fig. 8). One can see that aerosols invigorate convection and increase precipitation at the distance of about 250 km, decreasing, at the same time, the convection intensity between the remote rain bands and the eye wall. As a result, convection within the circle with radius of about 250 km weakens, preventing intense lightning at closer distance to the TC center.

As was discussed above, an increase of CWC and ice content in the zones of high vertical velocity should foster lightning formation. Figure 9 shows the fields representing the product of CWC and ice mass contents of low and high density ice. This product will be referred to as lightning probability (LP). This product is maximum within the area of maximum updrafts. The Fig. 9 (upper right panel) is plotted at time instance of lightning activity depicted in Fig. 1 (left and middle panel). One can see that LP field calculated in NWRP-30 resembles very well the

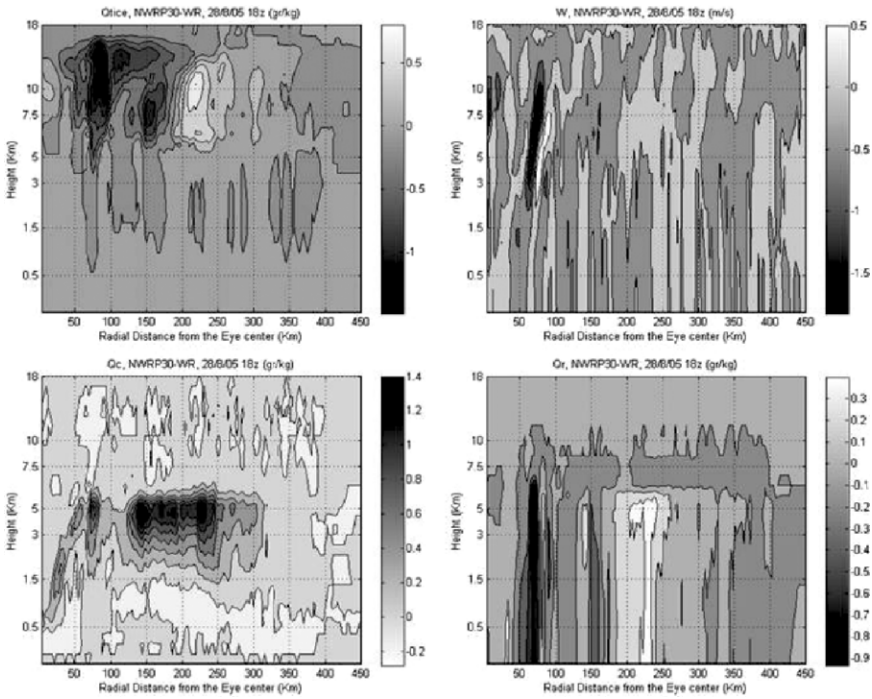

Fig. 8 The vertical cross-sections of (NWRP30-WR) differences of azimuthally averaged fields of total ice content Qt_{ice}, cloud water content (Qc), rain content (Qr), and vertical velocity. One can see that aerosols invigorate convection (and precipitation) at the distance about 250 km (the differences are positive), decreasing at the same time the convection intensity between the remote rain bands and the eye wall. As a result, convection within the about 250 km radius circle weakens, preventing intense lightning at closer distance to the TC center

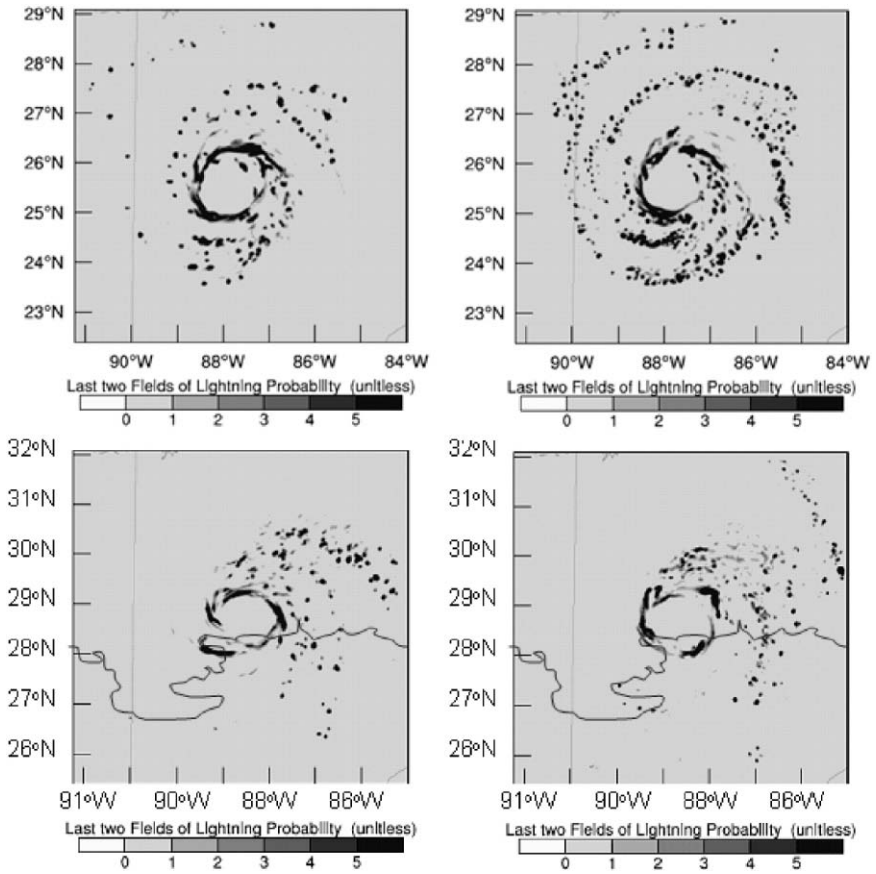

Fig. 9 Lightning probability (LP) (relative units) accumulated for different time periods of TC evolution in case of clouds developing in clean air (*left*) and dirty air (*right*). The LP is calculated as a product of updrafts, CWC and total ice content. In the upper row LP is calculated for the period t = 3–6 hours, and in the bottom row LP for the period t = 24–27 hours

structure of observed lightning: a) the maximum lightning takes place within a comparatively narrow ring of the 250–300 km radius; Time averaging of the LP over the period of a few hours results in appearance of several rings of enhanced lightning related to different time instances: b) lightning at TC central zone is as a rule weaker than at the rain bands at TC periphery. In contrast, in the WR simulation lightning is much weaker and concentrated in the eye wall, which does not agree with the observations. The lower panels correspond to time when the entire TC has penetrated to the land and rapidly decays. One can see that while in clean air lightning weakens over the land, it continues in dirty air. Moreover, the lightning rate increases in the TC central zone. These figures show that aerosols significantly affect the spatial distribution of intense convection in TCs.

The results indicate also that aerosols affect cloud structure, intensity and spatial distribution of precipitation of TCs approaching and penetrating the land. Figure 10

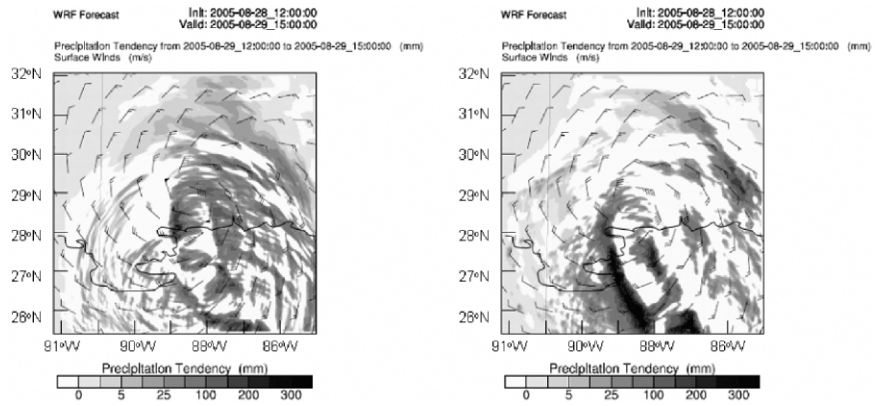

Fig. 10 The field of precipitation rate in the experiment with warm rain allowed over the entire computational area (WR-simulation) (*left*) and in case when warm rain has been turned off at the TC periphery (NWRP-30) (*right*) during the TC landfall

shows the fields of precipitation rate in the experiment with warm rain allowed over the entire computational area (WR-simulation) and in case when warm rain has been turned off at the TC periphery (NWRP-30). One can see that in case the aerosol effects are taken into account, precipitation takes place over larger area, but the intensity in the TC center is weaker.

Figure 11 shows time dependences of precipitation averaged over 3 h periods within the TC zone (the internal grid) in "warm rain" and "no warm rain" simulations. During first 5 hours precipitation rate in the NWRP-30 is larger than in the WR run, supposedly due to increase of precipitation at the TC perephery. Later on, an increase in the aerosol concentration decreases precipitation within the TC zone, because the decrease in precipitation rate in the central zone of the TC. These results can serve as numerical justification and explanation of the observed weekly cycle of intensity and precipitation of landfalling TCs found by Cerveny and Balling (1998) who attributed these changes to the weekly variation of anthropogenic aerosol concentration.

Discussion and Conclusions

The potential effects of continental aerosol penetrated into the circulation of TC approaching the land on the cloud structure and the lightning rate in hurricane clouds has been investigated using a 2-D cloud model with spectral bin microphysics and a 3D mesoscale model WRF with bulk microphysics. Numerical experiments with the 2D cloud model with the resolution of 250 m and 125 m in the horizontal and vertical directions, respectively, show that the continental aerosols with the CCN concentrations of about 1000 cm^{-3} significantly increase the amount of supercooled cloud water, as well as ice (mainly ice crystals, graupel and hail) even under the high concentration of large CCN, which may have maritime nature.

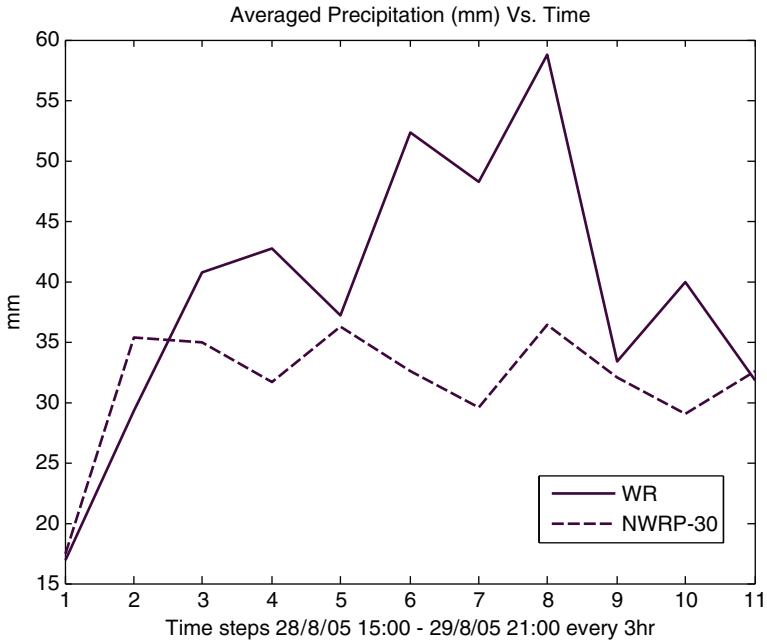

Fig. 11 Time dependences of precipitation averaged over 3 h periods within the TC zone (the internal grid) in "warm rain" and "no warm rain" (NWRP-30) simulations

In addition, the vertical updrafts were stronger in the polluted clouds. All these factors taken together lead to coexistence of ice and cloud water within a supper-cooled cloud zone, which is considered to be favorable for charge separation and lightning formation.

The purpose of simulations using a mesoscale 3-km resolution model was to investigate the possible effects of aerosols on cloud structure and lightning of hurricanes, as well on precipitation and TC intensity. The utilization of 3-km resolution and crude vertical resolution, as well as the bulk-parameterization scheme used does not allow one to reproduce aerosol effects related to a fine balance between the fall velocity of growing droplets and the vertical velocity. For instance the results of supplemental simulation with droplet concentration N_d of 1000 cm^{-3} indicate some increase in supercooled CWC, etc., but, in general, the results were quite similar to those obtained in case when droplet concentration was set equal to 30 cm^{-3}.

As a result, the aerosol effects were parameterized by shutting of droplet collisions, preventing warm rain at the TC periphery, where the surface wind speed was weaker than 35 m/s. This simple parameterization of the aerosol effects turned out to lead to more realistic results, which better agrees with those, obtained using a spectral microphysical model with the resolution of 100–250 m.

The product of the updraft velocity, ice content and supercooled cloud water content was chosen as the measure of lightning activity (lightning probability LP).

It was shown that the LP field calculated in the model resembles very well the structure of observed lightning: a) the maximum lightning takes place within a comparatively narrow rings with radius 250–300 km; b) lightning in the TC central zone is, as a rule, weaker than that in the rain bands at the TC periphery. In the simulation, where no aerosol effects were taken into account, the magnitude of the LP parameter was smaller and concentrated in the eye wall, which does not agree with the observations.

The analysis of the intensity variations of simulated TCs, as well as the observed variation of the intensity of hurricanes Katrina (2005) and Rita (2005) (Fierro et al., 2007), shows that the disappearance of lightning in the TC central zone and its intensification (convection invigoration) at the TC periphery can be a good indicator of the TC decaying. Such behavior of TC lightning may be useful for a short range TC intensity forecast. Note that simulations of TC lightning in an idealized TC performed by Fierro et al. (2007) showed negligible lightning activity at the TC periphery as compared to that in the TC eye wall. We attribute this result to the fact that no aerosol effects were taken into account in the simulations performed by Fierro et al. (2007). Their results indicate that the changes of the instability of the atmosphere can lead to a variability of the lightning in the TC eye wall, but not within a narrow ring at the TC periphery. Correspondingly, the comparison of the results obtained by Fierro et al. (2007) and those in this study supports the assumption that lightning at the TC periphery is caused by continental aerosols.

The results indicate also that aerosols affect cloud structure, intensity and spatial distribution of precipitation of TCs approaching and penetrating the land. Precipitation in the TC zone of 350–400 km radius decreases in dirty air mainly due to weakening of convection in the central zone of the TCs. These results can serve as the first numerical justification of the observed weekly cycle of intensity and precipitation of landfalling TCs found by Cerveny and Balling (1998), who attributed these changes to the weekly variation of anthropogenic aerosol concentration.

According to the results obtained using the 2-D cloud model, aerosols lead to larger transport of CWC upward than it was simulated using the WRF mesoscale model. We suppose, therefore, that aerosol effect on cloudiness, precipitation and intensity of TCs may be even more pronounced than that was demonstrated in the study. The utilization of high resolution models with spectral bin microphysics is desirable to make the results quantitative. More observational studies are required for investigation of microphysical structure (supercooled water, cloud ice) of clouds in TCs. Observational and numerical studies are needed also for determination of aerosol fluxes from the land to landfalling tropical cyclones.

The monitoring of lightning in hurricanes both over open sea and in the vicinity to the land can provide useful information about the climatic changes of structure, intensity and precipitation in tropical cyclones.

The decrease in intensity of TC under the influence of small aerosols penetrating cloud base of deep convective clouds found in the simulation allows one to consider a possibility to decrease of hurricane intensity by seeding of small aerosols near cloud base at TC periphery. This seeding can be done during the time period before penetration of natural continental aerosols to distances 250–300 km from the TC

center. The idea to decrease TC intensity by cloud seeding is not new. Hurricane mitigation was first attempted between 1962 and 1983 in the framework of project STORMFURY by the US government (Willoughby et al., 1985). The envisioned modification technique involved artificial stimulation of convection at the outer periphery of the eyewall through seeding of strong convective cloud towers with silver iodide for the purpose of freezing super-cooled water (water in liquid state but colder than 0°C). It was hypothesized that the release of the latent heat of freezing would invigorate convection (Simpson and Malkus, 1964) that would compete with the original eyewall, leading to its reformation at a larger radius, and thus, through partial conservation of angular momentum, produce a decrease in the strongest winds. Modification was attempted in four hurricanes. The analysis of the microphysical structure of tropical convective (TC) clouds performed later (Willoughby et al., 1985) showed that at the levels where seeding was applied there was too little supercooled water in agreement with the results of the present study (see, e.g., Fig. 3 left panel). Consequently, the glaciogenic seeding was not likely to affect cloud dynamics, at least in the way assumed in the STORMFURY conceptual model. As a result, changes in intensity of seeded hurricanes were attributed to natural fluctuations of TC intensity. Seeding with small aerosols at cloud base leads, as it was shown in the study, to convection invigoration at the TC periphery and to the TC weakening. Note that the seeding of cloud bases with small aerosols increases amount of the supercooled water in the upper atmosphere. Thus, the seeding with small aerosols at cloud base may be combined with glaciogenic seeding with silver iodide to reach stronger invigoration of convection on the TC periphery. In more detail the possibility to decrease TC intensity by cloud seeding is discussed by Rosenfeld et al. (2007).

Acknowledgements The study was supported by the Israel Science Foundation, grant N 140/07.

References

Andreae, M.O., D. Rosenfeld, P. Artaxo, A.A. Costa. G.P. Frank, K.M. Longlo, and M.A.F. Silva-Dias (2004): Smoking rain clouds over the Amazon. *Science*, 303, 1337–1342.

Black R.A. and Hallett J (1999). Electrification of the hurricane, *J. Atmos. Sci*, 56, 2004–2028.

Cecil D.J., E.J. Zipser, and S.W. Nebitt (2002a) Reflectivity, ice scattering, and lightning characteristics of hurricane eyewalls and rainbands. Part 1: Quantitative description. *Mon Wea. Rev*. 130, 769–784.

Cecil D.J., E.J. Zipser, and S.W. Nebitt (2002a) Reflectivity, ice scattering, and lightning characteristics of hurricane eyewalls and rainbands. Part 2: Intercomparison of observations. *Mon Wea. Rev*. 130, 785–801.

Cerveny R.S. and R.C. Balling (1998). Weekly cycles of air pollutants, precipitation and tropical cyclones in the coastal NW Atlantic region. *Nature* 394 (6693) 561–563.

Cotton, W. R., H. Zhang, G.M. McFarquhar, S.M. Saleeby (2007) Should we consider polluting hurricanes to reduce their intensity? *J. Weather Modification*, **39**, 70–73.

Fierro A.O., L. Leslie, E. Mansell, J. Straka, D. MacGorman, and C. Ziegler (2007) A high-resolution simulation of microphysics and electrification in an idealized hurricane-like vortex. *Meteorol. Atmos. Phys.*, **98**, 13–33, Doi: 10.1007/s00703-006-0237–0.

Jordan, C.L. (1958) Mean soundings for the West Indies area. *J. Meteor.*, 15, 91–97.

Jorgensen, D. P., E.J. Zipser, and. M.A. LeMone (1985). Vertical motions in intense hurricanes. *J. Atmos. Sci.* 42, 839–856.

Khain, A. P. (1984) *Mathematical modeling of tropical cyclones.*

Khain, A.P. and E.A. Agrenich (1987) Possible effect of atmospheric humidity and radiation heating of dusty air on tropical cyclone development. *Proc. Institute Experim. Meteorol.*, 42 (127), 77–80.

Khain, A.P., M. Ovtchinnikov, M. Pinsky, A. Pokrovsky, and H. Krugliak (2000) Notes on the state-of-the-art numerical modeling of cloud microphysics. *Atmos. Res.*, **55**, 159–224.

Khain, A.P., M.B. Pinsky, M. Shapiro and A. Pokrovsky (2001a) Graupel-drop collision efficiencies. *J. Atmos. Sci.*, **58**, 2571–2595.

Khain A., A. Pokrovsky, M. Pinsky, A. Seifert, and V. Phillips (2004) Effects of atmospheric aerosols on deep convective clouds as seen from simulations using a spectral microphysics mixed-phase cumulus cloud model Part 1: Model description. *J. Atmos. Sci.*, **61**, 2963–2982.

Khain, A., Rosenfeld and D. Pokrovsky A. (2005). Aerosol impact on the dynamics and microphysics of convective clouds. *Quart. J. Roy. Meteor. Soc.* 131, 2639–2663.

Khain A.P. and B. Lynn (2007) Simulation of a super cell storm in clean and dirty atmosphere. *J. Geophys. Research* (submitted).

Khain, A., D. Rosenfeld and A. Pokrovsky (2005). Aerosol impact on the dynamics and microphysics of convective clouds. *Quart. J. Roy. Meteor. Soc.* 131, 2639–2663.

Khain A.P., N. BenMoshe, A. Pokrovsky (2008) Factors determining the aerosol effects on precipitation: an attempt of classification. *J. Atmos. Sci.*, **65**, 1721–1748.

Koren I., Y.J. Kaufman, D. Rosenfeld, L.A. Remer, Y. Rudich (2005) Aerosol invigoration and restructuring of Atlantic convective clouds, *Geophys. Res. Lett.*, **32**, L14828, doi:10.1029/2005GL023187.

Lhermitte R.M., and P. Krehbiel (1979): Doppler radar and radio observations of thunderstorms. *IEEE Trans Geosci Electron* 17, 162–171.

Lynn B., A. Khain, J. Dudhia, D. Rosenfeld, A. Pokrovsky, and A. Seifert (2005a) Spectral (bin) microphysics coupled with a mesoscale model (MM5). Part 1. Model description and first results. *Mon. Wea. Rev.* 133, 44–58.

Lynn B., A. Khain, J. Dudhia, D. Rosenfeld, A. Pokrovsky, and A. Seifert (2005b) Spectral (bin) microphysics coupled with a mesoscale model (MM5). Part 2: Simulation of a CaPe rain event with squall line *Mon. Wea. Rev.*, 133, 59–71.

Mansell E.R. , D.R. Mac.Gorman and J.M. Straka (2002) Simulated three-dimensional branched lightning in a numerical thunderstorm model. *J. Geophys. Res.* 107, D9 (doi: 10.1029/2000JD000244).

McFarquhar G., and R.A. Black (2004) Observations of particle size and phase in tropical cyclones: implications for mesoscale modeling of microphysical processes. *J. Atmos. Sci.* 61, 422–439.

Meyers, M.P., P.J. DeMott, and W.R. Cotton (1992) New primary ice-nucleation parameterizations in an explicit cloud model. *J. Appl. Meteor.*, **31**, 708–721.

Molinari J., Moore P., and V. Idone (1998g) Convective Structure of hurricane as revealed by lightning locations, *Mon. Wea. Rev.*, **127**, 520–534.

Orville R.E. and J.M. Coyne (1999) Cloud-to-ground lightning in tropical cyclones (1986–1996). *Preprints, 23-rd Conf. on Hurricanes and tropical meteorology*, Dallas, Amer. Meteor. Soc., 194 pp.

Pinsky, M. and A.P. Khain (1998) Some effects of cloud turbulence on water-ice and ice-ice collisions, *Atmos. Res.*, **47–48**, 69–86.

Pinsky, M., A.P. Khain, and M. Shapiro (2001) Collision efficiency of drops in a wide range of Reynolds numbers: Effects of pressure on spectrum evolution. *J. Atmos. Sci.*, **58**, 742–764.

Pinsky, M. B., A.P. Khain, and M. Shapiro (2007) Collisions of cloud droplets in a turbulent flow. Part 4. Droplet hydrodynamic interaction. *J. Atmos. Sci.*, **64**, 2462–2482.

Pruppacher, H.R. and J.D. Klett (1997) *Microphysics of clouds and precipitation*. 2nd edition, Oxford Press, 1997, 963p.

Ramanathan, V., P.J. Crutzen, J.T. Kiehl and D. Rosenfeld (2001), Aerosols, climate, and the hydrological cycle, *Science*, 294, 2119–2124

Rogers, R.R. and Yau, M.K. (1989) *A short course of cloud physics*. Pregamon, Oxford, 293 pp.

Rodgers E., J. Weinman, H. Pierce, W. Olson (2000) Tropoical cyclone lightning distribution and its relationship to convection and intensity change. *Preprints, 24th Conf. on Hurricanes and Tropical meteorology*, Ft. Lauderdale, Amer. Meteor. Soc. pp. 537–541.

Rosenfeld D., R. Lahav, A. Khain, and M. Pinsky (2002) The role of sea spray in cleaning air pollution over ocean via cloud processes. *Science* 297, 1667–1670.

Rosenfeld D., M. Fromm, J. Trentmann, G. Luderer, M. O. Andreae, and R. Servranckx (2007a) The Chisholm firestorm: observed microstructure, precipitation and lightning activity of a pyro-Cb. *Atmos. Chem. Phys*., 7, 645–659.

Rosenfeld D., A. Khain, B. Lynn, W.L. Woodley (2007f) Simulation of hurricane response to suppression of warm rain by sub-micron aerosols. *Atmos. Chem. Phys. Discuss*., 7, 5647–5674.

Saunders, C.P.R. (1993). A review of thunderstorm electrification processes, *J. Appl. Meteor*., 32, 642–655.

Shepherd, J.M., and S.J. Burian (2003) Detection of urban-induced rainfall anomalies in a major coastal city. *Earth Interactions*, 7, 1–17.

Sherwood S.C., V. Phillips and J. S. Wettlaufer (2006). Small ice crystals and the climatology of lightning. *Geophys. Res. Letters*, 33, L058804, doi. 10.1029/2005GL.

Shao X.M., Harlin J., Stock M., Stanley M., Regan A., Wiens K., Hamlin T., Pongratz M., Suszcynsky D. and Light T. (2005) Katrina and Rita were lit up with lightning, *EOS*, Vol. 86, No. 42, page 398–399.

Simpson, R.H., and Malkus J.S. (1964) Experiments in hurricane modification. *Sci. Amer*., 211, 27–37.

Skamarock, W.C., Klemp J.B., Dudhia J., Gill D.O., Barker D.M., Wang W., and Powers J.G. (2005). A description of the Advanced Research WRF Version 2. NCAR Tech Notes-468+STR.

Straka J.M. and E.R. Mansell (2005). A bulk microphysics parameterization with multiple ice precipitation categories. *J. Appl. Meteorol*. 44, 445–466.

Takahashi, T (1978) Riming electrification as a charge generation mechanism in thunderstorms. *J. Atmos. Sci*., 35, 1536–1548.

Takahashi, T., T. Endoh, and G. Wakahama (1991) Vapor diffusional growth of free-falling snow crystals between –3 and −23 C. *J. Meteor. Soc. Japan*, **69**, 15–30.

Thompson, G., P.R. Field, W.D. Hall, and R. Rasmussen (2006) A new bulk microphysical parameterization for WRF (& MM5). *Presented at WRF conference*, NCAR, June 2006.

Wang C.A (2005) Modelling study of the response of tropical deep convection to the increase of cloud condensational nuclei concentration: 1. Dynamics and microphysics. *J. Geophys. Res*., v. 110; D21211, doi:10.1029/2004JD005720.

Williams E, G. Satori (2004) Lightning, thermodynamic and hydrological comparison of the two tropical continental chimneys. *J. Atmos. And Solar-Terrestrial Phys*. 66, 1213–1231.

Williams E., V. Mushtak, D. Rosenfeld, S. Goodman and D. Boccippio, (2005) Thermodynamic conditions favorable to superlative thunderstorm updraft, mixed phase microphysics and lightning flash rate. *Atmos. Res*., 76, 288–306.

Wiens K.C., S.A. Rutledge, and S.A. Tessendorf (2005) The 29 June 2000 supercell observed during steps. Pt 2: Lightning and charge structure. *J. Atmos. Sci*. 62, 4151–4177.

Willoughby, H.E., Jorgensen D.P., Black R.A., and Rosenthal S.L. (1985) Project STORMFURY, A Scientific Chronicle, 1962–1983, *Bull. Amer. Meteor. Soc*., 66, 505–514.

Response of Tropical Cyclogenesis to Global Warming in an IPCC AR4 Scenario

Jean-François Royer and Fabrice Chauvin

Abstract Since currently very few models can reach the high resolutions necessary for a detailed representation of tropical cyclones, most assessments of their response to climate change in coupled scenarios have to be based on indirect estimates of the hurricane activity potential. A modified Convective Yearly Genesis Potential index (CYGP) proposed by Royer et al. (1998) is applied here to the analysis of TC genesis in 15 coupled general circulation models (CGCMs) that have run simulations for the IPCC AR4 for the 20th century and for scenario A2. For the current climate most of the models simulate rather realistic patterns of cyclogenesis, though the TC genesis in the different ocean basins differs from model to model. The cyclogenesis index shows interdecadal fluctuations and long term trends. In scenario A2 the patterns of response of cyclogenesis at the end of the 21st century differ according to the ocean basins and models. While in some ocean basins like the Indian Ocean, the majority of models compute an increasing trend in TC genesis, the response is less coherent in other basins where some models give a decreasing trend. The lack of coherence of the TC genesis response to future climate change can be associated to the different response patterns of sea surface temperatures (SST) in the coupled models, particularly over the Equatorial Pacific, and to their differences in the simulation of ENSO. Until some better convergence of the model SST response has been achieved, it seems rather premature to draw conclusions about possible future changes in TC genesis.

Introduction

There is still considerable uncertainty concerning the change in tropical cyclone (TC) properties in response to global warming and climate change produced by the increase of greenhouse gas (GHG) forcing (Henderson-Sellers et al. 1998; Walsh 2004; Pielke et al. 2005). The tools appropriate for studying this question are global, or regional, coupled atmosphere-ocean climate models that can be applied in climate simulations for present and future conditions. There are two complementary aspects that need to be addressed, namely changes in tropical cyclone frequencies,

J.B. Elsner and T.H. Jagger (eds.), *Hurricanes and Climate Change,*
doi: 10.1007/978-0-387-09410-6,

that depend on their genesis and trajectories, and changes in tropical cyclone maximum intensity. In this paper only the question relevant to TC genesis in global coupled simulations will be considered. The question of TC intensity requires different methodologies applied to high resolution nested regional models (Knutson and Tuleya 2004; Stowasser et al. 2007).

The methods that have been used to study the genesis of tropical cyclones, in global climate simulations, can be divided in two categories:

- The direct approach by tracking methods
- The indirect approach by means of a cyclogenesis potential based on large-scale environment factors.

The direct approach consists simply in identifying TC-like vortices in sequences of daily (or sub-daily) large-scale fields, and tracking them in order to construct their trajectories. Though conceptually simple, the application of this method requires in practice consideration of different rather complex technical issues. For example, the choice of the detection thresholds needs to be adapted to the model resolution (Walsh et al., 2007), and criteria need to be defined for checking the continuity of the constructed trajectories. In order to yield convincing results this method requires a rather high resolution in the models, so that the simulated tropical vortices can have a reasonable resemblance to observed tropical cyclones. Though it has been applied initially to models with low resolution (Manabe et al. 1970; Broccoli and Manabe 1990, Krishnamurti et al. 1998; Tsutsui 2002), it is only with a grid reaching about 100 km resolution that the vortices start to look somewhat more realistically like TCs, rather than like large-scale lows, as was shown in the pioneering work of Bengtsson et al. (1982, 1995, 1996). However the application of this tracking method to the analysis of climate change has still been rather limited (Haarsma et al. 1996; Sugi et al. 2002; McDonald et al. 2005; Chauvin et al. 2006, Oouchi et al. 2006) since only a very small number of high-resolution simulations have been available, and this has precluded the assessment of model uncertainties.

Therefore it may appear preferable to try to assess the simulations by means of indirect methods allowing an estimation of cyclone properties by a combination of large-scale environment factors that have been shown physically relevant to TC formation or development. The most well known of such indices is the Yearly Genesis Parameter (YGP) developed by Gray (1968, 1975). The potential interest of the application of such indices to the analysis of climate simulations is that one can hope that the results should be less dependent on the model resolution than the direct approach, since the index depends on large-scale environmental properties, generally averaged over time. As some of the indices rely on time-averages properties over a month or a season, their computation should be much less costly in computer resources, and much easier to apply in practice than the tracking method that requires analysis of high-frequency (daily or subdaily) maps.

The indirect approach can thus be applied efficiently to a large set of different model simulations, which can be useful to assess the differences in their results and thus the uncertainties in the response (Ryan et al. 1992; Watterson et al. 1995; Tsutsui and Kasahara 1996). The initial application of the YGP to the analysis of

climate simulations has given a high increase of the YGP in the case of doubled CO2 simulations (Ryan et al. 1992). Royer et al. (1998) have confirmed the large increase of YGP in the case of doubled CO2 simulations. However they have shown that most of the increase comes from the thermal potential and its dependence on a fixed 26°C SST threshold. They defined a modified index in which the thermal potential is replaced by convective precipitation, and have shown that this modified Convective YGP (CYGP) was able to reproduce tropical cyclogenesis distribution. The CYGP is much less sensitive to surface temperature and provides a more modest and more credible change in cyclogenesis for the doubled-CO2 case.

McDonald et al. (2005) have compared tracked cyclones in high resolution simulations and have found that the CYGP was able to provide a good agreement with the genesis of tropical cyclones. Similar results were found by Chauvin et al. (2006) with higher resolution simulations for the change of the CYGP in future climate simulations. However Camargo et al. (2007) found less good agreement between the actual TC track density or TC numbers and the Genesis Potential Index defined by Emanuel and Nolan. The agreement of the CYGP with the results of cyclone tracking shows that the CYGP could be a useful diagnostic for analyzing cyclogenesis in climate simulations.

The aim of this paper is to illustrate the potential of the CYGP by applying it to a subset of IPCC climate simulations for the past climate, and for an A2 scenario for the future. The methodology is described in section 2, and the models in section 3. The results of applying the CYGP to model simulations for the current climate are given in section 4. The results for scenario A2 at the end of the 21st century are presented in section 5. Finally some conclusions and perspectives are discussed in section 6.

Method of Calculation of the Convective Seasonal and Yearly Genesis Parameter

Given that the formulation of the Seasonal and Yearly Genesis Parameter (resp. SGP and YGP) of Gray (1968, 1975) is not appropriate for climate change purposes, as indicated in the introduction, Royer et al. (1998) suggested to replace all the thermal contributions by a new thermal potential which can be represented by convective precipitation. This diagnostic is indeed a good integration of the three components of the Gray's YGP thermal potential. It combines the stability of the atmosphere, the humidity of the low levels and SST anomalies, since evaporation is a major contribution to convection. This new formulation of the YGP is able to diagnose the thermal potential with the model components and avoids the dependence to a fixed 26°C SST threshold that the old formulation induced.

The dynamical potential is defined as the product of three factors:

- $f = 2\Omega \sin\varphi$ is the Coriolis parameter, φ is the latitude and Ω the angular velocity of the Earth, in 10^{-5} s^{-1}.

- $I_{\hat{\zeta}} = (\zeta_r\, f/|f|) + 5$ where ζ_r is the low level relative vorticity at 950 hPa, in $10^{-6}\ s^{-1}$.
- $I_S = (|\delta V/\delta P| + 3)^{-1}$ is the inverse of the vertical shear of the horizontal wind (V) between the pressure (P) levels 950 hPa and 200 hPa, in ms^{-1}/750 hPa.

In CYGP the thermal potential is based on the convective precipitation diagnosed by the models. In order to avoid cyclogenesis being diagnosed over regions of shallow convection, a threshold (PT) has been introduced in the formulation of the thermal potential, i.e. if convective precipitations are less than this amount, the convective potential is set to 0. The choice of the threshold has been made subjectively, in such a way that the spatial repartition of the YGP computed from the ERA40 reanalysis corresponds fairly to global observations. A basic threshold of 3 mm day^{-1} was fixed for ERA40. Without taking into account the 3 mm day^{-1} threshold, some near mid-latitude cyclogenesis was artificially diagnosed while the conditions are generally not favorable over these regions. Actually, since ERA40 diagnoses total precipitation, this threshold is useful to remove the areas of weaker non-convective precipitation.

Since the total convective precipitation varies from model to model depending on the convective precipitation scheme, we have attempted to remove this variation by making the convective precipitation threshold (PT) model dependent and proportional to the total oceanic convective precipitation simulated by each model between the latitudes 35°S and 35°N.

Furthermore, in order to make sure that the global count of genesis for the present climate is the same for all the models, a calibration factor β is made model-dependent and chosen so that global TCs computed for the period 1960–99 is the same for all the models and equals 84 TCs per year (as observed, cf. Tsutsui and Kasahara 1996). Using this calibration is a useful feature for normalizing model results for intercomparison, as it avoids that the total level of computed TC genesis be too much dependent on model resolution or specific parameterizations. However this also puts a limitation on the usefulness of the CYGP as a diagnostic tool of model quality. It should be remembered later on that comparisons over a specific area between models are not absolute but only relative to the model global distribution of diagnosed cyclogenesis. In particular, a model tendency to overestimate cyclogenesis over a particular area will be compensated by an underestimate over the other areas to satisfy the constraint put on the total.

The thermal convective potential at each grid-point (i,j), is thus defined as follows:

$$PC_{ij}(k) = \beta(k) * \max(0, PR_{ij}(k) - PT(k))$$

where k represents the model, $PR_{ij}(k)$ the convective precipitation and PT(k) the convective threshold for the model k, and β (k) the calibrating factor.

The TC seasonal genesis potential is then computed for each season as the product of the dynamical potential and the convective potential, and the CYGP is computed as the sum of the seasonal potential over the 4 seasons.

Model Data Used for the Analysis

The analysis based on the CYGP has been applied on the coupled GCM simulations prepared for the Intergovernmental Panel of Climate Change (IPCC) Fourth Assessment (AR4), and made available by the Program for Climate Model Diagnosis and Intercomparison (PCMDI[1]). For the analysis of the future climate change we have chosen to use the simulation A2 of the Special Report on Emission Scenarios (SRES), which is the economic scenario giving one of the larger increases of greenhouse gas (GHG) forcing at the end of the 21st century. The models for which results for scenario A2 were available and used in the present analysis are summarized in Table 1.

We have also used as validation for the current climate the ECMWF ERA40 reanalysis dataset (Uppala et al. 2005). The ERA40 dataset has been interpolated to a T42 resolution, which corresponds to about an average of the model resolutions. As another measure of model resolution, in addition to the standard descriptions in term of spectral truncation (indicated by the standard notation of T for triangular truncation and the maximum wavenumber), or grid spacing (in degrees of longitude

Table 1 Characteristics of the IPCC models used for the CYGP computations

Model	Resolution	Number of ocean points	Convective precipitation (mm/day)	Calibration coefficient β
INMcm3_0	5° × 4°	892	3.02	0.256
GISS_model_e_r	5° × 4°	909	2.71	0.514
CCMA_cgcm3_1	T47	1240	2.14	0.603
IPSL_cm4	3.75° × 2.5°	1988	2.15	0.429
UKMO_hadcm3	3.75° × 2.5°	1995	3.34	0.335
MRI_cgcm2_3_2_a	T42	2466	2.59	0.384
MIROC3_2_medres	T42	2466	1.59	0.848
BCCR_bcm2_0	T63/G42	2478	3.36	0.822
CNRM_cm3	T63/G42	2480	3.60	0.713
GFDL_cm2_0	2.5° × 2°	3807	2.95	0.406
CSIRO_mk3_0	T63	5344	2.42	0.620
MPI_echam5	T63	5396	3.01	0.328
UKMO_hadgem1	1.875° × 1.25°	7994	3.48	0.346
NCAR_ccsm3_0	T85	9443	2.79	0.434
INGV_echam4	T106	14672	1.99	0.558
ERA40	T42	2480	2.27	0.543

[1] see information at: http://www-pcmdi.llnl.gov/ipcc/data_status_tables.htm

and of latitude), we have also indicated the total number of grid points over ocean in the latitude belt 35°S–35°N, over which the TC cyclogenesis index is computed.

The models have been ranked in the order of increasing number of ocean grid points. The small differences in the number of ocean grid points in models with similar resolutions is mainly due to the use of slightly different land masks. The average annual convective precipitation over these ocean points is given in the fourth column of the table since it is a fundamental component of the CYGP. The last column gives the calibration coefficient β of the CYGP that is applied to each model.

It can be seen that the model resolutions encompass a range of resolutions of over an order of magnitude in the number of ocean points (from less that 900 points to more than 14000 points). The convective precipitation varies also within large limits, from less than 2 mm/day to more than 3 mm/day, without any apparent link to model resolutions. This variation can be due to the fact that models use very different convective parameterization schemes and have different biases in SSTs, which can influence the surface heat and moisture fluxes. It has been noticed that many models produce too much convective precipitation and too little stratiform precipitation compared to observational estimates (Dai 2006). In view of this wide variation we have chosen to make the CYGP convective precipitation threshold (PT) proportional to the mean convective precipitation of each model. The coefficient of proportionality (1.32) was chosen after determining that a threshold of 3 mm/day seemed suitable for the ERA40 reanalysis that has a mean convective precipitation of 2.27 mm/day. We have checked that in the models the results are not sensitive to the choice of a threshold, but for consistency with ERA40 we have kept the use of the threshold in the models as well.

Since the large variation in convective precipitation in the different models is largely due to their use of different parameterization schemes for convection, it seems appropriate to choose the calibration coefficient β used in the computation of the CYGP as model dependent. This calibration coefficient was chosen so that the total cyclogenesis over all the ocean points computed over the interval 1960–1999 was equal to 84 TCs per year, which is about the average number of observed cyclones. It can be seen that this calibration coefficient varies also in a large interval (from less than 0.3 to over 0.8), but not always in the opposite direction as convective precipitation, since dynamical factors may also modulate the CYGP.

Results for the Current Climate

The CYGP has been computed from the 10-year mean large-scale fields. The average over the 3 last decades of the 20-th century (1970–1999) for the different models and for ERA40 are represented in Fig. 1 in order to show the geographical distribution of the cyclogenesis. It can be seen that the different models are able to represent the broad distribution patterns of the area of TC genesis. However differences between models can be noted in the different ocean basins.

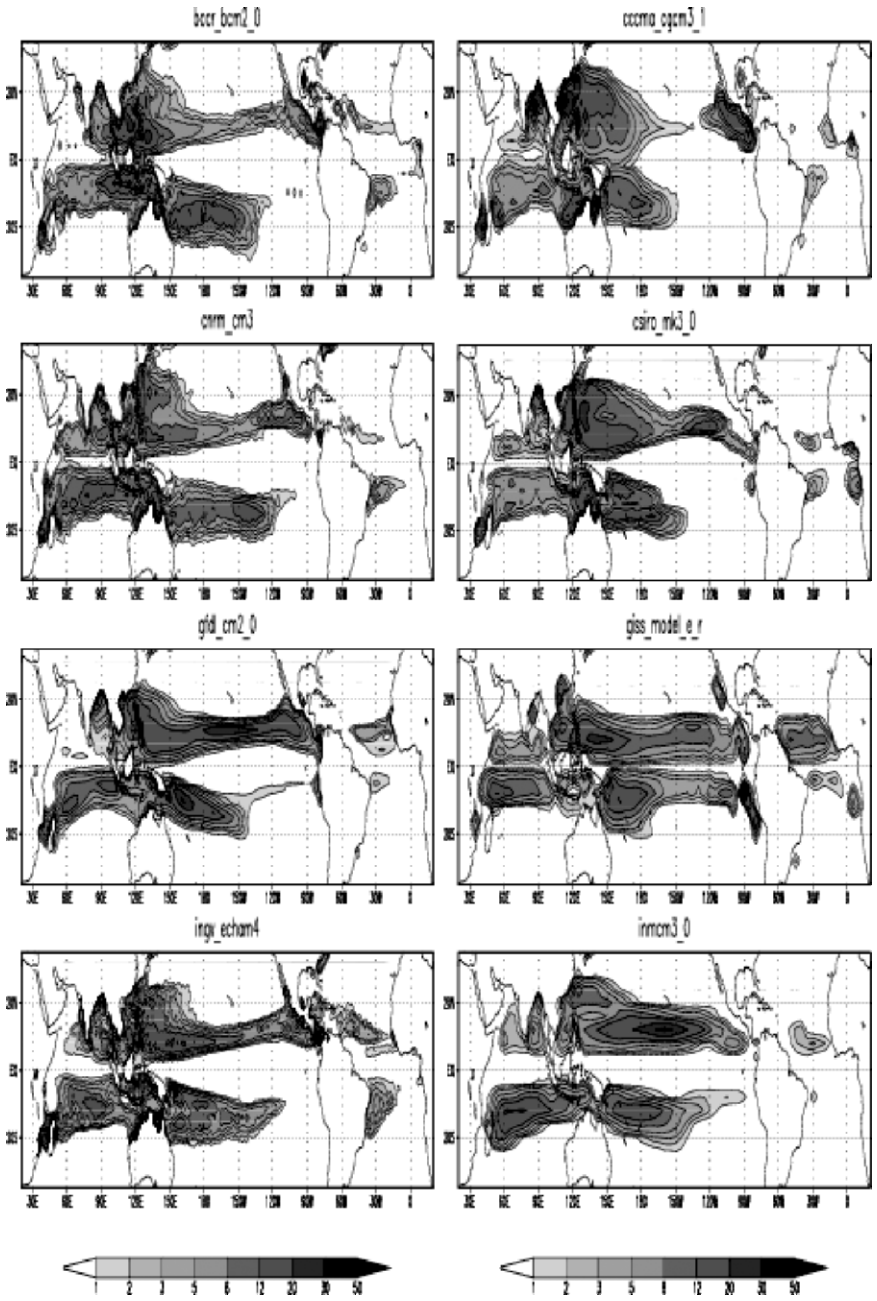

Fig. 1 Geographical distribution of the genesis index CYGP. The unit is number of TC genesis per 20 years per 5° × 5°. The model identification is shown above each figure for the other models and ERA40 reanalysis

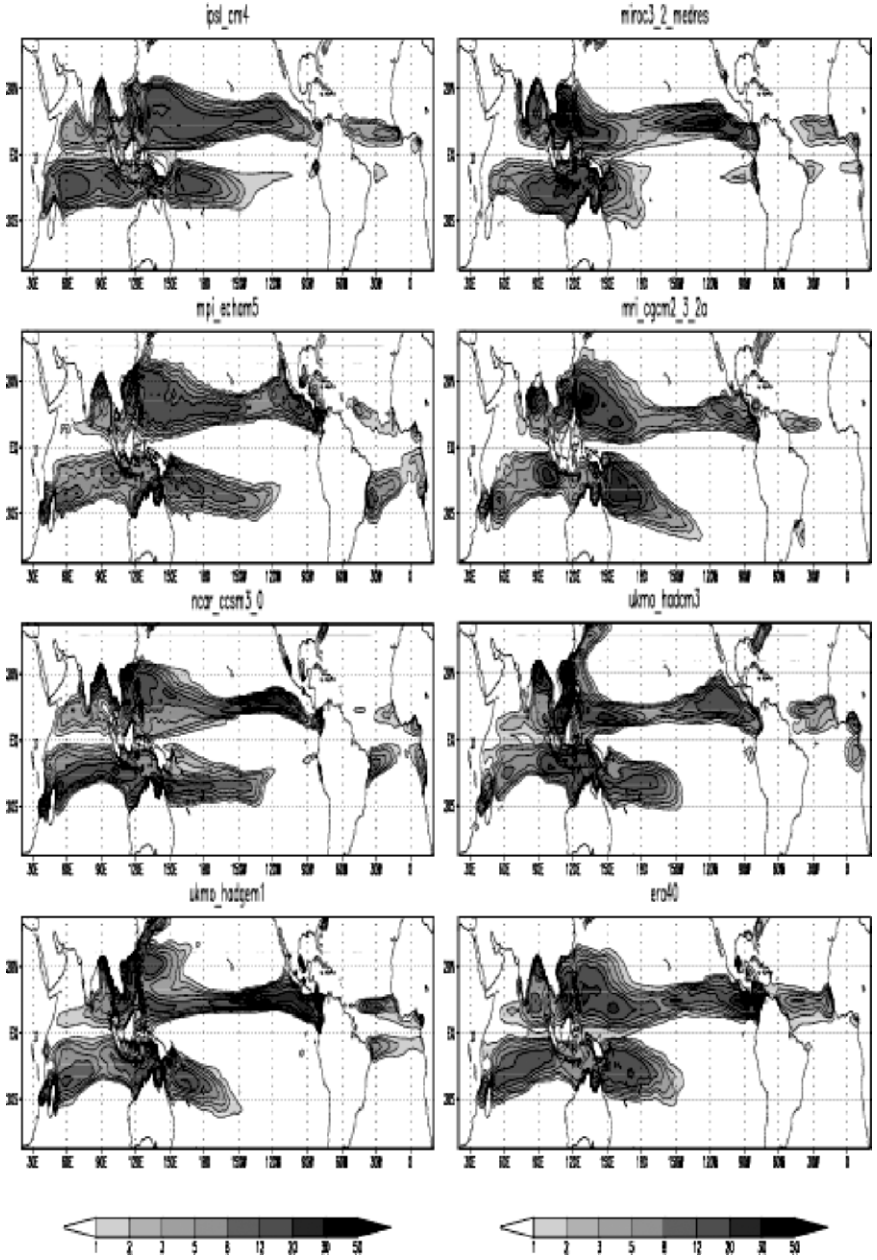

Fig. 1 (Continued)

Over the South-West Pacific several models extend the cyclogenesis zone eastwards farther east of 150°W than is computed in ERA40 (CNRM_cm3, GISS_model_e_r, INGV_echam4, INMcm3_0, IPSL_cm4, MPI_echam5, NCAR_ccsm3_0). This deficiency originates from the fact that these coupled models have the tendency to give a too symmetric distribution of precipitation straddling the equator. This is the well-known problem of the so-called double inter tropical convergence zone (ITCZ) frequently found in coupled models in association with an excessive westward extension of equatorial Pacific cold tongue in SSTs (Mechoso et al. 1995; Dai 2006; Lin 2007a). Some of the models give in addition a too zonal distribution over the North Pacific, and do not reproduce the contrast between the North West and North East Pacific (GISS_model_e_r, INMcm3_0, IPSL_cm4), a problem that could be due in part to the coarse resolution in these models. In several models the cyclogenesis index is underestimated over the North Atlantic (BCCR_bcm2_0, CCMA_cgcm3_1, CNRM_cm3, CSIRO_mk3_0, INVG_echam4, INMcm3_0, MPI_echam5, MRI_cgcm2_3–2a, NCAR_ccsm3_0). About half the models indicate a cyclogenesis area in the South Atlantic near the coasts of Brazil (BCCR_bcm2_0, CCMA_cgcm3_1, CNRM_cm3, CSIRO_mk3_0, GISS_model_e_r, INGV_echam4, MPI_echam5, NCAR_ccsm3_0, UKMO_Hadgem1). This does not seem to match well with current observations, since only one single case of a hurricane in this area has been ever observed, namely Catarina in March 2004 (Pezza and Simmonds 2005).

All models reproduce correctly the TC genesis area over the South Indian Ocean, and over the Gulf of Bengal in the North Indian Ocean. However several models tend to give too much TC genesis over the Arabian Sea (CNRM_cm3, CSIRO_mk3_0, GISS-model_e_r, INMcm3_0, IPSL_cm4, NCAR_ccsm3). This may be due to a tendency of these models to overestimate precipitation in this region.

In order to provide results of TC genesis in a more quantitative form, the CYGP has been integrated over the traditional ocean basins in order to provide an estimation of the number of TC generated each year over each basin (Table 2).

The figures from the models are an average over the 3 decades 1970–1999. In order to summarize the model results, the mean of the 15 models with the standard deviation (after the ± sign) has been included. The cyclogenesis computed from ERA40 is shown for comparison, as well as the observed number of cyclones over the period 1973–1992 published in Tsutsui and Kasahara (1996).

The six ocean basins are:

- NI (North Indian: 0°-35°N, 40°E-100°E);
- SWI (South West Indian: 45°S-0°S, 20°E-100°E);
- NWP (North West Pacific: 0°-55°N, 100°E-180°E);
- SWP (South West Pacific: 55°S-0°S, 100°E-220°E);
- NEP (North East Pacific: 0°-55°N, 180°E-American coast);
- ATL (Atlantic: 0-55°N, American coast-360°E).

This table confirms a tendency of many models to overestimate cyclogenesis over the South West Pacific and to underestimate it strongly over the Atlantic, while the cyclogenesis computed from ERA40 is in rather good agreement with the

Table 2 Number of annual cyclogeneses per year simulated in the different ocean basins by the 15 models, ERA40 and observed (Tsutsui & Kasahara 1996)

Model	NI	SWI	NWP	SWP	NEP	ATL
INMcm3_0	3.0	16.5	20.9	20.7	20.0	1.3
GISS_model_e_r	3.2	9.7	21.7	18.6	15.2	6.9
CCMA_cgcm3_1	6.9	9.8	35.4	21.0	8.9	1.1
IPSL_cm4	4.9	14.4	26.6	18.8	16.5	2.5
UKMO_hadcm3	7.5	9.0	24.0	25.0	14.5	3.1
MRI_cgcm2_3_2_a	4.1	10.4	31.9	26.4	10.2	1.7
MIROC3_2_medres	6.5	8.0	24.9	23.0	17.5	1.9
BCCR_bcm2_0	4.4	10.4	23.8	32.6	6.3	3.1
CNRM_cm3	6.2	15.4	23.0	25.5	7.6	1.5
GFDL_cm2_0	3.0	11.3	24.9	21.3	19.8	2.0
CSIRO_mk3_0	4.2	9.0	34.1	23.8	9.8	0.8
MPI_echam5	3.3	9.5	28.0	20.4	14.9	2.5
UKMO_hadgem1	4.1	11.3	25.0	19.3	20.6	2.6
NCAR_ccsm3_0	6.0	15.0	22.5	21.1	14.5	1.1
INGV_echam4	4.1	13.2	24.7	23.8	9.3	4.6
Mean $\pm$ Std. Dev.	4.8 $\pm$ 1.5	11.5 $\pm$ 2.7	26.1 $\pm$ 4.4	22.8 $\pm$ 3.7	13.7 $\pm$ 4.7	2.4 $\pm$ 1.6
ERA40	4.8	11.4	24.5	18.1	18.7	7.0
Obs. 1973–92	5.2	10.5	26.6	15.6	17.4	8.7

observed values. This is an indication that the opposite bias of some models over the Atlantic and South Pacific may be due to excessive convection over the Pacific simulated in these models. It is also likely that the dependence of the convective precipitation threshold on the mean convective precipitation may enhance the reduction of the convective potential over the Atlantic in the models that generate large convective rainfall over the Pacific. To go further into the explanation of such a low amount of CYGP over the Atlantic basin, we have calculated the average of the three main contributions to the CYGP index: vorticity, shear and thermal potential. Only the thermal potential average may explain the underestimated values of CYGP over the Atlantic for some of the models (not shown). Indeed, the models that show the more pronounced lack of activity are those with the weaker thermal potential. Besides the effect of the convective threshold, which is only effective on the edges of the convective precipitation pattern, one may conclude that the weakness of the CYGP over the Atlantic is mainly due to the lack of convective precipitations simulated by the models over this region. These weak convective precipitations are coherent with cool summer SSTs in the coupled models over the Atlantic (not shown). Several models have quite large cold SST biases over the tropical Atlantic that are associated with dry biases (Dai 2006).

In order to investigate the evolution of the results over time we have displayed in Fig. 2 the evolution of the number of cyclogenesis events computed by means of the CYGP for successive 10-year period as averaged over each of the six ocean basins.

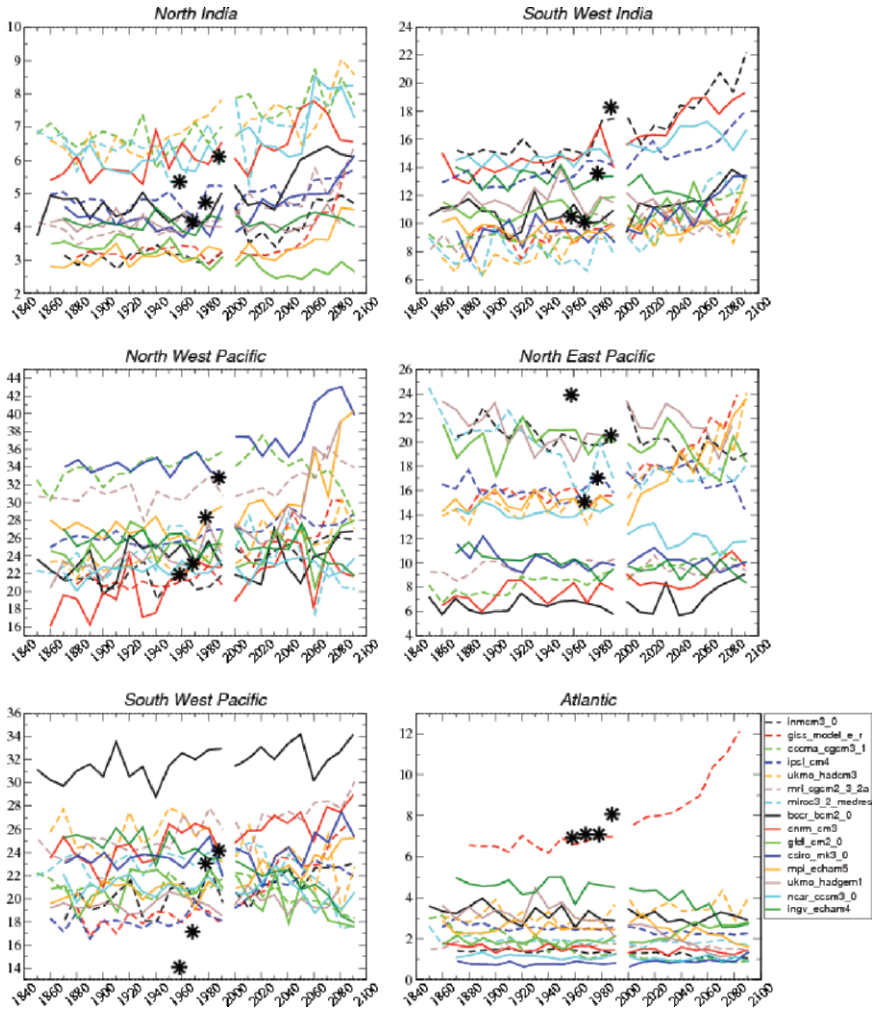

Fig. 2 Time evolution of TC genesis simulated in the six ocean basins by the 15 IPCC models (detailed in legend) and by ERA40 (* symbol). Horizontal axis represents the decades from 1860 to 2000 in the 20C3M simulation and from 2000 to 2100 in the A2 scenario, and vertical axis is the equivalent number of TCs following Gray's definition

The 10-year averages illustrate a rather large interdecadal variability, as well as the large differences in the number of cyclogenesis among the different models, as already discussed in Table 2.

Some long-term trends are clearly apparent in most simulations over some ocean basins, even over the 20th century, and they tend to increase over the 21st century. This is the case for the Indian Ocean (NI and SWI) where nearly all models simulate a small

increasing trend, and also for the North West Pacific. Over the NEP and SWP the trends are less apparent, and trends over the 21st century are even opposite in different models. Over the Atlantic most models give no trend or a slightly decreasing trend, with the exception of a single outlier. The trends over the 20-th century are not very stable and partly masked by the interdecadal variability. ERA40 gives larger CYGP variability and trends than the models for the last 4 decades of the 20th century. The observations over the past twenty to thirty years (Klotzbach 2006; Kossin et al. 2007, Webster et al. 2005) show only relatively small trends in TC numbers over most ocean basins, with an increasing trend only over the North Atlantic, and a decreasing trend over the Northeast Pacific that are not simulated by most of the models, nor by ERA40. So there appears to be more decadal variability in the model- or ERA40-diagnosed TC genesis than in reality, although with only a few decades of reasonably reliable observations, it is difficult to reach a more quantitative conclusion. In order to analyse these contrasting responses it is useful to examine the distribution of the cyclogenesis at the end of the 21st century.

Results for Scenario A2

To look more clearly at the trends of the different models that were apparent in Fig. 2, the change in the yearly number in TC genesis over the different basins between the last 3 decades of the 21st century with respect to those of the last 3 decades of the 20th century have been computed. The results, shown in Table 3, have been normalized by expressing the evolution as a percent change with respect with their numbers at the end of the 20th century (shown in Table 2), so as to show more clearly the behavior of the different basins independently of their large differences in total TC genesis.

There is a rather good consistency of the models for simulating an increase in TC genesis over the North Indian Ocean. Only one model (GFDL_cm2_0) simulates a small decrease, and another model (INGV_echam4) a negligible increase. Most models give increases above 10%, and three of them produce increases above 40% (INM_cm3, GISS_model_e_r, BCCR_bcm2_0). Over the South West Indian Ocean the consistency decreases as four models simulate a decrease in TC genesis (MRI_cgcm2_3_2_a, GFDL_cm2_0, UKMO_hadgem1, INGV_echam4), the decrease being rather strong (-22%) in the case of the INGV model. Two models still give increases above 40% in this region (MIROC, CSIRO).

The situation is similar over the North West Pacific where four models give a negative change (CCMA_cgcm3_1, MIROC3_2_medres, CNRM_cm3, INGV_echam4). Over the South West Pacific and North East Pacific there is no consistency even in the sign of the response since respectively 6 and 7 of the models, that is nearly half of the models, give a decreasing response and the rest a positive response. Over the Atlantic ten of the models give a decreasing in TC genesis, but still five of them an increase (GISS_model_e_r,, UKMO_hadcm3, BCCR,

Table 3 Change in the cyclogenesis per year simulated by the models in scenario A2 for the end of the 21st century (2070-2099) with respect to the end of the 20th century (1970–1999) for the total numbers, and relative change for the different ocean basins (in percent)

Model	Total	NI	SWI	NWP	SWP	NEP	ATL
INMcm3_0	12.1	58%	26%	25%	10%	−5%	−21%
GISS_model_e_r	30.5	59%	11%	39%	38%	48%	67%
CCMA_cgcm3_1	−1.7	14%	23%	−12%	−10%	18%	−23%
IPSL_cm4	7.3	13%	18%	5%	19%	−4%	−11%
UKMO_hadcm3	10.8	13%	10%	15%	−10%	49%	21%
MRI_cgcm2_3_2_a	5.4	35%	−7%	10%	9%	−6%	−11%
MIROC3_2_medres	−1.6	23%	62%	−15%	−19%	0%	−4%
BCCR_bcm2_0	9.5	41%	28%	9%	1%	36%	2%
CNRM_cm3	9.0	12%	21%	−1%	10%	35%	−13%
GFDL_cm2_0	−3.3	−8%	−8%	8%	−16%	−6%	39%
CSIRO_mk3_0	15.5	33%	45%	23%	9%	−1%	32%
MPI_echam5	21.6	30%	16%	31%	20%	46%	−25%
UKMO_hadgem1	10.6	9%	−5%	49%	4%	−3%	−55%
NCAR_ccsm3_0	−1.6	31%	8%	0%	−6%	−22%	−11%
INGV_echam4	−11.7	2%	−22%	−8%	−20%	0%	−43%
Mean	7.5	24%	15%	12%	3%	12%	−4%
S. Dev.	10.6	19%	21%	19%	17%	24%	32%

GFDL, CSIRO). From the dispersion of the model results it seems rather hazardous to draw a conclusion on the changes in TC genesis in the different ocean basins.

We can try to investigate further the cause of this dispersion by looking at the spatial distribution of the CYGP response. The changes of cyclogenesis in the different basins have a rather complex spatial distribution. This can be illustrated by the map of differences of the CYCP at the end of the 21st century compared to the end of 20th century (Fig. 3). It can be seen that the patterns of the cyclogenesis changes differ from model to model and have a rather complex structure with both positive and negative regions, which are an indication of displacements of the cyclogenesis areas. Though at first sight it may seem rather difficult to distinguish some coherency in model responses, a more detailed analysis reveals a number of general features.

The distribution of the response in longitude varies markedly according to the model and ocean basin. Over the Atlantic the response is very small except for the GISS_model_e_r, which gives a zonally symmetric increase over all ocean basins. This weakness of the response should, nevertheless, be related to the underestimation of the Atlantic TC activity as it is diagnosed by the CYGP in the models. Over the North Indian Ocean nearly all models simulate an increase of TC genesis west of India over the Arabian Sea. However, east of India over the Gulf of Bengal some models simulate an increase of TC genesis (BCCR, CSIRO, GISS, INM, MRI), while several other simulate a decrease (CCMA, CNRM-cm3, INGV, NCAR). This

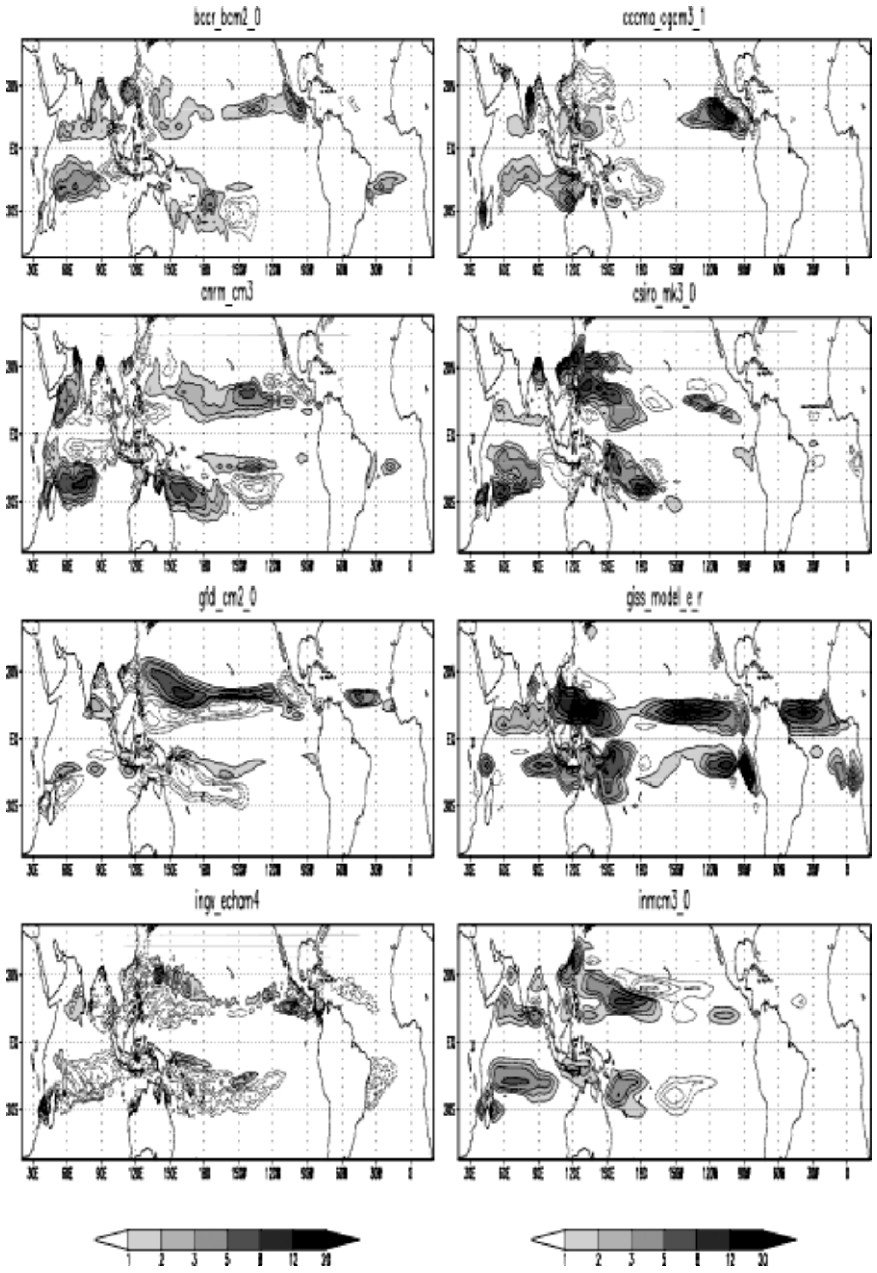

Fig. 3 Spatial distribution of the model CYGP change at the end of the 21st century (2070–2099) with respect to the end of the 20th century (1970–1999). The unit is the number of TC genesis per 20 years per 5° × 5°. Positive contours are shown by solid lines and negative contours by dashed lines. The model identifier is shown above each figure

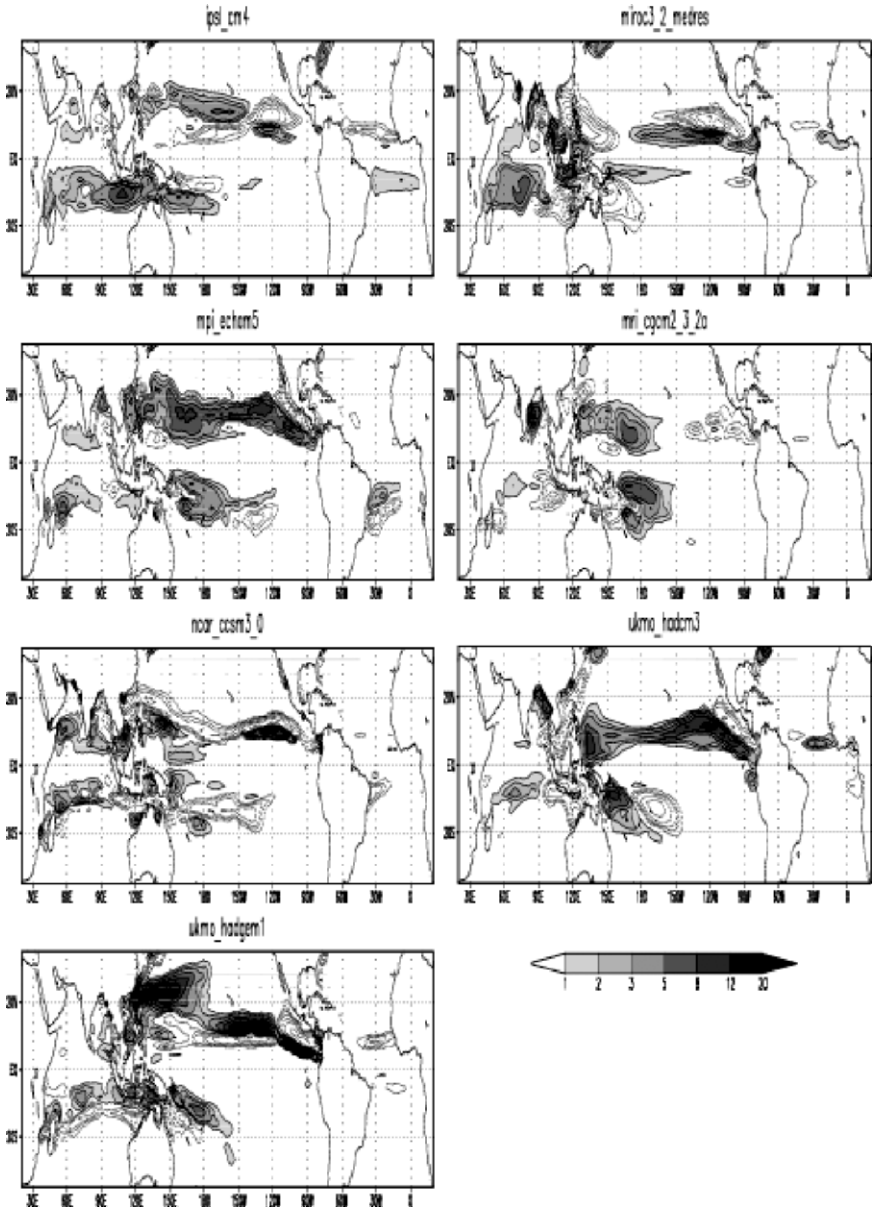

Fig. 3 (Continued)

contrasting response in the Bay of Bengal explains the difference in the magnitude of the change over the North Indian domain shown in Table 3. A similar contrast between west and east is found in the South Indian Ocean, where nearly all models give an increase of TC genesis in the western part, while in the eastern part (east of

90°E) most models give a decrease (BCCR, CNRM, CSIRO, MIROC, MRI, NCAR, UKMO_Hadcm3), with only a few giving an increase (CCMA, GISS, IPSL, MPI). Two models have a different pattern of response in this area: the INGV model that gives a general decrease over this area, and the UKMO_hadgem1 that gives a zonal response with an increase equatorward and a decrease poleward, corresponding to a general equatorward migration of the TC genesis area over the South Indian Ocean.

It can be noticed that the same pattern of response extends over the South West Pacific in these two models. For several of the other models the response over the SWP basin shows a contrast in longitude with a positive response westward of about 180–150°W, and a negative response eastward (BCCR, CNRM-cm3, INMcm3, MPI_echam5, NCAR_cssm3, UKMO_hadcm3). This pattern of response corresponds to a reinforcement of TC genesis over the Coral Sea, and a reduction of the eastward extension of the cyclogenesis zone associated with the SPCZ.

A similar east-west contrast over the North Pacific is found only in a few models (CSIRO_mk3, INMcm3, IPSL-cm4, MRI_cgcm2_3_2a). The majority of models give rather a more zonally uniform response extending across the whole North Pacific (BCCR, CNRM-cm3, GFDL_cm2_0, GISS_model_e_r, MPI_echam5, NCAR_ccsm3_0, UKMO_hadcm3, UKMO_hadgem1) with most of the time a north-south contrast. In most of the models there is an increase of TC genesis between 10–20°N latitude situated on the poleward side of the main cyclogenesis area. Depending on the model this zone of increase can extend over a whole ocean basin or be restricted to a part of it. This pattern corresponds to a poleward extension of the TC genesis, which is consistent with the poleward expansion of the Hadley circulation that has been diagnosed in the IPCC AR4 climate simulations (Lu et al. 2007).

There are however some exceptions to this general pattern, for example MIROC3_2_medres that simulates an increase equatorward and a decrease poleward of the main cyclogenesis zone in the North Pacific, both in the west and in the east, as well as in the South West Pacific. A similar opposite pattern is also found in the NCAR_ccsm3_0 simulation. For CCMA this opposite pattern is found only over the West Pacific in both hemispheres, and for INGV only in the South West Pacific and South Indian Ocean. For these models this type of response explains the strong reduction in TC genesis in these basins noticed in Table 3.

In conclusion there appears a diversity of patterns of TC genesis changes in the different models, but for several models there is a similar response pattern in longitude leading to a displacement of TC genesis westward in the North Indian Ocean, South Indian Ocean and South West Pacific. This pattern could be associated to a response of the Walker circulation to global warming, as described by Vecchi and Soden (2007). As the response of the tropical circulation is very sensitive to the SST gradients, a possible explanation of this diversity of response patterns could be linked to the model SST response to GHG increase.

Indeed it can be seen that the SST changes differ considerably from model to model (Fig. 4) not only in their magnitude, but also in their geographical pattern. Several models have a pattern of warming showing a marked resemblance to an El

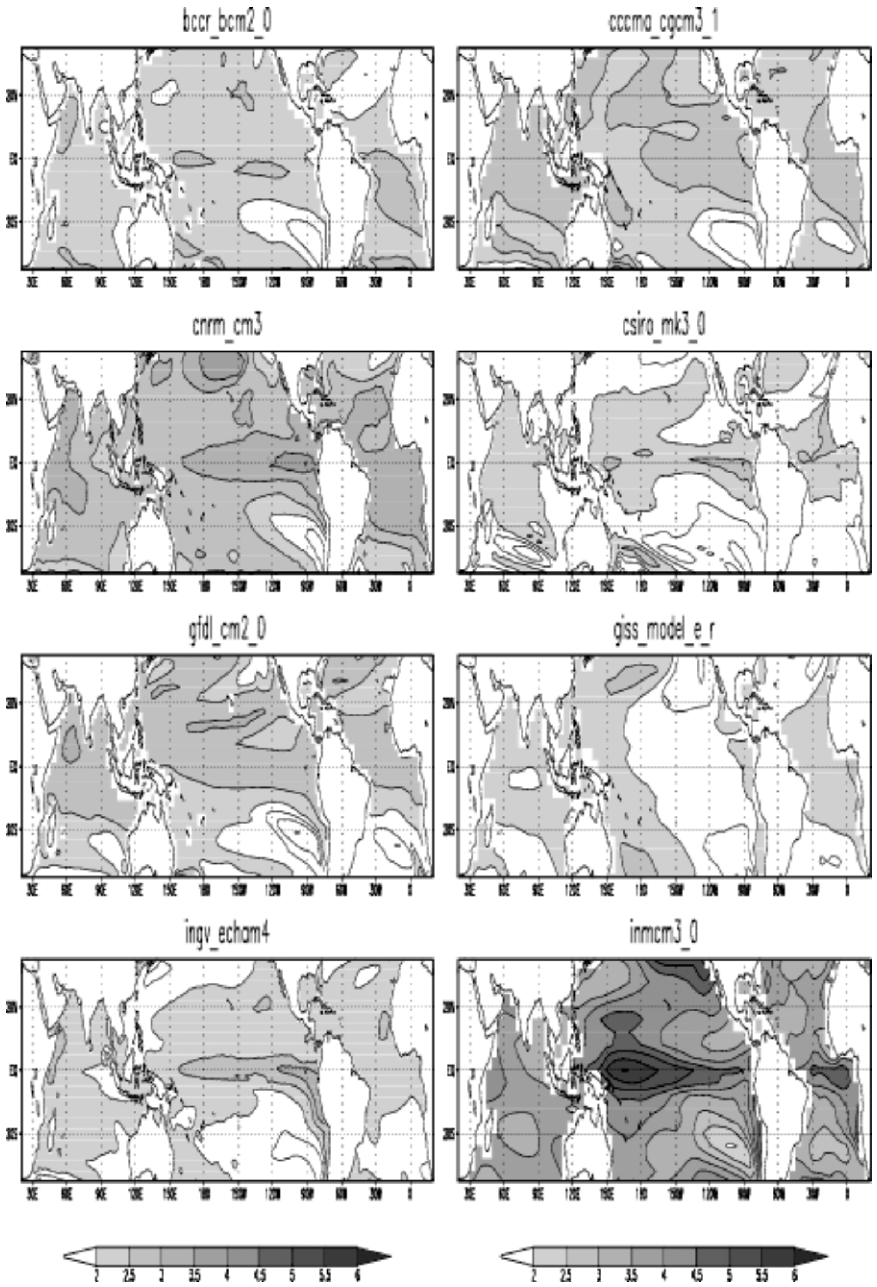

Fig. 4. Change in SST simulated by each model for scenario A2 at the end of the 21st century (2070–2099) with respect to the end of the 20th century (1970–1999). The contour interval is 0.5 K above 2K. The model identifier is shown above each figure

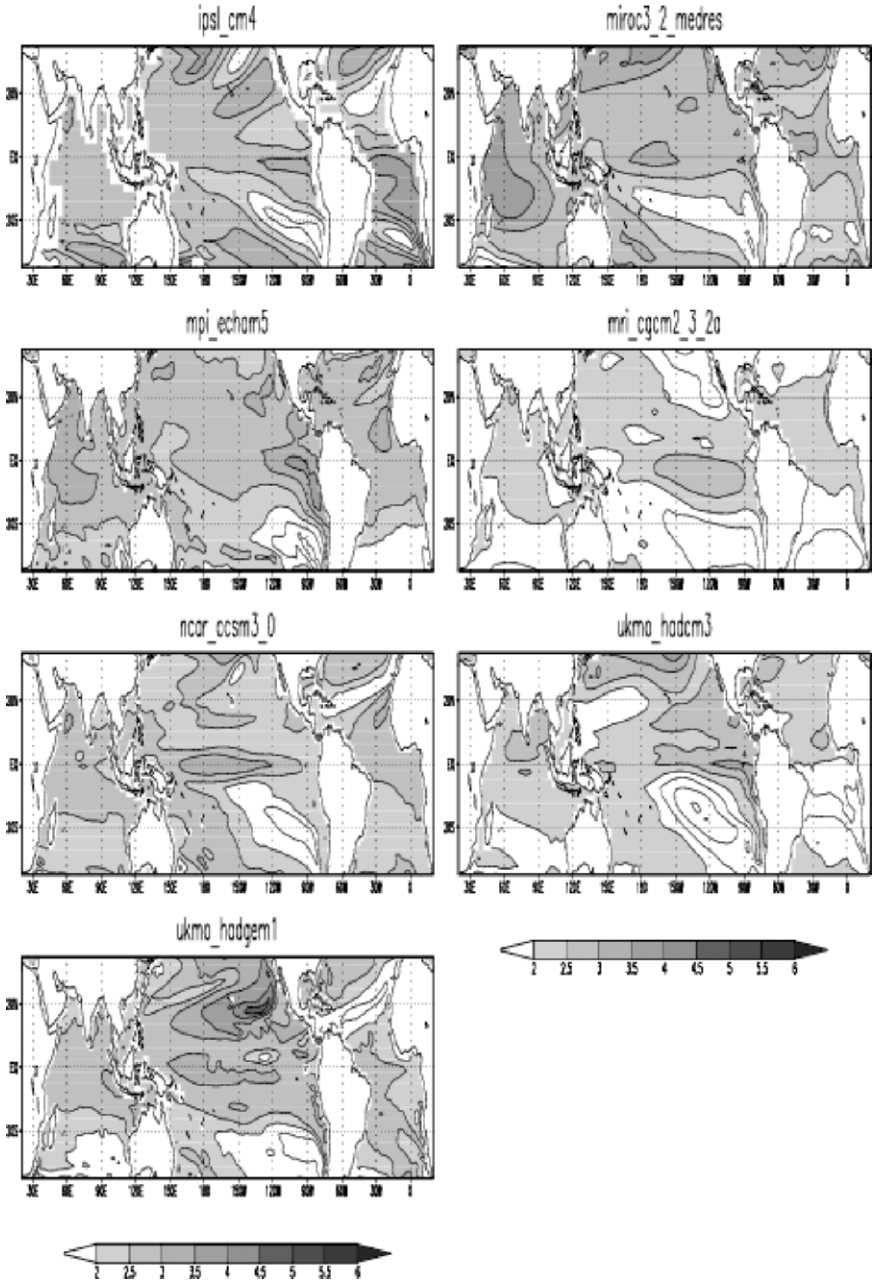

Fig. 4 (Continued)

Nino type anomaly with a maximum warming in the equatorial East Pacific (CCMA, CNRM_cm3, CSIRO, INGV, IPSL, MPI_echam5, UKMO_hadcm3) while others have a maximum warming in the central or West equatorial Pacific (INMcm3, MIROC, NCAR_ccsm3, UKMO_hadgem1). Such patterns of El Nino-like or La Nina-like responses to global warming have been previously pointed out (Collins et al. 2005, Yamaguchi and Noda 2006). It can be expected that the different patterns of SST changes in the model can modify the location of convective rainfall and also the other circulation features, such as wind shear, that can have a controlling effect on TC genesis (Vecchi and Soden 2007, Latif et al. 2007).

The lack of agreement in the pattern of SST changes can be considered to be one of the principal factors that is responsible for the diversity of the patterns of change in TC genesis.

Discussion and Conclusions

This paper has reported a preliminary analysis of 15 simulations of IPCC AR-4 coupled models for the 20th century in term of a cyclogenesis index, CYGP, based on a combination of large-scale environment factors, among which the simulated convective precipitation plays the part of a thermal potential. For the current climate the geographical distribution of the cyclogenesis patterns simulated by the different models has some degree of realism, although the absolute number of cyclogenesis in the different ocean basins differ widely from model to model. The cyclogenesis index presents large interdecadal fluctuations and trends. In scenario A2 the trends in the cyclogenesis response differ according to the ocean basins and models. While in some ocean basins like the Indian Ocean, the majority of models compute an increasing trend in cyclogenesis, the response is much less coherent in other basins where some models give a decreasing trend. In the global mean, nearly all models give an overall increase of cyclogenesis in the 21st century, except for the INGV model. Interestingly this is the model with the highest resolution (T106). The CYGP response in this model appears in good agreement with a direct analysis of the cyclone tracks (Gualdi et al. 2008). This would seem to add another piece of evidence to support the idea that models with a resolution of T106 or above produce a rather different response of the tropical cyclones to climate change than lower resolution models.

The lack of coherence of the TC genesis response to future climate change can be associated to the different response patterns of SST in the coupled models, particularly over the Equatorial Pacific and their differences in the simulation of ENSO. How the ENSO will change in a warmer climate is still a very uncertain and debated issue. A study of ENSO in different CGCMs has shown that most models simulate different characteristics of the ENSO pattern, intensity and period (van Oldenborgh et al. 2005, Guilyardi 2006, Lin 2007b). As the ENSO phenomenon has a large impact on the distribution of TCs over the Pacific, and even over the Atlantic, it seems useful to extend this study by analyzing the CYGP at higher temporal resolution (seasonal) and relating it to an ENSO index in each of the model simulation. In this way one could attempt to relate the response of each

model in the future climate to its response to ENSO SST patterns. However it seems that the large spread of model responses in term of SST patterns precludes drawing precise conclusions on the future TC genesis until some better convergence of the model SST response has been achieved. The question of the horizontal resolution of the coupled models may also be a crucial one, since it seems that the higher resolution models may have a different response than the lower resolution models in term of convective precipitation response.

Acknowledgments We thank the modeling groups and the PCMDI for making the model data available. The IPCC Data Archive at Lawrence Livermore National Laboratory is supported by the U.S. Department of Energy (DOE) Office of Sciences. We acknowledge support from the European Commission 6th Framework Programme (Project ENSEMBLES, contract GOCE-CT-2003–505539), and the French Agence Nationale de la Recherche (ANR Project Cyclones&Climate)

References

Bengtsson, L., H. Bøttger, and M. Kanamitsu, 1982: Simulation of hurricane-type vortices in a general circulation model. *Tellus*, **34**, 440–457.

Bengtsson, L., M. Botzet, and M. Esch, 1995: Hurricane-type vortices in a general circulation model. *Tellus (Ser. A)*, **47**, 175–196.

Bengtsson, L., M. Botzet, and M. Esch, 1996: Will greenhouse gas-induced warming over the next 50 years lead to higher frequency and greater intensity of hurricanes? *Tellus (Ser. A)*, **48**, 57–73.

Broccoli, A. J., and S. Manabe, 1990: Can existing climate models be used to study anthropogenic changes in tropical cyclone climate ? *Geophys. Res. Lett.*, **17**, 1917–1920.

Camargo, S. J., A. H. Sobel, A. G. Barnston, and K. A. Emanuel, 2007: Tropical cyclone genesis potential index in climate models. *Tellus (Ser. A)*, **59**, 428–443.

Chauvin, F., J. F. Royer, and M. Déqué, 2006: Response of hurricane-type vortices to global warming as simulated by ARPEGE-Climat at high resolution. *Climate Dyn.*, **27**, 377–399.

Collins, M., and the CMIP Modelling Groups, 2005: El Nino- or La Nina-like climate change? *Climate Dyn.*, **24**, 89–104.

Dai, A., 2006: Precipitation characteristics in eighteen coupled climate models. *J. Climate*, **19**, 4605–4630.

Druyan, L. M., P. Lonergan, and T. Eichler, 1999: A GCM investigation of global warming impacts relevant to tropical cyclone genesis. *Int. J. Climatol.*, **19**, 607–617.

Emanuel, K. A., 1988: The maximum intensity of hurricanes. *J. Atmos. Sci.*, **45**, 1143–1155.

Emanuel, K. A., 1999: Thermodynamic control of hurricane intensity. *Nature*, **401**, 665–669.

Gray, W. M., 1968: Global view of the origin of tropical disturbances and storms. *Mon. Weather Rev.*, **96**, 669–700.

Gray, W. M., 1975: *Tropical Cyclone Genesis*. Dept. of Atmospheric Science Paper No. 234, Colorado State University, 121 pp.

Gualdi, S., E. Scoccimarro, and A. Navarra, 2008: Changes in tropical cyclone activity due to global warming. Results from a High-Resolution Coupled General Circulation Model. *J. Climate.*, **21**, 5204–5228.

Guilyardi, E., 2006: El Nino-mean state-seasonal cycle interactions in a multi-model ensemble. *Climate Dyn.*, **26**, 329–348.

Haarsma, R. J., J. F. B. Mitchell, and C. A. Senior, 1993: Tropical disturbances in a GCM. *Climate Dyn.*, **8**, 247–257.

Henderson-Sellers, A., H. Zhang, G. Berz, K. Emanuel, W. Gray, C. Landsea, G. Holland, J. Lighthill, S. L. Shieh, P. Webster, and K. McGuffie, 1998: Tropical cyclones and global climate change: A post-IPCC assessment. *Bull. Amer. Meteorol. Soc.*, **79**, 19–38.

Klotzbach, P. J., 2006: Trends in global tropical cyclone activity over the past twenty years (1986–2005). *Geophys. Res. Lett.*, **33**, L10805.

Knutson, T. R., and R. E. Tuleya, 1999: Increased hurricane intensities with CO2-induced warming as simulated using the GFDL hurricane prediction system. *Climate Dyn.*, **15**, 503–519.

Knutson, T. R., and R. E. Tuleya, 2004: Impact of CO2-induced warming on simulated hurricane intensity and precipitation: Sensitivity to the choice of climate model and convective parameterization. *J. Climate*, **17**, 3477–3495.

Knutson, T. R., R. E. Tuleya, and Y. Kurihara, 1998: Simulated increase of hurricane intensities in a CO2-warmed climate. *Science*, **279**, 1018–1020.

Kobayashi, C., and M. Sugi, 2004: Impact of horizontal resolution on the simulation of the Asian summer monsoon and tropical cyclones in the JMA global model. *Climate Dyn.*, **23**, 165–176.

Kossin, J. P., K. R. Knapp, D. J. Vimont, R. J. Murnane, and B. A. Harper, 2007: A globally consistent reanalysis of hurricane variability and trends. *Geophys. Res. Lett.*, **34**, L04815.

Krishnamurti, T. N., R. Correa-Torres, M. Latif, and G. Daughenbaugh, 1998: The impact of current and possibly future sea surface temperature anomalies on the frequency of Atlantic hurricanes. *Tellus (Ser. A)*, **50**, 186–210.

Latif, M., N. Keenlyside, and J. Bader, 2007: Tropical sea surface temperature, vertical wind shear, and hurricane development. *Geophys. Res. Lett.*, **34**, L01710.

Lin, J. L., 2007a: The double-ITCZ problem in IPCC AR4 coupled GCMs: Ocean-atmosphere feedback analysis. *J. Climate*, **20**, 4497–4525.

Lin, J. L., 2007b: Interdecadal variability of ENSO in 21 IPCC AR4 coupled GCMs. *Geophys. Res. Lett.*, **34**, L12702.

Lu, J., G. A. Vecchi, and T. Reichler, 2007: Expansion of the Hadley cell under global warming. *Geophys. Res. Lett.*, **34**, L06805.

Manabe, S., J. L. Holloway Jr., and H. M. Stone, 1970: Tropical circulation in a time-integration of a global model of the atmosphere. *J. Atmos. Sci.*, **27**, 580–613.

McDonald, R. E., D. G. Bleaken, D. R. Cresswell, V. D. Pope, and C. A. Senior, 2005: Tropical storms: Representation and diagnosis in climate models and the impacts of climate change. *Climate Dyn.*, **25**, 19–36.

Mechoso, C. R., A. W. Robertson, N. Barth, M. K. Davey, P. Delecluse, P. R. Gent, S. Ineson, B. Kirtman, M. Latif, H. Le Treut, T. Nagai, J. D. Neelin, S. G. H. Philander, J. Polcher, P. S. Schopf, T. Stockdale, M. J. Suarez, L. Terray, O. Thual, and J. J. Tribbia, 1995: The seasonal cycle over the tropical Pacific in coupled ocean-atmosphere general circulation models. *Mon. Weather Rev.*, **123**, 2825–2838.

Oouchi, K., J. Yoshimura, H. Yoshimura, R. Mizuta, S. Kusunoki, and A. Noda, 2006: Tropical cyclone climatology in a global-warming climate as simulated in a 20 km-mesh global atmospheric model: Frequency and wind intensity analyses. *J. Meteorol. Soc. Japan*, **84**, 259–276.

Palmén, E., 1948: On the formation and structure of tropical cyclones. *Geophysica*, **3**, 26–38.

Pezza, A. B., and I. Simmonds, 2005: The first South Atlantic hurricane: Unprecedented blocking, low shear and climate change. *Geophys. Res. Lett.*, **32**, L15712.

Pielke, R. A., Jr., C. Landsea, M. Mayfield, J. Laver, and R. Pasch, 2005: Hurricanes and global warming. *Bull. Amer. Meteorol. Soc.*, **86**, 1571–1575.

Royer, J. F., F. Chauvin, B. Timbal, P. Araspin, and D. Grimal, 1998: A GCM study of the impact of greenhouse gas increase on the frequency of occurrence of tropical cyclones. *Climatic Change*, **38**, 307–343.

Ryan, B. F., I. G. Watterson, and J. L. Evans, 1992: Tropical cyclone frequencies inferred from Gray's yearly genesis parameter: Validation of GCM tropical climates. *Geophys. Res. Lett.*, **19**, 1831–1834.

Santer, B. D., T. M. L. Wigley, P. J. Gleckler, C. Bonfils, M. F. Wehner, K. AchutaRao, T. P. Barnett, J. S. Boyle, W. Bruggemann, M. Fiorino, N. Gillett, J. E. Hansen, P. D. Jones, S. A.

Klein, G. A. Meehl, S. C. B. Raper, R. W. Reynolds, K. E. Taylor, and W. M. Washington, 2006: Forced and unforced ocean temperature changes in Atlantic and Pacific tropical cyclogenesis regions. *Proc. Natl Acad. Sci. USA*, **103**, 13905–13910.

Stowasser, M., Y. Q. Wang, and K. Hamilton, 2007: Tropical cyclone changes in the western North Pacific in a global warming scenario. *J. Climate*, **20**, 2378–2396.

Sugi, M., A. Noda, and N. Sato, 2002: Influence of the global warming on tropical cyclone climatology: An experiment with the JMA global model. *J. Meteorol. Soc. Japan*, **80**, 249–272.

Tsutsui, J. I., 2002: Implications of anthropogenic climate change for tropical cyclone activity: A case study with the NCAR CCM2. *J. Meteorol. Soc. Japan*, **80**, 45–65.

Tsutsui, J. I., and A. Kasahara, 1996: Simulated tropical cyclones using the National Center for Atmospheric Research Community Climate Model. *J. Geophys. Res. - Atmos.*, **101**, 15013–15032.

Uppala, S. M., P. W. Kallberg, A. J. Simmons, U. Andrae, V. D. Bechtold, M. Fiorino, J. K. Gibson, J. Haseler, A. Hernandez, G. A. Kelly, X. Li, K. Onogi, S. Saarinen, N. Sokka, R. P. Allan, E. Andersson, K. Arpe, M. A. Balmaseda, A. C. M. Beljaars, L. Van De Berg, J. Bidlot, N. Bormann, S. Caires, F. Chevallier, A. Dethof, M. Dragosavac, M. Fisher, M. Fuentes, S. Hagemann, E. Holm, B. J. Hoskins, L. Isaksen, P. A. E. M. Janssen, R. Jenne, A. P. McNally, J. F. Mahfouf, J. J. Morcrette, N. A. Rayner, R. W. Saunders, P. Simon, A. Sterl, K. E. Trenberth, A. Untch, D. Vasiljevic, and P. Viterbo, 2005: The ERA-40 re-analysis. *Quart. J. Roy. Meteorol. Soc.*, **131**(Part B), 2961–3012.

van Oldenborgh, G. J., S. Y. Philip, and M. Collins, 2005: El Niño in a changing climate: a multi-model study. *Ocean Sci.*, **1**, 81–95.

Vecchi, G. A., and B. J. Soden, 2007: Increased tropical Atlantic wind shear in model projections of global warming. *Geophys. Res. Lett.*, **34**, L08702.

Vitart, F., J. L. Anderson, and W. F. Stern, 1997: Simulation of interannual variability of tropical storm frequency in an ensemble of GCM integrations. *J. Climate*, **10**, 745–760.

Walsh, K., 2004: Tropical cyclones and climate change: Unresolved issues. *Clim. Res.*, **27**, 77–83.

Walsh, K. J. E., and B. F. Ryan, 2000: Tropical cyclone intensity increase near Australia as a result of climate change. *J. Climate*, **13**, 3029–3036.

Walsh, K. J. E., M. Fiorino, C. W. Landsea, and K. L. McInnes, 2007: Objectively determined resolution-dependent threshold criteria for the detection of tropical cyclones in climate models and reanalyses. *J. Climate*, **20**, 2307–2314.

Watterson, I. G., J. L. Evans, and B. F. Ryan, 1995: Seasonal and interannual variability of tropical cyclogenesis: Diagnostics from large-scale fields. *J. Climate*, **8**, 3052–3066.

Webster, P. J., G. J. Holland, J. A. Curry, and H. R. Chang, 2005: Changes in tropical cyclone number, duration, and intensity in a warming environment. *Science*, **309**, 1844–1846.

Yamaguchi, K., and A. Noda, 2006: Global warming patterns over the North Pacific: ENSO versus AO. *J. Meteorol. Soc. Japan*, **84**, 221–241.

Risk of Tropical Cyclones Over the Mediterranean Sea in a Climate Change Scenario

Miguel Angel Gaertner, Marta Domínguez, Victoria Gil, and Enrique Sánchez

Abstract The possible development of tropical cyclones over the Mediterranean Sea due to anthropogenic climate change is analysed here. A previous paper (Gaertner et al., 2007) has shown for the first time that there is a risk of such a development, based on regional climate model simulations for a high emissions scenario. The combined use of an ensemble of regional climate models nested in the same global climate model and of the cyclone phase space method from Hart (2003) as an objective way to detect tropical characteristics in the cyclones has allowed us to detect this possibility. The results show a large spread among the models, ranging from no cyclone intensity change in the future climate scenario to the development of strong tropical cyclones. A spatial and temporal comparison of the sea surface temperature with the ocurrence of intense cyclones show that though this variable is important, it's not the only important factor. An adequate synoptic setting is needed, with high-latitude blocking conditions and an upper-level cut-off low over the Mediterranean Sea. Several important uncertainties remain to be analysed, but the existence of a theoretical mechanism for tropical cyclone formation over the Mediterranean Sea and the fact that already some observed Mediterranean cyclones show partially tropical characteristics give plausibility to the analysed risk.

Introduction

The changes in tropical cyclones that can be expected due to anthropogenic climate change still have several open aspects. One of these aspects is the possibility of changes in the geographical distribution of tropical cyclones. The projected increase of sea surface temperatures (SSTs) alone cannot be linked directly to an extension of the areas where tropical cyclones can be found, as the genesis and development of tropical cyclones depend also on atmospheric conditions like the atmospheric stability and the vertical wind shear. Previous studies have not found evidences of changes in the projected areas of formation of tropical cyclones

J.B. Elsner and T.H. Jagger (eds.), *Hurricanes and Climate Change,*
doi: 10.1007/978-0-387-09410-6,

(IPCC, 2007; Lionello, 2002; Walsh, 2004). These results were based either on simulations with General Circulation Models (GCMs), which have a relatively low horizontal resolution or on one particular Regional Climate Model (RCM). The coarse resolution of GCMs limits their ability to simulate perturbations of the scale of tropical cyclones.

Recently, two cyclones have developed over unusual areas of the Atlantic Ocean, raising questions about this issue. In March 2004, the first documented South Atlantic hurricane, called Catarina, made landfall over the southern coast of Brazil (Pezza and Simmonds, 2005). Hurricane Vince (Franklin, 2006) formed next to Madeira Islands in the Atlantic Ocean and was the first detected hurricane to develop over this area. It was also the first known tropical cyclone to make landfall in Spain, though at this point it had lost the hurricane category. Both cyclones developed from an initially baroclinic cyclone, and the tropical transition occurred over SSTs lower than 26°C. The mechanisms of tropical transition and the potential impacts of large scale circulation changes on them have been analyzed in recent studies (Davis and Bosart, 2003; Pezza and Simmonds, 2005).

The Mediterranean Sea reaches already for present climate conditions rather high SST values at the end of summer and beginning of autumn. This has led to studies analysing observed Mediterranean cyclones with respect to tropical characteristics. Partially tropical characteristics have been found in some September and October cyclones (Reale and Atlas, 2001; Homar et al., 2003). Fita et al. (2007) make an analysis of seven observed Mediterranean tropical-like storms using observations and numerical simulations. A mechanism for the development of Mediterranean tropical cyclones, initiated by upper-level cut-off lows, has been proposed (Emanuel, 2005).

The future characteristics of Mediterranean cyclones have been analysed in several papers. Lionello et al. (2002, 2007) have used global climate model (GCM) results and one particular regional climate model (RCM), finding no evidence of more intense cyclones during early autumn months. Another study applied a different regional climate model to analyze Mediterranean cyclones and also did not find any clear tendency in the number of intense summer cyclones for future climate conditions (Muskulus and Jacob, 2005). A recent paper has found evidences of fully tropical cyclones developing over the Mediterranean Sea in future climate scenario simulations (Gaertner et al, 2007), making use of an ensemble of RCMs and an analysis method focused on the detection of tropical cyclones. Here we present additional results of this study.

Methods and Data

Climate change simulations. The multi-model ensemble simulations which are the basis of the present study were performed within PRUDENCE project (Christensen et al., 2002). A description of the nine regional climate models and an analysis of their results can be found e.g. in Jacob et al. (2007) or Déqué et al. (2007). The

domains cover most of Europe, but differ particularly in the location of the southern and eastern boundaries. This is the reason of the differences in the extension of the Mediterranean basin covered by the models. The horizontal resolution is between 50 and 55 km. Two 30-year time slice simulations have been performed in this study: the control run for 1960–1990 period, with observed greenhouse gases levels, and a scenario run for 2070–2100 period, considering SRES-A2 greenhouse gases evolution (IPCC, 2000). Lateral boundary conditions were provided by simulations performed with the Hadley Centre atmospheric global climate model (HadAM3H) (Pope et al., 2000).

The analysis is performed for the month of September, in order to focus on the possible development of cyclones with tropical characteristics. In this month, the SSTs are near their maximum annual value and the summer subsidence over the Mediterranean Sea is also weakening. The summer subsidence is associated to the northward displacement of the subtropical high, and limits strongly summer precipitation over the region.

Observed SSTs (1960–1990) are used for present climate, and future climate SSTs are calculated by adding a constant increment and a positive trend to the monthly values used in the control simulation. This increment is the 30-year monthly mean difference between the two periods in corresponding runs performed with the ocean-atmosphere coupled model HadCM3 (Johns et al., 2003), and the trend has been taken from the same simulation. SSTs reach values of up to 30°C (averaged over the Mediterranean Sea) at the end of the scenario simulation. The SST values (averaged over the Mediterranean Sea) for both present and future climate simulations are shown in Fig. 1.

Cyclone detection method. An objective cyclone detection method (Picornell et al., 2001) based on sea level pressure (SLP) fields is used. The SLP output from the models has been smoothed with a Cressman filter with a radius of 200 km in order to filter out smaller scale noisy features that appear usually in SLP fields. SLP minima are detected in the filtered fields. Too weak cyclones are removed by applying an SLP gradient threshold within a radius of 400 km around the SLP minima. This radius is the reason why the so called cyclone detection area is smaller

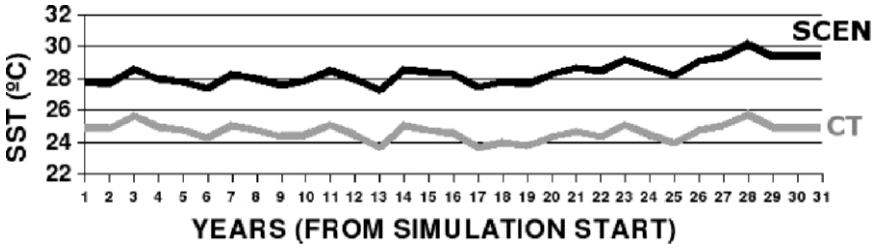

Fig. 1 Evolution of September SST (averaged over the Mediterranean Sea) for control simulation (grey line, 1960–1990) and for scenario simulation (black line, 2070–2100)

than the respective RCM domain. Figure 2 shows the smallest and the largest detection area among the nine models. The largest detection area covers almost the whole Mediterranean Sea, while the smallest one covers only the northernmost part. For the present study, the geostrophic vorticity at cyclone centre has been used for measuring cyclone intensity.

The cyclone detection method allows also to calculate cyclone tracks, but it uses the horizontal wind at 700 hPa to this effect. This field is not available for the analysed RCMs. Due to this, a subjective method has been applied in order to determine cyclone duration and track for the most intense cyclones of each simulation. To this effect, the daily SLP field has been plotted with a 2 hPa interval, and only those lows with at least one closed contour have been considered. Tracks have been obtained by linking the daily cyclone centres using criteria of proximity and similarity. The fact that only the most intense cyclones were analysed this way simplified this task.

Vertical structure of the cyclones. The objective analysis of the vertical structure of the cyclones for determining if the cyclones have tropical or extratropical characteristics has been applied following the published description of the cyclone phase space method (Hart, 2003), based on the geopotential fields between 900 and 300 hPa.

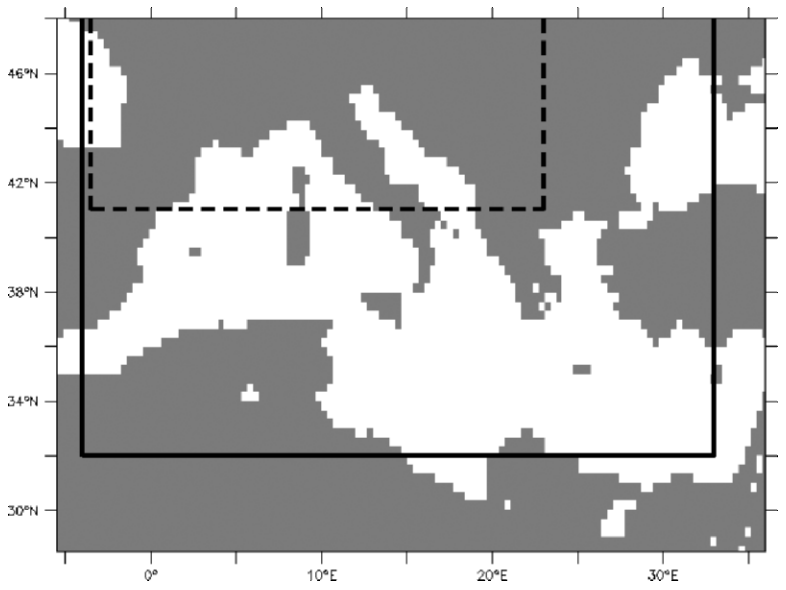

Fig. 2 Largest (*continous box*) and smallest (*dashed box*) detection areas in the regional climate model ensemble

Results

Frequency and Intensity of Cyclone Centres

As explained before, the detection area differs among the nine models. The southern extension of the detection area has been used for dividing the RCM ensemble in two groups for the following analysis. Those models reaching 36.5°C or further to the south were included in one group for which the most detailed analysis has been done, whereas models reaching only up to 39.5°C were included in the other.

As a measure for extreme intensity, the 95th percentile of geostrophic vorticity at cyclone centre has been used. Table 1 shows the values of this statistic for control (CTRL hereafter) and scenario (SCEN) simulations for the two groups of models, ordered from smaller to larger southern extension of the detection area. Among the models covering only the northern part of the Mediterranean Sea, two show almost no difference between CTRL and SCEN simulations, while the others show some intensity increase in the SCEN run. The increasing tendency of extreme intensity is more definite among the models covering also part of the southern Mediterranean Sea. Most of them show a moderate to strong increase in the intensity of extreme cyclones, with only one exception (RegCM) showing almost no increase. The spread in intensity among the models is much larger for SCEN than for CTRL runs, particularly for the models with larger detection area.

The following discussion concentrates on the group of five models with larger Mediterranean domain. The clearer intensity change in this group compared to the remaining models might suggest that it's related to cyclones over southern and eastern areas of the Mediterranean Sea. In order to analyse this possible

Table 1 Intensity of cyclone centres

Model	CTRL	A2 SCEN
CHRM (41.5°C)	186	182 (−2%)
HIRHAM (40.5°C)	162	212 (+31%)
RACMO (40.5°C)	198	231 (+17%)
RCAO (39.5°C)	185	187 (+1%)
HadRM3H (36.5°C)	169	361 (+114%)
CLM (35.5°C)	216	274 (+27%)
PROMES (35.5°C)	257	300 (+17%)
REMO (33.5°C)	221	491 (+122%)
RegCM (32.5°C)	205	214 (+4%)

95th percentile of geostrophic vorticity at cyclone centre ($\times 10^{-6}$ s^{-1}). The percentage variation from CTRL to A2 SCEN simulations is indicated in brackets in the third column. The southern limit of the cyclone detection area is indicated in brackets after the model name, in the first column. The two groups of models mentioned in the text are separated by a blank line.

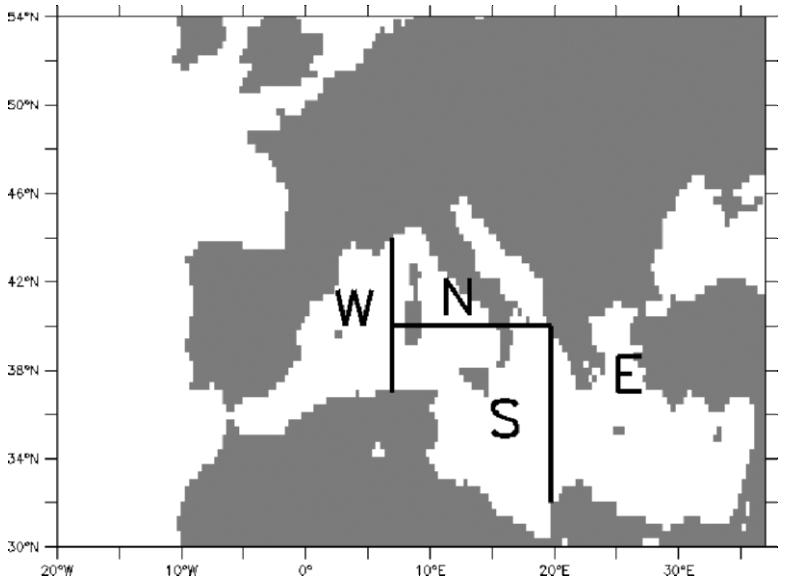

Fig. 3 Mediterranean subdomains for intensity change analysis: western (W), northern (N), southern (S) and eastern (E) subdomains

relationship, the Mediterranean Sea has been divided in four subdomains, shown in Fig. 3. The northern subdomain corresponds roughly to the area of Genoa cyclones. The warmer waters occur in the southern and eastern subdomains, which are not fully included in all the five models. If a direct relationship exists between higher SSTs and the cyclone intensity increase, this should show up in the spatial distribution of cyclone centres.

Figure 4 shows, for all five models and for every subdomain, the frequency of cyclone centres (all low pressure centres during the 30-year simulation period) and the average intensity of the four most intense cyclone centres, as a measure of the change in extreme intensity from CTRL to SCEN run. The model with the largest intensity increase (REMO) shows a clear increase in the number of cyclone centres and in their extreme intensity particularly over the southern and eastern subdomains, as expected if the SST increase is a major reason for these changes. But the picture isn't that clear when we look at the other models. HadRM3H shows also the largest intensity increase over the southern subdomain, but the number of detected cyclone centres is very low there. This is in part due to the more limited detection domain for this model. A visual inspection of the SLP field at the original HadRM3H domain reveals that the cyclone detection method misses several intense cyclone centres over the southern and eastern Mediterranean areas. If these missed cyclones would have been taken into account, a clearer relationship between intensity increase and SSTs for this model would have been apparent. But the largest frequency and extreme intensity increases for CLM occur over the western

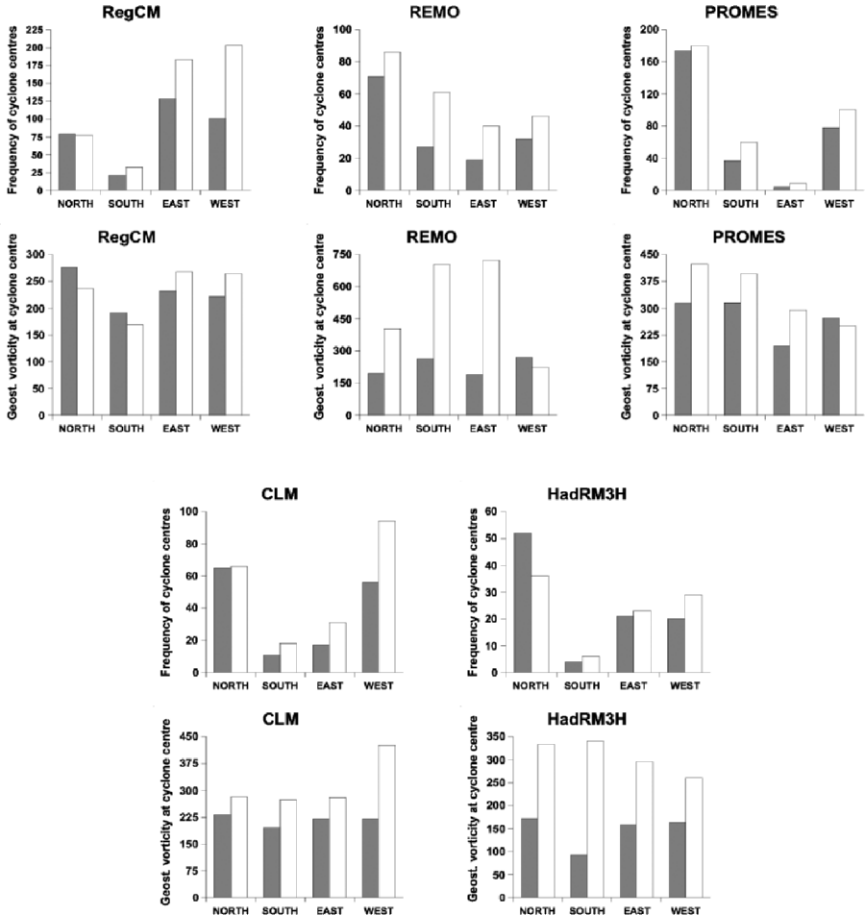

Fig. 4 Number of cyclone centres during 30 years (upper graph) and geostrophic vorticity at cyclone centre ($\times 10^{-6} s^{-1}$) (average of the 4 most intense cyclone centres, lower graph) for the different models, for every subdomain (horizontal axis) and for CTRL (*grey bar*) and A2 SCEN (*white bar*) simulations. The scales are different for each model

subdomain, whereas in PROMES these two quantities increase similarly over three subdomains, including the northern one. Finally, RegCM (which gives no overall intensity increase) shows even some intensity decrease over the southern subdomain. For this last model, the clearest change is a frequency increase over the western subdomain, which seems to be linked mainly to more cyclone centres forming north of the Atlas mountain range.

In summary, the model ensemble shows no systematic relationship between higher SSTs and more intense cyclone centres, though a clearer relationship may be masked by the limited extension to the south and east of the detection areas.

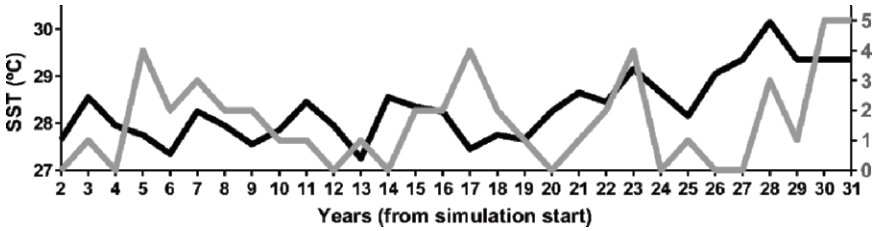

Fig. 5 SCEN simulation: evolution of SST (°C) (*black line, left vertical axis*) during the period 2071–2100 and evolution of the number of intense cyclones per year (*grey line, right vertical axis*) for all the five models analysed. The 10 most intense cyclones have been taken for every model

An interesting related question is if the most intense SCEN cyclones develop at the end of the 30-year period, when the trend leads to the the highest SSTs (Fig. 1). For the same group of five models previously considered, we have taken the ten most intense cyclones of every model, and summed for all models the number of these cyclones occurring every year. This aggregate frequency is shown in Fig. 5, compared to the SST evolution. There seems to be no trend in the number of most intense cyclones, though the highest value occur in the last two years. A visual inspection reveals no correlation with SST either, with some peaks in the number of intense cyclones coinciding even with the lowest SSTs.

This is an aggregate result for the five models. If we look only at the model with the strongest intensity increase, we see that the three most intense cyclones occur during the last decade (figure not shown). This model showed also a relationship between higher SST areas and the intensity increase. SSTs seem therefore to play a role in the intensity increase, but other factors contribute to it.

Analysis of Tropical Characteristics of Cyclones

We will analyse now if the cyclone intensity increase, found in most models of the RCM ensemble, is associated at least in part to tropical characteristics. To this end, the cyclone phase space method described by Hart (2003) has been applied to two of the models. The analysis of other models with this method has not been possible, due to the absence of the necessary daily upper-level data.

The cyclone phase space method uses 3 parameters: one indicates if the cyclone is thermally asymmetric (i.e. has a frontal structure) or symmetric in the horizontal, the other two describe if the cyclone has a cold core or a warm core in the lower troposphere (900-600 hPa) and in the upper troposphere (600-300 hPa). A tropical cyclone is a thermally symmetric, full-tropospheric warm-core cyclone.

The two models analysed are REMO (which shows the strongest intensity increase) and PROMES (which shows the weakest intensity increase among the

five models, when we exclude the model showing virtually no intensity change). This way we can get a first approximation of the relationship between intensity changes and vertical structure changes of cyclones in the RCM ensemble.

Specifically, the four most intense cyclones of CTRL and SCEN runs have been analysed for these two models. Figure 6a shows the cyclone phase space evolution

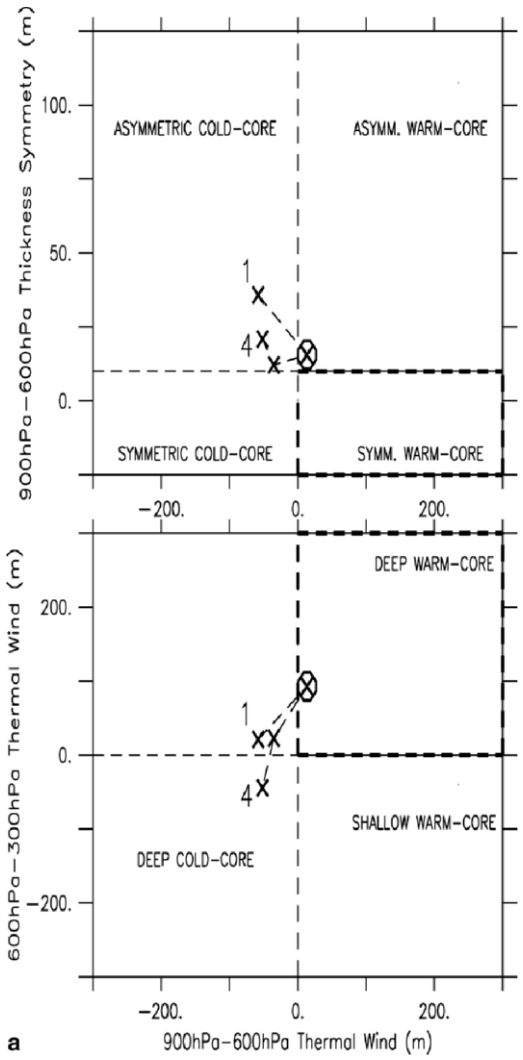

Fig. 6a Cyclone phase space for the most intense cyclone in REMO CTRL simulation. *Upper frame*: 900 hPa-600 hPa storm-relative thickness symmetry (m) versus 900 hPa-600 hPa thermal wind parameter (m). *Lower frame*: 600-300 hPa thermal wind parameter (m) versus 900 hPa-600 hPa thermal wind parameter (m). The most intense cyclone centre is highlighted with a circle

for the most intense REMO-CTRL cyclone. This cyclone has a lifetime of 4 days. In the second day, it develops a full-tropospheric warm core, but it has a certain degree of thermal assymetry. Another REMO-CTRL cyclone (figure not shown) is able to develop a symmetrical warm core structure during two days, but the warm core is less intense and doesn't reach 300 hPa. Similar short-lived warm cores develop also in PROMES-CTRL simulation, where three of the four most intense cyclones show a warm core during 1 day. An example can be found in Fig. 7a), which shows the phase space evolution for the most intense PROMES-CTRL cyclone. The appearance of such short-lived features is consistent with the so called "medicanes" (Fita et al., 2007), which are ocasionally observed over the Mediterranean and show a partially tropical structure. It's noteworthy that the days with a most intense cyclone centre correspond to a warm core structure in the cyclones shown (the most intense cyclone centre is highlighted with a circle in all these phase space graphs).

REMO-SCEN most intense cyclones show a strong structure change. As can be seen in Fig. 6b, the most intense cyclone is able to develop a symmetric, full-tropospheric warm core structure during 6 days. The warm cores are also much more intense than for CTRL cyclones. The parameters reach values typical of a strong hurricane (Hart, 2003). The other three most intense cyclones (not shown) have a warm core structure during 5 to 8 days and, at the same time, low values of the thermal asymmetry parameter. These simulated cyclones are therefore tropical cyclones during part of their lifetime. They maintain a warm core structure for several consecutive days (up to 8), which indicates clearly that the feedback between latent heat fluxes and winds at the sea surface is operating as in fully developed tropical cyclones.

In contrast, the differences between PROMES SCEN and CTRL cyclones are smaller, in good correspondence with the smaller intensity change. The changes are in the direction of an increasingly tropical structure, as two SCEN cyclones show warm cores during more days (2 and 3) in their lifetime, and the intensity of the upper tropospheric warm cores is larger. This is associated to deeper warm cores. The most intense centres for every cyclone correspond to lows with warm core structure, though not necessarily with thermal symmetry, as seen in Fig. 7b).

The clear relationship between maximum intensity and warm cores could suggest that tropical characteristics are also behind at least part of the intensity increase observed in two other models (CLM and HadRM3H). The data needed for a cyclone phase space analysis are not available for these models, but we can look for surface features associated likely to a tropical structure. The most intense CLM-SCEN cyclone is particularly noteworthy in this respect: it deepens strongly while diminishing in size and the spatial distribution of the modelled precipitation is compact and rather symmetrical around the cyclone centre, with high precipitation values near the centre and no evidence of fronts. The radius of maximum wind is small, taking into account the horizontal resolution of 50 km. Several other cyclones simulated by these two models show similar characteristics of the precipitation and wind field, which makes likely that they have tropical characteristics during part of their lifetime.

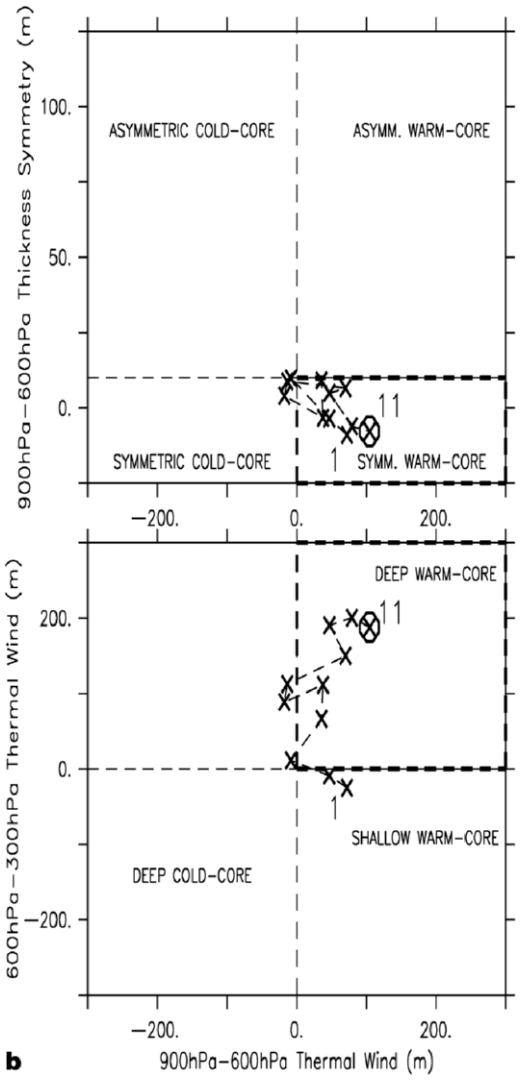

Fig. 6b As figure 6a, but for the most intense cyclone in REMO SCEN simulation

Discussion and Conclusions

In this study we have analysed how different RCMs simulate changes of extreme intensity of cyclones over the Mediterranean Sea in the month of September for a particular emissions scenario. The uncertainty due to differing RCMs, which is relatively low regarding the future evolution of variables like temperature (Déqué et al., 2007), is here very important, as the responses from the different RCMs range

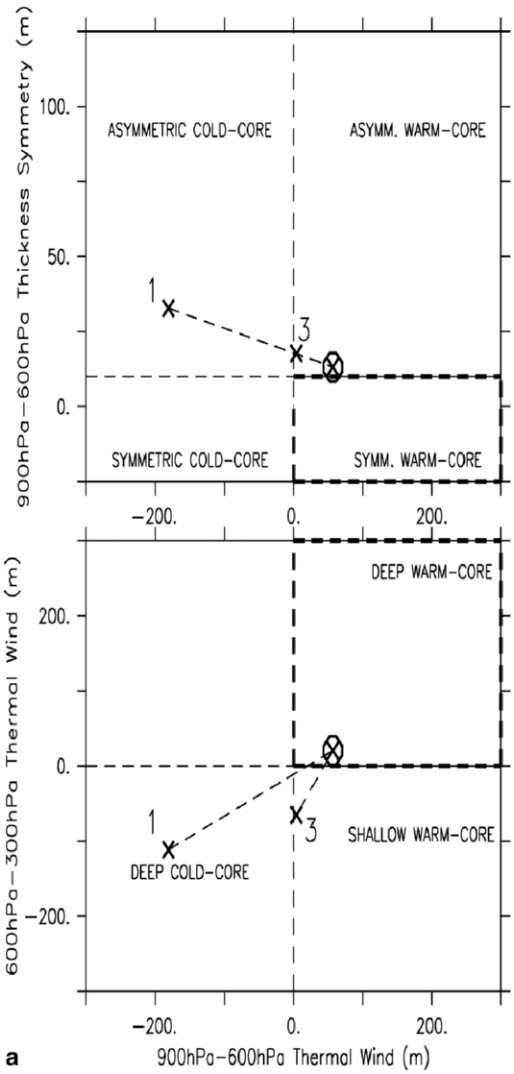

Fig. 7a As Fig. 6b, but for the most intense cyclone in PROMES CTRL simulation

from no change in extreme intensity to a large change which is due to the formation of strong tropical cyclones over the Mediterranean Sea.

There are several other important sources of uncertainty that have to be analysed before reaching clear conclusions regarding the risk of tropical cyclone development. One of them is the use of different GCMs. Tipically the uncertainty due to GCMs is larger (Déqué et al., 2007) than the uncertainty due to RCMs. Different coupled atmosphere-ocean GCM simulations will yield a different evolution of Mediterranean SSTs. For example, the global model of CNRM used also in some

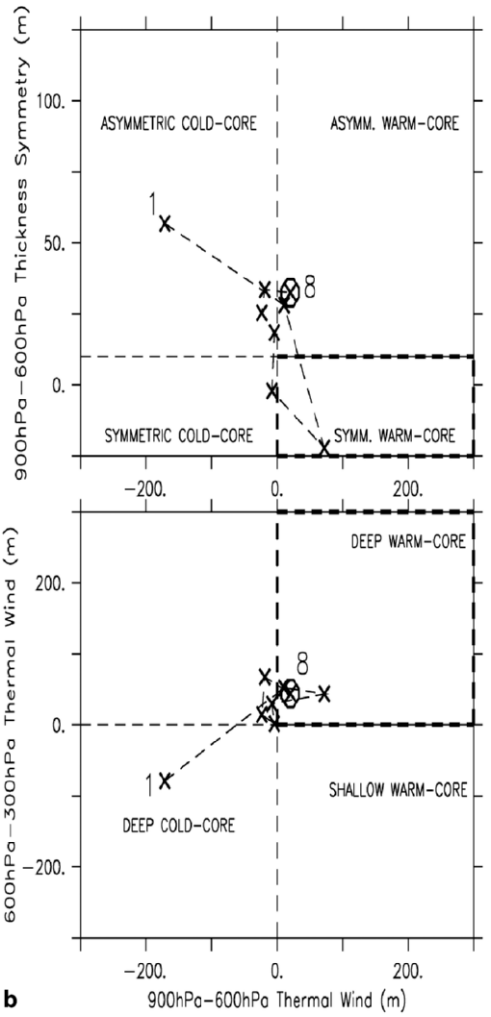

Fig. 7b As Fig. 6a, but for the most intense cyclone in PROMES SCEN simulation

PRUDENCE simulations shows an average SST increase of 3.1°C (Somot et al., 2007) for the same emissions scenario, which is about half a degree less than the SST increase of HadCM3 model. The GCMs can also differ in the frequency and duration of blocking episodes, which would modify the environment for the development of tropical cyclones.

The observed SSTs (Smith et al., 1996) used in the present study show a limited interannual variability, due to the way the database was obtained (Somot et al., 2007). If large positive SST anomalies (like the one observed in the summer of 2003) are more frequent in the future, SSTs at the end of the summer for certain

years might be clearly above the ones used in the present study, increasing the risk of tropical cyclone development.

The use of RCMs which are coupled to the Mediterranean Sea can offer important information. Somot et al. (2007) show that the use of an atmosphere-ocean RCM reduces slightly the average summer SST increase (to 2.9°C, compared with 3.1°C in the uncoupled simulation), but the impact on the intensity of tropical cyclones could be larger than implied by such a small average difference, as a coupled simulation would include the sea surface cooling typically observed under such cyclones. This limiting factor would depend on the depth of the warm sea mixed layer, as a deep mixed layer can even lead to a positive feedback on the intensity of tropical cyclones, as indicated e.g. by Shay et al. (2000).

Another important uncertainty is the emissions scenario. The A2 scenario used here is based on high emissions, but the global temperature increase in the specific HadAM3H A2 simulation is of 3.18°C between CTRL and SCEN runs (Frei et al., 2006), which is at the middle of the range projected by IPCC (Intergovernmental Panel on Climate Change, 2007). Lower emissions scenarios should be analysed to determine the effect of mitigation measures on tropical cyclone risk.

Regarding the synoptic environment under which the SCEN tropical cyclones develop, the tropical cyclones identified in the present study seem to follow a mechanism similar to the one proposed by Emanuel (2005) for the formation of Mediterranean tropical cyclones from upper-level cut-off lows. The cyclones with a clear tropical structure detected in the present study form from a cut-off low which triggers convection over the sea and undergoes a tropical transition afterwards (results not shown). The development of a strong tropical cyclone needs an adequate environment, and that seems to be provided by long-lasting blocking anticyclones over northern Europe. This synoptic setting explains also why these cyclones may move westward over long distances, as seen particularly in one of REMO-SCEN most intense cyclones, steered by the easterly winds on the southern part of the blocking anticyclone. The duration of these blocking anticyclones can be very long. For example, high pressures last during two weeks over northern Europe when the most intense REMO-SCEN cyclone develops.

Finally, some aspects of the RCM setup can affect the results. The domain of the models, together with the cyclone detection method used, has probably led to missing cyclone centres over the warmer waters of the southern and eastern Mediterranean Sea. The resolution (about 50 km) is certainly larger than that of many GCMs used up to now in analysing Mediterranean cyclones, but is still too coarse to fully resolve tropical cyclones. Resolution increases could lead to better simulation of tropical cyclone processes, and perhaps to more intense cyclones, if the tipically observed relationship between resolution and intensity is valid here.

The results presented here give strong support to the use of RCM ensembles. The use of only one RCM can lead either to underestimations of the risk or to overestimations of the risk. The use of the cyclone phase space analysis seems to be a promising tool in analysing structural changes of cyclones, due to its objective and gradual character, as there are no arbitrary limits separating in a binary way extratropical from tropical cyclones. The large frequency of vertical level

geopotential data needed by this method may limit its application, due to the possible absence of such data in the output from climate simulations.

Despite the need for more studies that take into account the different sources of uncertainty, the present results give plausibility to the future development of tropical cyclones over the Mediterranean Sea. At least some increase in tropical characteristics seems likely for the analysed emissions scenario, following the results presented here. A theoretical mechanism exists for explaining the possible development of tropical cyclones, and the fact that for present climate conditions some Mediterranean cyclones develop already partially tropical characteristics is a strong reason for taking this possibility into account.

References

Christensen, J., T. Carter, and F. Giorgi, 2002: PRUDENCE employs new methods to assess European climate change. *Eos, Trans. Amer. Geophys. Union*, **83**, 147.

Davis, C. A., and L. F. Bosart, 2003: Baroclinically induced tropical cyclogenesis. *Mon. Wea. Rev.*, **131**, 2730–2747.

Déqué, M., D. P. Rowell, D. Lüthi, F. Giorgi, J. H. Christensen, B. Rockel, D. Jacob, E. Kjellstrøm, M. de Castro and B. van den Hurk, 2007: An intercomparison of regional climate simulations for Europe: assessing uncertainties in model projections. *Climatic Change*, **81**, 53–70.

Emanuel, K., 2005: Genesis and maintenance of Mediterranean hurricanes. *Adv. Geosci.*, **2**, 217–220.

Fita, L., R. Romero, A. Luque, K. Emanuel, and C. Ramis, 2007: Analysis of the environments of seven Mediterranean tropical-like storms using an axisymmetric, nonhydrostatic, cloud resolving model. *Nat. Hazards Earth Syst. Sci.*, **7**, 41–56.

Franklin, J. L., 2006: Tropical cyclone report: Hurricane Vince, 8–11 October 2005. Natl. Hurricane Cent., Miami, Fla., 9 pp. [Available at http://www.nhc.noaa.gov/pdf/TCR-AL242005_Vince.pdf]

Frei, C., R. Scholl, S. Fukutome, R. Schmidli, and P. L. Vidale, 2006: Future change of precipitation extremes in Europe: Intercomparison of scenarios from regional climate models. *J. Geophys. Res.*, **111**, D06105, doi:10.1029/2005JD005965.

Gaertner, M. A., D. Jacob, V. Gil, M.Domínguez, E. Padorno, E. Sánchez, and M. Castro, 2007: Tropical cyclones over the Mediterranean Sea in climate change simulations. *Geophys. Res. Lett.*, **34**, L14711, doi:10.1029/2007GL029977.

Hart, R., 2003: A cyclone phase space derived from thermal wind and thermal assymmetry. *Mon. Wea. Rev.*, **131**, 585–616.

Homar, V., R. Romero, D. J. Stensrud, C. Ramis, and S. Alonso, 2003: Numerical diagnosis of a small, quasi-tropical cyclone over the western Mediterranean: Dynamical vs. boundary factors. *Q. J. R. Meteorol. Soc.*, **129**, 1469–1490.

Intergovernmental Panel on Climate Change, 2000: *Emissions Scenarios: A Special Report of Working Group III of the Intergovernmental Panel on Climate Change*. edited by N. Nakicenovic and R. Swart, 599 pp.,Cambridge Univ. Press, New York.

Intergovernmental Panel on Climate Change, 2007: *Climate Change 2007: The Physical Science Basis*. edited by S. Solomon et al., 987 pp., Cambridge Univ. Press, New York.

Jacob, D., L. Bärring, O. B. Christensen, J. H. Christensen, M. de Castro, M. Déqué, F. Giorgi, S. Hagemann, M. Hirschi, R. Jones, E. Kjellström, G. Lenderink, B. Rockel, E. Sánchez, C. Schär, S. I. Seneviratne, S. Somot, A. van Ulden, and B. van den Hurk, 2007: An inter-comparison of regional climate models for Europe: Model performance in present-day climate. *Climatic Change*, **81**, 31–52.

Johns, T. C., J. M. Gregory, W. J. Ingram, C. E. Johnson, A. Jones, J. A. Lowe, J. F. B. Mitchell, D. L. Roberts, D. M. H. Sexton, D. S. Stevenson, S. F. B. Tett, and M. J. Woodage, 2003: Anthropogenic climate change for 1860 to 2100 simulated with the HadCM3 model under updated emissions scenarios. *Clim. Dyn.*, **20**, 583–612.

Lionello, P., F. Dalan, and E. Elvini, 2002: Cyclones in the Mediterranean region: The present and the doubled CO2 climate scenarios. *Clim. Res.*, **22**, 147–159.

Lionello, P., U. Boldrin, and F. Giorgi, 2007: Future changes in cyclone climatology over Europe as inferred from a regional climate simulation. *Clim. Dyn.*, doi:10.1007/s00382-007-0315-0.

Muskulus, M., and D. Jacob, 2005: Tracking cyclones in regional model data: The future of Mediterranean storms. *Adv. Geosci.*, **2**, 13–19.

Pezza, A. B., and I. Simmonds, 2005: The first South Atlantic hurricane: Unprecedented blocking, low shear and climate change. *Geophys. Res. Lett.*, **32**, L15712, doi:10.1029/2005GL023390.

Picornell, M. A., A. Jansá, A. Genovés, and J. Campins: Automated database of mesocyclones from the HIRLAM-0.5 analyses in the western Mediterranean. *Int. J. Climatol.*, **21**, 335–354.

Pope, V., M. Gallani, P. Rowntree, and R. Statton, 2000: The impact of new physical parameterizations in the Hadley Centre climate model: HadAM3. *Clim. Dyn.*, **16**, 123–146.

Reale, O., and R. Atlas, 2001: Tropical cyclone-like vortices in the extratropics: Observational evidence and synoptic analysis. *Weather Forecast.*, **16**, 7–34.

Shay, L. K., G. J. Goni, and P. G. Black, 2000: Effects of a Warm Oceanic Feature on Hurricane Opal. *Mon. Wea. Rev.*, **128**, 1366–1383.

Somot, S., F. Sevault, M. Déqué, and M. Crepon, 2008: 21st Century Climate Change Scenario for the Mediterranean using a coupled Atmosphere-Ocean Regional Climate Model. Global Planet. Change (in press).

Smith, T., R. Reynolds, R. Livezey, and D. Stokes, 1996: Reconstruction of historical sea surface temperatures using empirical orthogonal functions. *J. Climate*, **9**, 1403–1420.

Walsh, K., 2004: Tropical cyclones and climate change: Unresolved issues, *Clim. Res.*, **27**, 77–83.

A Fast Non-Empirical Tropical Cyclone Identification Method

Norihiko Sugimoto, Minh Tuan Pham, Kanta Tachibana, Tomohiro Yoshikawa, and Takeshi Furuhashi

Abstract We propose a high speed non-empirical method to detect centers of tropical cyclones, which is useful to identify tropical cyclones in huge climatology data. In this method, centers of tropical cyclones are detected automatically by iteration of streamline in down-stream direction from some initial positions. We also bend the path of streamline successively to converge on the center of tropical cyclone rapidly. Since this method is free from empirical conditions used in the conventional method, the accuracy is independent of these conditions. Moreover, because the proposed method does not need to check these at all grid points, computational cost is significantly reduced. We compare the accuracy and effectiveness of the method with those of the conventional one for tropical cyclone identification task in observational data. Our method could find almost all tropical cyclones, some of which were not identified by the conventional method. This method will be useful for future huge climatology data, since computational cost does not depend on the number of grid points.

Introduction

Global warming is a very important issue in the climate research fields. As the Intergovernmental Panel on Climate Change (IPCC 2007) reported, global warming gives not only increase of global average temperature, but change of frequencies and intensities of extreme events. There is a social need to study causality between global warming and these extreme events, since their impact on our life and environment will be serious in future climate.

Among these extreme events, tropical cyclone is one of the most important topics. It is argued eagerly that the effect of global warming on the frequencies and intensities of the tropical cyclones [Emanuel 1987, Holland 1997]. In order to predict future climate change and extreme events such as tropical cyclones, many

J.B. Elsner and T.H. Jagger (eds.), *Hurricanes and Climate Change,*
doi: 10.1007/978-0-387-09410-6,

numerical investigations has been done using general circulation model [Broccoli and Manabe 1990, Haarsma et al. 1993, Bengtsson et al. 1996, Krishnamurti et al. 1998, Sugi et al. 2002, Yoshimura et al. 2006, Bengtsson et al. 2007]. However, there is some ambiguity in these studies because of the parameterization process due to finite resolution of the numerical model. Some studies suggest that while tropical cyclones will appear less frequently, intense tropical cyclones will appear more frequently. It is necessary to use a higher resolution model to discuss features of future tropical cyclones in detail. Although recent numerical investigation achieves fine grid size about 20 km [Oouchi et al. 2006], further investigation will be needed to have a consensus understanding of future tropical cyclones. This tendency to develop and use high resolution model is accelerating and will continue.

One of the main weak points of these high resolution numerical studies is that there is no definite method to identify tropical cyclones in huge output data. In the case of the observational data, the conventional way is an empirical identification by experts using satellite images. However, it is not reasonable for an identifier of tropical cyclones in the model output data to create surrogate images to satellite ones, since the reliable data are distributed uniformly at all grid points. There is a room of exploring an alternative method to identify tropical cyclones effectively. Although several methods have been proposed to identify tropical cyclones in the model output data [Haarsma et al. 1993, Bengtsson et al. 1995, Sugi et al. 2002, Oouchi et al. 2006], these methods have some problems as the following. Since these methods use empirical conditions of criteria, first it is difficult to determine criteria themselves. Second, there is some possibility to overlook and miss the tropical cyclones in the datasets, since the accuracy depends on these criteria. Third, as these conditions need to be checked at all grid points, the computational cost is enormously in the case of high resolution model. The finer the model resolution is, the larger the size of the output data becomes. Thus, sometimes we have to analyze several gigabyte data to discuss future tropical cyclones induced by climate change [Oouchi et al. 2006].

In the present study, we propose a new high speed non-empirical method to detect centers of vortices automatically, which enables us to identify tropical cyclones in huge climatology data. To perform this method effectively, we first transform coordinates. Since a tropical cyclone has its wind flow as concentric circles, we make use of streamline. For effective searching, we bend the path of streamline successively. This method allows us to save large amount of computational time even in the case of high resolution model, since our method does not need to check conditions at all grid points.

The rest of this paper is organized as follows. In section 2, we show several methods used in this study. First, empirical conditions of criteria used in the conventional method are shown. Then we propose a new high speed non-empirical method to detect centers of tropical cyclone automatically. In Section 3, we compare the effectiveness of the proposed method with those of the conventional one for tropical cyclone identification task in the observational data. We give summary and future works in Section 4.

Methodologies

Data

In the present study, we use datasets of National Centers for Environmental Prediction (NCEP) global reanalysis project [Kalnay et al. 1996] as a meteorological data. The horizontal resolution is 2.5°lat × 2.5°lon grid, and the total grid number is 10244. In the conventional method of identifying tropical cyclones, fourth-daily geopotential height, horizontal velocity, and temperature at several pressure levels are used. In the proposed method, we only use fourth-daily horizontal velocity at one pressure level, i.e. either of 850[hPa] or 1000[hPa]. Although mesh size of this data is too coarse to express structures of tropical cyclones, this dataset is enough to detect tropical cyclone-like phenomena. In the present study, we emphasize the accuracy of the proposed method even in the coarse resolution.

We also use "best track" dataset as a correct answer to evaluate the accuracy of the methods. This dataset is official record of tropical cyclones in Northwest Pacific, compiled by the Japan Meteorological Agency since 1951. The dataset contains records such as center position, central pressure, and maximum sustained wind speed for every three to six hours. We regard the data as ground truth data, since these data are provided and assessed by the experts after receiving all information of tropical cyclones. We compare the identification of tropical cyclones in the several methods with the right answer of "best track".

Conventional Method

First, we introduce the conventional method of tropical cyclone identification. Traditionally, tropical cyclones are identified by several empirical conditions. For example, [Bengtsson et al. 1995] use the following 5 conditions of criteria. For the position i,

(1) $\exists j \in N(i, 48), V_j^{850} > 3.5 \times 10^{-5}$.

(2) $H_i^{1000} \leq min_{l \in N(i,4)}\, H_l^{1000}$ and above $j\ \exists k \in N(j, 48), \left|w_k^{1000}\right| > 15$.

(3) $A_{i,48}^{700} + A_{i,48}^{500} + A_{i,48}^{300} > 3$.

(4) $A_{i,48}^{300} > A_{i,48}^{850}$.

(5) $\sum_{j \in i \cup N(i,48)} \left(\left|w_j^{850}\right| - \left|w_j^{300}\right|\right) > 0$.

Here, $N(i,n)$ denotes n neighborhoods of grid point i,V_j^{850} is a relative vorticity [1/s] at the pressure level of 850[hPa] at grid point j. H_l^{1000} is height field [m] at the pressure level of 1000[hPa] at grid point l. w_k^{λ} is velocity [m/s] at the pressure level λ[hPa] at grid point k. $A_{i,n}^{\lambda} = a_i^{\lambda} - \frac{1}{n}\sum_{j\in N(i,n)} a_j^{\lambda}$ stands for air temperature anomalies [k] from average of n neighborhoods of grid point i at the pressure level of λ[hPa], where a_i^{λ} is air temperature [k] at the pressure level of λ[hPa] at grid point i. If these conditions are satisfied with more than one and a half day long, the phenomenon is regarded as a tropical cyclone.

It is not appropriate to apply this method to data from high resolution numerical models. First, these conditions are empirical, so it needs a trial and error to obtain effective identification of tropical cyclone. Second, since the longitudinal grid intervals depend on the latitude, conditions of criteria are not uniform. Third, it needs large amount of computational time, since it has to check these conditions at all grid points. In the case of high resolution numerical model, it would be troublesome to use this method.

Proposed Method

In the proposed method, we use coordinate transformation and streamline with enhanced curvature in order to achieve high speed detection of centers of tropical cyclones without empirical conditions. For preparation, we construct a database of velocity fields from the NCEP reanalysis dataset. In the database, horizontal velocities at arbitrary positions are obtained using linear interpolation at desired time and pressure level.

Coordinate Transformation

We first transform the coordinate. Traditionally, observational datasets are provided in the latitude-longitude grid system and these datasets are used to identify tropical cyclones in the conventional method. However, if we project this grid system to the 2-dimensional plane, there are large distortions especially at higher latitude. To avoid this distortion, we need to transform flow velocity field provided in the latitude-longitude grid to the 3-dimensional Cartesian coordinate. In the proposed method, since we use vector field of streamline and its curvature in 3-dimensional Cartesian coordinate, we equip a conversion and inversion from latitude-longitude coordinate to 3-dimensional Cartesian one, as shown in Fig. 1.

The transformation from latitude-longitude coordinate (ϕ, ψ) to 3-dimentional Cartesian coordinate (x,y,z) with the origin at the center of the earth is written in the following equation.

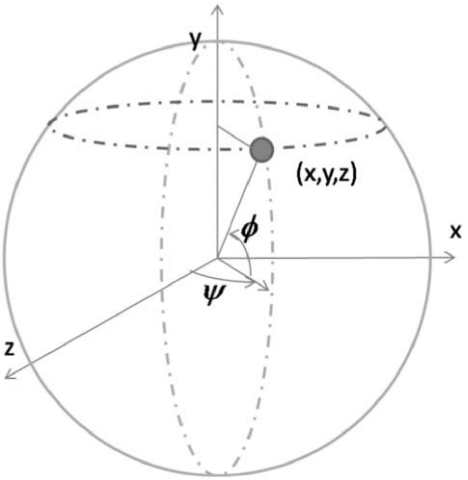

Fig. 1 Latitude-longitude coordinate and 3-dimensional Cartesian coordinate

$$\begin{bmatrix} x \\ y \\ z \end{bmatrix} = R_y(\psi)R_x(\phi)\begin{bmatrix} 0 \\ 0 \\ h_l \end{bmatrix}, \tag{1}$$

where, h_l stands for the length from the center of the earth to the pressure level l. $R_x(\phi)$ is the rotation matrix of angle ϕ around x axis,

$$R_x(\phi) = \begin{bmatrix} 1 & 0 & 0 \\ 0 & \cos\phi & \sin\phi \\ 0 & -\sin\phi & \cos\phi \end{bmatrix}. \tag{2}$$

$R_y(\psi)$ is the rotation matrix of angle ψ around y axis,

$$R_y(\psi) = \begin{bmatrix} \cos\psi & 0 & \sin\psi \\ 0 & 1 & 0 \\ -\sin\psi & 0 & \cos\psi \end{bmatrix}. \tag{3}$$

Then the velocity vector (w_x, w_y, w_z) is written in 3-D Cartesian coordinate,

$$\begin{bmatrix} w_x \\ w_y \\ w_z \end{bmatrix} = R_y(\psi)R_x(\phi)\begin{bmatrix} u \\ v \\ 0 \end{bmatrix}. \tag{4}$$

where, u and v are longitudinal and latitudinal velocity, respectively. The latitude ϕ and longitude ψ are obtained from 3-D Cartesian coordinate vector (x, y, z) as follows,

$$\sin\phi = \frac{y}{h_l}, \quad \cos\phi = \frac{\sqrt{x^2 + y^2}}{h_l}, \tag{5}$$

$$\sin\psi = \frac{x}{\sqrt{x^2 + y^2}}, \quad \cos\psi = \frac{z}{\sqrt{x^2 + y^2}}. \tag{6}$$

Streamline

Streamline is one of the ways to search convergent points in the vector field [Vollmers 2001]. Since velocity vector field around the tropical cyclone is nearly concentric circles and there is almost no flow at the center of tropical cyclone, the convergent point of velocity is considered as the center of tropical cyclone. In addition, because of the surface friction, the velocity field tends to converge on the center of tropical cyclone near the ground pressure level. Thus, we use streamline to detect the center of tropical cyclone.

Starting with several initial positions we search for the center of tropical cyclone by iterating the streamline path downstream until the interpolated wind speed at 850 [hPa] or 1000[hPa] is close to zero. At the next step of iteration, the position is moved to,

$$\vec{x}_{i+1} = \vec{x}_i + \Delta t \vec{w}_i. \tag{7}$$

Here $\vec{x}_i$ and $\vec{w}_i$ is the reference position and its velocity in 3-dimensional Cartesian coordinate system, respectively. $\vec{x}_{i+1}$ stands for the position at the next step. In the present study, we set Δt at 21600[s]. From equation (7) and the fact that $\vec{w}_i$ is perpendicular to $\vec{x}_i$, we obtain

$$\vec{x}^2_{i+1} = (\vec{x}_i + \Delta t \vec{w}_i)^2 = \vec{x}^2_i + (\Delta t \vec{w}_i)^2. \tag{8}$$

Since above equation gives $\left|\vec{x}_{i+1}\right| \geq \left|\vec{x}_i\right|$, if we use (7), the reference point goes away and away from the center of the earth. To avoid this, we convert $\vec{x}_{i+1}$ to latitude-longitude coordinate, and then we obtain the position at the corresponding pressure level in 3-dimensonal coordinate.

We decide centers of tropical cyclones using the following criterion, since there is almost no flow at the center of tropical cyclone.

$$\left|\overrightarrow{x}_{i+1} - \overrightarrow{x}_i\right| < \varepsilon. \tag{9}$$

Here we set $\varepsilon = 1000$[m], after checking several values of ε. This means that our searching finishes when the velocity is less than 1 km per 6 hour. This small value is effective to search convergent points precisely. We also set total iteration steps to be 100.

Streamline With Enhanced Curvature

Since velocity field of tropical cyclone tends to form concentric circle as mentioned before, it is possible that the method of streamline (9) does not converge on the center of tropical cyclone. To avoid this, we make use of velocity vector $\overrightarrow{w}'_i$ at the next position $\overrightarrow{x}'_i = \overrightarrow{x}_i + \Delta t \overrightarrow{w}_i$ as shown in Fig. 2.

$$\overrightarrow{x}_{i+1} = \overrightarrow{x}'_i + \frac{\overrightarrow{w}_i \cdot \overrightarrow{w}'_i}{\overrightarrow{w}'_i 2} \Delta t \overrightarrow{w}'_i. \tag{10}$$

Namely, we enhance the curvature of streamline at the position $\overrightarrow{x}_i$ to assume that the curvature at the position $\overrightarrow{x}'_i$ is almost equal to that at the position $\overrightarrow{x}_i$. Since the path of the streamline with enhanced curvature bends to the inner circle, this method converges on the center of tropical cyclone in contrast to the method with simple streamline. In addition, as $\left|\overrightarrow{x}_{i+1} - \overrightarrow{x}_i\right| \leq \Delta t \left|\overrightarrow{w}_i\right|$, this method also tends to converge rapidly and accurately. We set the criterion of the end of searching to be the same as (9). Total iteration steps are also the same as the method with simple streamline.

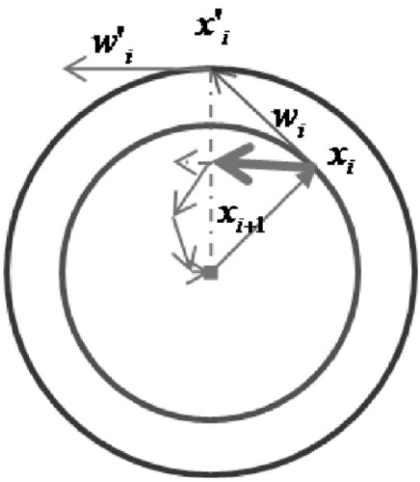

Fig. 2 Example of streamline with enhanced curvature (10)

Results

Comparison of Two Streamline Methods

First, we compare the efficiency of the two methods, simple streamline (7) and streamline with enhanced curvature (10). Here we use a velocity field data from NCEP at 1000[hPa] pressure level on 1800UTC July 10, 2006. We put 12 initial positions at grid points, $\{10°\mathrm{N}, 22.5°\mathrm{N}, 35°\mathrm{N}\} \times \{120°\mathrm{E}, 130°\mathrm{E}, 140°\mathrm{E}, 150°\mathrm{E}\}$. Fig. 3 shows the result of the comparison. Black marks express observational points, and short black lines at these points denote velocity vectors. Long black lines show the results of simple streamline, and long white lines show those of the streamline with enhanced curvature. Black and white hexagons show convergent points of two methods which colors correspond to those of the methods.

Although some simple streamlines approach near to a tropical cyclone, named BILIS, they never converge on the center and do not satisfy the criteria (9) even after 100 iterations. On the other hand, streamlines with enhanced curvature converge on the center of the tropical cyclone BILIS, from 5 initial positions at 20 iterations on average. These results show the efficiency of the streamline method with enhanced curvature. In the next subsection we make a comparison of this method with the conventional method.

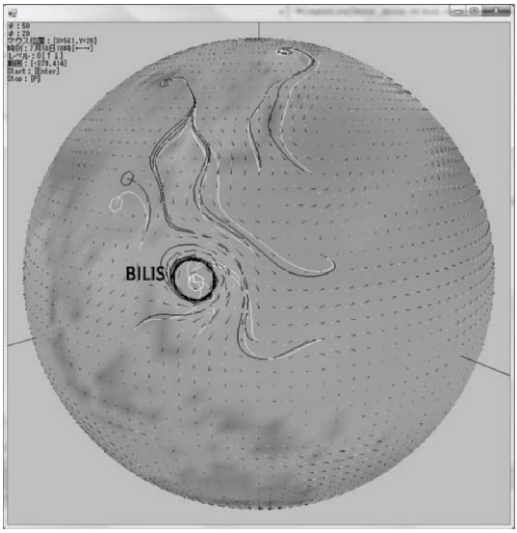

Fig. 3. Comparison of the two streamline methods

Comparison of Streamline Method to Conventional One

We compare the efficiency of the proposed method (10) with that of the conventional method, using the NCEP reanalysis dataset in 2006. The accuracy of the identifications of tropical cyclones near Japan is evaluated by the ''best track'' data. We use conditions in [Bengtsson et al. 1995] as the conventional method, since the resolution is comparable to NCEP. Note that since conventional methods proposed by [Sugi et al. 2002, Oouchi et al. 2006] are for the data of higher resolution numerical models, the conditions of criteria, such as the values of neighborhood points or the values of criterion (3), are somewhat different from [Bengtsson et al. 1995]. In the proposed method, we put 12 initial positions, which are the same as subsection 3.1 but at 850[hPa] pressure level to compare with the conventional method. We also evaluate accuracy of detection using only criterion (1) of the conventional method, since the other criteria based on different data than wind vectors may remove some tropical cyclones. We focus on the tropical cyclones in the range of $[0°\mathrm{N}-50°\mathrm{N}] \times [110°\mathrm{E}-170°\mathrm{E}]$ (we call it ''near Japan'').

The results are summarized in Table 1. There are 23 tropical cyclones in 2006. For each tropical cyclone, ''lifetime'' shows a duration time between developed

Table 1 The results of identification of tropical cyclones, number in the parentheses denotes hour [UTC]

Name	Lifetime	Max strength [kt]	Streamline	Criterion 1	All criteria
CHANCHU	5/9(12)–18(18)	95, 5/15(0)	5/5(0)	5/13(0)	5/15(6)
JELAWAT	6/27(12)–28(18)	40, 6/28(6)	6/23(6)	none	none
EWINIAR	6/30(18)–7/10(6)	100, 7/4(12)	6/29(18)	6/30(18)	none
BILIS	7/9(6)–7/15(0)	60, 7/12(21)	7/4(12)	7/7(12)	7/8(6)
KAEMI	7/19(12)–7/25(18)	80, 7/21(12)	7/17(12)	7/20(18)	7/24(18)
PRAPIROON	8/1(6)–8/4(18)	65, 8/2(12)	7/25(0)	8/1(18)	8/2(18)
MARIA	8/5(18)–8/10(0)	70, 8/6(18)	8/4(0)	none	none
SAOMAI	8/5(12)–8/10(18)	105, 8/9(12)	8/5(0)	none	none
BOPHA	8/6(12)–8/9(0)	55, 8/7(21)	8/3(6)	none	none
WUKONG	8/13(0)–8/19(6)	50, 8/15(12)	8/10(0)	8/10(18)	8/11(18)
SONAMU	8/14(0)–8/15(0)	35, 8/14(0)	none	none	none
IOKE	8/27(6)–9/6(12)	105, 8/30(0)	8/30(12)	8/31(6)	8/31(6)
SHANSHAN	9/10(12)–9/18(9)	110, 9/15(15)	9/9(0)	9/15(6)	9/15(6)
YAGI	9/17(6)–9/25(0)	105, 9/21(12)	9/18(18)	9/22(6)	9/22(6)
XANGSANE	9/26(0)–10/1(18)	80, 9/29(18)	9/24(6)	9/27(0)	none
BEBINCA	10/3(0)–10/6(0)	50, 10/4(18)	9/28(18)	10/2(0)	10/2(6)
RUMBIA	10/3(6)–10/5(18)	45, 10/4(0)	10/2(18)	10/2(18)	10/5(12)
SOULIK	10/9(12)–10/16(6)	75, 10/14(6)	10/7(12)	10/13(12)	10/13(6)
CIMARON	10/27(6)–11/4(6)	100, 10/29(6)	10/25(6)	none	none
CHEBI	11/9(12)–11/13(6)	100, 11/10(12)	11/8(12)	none	none
DURIAN	11/26(12)–12/5(0)	105, 11/29(12)	11/25(0)	none	none
UTOR	12/7(18)–12/14(0)	85, 12/12(12)	12/7(0)	12/9(12)	none
TRAMI	12/17(12)–12/18(12)	35, 12/17(12)	none	none	none

time and decayed time when maximum wind velocity exceeds 0 at first and at final, in the ''best track'' data, respectively. The maximum strength [kt] and its time for each tropical cyclone are also shown. We list the time of identifying tropical cyclones at first in the proposed and the conventional methods, in which we also include the case using only criterion (1). There are only 11 tropical cyclones found by the conventional method. Even when we only use criterion (1), 14 tropical cyclones are found. In contrast, the proposed method finds 19 tropical cyclones before the developed time, and other 2 at the time of developing. Only 2 tropical cyclones, which have very short lifetime, are missed.

Figure 4 shows the result on 1200UTC August 13, 2006. Black pentagons show the centers of tropical cyclones in ''best track'' data. A black diamond denotes a tropical cyclone identified by the conventional method. By the conventional method, only a tropical cyclone ''WUKONG'' is found. White hexagons are the centers of tropical cyclones detected by the proposed method. The proposed method finds

1. A decaying tropical cyclone, MARIA
2. A developing tropical cyclone, WUKONG
3. A strong vortex near to Japan.

However, a tropical cyclone SONAMU is missed by the proposed method. The reason is that there is no vortex at 850[hPa].

We emphasize another benefit of the proposed method. In this method, at each iteration we need only few data points around the reference point. Thus, in the case of huge climatology datasets of the high resolution numerical model, we only use small subset of the data to detect centers of tropical cyclones. Although there are several empirical conditions in the proposed method, such as initial positions, Δt,

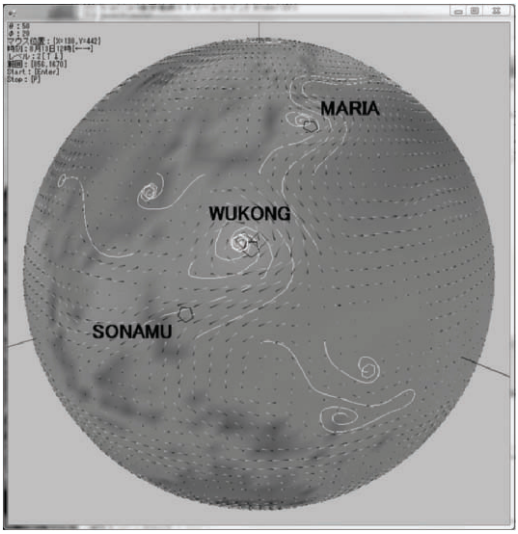

Fig. 4 Comparison enhanced streamline with conventional method

Table 2 The statistical average of identification on 2006 by the proposed method

Level [hPa]	Initial points	convergence	all area	near Japan	TC
850	12	7.22	3.51	2.25	0.78
1000	12	11.16	4.15	2.79	0.9
1000	20	18.49	4.97	3.27	0.91

and ε in the criterion (9), it is easy to test several values of these conditions because of small computational time.

We investigate the efficiency of the proposed method for different pressure levels (850[hPa] and 1000[hPa]) and initial positions (12 and 20). Table 2 shows statistical average of identification on 2006. Each column shows the average numbers for a time step throughout the year of: convergent streamlines, convergent points, convergent points in the range of $[0^\circ\mathrm{N}-50^\circ\mathrm{N}] \times [110^\circ\mathrm{E}-170^\circ\mathrm{E}]$ (near Japan), and convergent points at the centers of tropical cyclones (TC), respectively. Although there are some initial points from which streamline do not converge after 100 iterations, we obtain better convergence and thus find more tropical cyclones in higher pressure level of 1000[hPa]. On the other hand, in the case of 20 initial points, there are not significant differences to detect tropical cyclones. Although we have checked several choices of initial positions, the results are qualitatively the same.

One thing we have to note is that the proposed method detects several strong cyclones. These strong cyclones are important for natural disaster at one side. However, if we want to discuss the effect of global warming on tropical cyclones, we have to omit these strong cyclones correctly. Once we find strong vortices in the huge datasets, it is a relatively easy task to remove these cyclones by adding several conditions, such as coherent vertical structure and warm core. Since there are only small numbers of convergent points (3.51–4.97), we can identify tropical cyclones applying, for example, traditional empirical conditions to each of the convergent points and its neighborhoods. This procedure saves us a large amount of computational time, since we do not need to check empirical conditions for all grid points. Note that there is no convergence at high pressure point. This is because of two main reasons. First, flow velocity of anticyclone tends to be weaker than that of cyclone. Second, the center of anticyclone at lower levels is not a convergent point but rather a divergence point.

Summary

In the present study, we proposed a non-empirical streamline method to detect the center of tropical cyclone automatically with less computational time. In the proposed method, first we solve the problem of distortion at high latitude in latitude-longitude grid system by use of coordinate transformation. We also bend

the path of streamline successively to accelerate the convergence on the center of tropical cyclone. This method does not depend on empirical conditions which are adopted in the conventional method. Moreover, since the proposed method does not need to check conditions at all grid points, we achieved significant reduction of computational time.

To evaluate the effectiveness of the proposed method, we made several comparison experiments using the NCEP reanalysis datasets. Although the data is too coarse to define tropical cyclones, the proposed method automatically detects almost all tropical cyclones some of which are not identified by the conventional method. While our method is robust for initial positions, we could obtain better results using lower level (1000hPa). It is true that some tropical cyclones are not detected by the proposed method because of small vorticity, but these tropical cyclones have short lifetime.

As future work, we extend this method to 3-dimensional one, using the streamlines at all pressure levels in huge climatology data. Not only the extension will allow us to detect tropical cyclones more accurately, but will reveal 3-dimensional structure. This will be important for risk management. It would be interesting to predict course and development of the tropical cyclone by using a revealed 3-dimensional structure.

Acknowledgments This work was supported by Grant-in-Aids for the 21st Century COE "Frontier of Computational Science" and the Global Environment Research Fund (RF-070) of the Ministry of the Environment, Japan. The numerical analysis was performed by Fujitsu HPC2500 super computer system at the Information Technology Center, Nagoya University.

References

Bengtsson, L., M. Botzet, and M. Esch, 1995: Hurricane-type vortices in a general circulation model, *Tellus*, **47A**, 175–196.

——, ——, and –, 1996: Will greenhouse gas induced warming over the next 50 years lead to higher frequency and greater intensity of hurricanes?, *Tellus*, **48A**, 57–73.

——, K. I. Hodges, M. Esch, N. Keenlyside, L. Komblush, J. J. Luo, and T. Yamagata, 2007: How many tropical cyclones change in a warmer climate?, *Tellus*, **59A**, 539–561.

Broccoli, A. J., and S. Manabe, 1990: Can existing climate models be used to study anthropogenic changes in tropical cyclone climate?, *Geophys. Res. Lett.*, **17**, 1917–1920.

Emanuel, K. A., 1987: The dependence of hurricane intensity on climate, *Nature*, **326**, 483–485.

Haarsma, R. J., J. F. B. Mitchell, and C. A. Senior, 1993: Tropical disturbances in a GCM, *Clim. Dyn.*, **8**, 247–257.

Holland, G. J., 1997: The maximum potential intensity of tropical cyclones, *J. Atmos. Sci.*,. **54**, 2519–2541.

IPCC, 2007: *Climate Change 2007: The Physical Science Basis. Contribution of Working Group I to the Fourth Assessment Report of the Intergovernmental Panel on Climate Change* [Solomon, S., D. Qin, M. Manning, Z. Chen, M. Marquis, K. B. Averyt, M. Tignor and H. L. Miller (eds.)]. Cambridge University Press, Cambridge, United Kingdom and New York, NY, USA, 996 pp.

Kalnay, E., M. Kanamitsu, R. Kistler, W. Collins, D. Deaven, L. Gandin, M. Iredell, S. Saha, G. White, J. Woollen, Y. Zhu, A. Leetmaa, B. Reynolds, M. Chelliah, W. Ebisuzaki, W. Higgins, J. Janowiak, K. C. Mo, C. Ropelewski, J. Wang, J. Roy, and J. Dennis, 1996: The NCEP / NCAR40 year re-analysis project, *Bull. Am. Meteorol. Soc*., **77**, 437–470.

Krishnamurti, T. N., R. Correa-Torres, M. Latif, and G. Daughenbaugh, 1998: The impact of current and possibly future sea surface temperature anomalies on the frequency of Atlantic hurricanes, *Tellus*, **50A**, 186–210.

Oouchi, K., J. Yoshimura, H. Yoshimura, R. Mizuta, S. Kusunoki, and A. Noda, 2006: Tropical cyclone climatology in a global warming climate assimulated in a 20km mesh global atmospheric model: Frequency and wind intensity analyses, *J. Meteorol. Soc. Japan*, **84**, 259–276.

Sugi, M., A. Noda, and N. Sato, 2002: Influence of the global warming on tropical cyclone climatology: An Experiment with the JMA Global Model, *J. Meteorol. Soc. Japan*, **80**, 249–272.

Vollmers H., 2001: Detection of vortices and quantitative evalution of their main parameters from experimental velocity data, *Measurement Science and Technology*, **12**, 1199–1207.

Yoshimura J., A. Noda and M. Sugi, 2006: Influence of greenhouse warming on tropical cyclone frequency, *J. Meteorol. Soc. Japan*, **84(2)**, 405–428

Boundary Layer Model for Moving Tropical Cyclones

Andreas Langousis, Daniele Veneziano, and Shuyi Chen

Abstract We propose a simple theoretical model for the boundary layer (BL) of moving tropical cyclones (TCs). The model estimates the horizontal and vertical wind velocity fields from a few TC characteristics: the maximum tangential wind speed V_{max}, the radius of maximum winds R_{max}, and Holland's B parameter away from the surface boundary where gradient balance is approximately valid, in addition to the storm translation velocity V_t, the surface drag coefficient C_D, and the vertical diffusion coefficient of the horizontal momentum K.

The model is based on Smith's (1968) formulation for stationary (axi-symmetric) tropical cyclones. Smith's model is first extended to include storm motion and then solved using the momentum integral method. The scheme is computationally very efficient and is stable also for large B values and fast-moving storms.

Results are compared to those from other studies (Shapiro 1983; Kepert 2001) and validated using the Fifth-Generation Pennsylvania State University/NCAR Mesoscale Model (MM5). We find that Kepert's (2001) BL model significantly underestimates the radial and vertical fluxes, whereas Shapiro's (1983) slab-layer formulation produces radial and vertical winds that are a factor of about two higher than those produced by MM5. The velocity fields generated by the present model are consistent with MM5 and with tropical cyclone observations.

We use the model to study how the symmetric and asymmetric components of the wind field vary with the storm parameters mentioned above. In accordance with observations, we find that larger values of B and lower values of R_{max} produce horizontal and vertical wind profiles that are more picked near the radius of maximum winds. We also find that, when cyclones in the northern hemisphere move, the vertical and storm-relative radial winds intensify at the right-front quadrant of the vortex, whereas the storm-relative tangential winds are more intense in the left-front region. The asymmetry is higher for faster moving TCs and for higher surface drag coefficients C_D.

J.B. Elsner and T.H. Jagger (eds.), *Hurricanes and Climate Change,*
doi: 10.1007/978-0-387-09410-6,

Introduction

Tropical cyclones (TCs) are a particular class of rotating low-pressure systems that develop over tropical and subtropical waters. The systems have a warm-core, a well-organized convection, and cyclonic surface wind circulation (Anthes 1982; Landsea 2000).

Empirical observations (La Seur and Hawkins 1963; Hawkins and Rubsam 1968; Holland 1980; Willoughby 1990, 1991; Vickery et al. 2000; among others) show that in the altitude range from 2–3 km to about 10 km, the tangential winds are in approximate gradient balance and the radial inflow is negligible. Based on earlier work by Schloemer (1954) and Myers (1957), Holland (1980) used a symmetric pressure distribution to derive the tangential gradient wind V_{gr}, as a function of distance R from the TC center. His result, which we refer to here as Holland's wind profile, is

$$V_{gr}(R) = V_{max}\sqrt{(R_{max}/R)^B exp[1-(R_{max}/R)^B]} \tag{1}$$

where V_{max}, R_{max}, and B are TC-specific constants. The tangential velocity V_{gr} increases with R to a maximum V_{max} at $R = R_{max}$ (usually referred to as the radius of maximum winds). For $R >> R_{max}$, V_{gr} has an approximately power-law decay with distance, with exponent $-B/2$. According to Willoughby and Rahn (2004), B varies in the range [1, 2] with typical values around 1.4.

Inside the TC boundary layer (BL) (within approximately 1–2 km from the surface), frictional stresses are important and result in an inward net force that drives low-level convergence. Consequently, the horizontal and vertical wind fields are strongly coupled and Eq. (1) does not apply. Horizontal convergence drives the vertical winds, which are maximum at the top of the boundary layer near the radius of maximum winds R_{max} (e.g. Kepert 2001 and Kepert and Wang 2001).

Since the convergence of moisture inside the BL is of major importance for the maintenance, evolution and destructive potential of TCs (Emanuel 1986, 1989; Renno and Ingersoll 1996), a number of studies (Myers and Malkin 1961; Chow 1971; Shapiro 1983; Kepert 2001) have focused on developing theoretical models for the boundary layer of moving TCs. These models derive the radial and tangential winds inside the boundary layer from an assumed radial profile of the tangential wind velocity under gradient balance, for example the profile in Eq. (1), and from suitable surface boundary conditions.

Review of Boundary Layer Models reviews these BL models and their limitations. Proposed Model describes our proposed model by giving the governing equations (an extension of the equations of Smith 1968) and discussing their numerical solution. Model Comparison, we compare model results with earlier models and with simulations using the Fifth-Generation Pennsylvania State University/NCAR Mesoscale Model (MM5). Sensitivity Analysis shows how the calculated winds depend on various storm parameters. Conclusions are stated in Conclusions.

Review of Boundary Layer Models

The focus of this review is on BL models for moving tropical cyclones, but studies of stationary TCs that are relevant to what follows are also mentioned.

Boundary layer models differ mainly in their treatment of altitude Z and the surface boundary conditions. In one of the earlier studies of moving TCs, Myers and Malkin (1961) used a Lagrangian parcel trajectory approach to study the horizontal winds inside the BL. The authors assume that the frictional drag force is proportional to the square of the wind speed with equal tangential and radial components. Another (implicit) assumption is that the velocity of the background flow is zero rather than equal to the translation velocity of the TC. A finding of the study is that, when a TC in the northern (southern) hemisphere moves, the radial convergence is maximum at the right-front (left-front) quadrant of the vortex and the location of this maximum rotates anticyclonically as the translation velocity V_t increases.

Based on the work of Chow (1971), Shapiro (1983) approximated the boundary layer of a moving TC by a slab of constant depth $H = 1$ km. The horizontal momentum equations are formulated in cylindrical coordinates that translate with the vortex and then averaged in the vertical direction. This results in a system of two partial differential equations (PDEs) that are solved numerically for the vertically averaged tangential $\bar{V}(R, \theta)$ and $\bar{U}(R, \theta)$ radial wind velocity as a function of radius R and the azimuth θ relative to the direction of TC motion. Contrary to Myers and Malkin (1961), Shapiro's (1983) formulation assumes that the frictional drag force is parallel to the surface-relative flow and its magnitude is proportional to the square of the composite surface-relative wind velocity. Although the two studies use different formulations for the friction-induced convergence, they both produce maximum convergence at the right-front quadrant of vortices in the northern hemisphere. However, in Shapiro's model the location of the maximum does not depend on the translation velocity, whereas in Myers and Malkin's (1961) analysis it does.

The main limitation of Shapiro's (1983) approach is that it approximates the BL as a slab of constant depth and hence cannot resolve the variation of U and V with height. According to Anthes (1971), this leads to overestimation of the radial and vertical velocities close to the vortex core; see discussion of Fig. 3 below. Another limitation of Shapiro's analysis is that the numerical stability of the system depends on TC parameters such as the depth of the boundary layer H, the translation velocity V_t, the vertical diffusion coefficient K and the surface drag coefficient C_D. This limitation becomes important when, as for example in risk studies, one needs to calculate the wind field under a wide variety of conditions.

A third BL model for moving tropical cyclones was proposed by Kepert (2001) (see also refinements in Kepert 2006b). Kepert's formulation neglects vertical advection and linearizes the horizontal advection. This produces a system of linear PDEs that is solved analytically for the radial, tangential and vertical wind velocities (U, V and W, respectively) as a function of R, θ, and Z. Kepert (2001) uses a bulk formulation of the surface stresses similar to those of Rosenthal (1962), Shapiro (1983) and Smith (1968, 2003). However, the surface boundary condition is linearized to allow

analytical integration. Linearization produces inaccurate results close to the TC center ($R < 2$–$3\ R_{max}$) where the horizontal gradient of the wind components is high, when the vertical gradient of the horizontal wind velocity is large (this happens for large surface drag coefficient C_D; see discussion on Fig. 2 below), for high translation velocities ($V_t > 5$ m/s), and under inertially neutral conditions ($B >$ 1.6–1.8). Other linearizations of the horizontal momentum equations have been proposed by Haurwitz (1935), Rosenthal (1962), Miller (1965) and Elliassen and Lystad (1977), but these formulations are for stationary vortices ($V_t = 0$).

An order of magnitude analysis by Smith (1968) shows that in the near-core region the nonlinear terms are as important as the linear ones. To include the nonlinear terms, Smith (1968) (see also refinements in Leslie and Smith 1970 and Bode and Smith 1975) used the Karman and Pohlhausen momentum integral method to calculate the radial $U(R,Z)$ and tangential $V(R,Z)$ wind velocities in a stationary vortex. In the momentum integral method (Schlichting, 1960), one avoids an explicit analysis of altitude Z by assuming vertical profiles for U and V that satisfy the boundary conditions at the surface ($Z = 0$), and tend asymptotically to gradient balance as $Z \to \infty$; see Eq. (3) below. Specifically, Smith (1968) used profiles of the Ekman type, with an amplitude coefficient E and a dimensionless BL scale thickness δ as parameters. The horizontal momentum equations are vertically integrated to produce a system of ordinary differential equations that are solved numerically to obtain E and δ as a function of R.

The main limitation of Smith's (1968) model is that it does not consider storm motion. Also, Smith's (1968) formulation is theoretically correct only for the case of no slip at the surface boundary (i.e. for $C_D \to \infty$); see Proposed Model. In the following section, we extend Smith's (1968) model to include storm motion and correct the formulation for the general case of stress surface boundary conditions.

Proposed Model

In a cylindrical coordinate system (R, θ, Z) that follows the vortex motion, the boundary layer equations are (see Smith 1968 and Kepert 2001 for a detailed derivation),

$$
\begin{aligned}
&U\frac{\partial U}{\partial R}+\frac{V}{R}\frac{\partial U}{\partial \theta}+W\frac{\partial U}{\partial Z}+\frac{V_{gr}^2-V^2}{R}+f\left(V_{gr}-V\right)=K\frac{\partial^2 U}{\partial Z^2} \quad \text{(a)}\\
&U\frac{\partial V}{\partial R}+\frac{V}{R}\frac{\partial V}{\partial \theta}+W\frac{\partial V}{\partial Z}+\frac{UV}{R}+fU=K\frac{\partial^2 V}{\partial Z^2} \quad \text{(b)}\\
&\frac{\partial (RU)}{\partial R}+\frac{\partial V}{\partial \theta}+\frac{\partial (RW)}{\partial Z}=0 \quad \text{(c)}
\end{aligned}
\tag{2}
$$

where R is distance from the vortex center, θ is azimuth relative to the direction of motion, f is the Coriolis parameter, U, V, and W are the storm-relative radial, tangential and vertical wind velocities, respectively, K is the vertical diffusion coefficient of the horizontal momentum, and V_{gr} is the tangential wind velocity under gradient wind balance; see for example Eq. (1).

As Kepert (2001) and Smith (1968), we solve Eqs. (2) for the case of a semi-infinite domain, when gradient wind balance is satisfied asymptotically as $Z \to \infty$,

$$\frac{\partial U}{\partial Z} = \frac{\partial V}{\partial Z} = U = 0, \text{and } V = V_{gr}, \text{at} \quad Z \to \infty \tag{3}$$

The translation velocity V_t enters through the surface boundary conditions. Suppose that the vortex is translating in the positive x-direction with constant speed V_t. Using a viscous surface stress formulation similar to Smith (1968, 2003) and Kepert (2001), the conditions to be satisfied at the surface boundary ($Z = 0$) are:

$$\begin{aligned} U + V_t \cos\theta &= \frac{K}{C_D V_{gr}} \frac{\partial U}{\partial Z} \quad \text{(a)} \\ V - V_t \sin\theta &= \frac{K}{C_D V_{gr}} \frac{\partial V}{\partial Z} \quad \text{(b)} \\ W &= 0 \quad \text{(c)} \end{aligned} \tag{4}$$

where C_D is a surface drag coefficient; see for example Rosenthal (1962), Smith (1968, 2003), Kepert (2001), and Kepert and Wang (2001). For $1/C_D = 0$, Eq. (4) corresponds to no slip conditions ($U = -V_t \cos\theta$, $V = V_t \sin\theta$) at the surface boundary.

For $R \to \infty$, the system in Eq. (2) reduces to the classic Ekman BL equations under geostrophic conditions (Kundu and Cohen, 2004):

$$\begin{aligned} f\left(V_{gr} - V\right) &= K \frac{\partial^2 U}{\partial Z^2} \quad \text{(a)} \\ fU &= K \frac{\partial^2 V}{\partial Z^2} \quad \text{(b)} \\ W &= \text{const.} \quad \text{(c)} \end{aligned} \tag{5}$$

Denote by R_g the distance from the TC center beyond which the geostrophic model in Eq. (5) is approximately valid; say $R_g \approx 1000$ km (Smith 1968, Kundu and Cohen 2004). Also denote by K_M the vertical diffusion coefficient under geostrophic conditions and let $V_g = V_{gr}(R_g)$ be the gradient tangential wind for $R = R_g$ and $Z_g = (K_M/f)^{1/2}$ (Z_g has the meaning of vertical length scale for the depth of the boundary layer; see below). Then one can write Eq. (2) in dimensionless form, as

$$\begin{aligned} R_o\left[u\frac{\partial u}{\partial r} + \frac{v}{r}\frac{\partial u}{\partial \theta} + w\frac{\partial u}{\partial z} + \frac{v_{gr}^2 - v^2}{r}\right] + v_{gr} - v &= k\frac{\partial^2 u}{\partial z^2} \quad \text{(a)} \\ R_o\left[u\frac{\partial v}{\partial r} + \frac{v}{r}\frac{\partial v}{\partial \theta} + w\frac{\partial v}{\partial z} + \frac{uv}{r}\right] + u &= k\frac{\partial^2 v}{\partial z^2} \quad \text{(b)} \\ \frac{\partial (ru)}{\partial r} + \frac{\partial v}{\partial \theta} + \frac{\partial (rw)}{\partial z} &= 0 \quad \text{(c)} \end{aligned} \tag{6}$$

and Eqs. (3) and (4) become

$$\begin{aligned} &\frac{\partial u}{\partial z} = \frac{\partial v}{\partial z} = u = 0, \text{ and } v = v_{gr}, \text{ at } z \to \infty \quad \text{(a)} \\ &u + v_t \cos\theta = \frac{ak}{v_{gr}} \frac{\partial u}{\partial z}, v - v_t \sin\theta = \frac{ak}{v_{gr}} \frac{\partial v}{\partial z}, \text{ and } w = 0, \text{at } z = 0 \quad \text{(b)} \end{aligned} \tag{7}$$

In Eqs. (6) and (7), $R_o = V_g/(R_g f)$ is the Rossby number and $r = R/R_g$, $z = Z/Z_g$, $v_t = V_t/V_g$, $u = U/V_g$, $v = V/V_g$, $w = (WR_g)/(V_g Z_g)$, $v_{gr} = V_{gr}/V_g$, $k = K/K_M$, and $\alpha = K_M/(C_D\, Z_g\, V_g)$ are dimensionless quantities. In his model for axi-symmetric vortices, Smith (1968) allows K to be different from K_M and to vary radially. In the present extension to moving vortices, we further allow K to vary azimuthally.

Vertical integration of Eq. (6) under boundary conditions (7a) gives

$$R_o \left[\frac{\partial}{\partial r} \int_0^\infty r u^2 dz + \frac{\partial}{\partial \theta} \int_0^\infty uv dz + \int_0^\infty v_{gr}^2 - v^2 dz \right] + r \int_0^\infty v_{gr} - v \, dz = -kr \frac{\partial u}{\partial z}|_{z=0} \quad \text{(a)}$$

$$R_o \left[\frac{\partial}{\partial r} \int_0^\infty r^2 uv dz + r \frac{\partial}{\partial \theta} \int_0^\infty v^2 dz + r^2 w_\infty v_{gr} \right] + r^2 \int_0^\infty u dz = -kr^2 \frac{\partial v}{\partial z}|_{z=0} \quad \text{(b)}$$

$$w_\infty = -\frac{1}{r} \left[\frac{\partial}{\partial r} \left(r \int_0^\infty u dz \right) + \int_0^\infty \frac{\partial v}{\partial \theta} dz \right] \quad \text{(c)} \tag{8}$$

where w_∞ is the dimensionless vertical wind velocity at $Z \to \infty$. Next we discuss how Eq. (8) is solved under the conditions (7b).

Momentum Integral Method

Similar to Smith (1968) we take the boundary layer thickness to be proportional to $Z_g = (K_M/f)^{1/2}$, with proportionality coefficient δ. In Smith's (1968) axi-symmetric formulation δ exhibits only radial variation, but in the present case of moving cyclones we allow δ to vary also azimuthally.

Define $\eta = Z/[Z_g\ \delta(r,\theta)] = z/\delta(r,\theta)$ and notice that the geostrophic model in Eq. (5) is satisfied for $\delta = \sqrt{2}$; see e.g. Kundu and Cohen (2004). Following the derivations of Schlichting (1960), Mack (1962) and Smith (1968), but allowing azimuthal dependence of u and v, the solution of Eq. (8) can be approximated as

$$\begin{aligned} u(r,\theta,\eta) &= E(r,\theta)\Psi(r,\theta,\eta) \quad \text{(a)} \\ v(r,\theta,\eta) &= \Omega(r,\theta,\eta) \quad \text{(b)} \end{aligned} \tag{9}$$

where $E(r,\theta)$ is an unknown function, usually referred to as the amplitude coefficient, and Ψ and Ω are such that $(u,v) = (\Psi,\Omega)$ satisfy Eqs. (6) and (7) under geostrophic conditions ($R > R_g$). After some algebra one obtains

$$\begin{aligned}\Psi(r,\theta,\eta) &= g(r,\theta,\eta)v_t\cos\theta + f(r,\theta,\eta)(v_{gr} - v_t\sin\theta) - v_t\cos\theta \quad \text{(a)}\\ \Omega(r,\theta,\eta) &= g(r,\theta,\eta)(v_{gr} - v_t\sin\theta) - f(r,\theta,\eta)v_t\cos\theta + v_t\sin\theta \quad \text{(b)}\end{aligned} \tag{10}$$

where

$$\begin{aligned}f(r,\theta,\eta) &= -e^{-\eta}[a_1(r,\theta)\sin\eta + a_2(r,\theta)\cos\eta] \quad \text{(a)}\\ g(r,\theta,\eta) &= 1 - e^{-\eta}[a_1(r,\theta)\cos\eta + a_2(r,\theta)\sin\eta] \quad \text{(b)}\end{aligned} \tag{11}$$

The parameters $a_1(r,\theta)$ and $a_2(r,\theta)$ in Eq. (11) are calculated so that (u, v) in Eq. (9) satisfy condition (7b). This gives

$$a_2(r,\theta) = \frac{L_3L_4 - L_1L_6}{L_2L_4 - L_1L_5}, \quad a_1(r,\theta) = \frac{L_3 - L_2a_2}{L_1} \tag{12}$$

where

$$\begin{aligned}L_1 &= v_{gr} - v_t\sin\theta + \left(1 + \frac{2ka}{v_{gr}\delta}\right)v_t\cos\theta,\\ L_2 &= v_{gr} - v_t\sin\theta - \left(1 + \frac{2ka}{v_{gr}\delta}\right)v_t\cos\theta\\ L_3 &= v_{gr} - v_t\sin\theta + \frac{v_t\cos\theta}{E},\\ L_4 &= \left(v_{gr} - v_t\sin\theta\right)\left(1 + \frac{2ka}{v_{gr}\delta}\right) - v_t\cos\theta\\ L_5 &= \left(v_t\sin\theta - v_{gr}\right)\left(1 + \frac{2ka}{v_{gr}\delta}\right) - v_t\cos\theta,\\ L_6 &= v_{gr} - v_t\sin\theta - \frac{v_t\cos\theta}{E}\end{aligned} \tag{13}$$

The parameters a_1 and a_2 are constants independent of r and θ ($a_1 = 1$ and $a_2 = 0$) only for a stationary TC and $\alpha = 0$ (i.e. $C_D \to \infty$, no slip conditions). Hence, Smith's (1968) axi-symmetric formulation, where a_1 and a_2 are assumed constant independent of r, is theoretically correct only in the case of no slip conditions at the surface boundary.

By combining Eq. (8)–(11) and after some algebra, one obtains the following system of differential equations in E and δ:

$$\begin{aligned} &B_1(r,\theta)\frac{\partial E}{\partial r}+B_2(r,\theta)\frac{\partial E}{\partial \theta}+B_3(r,\theta)\frac{\partial \delta}{\partial r}+B_4(r,\theta)\frac{\partial \delta}{\partial \theta}=-B_5(r,\theta) \quad \text{(a)}\\ &C_1(r,\theta)\frac{\partial E}{\partial r}+C_3(r,\theta)\frac{\partial \delta}{\partial r}+C_4(r,\theta)\frac{\partial \delta}{\partial \theta}=C_5(r,\theta) \quad \text{(b)} \end{aligned} \tag{14}$$

with coefficients

$$\begin{aligned} &B_1=r\delta R_o A_{10},\ B_2=\delta R_o A_{12},\ B_3=rR_o A_1,\ B_4=R_o A_2\\ &B_5=\frac{kr}{\delta}A_6+\delta R_o(rA_5/R_o+A_3+A_{13}+A_1+rA_{11}),\ C_1=r^2R_o\delta\left(A_{12}-v_{gr}A_{16}\right)\\ &C_3=r^2R_o\left(A_2-v_{gr}A_7\right),\ C_4=rR_o\left(A_4+A_{19}-v_{gr}A_8\right)\\ &C_5=-\frac{kr^2}{\delta}A_9+rR_o\delta\left[v_{gr}(A_{18}+rA_{17}+A_7-A_{20})-rA_7/R_o-A_{15}-rA_{14}-2A_2\right] \end{aligned} \tag{15}$$

Analytical expressions for the parameters A_1–A_{20} in Eq. (15) are derived in Appendix A.

The nonlinear system in Eq. (14) can be integrated numerically to obtain $E(r,\theta)$ and $\delta(r,\theta)$. For this purpose we use a scheme that is implicit in θ and explicit in r. Integration starts at $r = 1$ where we set $E = 1$ and $\delta = \sqrt{2}$ (these are the values under geostrophic conditions) and moves inward using a stepwise integration procedure. At each step i in r, integration with respect to θ is performed simultaneously for all azimuthal locations using a central difference approach; see e.g. Chapra and Canale (2002).

Since the parameters in Eq. (14) depend on E and δ, a first approximation to the solution at step i is obtained by evaluating all parameters using the values of E and δ from step i–1. This procedure is iterated until E and δ at step i converge.

After E and δ (and hence the horizontal wind components U and V) are obtained, the vertical wind velocity W is calculated using mass conservation, as

$$W(R,\theta,Z)=-\frac{1}{R}\left[\int_0^Z\frac{\partial(RU)}{\partial R}dZ+\int_0^Z\frac{\partial V}{\partial\theta}dZ\right] \tag{16}$$

In what follows, we refer to Eqs. (6) and (7) and their solution by the momentum integral method as the Modified Smith (MS) model. In the next section we compare results for a specific storm with wind estimates from the Shapiro (1983) and Kepert (2001) formulations and with MM5 simulations, and in Sensitivity Analysis we examine how the winds generated by the MS model vary with a number of storm parameters.

Model Comparison

First we illustrate the results from the MS model and then compare the performance of that model with others for stationary and moving tropical cyclones.

Figure 1 shows the storm-relative radial and tangential wind velocity fields U and V and the vertical wind velocity W at elevations $Z = 0$, 0.5, 1 and 2 km obtained using the MS model. The tropical cyclone translates eastward in the northern hemisphere, with velocity $V_t = 5$ m/s. Asymptotically as $Z \rightarrow \infty$, the tangential winds satisfy Holland's profile in Eq. (1) with parameters $V_{max} = 50$ m/s, $R_{max} = 40$ km and $B = 1.6$. Results are for non-slip conditions at the surface boundary ($1/C_D = 0$) and constant vertical diffusion coefficient $K = K_M = 50$ m^2/s. This value of K is often quoted in the literature (e.g. Smith 1968, Shapiro 1983, Kepert 2001; Kepert 2006b) and is close to values extracted from MM5 simulations (M. Desflots 2006, personal communication). The Coriolis parameter f is set to 5 10^{-5} sec^{-1}, which corresponds to a latitude φ of 20^o North.

The model reproduces the conditions $U|_{Z=0} = -V_t \cos\theta$, $V|_{Z=0} = V_t \sin\theta$, and $W|_{Z=0} = 0$ at the surface boundary; see also discussion of Fig. 2 below. Translation of the tropical cyclone causes intensification of the radial fluxes at the right and right-front of the vortex. Specifically, the maximum of U (x symbol in Fig. 1) is located at the right/right-front of motion and close to the vortex center for $Z =$ 500 m, and moves outward while rotating clockwise as Z increases. Intensification of V is at the left-front of the vortex, with an asymmetry that decreases as one approaches gradient balance. Due to radial convergence at different altitudes, the vertical velocity W increases monotonically with Z. In addition, storm translation causes W to intensify at the right and right-front of the vortex. Similar qualitative findings on U, V and W have been reported by Kepert (2001) and Kepert and Wang (2001).

For the same storm, Fig. 2 compares the vertical profiles of the azimuthally averaged radial and tangential winds generated by the MS and Kepert (2001) models. Azimuthal averaging produces results that correspond to a stationary, and hence, axi-symmetric TC. The profiles shown in Fig. 2 are at radial distances $R = R_{max} = 40$ km and $R = 2.5R_{max} = 100$ km from the vortex center.

As was pointed out in Review of Boundary Layer Models, the linearized stress formulation of Kepert (2001) is accurate only for small drag coefficients C_D. In the present case $C_D \rightarrow \infty$ and Kepert's (2001) model correctly reproduces the non-slip condition $U|_{Z=0} = 0$ in the radial direction (see Fig. 2) but fails to reproduce the condition $V|_{Z=0} = 0$ in the tangential direction (Fig. 2). This inconsistency results in underestimation of the frictional stresses at the surface boundary and hence of the radial fluxes relative to the MS formulation; see Fig. 2 and discussion of Fig. 3 below.

Kepert's (2001) model also fails to reproduce the variation of the radial wind U with R. Observations using GPS dropsonde data (Kepert 2006a, b) show that the maximum of U increases as one approaches the center of the TC. While the MS model is consistent with this observation, the maximum values of U at 40 and 100km from Kepert's (2001) approach are about the same.

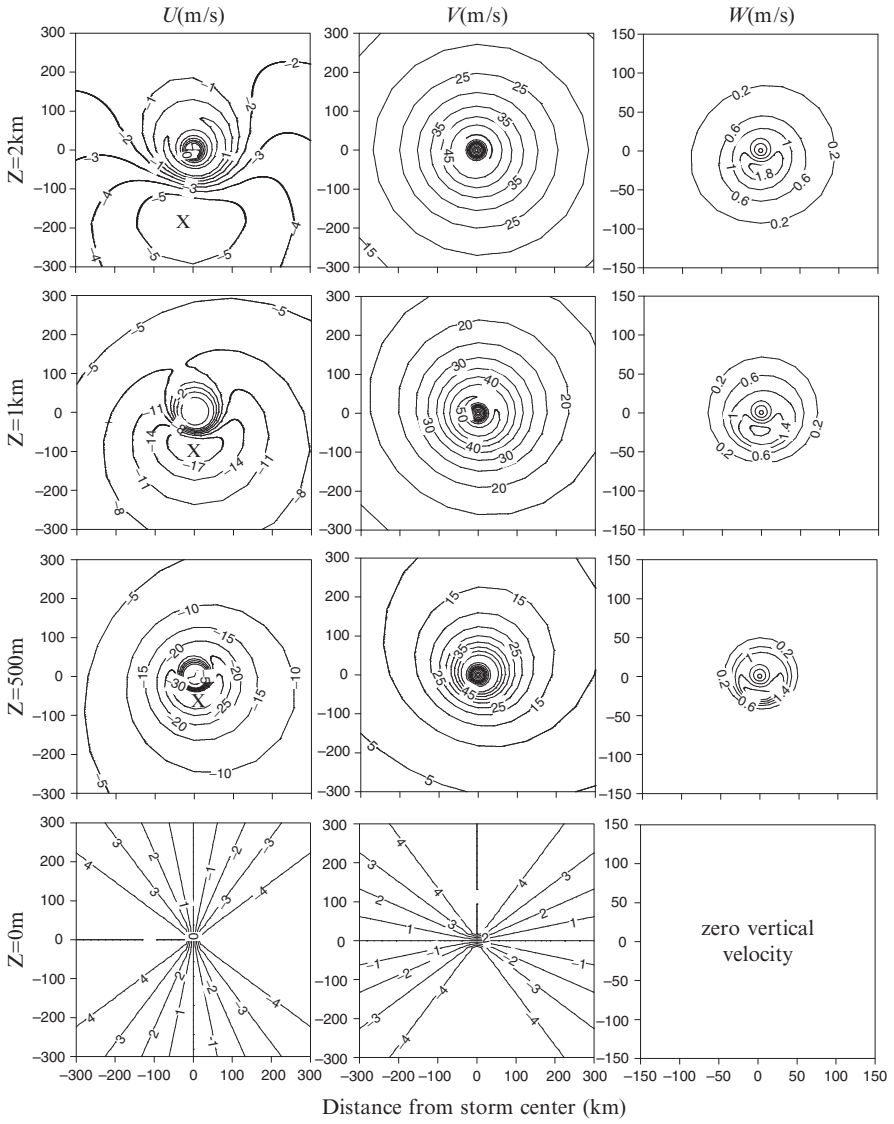

Fig. 1 MS boundary layer solution for the tangential V, radial U and vertical W wind velocity fields at altitudes Z = 0, 0.5, 1, and 2 km. V and U are velocities relative to the moving vortex. The location of the maximum of U is denoted by an x symbol. The tropical cyclone translates eastwards (to the right) with velocity V_t = 5 m/s. All figures are generated under non-slip conditions at the surface boundary and using a constant vertical diffusion coefficient K = 50 m^2/s. Other parameters are V_{max} = 50 m/s, R_{max} = 40 km and B = 1.6

In both the MS and Kepert (2001) models, the depth of the boundary layer H, defined as the height Z where $U \approx 0$, increases with increasing R. In the MS solution, H is about 2.2 km at R = 100 km and about 1.5 km at R = 40 km, whereas

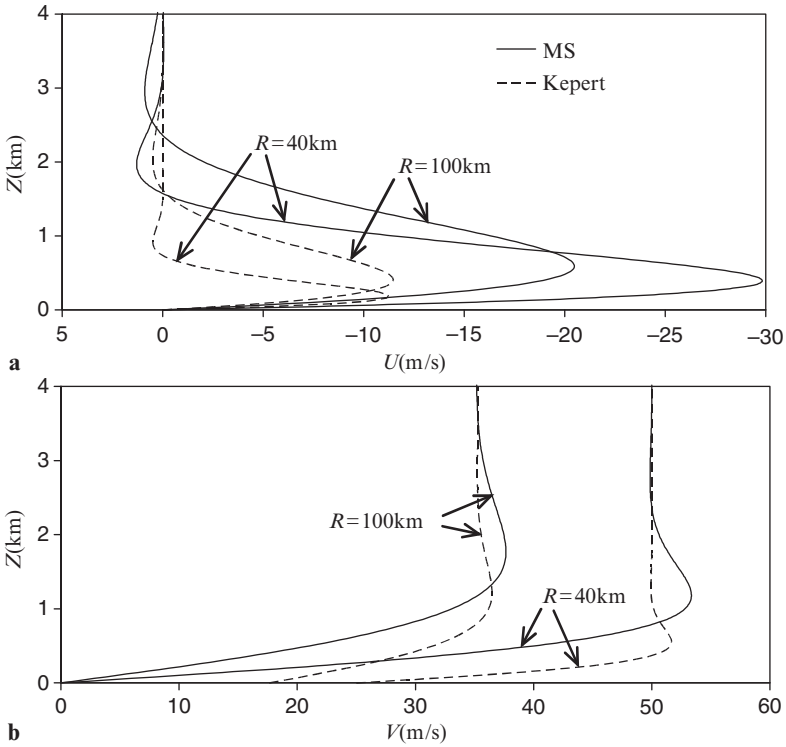

Fig. 2 Comparison of the axi-symmetric component of the wind field from Kepert's (2001) model and the MS model. Vertical profiles of (**a**) the radial wind velocity U, and (**b**) the tangential wind velocity V at 40 km and 100 km from the vortex center. Same storm as in Fig. 1

the corresponding values from Kepert's (2001) analysis are 1.5 and 0.8 km. Both sets of estimates are order-of-magnitude correct, with the MS values been closer to observations (e.g. Frank 1977 and Kepert 2006a).

Figures 3 and 4 compare the vertically averaged radial and tangential winds and the vertical winds obtained using the Shapiro (1983), Kepert (2001) and MS models as well as MM5 simulations. Figure 3 shows the radial variation of the axi-symmetric component, whereas Fig. 4 includes the asymmetry due to motion through contour plots. The reasons for vertically averaging U and V (over a depth of 1 km) are to ease model comparison, since Shapiro (1983) treats the BL as a slab of constant depth H = 1 km, and to reduce the effect of vertical fluctuations in the MM5 solution. All storm parameters are the same as in Fig. 1, except for the drag coefficient, which is set to 0.003. This value of C_D is close to values extracted from MM5 simulations for oversea conditions (M. Desflots 2006, personal communication), does not introduce significant distortions in Kepert's (2001) linear formulation, and does not cause numerical oscillations in Shapiro's (1983) approach. Also, values of C_D close to 0.003 are often quoted in the literature for wind speeds in the

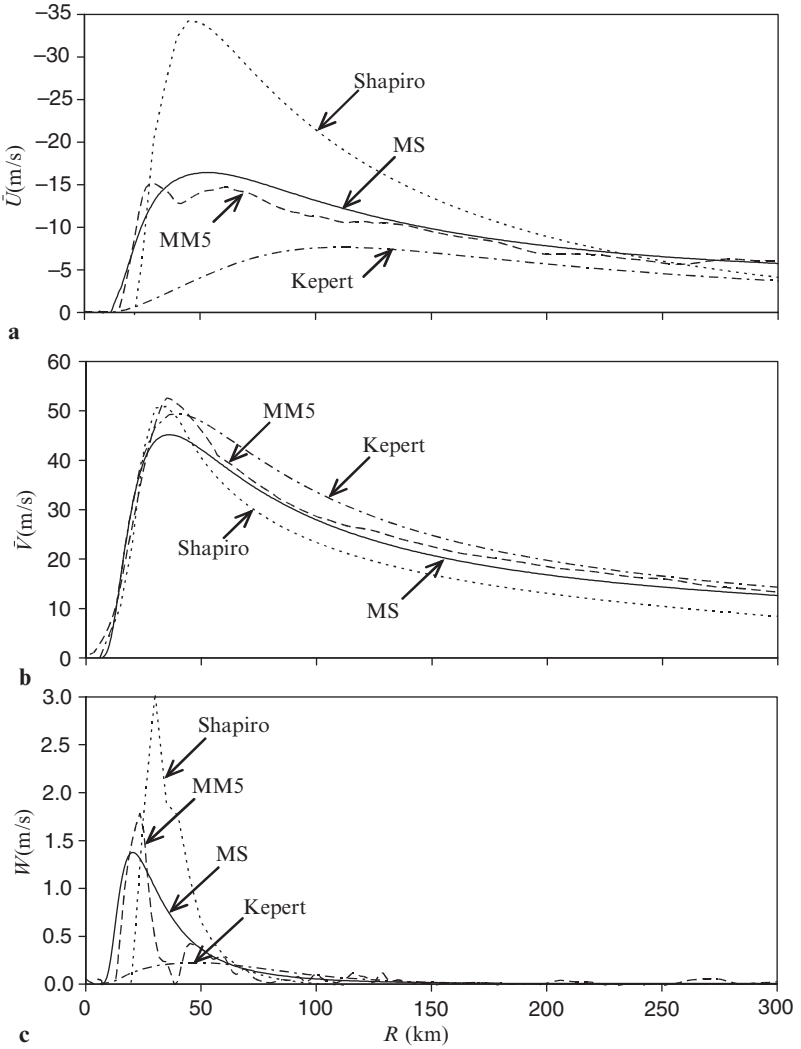

Fig. 3 Comparison of the Shapiro (1983), Kepert (2001) and MS boundary layer solutions with MM5 simulations for an axi-symmetric (stationary) TC. (**a**) Vertically averaged radial wind velocity $\bar{U}$, (**b**) vertically averaged tangential wind velocity $\bar{V}$, and (**c**) vertical wind velocity W at an altitude of 1 km. All figures are generated using a constant vertical diffusion coefficient $K = 50$ m^2/s and a surface drag coefficient $C_D = 0.003$ and averaging is over a depth of 1 km. Other parameters are $V_{max} = 50$ m/s, $R_{max} = 40$ km and $B = 1.6$

range encountered in hurricanes (e.g. Large and Pond 1981; Powell et al. 2003; Donelan et al. 2004).

In general, the MS model predictions are close to the MM5 simulations, except that in MM5 the vertical velocities are more peaked near R_{max} (mainly due to rainband effects, which the BL models do not resolve) and the contour plots are

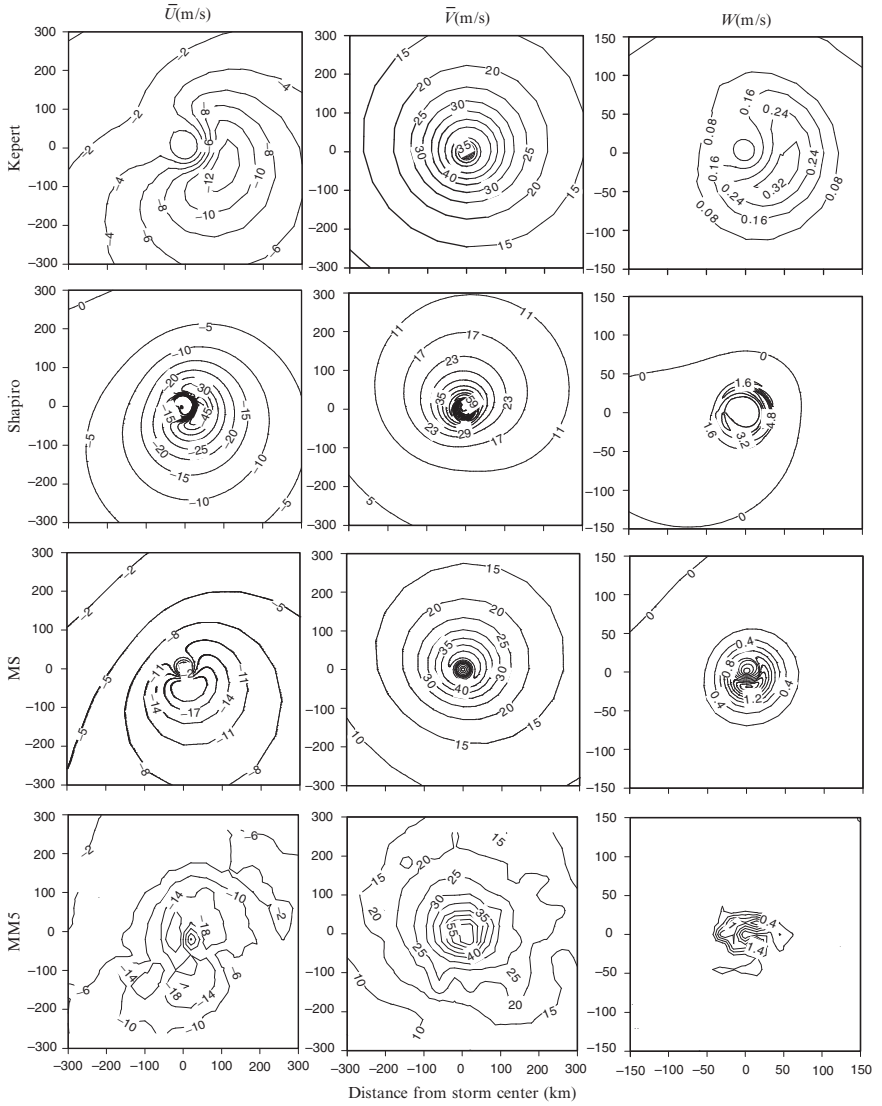

Fig. 4 Comparison of results form the Kepert (2001), Shapiro (1983) and MS models with MM5 simulations for a TC that translates eastwards (*to the right*) with velocity V_t = 5 m/s. Vertically averaged radial wind velocity $\bar{U}$ (*left column*), vertically averaged tangential wind velocity $\bar{V}$ (*middle column*) and vertical wind velocity W at an altitude of 1 km (*right column*). $\bar{V}$ and $\bar{U}$ are relative to the moving vortex and averaging is over a depth of 1 km. All other parameters are the same as in Fig. 3

more erratic due to local fluctuations. Also the Kepert (2001) model reproduces well the vertically averaged tangential winds of MM5, but that model severely underestimates the radial and vertical flows, especially in the near-core region. This

is due to inaccuracy of Kepert's linearization at radial distances smaller than $2–3R_{max}$; see Review of Boundary Layer Models. For example, flight observations show that, in the vicinity of R_{max}, W is in the range 0.5–3 m/s or higher (Willoughby et al. 1982; Jorgensen 1984a, b; Black et al. 2002), whereas Kepert's (2001) estimates are around 0.1–0.4 m/s. In the far field ($R > 2.5R_{max}$), Kepert's (2001) model and MM5 produce vertical velocities that are similar and in good agreement with observations (Jorgensen 1984a, b; Black et al. 2002).

Shapiro's (1983) model has an opposite behavior in the near-core region, where it overpredicts the radial and vertical flows by a factor of about 2. This is consistent with the finding by Anthes (1971) for slab-layer models; see Review of Boundary Layer Models.

Overall, we find that the MS model produces realistic estimates of the tangential, radial and vertical wind velocities and is numerically more stable and more accurate than the boundary layer models of Kepert (2001) and Shapiro (1983). Next we use the MS model to study the sensitivity of the velocity fields to various storm parameters.

Sensitivity Analysis

Figures 5, 6 and 7 show the sensitivity of MS model results to tropical cyclone characteristics: the tangential wind speed under gradient balance (parameterized here in terms of V_{max}, R_{max} and B; see Eq. (1)), the vertical diffusion coefficient K, the surface drag coefficient C_D, and the translation velocity V_t.

Figures 5 shows the sensitivity of the azimuthally averaged (axi-symmetric) velocities to V_{max}, R_{max}, B, K and C_D. The base case (solid lines in Fig. 5) corresponds to the storm used in Fig. 1. Sensitivity is evaluated by varying the parameters one at a time around their base-case values. V_{max} affects only the amplitude of the radial profiles, whereas other parameters affect mainly the shape of the profile (e.g. rate of decay with distance) or both. The effects on the three velocity components are however not uniform. For example, R_{max} has negligible influence on the peak value of the horizontal winds $\bar{U}$ and $\bar{V}$, but affects significantly the peak vertical velocity.

Figure 6 shows the effect of C_D on the wind fields for a TC that moves eastward with velocity $V_t = 5$ m/s. Higher values of C_D correspond to increased friction at the surface boundary and stronger asymmetry of the three velocity components.

Finally, Fig. 7 shows sensitivity to the translation velocity V_t when the other parameters are fixed at $V_{max} = 50$ m/s, $R_{max} = 40$ km, $B = 1.6$, $K = 50$ m^2/s and $C_D = 0.003$. One sees that $\bar{U}$ and W intensify in the NE quadrant relative to the direction of motion, whereas $\bar{V}$ intensifies to the left of the velocity vector. The asymmetry increases with increasing V_t.

Qualitatively similar sensitivity results are obtained when using Kepert's (2001) model (not shown here). This is expected, since Kepert's (2001) model is a linearized variant of the present MS formulation. However, Kepert's linearization has approximate validity only for large R, $C_D << 1$ and small V_t; see Review of Boundary Layer Models.

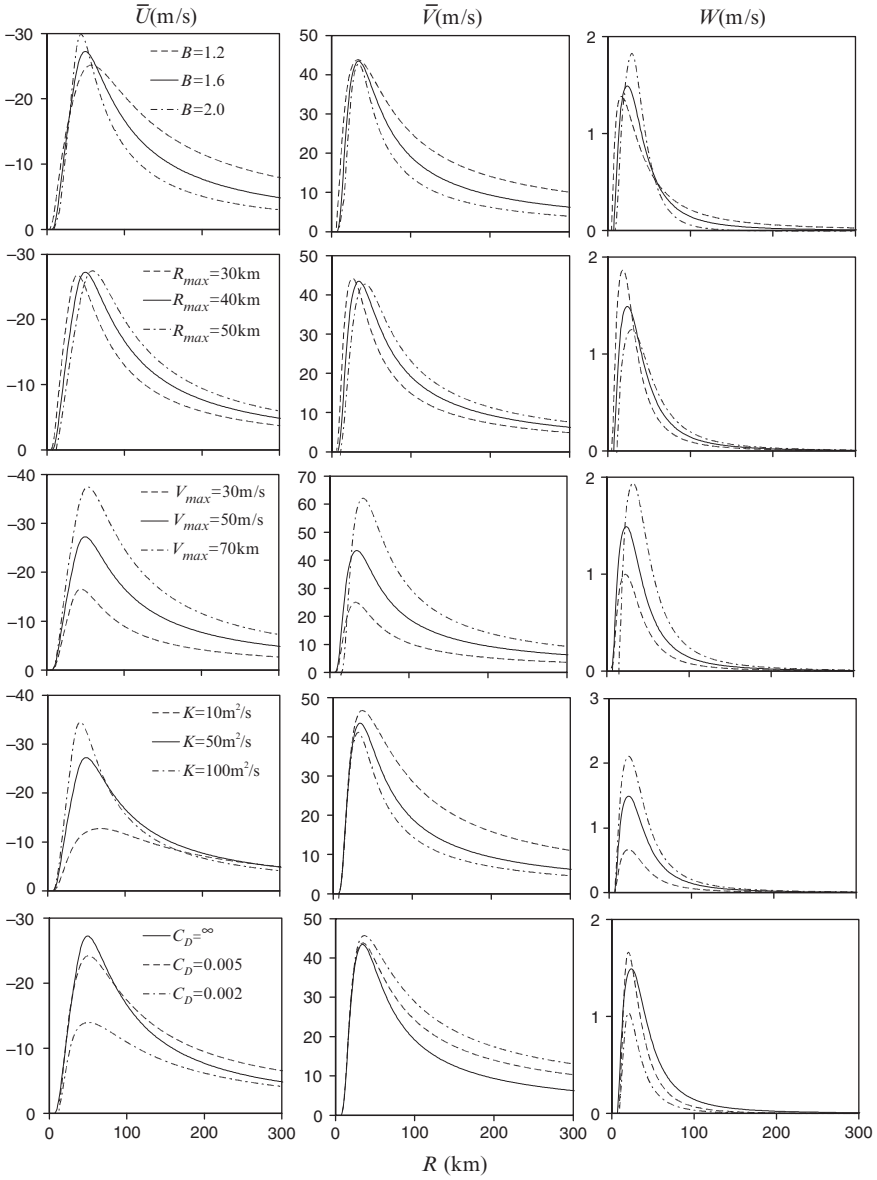

Fig. 5 Sensitivity analysis of MS model results to storm parameters for a stationary TC. Vertically averaged (over a 1km depth) radial wind velocity $\bar{U}$ (*left column*) and tangential wind velocity $\bar{V}$ (*middle column*) and vertical wind velocity W at Z = 1 km (*right column*). Solid lines correspond to V_{max} = 50 m/s, R_{max} = 40 km, B = 1.6, K = 50 m^2/s and non-slip conditions at the surface boundary. Each row shows results under perturbation of one parameter

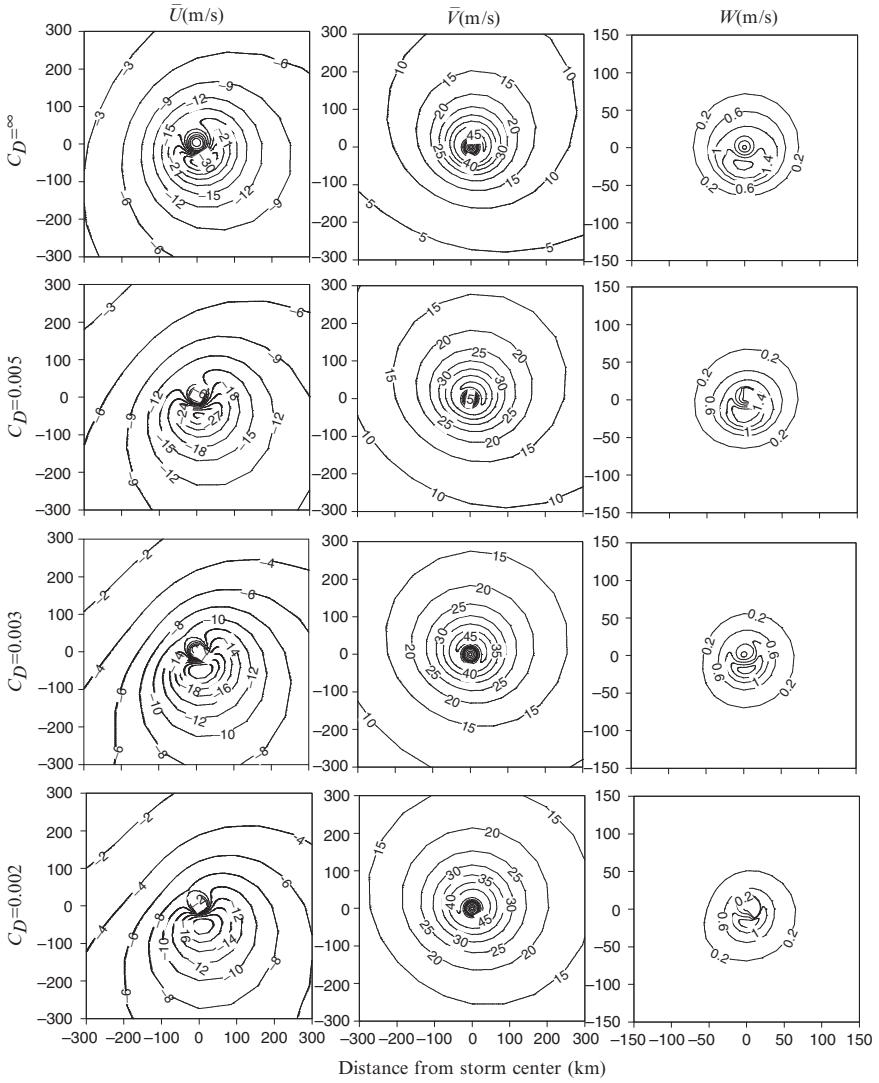

Fig. 6 Sensitivity of MS results to the drag coefficient C_D for a tropical cyclone that translates eastwards (*to the right*) with velocity V_t = 5 m/s. Vertically averaged radial wind velocity $\bar{U}$ (*left column*), vertically averaged tangential wind velocity $\bar{V}$ (*middle column*), and vertical wind velocity W at an altitude of 1 km (*right column*). $\bar{V}$ and $\bar{U}$ are relative to the moving vortex and averaging is over a depth of 1 km. Other parameters are the same as in Fig. 4

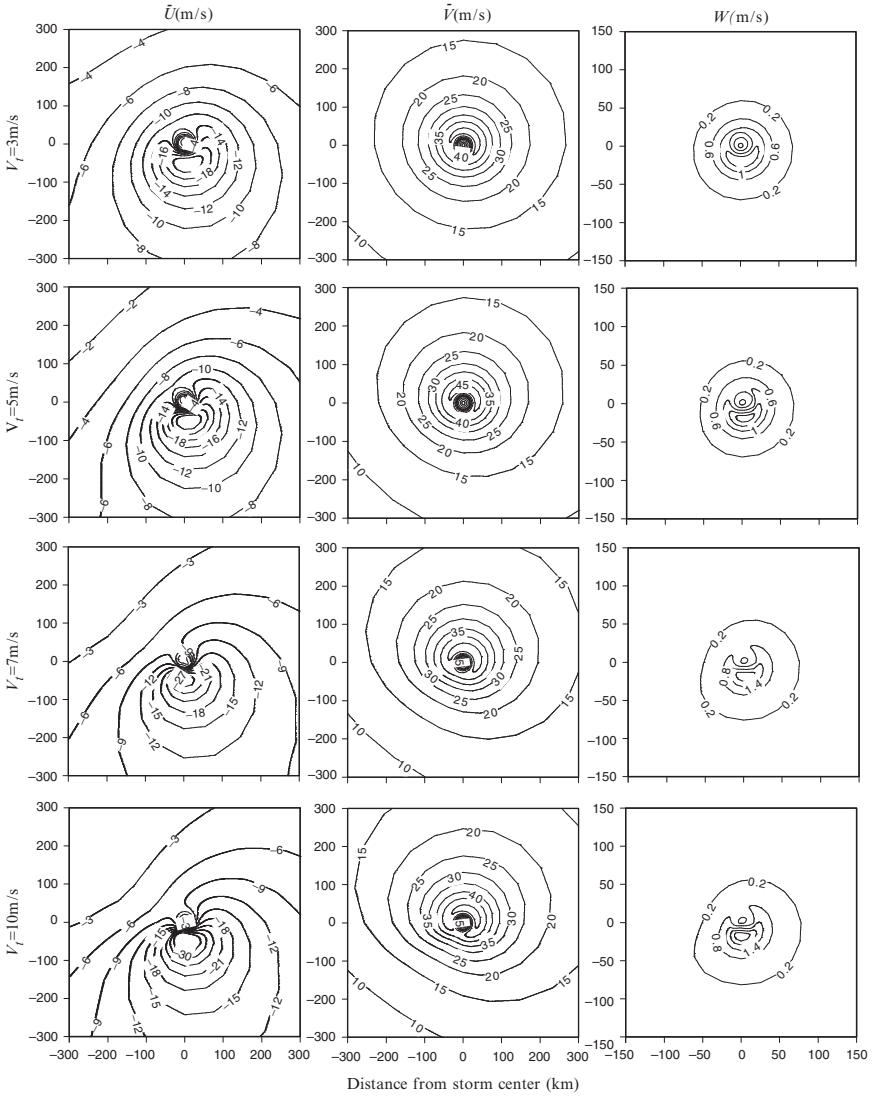

Fig. 7 Sensitivity of MS model results to the translation velocity V_t. Notation and parameters are the same as in Fig. 6, except for $C_D = 0.003$

Conclusions

We developed a simple theoretical model for the boundary layer (BL) of translating tropical cyclones (TCs). The model estimates the tangential, radial and vertical wind fields from a given radial profile of the tangential wind speed under geostrophic conditions (e.g. Holland's profile in Eq. (1)) and surface stress boundary conditions.

The model is based on Smith's (1968) formulation, which is corrected for the general case of a stress surface boundary (see Proposed Model) and modified to account for motion-induced asymmetries. The governing equations are solved using the momentum integral method, resulting in a very efficient computational scheme (less than a minute to run on a conventional computer). Contrary to the Shapiro (1983) and Kepert (2001) BL formulations, the present modified Smith (MS) model is stable over a wide range of storm parameters and produces results that are in good agreement with MM5 simulations and observations; see Figs. 5, 6 and 7.

In a parametric analysis, we have examined how the symmetric wind components and motion-induced asymmetries generated by the MS model depend on various storm characteristics. For TCs that translate in the northern hemisphere, the vertical and storm-relative radial wind velocity fields intensify at the right-front quadrant of the vortex, whereas the storm-relative tangential winds intensify at the left-front of the storm. The asymmetry is higher for faster-moving TCs. These findings are in accordance with field observations; see for example Shapiro (1983).

As the intensity of the TC (expressed through the maximum tangential velocity at gradient balance V_{max}) increases, the horizontal and vertical velocity components also increase. Larger values of Holland's B parameter and lower values of the radius of maximum winds R_{max} produce horizontal and vertical wind profiles that are more picked and concentrated closer to the TC center.

The effect of the frictional drag coefficient C_D is more complex. As C_D increases, the frictional drag force also increases resulting in lower tangential winds and higher radial convergence (stronger vertical winds). Another effect of increasing C_D is higher asymmetry of the velocity field.

As described above, the model considers C_D to be spatially constant. In reality, the drag coefficient varies with the sea state and hence with the near surface wind speed (Large and Pond 1981; Donelan et al. 2004). We are currently extending the model to include the coupling between C_D and wind speed.

The combination of accuracy, stability and computational efficiency make the present model a good instrument for applications, like risk analysis, for which one must assess tropical cyclone winds under many parameter combinations. In this respect, a limitation of the model is that it produces smooth solutions, since it does not account for features like rainbands and local convective activity. It is the authors' belief that these features are best represented statistically.

Acknowledgments This work was supported by the Alexander S. Onassis Public Benefit Foundation under Scholarship No. F-ZA 054/2005–2006 and by ONR research grants N00014-03-1-0479 and N00014-04-6-0524. The authors are grateful to Melicie Desflots for providing the MM5 numerical simulations, to Robert Rogers and Jason Dunion for making available a code for Shapiro's (1983) model and to Anastasios Tsonis and James Elsner for reviewing this manuscript.

Appendix A

Analytical expressions for the parameters in Eq. (15)

Let $I_1 = \int_0^\infty f^2 d\eta$, $I_2 = \int_0^\infty (1-g^2) d\eta$, $I_3 = \int_0^\infty (1-g) d\eta$, $I_4 = \int_0^\infty fg d\eta$, $I_5 = \int_0^\infty f d\eta$, $I_6 = \int_0^\infty (g^2-g) d\eta$ and $I_7 = \int_0^\infty (1-g)^2 d\eta$, where f and g are the

functions given in Eq. (11). Then

$$\begin{aligned}
&\frac{\partial f}{\partial \eta}|_{\eta=0} = a_2 - a_1, \quad \frac{\partial g}{\partial \eta}|_{\eta=0} = a_1 - a_2 \\
&I_1 = \frac{1}{8}\left(a_1^2 + 2a_1a_2 + 3a_2^2\right), \quad I_2 = (a_1 + a_2) - \frac{1}{8}\left(3a_1^2 + 2a_1a_2 + a_2^2\right) \\
&I_3 = \frac{a_1 + a_2}{2}, \quad I_4 = \frac{1}{8}\left(a_1^2 + 4a_1a_2 + a_2^2\right) - \frac{a_1 + a_2}{2} \\
&I_5 = -\frac{a_1 + a_2}{2}, \quad I_6 = \frac{1}{8}\left(3a_1^2 + 2a_1a_2 + a_2^2\right) - \frac{a_1 + a_2}{2} \\
&I_7 = \frac{1}{8}\left(3a_1^2 + 2a_1a_2 + a_2^2\right)
\end{aligned} \tag{A.1}$$

where a_1 and a_2 are calculated from Eq. (12). Under Eq. (A.1), the parameters A_1–A_{20} in Eq. (15) are given by

$$\begin{aligned}
A_1 = E^2[&v_t^2 \cos^2\theta\ I_7 + (v_t \sin\theta - v_{gr})^2 I_1 + (I_5 - I_4)(v_t^2 \sin 2\theta - 2v_t v_{gr} \\
&\cos\theta)]
\end{aligned} \tag{A.2}$$

$$\begin{aligned}
A_2 = E\big[&(v_t^2 \cos 2\theta + v_t v_{gr} \sin\theta) I_5 + (½ v_t^2 \sin 2\theta - v_t v_{gr} \cos\theta)\ I_1 \\
&+ (v_{gr}^2 - 2v_t v_{gr} \sin\theta - v_t^2 \cos 2\theta) I_4 + v_t v_{gr} I_6 \cos\theta - ½\ I_7 v_t^2 \sin 2\theta]
\end{aligned} \tag{A.3}$$

$$\begin{aligned}
A_3 = &-v_t^2 I_1 \cos^2\theta + v_t^2 I_5 \sin 2\theta + (2v_t v_{gr} \cos\theta - v_t^2 \sin 2\theta) I_4 - v_t^2 I_7 \sin^2\theta \\
&+ v_{gr}^2 I_2 + 2v_t v_{gr} I_6 \sin\theta
\end{aligned} \tag{A.4}$$

$$\begin{aligned}
A_4 = &v_t^2 I_1 \cos^2\theta - v_t^2 I_5 \sin 2\theta + (v_t^2 \sin 2\theta - 2v_t v_{gr} \cos\theta) I_4 + v_t^2 I_7 \sin^2\theta \\
&- 2v_t v_{gr} I_6 \sin\theta
\end{aligned} \tag{A.5}$$

$$A_5 = v_t I_5 \cos\theta + (v_{gr} - v_t \sin\theta) I_3 \tag{A.6}$$

$$A_6 = E\left[v_t \cos\theta \frac{\partial g}{\partial \eta}\bigg|_{\eta=0} + \left(v_{gr} - v_t \sin\theta\right)\frac{\partial f}{\partial \eta}\bigg|_{\eta=0}\right] \tag{A.7}$$

$$A_7 = E[(v_{gr} - v_t \sin\theta) I_5 - v_t I_3 \cos\theta],\ A_8 = -v_t \cos\theta I_5 + v_t I_3 \sin\theta \tag{A.8}$$

$$A_9 = -v_t \cos\theta \frac{\partial f}{\partial \eta}\bigg|_{\eta=0} + \left(v_{gr} - v_t \sin\theta\right)\frac{\partial g}{\partial \eta}\bigg|_{\eta=0} \tag{A.9}$$

$$A_{10} = 2E[v_t^2 I_7 \cos^2\theta + I_1 (v_{gr} - v_t \sin\theta)^2 + (v_t^2 \sin 2\theta - 2v_t v_{gr} \cos\theta)(I_5 - I_4)] \tag{A.10}$$

$$A_{11} = E^2\Bigg[v_t^2\cos^2\theta\frac{\partial I_7}{\partial r} - 2I_1\big(v_t\sin\theta - v_{gr}\big)\frac{\partial v_{gr}}{\partial r} + \big(v_{gr} - v_t\sin\theta\big)^2\frac{\partial I_1}{\partial r} - 2v_t(I_5 - I_4)\frac{\partial v_{gr}}{\partial r}\cos\theta + \big(v_t^2\sin 2\theta - 2v_t v_{gr}\cos\theta\big)\frac{\partial(I_5 - I_4)}{\partial r}\Bigg] \tag{A.11}$$

$$A_{12} = (v_t^2\cos 2\theta + v_t v_{gr}\sin\theta)I_5 + (\tfrac{1}{2}v_t^2\sin 2\theta - v_t v_{gr}\cos\theta)I_1 + (v_{gr}^2 - 2v_t v_{gr}\sin\theta - v_t^2\cos 2\theta)I_4 + v_t v_{gr}I_6\cos\theta - \tfrac{1}{2}v_t^2 I_7\sin 2\theta \tag{A.12}$$

$$A_{13} = E\Bigg[\big(-2v_t^2\sin 2\theta + v_t v_{gr}\cos\theta\big)I_5 + \big(v_t^2\cos 2\theta + v_t v_{gr}\sin\theta\big)\left(\frac{\partial I_5}{\partial\theta} + I_1\right) + \big(\tfrac{1}{2}v_t^2\sin 2\theta - v_t v_{gr}\cos\theta\big)\frac{\partial I_1}{\partial\theta} + \big(2v_t^2\sin 2\theta - 2v_t v_{gr}\cos\theta\big)I_4 + \left(v_{gr}^2 - 2v_t v_{gr}\sin\theta - v_t^2\cos 2\theta\right)\frac{\partial I_4}{\partial\theta} - v_t v_{gr}I_6\sin\theta + v_t v_{gr}\cos\theta\frac{\partial I_6}{\partial\theta} - v_t^2 I_7\cos 2\theta - \tfrac{1}{2}v_t^2\sin 2\theta\frac{\partial I_7}{\partial\theta}\Bigg] \tag{A.13}$$

$$A_{14} = E\Bigg[v_t\sin\theta\ \frac{\partial v_{gr}}{\partial r}I_5 + \big(v_t^2\cos 2\theta + v_t v_{gr}\sin\theta\big)\frac{\partial I_5}{\partial r} - v_t\frac{\partial v_{gr}}{\partial r}I_1\cos\theta + \big(\tfrac{1}{2}v_t^2\sin 2\theta - v_t v_{gr}\cos\theta\big)\frac{\partial I_1}{\partial r} + 2I_4\big(v_{gr} - v_t\sin\theta\big)\frac{\partial v_{gr}}{\partial r} + I_6 v_t\cos\theta\frac{\partial v_{gr}}{\partial r} + \left(v_{gr}^2 - 2v_t v_{gr}\sin\theta - v_t^2\cos 2\theta\right)\frac{\partial I_4}{\partial r} + v_t v_{gr}\cos\theta\frac{\partial I_6}{\partial r} - \tfrac{1}{2}v_t^2\sin 2\theta\frac{\partial I_7}{\partial r}\Bigg] \tag{A.14}$$

$$A_{15} = -v_t^2 I_1\sin 2\theta + v_t^2\cos^2\theta\frac{\partial I_1}{\partial\theta} - 2v_t^2 I_5\cos 2\theta - v_t^2\sin 2\theta\frac{\partial I_5}{\partial\theta} + \big(2v_t^2\cos 2\theta + 2v_t v_{gr}\sin\theta\big)I_4 + \big(v_t^2\sin 2\theta - 2v_t v_{gr}\cos\theta\big)\frac{\partial I_4}{\partial\theta} + v_t^2 I_7\sin 2\theta + v_t^2\sin^2\theta\frac{\partial I_7}{\partial\theta} - 2v_t v_{gr}\ I_6\cos\theta - 2v_t v_{gr}\sin\theta\frac{\partial I_6}{\partial\theta} \tag{A.15}$$

$$A_{16} = (v_{gr} - v_t\ \sin\theta)I_5 - v_t I_3\cos\theta \tag{A.16}$$

$$A_{17} = E\left[I_5\frac{\partial v_{gr}}{\partial r} + \big(v_{gr} - v_t\sin\theta\big)\frac{\partial I_5}{\partial r} - v_t\cos\theta\frac{\partial I_3}{\partial r}\right] \tag{A.17}$$

$$A_{18} = v_t I_5\sin\theta - v_t\cos\theta\frac{\partial I_5}{\partial\theta} + v_t I_3\cos\theta + v_t\sin\theta\frac{\partial I_3}{\partial\theta} \tag{A.18}$$

$$A_{19} = v_{gr}^2 I_6,\ A_{20} = v_{gr} \frac{\partial I_6}{\partial \theta} \tag{A.19}$$

In Eqs. (A.2)–(A.19), the derivatives $\frac{\partial I_j}{\partial r}$ and $\frac{\partial I_j}{\partial \theta}$ for j = 1,..,7 can be calculated analytically using the chain rule

$$\frac{\partial I_j}{\partial s} = \frac{\partial I_j}{\partial a_1} \frac{\partial a_1}{\partial s} + \frac{\partial I_j}{\partial a_2} \frac{\partial a_2}{\partial s},\ j = 1,..,7 \tag{A.20}$$

where s is either r or θ and $\frac{\partial a_1}{\partial s}$ and $\frac{\partial a_2}{\partial s}$ can be analytically derived from Eqs. (12) and (13).

References

Anthes, R.A., 1971: Iterative solutions to the steady-state axisymetric boundary layer equations under an intense pressure gradient, *Mon Wea. Rev.*, **99**, 261–268.

Anthes, R.A., 1982: *Tropical Cyclones: Their Evolution, Structure, and Effects*, Meteorological Monographs Number 41, American Meteorological Society, Boston, MA.

Black, M.L., J.F. Gamache, F.D. Marks Jr., C.E. Samsury and H.E. Willoughby, 2002: Eastern Pacific Hurricanes Jimena of 1991 and Olivia of 1994: The effect of vertical shear on structure and intensity. *Mon. Wea. Rev.*, **130**, 2291–2312.

Bode, L. and R.K. Smith, 1975: A parameterization of the boundary layer of a tropical cyclone. *Bound. Layer Meteor.*, **8**, 3–19.

Chapra, S.C. and R.P. Canale, 2002: *Numerical methods for engineers*, **4**th Edition, McGraw-Hill, New York, U.S.A.

Chow, S., 1971: A study of the wind field in the planetary boundary layer of a moving tropical cyclone. M.S. Thesis, Dept. of Meteor. and Oceanogr., New York University, 59 pp. [NOAA/NHRL Library, 1320 South Dixie Highway, Coral Gables, FL 33146].

Donelan, M.A., B.K. Haus, N. Reul, W.J. Plant, M. Stiassnie, H.C. Graber, O.B. Brown, E.S. Saltzman, 2004: On the limiting aerodynamic roughness of the ocean in very strong winds. *Geophys. Res. Lett.,* **31**, L18306, doi:10.1029/2004GL019460.

Eliassen, A. and M. Lystad, 1977: The Ekman layer of a circular vortex: A numerical and theoretical study. *Geophys. Norv.*, **31**, 1–16.

Emanuel, K.A., 1986: An air-sea interaction theory for tropical cyclones. Part I: Steady state maintenance. *J. Atmos. Sci.*, **43**, 585–604.

Emanuel, K.A., 1989: Polar lows as Artic hurricanes. *Tellus*, **41A**, 1–17.

Frank, W.M., 1977: The structure and energetics of the tropical cyclone: I. Storm structure. *Mon. Wea. Rev.*, **105**, 1119–1135.

Haurwitz, B., 1935: On the variation of wind with elevation under the influence of viscosity in curved air currents. *Beitrage zur Geophysik*, **45**, p. 243.

Hawkins, H.F. and D.T. Rubsam, 1968: Hurricane Hilda, 1964. II. Structure and budgets of the hurricane on October 1, 1964. *Mon. Wea. Rev.*, **96**, 617–636.

Holland, G.J., 1980: An analytic model of the wind and pressure profiles in hurricanes. *Mon. Wea. Rev.*, **108**, 1212–1218.

Jorgensen, D.P., 1984a: Mesoscale and convective-scale characteristics of mature hurricanes. Part I: General observations by research aircraft. *J. Atmo. Sci.*, **41(8)**, 1268–1286.

Jorgensen, D.P., 1984b: Mesoscale and convective-scale characteristics of mature hurricanes. Part II: Inner core structure of Hurricane Allen (1980). *J. Atmo. Sci.*, **41**(8), 1287–1311.

Kepert, J. and Y. Wang, 2001: The dynamics of boundary layer jets within the tropical cyclone core. Part II: Nonlinear enhancement. *J. Atmos. Sci*., **58**, 2485–2501.
Kepert, J., 2001: The dynamics of boundary layer jets within the tropical cyclone core. Part I: Linear theory. *J. Atmo. Sci*, **58**, 2469–2484.
Kepert, J., 2006a: Observed boundary layer wind structure and balance in the hurricane core. Part I: Hurricane Georges, *J. Atmo. Sci*, **63**, 2169–2193.
Kepert, J., 2006b: Observed boundary layer wind structure and balance in the hurricane core. Part II: Hurricane Mitch, *J. Atmo. Sci*, **63**, 2194–2211.
Kundu, K.K. and I.M. Cohen, 2004: *Fluid mechanics*. 3rd Edition, Elsevier Academic Press.
Large, W.G. and S. Pond, 1981: Open ocean momentum flux measurements in moderate to strong winds, *J. Phys. Oceanogr*., **11**, 324–336.
La Seur, N.E. and H.F. Hawkins, 1963: An analysis of Hurricane Cleo (1958) based on data from research reconnaissance aircraft. *Mon. Wea. Rev*., **91**, 694–709.
Landsea, C.W., 2000: Climate variability of tropical cyclones: Past, present and future. In: Pielke, Jr. R. and R. Pielke Sr. (eds) *Storms*. Vol. 1, Routledge, NY, U.S.A, p. 220–241.
Leslie, L.M. and R.K. Smith, 1970: The surface boundary layer of a hurricane- Part II. *Tellus*, **22**, 288–297.
Mack, L.M., 1962: The laminar boundary layer on a disk of finite radius in a rotating fluid. Calif. Instit. of Tech. Rep. No. 32–224.
Miller, B.I., 1965: A simple model of the hurricane inflow layer. Nat. Hurr. Res. Proj. Rep. No. 75, 16 pp.
Myers, V.A. and W. Malkin, 1961: Some properties of hurricane wind fields as deducted from trajectories. NHRP Rep. 49, 45 pp. [NOAA/NHRL Library, 1320 South Dixie Highway, Coral Gables, FL 33146].
Myers, V.A., 1957: Maximum hurricane winds. *Bull. Amer. Meteor. Soc*., **38**, 227–228.
Powell, M.D., P.J. Vickery and T.A. Reinhold, 2003: Reduced drag coefficient for high wind speeds in tropical cyclones, *Nature*, **422**, 279–283.
Renno, N. and A. Ingersoll, 1996: Natural convection as a heat engine: A theory for CAPE. *J. Atmo. Sci*., **53**(4), 572–585.
Rosenthal, S.L., 1962: A theoretical analysis of the field of motion in the hurricane boundary layer. Nat Hurr. Res. Proj. Rep., No. 56, 12 pp.
Schlichting, H., 1960: *Boundary layer theory*. 2nd Edition, McGraw Hill, London, Great Britain.
Schloemer, R.W., 1954: Analysis and synthesis of hurricane wind patterns over Lake Okechobee, FL. Hydromet. Rep. 31, 49 pp [Govt. Printing Office, No. C30.70:31].
Shapiro, L.J., 1983: The asymmetric boundary layer flow under a translating hurricane. *J. Atmos. Sci*., **40**, 1984–1998.
Smith, R.K. 2003: A simple model of the hurricane boundary layer. *Quart. J. Roy. Met. Soc*., **129**, 1007–1027.
Smith, R.K., 1968: The surface boundary layer of a hurricane. *Tellus*, **20**, 473–484.
Vickery, P.J., P.F. Skerlj and L.A. Twisdale, 2000: Simulation of hurricane risk in the U.S. using empirical track model. *J. of Structural Engineering*, **126(10)**, 1222–1237.
Willoughby, H.E. and M.E. Rahn, 2004: Parametric representation of the primary hurricane vortex. Part I: Observations and evaluation of the Holland (1980) model. *Mon. Wea. Rev*., **132**, 3033–3048.
Willoughby, H.E., 1990: Gradient balance in tropical cyclones. *J. Atmos. Sci*., **47**, 265–274.
Willoughby, H.E., 1991: Reply. *J. Atmos. Sci*., **48**, 1209–1212.
Willoughby, H.E., J.A. Clos, M.G. Shoreibah, 1982: Concentric eye walls, secondary wind maxima, and the evolution of the hurricane vortex, *J. Atmo. Sci*., **39**, 395–411.

Changes in Tropical Cyclone Activity due to Global Warming in a General Circulation Model

S. Gualdi, E. Scoccimarro, and A. Navarra

Abstract This study investigates the possible changes that the greenhouse global warming might generate in the characteristics of the tropical cyclones (TCs). The analysis has been performed using scenario climate simulations carried out with a fully coupled high-resolution global general circulation model. The capability of the model to reproduce a reasonably realistic TC climatology has been assessed by comparing the model results from a simulation of the 20th Century with observations. The model appears to be able to simulate tropical cyclone-like vortices with many features similar to the observed TCs. The simulated TC activity exhibits realistic geographical distribution, seasonal modulation and interannual variability, suggesting that the model is able to reproduce the major basic mechanisms that link the TC occurrence with the large scale circulation.

The results from the climate scenarios reveal a substantial general reduction of the TC frequency when the atmospheric CO2 concentration is doubled and quadrupled. The reduction appears particularly evident for the tropical North West Pacific and North Atlantic (NA). In the NWP the weaker TC activity seems to be associated with a reduced amount of convective instabilities. In the ATL region the weaker TC activity seems to be due to both the increased stability of the atmosphere and a stronger vertical wind shear. Despite the generally reduced TC activity, there is evidence of increased rainfall associated with the simulated cyclones. Despite the overall warming of the tropical upper ocean and the expansion of warm SSTs to the subtropics and mid-latitudes, the action of the TCs remains well confined to the tropical region and the peak of TC number remains equatorward of 20° latitude in both Hemispheres.

An extended version of this work is published in Journal of Climate (Gualdi et al. 2008).

Introduction

Tropical cyclones (TCs) are non-frontal synoptic scale low-pressure systems, which develop over warm pools of the tropical or sub-tropical oceans, with organized convection and definite cyclonic surface wind circulation (Holland 1993). A severe

J.B. Elsner and T.H. Jagger (eds.), *Hurricanes and Climate Change,*
doi: 10.1007/978-0-387-09410-6,

tropical cyclone is also known as “hurricane” in North Atlantic and North-East Pacific and “typhoon” in West Pacific. TCs are one of the most devastating natural phenomena, which often cause severe human and economic losses. Therefore, the understanding of the mechanisms that underlie their formation and evolution is a high-priority issue from both the scientific, social and economic point of view.

The increased frequency and intensity of observed hurricanes since 1995 (Goldenberg et al. 2001, Webster et al. 2005) and the extraordinary nature of the North Atlantic hurricane season that occurred in 2005 have triggered a lively discussion about the possible changes of TC frequency and intensity due to global climate change (e.g., Emanuel 2005, Trenberth 2005, Pielke et al. 2005, Anthes et al. 2006, Pielke et al. 2006., Landsea et al. 2006, among other).

A number of studies have shown that TC activity varies substantially from interannual to decadal timescales. For example, the sensitivity of the TC activity to the phase of El Niño/Southern Oscillation (ENSO) has been documented in several studies (e.g., Gray 1984, Chan 2000, Chia and Ropelewski 2002). Similarly, low-frequency modulations of the North Atlantic Oscillation (NAO) exert significant influences on the behaviour of TCs (e.g., Elsner and Kocher 2000).

The wide interannual and decadal changes, associated with natural modes of climate variability, make difficult the identification of changes in the TC features that could be unambiguously attributed to the global warming (Walsh 2004). The detection of possible trends becomes even harder when observational data-sets only are used. The destructive nature of TCs, in fact, makes the collection of observed data extremely difficult and expensive. For this reason, databases of observed TCs are available only for a few regions (particularly North Atlantic) and are generally limited in length. Furthermore, due to subjective measurements and variable procedures, reservations have been raised about the reliability of the existing tropical cyclone data-bases for estimating climatological trends (Landsea et al. 2006, Landsea 2007).

To overcome the limitations of the observational data-sets, the possible influences of global warming on TC activity also have been explored using numerical models. Since the early work of Broccoli and Manabe (1990), a number of studies have been performed both with global and regional models, reaching conflicting conclusions. Haarsma et al. (1993), for instance, found a significant increase of the number of simulated TCs in greenhouse warming experiments. However, similar simulations, but performed with higher resolution models, showed a significant reduction of the global TC activity in a warmer earth (Bengtsson et al. 1996, Sugi et al. 2002, McDonald et al. 2005, Yoshimura et al. 2006, Bengtsson et al. 2007). Royer (1998), on the other hand, found increased (decreased) TC activity in the Northern (Southern) Hemisphere, whereas Chauvin et al. (2006) showed that possible changes in the frequency of TC occurrence in the North Atlantic strongly depend on the characteristics of the sea-surface temperature (SST) spatial distribution produced by the scenario simulations.

While the issue of the TC frequency response to greenhouse warming remains arguable, some consensus has been achieved about the effects on the TC intensity. Consistent with the theoretical findings of Emanuel (1987) and Holland (1997), numerous model studies, have found that the intensity of simulated TCs tends to

increase in a warmer earth (e.g., Walsh and Ryan 2000, Sugi et al. 2002, Knutson and Tuleya 2004, Chauvin et al. 2006, Yoshimura et al. 2006, Oouchi et al. 2006, Bengtsson et al. 2007). In particular, these works have shown that in a warmer climate TCs might be characterized by stronger winds and more intense precipitations. These results appear to be rather robust, as they have been obtained using a variety of models (global and regional), different resolutions and convective parametrizations. However, it is important to note that most of these studies have been conducted analyzing experiments performed with atmospheric only models forced with prescribed SSTs, thus the large majority of these experiments do not include air-sea interactions. Moreover, the SST patterns used to force the atmosphere were based on (generally low-resolution) climate scenario simulations performed with other models. This procedure, therefore, might be affected by possible inconsistencies between the simulations from which the SST patterns were taken and the atmospheric runs used to analyze the TC behaviour.

Though the air-sea feedbacks are known to be important for TC intensity (Emanuel 2003), there are only a few analysis of the TC response to global warming performed with coupled models, which, moreover, have been carried out using limited area models with simplified experimental setting (Knutson et al. 2001). On the other hand, in-depth investigations of TCs and their simulation conducted with fully coupled global models, the same as those used to perform the climate scenarios, would provide further insight into these phenomena and into our ability to reproduce and predict their behaviour.

In this study, we document the ability of a high-resolution coupled atmosphere-ocean general circulation model to simulate tropical cyclone-like vortices and explore how the features of these phenomena are possibly altered by greenhouse warming. The analysis is performed on idealized greenhouse gas forcing scenarios and a simulation of the 20° Century climate. The difference with respect to most of the previous works published on he same subject is that we use a fully coupled model, where air-sea feedbacks are accounted for.

In Section 2, a description of the model, scenario simulations and of the methodological approach used in the present paper is provided. In Section 3, we examine the ability of the model to simulate TCs. Section 4 presents an assessment of the possible changes of the TC characteristics as a consequence of global warming. In Section 5, the main findings of this work will be discussed, and the summary in Section 6 close the paper.

Model, Simulations and Methodology

The Model

The modelling data employed in this work are time series obtained from climate simulations carried out with the SINTEX-G (SXG) coupled atmosphere-ocean general circulation model (AOGCM), which is an evolution of the SINTEX and

SINTEX-F models (Gualdi et al., 2003a, 2003b; Guilyardi et al., 2003, Luo et al. 2003, Masson et al. 2005, Behera et al. 2005).

The ocean model component is the reference version 8.2 of the Ocean Parallelise (OPA; Madec et al. 1998) with the ORCA2 configuration. To avoid the singularity at the North Pole, it has been transferred to two poles located on Asia and North America. The model longitude-latitude resolution is $2^\circ \times 2^\circ$ cosine(latitude) with increased meridional resolutions to 0.5° near the equator. The model has 31 vertical levels, ten of which lie in the top 100 m.

Model physics includes a free-surface configuration (Roullet and Madec 2000) and the Gent and McWilliams (1990) scheme for isopycnal mixing. Horizontal eddy viscosity coefficient in open oceans varies from 40000 m^2/s in high latitudes to 2000 m^2/s in the equator. Vertical eddy diffusivity and viscosity coefficients are calculated from a 1.5-order turbulent closure scheme (Blanke and Delecluse 1993). For more details about the ocean model and its performance, readers are referred to Madec et al. (1998) or online to the web-site http://www.lodyc.jussieu.fr/opa/.

The evolution of the sea-ice is described by the LIM (Louvain-La-Neuve sea-ice model; Fichefet and Morales Maqueda, 1999), which is a thermodynamic-dynamic snow sea-ice model, with three vertical levels (one for snow and two for ice). The model allows for the presence of leads within the ice pack. Vertical and lateral growth and decay rates of the ice are obtained from prognostic energy budgets at both the bottom and surface boundaries of the snow-ice cover and in leads. When the snow load is sufficiently large to depress the snow-ice interface under the sea-water level, sea-water is supposed to infiltrate the entirety of the submerged snow and to freeze there, forming a snow ice cap. For the momentum balance, sea-ice is considered as a two-dimensional continuum in dynamical interaction with the atmosphere and ocean. The ice momentum equation is solved on the same horizontal grid as the ocean model. LIM has been thoroughly validated for both Arctic and Antarctic conditions, and has been used in a number of process studies and coupled simulations (Timmermann et al. 2005 and references therein).

The atmospheric model component is the latest version of ECHAM-4 in which the Message Passing Interface is applied to parallel computation (Roeckner et al. 1996). We adopted a horizontal resolution T106, corresponding to a gaussian grid of about $1.12^\circ \times 1.12^\circ$. In the pantheon of long coupled climate simulations, this is a considerably high horizontal resolution. A hybrid sigma-pressure vertical coordinate is used with 4–5 of a total of 19 levels lying in the planetary boundary layer. The parameterization of convection is based on the mass flux concept (Tiedtke, 1989), modified following Nordeng (1994). The Morcrette (1991) radiation scheme is used with the insertion of greenhouse gases (ghg) and a revised parameterization for the water vapour and the optical properties of clouds. A detailed discussion of the model physics and performances can be found in Roeckner et al. (1996).

The ocean and atmosphere components exchange SST, surface momentum, heat and water fluxes every 1.5 hours. The coupling and the interpolation of the coupling fields is made through the OASIS2.4 coupler (Valcke et al., 2000). No flux corrections are applied to the coupled model.

The Climate Scenario Simulations

With respect to the previous versions of the SINTEX model, SXG includes a model of the sea-ice, which allows the production of fully coupled climate scenario experiments. In this paper, we present results obtained from the analysis of four climate simulations (Table 1).

In order to assess the capability of the model to reproduce a reasonably realistic TC activity and to evaluate the effectiveness of our TC detection methodology, the tropical cyclone-like vortices produced during the last 30 years of a 20th Century simulation have been analyzed and compared with observations. The simulation has been conducted integrating the model with forcing agents, which include greenhouse gases (CO2, CH4, N2O and CFCs) and sulfate aerosols, as specified in the protocol for the 20C3M experiment defined for the IPCC simulations (for more details see also the web-site http://www-pcmdi.llnl.gov/ipcc/about_ipcc.php). The integration starts from an equilibrium state obtained from a long coupled simulation of the pre-industrial climate, and has been conducted throughout the period 1870–2000.

Once the skill of the model to reproduce TC-like vortices has been evaluated using the present climate simulation, the possible effects induced by greenhouse global warming on the simulated TCs have been explored using 30 years of twice-daily data from climate scenario experiments. Specifically, a simulation with atmospheric CO2 concentration 287 ppm, corresponding to the pre-industrial period (PREIND), a climate simulation with CO2 concentration doubled with respect to the PREIND period (2CO2), and a climate simulation with atmospheric CO2 concentration quadrupled with respect to the PREIND period (4CO2). The transition between PREIND and 2CO2 and between 2CO2 and 4CO2 periods has been produced by a 1%/year increment of the CO2 concentration. At the end of the two transition periods, the model has been integrated for 100 years with constant values of CO2 concentration, i.e. 574 ppm and 1148 ppm respectively.

A greenhouse warming scenario based on a doubling and a quadrupling of atmospheric CO2 is certainly an idealized experiment and does not represent a realistic forecast of future radiative forcing. The motivation of this choice resides in the fact that large concentration of atmospheric CO2 might emphasize and make more evident the response of simulated TCs to greenhouse warming. Also, the advisability of this kind of idealized experiments in the framework of TC studies has been discussed by Michaels et al. (2005) and Knutson and Tuleya (2005). Furthermore, the possible impacts of a doubling of atmospheric CO2 concentration has been explored in a

Table 1 Summary of the climate simulations used in this study

CLIMATE SIMULATIONS AND SCENARIOS		
PREIND	Preindustrial ghg concentration	30 years
20C3M	20th Century ghg conc. + aerosols	30 years (1970–1999)
2CO2	2 × PREIND CO2 conc.	30 years
4CO2	4 × PREIND CO2 conc.	30 years

number of previous works (e.g., Broccoli and Manabe 1990, Haarsma et al. 1993, Bengtsson et al. 1996, Royer 1998, Sugi et al. 2002, Knutson and Tuleya 2004, McDonald et al. 2005, Yoshimura et al. 2006, Chauvin et al. 2006), but so far no analysis has been performed on the effects of its further increase.

Reference Data

The simulated TC-like vortices and the main features of their climatology are evaluated comparing the model results with observational data sets. Specifically, we use data from the National Hurricane Center (NHC) and the U.S. Joint Typhoon Warning Center (JTWC). Furthermore, the capability of the model to reproduce the observed mean climate is assessed using the ECMWF 40-year Re-Analysis (ERA40; more information available at the web-site http://www.ecmwf.int/research/era), the observational sea-surface temperature data set HadISST (Global Sea-Ice and Sea Surface Temperature Dataset produced at the Hadely Centre, Rayner et al. 2003) and the observed precipitation data set produced by Xie and Arkin (1997). For the sake of simplicity, in the rest of the paper we will refer to all of these data as observations.

Method of Detection of the Simulated Tropical Cyclones

Basically, two methods for detecting TCs have been commonly used in the analysis of general circulation model (GCM) experiment results. The first technique produces an estimate of the TC activity based on a genesis parameter computed from seasonal means of large scale fields (Gray 1979, Watterson et al. 1995, Royer 1998). This method has been used especially in the analysis of low-resolution model runs, as it obviates the explicit simulation of individual TCs.

The second method is the location and tracking of individual TCs based on objective criteria for the identification of specific atmospheric conditions that characterize a TC with respect to other atmospheric disturbances. In particular, TCs are identified and tracked as centres of maximum relative vorticities and minimum of surface pressure, with a warm core in high levels and maximum wind in the low layers of the atmosphere (Haarsma 1993, Bengtsson et al. 1995, Walsh 1997). In the existing literature, the definition of the criteria, i.e. the thresholds and the domain over which they are computed, varies from work to work. A discussion and a short summary for the criteria of objective TCs detection in atmospheric analysis and model simulations is given in Walsh (1997) and Chauvin et al. (2006) respectively.

In this study, we use a TC location and tracking method based on the approach defined in Bengtsson et al. (1995) and Walsh (1997). Specifically we assume that a

model TC is active over a certain grid point A if the following conditions are satisfied:

- in A relative vorticity at 850 hPa is $>3 \cdot 10^{-5}$ 1/s;
- there is a relative minimum of surface pressure and wind velocity is >14 m/s in an area of 2.25° around A;
- wind velocity at 850 hPa is > wind velocity at 300 hPa;
- the sum of temperature anomalies at 700, 500 and 300 hPa is >2°K. Where the anomalies are defined as the deviation from a spatial mean computed over an area of 13 grid points in the east-west and 2 grid points in the north-south direction;
- temperature anomaly at 300 hPa is > temperature anomaly at 850 hPa;
- the above conditions persist for a period longer than 1.5 days;

Conditions 3, 4 and 5 distinguish TCs from other low-pressure systems and particularly the extra-tropical cyclones, which are characterized by strongest winds near the tropopause and a tropospheric cold core. The choice of the parameters in conditions 1–6 are very similar to the value indicated by Bengtsson et al. (1995) and Walsh (1997) and optimize the detection of simulated TCs in our model compared with the observations. Also, we checked the sensitivity of our results to small changes in these parameters. We found that the number of detected TCs is scarcely sensitive to the threshold values, but exhibits some sensitivity to the size of the areas over which means are computed. For a complete discussion of these criteria and their sensitivity to the parameters used the reader is addressed to Walsh (1997).

Simulation of the Tropical Climate and TC Climatology

As a first step, we analyze the results obtained from a simulation of the 20th Century, as described in Section 2.2, comparing the model results with observations (re-analysis) for the period 1970–1999.

The TC occurrence has a pronounced seasonal character, with more intense activity found in the summer hemisphere (Emanuel 2006), namely in the Northern Hemisphere from June to October and in the Southern Hemisphere from December to April. Therefore, we will focus our attention on the specific seasons (and regions) of intense TC activity.

Simulation of Mean State and High-frequency Variability in the Tropics

Figure 1 shows the seasonal means of SST and precipitation as obtained from the observations and the model, for the extended northern summer (June–October, JJASO) and southern summer (December-April, DJFMA).

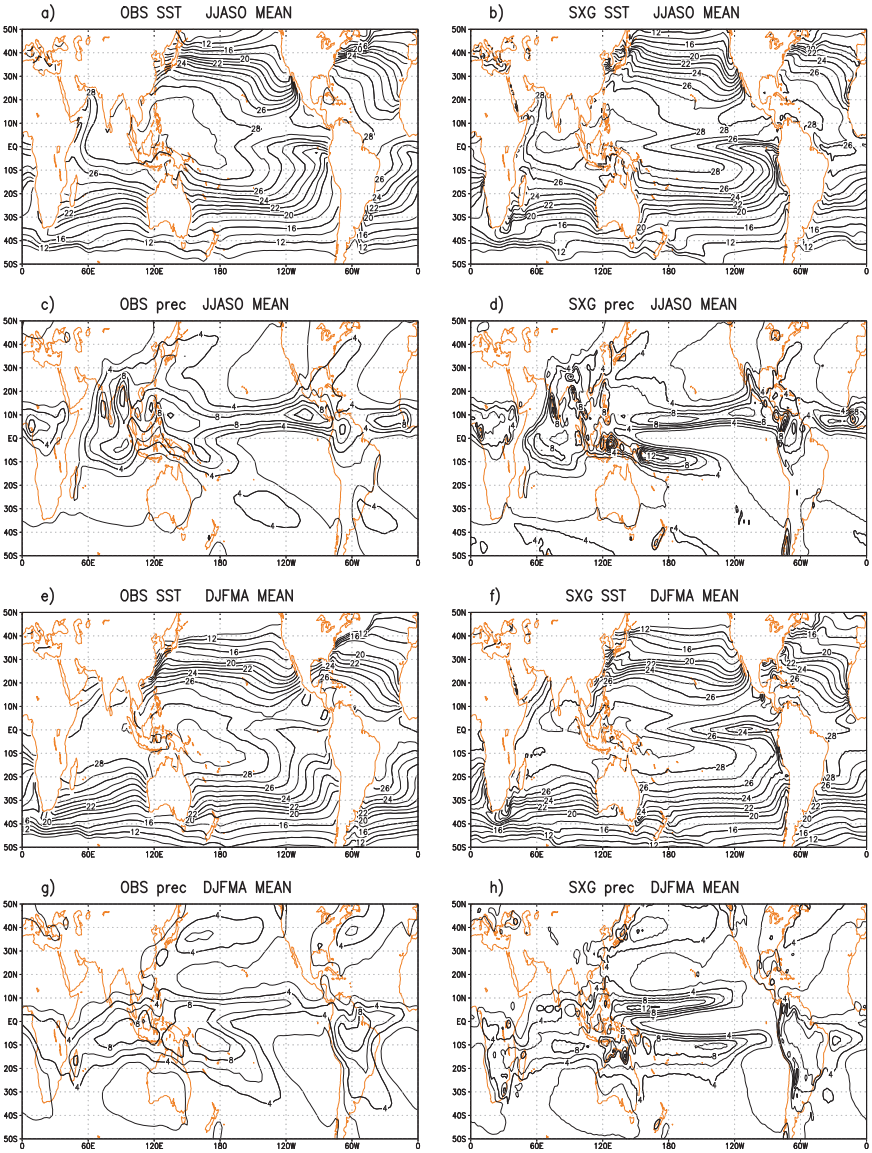

Fig. 1 Seasonal means of sea-surface temperature (SST) and precipitation as obtained from the observations (*left panels*) and the model (*right panels*). The upper panels (**a–d**) show the extended Northern Hemisphere summer means June-July-August-September-October (JJASO); the lower panels (**e–h**) are the means obtained for the extended Southern Hemisphere summer December-January-February-March-April (DJFMA). The SST contours (panels a, b, e and f) is 2°C for the SST interval 10–20°C and 1°C for the SST interval 21–29°C. The precipitation contours (panels c, d, g and h) are 2 mm/day. Rainfall values lower than 2 mm/day are not plotted

In general the model overestimates the SSTs in the tropical regions, during both seasons. The seasonal mean SST, averaged over the tropics is 0.26°C and 0.32°C warmer than observed in JJASO and in DJFMA respectively. The warm bias is visible both in the tropical Indian Ocean and Atlantic Ocean and it is particularly evident in the central-eastern Pacific, south of the equator. In this region, over the warm SSTs, the model overestimates also the rainfall, tending to produce a double ITCZ, which is a common error of most AOGCMs. In the equatorial Pacific, on the other hand, the model cold tongue is clearly too strong and extends too far west. Correspondingly, the simulated precipitation is too weak in the equatorial Pacific, especially west of the date line.

In the tropical Atlantic, the model rainfall is reasonably close to observations in JJASO, whereas during DJFMA it appears to be shifted south (by about 10° of latitude), probably as a consequence of the excessively warm SSTs found in the subtropical southern Atlantic, off the Brazilian coast. Interestingly, in the tropical Indian Ocean, the model precipitation is generally weaker than observed. During northern summer, the model shows a clear rainfall deficit in the area affected by the Asian summer monsoon, extending from the Bay of Bengal, through South-East Asia and South China Sea, up to the region east of the Philippines archipelago. Simulated precipitation appears to be too weak also over the eastern equatorial Indian Ocean, whereas it tends to be too intense in the western part of the basin, between the equator and 10°S. Also during northern winter (Fig. 1, panels g and h) model rainfall is too weak over the eastern Indian Ocean and the Indonesian region.

Simulation of Tropical Cyclones

In this Section we analyze the ability of the model to simulate tropical cyclones-like vortices (that we will refer to simply as TCs), following the methodology discussed in Section 2.4. As a first step, we compare the total number of TCs per year detected in the model simulation and in the observations over the period 1970–1999 (Table 2). In general, the number of simulated TCs per year is almost 30% lower than the number detected in the observations, whereas its standard deviation is quite well captured by the model.

The geographical distribution of the TC formation positions is shown in Fig. 2. In the observations (panel a) there are four distinct regions of TC formation in the Tropics of the Northern Hemisphere: North Indian Ocean (NI), West-North Pacific (WNP), East-North Pacific (ENP) and North Atlantic (NA); and three regions in the

Table 2 Total number of Tropical Cyclones found in the observations and in the 20th Century model simulation during the period 1970–1999

NUMBER OF TCs 1970–1999		
	OBS	SXG 20C3M
TOT	2813	1986
MEAN	93.8	66.2
STD	10.9	9.2

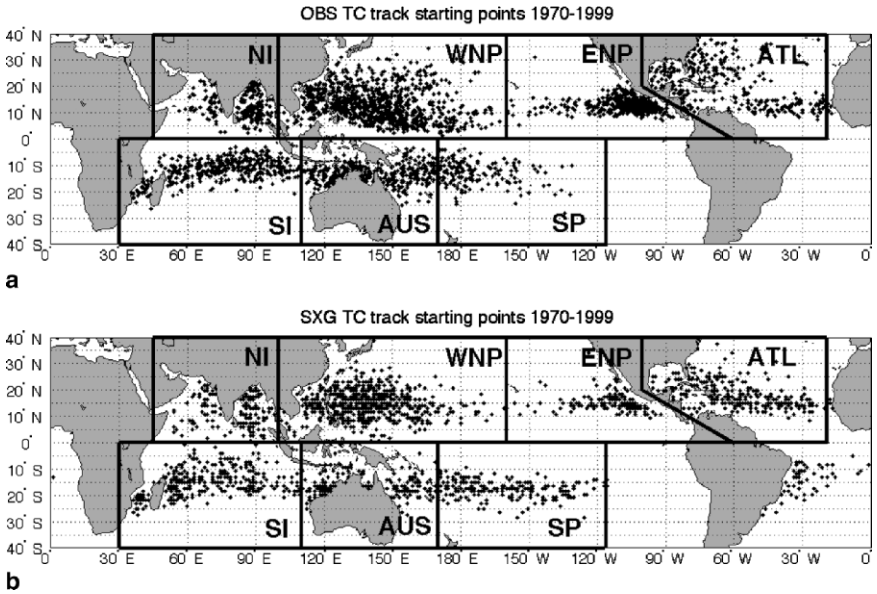

Fig. 2 Distribution of the TC track starting points for the period 1970–1999 for the observations (*panel a*) and model (*panel b*). Each point corresponds to the geographical location of a TC at the time of its first detection. Following Camargo et al. (2004) seven regions of TC genesis have been defined. In the pictures these regions are delimited by thick black lines

Southern Hemisphere: Southern Indian Ocean (SI), the ocean North of Australia (AUS) and the Southern Pacific (SP). Based on these regions of TC genesis and following Camargo et al. (2004), we define seven basins (demarked by the boxes in Fig. 2) that will be used to delimit and characterize the different areas of TCs activity.

The model (Fig. 2, panel a) reproduces well the patterns of TCs genesis, especially in the Northern Hemisphere. The major contrast with the results obtained from the observations occurs in the southern Atlantic, where the model generates some TC, though no TCs are observed in this region during the considered period (1970–1999). This model error might be related to the too warm SSTs and intense convective activity found in this region (Fig. 1). However, it is noteworthy that in March 2004 the first ever observed TC in South America, named Catarina, hit the Brazilian coast (Pezza and Simmonds, 2005).

A comparison with the results obtained with atmospheric GCMs forced with observed prescribed SSTs (Camargo et al. 2004, Fig. 1) shows a substantial improvement in the patterns of TC genesis obtained with the coupled simulation. Interestingly, the comparison is made more valid by the fact that one of the atmospheric models used in Camargo et al. (Echam4) is basically the same as the one we use as atmospheric component in our coupled model. An important difference, however, is the horizontal resolution, which is T42 in Camargo et al. and T106 in our case. The enhanced model resolution might explain some of the

improvements we find with our model, such as, for example, the increased global number of TCs, accompanied by a significant reduction of the number of TCs near the equator, which is a rather unrealistic feature (e.g., Camargo et al. 2004, Oouchi et al. 2006).

In Fig. 3, the box plots representing the mean number of TCs per year for each area are shown both for the observations (left panel) and the model (right panel). The plots confirm that in the simulation there is a lower number of TCs, especially in the tropical North Pacific (WNP and ENP). However, in general the difference with the observations is relatively small, and, for each area, the model simulates a fairly realistic mean year-to-year variability (see also STD in Table 2). More importantly, the simulation appears to capture the basic features of the TC distribution among the different areas. Specifically, the region with the highest mean number of TCs per year is the north-western tropical Pacific (WNP) both in the model and observations. Also the mean number of TCs in the North Indian Ocean

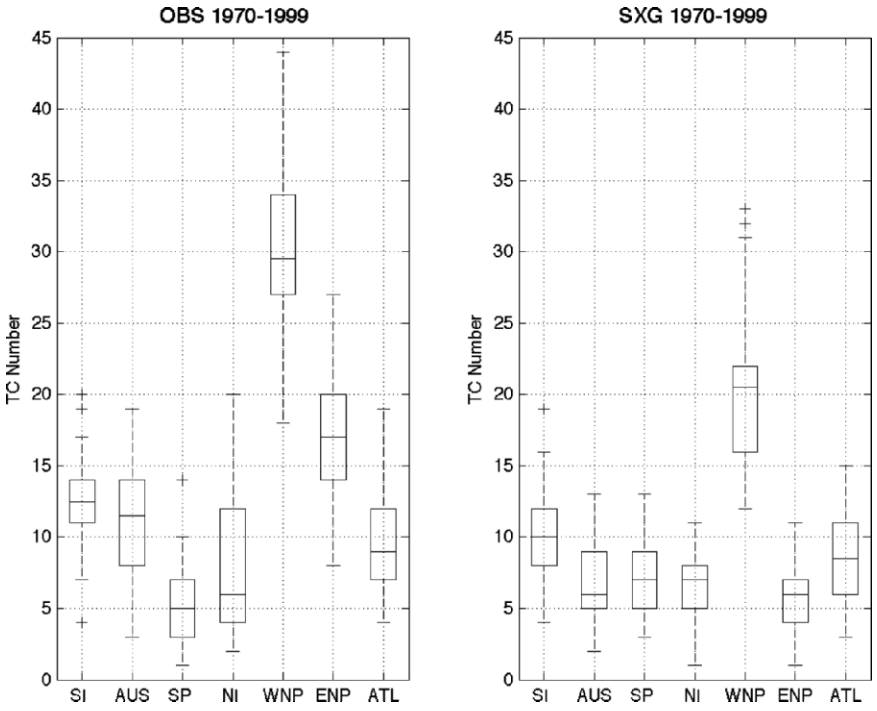

Fig. 3 Box plots of the number of TCs per year for the observations (*left panel*) and model simulation (*right panel*). The number of TCs (y-axis) is plotted for each area of TC-genesis (x-axis) defined in Fig. 4. In a box-plot, the box represents the interquartile (IQR) and contains the 50% of the data; the upper edge of the box represents the 75th percentile (upper quartile, UQ), while the lower edge is the 25th percentile (lower quartile, LQ). The horizontal lines within the box are the median. The vertical dashed lines indicate the range of the non-outliers. The values indicated with the crosses are the outliers, i.e. values that are either larger than $UQ + 1.5 \cdot IQR$ or smaller than $LQ - 1.5 \cdot IQR$

(NI) and Atlantic region (ATL) are well reproduced, whereas the TC activity in the north-eastern Pacific (ENP) is clearly underestimated.

The results shown in Figs. 1–3 indicate that the model reproduces a quite realistic tropical mean state (at least in terms of SST and precipitation) and number of simulated TC-like vortices. Furthermore, the geographic distribution of TCs appears to be in good agreement with the observations. However, so far nothing has been said about how realistic the features of the simulated TCs are.

In order to have a closer look at the structure of the model TCs, Fig. 4 depicts the composite patterns of precipitation and low-level wind field obtained from the 100 most intense simulated TCs in the Northern Hemisphere. The composites were calculated by averaging the fields over the period of occurrence of the TCs and over the 100 events. The means have been computed for a domain centered on the core of the cyclones and extending 10° each side.

From these patterns it turns out that the model simulates TCs with a somewhat realistic structures. When averaged over the 100 events and their lifetimes, the mean TC has intense mean precipitation and surface winds that extend for about 300–400 Km from the centre ("eye") of the cyclone. The amplitude of the fields is substantially smaller than observed, but consistent with the results obtained from high-resolution atmospheric GCMs experiments (e.g., Bengtsson et al. 1995,

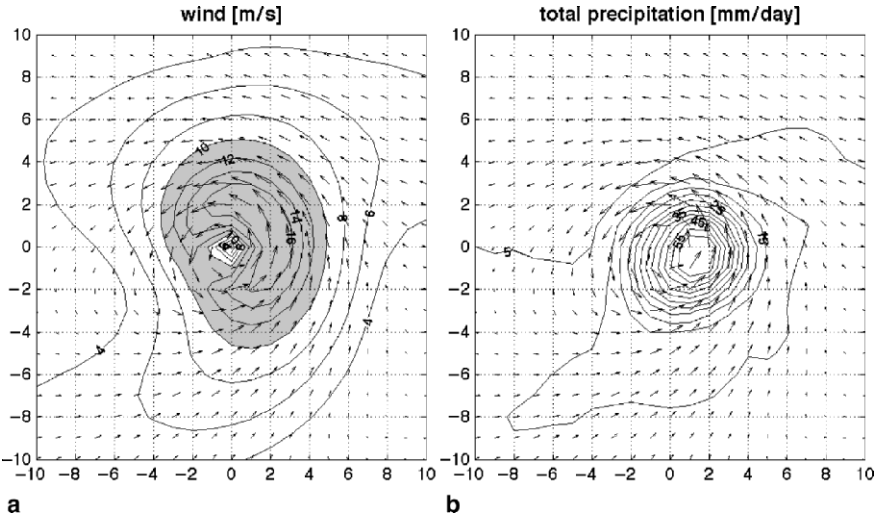

Fig. 4 Composite patterns of 850-hPa wind and total precipitation associated with the simulated TCs. The composites have been computed by averaging the fields of the 100 most intense (in terms of precipitation) model TCs in the Northern Hemisphere. The fields have been averaged over the period of occurrence of the TCs and over the 100 events. The mean fields have been computed over a spatial domain centred in the core of the cyclone and extending 10° each side. In panel (**a**) the of 850-hPa wind (arrows) is plotted along with the intensity of the wind (contour). The contour interval is 2 m/s. Contours larger than 10 m/s are shaded. Panel (**b**) shows the 850-hPa wind (arrows) along with the total precipitation rate. The contour interval is 5 mm/day

Chauvin et al. 2006). In agreement with observational studies (e.g., Frank 1977, Gray 1979, Willoughby et al. 1982), the strongest wind velocities are located to the right–front sector of the core, though the maxima in the model is much too far away from the "eye". This model error is most likely due to the model resolution, which does not allow to resolve the fine and tight structures observed in "real" TCs, as suggested in McDonald et al. (2005) Chauvin et al. (2006) and shown in Bengtsson et al. (2007). For the same reason, the minimum surface pressure at the center of the storm (not shown) tends to be rather high (∼990 hPa) and the simulated TC does not exhibits the "eye" in precipitation, though in general the rainfall pattern is reasonably realistic.

An important feature of the observed TCs is their marked seasonal character (Emanuel 2003). Fig. 5 shows the seasonality of TC occurrence for both observations and model simulations in the Northern Hemisphere and Southern Hemisphere and for specific regions of activity described in Fig. 2. In general the model reproduces well the seasonal behaviour of TCs, especially in the Southern Hemisphere, the northern Indian and Atlantic Oceans. In the Northern Hemisphere, and

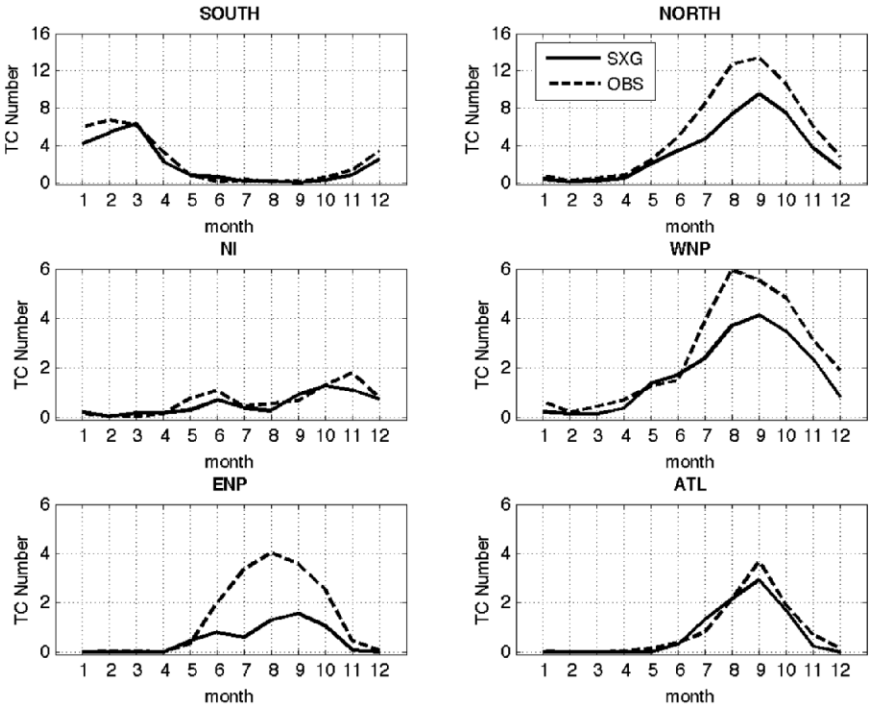

Fig. 5 Seasonal modulation of the TC occurrence for the observations (*dashed lines*) and model simulation (*solid lines*) and for different region of the Tropics. *Upper panels*: tropical region of the Southern Hemisphere (*left*) and of the Northern Hemisphere (*right*). *Middle* and *lower panels*: northern Indian Ocean, western tropical Pacific, eastern tropical Pacific and tropical Atlantic

particularly in the North-West and North-East Pacific the annual phase of the TC activity is captured but the amplitude is much smaller, consistent with the reduced number of simulated TCs previously discussed.

Beside the seasonal modulation, the TC activity exhibits a rather strong year-to-year variability. As it has been shown in a number of studies (Gray 1984, Chan 2000, Chia and Ropelewski 2002, Frank and Young 2007, among the others), this interannual variability has a strong link with ENSO. Changes in the SST distribution in the tropical Pacific and the associated changes in the large scale circulation, in fact, appear to have a strong impact on the number of TCs that occur in different regions of the globe. The relationship between ENSO and TCs activity differs depending on the region considered. Frank and Young 2007 have shown that the number of observed TCs and the NINO3 ENSO index are negatively correlated in the North Atlantic ($r = -0.55$), whereas they appear to be positively correlated in the North-East Pacific ($r = 0.38$) and Indian Ocean ($r = 0.24$).

Figure 6 shows the interannual variation of the number of TCs in the North Atlantic, North-East Pacific and southern Indian Ocean (solid curves), along with the NINO3 SSTA index (dotted curves). Here, the value of the NINO3 index is computed for the season of maximum TC activity, i.e. JJASO for the Northern

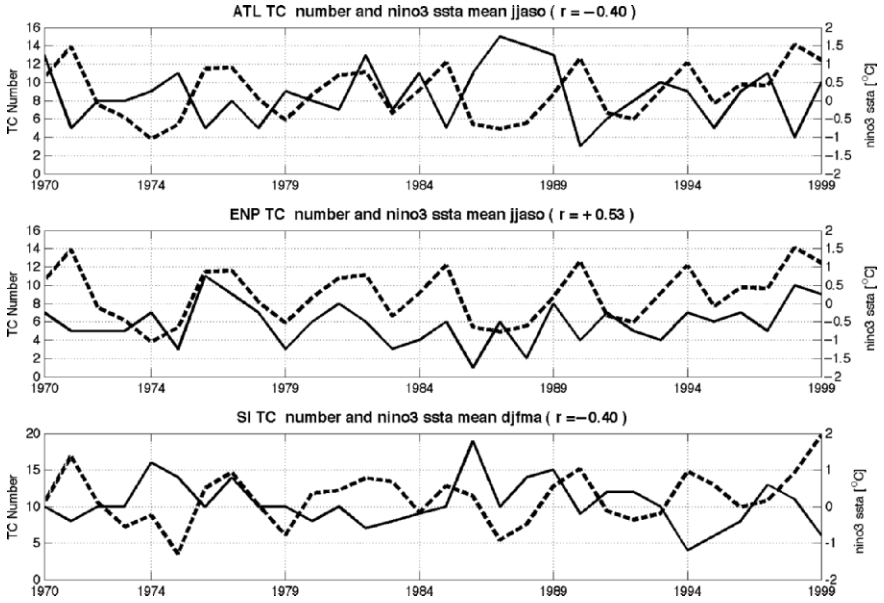

Fig. 6 Time series of the number of TCs along with the NINO-3 index for different regions of the Tropics. The dashed lines show the interannual variation of the number of simulated TCs in the northern tropical Atlantic (*upper panel*), northern tropical eastern Pacific (*middle panel*) and Southern Indian Ocean (*lower panel*). The solid line show the value of NINO-3 SSTA index defined as the average of the SST anomaly over the NINO-3 region (5°S-5°N ; 150°W-90°W). The values of the NINO-3 index plotted in the ATL and ENP case have been obtained for JJASO, whereas for the SI case it has been computed for DJFMA. The value of the correlation between the two curves (r) is also shown

Hemisphere and DJFMA for the Southern Hemisphere. The curves shown in Fig. 6 indicate that the model simulates a fairly realistic interannual modulation of the number of TCs and that this interannual variability is correlated with ENSO similarly to what is found in the observations.

All these results indicate that the model simulates intense convective disturbances with characteristics similar to the basic features of observed TCs, reassuring about its suitability to investigate how climate change might impact on the TC activity, which will be the subject of the next Section.

Impacts of the Global Warming on the Tropical Climate and TC Climatology

Possible changes in the basic features of the tropical mean climate and of the simulated tropical cyclones due to greenhouse global warming are investigated using the climate scenario experiments PREIND, 2CO2 and 4CO2 described in Section 2.2.

Changes in the Tropical Mean State

The impacts of the increased atmospheric CO2 on the mean state of the Tropics is shown in Fig. 7. Here the difference between 2CO2 and PREIND (2CO2-PREIND), and 4CO2 and PREIND (4CO2-PREIND) seasonal means of SST and precipitation are shown. Panels a, b, e and f indicate that the overall warming of the tropical SST is characterized by regional patterns. Both during JJASO and DJFMA, in fact, the warming is more marked in the western part of the Indian Ocean, in the equatorial Pacific and along the coast of South America, whereas a weaker warming is found in the eastern tropical Indian Ocean and eastern subtropical Pacific. In the tropical Pacific the warming patterns resemble El Niño anomalies. Interestingly, these patterns are similar for the 2CO2 PREIND and 4CO2-PREIND cases, though with different amplitudes.

Similar characteristics exhibit the patterns of difference between the PREIND, 2CO2 and 4CO2 precipitation (panels c, d, g and h). In particular, the increased CO2 induces a remarkable enhancement of precipitation along the ITCZ, from the Indian Ocean, through the Pacific to the Atlantic, during JJASO. Interestingly the increase of rainfall is confined to a relatively narrow region, very close to the equator. In the same season, areas of reduced rainfall are located in the south-eastern tropical Indian Ocean and south-central Pacific. During DJFMA, increased precipitation is found south of the equator, along the southern branch of the double ITCZ simulated by the model and discussed in Section 3.1; whereas regions of decreased rainfall are found in the subtropics of both the summer and winter hemispheres. Also in this case, the patterns of precipitation difference

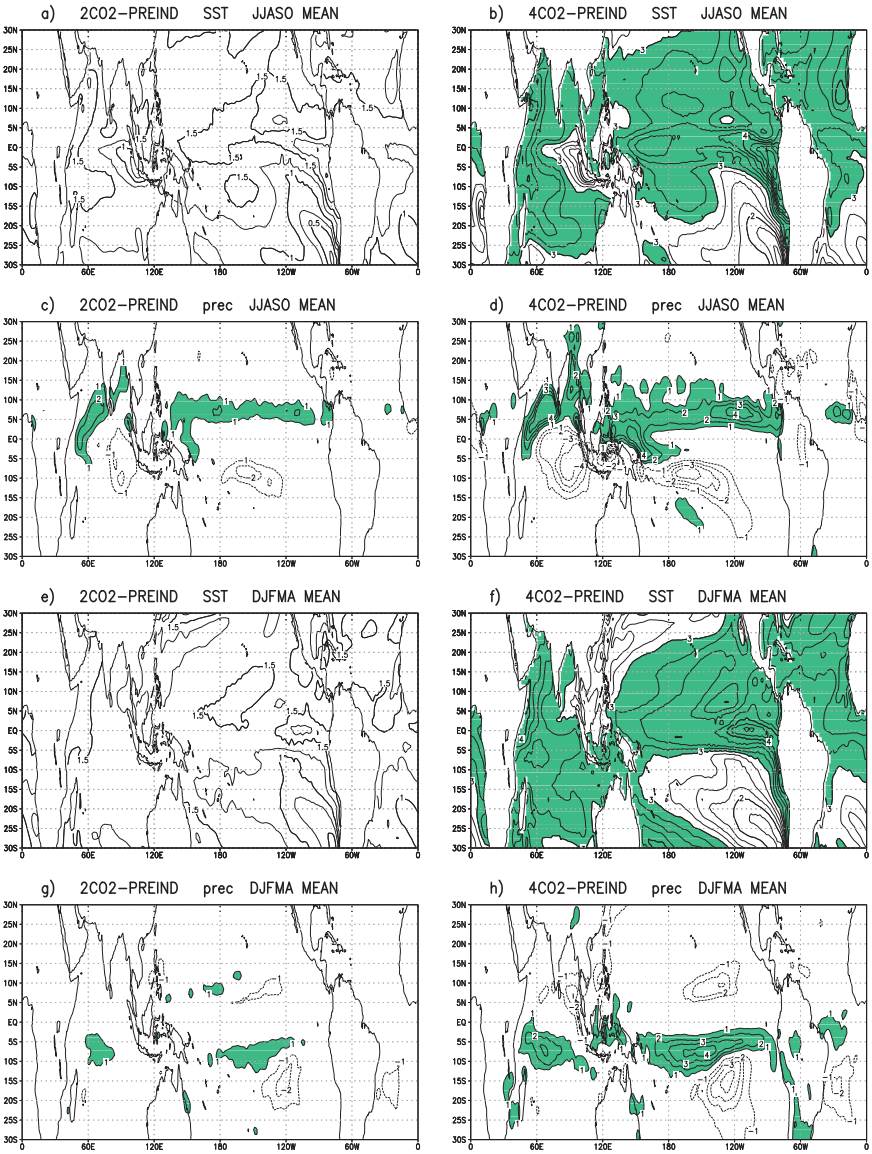

Fig. 7 Differences between the seasonal mean SST and precipitation obtained from the 2CO2 and PREIND experiments (*left panels*) and 4CO2 and PREIND experiments (*right panels*). Panels a, b, e and f show the differences in mean SST; contour interval is 0.25°C. Panels c, d, g and h show the differences in mean precipitation, with a contour interval of 1.0 mm/day

2CO2-PREIND and 4CO2-PREIND exhibit very similar spatial features but different amplitudes.

Table 3 shows the changes in mean temperature, mean precipitation and mean convective precipitation over the entire globe and over the Tropics for the three

Table 3 Global average and tropical average of mean surface temperature, mean total precipitation and mean convective precipitation. The mean have been computed over the 30-year periods considered in the study. Values in parenthesis are the differences (absolute values for temperature and percentage for precipitation) with respect to the PREIND case

	PREIND	2CO2	4CO2
T global mean °K	288.37	290.377 (+2.01)	292.72 (+4.36)
T Tropics °K	298.72	300.286 (+1.57)	302.41 (+3.69)
Prec. global mean mm/day	2.757	2.809 (+1.89%)	2.852 (+3.45%)
Prec. Tropics mm/day	3.317	3.353 (+1.09%)	3.354 (+1.12%)
ConvPrec global mean mm/day	1.209	1.164 (−3.72%)	1.106 (−8.52%)
ConvPrec Tropics mm/day	2.117	2.008 (−5.15%)	1.884 (−11.01%)

experiments. Here, the convective precipitation is the precipitation associated with convective processes and produced by the convective parametrization scheme. Interestingly, while a substantial rise in mean surface temperature and mean total precipitation are found when the CO2 is increased, a completely different behaviour is found for the convective precipitation. The latter in fact shows a significant reduction when the atmospheric CO2 concentration has doubled and quadrupled, especially in the tropical region.

A first assessment of the changes in high-frequency (<10 days) convective variability induced by the CO2 forcing has been obtained computing the difference in standard deviation of high-pass filtered OLR anomalies (not shown). Over most of the tropical belt the sign of the difference is negative, indicating a tendency of the model to attenuate the high-frequency convective variability when the atmospheric CO2 is increased. Only over the equatorial Pacific, between about 5°N and 5°S, there is a clear sign of enhanced variability.

These results appear to suggest that increasing the concentration of CO2 in the atmosphere of the model, the general warming of the earth surface is accompanied by a reduction of the (deep) convective activity in the Tropics. The weaker convective activity, in turn, might be due to an enhancement of the vertical stability of the atmosphere. This point will be examined in more detail in Section 5.

Changes in the Simulated Tropical Cyclones

Let us consider now what happens to the simulated TCs as a consequence of the greenhouse global warming. Table 4 shows the total number of TCs and TC days (upper row), the annual mean number of TCs and TC days (middle row) and their standard deviations (lower row) for the PREIND, 2CO2 and 4CO2 experiments. The method for detecting the TCs in these experiments is the same as the one used for the 20th century and discussed in Section 2.4. Also in this case we checked the sensitivity of the results to changes in the parameters used in the tracking procedure. In particular, we checked whether the results obtained from the 2CO2 and 4CO2 simulations might be affected by the choice of the vertical levels used to detect the

Table 4 Total number of TCs (left columns) and total number of TC days (right columns) found in the PREIND, 2CO2 and 4CO2 experiments. In all of the experiments a 30-year period is considered. In the upper row is the total number of TCs and TC days; in the middle row is the mean number of TCs and TC days per year; in the bottom row is the year-to-year standard deviation of the annual number of TCs and TC days. The average duration of the TCs, defined as the ratio between number of TC days and number of TCs, is 2.7 days for the PREIND, 2.8 for the 2CO2 and 2.7 for the 4CO2 experiment

	Number of Tropical Cyclones			Number of Tropical Cyclone Days		
	PREIND	2CO2	4CO2	PREIND	2CO2	4CO2
TOT	2196	1839	1229	5941	5085	3313
MEAN	73.2	61.3	41.0	198.0	169.5	110.4
STD	6.8	8.3	7.6	24.0	23.3	23.3

warm core (700, 500 and 300 hPa). The analysis indicated that the results shown in Table 4 are scarcely sensitive to small changes in the criteria we adopted.

The results illustrated in Table 4 suggest that the total number and the annual mean number of TCs and TC days appear to be substantially reduced with increased concentration of atmospheric CO2, whereas their interannual variability does not show significant changes. Also the average duration of TC (2.7 days for the PREIND and 4CO2 experiments and 2.8 days for the 2CO2 case) does not exhibit substantial variations. Our simulations, thus, indicate that increased CO2 leads to a reduction of the TC activity, both in terms of number of TCs and number of TC days. These results are consistent with previous findings (e.g., Bengtsson et al. 1996, Sugi et al. 2002, McDonald et al. 2005, Yoshimura et al. 2006), and for the first time they have been obtained using climate scenario simulations performed with a state-of-the-art fully coupled GCM.

The box plots shown in Fig. 8 represent the mean number of TCs per year for each activity area and for the three climate experiments. The reduction of the number of TCs is visible in all of the regions, though it appears to be particularly evident in the WNP and ATL areas. Interestingly, the TC activity appears to be drastically reduced also in the tropical South Atlantic (SATL).

Observational studies have hypothesized the existence of an Atlantic Multidicadal Oscillation (AMO; e.g., Delworth and Mann 2000), which modulating the Atlantic SST might influence the low-frequency variation of the TC activity in this region (Goldenberg et al. 2001). If the model produces an AMO-like variation of the SSTs and a consequent modulation of the Atlantic TC frequency, then the changes found in the TC number and shown in Fig. 8 could be due to a low-frequency "natural" oscillation of the storm activity. The time series of the number of TCs in the North Atlantic have been computed for 90 years of the PREIND climate simulation and the 4CO2 experiment. In the PREIND case, the series shows a pronounced decadal variation of the TC number, apparently much more pronounced than in the 4CO2 case. However, the amplitude of the oscillation is much smaller than the differences between 4CO2 and PREIND and also during the phases of lower TC activity, the number of storms in the PREIND experiment is higher

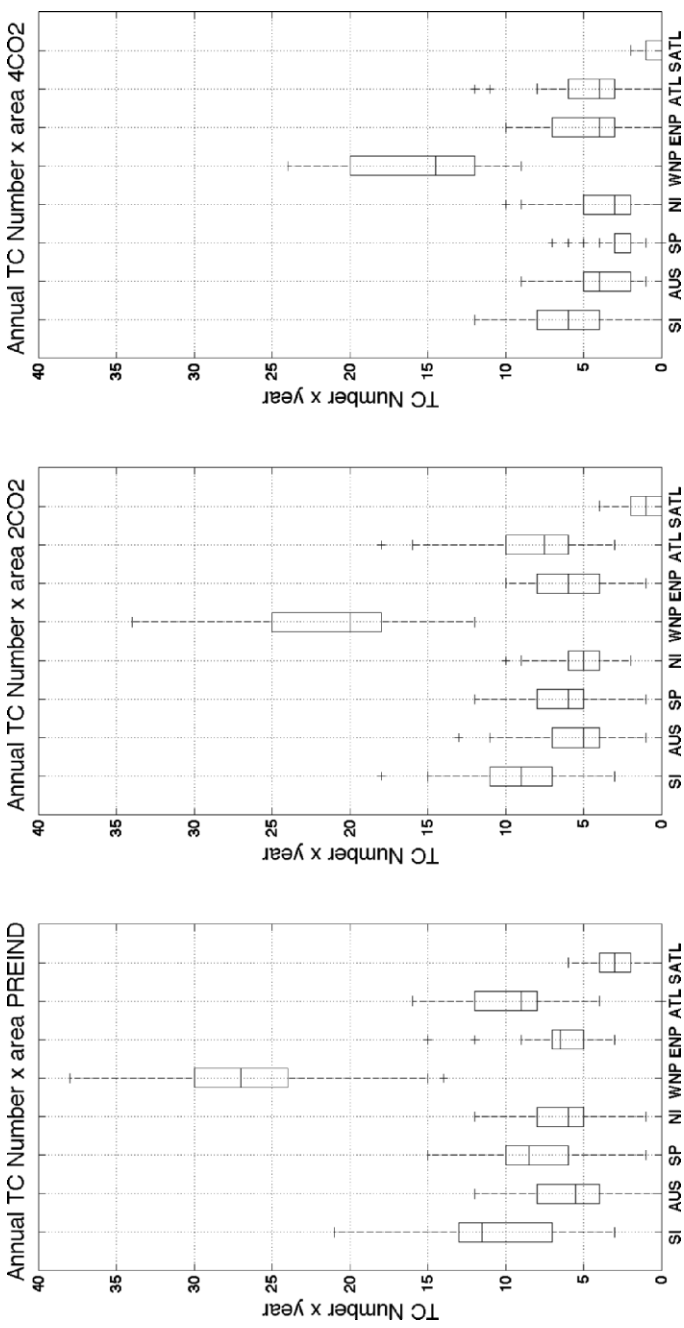

Fig. 8 Box plot of the annual number of TCs in the areas defined in Fig. 4 and for the tropical South-Atlantic (SATL) region. *Left panel*: PREIND experiment; *middle panel*: 2CO2 experiment; *right panel*: 4CO2 experiment

then in the 4CO2 one. Therefore, even considering the model "natural" (internal) low-frequency modulation of the TC activity, the number of TCs in the PREIND climate is systematically larger than in the 4CO2 case. This result suggests that the marked reduction of Atlantic TC number in the 4CO2 experiment is most likely ascribable to the greenhouse warming.

Generally, it is accepted that TCs tend to develop over oceanic warm waters. Specifically, climatological studies (e.g., Palmen 1948) indicate that the SST has to be warmer than about 26°C. The overall warming of the SST shown in Fig. 7, implies a poleward migration of the 26°C isotherm, therefore, one could expect to find a poleward extension of the TC activity in a warmer climate.

Figure 9 shows the zonal average of the total number of simulated TCs (left panels, dashed lines) and number of TC days (right panels, dashed lines) along with the zonal mean SST (solid lines) for the three experiments, PREIND (upper panels), 2CO2 (middle panels) and 4CO2 (lower panels). In the PREIND case the zonal mean SST threshold for TC occurrence appears to be between 25 and 26°C. The maximum number of TCs and TC days occur slightly equatorward of 20° latitude in both Hemispheres.

Increasing the atmospheric CO2 (middle and lower panels) the 26°C isotherm migrates poleward, on average, of almost 10° of latitude, but the latitudinal distribution of the number of TCs and TC days do not appear to be substantially changed. The maxima of TC occurrence, though reduced, still appears to be confined equatorward of 20° latitude, and the number of TC days tends to vanish poleward of 30° latitude. On the other hand, the zonal mean SST threshold for TC occurrence increases to about 28°C and almost 30°C for the 2CO2 and 4CO2 cases respectively. These results, in agreement with previous works (e.g., Haarsma et al. 1993, Henderson-Sellers et al. 1998) suggest that the poleward migration of warm SSTs caused by the greenhouse global warming does not imply an extension of the regions of cyclogenesis or TC activities towards the middle latitudes. Similar findings for the relationship between SSTs and convective precipitation have been indicated by Dutton et al. 2000.

In order to assess possible modifications in the strength of the simulated TCs, we have analyzed the changes in intensity of both low-level winds, minimum surface pressure and precipitation associated with the model TCs. The intensity of the TC low-level wind has been analyzed using the PDI (power dissipation index) proposed by Emanuel (2005), whereas as an index of intensity of TC precipitation we consider the rainfall averaged over a 4 by 4 grid point area around the centre of the cyclone and over the duration of the event.

When the pdf (probability density function) of the PDI for the three experiments is computed and plotted (not shown), the curves do not show significant differences. Similar results are obtained from the pdf of the lowest TC minimum surface pressure (not shown). Thus, in terms of strength of the near-surface wind, the changes in atmospheric CO2 do not appear to alterate the intensity of the simulated TCs. Simulations performed with very high resolution atmospheric models, on the other hand, showed that in a warmer climate the pdf of TC intensity shifts to higher values, with a decrease of the weaker cyclones and an increment of the most intense

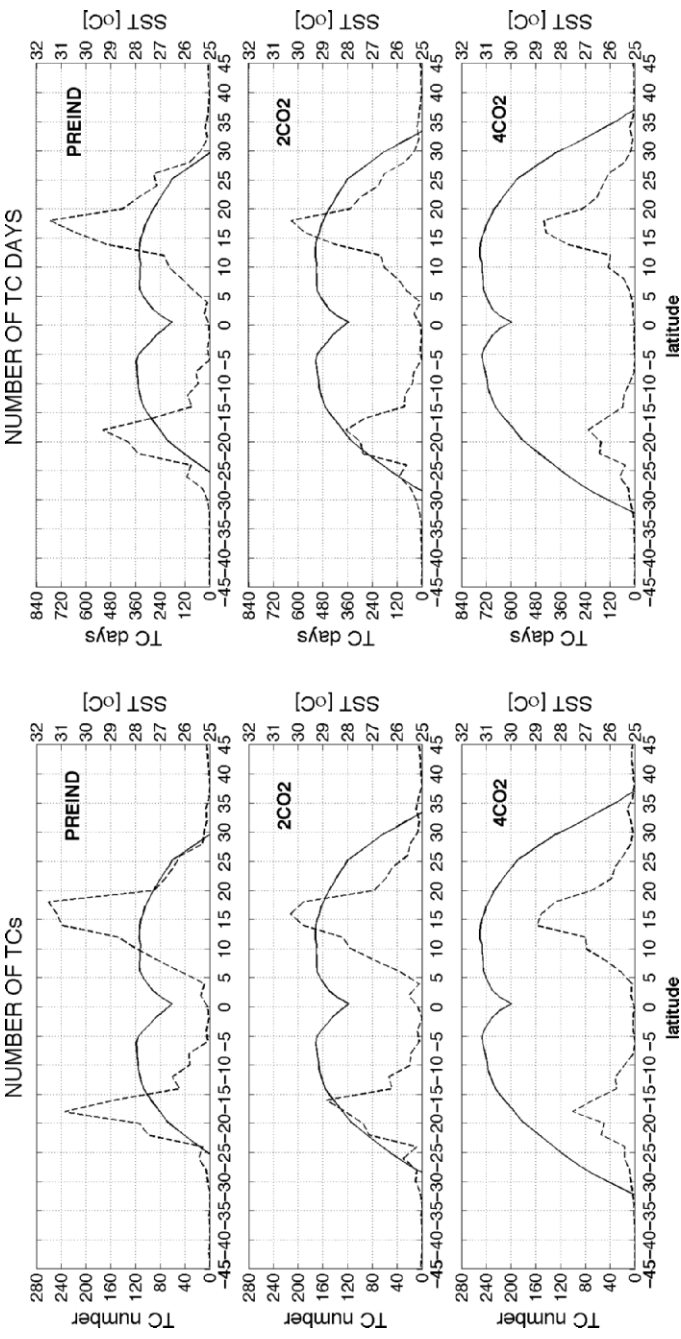

Fig. 9 Latitudinal distribution of the total number of simulated TCs (*left panels*), TC days (*right panels*) and zonal mean value of SST for the PREIND experiment (*upper panels*), the 2CO2 case (*middle panels*) and the 4CO2 experiment (*lower panels*). On the x-axis is the latitude. The y-axis on the left show the number of TCs and TC days and on the right the SST value. The dashed curves show the meridional distribution of the total number of TCs and TC days, with maxima centred between 15° and 20° latitude in both the Hemispheres. The solid curves show the distribution of the zonal mean SST. The two curves indicate, for each latitude, the number of TCs and the number of TC days and the corresponding values of SST

ones (Knutson et al. 2004, Oouchi et al. 2006, Bengtsson et al. 2007). In particular, Bengtsson et al. (2007) have shown that the shift becomes more evident increasing the model horizontal resolution. We think that this shift does not occur in our simulations because of thes deficiencies that our model appears to have in simulating intense events. It is likely, in fact, that the model produces the most intense TCs that is capable of simulating even in the PREIND climate, at least in terms of surface wind and minimum surface pressure. Therefore, the apparent lack of impact of the global warming on the simulated PDI and surface pressure, might be actually due to the difficulties of the model in representing the TC intensity, which in turn are probably ascribable to the too coarse resolution.

Different findings are obtained when we use the precipitation field to quantify the intensity of the model TCs. Fig. 10 shows the pdf of precipitation (total, convective and non-convective) associated with a model TC for four different regions of activity and for the three experiments. In all of the cases, the maximum of pdf appears to shift to higher values of rainfall when the CO2 increases, indicating that in general in a warmer climate the TCs tend to be accompanied by more intense precipitation.

To further confirm these findings, in Fig. 11 the composite of TC precipitation are shown. The composite represents the mean rainfall rate averaged over the TC life time and over the number of TCs for the considered regions. The means have been computed for a domain centered on the core of the cyclones and extending 5° each side. The shaded patterns show the composites of TC rainfall for the PREIND case, whereas the contours are the difference between the composite 2CO2-PREIND (upper panels) and 4CO2-PREIND (lower panels), for the WNP region (left panels) and the ATL region (right panels). Using a boot-strap technique, the changes shown in Fig. 11 are found to be statistically significant, and suggest that the amount of TC rainfall, on average, becomes larger as a consequence of the greenhouse warming. These results are consistent with the findings of Knutson and Tuleya (2004), Bengtsson et al. (2007), Chauvin et al. (2006), for the Atlantic hurricanes, and Yoshimura et al. (2006), who used a high-resolution atmospheric only model.

Discussion

In Section 4, it has been shown that, in general, the frequency of the simulated TCs is substantially and significantly reduced when the concentration of atmospheric CO2 is increased. In order to understand this result, we discuss here how the global warming affects those characteristics of the tropical atmosphere which are of relevance for the development of the TCs. In particular, we consider the two major basic mechanisms, dynamical and thermodynamical, that can oppose the development, and hence the occurrence, of these phenomena: the vertical wind shear and the stability of the atmosphere.

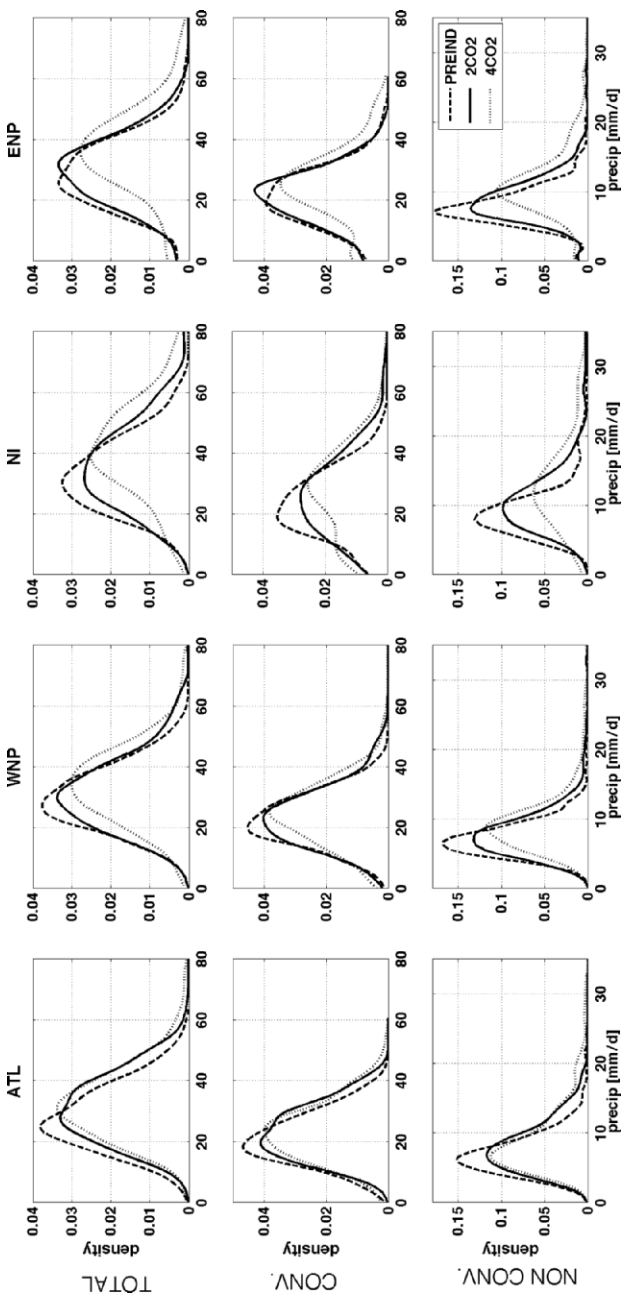

Fig. 10 Probability density function (PDF) of total precipitation (*upper row*), convective precipitation (*middle row*) and large scale precipitation (*bottom row*) associated with the simulated TCs in the different regions for the PREIND case (*dashed line*), 2CO2 case (*solid line*) and 4CO2 experiment (*dotted line*). On the x-axis is the value of precipitation in mm/day. On the y-axis is the (density of) frequency of events corresponding to a certain amount of rainfall

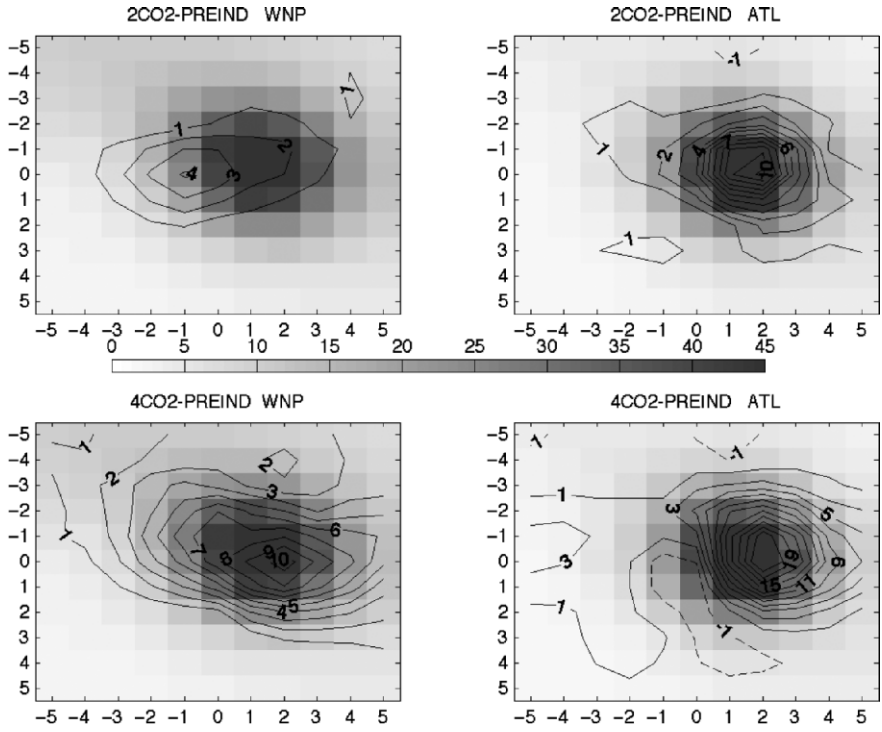

Fig. 11 *Left panels*: composite of TC precipitation for the PREIND experiment over the WNP region (*shaded pattern*) along with the difference 2CO2-PREIND (*upper panel*) and 4CO2-PREIND (*lower panel*) shown by the contour patterns. The composites represent the mean rainfall rate averaged over the TC life time and over the number of TCs for the considered regions. The means have been computed for a domain centered on the core of the cyclones and extending 5° each side. *Right panels*: as for the left panels but for the ATL region. The PREIND rainfall composite (*shaded patterns*) have a shaded contour interval of 5 mm/day. The difference between the 2CO2 and PREIND composite and the 4CO2 and PREIND composite (*contour patterns*) have a contour interval of 1 mm/day. The contour lines show only the values that are statistically significant at a 95% level. The significance test has been performed using the bootstrap method

It is well known that the vertical wind shear is one of the dynamical parameters that controls the formation of TCs. Specifically, strong large scale vertical wind shear represent unfavorable environmental conditions to the development of TCs (Gray 1968, Emanuel 2003). Therefore, a change in the climatological wind shear induced by greenhouse warming over a certain region might affect the TC frequency there.

Figure 12 shows the vertical wind shear for the PREIND and 4CO2 experiments and the difference 4CO2-PREIND (for the sake of brevity, we omit the 2CO2 experiment, whose results are fully consistent with the 4CO2 case, though with smaller amplitudes). Here, the wind shear is defined as the absolute value of the vector wind difference at 300 hPa and 850 hPa (i.e., winds shear = sqrt{(u_{300}-u_{850})^2+(v_{300}–v_{850})^2}). Both in the PREIND and 4CO2 case, the

Tropics are characterized by a minimum of vertical wind shear, which is particularly weak in the summer hemisphere. The difference 4CO2-PREIND (bottom panels) indicates a general reduction of the wind shear over most of the Tropics. This result is in agreement with previous studies, which have shown the weakening of the tropical circulation with the increasing of the atmospheric CO2 (e.g. Knutson and Manabe 1995, Vecchi and Soden 2007a).

A notable exception is the reinforcement of the vertical wind shear in the 4CO2 experiment visible both in winter and in summer over the north tropical Atlantic. The increase of the tropical Atlantic wind shear in a warmer climate is consistent with the findings of Vecchi and Soden 2007b, and might be one of the possible causes of the TCs reduction found over this area. Interestingly, the warming patterns in the tropical Pacific SSTs found in the 4CO2 case (Fig. 7) resemble the SST anomalies occurring during El Niño events. It is known that ENSO affects the TC activity over the north tropical Atlantic and one hypothesized mechanism is

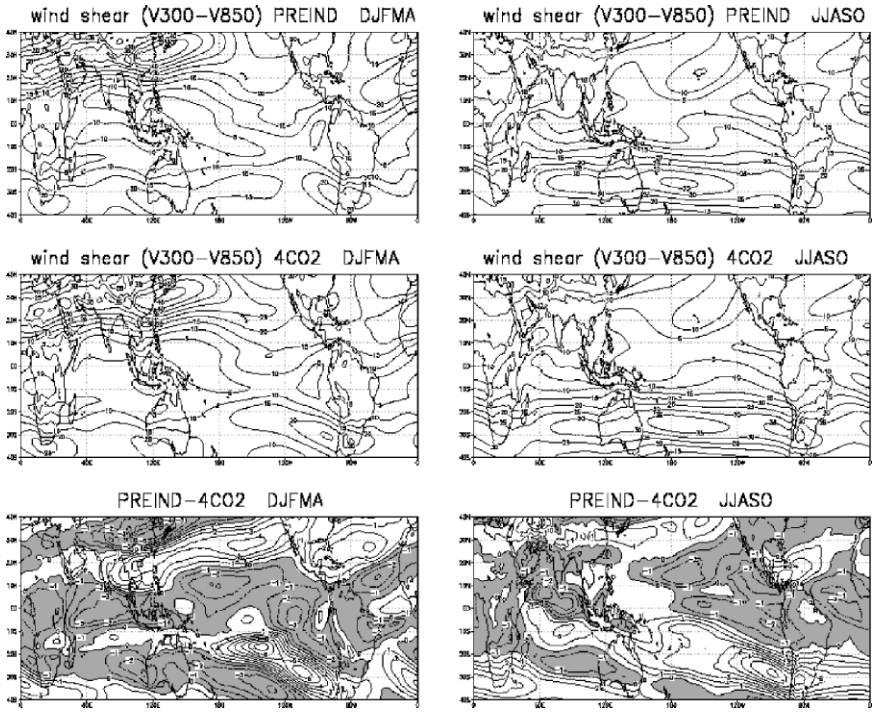

Fig. 12 Seasonal mean of the vertical wind shear defined as the difference between the wind at 300 hPa and at 850 hPa (winds shear = sqrt{(u_{300}-u_{850})^2+(v_{300}–v_{850})^2}). On the left panels are the results for the Southern Hemisphere extended summer (DJFMA), whereas on the right panels the values for the Northern Hemisphere extended summer (JJASO). The upper panels show the fields for the PREIND experiment. The middle panels the results from the 4CO2 experiments. For these plots, the contour interval is 5 m/s. The lower panels show the difference between the 4CO2 and the PREIND case. For these plots the contour interval is 1 m/s and negative values are shaded

the modulation of the vertical wind shear strength (Goldenberg and Shapiro 1996). Therefore, the stronger response of the tropical eastern Pacific SSTs to the global warming might induce a reduction of the TC activity in the ATL region in a way (and through mechanisms) similar to the influence exerted by El Niño (see also Aiyyer and Thorncroft 2006, Latif et al. 2007).

The strengthening of the vertical wind shear, however, does not explain the reduction of the TCs over the WNP. Fig. 12, in fact, shows that the wind shear reinforces over this region only during the northern winter, whereas it remains substantially unalterated in boreal summer, i.e. the TC season for this area. Therefore, there must be some other explanation for the reduced TC activity in this area.

Another important parameter that may regulate the development of TCs is the vertical stability of the atmospheric column (e.g., Gray 1979, DeMaria 2001). If the atmosphere becomes more stable, the occurrence of phenomena based on the development of organized convective systems, such as TCs, becomes more unlikely. In Section 4.1, it has been shown that the increase of atmospheric CO2 is accompanied by a reduction of the convective precipitation in the Tropics. The latter, in turn, might be the sign of an increase of the vertical stability in this region. In order to investigate possible changes in the stability of the tropical troposphere, we have assessed how the Convective Available Potential Energy (CAPE) and the Convective Inhibition (CIN) (Stevens, 2005) might be affected by the greenhouse warming.

The annual mean values of CAPE and CIN have been computed for the three experiments. The results (not shown) indicate that, in general, CAPE tends to increase with the increasing of CO2 over most of the Tropics. Exceptions are found in the eastern equatorial Indian Ocean, subtropical eastern Pacific and central Atlantic, where a slight reduction of CAPE is recorded. Table 5 shows the mean value of CAPE computed over the Tropics and over the tropical oceans only. When the atmospheric CO2 concentration is doubled, on average CAPE has increased by about 20% over the Tropics and 17% over the tropical oceans, with respect to the PREIND case. The further doubling of CO2 (4CO2) leads to only a slight increase of CAPE (3% with respect to 2CO2 and 24% with respect to PREIND) in the tropical belt. However, even more interesting, over the tropical oceans, the 4CO2 CAPE increases only by about 15% compared to the PREIND value and decreases by about 2% compared to the 2CO2 case. Therefore, the increment of tropical CAPE that appears to accompany the doubling of atmospheric CO2 seems to saturate, especially over the oceans, when the CO2 concentration is further augmented.

Table 5 shows also the mean value of CIN. Similarly to CAPE, also CIN tends to increase with the CO2 concentration, and at an even greater rate. However, different from CAPE, CIN does not appear to saturate when the CO2 concentration is quadrupled. Therefore, in the model, the increased atmospheric CO2 appears to cause an increase of CAPE, i.e. an augmented conditional instability, but also an even more pronounced increment of CIN, i.e. a higher energy barrier preventing the convection from occurring spontaneously.

Figure 13 shows the pdf of the level of free convection (LFC) for the PREIND, 2CO2 and 4CO2 cases over the WNP and ATL areas. The results suggest that the LFC tends to be higher when the atmospheric CO2 concentration increases. Con-

Table 5 Spatial average of mean convective available potential energy (CAPE) and mean convective inhibition (CIN). The mean CAPE and CIN are obtained by averaging over the 30-year periods of the PREIND, 2CO2 and 4CO2 experiments. The spatial average are computed over the whole tropical belt and over the tropical oceans only. Values in parenthesis are the percent increment with respect to the PREIND case

	PREIND	2CO2	4CO2
CAPE Tropical mean (J/Kg)	109.09	131.39 (+20%)	135.24 (+24%)
CAPE Tropical oceans only (J/Kg)	132.41	155.21 (+17%)	152.40 (+15%)
CIN Tropical mean (J/Kg)	13.06	16.04 (+23%)	18.73 (+43%)
CIN Tropical oceans only (J/Kg)	8.16	9.85 (+21%)	11.46 (+40%)

sistent with the larger CIN, the effects of the higher LFCs is to reduce the chance for convective instabilities to develop.

The generally larger potential energy barrier (CIN) and the shift of the LFC to higher levels, making less likely the development of convective systems, might be responsible for both the general diminishing of convective precipitation and, at least in part, for the reduced occurrence of TCs, especially in the WNP region. For the ATL region, on the other hand, the decreased number of TCs appears to be probably due to both the increased vertical wind shear and the reduced instability of the atmosphere.

Importantly, the reduction of the convective activity suggested by the results of this work is fully consistent with the findings of other studies, where the effects of atmospheric CO2 concentration on the tropical convection have been investigated (e.g., Knutson and Manabe 1995, Sugi and Yoshimura 2004, Held and Soden 2006, Vecchi and Soden 2007a).

The warming of the tropical troposphere is accompanied by an increase of water vapor, especially in the lower layers (not shown), which, in general, leads to an increase of the potential energy available for convection. In fact, as we have seen in Table 5, the tropical CAPE increases in the 2CO2 and 4CO2 experiments compared with the PREIND case. Therefore, when convection occurs it has more potential energy available and the events might be more intense. In other words, the increase of CIN makes the triggering of convective episodes more difficult, but the larger CAPE makes the convective episodes stronger. This might explain the increased intensity of TC precipitation, found in Section 4.2 (Fig. 10 and Fig. 11).

In order to further substantiate our findings, we have assessed how other (empirical) indices related to the TC activity are changed as a consequence of the greenhouse warming. Specifically, parameters like the mid-tropospheric relative humidity over the oceans, the maximum potential index (MPI, Bister and Emanuel 2002) and the genesis potential (GP) index (Emanuel and Nolan, 2004) have been found to be related with the TC activity (e.g., Camargo et al. 2004). In Fig. 14 we show the differences between the 30-year mean values of these parameters from the 4CO2 and the PREIND case.

The tropical mean of the 4CO2-PREIND difference of the 700-hPa relative humidity (RH700) exhibits a very small increase, consistent with Held and Soden 2007. However, locally some considerable change is visible (Fig. 14, upper panels).

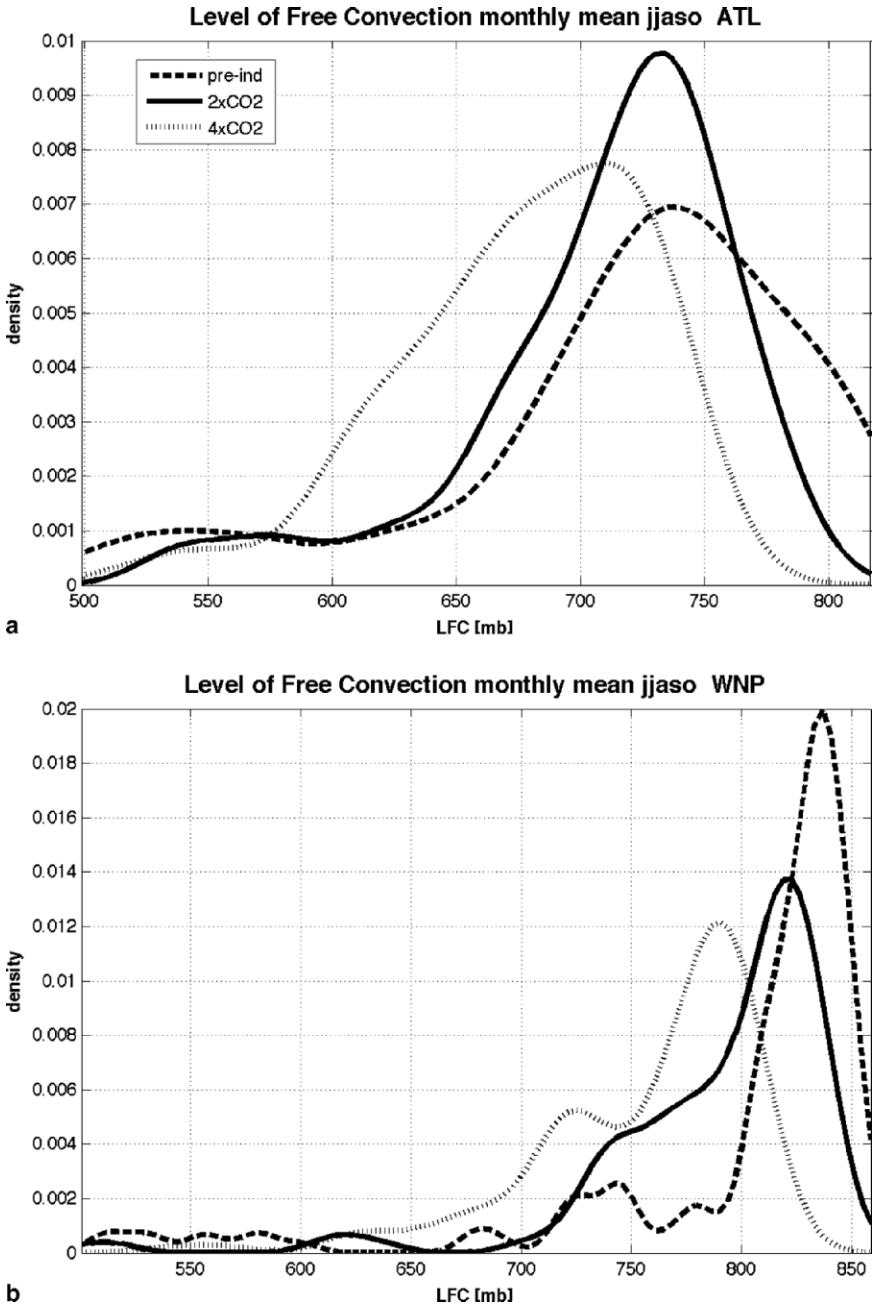

Fig. 13 Probability density function (PDF) of the level of free convection (LFC) for the PREIND case (*dashed line*), the 2CO2 case (*solid line*) and the 4CO2 experiment (*dotted curve*) over the ATL region (*panel a*) and the WNP region (*panel b*) during northern summer (JJASO). On the x-axis is the value of vertical levels in Millibar (mb), and on the y-axis is the (density of) frequency of occurrence at which free convection can be triggered at that level

A substantial increase, for example, is found in the equatorial band of the Pacific ocean, whereas reductions are found the tropical Indian Ocean, subtropical Pacific and Atlantic oceans. In northern summer (left panel), the RH700 appears to decrease in the North Atlantic, whereas a very slight increased is found in the WNP region.

When averaged over the Tropics, the MPI difference (panels c and d) shows a reduction of this index. Consistent with Vecchi and Soden (2007b), the patterns of MPI change are similar to the patterns of SST change (Fig. 7). MPI increases (decreases) over the region where the SST warming is more (less) intense. Thus, substantial increase of MPI is found in the equatorial Pacific and western Indian Ocean, while the index decreases over the southern Pacific, eastern Indian Ocean, WNP and tropical Atlantic, especially during northern summer (left panel).

The 4CO2-PREIND difference of the GP index (lower panels) reveals an increase of this parameter in the tropical Pacific, north of the equator, during northern summer. In most of the WNP sector, the difference is not statistically significant, though there is a portion of the region where the GP exhibits a significant increment. The increase is more pronounced in the central-eastern North Pacific. Noteworthy, from the results shown in Section 4 (e.g., Fig. 8), this is also the region where the TC activity does not appear to be reduced by the CO2 increase.

Overall, the results obtained from the parameters shown in Fig. 14 are consistent with the findings we obtained with the TC tracking methods described in Section 2.4. The agreement appears to be particularly evident in the ATL region, where all of the empirical parameters suggest a reduction of the TC activity, consistent with the results shown in Section 4. In the WNP area, on the other hand, the agreement is less obvious. While the MPI shows a slight but visible decrease, the GP index exhibits some increment, especially in the eastern part.

Summary

In this study, a fully coupled high-resolution AOGCM has been used to investigate the possible impacts of greenhouse global warming on the characteristics of tropical cyclones. To our knowledge, this is the first time the impact of global warming on TCs is investigated by means of a state of the art fully coupled GCM.

The simulated TCs have many, basic, gross features similar to the observed ones. However, the rather low intensity of the low-level winds and the too large distance between the cyclone eye and the wind maximum remain unsatisfactory. These shortcomings are likely due to the model resolution, which, though rather high for long climate simulations, is still too coarse for an adequate representation of the tight structures accompanying these phenomena. Despite these problems, the model seems to be able to simulate a reasonable realistic climatology of TCs, both in terms of spatial distribution, seasonal and interannual variability of the TC activity. In particular, the model appears to capture at least some of the links between SST interannual variability and TC activity.

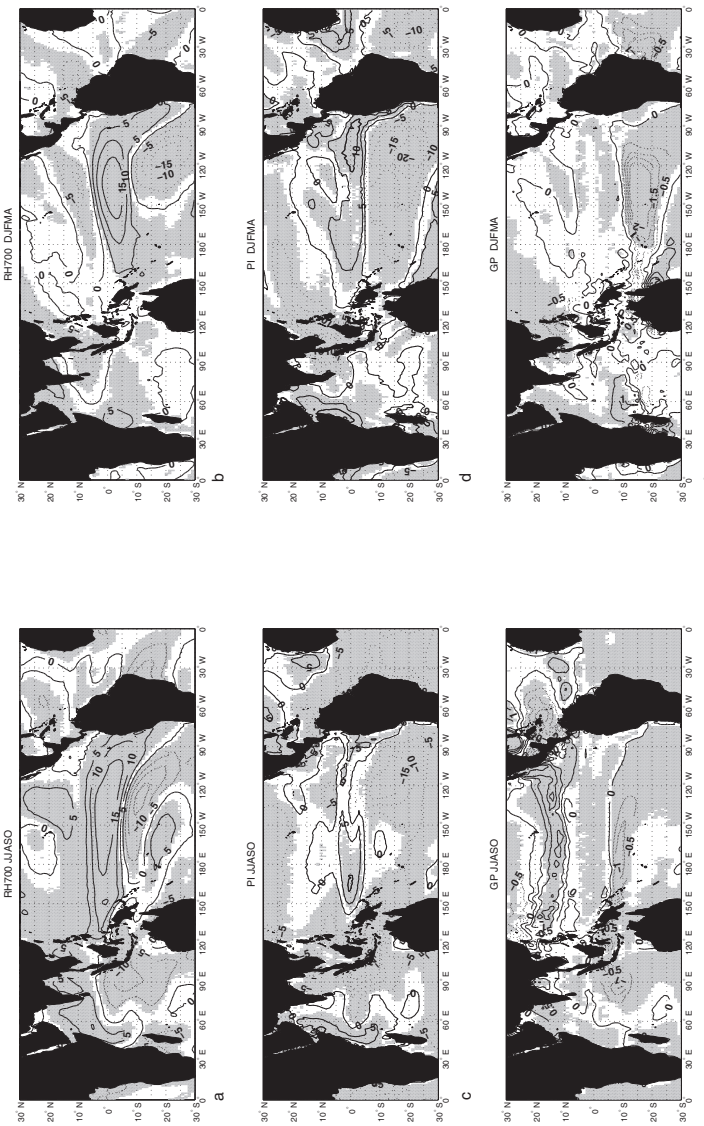

Fig. 14 4CO2-PREIND differences of the mean values of 700-hPa relative humidity (RH700, panels **a** and **b**); maximum potential index (MPI, panels **c** and **d**) and genesis potential index (GP, panels **e** and **f**). *Left panels*: northern summer; *right panels*: northern winter. The RH is expressed in %, the MPI in m/s and the GP index in (number of TC)/(unit area x decade). Only statistically significant at a 95% level contours are shown. The significance test has been performed using the boot-strap method

The enhanced concentration of atmospheric CO2 induces a warming of the entire tropical and subtropical upper ocean, accompanied by a redistribution of the tropical rainfall. The increase of the tropical ocean surface temperature, however, is not uniform, and the eastern Pacific exhibits a more pronounced warming with patterns that resemble El Niño SST anomalies. The total precipitation averaged over the Tropics increases with the CO2 increase, but the convective precipitation exhibits a significant reduction.

Along with the attenuated convective activity, our simulations show a substantial and significant reduction of the number of generated TCs, especially over the North West Pacific and North Atlantic tropical regions. Both the decrease in convective activity and and the reduced occurrence of TCs might be due to the larger potential energy barrier found when the CO2 concentration is increased. In the reduction of the TC activity in the ATL region, however, an important role appears to be played also by a considerable increase of the vertical wind shear.

The greenhouse warming is associated with a poleward expansion of the tropical warm SSTs. In particular, the 26°C isotherm, that appears to be crucial for the development of the TCs in the present climate, in the 4CO2 case migrates poleward of almost 10° latitude compared to the PREIND one. In the model, however, the warming of the subtropical and mid-latitudes is not accompanied by a poleward extension of the TC action, consistent with earlier works. The peaks of TC activity remain substantially confined equatorward of 20° latitude in both the Hemispheres.

Despite the reduced number of TCs generated when the CO2 has doubled and quadrupled, there is evidence of an increase in their intensity in terms of precipitation. This might be related with the increase of CAPE found in the warmer climate. The intensity of the simulated TCs expressed in terms of near-surface wind (PDI) and surface pressure, on the other hand, does not appear to be significantly affected by the global warming. However, we think that this result might be actually related to the deficiencies that the model exhibits in reproducing realistic TC intensities.

Acknowledgments The authors are indebted to Gabriel Vecchi, Chiara Cagnazzo and Andrea Alessandri for their precious help, useful suggestions and stimulating discussions. They also want to thank the three anonymous reviewers for their suggestions and constructive criticisms and K. Emanuel for making available the routines to compute the maximum potential index, MPI (http://wind.mit.edu/∼emanuel/home.html). This work has been supported by the Euro-Mediterranean Centre for Climate Change and by the European Community project ENSEMBLES, contract number GOCE-CT-2003-505539.

References

Anthes R.A., Corell R.W., Holland G., Hurrel J.W., MacCracken M.C., and K.E. Trenberth, 2006: Hurricanes and Global Warming - Potential Linkages and Consequences. *Bull. Am. Meteor. Soc.*, DOI:10.1175/BAMS-87-5-617.

Aiyyer, A.R., and C. Thorncroft 2006: Climatology of vertical wind shear over the tropical Atlantic *J. of Clim.*, **19**, 2969–2983.

Behera S.K., J.J. Luo JJ, S. Masson, P. Delecluse, S. Gualdi, A. Navarra, T. Yamagata, 2005 Paramount impact of the Indian Ocean dipole on the East African short rains: A CGCM study. *J. of Clim.*, **18**, 4514–4530.

Bengtsson L., M. Botzet, M. Esch, 1995: Hurricane–type vortices in a general–circulation model. *Tellus-A*, **47**, 175–196.

Bengtsson L., M. Botzet, M. Esch, 1996: Will greenhouse gas–induced warming over the next 50 years lead to higher frequency and greater intensity of hurricanes? *Tellus-A*, **48**, 57–73.

Bengtsson L., K.I. Hodges, M. Esch, N. Keenlyside, L. Kornblueh, J.-J. Luo, and T. Yamagata, 2007: How may tropical cyclones change in a warmer climate? *Tellus-A*, **59**, 539–561.

Bister M. and K.A. Emanuel, 2002: Low frequency variability of tropical cyclone potential intensity. 1. Interannual to interdecadal variability. *J. Geophys. Res.*, **107**, 4801, doi:10.1029/2001JD000776.

Blanke B., P. Delecluse, 1993: Low frequency variability of the tropical Atlantic ocean simulated by a general circulation model with mixed layer physics. *J. Phys. Oceanogr.*, **23**, 1363–1388.

Broccoli A.J., and S. Manabe, 1990: Can existing climate models be used to study anthropogenic changes in tropical cyclone climate. *Geophys. Res. Lett.*, **17**, 1917–1920.

Camargo S.J., A.G. Barnston, and S.E. Zebiak, 2004: Properties of Tropical Cyclones in atmospheric general circulation models. IRI Tech. Rep. 04–02, International Research Institute for Climate Prediction, Palisades, N.Y. 72 pp.

Chan J.C.-L., 2000: Tropical cyclone activity over the western North Pacific associated with El Niño and La Niña events. *J. of Clim.*, **13**, 2960–2972.

Chauvin F., J.-F. Royer, and M. Deque, 2006: Response of hurricane-type vortices to global warming as simulated by ARPEGE-Climat at high resolution. *Clim. Dyn.*, **27**, 377–399.

Chia H.H, and C.F. Ropelewski, 2002: The interannual variability in the genesis location of tropical cyclones in the northwest Pacific. *J. of Clim.*, **15**, 2934–2944.

Delworth T.L., and M.E. Mann, 2000: Observed and simulated multidecadal variability in the Northern Hemisphere *Clim. Dyn.*, **16**, 661–676.

De Maria, M, J.A. Knaff, and B.H. Connell, 2001: A Tropical Cyclone Genesis Parameter for the Tropical Atlantic. *Weath. Forec.*, **16**, 219–233.

Dutton, J. F., C. J. Poulsen, J. L Evans, 2000: The effect of global climate change on the region of tropical convection in CSM1. *Gophys. Res. Lett.*, **27**, 3049–3052.

Elsner J.B., and B. Kocher, 2000: Global tropical cyclone activity: A link to the North Atlantic Oscillation. *Geophys. Res. Lett.*, **27**, 129–132.

Emanuel K.A., 1987: The dependence of hurricane intensity on climate. *Nature*, **326**, 483–485.

Emanuel K.A., 2003: Tropical Cyclones. *Annu. Rev. Earth Planet. Sci.*, **31**, 75–104.

Emanuel K.A., and D.S. Nolan, 2004: Tropical cyclone activity and global climate. Preprints, *26th Conf. on Hurricanes and Tropical Meteorology*, Miami, FL., Amer. Meteor. Soc., 240–241.

Emanuel K.A., 2005: Increasing destructiveness of tropical Cyclones over the past 30 years. *Nature*, **436**, 686–688.

Fichefet T, M. A. Morales-Maqueda, 1999: Modelling the influence of snow accumulation and snow–ice formation on the seasonal cycle of the Antarctic sea-ice cover. *Clim. Dyn.*, **15**, 251–268.

Frank W.M., 1977: The structure and energetics of the Tropical Cyclone I. The Storm structure. *Mon. Wea. Rev.*, **105**, 1119–1135.

Frank W.M., and G.S. Young, 2007: The Interannual Variability of Tropical Cyclones. *Mon. Wea. Rev.*, **135**, 3587–3598.

Gent P.R., and J.C. McWilliams, 1990: Isopycnal mixing in ocean circulation models. *J. Phys. Ocean.*, **20**, 150–155.

Goldenberg S.B., C.W. Landsea, A.M. Mestas-Nunez, and W.M Gray, 2001: The recent increase in the Atlantic hurricane activity: causes and implications. *Science*, **293**, 474–479.

Goldenberg S.B., L.J. Shapiro, 1996: Physical mechanisms for the association of El Niño and west African rainfall with Atlantic major hurricane activity. *J. of Clim*, **9**, 1169–1187.

Gray W.M., 1968: Global view of the origin of tropical disturbances and storms. *Mon. Wea. Rev*., **96**, 669–700.

Gray W.M., 1979: Hurricanes: Their formation, structure and likely role in the tropical circulation. *Meteorology over the Tropical Oceans*, D.B. Shaw (Ed.), Royal Meteorological Society, 155–218.

Gray W.M., 1984: Atlantic seasonal hurricane frequency .1. El-Nino and 30-mb Quasi–biennial oscillation influences. *Mon. Weather Rev*., **112**, 1649–1668.

Gualdi, S., A. Navarra, E. Guilyardi, and P. Delecluse, 2003a: Assessment of the tropical Indo-Pacific climate in the SINTEX CGCM, *Ann. Geophysics*, **46**, 1–26.

Gualdi, S., E. Guilyardi, A. Navarra, S. Masina, and P. Delecluse, 2003b: The interannual variability in the tropical Indian Ocean as simulated by a CGCM. *Clim. Dyn*., **20**, 567–582.

Gualdi, S., E. Scoccimarro, A. Navarra, 2008: Changes in Tropical Cyclone Activity due to Global Warming: Results from a High-Resolution Coupled General Circulation Model. *J. Climate*., **21**, 5204–5228.

Guilyardi, E., P. Delecluse, S. Gualdi, and A. Navarra, 2003: Mechanisms for ENSO phase change in a coupled GCM, *J. of Clim*., **16**, 1141–1158.

Haarsma R.J., J.F.B. Mitchell, C.A. Senior, 1993: Tropical disturbances in a GCM. *Clim. Dyn*., **8**, 247–257.

Held I.M., and B.J. Soden, 2006: Robust responses of the hydrological cycle to global warming. *J. of Clim*., **19**, 5686–5699.

Henderson-Sellers A, H. Zhang, G. Berz, K.A. Emanuel, W. Gray, C. Landsea, G. Holland, J. Lighthill, S.L. Shieh, P. Webster, and K. McGuffie, 1998: Tropical cyclones and global climate change: A post-IPCC assessment. *Bull. Am. Meteor. Soc*., 79, 19–38.

Holland G.J., 1993: "Ready Reckoner" - Chapter 9, Global Guide to Tropical Cyclone Forecasting, WMO/TC-No. 560, Report No. TCP-31, World Meteorological Organization; Geneva, Switzerland.

Holland G.J., 1997: The maximum potential intensity of tropical cyclones. *J. Atmos. Sci*., **54**, 2519–2541.

Knutson T.R., and R.E. Tuleya, 2005: Reply. *J. of Clim*., **18**, 5183–5187.

Knutson T.R., and R.E. Tuleya, 2004: Impact of CO2 induced warming on simulated hurricane intensity and precipitation: sensitivity to the choice of climate model and convective parametrization. *J. of Clim*., **17**, 3477–3495.

Knutson T.R., R.E. Tuleya, W. Shen, and I. Ginis, 2001: Impact of CO2-induced warming on hurricane intensities simulated in a hurricane model with ocean coupling. *J. of Clim*., **14**, 2458–2468.

Knutson T.R., S. Manabe, 1995: Time-response over the tropical Pacific to increased CO2 in a coupled ocean atmosphere model. . *J. of Clim*., **8**, 2181–2199.

Landsea C.W., B.A. Harper, K. Hoarau, and J. Knaff, 2006: Can we detect trends in extreme tropical cyclones?, *Science*, **313**, 452–454.

Landsea C.W., 2007: Counting Atlantic Tropical Cyclones Back to 1900. *EOS*, **88**, 197–202.

Latif M., N. Keenlyside, J. Bader, 2007: Tropical sea surface temperature, vertical wind shear, and hurricane development. Geophys. *Res. Lett*., **34**, L01710.

Luo, J.-J., S. Masson, S. Behera, P. Delecluse, S. Gualdi, A. Navarra, and T. Yamagata, 2003: South Pacific origin of the decadal ENSO-like variation as simulated by a coupled GCM. *Geophys. Res. Lett*., **30**, 2250, doi:10.1029/2003GL018649.

Madec, G., P. Delecluse, M. Imbard, and C. Levy, 1998: OPA 8.1 Ocean General Circulation Model reference manual, Internal Rep. 11, Inst. Pierre–Simon Laplace, Paris, France.

Masson, S., J.-J. Luo, G. Madec, J. Viala*f*rd, F. Durand, S. Gualdi, E. Guilyardi, S. Behera, P. Delecluse, A. Navarra and T. Yamagata, 2005: Impact of barrier layer on winter-spring variability of the southeastern Arabian Sea. Geophys. *Res. Lett*., **32**, L07703, doi:10.1029/2004GL021980.

McDonald, R.E., D.G. Bleaken, D.R. Cresswell, 2005: Tropical storms: representation and diagnosis in climate models and the impacts of climate change. *Clim. Dyn.*, **25**, 19–36, doi:10.1007/s00382-004-0491-0

Michaels P.J., P.C. Knappenberger, and C Landsea, 2005: Comments on "impacts of CO2-induced warming on simulated hurricane intensity and precipitation: Sensitivity to the choice of climate model and convective scheme". *J. of Clim.*, **18**, 5179–5182.

Mocrette J.J., 1991: Radiation and cloud radiative properties in the European centre for medium range weather forecasts forecasting system. *J. Geophys. Res.*, **96**, 9121–9132.

Nordeng T.E., 1994: Extended versions of the convective parametrization scheme at ECMWF and their impact on the mean and transient activity of the model in the Tropics. ECMWF Research Department, Technical Memorandum No. 206, October 1994, European Center for Medium Range Weather Forecasts, Reading, UK, 41 p.

Oouchi K., J. Yoshimura, H. Yoshimura, R. Mizuta, S. Kusunoki, and N.A. Noda, 2006: Tropical cyclone climatology in a global-warming climate as simulated in a 20 km-mesh global atmospheric model: Frequency and wind intensity analyses. *J. Meteor. Soc. Japan*, **84**, 259–276.

Palmen, E., 1948: On the formation and structure of tropical hurricanes. *Geophysica*, **3**, 26–39.

Pezza A.B., and I Simmonds, 2005: The first South Atlantic hurricane: Unprecedented blocking, low shear and climate change. *Geophys. Res. Lett.*, **32**, L15712, doi:10.1029/2005GL023390.

Pielke Jr. R., C. Landsea, M. Mayfield, J. Laver, and R. Pasch, 2006: Reply to "Hurricanes and Global Warming - Potential Linkages and Consequences. *Bull. Am. Meteor. Soc.*, DOI:10.1175/BAMS-87-5-622.

Pielke Jr. R., C. Landsea, M. Mayfield, J. Laver, and R. Pasch, 2005: Hurricanes and Global Warming. *Bull. Am. Meteor. Soc.*, DOI:10.1175/BAMS-86-11-1571.

Rayner N.A., D.E. Parker, E.B. Horton, C.K. Folland, L.V. Alexander, D.P. Rowell, E.C. Kent, and A. Kaplan, 2003: Global analyses of sea surface temperature, sea ice, and night marine air temperature since the late nineteenth century. *J. Geophys. Res.*}, **108**, D14, 4407, doi:10.1029/2002JD002670.

Roeckner E, and Coauthors (1996) The atmospheric general circulation model Echam-4: model description and simulation of present-day climate. Max-Planck-Institut fur Meteorologie, Rep. No 218, Hamburg, Germany, 90 p.

Roullet G., and G. Madec, 2000: Salt conservation, free surface, and varying levels: a new formulation for ocean general circulation models. *J. Geophys. Res*, **105**, 23927–23942.

Royer J.-F., F. Chauvin, B. Timbal, P Araspin, and D. Grimal, 1998: A GCM study of the impact of greenhouse gas increase on the frequency of occurrence of tropical cyclones. *Clim Dyn.*, **38**, 307–343.

Stevens B., 2005: Atmospheric Moist Convection, 2005. *Annu.Rev.Earth Planet.Sci.*, **33**, 605–43, doi:10.1146/annurev.earth.33.092203.122658.

Sugi M., A. Noda, N. Sato, 2002: Influence of global warming on tropical cyclone climatology: an experiment with the JMA global model. *J. Meteor. Soc. Japan*, **80**, 249–272.

Sugi M., and J. Yoshimura, 2004: A mechanism of tropical precipitation change due to CO2 increase. *J. of Clim*, **17**, 238–243.

Tiedtke M., 1989: A comprehensive mass flux scheme for cumulus parametrization in large-scale models. *Mon. Weather Rev.*, **117**, 1779–1800.

Timmermann R., H. Goosse, G. Madec, T. Fichefet, C Ethe and V. Dulie're, On the representation of high latitude processes in the ORCALIM global coupled sea ice-ocean model, *Ocean Modell.*, **8**, 175–201, 2005.

Trenberth K., 2005: Uncertainty in Hurricanes and Global Warming. *Science*, **308**, 1753–1754.

Valke S, L. Terray, A. Piacentini, 2000: The OASIS coupled user guide version 2.4, Technical Report TR/ CMGC/00-10, CERFACS.

Vecchi G.A., B.J. Soden, 2007a: Global Warming and the Weakening of the Tropical Circulation. *J. of Clim.*, **20**, 4316–4340.

Vecchi G.A., B.J. Soden, 2007b: Increased tropical Atlantic wind shear in model projections of global warming. *Geophys. Res. Lett.*, **34**, L08702.

Walsh K.J.E, 1997: Objective detection of tropical cyclones in high–resolution analyses. *Mon. Weather Rev*., **120**, 958–977.

Walsh K.J.E., and B.F. Ryan, 2000: Tropical cyclone intensity increase near Australia as a result of climate change. *J. of Clim*., **13**, 3029–3036.

Walsh K.J.E., 2004: Tropical cyclones and climate change: unresolved issues. *Clim. Res*., **22**, 77–83.

Watterson I.G., J.L. Evans, and B.F. Ryan, 1995: Seasonal and interannual variability of tropical cyclogenesis: Diagnostics from large-scale fields. *J. of Clim*., **8**, 3052–3066.

Webster P.J., G.J. Holland, J.A. Curry, and H.-R. Chang, 2005: Changes in Tropical Cyclones Number, Duration and Intensity in a Warming Environment. *Science*, **309**, 1844–1846.

Willoughby H.E., J.A. Clos, M.G. Shoreibah, 1982: Concentric eye walls, secondary wind maxima, and the evolution of the hurricane vortex. *J. Atmos. Sci*., **39**, 395–411.

Xie P., and P. Arkin, 1997: Global precipitation: A 17-year monthly analysis based on gauge observations, satellite estimates, and numerical model outputs. *Bull. Am. Meteor. Soc*., **78**, 2539–2558.

Yoshimura J., M. Sigu, and A. Noda, 2006: Influence of greenhouse warming on tropical cyclone frequency. *J. Meteor. Soc. Japan*, **84**, 405–428.

Relationship between ENSO and North Atlantic Tropical Cyclone Frequency Simulated in a Coupled General Circulation Model

Satoshi Iizuka and Tomonori Matsuura

Abstract Relationship between El Niño / Southern Oscillation (ENSO) and tropical cyclone (TC) frequency over the North Atlantic simulated in a high-resolution (T213) coupled ocean-atmosphere general circulation model is described. The high-resolution model succeeded to simulate TCs with a maximum surface wind speed at 10 m more than 17 m/s. In La Niña (El Niño) years, the annual number of model TCs as well as hurricanes in the North Atlantic increases (decreases). The change seems to be related to that in the vertical wind shear over the North Atlantic accompanied by model ENSO. This relationship between ENSO and North Atlantic TC frequency is in agreement with observational evidence. Although there is no TCs with a maximum surface wind more than 43 m/s belonging to the category 2 on the Saffir-Simpson scale in this model, the present study suggests that a finer-resolution CGCM could become a powerful tool for understanding the future variability of TC intensity.

Introduction

It has been recognized that a large proportion of North Atlantic tropical cyclones (TCs) originate from Africa easterly waves that propagate westward from the western coast of North Africa at around 15°N, and eventually developing into TCs (e.g., Landsea 1993). The peak of TC formation in the North Atlantic happens during the months from August to October, and the mean annual number is about 10 but more than 10 since 1995 (e.g., Goldenberg et al. 2001). The frequency of Atlantic TCs is observed to have significant variability on a number of different timescales (e.g., Goldenberg et al. 2001). Although previous studies (Shapiro 1982a, b; Gray 1984) have identified several factors (e.g., quasi-biennial oscillation, Sahel rainfall) that appear to influence Atlantic TC activity, El Niño / Southern Oscillation (ENSO) give a significant impact on Atlantic TC frequency on the interannual timescales (e.g., Gray, 1984; Shapiro 1987). During El Niño years, the vertical wind shear over the North Atlantic is increased. The increased vertical wind

J.B. Elsner and T.H. Jagger (eds.), *Hurricanes and Climate Change,*
doi: 10.1007/978-0-387-09410-6,

shear helps to prevent tropical disturbances from developing into TCs, resulting in fewer TC formations. In La Niña years, there are more TCs than average because the vertical wind shear is reduced.

Manabe et al. (1970) first noted that a general circulation model (GCM) could reproduce vortices similar to observed TCs. Subsequently, Tsutsui and Kasahara (1996) confirmed that the seasonal and geographic variations of TC-like vortices reproduced observational TC statistics reasonably well even in a GCM with the horizontal resolution of approximately 300 km. While Wu and Lau (1992) examined the ability of GCM to reproduce the interannual variability of TC frequency, Vitart et al. (1997, 1999) explored the possibility of a GCM to forecast seasonal TC activity using an ensemble of integrations for the period 1980–88. The latter showed that their GCM was able to simulate a realistic interannual variability of tropical storm frequency over the North Atlantic. Vitart and Anderson (2001) further demonstrated that a GCM also has the ability to simulate the interdecadal variability of North Atlantic tropical storm frequency. These studies have showed the potential skills of a GCM in reproducing observed interannual variability of TC frequency and genesis location. However, the resolution of a GCM used by the above-mentioned studies is relatively coarse, and hence the intensity of model TCs is much weaker than in observations, and also there is the deficiency in tracks of model TCs (e.g., Vitart et al. 1997; Camargo et al. 2005).

In global warming experiments, the simulations of TCs using a high-resolution GCM are now becoming feasible (Sugi et al. 2002; Yoshimura et al. 2006; Oouchi et al. 2006; Bengtsson et al. 2007). They have reported that the models are successful in simulating intense TCs. However, an air-sea interaction is not considered in the models, which is one of the important factors controlling TC intensity (e.g., Emanuel, 1986). Recently Iizuka and Matsuura (2008) have examined the relationship between ENSO and TC activity in the western North Pacific simulated in a high-resolution ocean-atmosphere coupled GCM (CGCM) with a nearly 60km horizontal resolution. They have demonstrated that the model has the ability to simulate the ENSO impact not only on TC frequency and genesis location as in the previous studies but also on TC track and intensity reasonably well. In this paper, we document the interannual variations in TC frequency over the North Atlantic simulated in the same CGCM. The paper is organized as follows. A description of the model and data are given in Section 2. The model climatology is shown in Section 3. Section 4 presents the relationship between ENSO and TC activity over the North Atlantic simulated in the model. A summary is given in Section 5.

Model and Data

The atmospheric component of the CGCM used in the present study is the global spectral model that was previously used as a forecasting model at the Japan Meteorological Agency. In the horizontal direction, all variables are truncated at total wave number 213 (T213). There are 21 levels in the vertical from the surface to

approximately 10 hPa. The model includes comprehensive physical parameterizations: long wave radiation (Sugi et al. 1990), short wave radiation (Lacis and Hansen 1974), planetary boundary layer (Mellor and Yamada 1974), surface fluxes (Louis et al. 1982), SiB as a land surface model (Sellers et al. 1986; Sato et al. 1989), and gravity wave drag (Iwasaki et al. 1989). The cumulus convection scheme is based on the mass flux scheme proposed by Arakawa and Schubert (1974). The scheme is modified for entrainment rate (Moorthi and Suarez 1992) and for determination of mass flux at cloud base (Randall and Pan 1993; Lord et al. 1982). The cloud work function for each cloud type is relaxed back to a critical value taken from Lord and Arakawa (1980) over a fixed time scale. Detailed descriptions of the physical processes are given in Sugi et al. (1990) and in Kuma (1996).

The ocean component is based on the Southampton–East Anglia model (e.g., Killworth et al. 1991). The model domain covers all oceans except the Arctic Ocean, where the observed climatological sea surface temperatures (SSTs) and sea-ice distributions are prescribed as the boundary conditions of the atmospheric model. The horizontal resolution is 0.5625° in both longitude and latitude. There are 37 levels in the vertical direction, with the upper 400 m divided into 25 levels, making it well suited for investigating the upper layer of ocean. The coefficient of vertical mixing depends on the Richardson number, as in the parameterization proposed by Pacanowski and Philander (1981). The coefficients for both horizontal eddy viscosity and diffusivity are 1×10^7 cm^2 s^{-1}. The penetrative solar radiation is parameterized by using the formula of type I given in Paulson and Simpson (1977). The convection scheme introduced by Marotzke (1991) is used to immediately eliminate unstable conditions. The process for sea-ice and runoff is not considered in the ocean model.

The initial conditions for the atmospheric model were taken from the National Center for Environmental Prediction–National Center for Atmospheric Research (NCEP–NCAR) global atmospheric reanalysis data (Kalnay et al. 1996). Those of the ocean model were the state of rest with annual mean temperature and salinity distributions (Levitus 1982). Under these conditions, the atmospheric model and the ocean model were coupled through daily mean SSTs and surface fluxes. The CGCM was integrated for 100 years without flux correction, and we analyzed the results during a period from year 30 to year 100.

In order to validate the relationship between ENSO and TC activities in the CGCM, we use the best track data compiled by the National Hurricane Center, the NCEP–NCAR reanalysis, and the extended reconstructed sea surface temperature (ERSST) ver.2 (Smith and Reynolds 2004).

Climatology

Model Climate

SST and vertical wind shear are key environmental variables that control tropical cyclone development, in particular, over the North Atlantic (e.g., Gray 1968; Gray

1975; Gray et al. 1993). Thus, we first present the climatology of the model SST and vertical wind shear averaged from August to October in Fig. 1. The vertical wind shear in this study is defined as the magnitude of the vector difference of the 200 and 850 hPa horizontal winds. The warm SST regions exceeding 26˚C are spread over the entire tropical regions in the model. The overall patterns and magnitudes of the model warm SST regions are in agreement with the observations, although the model SSTs, in particular, over the eastern parts of the Atlantic are warmer compared with the observation (Figs. 1a and b) partially due to a lack of low-level marine stratus in this model. The similar deficiency is found also in other CGCMs (e.g., Mechoso et al. 1995). The model SSTs over the mid-latitude oceans are also warmer compared with the observation due to insufficient resolution of ocean model to simulate the Gulf Stream and a lack of sea ice model in this CGCM. The overall patterns and magnitudes of surface wind fields in the model are in general agreement with the observations (Figs. 1a and b).

In observations, the area of weak vertical shear with values less than 10 m/s extends from the east of the Caribbean to northwest Africa. The regions of strong vertical shear are found to both south and north of the weak vertical shear area. The

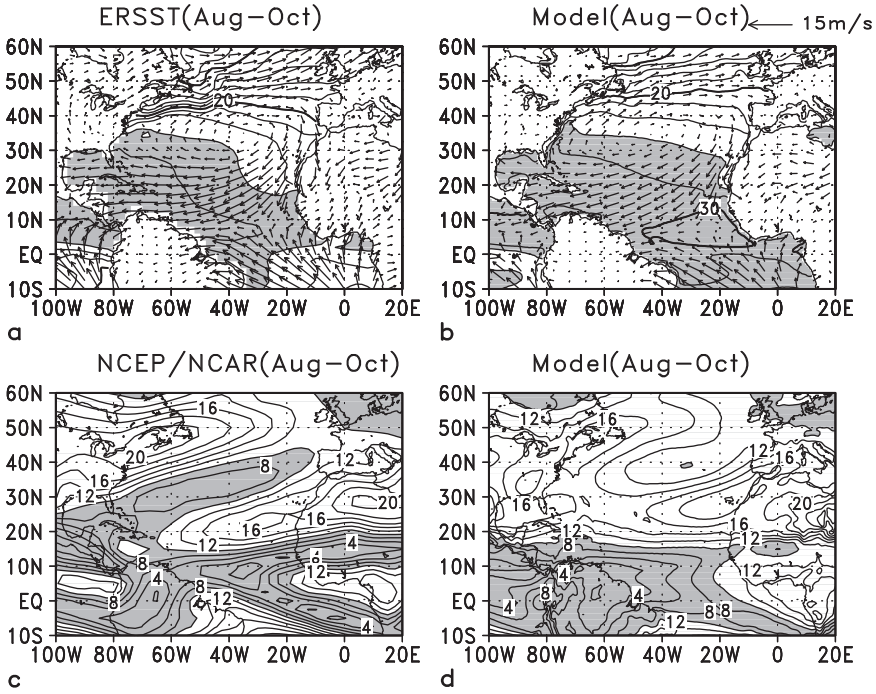

Fig. 1 Climatology of observed (**a**) and model SST (**b**) averaged from August to October, along with surface wind vector. Regions with values more than 26˚C are shaded and contour interval is 2˚C. (**c**)–(**d**) Same as in (**a**)–(**b**) but for magnitude of vertical wind shear defined as the vector difference of the 200 and 850 hPa horizontal winds. Regions with values less than 10 m/s are shaded and contour interval is 2 m/s

overall pattern of model vertical wind shear is similar to the observation, but the magnitude over the observed weak vertical shear region is stronger, in particular, over the Caribbean and the Gulf of Mexico. As shown in the next, this model bias in vertical wind shear could affect the distribution in genesis location of model TCs.

Structure of Model TC

Evans (1993) argued that it is important to examine the degree to which the model vortices have physical similarities with real TCs. Here we present the structure of the simulated TC. Figure 2 shows the horizontal and vertical structures of several quantities in a TC simulated in the model. In common with observed TCs, there is low sea level pressure accompanied by cyclonic circulations with stronger surface winds on the right hand side (Figs. 2a and b). The surface wind speed at 10 m exceeds 20 m s^{-1}. The cyclonic circulations of the model TCs extend up to near 200 hPa (Fig. 2c), with warm cores from 700 hPa to 200 hPa (Fig. 2d). Although the model used in the present study cannot simulate the eye wall structure because of the insufficient resolution, the above features of the simulated TC are in reasonable

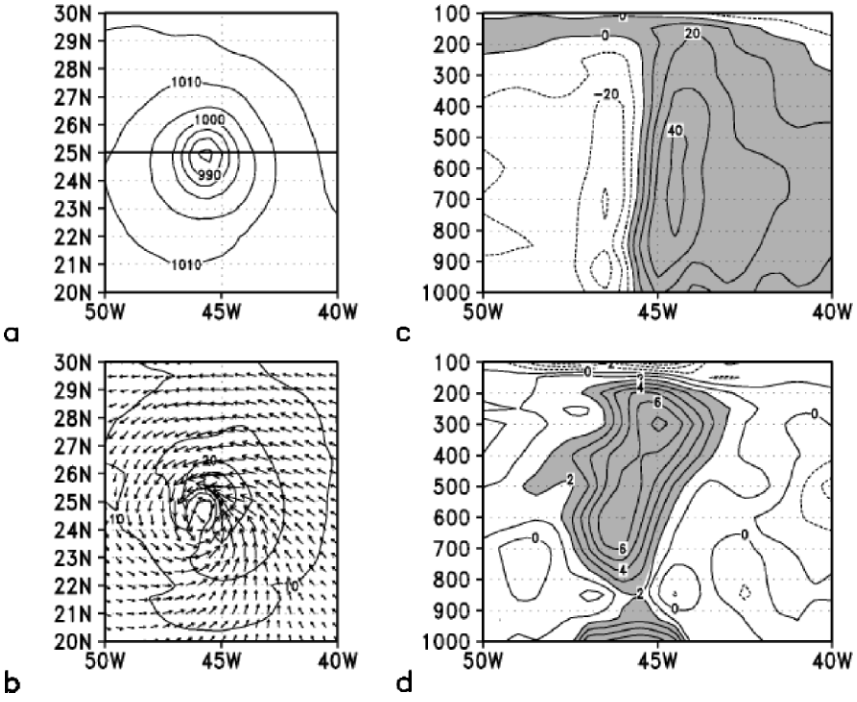

Fig. 2 (**a**) Sea Level Pressure. Contour interval is 5 hPa. (**b**) Wind vector and speed at 10 m. Contour interval is 5 m/s. (**c**) Vertical section of meridional wind. Contour interval is 10 m/s. (**d**) Vertical temperature anomalies. Contour interval is 1 K

agreement with the observations (e.g., Frank 1977) and the model TC simulated in other GCM (e.g., Wu and Lau 1992; Tsutsui and Kasahara 1996; Vitart et al. 1997).

Climatology of TCs

Various definitions have been proposed to detect TCs simulated in GCMs (e.g., Camargo and Zebiak 2002). In the present study, we used the following definitions to identify TCs simulated in the CGCM:

1. The grid point with minimum sea level pressure in a 9 × 9 grid-point box is defined as the center of a TC
2. The difference in sea level pressure between the center and each grid point on the boundaries at 4 grid points away from the center is greater than 5 hPa
3. Maximum surface wind speeds at 10 m in a 9 × 9 grid-point box around the center are greater than 17 m/s
4. The difference in the vorticity of surface winds between the center and each grid point on the boundaries at 4 grid points away from the center is greater than 1.5×10^{-4} s^{-1}
5. The lifetime is more than 2 days
6. The genesis location is located to the south of 40°N
7. The vorticity of surface winds around the center has a value greater than 5.0×10^{-4} s^{-1} at least 4 times throughout its lifetime.

Figure 3 present the genesis locations of model TCs, along with the observed ones during the period from 1930 to 2000. The more model TCs are formed over the northeastern part of the North Atlantic, along the western coast of Africa, and along the eastern coast of North America, while there are less model TCs over the Caribbean and the Gulf of Mexico. The reason for this discrepancy is not clear,

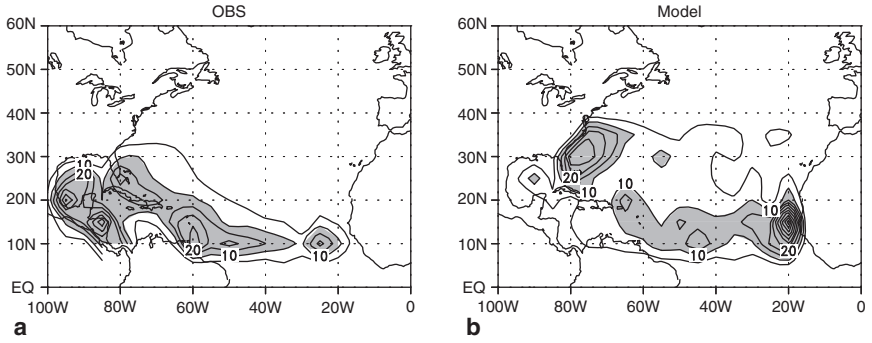

Fig. 3 Density of total TC genesis number in (**b**) model and (**a**) observations over the 1930–2000. TC genesis density is shown in each 5° × 5° latitude-longitude grid box. Contour interval is 5 and values more than 10 are shaded

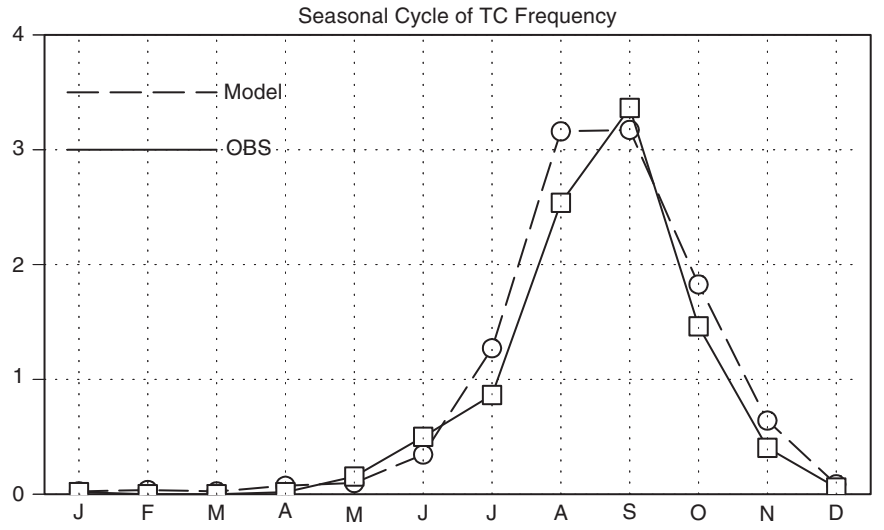

Fig. 4 Seasonal frequency of observed (*thick line*) and model (*dashed line*) TCs

but in the model, a trough or cold-core low in the upper atmosphere produces convection, occasionally developing into a warm-core tropical cyclone, which seems to contribute to the excess formation of model TCs in the mid-latitude of the North Atlantic compared with the observations. Less model TCs formed over the Caribbean and the Gulf of Mexico appear to be related to the stronger vertical wind shear compared with the observation (Figs. 1c and d).

Figure 4 shows the climatological seasonal cycle of frequencies of the simulated TCs. The annual number of the model TC is about 10, which is consistent with the observation. The peak of the observed North Atlantic TC season happens during the months of August to October with its maximum in September, while the frequency of model TCs is more in July and August compared with the observation.

Variability of TC

Model ENSO

Before addressing the variation of model TC frequency, we present the features of model ENSO. Figure 5a shows the time series of the simulated SST anomalies in the Niño3 region (5°S–5°N, 150°W–90°W) averaged during the months from August to October. Though observed ENSO typically occurs every 2 to 7 years (e.g., McPhaden et al. 2007), the CGCM simulates the quasi-periodic ENSO with a significant narrow spectrum peak at about 5 years (Fig. 5b). The standard deviation

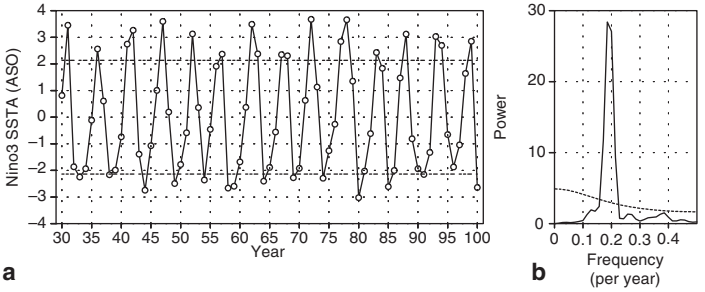

Fig. 5 (**a**) Time series of model Niño3 (5°S–5°N, 150°W–90°W) SST anomaly averaged during the months from August to October (ASO), denoted by solid line. Dashed lines are standard deviation. (**b**) Power spectra of model ASO Niño3 SST anomaly (*solid line*) and dashed curve shows the power spectra of red noise

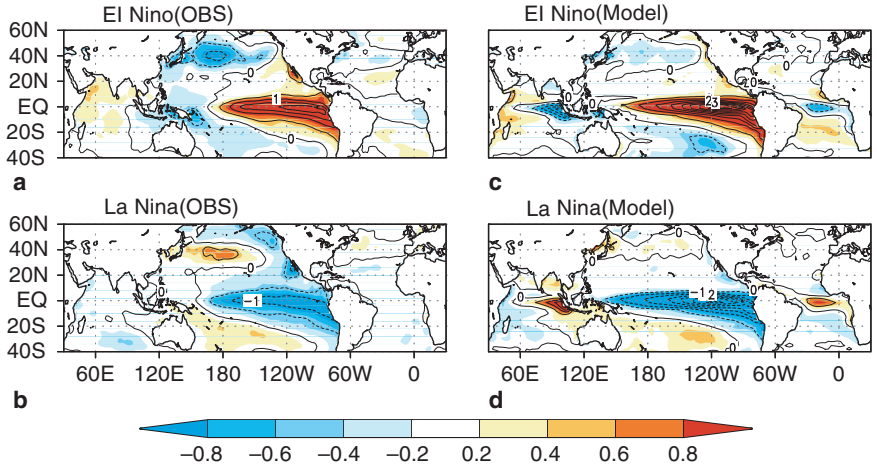

Fig. 6 Composite maps of observed SST anomalies averaged during the months from August to October of El Niño (**a**) and La Niña years (**b**), respectively. Contour interval is 0.5°C. (**c**)–(**d**) Same as in (**a**)–(**b**) but for model

of model Niño3 SST anomaly is 2.12°C that is twice larger than the observed one (0.91°C). However, this deficiency implies that the model may provide useful information for understanding the impact of a strong ENSO on TC frequency.

Figure 6 presents the composite maps of model SST anomalies on Niño3 SST anomalies, together with the observed counterparts. We here define El Niño (La Niña) years when Niño3 SST anomaly averaged during the months from August to October is more (less) than the standard deviation. Comparing with the observations, there are discrepancies in the SST anomalies in the equatorial Atlantic and the eastern equatorial Indian Ocean. This is because air-sea coupled modes in the tropical Atlantic and Indian Oceans concur with ENSO in this model, while those

modes do not always occur with ENSO in the observations (Zebiak 1993; Saji et al. 1999). The deficiencies may be related to the larger amplitude of ENSO in this model, resulted from the difference in convection scheme (Iizuka et al. 2003). However, the spatial structures of SST anomalies in the model during model El Niño and La Niña years show generally good agreement with the observed ones.

ENSO and TC Frequency

Figure 7a shows the time series of annual number of the model TCs over the North Atlantic. There is an interannual variation with a period of about 5 years in the time series (Fig. 7b). Although the variation on decadal time scales as in the actual TC frequency observed over the North Atlantic is not found in this model, there is an upward trend in annual number of the model TCs (0.5/decade). This increase will be discussed later.

It has been accepted that SST is one of the key environmental variables affecting the interannual variability of TC frequency. Thus, we first present the correlation maps of SST anomalies with model annual TC frequency in Fig. 8a. The correlation of SST anomalies is quite similar to the model ENSO SST anomaly pattern (c.f. Fig. 6), suggesting that the interannual variability of model TC frequency is related to ENSO. In the Atlantic, there is no significant correlation in the region between 10° and 20°N from the west coast of Africa to Central America and along the eastern coast of North America, where most model TCs are formed (c.f., Figs. 3b and 8a). Moreover, the negative correlation is found off Dakar. This implies that TCs cool SST through an increase in ocean mixing and evaporation. Therefore, it is suggested that the interannual variability of TC frequency in the Atlantic simulated by this CGCM is constrained by the large-scale atmospheric circulation rather than by the local SSTs.

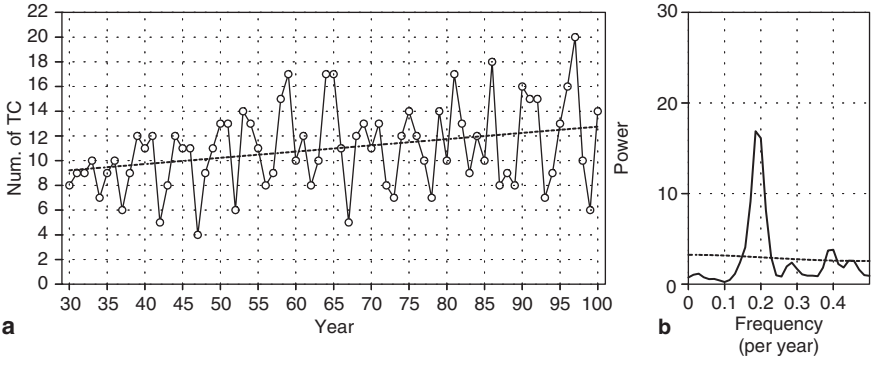

Fig. 7 (**a**) Time series of annual number of model TCs (*solid line*) and least squares best-fit linear trend is denoted by dashed line. (**b**) Power spectra of annual number of model TCs (*solid line*) and dashed curve shows the power spectra of red noise

Previous studies (e.g. Gray 1984; Goldenberg and Shapiro 1996; Vitart and Anderson 2001) have shown that an inverse relationship exists between North Atlantic TC activity and vertical wind shear in the main TC developing region between 10° and 20°N from the west coast of Africa to Central America (MDR) on seasonal and longer time scales. Thus, we next examine the relationship between the vertical wind shear and TC frequency in the model. There is the region with negative correlation between 10°N–20°N over the western part of North Atlantic (Fig. 8b). The similar spatial pattern is found in the correlation map between vertical wind shear and Niño3 SST anomaly (Fig. 8c). Therefore, the change in the vertical wind shear through atmospheric bridge associated with ENSO would cause the variation in annual TC frequency simulated by this CGCM. The results are in good agreement with the relationship between ENSO and Atlantic TC frequency in the observations (e.g., Goldenberg and Shapiro 1996).

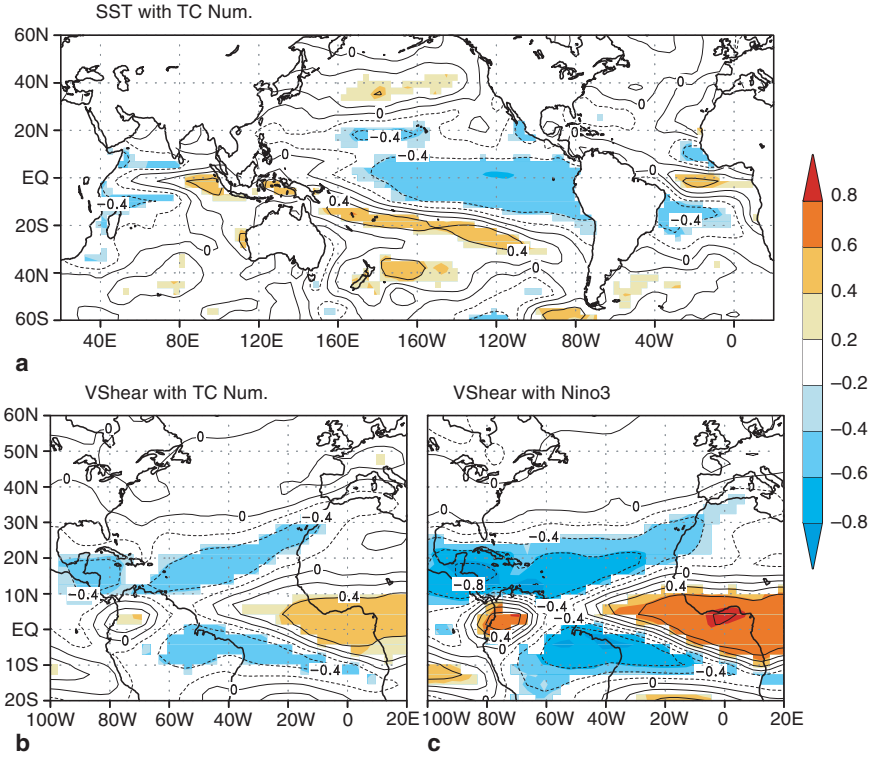

Fig. 8 Maps of correlation coefficients of SST (**a**) and vertical wind shear (**b**) averaged during the months from August to October against the annual number of model TCs. Contour interval is 0.2 and values exceeding the 99 % confidence level are shaded. (**c**) Same as in (**b**) but for correlation coefficients of vertical wind shear against Niño3 SST anomaly averaged during the months from August to October. Note that sign is reversed

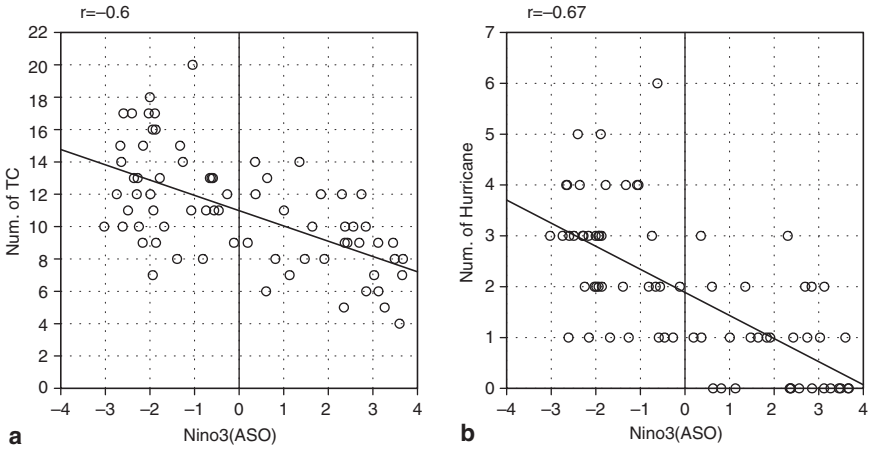

Fig. 9 Scatter diagrams for annual TC number (**a**) and annual hurricane number (**b**) against Niño3 SST anomaly during August–October. Correlation coefficient is denoted in the top of each panel. Linear regression lines are denoted by solid lines

Figure 9 shows the scatter diagrams for annual TC number and annual Hurricane number against Niño3 SST anomaly during August-October. Here, the model tropical storms (TSs) and Hurricanes are defined as model TCs reaching maximum surface winds more than 17 and 33 m/s, respectively. It is noted that there are no TCs with maximum surface winds more than 43 m/s belonging to the category 2 on the Saffir-Simpson scale because the horizontal resolution of the model used in the present study does not have the ability to simulate such strong TCs (c.f. Oouchi et al. 2006).

The annual number of model Atlantic TCs tends to increases in model La Niña years while it seems to be below the average in model El Niño years (Fig. 9a). There is also the similar relation in the annual number of model Hurricanes (Fig. 9b). The regression coefficients of model annual TC number and annual Hurricane number against Niño3 SST anomaly are -0.94/°C and -0.45/°C, respectively. The result suggests that in model El Niño years there are fewer intense TCs than in model La Niña years, which is generally consistent with the observation (e.g., Landsea et al. 1999).

Trend in TC Frequency

Although an interannual variation with a period of about 5 years is dominant in the time series of annual number of the model TCs over the North Atlantic (Fig. 7), there is also an upward trend in annual number of the model TCs (Fig. 7a). Since no any trend is found in time series of model Niño3 SST anomaly (Fig. 5), other

forcing might induce the change. In the present CGCM, an increase of any anthropogenic forcing is not considered. Therefore, one may consider that the SST change induced through slow oceanic adjustment from the initial state is related to the upward trend of model TC frequency. Thus, we computed the correlation between the SST and model TC frequency after applying a 7-year low-pass filter to both variables to remove ENSO signal.

In contrast to the correlation of the non-filtered SST and Atlantic TC frequency (Fig. 8a), there is the significant positive correlation in the region between 10° and 20°N from 30°W to Central America (Fig. 10a). The positive correlation is found also in the mid-latitude North Atlantic. The similar pattern is found in the trend and the 2nd EOF mode of SST anomalies (not shown). This also seems to be somewhat similar to the spatial pattern of SST anomalies associated with the Atlantic Multi-decadal Oscillation (AMO) (e.g., Goldenberg et al., 2001). It is noted that there is no significant correlation in the filtered vertical wind shear (Fig 10b). These imply that warmer SSTs in the region between 10° and 20°N over the North Atlantic may have potentially impacts on an increase in Atlantic TC frequency.

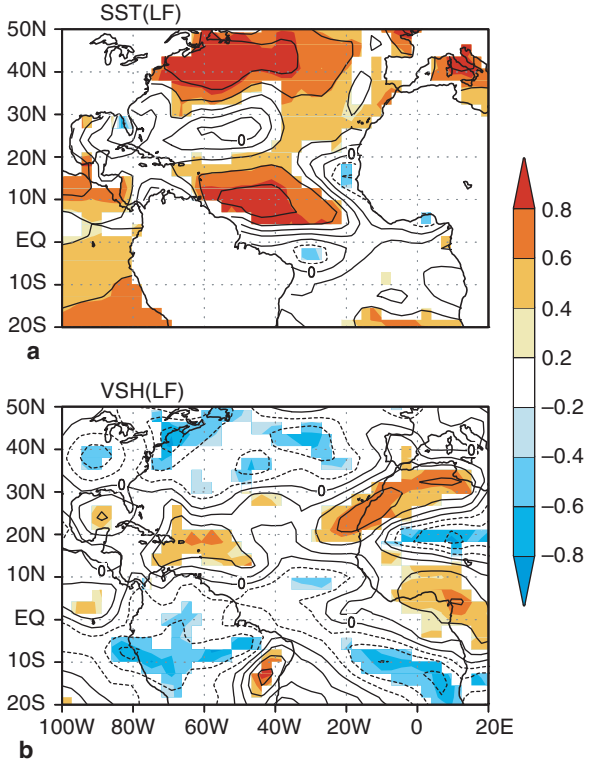

Fig. 10 (**a**) Maps of correlation coefficient between 7 year low-pass filtered SST and annual number of model TCs. Contour interval is 0.2 and values exceeding the 99% confidence level are shaded. (**b**) Same as in (**a**) but for 7 year low-pass filtered vertical wind shear

Summary

We examined the impact of ENSO on the activity of tropical cyclones (TCs) in the North Atlantic using 71-yr outputs simulated in a high-resolution (T213) coupled ocean-atmosphere general circulation model (CGCM). The high-resolution model simulated TCs with a maximum surface wind speed at 10 m more than 17 m/s, although there are no TCs with a maximum surface wind more than 43 m/s belonging to the category 2 on the Saffir-Simpson scale. The model also simulated quasi-periodic (about 5 years) ENSO-like events with amplitudes of Niño34 SST anomaly twice as large as observed. The spatial structure in the model anomalies shows good agreement with the observed one.

As in the observations, the annual frequency of model TCs as well as hurricanes over the North Atlantic increases (decreases) in model La Niña (El Niño) years. The increase (decrease) in model TCs is related to the reduction (enhancement) of vertical wind shear over the North Atlantic induced by a cold (warm) SST anomaly in the eastern equatorial Pacific. The upward trend found in model TC frequency, on the other hand, seems to be related to SST warming in the North Atlantic.

Recent papers have been focusing on the association between TC activities and global warming. Emanuel (2005) and Webster et al. (2005) suggested that the recent upswing in Atlantic TC activity since 1995 is related to SST warming in the North Atlantic, resulting from anthropogenic climate change, while Goldenberg et al. (2001) and Landsea et al. (2006) attributed the change to natural climate variability termed the AMO. On the other hand, Knight et al. (2005) suggested that changes in Atlantic thermohaline circulation could cause the AMO but the associated SST changes may be not enough to explain the recent increase in SST over the North Atlantic. It is certainly necessary to enhance our understanding of how global warming affects TC activities from both observational and modeling perspectives. Although the relationship between ENSO and TC frequency in the North Atlantic is simulated reasonably well in this high-resolution CGCM, there is still the deficiency in simulated TC intensity, therefore suggesting that further finer-resolution model would be required to simulate realistic TC intensity. Here we have demonstrated that the use of a finer-resolution GCM could be a powerful tool for understanding the future TC activities.

Acknowledgments The authors would like to thank Dr. M. J. McPhaden for helpful suggestions. This work is supported by the Research Project for Study on extreme weather events and water-related disasters due to Climate Change and Study on long term prediction of typhoon disasters under NIED, and Suitable Coexistence of Human, Nature, and the Earth under the Japanese Ministry of Education, Sports, Culture, Science, and Technology. The work is partially supported by Global Environment Research Fund of the Ministry of the Environment, Japan.

References

Arakawa, A., and W.H. Schubert, 1974: Interaction of a cumulus cloud ensemble with the large-scale environment. Part I. *J Atmos Sci.,* **31**, 674–701.

Bengtsson, L., K.I. Hodges, M. Esch, N. Keenlyside, L. Kornblueh, J.-J. Luo, and T. Yamagata, 2007: How tropical cyclones may change in a warmer climate? *Tellus*, **59**A, 539–561.

Camargo, S.J., and S.E. Zebiak, 2002: Improving the detection and tracking of TCs in atmospheric general circulation models. *Wea. Forecasting*, **17**, 1152–1162.

Camargo, S.J., A.G. Barnston, and S.E. Zebiak, 2005: A statistical assessment of tropical cyclone activity in atmosphere general circulation models. *Tellus*, **57**A, 589–604.

Emanuel, K.A., 1986: An air-sea interaction theory for tropical cyclones. Part I: Steady-state maintenance. *J. Atmos Sci*., **3**, 585–605.

Emanuel, K.A., 2005: Increasing destructiveness of tropical cyclones over the past 30 years. *Nature,* **326**, 686–688.

Evans, J.L., 1993: Sensitivity of tropical cyclone intensity to sea surface temperature. J *Clim*, **6**, 1133–1140.

Frank, W.M., 1977: The structure and energetics of the tropical cyclone, Paper I: Storm structure. *Mon Wea Rev*, **105**, 1119–1135.

Goldenberg, S.B., and L.J. Shapiro, 1996: Physical mechanisms for the association of El Niño and West African rainfall with Atlantic major hurricane activity. *J Clim*, **9**, 1169–1187.

Goldenberg, S.B., C.W. Landsea, A.M. Mestas-Nuñez, and W.M. Gray, 2001: The Recent Increase in Atlantic Hurricane Activity: Causes and Implications. *Science*, **293**, 474–479.

Gray, W.M., 1968: Global view of the origin of tropical disturbances and storms. *Mon Wea Rev,* **96**, 669–700.

Gray, W.M., 1975: Tropical cyclone genesis. Dept of Atmos Sci. Paper No 234. Colorado State Univ., Fort Collins, CO, 121 pp.

Gray, W.M., 1984: Atlantic seasonal hurricane frequency. Part I: El Niño and 30 mb quasi-biennial oscillation influences. *Mon Wea Rev*, **112**, 1649–1668.

Gray, W.M., C.W. Landsea, P.W. Mielke, and K.J. Berry, 1993: Predicting Atlantic basin seasonal tropical cyclone activity by 1 August. *Wea Forecasting*, **8**, 73–86.

Iizuka, S., K. Orito, T. Matsuura, and M. Chiba, 2003: Influence of cumulus convection schemes on the ENSO-like phenomena simulated in a CGCM. *J Meteor Soc,* **81**, 805–827.

Iizuka, S., and T. Matsuura, 2008: ENSO and Western North Pacific Tropical cyclone activity simulated in a CGCM. *Clim Dyn*. DOI: 10.1007/s00382-007-0326-x.

Iwasaki, T., S. Yamada, and K. Tada, 1989: A parameterization scheme at orographic gravity wave drag with the different vertical partitionings. Part I: Impact on medium range forecasts. *J Meteor Soc,* **67**, 11–27.

Kalnay, E., M. Kanamitsu, R. Kistler, W. Collins, D. Deaven, L. Gandin, M. Iredell, S. Saha, G. White, J. Woollen, Y. Zhu, A. Leetmaa, B. Reynolds, M. Chelliah, W. Ebisuzaki, W. Higgins, J. Janowiak, K.C. Mo, C. Ropelewski, J. Wang, R. Jenne, and D. Joseph, 1996: The NCEP/NCAR 40-Year Reanalysis Project. *Bull Amer Meteorolo Soc*, **77**, 437–471.

Killworth, P.D., D. Stainforth, D.J. Webb, and S.M. Paterson, 1991: The development of a free-surface Bryan-Cox-Semtner ocean model. *J Phys Oceanogr*, **21**, 1333–1348.

Knight, J.R., R.J. Allan, C.K. Folland, M. Vellinga, and M.E. Mann, 2005: A signature of persistent natural thermohaliner circulation cycles in observed climate. *Geophys Res Lett*, **32**, L20708, doi:10.1029.

Kuma, K., 1996: Parameterization of cumulus convection. JMA/NPD Report No 42:93pp.

Lacis, A.A., and J.E. Hansen, 1974: A parameterization for the absorption of solar radiation in the earth's atmosphere. *J Atmos Sci*, **31**, 118–133.

Landsea, C.W., 1993: The climatology of intense (or major) Atlantic hurricanes. *Mon Wea Rev,* **121**, 1703–1713.

Landsea, C.W., R.A. Pielke Jr, A.M. Mestas-Nuñez, and J. Knaff, 1999: Atlantic basin hurricanes: indices of climate changes. *Climatic Change*, **42**, 89–129.

Landsea, C.W., B.A. Harper, K. Hoarau, and J.A. Knaff, 2006: Can we detect trends in extreme tropical cyclones? *Science*, **313**, 452–454.

Levitus, S., 1982: Climatological atlas of the world ocean. NOAA Prof Paper 13, 178pp. U.S. Government Printing Office Washington D.C.

Lord, S.J., and A. Arakawa, 1980: Interaction of a cumulus cloud ensemble with the large-scale environment. Part II. *J Atmos Sci*, **37**, 2677–2692.

Lord, S.J., W.C. Chao, and A. Arakawa, 1982: Interaction of cumulus cloud ensemble with the large-scale environment: Part IV: The discrete model. *J Atmos Sci*, **39**, 978–1002.

Louis, J., M. Tiedtke, and J.F. Geleyn, 1982: A short history of PBL parameterization at ECMWF. Workshop on planetary boundary layer parameterization, ECMWF, 59–80.

Manabe, S., J.L. Holloway, Jr., and H.M. Stone, 1970: Tropical circulation in a time-integration of a global model of the atmosphere. *J Atmos Sci*, **27**, 580–613.

Marotzke, J., 1991: Influence of convection adjustment on the stability of the thermohaline circulation. *J Phys Oceanogr*, **21**, 903–907.

McPhaden, M.J., S.E. Zebiak, and M.H. Glantz, 2007: ENSO as an integrating concept in earth science. *Science*, **314**, 1740–1745.

Mechoso, C.R., A.W. Robertson, N. Barth, M.K. Davey, P. Delecluse, P.R. Gent, S. Ineson, B. Kirtman, M. Latif, H. Le Treut, T. Nagai, J.D. Neelin, S.G.H. Philander, J. Polcher, P.S. Schopf, T. Stockdale, M.J. Suarez, L. Terray, O. Thual, and J.J. Tribbia, 1995: The seasonal cycle over the Tropical Pacific in General Circulation Models. *Mon Wea Rev,* **123**, 2825–2838.

Mellor, G.L., and T. Yamada, 1974: A hierarchy of turbulence closure models for planetary boundary layers. *J Atmos Sci*, **31**, 1791–1806.

Moorthi, S., and M.J. Suarez, 1992: Relaxed Arakawa-Schubert: A parameterization of moist convection for general circulation models. *Mon Wea Rev*, **120**, 978–1002.

Oouchi, K., J. Yoshimura, H. Yoshimura, R. Mizuta, S. Kusunoki, and A. Noda, 2006: Tropical cyclone climatology in a global-warming climate as simulated in a 20 km-mesh global atmospheric model: frequency and wind intensity analysis. *J Meteorol Soc*, **84**, 259–276.

Pacanowski, R., and S.G.H. Philander, 1981: Parameterization of vertical mixing in numerical models of tropical oceans. *J Phys Oceanogr*, **11**, 1443–1451.

Paulson, E.A., and J.J. Simpson, 1977: Irradiance measurements in the upper ocean. *J Phys Oceanogr*. **8**, 1572–1583.

Randall, D., and D.M. Pan, 1993: Implementation of the Arakawa-Schubert cumulus parameterization with a prognostic closure. Meteorological Monograph/The representation of cumulus convection in numerical models, No. 46, 137–144.

Saji, N.H., N.H. Goswami, P.N. Vinayachandran, and T. Yamagata, 1999: A dipole mode in the tropical Inidan Ocean. *Nature*, **401**, 360–363.

Sato, N., P.J. Sellers, D.A. Randall, E.K. Schneider, J. Shukla, J.L. Kinter, Y.T. Hou, and E. Albertazzi, 1989: Effects of implementing the simple biosphere model in a general circulation model. *J Atmos Sci*, **46**, 2757–2782.

Sellers, P.J., Y. Mintz, Y.C. Sud, and A. Dalcher, 1986: A simple biosphere model (SiB) for use within general circulation models. *J Atmos Sci*, **43**, 505–531.

Shapiro, L.J., 1982a: Hurricane climate fluctuations. Part I: Patterns and cycles. *Mon Wea Rev*, **110**, 1007–1013.

Shapiro, L.J., 1982b: Hurricane climate fluctuations. Part II: Relation to large-scale circulation. *Mon Wea Rev*, **110**, 1014–1023.

Shapiro, L.J., 1987: Month-to month variability of the Atlantic tropical circulation and its relationship to tropical storm formation. *Mon Wea Rev*, **115**, 2598–2614.

Shapiro, L.J., and S.B. Goldenberg, 1998: Atlantic sea surface temperatures and tropical cyclone formation. *J Clim*, **11**, 578–590.

Smith, T.M., and R.W. Reynolds, 2004: Improved Extended Reconstruction of SST (1854–1997). *J Clim*. **17**, 2466–2477.

Sugi, M., K. Kuma, K. Tada, K. Tamiya, N. Hasegawa, T. Iwasaki, S. Yamada, and T. Kitade, 1990: Description and performance of the JMA operational global spectral model (JMA-GSM88). *Geophys Mag*. **43**, 105–130.

Sugi, M., A. Noda, and N. Sato, 2002: Influence of the global warming on tropical cyclone climatology: an experiment with the JMA global model. *J Meteorol Soc*, **80**, 249–272.

Tsutsui, J., and A. Kasahara, 1996: Simulated tropical cyclones using the National Center for Atmospheric Research community climate model. *J Geophys Res*, **101**, 15013–15032.

Vitart, F., J.L. Anderson, and W.F. Stern, 1997: Simulation of interannual variability of tropical storm frequency in an ensemble of GCM integrations. *J Clim*, **10**, 745–760.

Vitart, F., J.L. Anderson, and W.F. Stern, 1999: Impact of large-scale circulation on tropical storm frequency, intensity, and location, simulated by an ensemble of GCM integrations. *J Clim*, **12**, 3237–3254.

Vitart, F., and J.L. Anderson, 2001: Sensitivity of Atlantic tropical storm frequency to ENSO and interdecadal variability of SSTs in an ensemble of AGCM integrations. *J Clim*, **15**, 533–545.

Webster, P.J., G.J. Holland, J.A. Curry, and H.R. Chang, 2005: Changes in tropical cyclone number and intensity in a warming environment. *Science*, **309**, 1844–1846.

Wu, G., and N.C. Lau, 1992: A GCM simulation of the relationship between tropical-storm formation and ENSO. *Mon Wea Rev*, **120**, 958–977.

Yoshimura, J., M. Sugi, and A. Noda, 2006: Influence of greenhouse warming on tropical cyclone frequency. *J Meteorol Soc*, **84**, 405–428.

Zebiak, S.E., 1993: Air-sea interaction in the equatorial Atlantic region. *J Clim*, **6**, 1567–1586.

Modeling of Tropical Cyclones and Intensity Forecasting

Zafer Boybeyi, Menas Kafatos, and Donglian Sun

Background

Accurate forecast of tropical cyclones/hurricanes (TC) is a high priority topic of research, due to their potential large economic impact as well as public safety issues. Hurricanes rank among the most destructive and costly of natural phenomena. For example, the warm waters particularly along the Bahamas and the Greater Antilles provide a significant energy source for hurricanes en route to Florida. As a result, Florida receives more hurricanes than elsewhere in the United States (Elsner and Kara, 1999). In 1992, hurricane Andrew caused more than $30 billion in direct economic losses in south Florida. The recent hurricanes of 2004 (Charley, Frances, Ivan and Jeanne) that spun toward and crossed Florida, caused over $20 billion in losses. Even more alarming, Pielke and Landsea (1998) reported that total loss estimates for a category-4 hurricane striking Miami, Florida would be more than $60 billion. The most recent hurricane of 2005 (Katrina) caused $100 billion economic cost. This trend in damages highlights the importance of and need for better TC track and particularly intensity forecasting.

Despite large reductions in track forecast errors over the past three decades (cf. Fig. 1), hurricane forecast errors have not reached estimated predictability limits (McAdie and Lawrence, 2000). In contrast to the improvements in track forecasts, there has been little improvement in forecasts of storm intensity and surprisingly little effort to forecast storm structure and overall size (Liu et al., 1997; Camp and Montgomery, 2001). Since, most of the damaging hurricanes undergo rapid intensification prior to landfall, such as hurricane Katrina, (globally about 10–15% of all hurricanes experience a period of rapid intensification), considerable improvement is still needed in the understanding and prediction of TC intensity change and inner core structure.

The TC forecasting has received significant attention both on the scale of weather prediction (~3–5 days forecasting) and on the climate scale. On the climate scale, TC behavior is influenced by climate factors, such as changes in large scale

J.B. Elsner and T.H. Jagger (eds.), *Hurricanes and Climate Change,*
doi: 10.1007/978-0-387-09410-6,

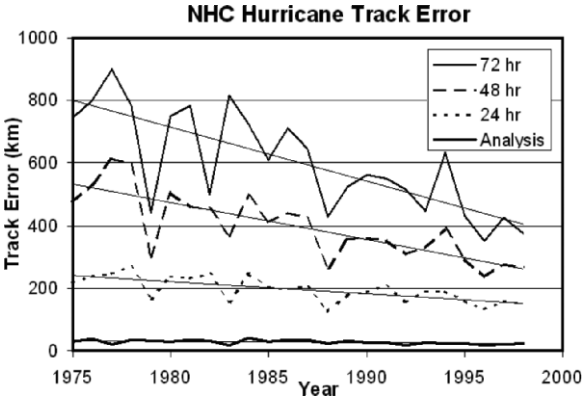

Fig. 1 Shown are the analysis and 24, 48, and 72 hour National Hurricane Center forecast track errors from 1975 to 1998 (after McAdie and Lawrence, 2000). The linear regression trend lines show that in this 23 year period the 48 and 72 hour forecast track error improved by 50%, while the 24 hour forecast track error improved by 37%. In spite of these improvements, 72 hour forecast track error is still about 400 km, the 48 hour forecast track error is about 275 km, while the 24 hour track error is about 175 km

circulation anomalies associated with the El Ninño-Southern Oscillation (ENSO) or the North Atlantic Oscillation (NAO) or by shifts in tropical storm origins or regional changes in land use (e.g., Elsner et al., 1998). On the scale of weather prediction, TC behavior is characterized by strong multi-scale interactions: the hurricane vortex is hundreds of km in horizontal size (synoptic-scale), the eye is tens of km (mesoscale), and the embedded convective clouds are in the order of km (cloud-scale), with a vertical scale of up to 20 km (e.g., Gopal et al., 2002). Moreover, other atmospheric phenomena, such as dust aerosols, may affect the development of TC's (Dunion and Velden, 2004). Such issues are still under investigation and are somewhat controversial.

The local environmental flow in which the hurricane vortex is embedded is the main factor that determines its short-term track. At longer timescales, an accurate forecast of the flow at considerable distance from the cyclone is needed. The internal structure of the TC and interaction between the structure and the hurricane's environment are the primary influences on hurricane intensity. These space-time scales and scale interactions should be represented as accurately as possible, when TC behavior is studied. Otherwise, significant components of the problem may be neglected.

This wide range of temporal and spatial scales characterizing atmospheric processes demonstrates the need for multiscale capabilities in hurricane modeling. However, the current atmospheric simulation systems are scale specific and cannot resolve the full spectrum required for the accurate forecast of local scale phenomena (e.g., convection). Even with recent advances in computational power, the current architecture and physics of today's generation of atmospheric models

cannot simulate the full spectrum of scale interactions of the atmosphere. Nevertheless, numerical weather prediction (NWP) models should be capable of predicting three dimensional, time dependent atmospheric mean flow and turbulence fields over complex terrain in an unsteady synoptic environment. In addition, these models should have a sufficient grid resolution to account for local scale phenomena and mean vertical planetary boundary layer structure. The numerical accuracy of the algorithms and consequently the eventual predictions of these models are closely related to the completeness of model physics, dynamics, accurate initial and boundary conditions, and the computational domain and mesh on which the model calculations are performed.

As to the completeness of model physics and dynamics, over the last two decades, with the advancements in supercomputers and improvements in the formulation of atmospheric physics and dynamics, NWP models have been continuously improved. However, analysis errors (i.e., errors in initial conditions) are still being considered as one of the main source of the TC forecast errors for the NWP models (Lorenz, 1990). As for the atmospheric analyses, their quality depends on two main factors. First, the quality of the analysis is limited by the technique through which the analysis is derived. Both the NWP model used to generate first guess fields for the analysis, and the statistical estimation method that combines information from the first guess and observations are built using approximations because of limits in our knowledge and computational capabilities. The second dominant factor regarding the quality of the analysis is data coverage. Observations with better geographical coverage, higher quality and/or more comprehensive data should lead to improved atmospheric initial conditions and in turn improved NWP forecast, provided that these observations can be assimilated rapidly enough to be useful.

The current *in-situ* atmospheric measurement system is inadequate to determine the current state of the atmosphere and hence our ability to forecast is limited by this constraint. These observations at regular time intervals and at fixed geographical locations have been able to define the large-scale features of the atmospheric system and have served the interests of climatologists, synoptic forecasters, and early NWP forecast systems. However, there is always need for additional data to resolve *critical* features in the atmosphere (such as the details of convective structure of hurricanes). The current and next generation of satellite-based atmospheric observations is likely to provide a significant increase in our observational coverage. The spatial and temporal resolution of the retrieved atmospheric properties will expand and the net result on the data flow is expected to increase. This paradigm shift may require a shift in our utilization of data. For example, instead of using all data in an egalitarian and brute-force method, we may need to consider adding some form of intelligence to our data processing system to identify, extract, and utilize just the necessary critical information for a given forecast cycle (Boybeyi et al., 2007).

Undoubtedly, another obvious method to improve the accuracy of the prediction of NWP models is to enhance the spatial grid resolution. However, introducing fine spatial resolution throughout the domain is not always practical since the size of the

modeling domain, the numerous interactions between the various atmospheric processes, and the complexity of the numerical algorithms places restrictions on the grid resolution that can be achieved using current computers. These limitations prohibit the use of a uniform high spatial resolution that is appropriate to resolve the smallest scales of interest (in case of TC forecasting, the smallest scale of interest is "convection"). One of the alternatives is then to develop methodologies capable of providing local refinement in certain key regions.

Hence, TC track and intensity forecast can be improved by;

- Detailed measurements on scales from the storm's large scale environment to its small inner-core and
- Appropriate numerical grid resolution to resolve the smallest scales of interest (e.g., eye, eye wall, and spiral bands) and multi-scale atmospheric flow interactions.

This chapter discusses the above requirements in details for a better TC forecasting. Section 2 provides discussion on remotely sensed observations, while Section 3 provides discussion on high fidelity numerical modeling coupled with high resolution observations. Finally, Section 4 provides some concluding remarks.

Importance of Remote Sensing Data

Over the past four decades, remote sensing of the atmosphere from space has undergone a steady progression from qualitative vertically-integrated measurements to quantitative vertically-resolved information – providing high-density observations. Satellite observations are especially useful in data sparse ocean areas where TC's occur.

Of particular recent interest is the issue of the effect of dust aerosols on TC's. Here, remote sensing (RS) data become even more crucial, particularly vertical measurements. As such, the importance of African dust has been increasingly recognized for its potential influence on climate and TC's worldwide (Arimoto, 2001; Goudie and Middleton, 2002; Kaufman et al., 2002). Radiative forcing (e.g., Carlson and Benjamin, 1980; d'Almeida, 1987; Li et al., 2003; Miller and Tegen, 1998; Weaver et al., 2002; Christopher and Jones, 2006) is recognized as the most important aspect of African dust. Such outbreaks are associated with an elevated layer of hot, dry air outbreaks (e.g., Prospero and Carlson, 1981). Dry air affects tropical clouds and precipitation directly through thermal structure and indirectly through dry air entrainment (e.g., Mapes and Zuidema, 1996; Yoneyma and Parsons, 1999; Zhang and Chou, 1999; Tompkins, 2001).

Tropical cyclones/hurricanes in the Atlantic basin often develop from mesoscale convective systems embedded within the African Easterly Waves (AEWs) that develop over West Africa. Previous studies show that the Atlantic basin major hurricane activity is associated with western Sahelian monsoon rainfall, and

negative Sahelian rainfall anomalies or droughts are associated with suppressed Atlantic basin TC activity (Goldenberg and Shapiro, 1996). They explained that drought induced the increase of vertical wind shear and therefore inhibited TC development.

Since rainfall in the Sahel is found to be highly anti-correlated with African dust (Prospero and Lamb, 2003), the Atlantic basin TC activity is also found to be anti-correlated with African dust outbreaks (Evan et al., 2006). Recently, Wu et al., 2006 analyzed the effects of the Saharan air layer (SAL) on Hurricane Isabel by incorporating the Atmospheric Infrared Sounder (AIRS on the Aqua satellite) measurements into MM5 model runs. They found that the SAL may have delayed the formation of Hurricane Isabel and inhibited the development of another tropical disturbance following behind it. Dunion and Velden (2004) suggest the dry SAL can suppress Atlantic tropical cyclone activity by increasing the vertical wind shear and stabilizing the environment at low levels.

We also believe the radiative forcing effects of dust aerosols on sea surface temperature (SST) may be an important factor to influence TC activity as shown in the study of Lau and Kim (2007). The reason is because SST plays a fundamental role in the inter-annual variability of tropical storm frequency and intensity (Vitart et al., 1999), and a direct role in providing moist enthalpy (i.e., latent and sensible heat flux) to intensify tropical cyclones.

In the study of TC development and intensification, as well as the possible aerosol effects on TC formation, several data sets have become of interest, which can be coupled to numerical runs (cf. Boybeyi et al., 2007; Kafatos et al., 2006; Sun et al. 2007). Some of these data sets include;

- MODIS from the NASA GSFC DAAC;
  - Daytime aerosol optical depth (AOD) at 0.55 mm,
  - Daytime SST.
- AIRS daytime vertical temperature and moisture profiles from the NASA GSFC DAAC.
- CALIPSO vertical data from the NASA GSFC DAAC.
- Tropical cyclone data from the National Hurricane Center (NHC) Hurricane Best Track Files (HURDAT), available at http://www.nhc.noaa.gov/pastall.shtml.
- NOAA Extended Reconstructed SST V2 products from 1854 to 2003 (http://lwf.ncdc.noaa.gov/oa/climate/research/sst/sst.html#ersst).
- Monthly mean wind and humidity profile data from the NCEP-NCAR reanalysis (NNR) from 1948 to present.
- Dust concentration data at the Barbados sampling station (13° 10'N, 50°30'W), which provide the most extensive long-term records with aerosol measurements that start in 1965 (Prospero and Lamb, 2003).
- Aerosol Index (AI) data with 1° X 1.25° resolution are from 1980 to 2006 (1980 to 1993 from the Nimbus and 1996–2000 from the total ozone mapping spectrometer, TOMS, and 2004–2006 from the Ozone Mapping Instrument, OMI,

from the NASA GSFC) with missing data from 1993 to 1995 (http://toms.gsfc.nasa.gov/aerosols/aerosols_v8.html). The AI data from 2001–2003 are not used due to the unreliability in the TOMS data.

The primary factors that will determine the use of any observational data in NWP models are the quality and spatial and temporal resolution of the data. Since the current *in-situ* atmospheric measurement system is inadequate to determine the current state of the atmosphere particularly over water areas where TCs develop, remote sensing observations provide a viable option with better geographical coverage. This aspect of remote sensing data is important for NWP models. As to the quality of remote sensing data, over past four decades, quality of the data has undergone a steady improvement. For example, the standard error for surface temperature is now less than 0.8 K, the SST data have accuracies to $+/-0.4$ degrees Celsius, temperature profiles have accuracies to 1°K in 1 km layer, and water vapor profiles have accuracies of 15% in 2-km layer in the troposphere. In short, the regular and opportunity driven observations constitute the backbone of the global observing network and will likely do so for the foreseeable future. Satellite derived atmospheric properties have the accuracy, coverage, and resolution to dominate our understanding of the dynamics of the atmosphere. The utilization of this data in NWP models will improve the forecast accuracy of such models.

Numerical Modeling of Tropical Storms

Over the past four decades, numerical modeling of the atmosphere has also undergone a steady progression from 2D simulations to high fidelity 3D real time simulations. NWP models use predictive equations to describe the model variables (i.e., they are prognostic). In other words, NWP models are described by appropriate differential equations, which represent the time-variability of the state and dynamical variables. The model variables are quantities that are conserved under spatial motion. Here, a quantity is defined as conservative if it does not change in value with time as it moves through the computational grid. For example, in the atmosphere linear momentum, potential temperature, and mass mixing ratios of airborne material are conserved quantities. Hence the prognostic variables are defined on an appropriate geometric grid and the time-behavior of the variables is represented by a truncated Taylor series as shown later in this section. The partial differential equations (PDE's) are then used to compute the rate of change of a quantity at a grid point.

As to the physical processes, the four most important ones that must be included in NWP models are radiation transport, turbulence, cloud microphysics, and convective parameterization. Radiation transport is important in determining the solar heating of the Earth's surface and the atmosphere. Atmospheric radiation is modeled at various levels of complexities ranging from simple bulk calculations and two-stream models to more complex models that treat the different parts of the

electromagnetic spectrum. Turbulence affects, among many other things, the rate at which surface energy and moisture enter the atmosphere. For example, it is a well-known fact that hurricanes are strengthened by the thermal energy and water vapor from the surface of warm oceans and they rapidly decay if either of these sources is cut off. The parameterization of turbulence in NWP models is usually divided into two parts: horizontal and vertical. In general, the horizontal diffusion is defined as a function of the deformation of momentum, while the vertical diffusion is implemented using a multi-level planetary boundary layer model. The planetary boundary layer (PBL) is also generally treated separately as the viscous sub-layer, the surface layer, and the transition layer in which the surface layer provides the necessary link for the surface latent and sensible heat fluxes that are very important in TC development (cf. Fig. 2).

Cloud microphysics and convective parameterization play an important role in the vertical distribution of moisture and energy, and in the formation of clouds and precipitation. The term "microphysics" is here referred as the processes that comprise the water cycle such as evaporation and condensation, growth of ice crystals (and water droplets) on heterogeneous microscopic particle substrates called ice (and condensation) nuclei, etc. (cf., Fig. 3). Many of the microphysical turbulent processes are not easy to represent in simple mathematical terms so as to be incorporated into numerical models. In models, these processes are represented by parameterizations that have been derived empirically with theoretical considerations in which the parametric values are set from the results of numerous field and laboratory experiments and measurements. Even though significant progress has been achieved in the understanding of these processes in the last few decades, cloud microphysics and atmospheric turbulence still pose considerable challenge to

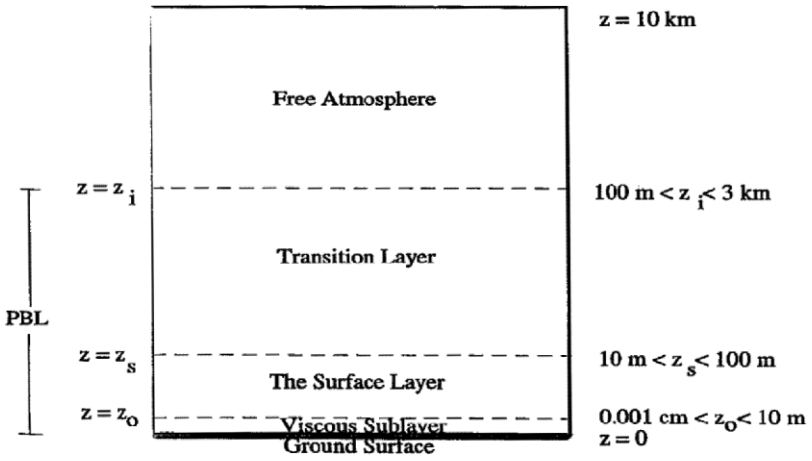

Fig. 2 A conceptual layout of a PBL scheme

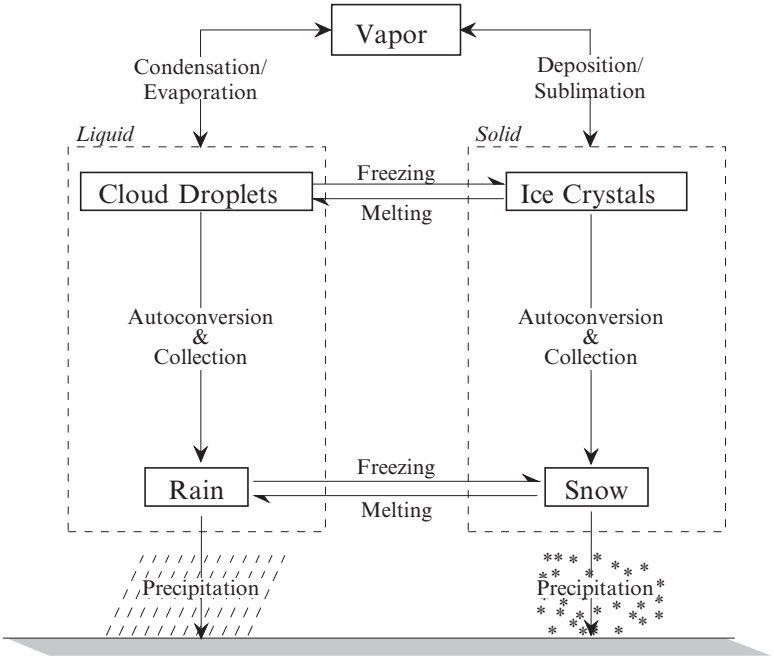

Fig. 3 A conceptual layout of a microphysics scheme derived from the scheme developed by Lin et al. (1983)

researchers in the field of NWP. It is also here where the effects of dust aerosols are still largely an unknown and become important.

In addition, atmospheric modeling is fundamentally an initial and boundary value problem. The fundamental equations are integrated with the constraint that the variables have known values at the initial time and also along the boundaries of the computational domain at all times. For the initial conditions, we depend on measurements of the key state variables. Ideally, the initial conditions should define the state of the atmosphere accurately at all points within the computational domain. This is impractical if not impossible to achieve and we have to be satisfied with a diverse set of measurements at a finitely few points in space and time.

In summary, although the poor performance of many NWP models in TC track and intensity forecasting may be explained by their neglect or poor treatment of the above mentioned physical processes, inadequate representation of the initial and evolving three-dimensional structure and dynamics of hurricanes and the surrounding large-scale environment are often the cause of these substandard predictions (Burpee et al., 1996). Consequently, TC track and intensity forecasts of NWP models can be improved by improving their initial condition and grid resolution.

Therefore, the rest of discussion in this section will concentrate on relatively new concepts in improving both model initial fields and grid resolution. Namely, adaptive data assimilation (i.e., targeted observations) and solution adaptive numerical modeling technique will be discussed rather than all other aspects of NWP that have been extensively studied in the past.

Improving Initial Condition (Adaptive Data Assimilation)

Numerical forecasts of chaotic systems like the atmosphere are limited by the use of imperfect initial conditions. Lorenz (1965) pointed out that any minor discrepancies, between either the natural system and its model or the actual and the analyzed state of the system at the initial time of a forecast, will lead to a loss of predictability within a finite time period. The size of these discrepancies will, in general, determine the time period for which useful forecasts can be made. Improving the analysis of the atmosphere used as initial condition is hence one of the basic avenues through which progress can be made in NWP.

Although the regular and opportunity driven observations constitute the backbone of the global observing network, satellite derived atmospheric properties as discussed in the previous section are expected to be able to provide the accuracy, coverage, and resolution to improve our understanding of the dynamics of the atmosphere. Current remotely-sensed observations, therefore, provide the opportunity to assist the hurricane research community in addressing the deficiencies in initial conditions. The utilization of these data, however, will require either massive increase in our data processing capability, or a change in our approach. The selective extraction of observations (i.e., targeted observations) is, for example, one possible method to make maximal utilization of the satellite derived information.

3DOI scheme is used in many data assimilation studies (e.g., Daley, 1991), since it is less CPU intensive. The basic principle of the OI scheme is that an estimate of the value of a variable at a set of grid points can be created from a set of meteorological observations distributed irregularly throughout the analysis domain by forming an "optimal" linear combination of the observations closest to the grid point. However, the 3DOI analysis scheme provides a simple means for assimilating data. More sophisticated assimilation methods (such as three-dimensional or four-dimensional variational analysis, 3DVAR/4DVAR) may yield better results (e.g., Leslie et al., 1998).

For example, Figures 4 and 5 show one of the recent such studies in which temperature and dew point temperature soundings from the GOES satellite were selectively (i.e., targeted way) assimilated using a 3DOI scheme to improve the model initial condition (Boybeyi et al., 2007). The results show that by reducing uncertainties in the steering polar jet entrance flow region at initial time, the track

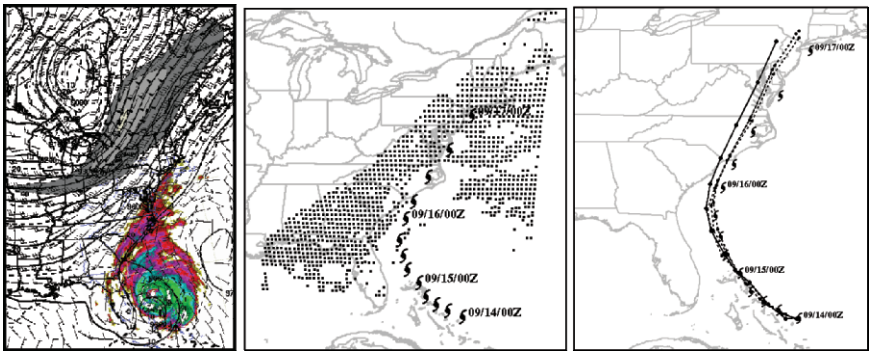

Fig. 4 Shown are; (*left*) 300-mb wind and height ETA analysis roughly overlaid on the enhanced infrared image of hurricane Floyd at 0000 UTC on September 15, 1999. The shaded area shows the high winds in the polar jet entrance steering flow region, (*middle*) the locations of about 1200 irregularly spaced GOES temperature and dew point temperature soundings superimposed on the observed Floyd track (hurricane symbols) and (*right*) OMEGA model forecasted tracks with the assimilation of the soundings at model initial time on 0000 UTC 9/14/2005 (*dashed lines*) and without the data assimilation (*solid line*)

error was improved by about 30%. In a NWP model, the initial uncertainty is mainly associated with the low resolution of the observations. This problem is amplified further in hurricane initialization due to lack of observations over the ocean regions (Burpee et al., 1996; Aberson and Franklin, 1999).

Today, we are on the verge of having improvements in *horizontal, vertical*, and *quantitative* resolutions to provide 10 to 100 times more than is potentially useful for TC forecasting. This is due to the computational cost of data assimilation that is quadratic in both the model horizontal grid resolution and the number of observations used. Over the coming decade, we are likely to see a 10-fold increase in the forecast model resolution and a 10–100 fold increase in the amount of satellite data. This will result in a 10^4 to 10^6 fold increase in the cost of data processing, which will far outstrip the factor of 100 increase in computing power predicted by Moore's Law over the same period.

Targeted observations can provide a viable solution to the above noted problem. From a numerical modeling point of view, the prediction will be more sensitive over some areas as compared to others, or the inaccuracy of analysis over some locations will affect the forecast errors more than in other locations. Thereby, the concept of targeted data assimilation can improve forecast skill by reducing the uncertainties over some particular areas for specific weather systems at the initial stages. Forecasts of events with potentially large societal impact, such as tropical cyclones (hurricanes), are prime candidates for targeted observation studies, given there is substantial uncertainty in their forecasts. Many investigators also studied this concept for TC simulations (Joly et al., 1997; Gelaro et al., 1999; Bergot et al., 1999; Leutbecher 2003; and Kim et al., 2004).

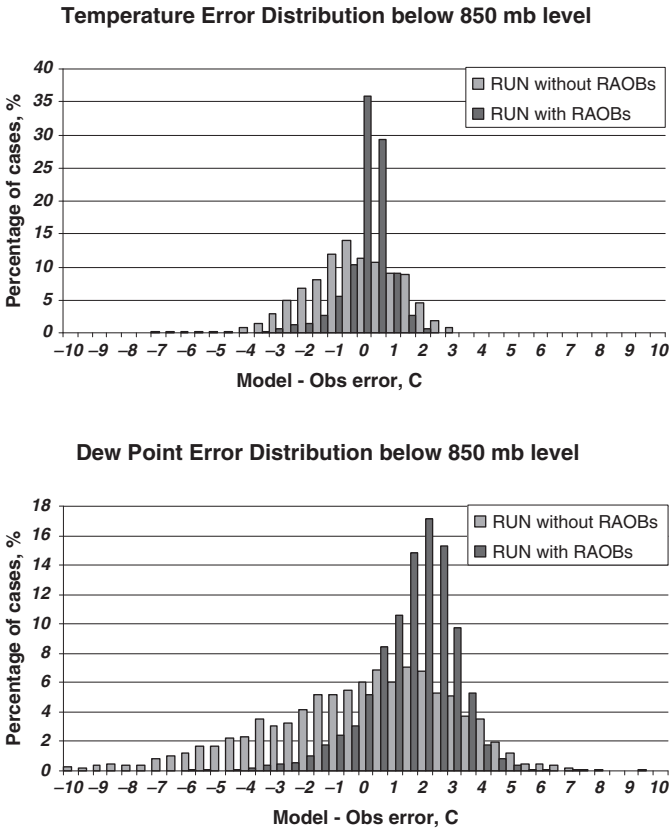

Fig. 5 Shows temperature (*top*) and dew point temperature (*bottom*) error distribution for the case presented in Fig. 2 below 850 mb level for hurricane Floyd case at model initial time (0000 UTC 9/14/1999) with and without the assimilation of the GOES soundings, respectively

Improving Model Grid Resolution (Solution Adaptive Modeling Technique)

Even, given the improved model initial condition, predictions of hurricanes can not be improved without accurately resolving the fine scale structure of the eye (cloud scale) and the steering large-scale environment (synoptic scale). Numerical models of the atmosphere are derived fundamentally from the Taylor series approximation which relates the value of a continuous function $f(x)$ to the known values of the function and its derivatives at a set of discrete points, x_i.

$$f(x) = f(x_i) + (x - x_i)f_i' + \frac{(x - x_i)^2}{2!}f_i'' + \frac{(x - x_i)^3}{3!}f_i''' + \ldots$$

where, f', f'', f''' denote the spatial derivatives $\frac{\partial f}{\partial x}, \frac{\partial^2 f}{\partial x^2}, \frac{\partial^3 f}{\partial x^3}$, respectively, evaluated at $x = x_i$. An examination of the above equation reveals that the general accuracy (or "order") of the calculation depends upon the number of terms on the RHS retained in the calculation. This translates into greater requirements for the computational resources. Hence it is customary to strike a balance by truncating the series at a suitable order of accuracy. An examination of the above equation also reveals that the error can be minimized by reducing the magnitude of $(x - x_i)$. This is in fact attained by increasing the grid resolution.

Therefore, in a numerical model of the atmosphere, the spatial scales of motion that can be resolved are dependent on the grid spacing used to represent the computational domain. In general, to effectively represent any feature requires that the feature be defined over four grid cells. Traditional numerical models use constant grid spacing. This implies that these models have prescribed lower limits for the spatial scale. However, atmospheric motions occur over various spatial scales. Introducing high grid resolution to resolve the smallest scales of interest throughout a simulation domain is not always practical, since the size of the modeling domain, the interactions between the atmospheric processes, the complexity of the numerical algorithms, and the operational requirements place restrictions on the grid resolution that can be achieved using today's computers (clusters or supercomputers).

The alternative, then, is to use methodologies or techniques capable of providing local refinement only in necessary key regions. In recent years, new grid methods have been developed to deal with multiscale events in atmospheric motion. In general, these methods can be classified into four groups: grid stretching techniques, grid nesting techniques, grid refinement techniques, and unstructured grid techniques. In the following section, these grid techniques are discussed briefly.

Anthes 1970 introduced a nonlinear grid transformation function that mapped nonuniform physical coordinates onto orthogonal, uniform computational coordinates. This mapping, commonly known as grid stretching, provides increased spatial resolution in selected regions of the computational domain, and has been widely applied in convective and mesoscale modeling studies (Wilhelmson and Chen, 1982). A principal limitation of the grid stretching technique is that one must know *a priori*, and for the duration of the calculation, which regions of the domain will require high spatial resolution.

The grid nesting technique is another way to provide increased spatial resolution in model forecasts of small scale features without requiring a fine mesh throughout the entire domain. This technique involves the sequential placement of multiple fine-scale meshes in desired regions of the domain (Jones, 1977). One problem with this technique, however, is the interaction among multiple nested meshes, particularly the tendency for propagating dispersive waves to discontinuously change their speeds upon passing from one mesh to the next and to reflect off the boundaries of each nested grid (Clark and Farley, 1984).

The grid refinement technique is a relatively new and powerful method that attempts to change resolution locally in response to the evolving solution. This technique can be subdivided into two basic categories: adaptive grid refinement and

continuous dynamic grid adaptation. The adaptive grid refinement technique refines the grid resolution either by adding grid points to an existing grid or by making use of separate fine grids that overlie existing coarser grids where the solution error is presumably high. Though similar in concept to the grid nesting technique, the adaptive grid refinement technique automatically determines the location, orientation, and resolution of the subgrids, and can be incorporated as a general solver in hydro-dynamical models without modifying the governing equations or their numerical representations. This technique has been successfully applied to atmospheric models by Skamarock et al. (1989). The continuous dynamic grid adaptation technique involves methods that redistribute a fixed number of grid points in a predetermined manner (Dietachmayer and Droegemeier, 1992). The criteria that determine how the grid points are redistributed with time are the critical element of this method, and are typically based on the physical characteristics of the evolving flow field. In this manner, the computational mesh structure is globally and dynamically coupled to the physics of the problem so that both are solved in a continuous manner (Thompson, 1984).

The unstructured grid technique (e.g., triangular prism computational mesh) is rather new to the atmospheric science community. In many fields of engineering applications (Baum et al., 1993), there is recognition that this method is more efficient and accurate than the structured logical grid approach used in more traditional codes. The primary benefit of the unstructured grid technique over a conventional structured grid lies in its ability to smoothly transition from high resolution where needed to low resolution elsewhere. This feature effectively removes the wave reflection and wave dispersion problems that are common in other grid techniques. The flexibility of unstructured grids also facilitates the gridding of arbitrary surfaces and volumes in three dimensions. In particular, unstructured grid cells in the horizontal dimension can increase local resolution to better capture the topography or important physical features of atmospheric flow and cloud dynamics. Therefore, this new grid technique can be suitable for studying the inherently multiscale nature of atmospheric motions (e.g., hurricanes).

For the first time, this technique has been applied to three dimensional atmospheric modeling by Bacon et al. (2000). Operational Multiscale Environment model with Grid Adaptivity (OMEGA) is a fully non-hydrostatic, three-dimensional prognostic model that is based on an adaptive, unstructured triangular prism grid. A full description of the system can be found in Bacon et al. (2000) and the details of validation studies can be found in Boybeyi et al. and Gopalakrishnan et al. 2002. The unstructured grid of the model provides flexibility to increase local grid resolution to better capture the important physical features of atmospheric flow and cloud dynamics (e.g., location, eye, eyewall, and spiral bands of a hurricane). This grid feature provides smooth transition from high resolution where needed to low resolution elsewhere and hence effectively removes the wave reflection and wave dispersion problems that are common in other grid techniques.

The model grid can adapt dynamically to a variety of user-specifiable adaptive criteria (e.g., precursors to convection, eye of a hurricane). In other words, the model focuses the model's horizontal grid resolution during the run on regions of

complex and critical phenomena to improve the overall quality and efficiency of simulations. The criteria have been well tested for the adaptation to wind-speed and pressure minima for hurricane simulations (cf. Figs. 6 and 7).

The model permits horizontal grids of continuously varying spatial resolutions ranging from about 100 km down to about 1 km to resolve important physical features of atmospheric circulation and cloud dynamics (Figs. 6 and 7). This

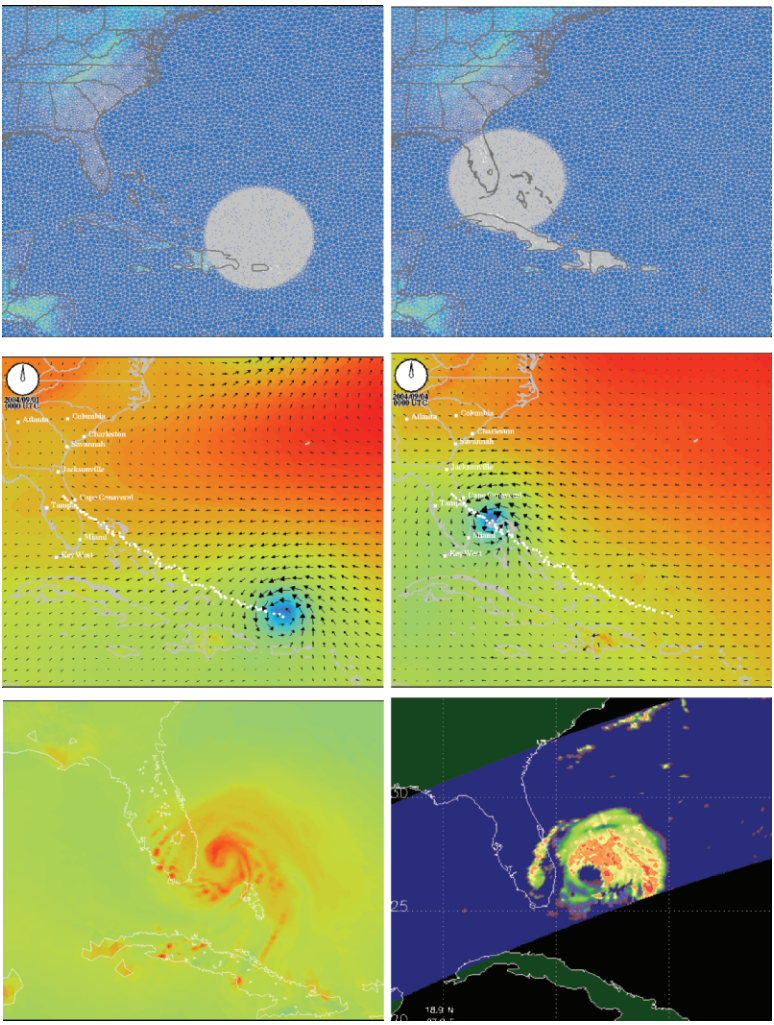

Fig. 6 Shows 4-day forecasts of hurricane FRANCES (from 9/1/2004 00Z to 9/ 4/2004 00Z) using OMEGA model with its dynamic grid adaptation: 1) top figures shows the simulation domain and model grid adapting to the evolving hurricane. The model grid resolution ranges from 60 km down to 1 km, 2) middle figures show OMEGA model predicted flow field and hurricane track in a zoomed area, and 3) bottom figures show model predicted vertically integrated water vapor in a further zoomed area and corresponding satellite image

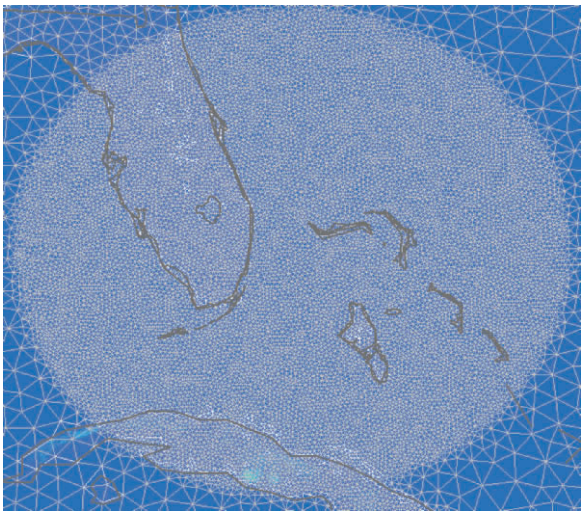

Fig. 7 Shows a zoomed view of dynamically adapted grid for the hurricane Frances case presented in Fig. 4 (*top right figure*). Note that grid resolution continuously ranges from 60 km down to 1 km or less

provides not only a higher resolution in the region of evolving weather systems (dynamic adaptation), but also allows a natural interaction with and influence upon the larger scale flow avoiding the wave-reflecting problem. We are currently investigating the possible impact of using solution adaptive modeling technique on a better TC intensity forecast. This work is still under investigation.

Combining remote sensing data sets (i.e., 3D or 4D data assimilation) with the concept of solution adaptive modeling technique presented above may be the most beneficial in improving TC track and particularly intensity forecast. For example, SST is one of the most important data set in accurately determining the storm intensity. We have also investigated the impact of warm sea surface temperature anomaly (SSTA) position on hurricane intensification, using the following remote sensing and buoy data combined with a numerical model:

- SST from the Geostationary Operational Environmental System (GOES) at 6 km resolution from the NASA JPL (http://podaac.jpl.nasa.gov/).
- SST from the tropical rainfall measuring mission (TRMM) microwave imager (TMI) at 0.25° resolution from the Remote Sensing Systems (http://www.ssmi.com). The advantage of using SST from microwave observations, like the TMI, is that it provides retrievals even under intense cloudy conditions associated with TC's.
- Buoy observations of winds, SST, surface air temperature, and dew point from the National Data Buoy Center (NDBC) (http://www.ndbc.noaa.gov/).

For example, both the buoy observations and TMI measurements show SST increase in advance of about 2 days prior to the significant intensification of

hurricane Katrina, while surface air temperature declined and reached minimum value at the time of the maximum hurricane intensity. This may be because it may need a period of time for a tropical cyclone to accumulate energy for developing into a hurricane, similar to the evaporation of water vapor, which may need some time to heat the water and make it evaporate, while evaporative cooling makes surface air temperature decrease.

Figure 8 (from Sun et al., 2007) compares the pre-storm SST (27 August 2005) with the post-storm SST (30 August 2005). Figure 8a shows that SST right before the storm development was above 31°C along the Gulf coast and storm track and was much warmer than the long-term mean for August (Fig. 8c). Also, the SST right after the storm passage showed cooling at the right side of the storm track (Fig. 8b). As compared to the pre-storm SST (Fig. 8a), the strongest cooling in SST is over 6°C, and occurred in the right-front quadrant of the storm track, near the location of the strongest intensity (category 5 as represented by red circles), where higher, longer, and more developed ocean waves usually produce higher drag (Moon et al., 2004).

The difference between the SST prior to and after the storm is related to the storm intensity (Zhu and Zhang, 2006). The stronger the TC, the larger is the difference. For Katrina, the pre-storm and post-storm SST difference was up to 6°C.

The SST map shows that the entire Gulf of Mexico was almost uniformly ∼30°C prior to Katrina's intensification (Fig. 8a), while SSTA data show clearly there existed a hot patch along the right side of the storm track, where Hurricane Katrina underwent quick intensification and reached the strongest intensity when it moved into the Gulf of Mexico. It has been found that most clouds and precipitation develop at the right side of the storm track. Desflots et al. (2004) indicate that it is the vertical wind shear that caused this wavenumber one rainfall asymmetry, while shear is due to change of direction of the upper-level wind.

Braun and Tao 2000 showed the significant sensitivity of Hurricane Bob (1991) to several planetary boundary layer (PBL) schemes in MM5 and suggested the dependence of simulated intensity on surface fluxes. We find that the maximum latent heat flux (LHF) occurs at the northeast quadrant or to the right side of storm track, at least at its mature stages. Although the wavenumber one asymmetry may not be caused by high SSTA, because high SST exists at the location of the maximum LHF, and increases the LHF, it enhances the effect of the LHF, and therefore may have played an important role in hurricane intensification.

In order to investigate the effect of the SSTA on hurricane intensification, we performed two control numerical experiments using the latest version of mesoscale model MM5 (Sun et al. 2007). The difference in the simulated tracks was found to be minor. However, as indicated by the pronounced difference in simulated minimum SLP, the simulated hurricane intensity shows remarkable sensitivity to the high SSTA. During the 36–84 h simulations, the control experiment with out the warm SSTA generated weaker intensity or higher minimum SLP than that with the higher SSTA. Although the SST reduction due to storm-induced upwelling and vertical mixing should result in a weaker-simulated hurricane intensity than that simulated when the SST was held constant during the simulations, the simulated

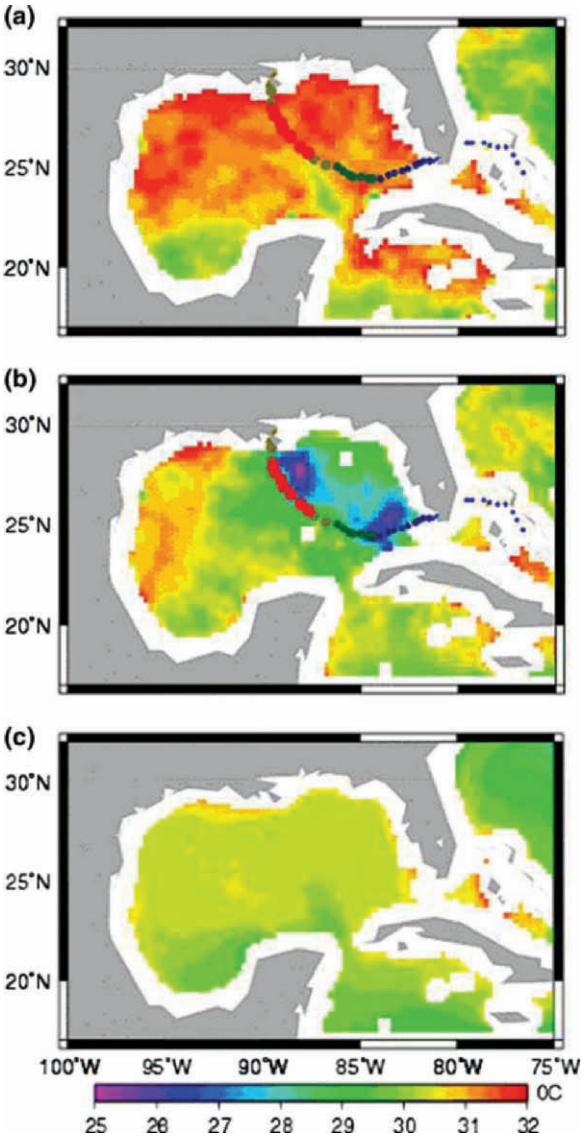

Fig. 8 TMI SST on: (**a**) 26 August 2005 for two days prior to the storm, and (**b**) 30 August 2005 for one day after the storm, and (**c**) 8-year (1998–2005) averaged monthly mean SST in August. The color bar in (**a**) and (**b**) is the same as in (**c**). The circles of different colors indicate the track and intensity of Hurricane Katrina (from Sun et al. 2007)

LHF from the experiment with the warm SSTA at the right side of the storm track is higher than that from the control experiment without higher SSTA, leading to the stronger deepening in the minimum SLP. These experiments further confirm the

TMI observations and show the important impacts of the warm SSTA on hurricane intensification.

Concluding Remarks

This chapter discussed the TC development, including track and intensity forecasting. The accurate simulation of TC track and intensity requires high resolution (in space and time) atmospheric conditions. Given the limited amount of atmospheric data, one obvious method to improve the prediction accuracy of NWP models is to use remotely sensed data to enhance their initial conditions. Undoubtedly, the numerical accuracy of the algorithms and consequently eventual predictions of the NWP models are also closely related to the computational mesh on which the model calculations are performed. Thus, the goal is to implement simulation models with as fine a grid resolution as possible.

In recent years, new grid techniques have been developed to improve prognostic meteorological model predictions. Grid nesting, grid refinement, and unstructured grid techniques all promise to improve the quality of the computed solution in these models. When these new techniques coupled with the adaptive data (particularly remote sensing data) assimilation, the desired improvements in hurricane track and intensity forecast may be achieved.

Acknowledgements This research was supported by the National Science Foundation (NSF) under Grant ATM-0543330, and by NASA grant NX06AF30G.

References

Aberson, S.D., and J.L. Franklin, 1999: Impact on Hurricane Track and Intensity Forecasts of GPS Dropwindsonde Observations from the First-season Flights of the NOAA Gulfstream IV Jet Aircraft. *Bull. Amer. Meteor. Soc.*, **80**, 421–428.

Anthes, R.A., 1970: Numerical Experiments with a Two-Dimensional Horizontal Variable Grid. *Mon. Wea. Rev.*, **98**, 810–822.

Arimoto, R., 2001: Eolian Dust and Climate: Relationships to Sources, Tropospheric Chemistry, Transport and Deposition. *Earth Sci. Rev.*, **54**, 29–42.

Bacon, D.P., N.N. Ahmad, Z. Boybeyi, T.J. Dunn, M.S. Hall, P. C-S. Lee, R.A. Sarma, M.D. Turner, K.W. Waight, S.H. Young, and J.W. Zack, 2000: A Dynamically Adapting Weather and Dispersion Model: The Operational Multi-scale Environment Model with Grid Adaptivity (OMEGA). *Mon. Wea. Rev.*, 128, 2044–2076.

Baum, J.D., H. Luo, and R. Lohner, 1993: Numerical Simulation of a Blast inside a Boeing 747. *AIAA* 93–3091, *24th Fluid Dynamics Conference*.

Bergot, T., G. Hello, and A. Joly., 1999: Adaptive Observations: A Feasibility Study. *Mon. Wea. Rev.*, **127**, 743–765.

Boybeyi, Z.N.N. Ahmad, D.P. Bacon, T.J. Dunn, M.S. Hall, P.C.S. Lee, R.A. Sarma, and T.R. Wait., 2000: Evaluation of the Operational Multi-scale Environment Model with Grid Adaptivity against the European Tracer Experiment. *J. Appl. Meteor*., **40**, 1541–1558.

Boybeyi Z., E. Novakovskaia, D.P. Bacon, M. Kaplan and R. MacCracken., 2007: Targeted GOES Satellite Observations to Improve Hurricane Track Forecast. *Pure and Applied Geophysics*, **164**, 1–18.

Braun, S.A., and W.K. Tao., 2000: Sensitivity of High-resolution Simulations of Hurricane Bob (1991) to Planetary Boundary Layer Parameterizations. *Mon. Weather Rev*., **128**, 12, 3941–12, 3961.

Burpee, R.W., S.D. Aberson, J.L. Franklin, S.J. Lord, R.E. Tuleya., 1996: The Impact of Omega Dropwindsondes on Operational Hurricane Track Forecast Models. *Bull. Amer. Meteor. Soc*., **77**, 925–934.

Camp J.P., and M.T. Montgomery., 2001: Hurricane Maximum Intensity: Past and Present. *Mon. Wea. Rev*., **129**, 1704–1717.

Carlson, T.N., and S.G. Benjamin., 1980: Radiative Heating Rates for Saharan Dust. *J. Atmos. Sci*. **37**, 193–213.

Christopher, S.A., and T. Jones., 2007: Satellite-based Assessment of Cloud-free Net Radiative Effect of Dust Aerosols over the Atlantic Ocean. *Geophy. Res. Lett*., **34**, (L02810), doi:10.1029.

Clark, T.L., and R.D. Farley., 1984: Severe Downslope Windstorm Calculations in Two and Three Spatial Dimensions Using Anelastic Interactive Grid Nesting: A Possible Mechanism for Gustiness. *J. Atmos. Sci*., **41**, 329–350.

d'Almeida, G.A., 1987: On the Variability of Desert Aerosol Radiative Characteristics. *J. Geophys. Res*., **92**, 3017–3026.

Daley, R., 1991: *Atmospheric Data Analysis*. Cambridge University Press, 457 pp.

Desflots, M., S.S. Chen, and J.E. Tenerelli, 2004: A Numerical Study of Rapid Intensity Change in Hurricane Lili, *26*th Conference on Hurricanes and Tropical Meteorology.

Dietachmayer, S.G. and K.K. Droegemeier., 1992: Application of Continuous Dynamic Grid Adaptation Techniques to Meteorological Modeling. Part I: Basic Formulation and Accuracy. *Mon. Wea. Rew*., **120**, 1675–1706.

Dunion, J.P., and C.S. Velden., 2004: The Impact of the Saharan Air Layer on Atlantic Tropical Cyclone Activity. *BAMS*, **85**, 3,353–3,365.

Elsner, J.B., and A.B. Kara, 1999: *Hurricanes of the North Atlantic: Climate and Society*. Oxford University Press, 488 pp.

Elsner, J.B., A.B. Kara, and M.A. Owens., 1998: Fluctuations in North Atlantic Hurricane Frequency. *J. of Clim*., **12**, 427–437.

Evan, A.T., J. Dunion, J.A. Foley, A.K. Heidinger, and C.S. Velden., 2006: New Evidence for a Relationship between Atlantic Tropical Cyclone Activity and African Dust Outbreaks. *Geophys. Res. Lett*., **33**, L19813.

Gelaro, R., R.H. Langland, G.D. Rohaly, T.E. Rossmond., 1999: An Assessment of the Singular-vector Approach to Target Observations using the FASTEX Dataset. Quart, *J. Roy. Meteor. Soc*., **125**, 3299–3328.

Goldenberg, S.B., L.J. Shapiro., 1996: Physical Mechanisms for the Association of El Niño and West African Rainfall with Atlantic Major Hurricane Activity. *J. Climate*, **9**, 1169–1187.

Gopalakrishnan, S.G., D.P. Bacon, N.N. Ahmad, Z. Boybeyi, T.J. Dunn, M.S. Hall, Y. Jin, P.C.S. Lee, D.E. Mays, R.V. Madala, R.A. Sarma, M.D. Turner, and T.R. Wait., 2002: An Operational Multiscale Hurricane Forecasting System. *Mon. Wea. Rev*., **130**, 1830–1847.

Goudie, A.S., and N.J. Middleton., 2002: Saharan Dust Storms: Nature and Consequences. *Earth Sci. Rev*., **56**, 179–204.

Joly, A., D. Jorgensen, M.A. Shapiro, A. Thorpe, P. Bessemoulin, K.A. Browning, J.-P. Cammas, J.-P. Chalon, S.A. Clough, K.A. Emanuel, L. Eymard, R. Gall, P.H. Hildebrand, R.H. Langland, Y. Lemaitre, P. Lynch, J.A. Moore, P.O.G. Persson, C. Snyder, and R.M. Wakimoto., 1997: The Fronts and Atlantic Storm-Track Experiment (FASTEX): Scientific Objectives and Experimental Design. *Bull. Amer. Meteor. Soc*., **78**, 1917–1940.

Jones, R.W., 1977: A Nested Grid for a Three-dimensional Model of a Tropical Cyclone. *J. Atmos. Sci*., **34**, 1528–1553.

Kafatos, M., D. Sun, R. Gautam, Z. Boybeyi, R. Yang, and G. Cervone., 2006: Role of Anomalous Warm Gulf Waters in the Intensification of Hurricane Katrina. *Geophysical Research Letters*, 33, L17802, doi:10.1029/2006GL026623.

Kaufman, Y.J., D. Tanré, and O. Boucher., 2002: A Satellite View of Aerosols in the Climate System. *Nature*, **419**, 215–223.

Kim, H.M., M.C. Morgan, R.E. Morss., 2004: Evolution of Analysis Error and Adjoint-Based Sensitivities: Implications for Adaptive Observations. *J. Atmos. Sci*., **61**, 795–812.

Lau, W.K., and K.M. Kim., 2006: How Nature Foiled the 2006 Hurricane Forecasts. *EOS*, **88**, 9,105–9,107.

Leslie, L.M., J.F. LeMarshall, R.P. Morison, C. Spinoso, R.J. Purser, N. Pescod and R. Seecamp., 1998: Improved Hurricane Track Forecasting from the Continuous Assimilation of High Quality Satellite Wind Data. *Mon. Wet. Rev*., **126**, 1248–1258.

Leutbecher, M., 2003: A Reduced Rank Estimate of Forecast Error Variance Changes due to Intermittent Modifications of the Observing Network. *J. Atmos. Sci*., **60**, 729–742.

Li, F., A.M. Vogelmann, and V. Ramanathan., 2003: Saharan Dust Aerosol Radiative Forcing Measured from Space. *J. Clim*., **17**, 2558–2571.

Lin, Y-L, R.D. Farley, and H.D. Orville., 1983: Bulk Parameterization of the Snow Field in a Cloud Model. *J. Appl. Meteor*., **22**, 1065–1092.

Liu, Yubao, D.L. Zhang, and M.K. Yau., 1997: A Multiscale Numerical Study of Hurricane Andrew (1992). Part I: Explicit Simulation and Verification. *Mon. Wea. Rev*., **125**, 3073–3093.

Lorenz, E.N., 1990: Effects of Analysis and Model Errors on Routine Weather Forecasts, *Proc. ECMWF seminars on 10 years of medium-range weather forecasting*. Reading, UK vol. 1, 115–128.

Mapes, B.E., and P. Zuidema., 1996: Radiative and Dynamical Consequences of Dry Tongues in the Tropical Troposphere. *J. Atmos. Sci*., **53**, 620–638.

McAdie, C.J., and M.B. Lawrence., 2000: Improvements in Tropical Cyclone Track Forecasting in the Atlantic Basin, 1970–98. *Bull. Amer. Meteor. Soc*., **81**, 989–997.

Miller, R.L., and I. Tegen., 1998: Radiate Forcing of a Tropical Direct Circulation by Soil Dust Aerosols. *J. Atmos. Sci*., **11**, 3247–3267.

Moon, I.J., I. Ginis, T. Hara., 2004: Effect of surface waves on air-sea momentum exchange. Part II: behavior of drag coefficient under tropical cyclones. *J. Atmos. Sci*., **61** (19), 2334–2348.

Pielke, R.A., and C.W. Landsea., 1998: Normalized Hurricane Damages in the United States: 1925–95. *Weather and Forecasting*, **13**, 621–631.

Prospero, J.M., R.A. Glaccum, and R.T. Nees., 1981: Atmospheric Transport of Soil Dust from Africa to South America. *Nature*, **289**, 570–572.

Prospero, J.M., and P.J. Lamb., 2003: African Droughts and Dust Transport to the Caribbean: Climate Change Implications. *Science*, **302**, 5647 1024–5467 1027, doi:10.1126/ science.1089915.

Skamarock, W.C., J. Oliger, and R.L. Street., 1989: Adaptive Grid Refinement for Numerical Weather Prediction. *J. Comput. Phys*, **80**, 27–60.

Sun, D., M. Kafatos, G. Cervone, Z. Boybeyi, and R. Yang, 2007: Satellite Microwave Detected SST Anomalies and Hurricane Intensification. *Natural Hazards,* Springer (in press).

Tompkins, A.M., 2001: Organization of Tropical Convection in Low Vertical Wind Shears: The Role of Water Vapor. *J. Atmos. Sci*., **58**, 529–545.

Thompson, J.F., 1984: Grid Generation Techniques in Computational Fluid Mechanics. *AIAA J*., **22**, 1505–1523.

Vitart, E., J.L. Anderson, and W.F. Stern., 1999: Impact of Large-scale Circulation on Tropical Storm Frequency, Intensity, and Location, Simulated by an Ensemble of GCM Integrations. *J. Clim*., **12**, 11 3237–11 3254.

Weaver, C.J., P. Ginoux., N.C. Hsu., M.-D. Chou, and J. Joiner., 2002: Radiative Forcing of Saharan Dust: GOCART Model Simulations Compared with ERBE Data. *J. Atmos. Sci*., **59**, 3,736–3,747.

Wilhelmson, R.B., and C.S. Chen., 1982: A Simulation of the Development of Successive Cells along a Cold Outflow Boundary. *J. Atmos. Sci*, **39**, 1466–1483.

Wu, L., S. Braun., J. Qu., X. Hao., 2006: Simulating the Formation of Hurricane Isabel (2003) with AIRS Data. *Geophys. Res. Lett*., 33, L04804, doi:10.1029/2005GL024665.

Yoneyma, K. and D.B. Parsons., 1999: A Proposed Mechanism for the Intrusion of Dry Air into the Tropical Western Pacific Region. *J. Atmos. Sci*., **56**, 1524–1546.

Zhang, C., and M.-D. Chou., 1999: Variability of Water Vapor, Infrared Radiative Cooling, and Atmospheric Instability for Deep Convection in the Equatorial Western Pacific. *J. Atmos. Sci*., **56**, 711–723.

Zhu, T., and D.L. Zhang., 2006: The Impact of the Storm-induced SST Cooling on Hurricane Jntensity. *Adv. Atmos. Sci*., **23** (1), 14–22.

Roadmap to Assess the Economic Cost of Climate Change with an Application to Hurricanes in the United States

Stéphane Hallegatte

Abstract This paper presents a methodological roadmap to assess macro-economic damages from climate change. To do so, it explores a single manifestation of climate change in a single location: an increase in hurricane intensity in the United States. The presentation starts from a global climate change, namely a homogenous 10 percent increase in hurricane potential intensity, and follows the causal chain to total macro-economic losses. First, the large-scale change is downscaled to a spatial scale pertinent to investigate socio-economic impacts. Here, the Emanuel hurricane model is used to estimate present and future local landfall probabilities. Second, a statistical analysis of historical landfalls is used to translate these probability changes into direct economic losses. The paper also discusses several adaptation strategies that could be implemented to limit these losses. Finally, a modified Input-Output model is used to investigate indirect losses due to macroeconomic mechanisms and feedbacks. This model translates the changes in direct losses into changes in total losses. The model suggests that total losses increase non-linearly, amplifying the role of the most extreme events. The paper then proposes adaptation strategies that can reduce indirect losses by improving the ability of the economy to reconstruct and deal with the consequences of disaster.

Introduction and Motivation

Estimating the economic consequences of climate change is a tricky task for various reasons. The first one is that climate and weather influence, more or less, almost all human activities from leisure to industrial production. Assessing this influence is made difficult by the multiplicity of these human activities. But even when considering only a few activities, the task remains problematic. Indeed, uncertainties are large in all components of the analysis. The future economy that will be impacted by climate change will differ from today's economy, and even small changes in economic development can make a difference in climate change

J.B. Elsner and T.H. Jagger (eds.), *Hurricanes and Climate Change,*
doi: 10.1007/978-0-387-09410-6,

impacts. For example, a reduction in poverty and an improvement in housing quality can reduce vulnerability to climate change. Climate change impacts will therefore vary with levels of economic development as well as with levels and types of climate change.

But future economies are not the only unknown components: future climate is also uncertain. While there is an agreement about the largest patterns of climate change (IPCC, 2007), local changes are still very uncertain. Unfortunately, impacts are mainly at the local scale, and this uncertainty makes it very difficult to investigate climate change impacts.

Also, all economic agents will respond to climate impacts by implementing adaptation strategies, therefore reducing damages. Their ability to do so, however, is difficult to predict, as it depends on the ability to detect a change in climate conditions in due time, to develop technical or institutional responses to this change, and to implement these responses in an efficient way (Hallegatte, 2007a). Past experience shows that detection failure, ill-adaptation, and over-reactions are common in such situations. This makes the efficiency of adaptation dependent on subtle local factors, which are difficult to measure and predict.

Finally, even when impacts can be estimated with some level of confidence, e.g. an impact on agriculture in a region, the indirect effects of this impact on the entire society or economy is very difficult to assess. For instance, if one important sector of the economy is made unprofitable by climate change, the overall impact on the economy depends on complex interaction of factors including the ability of workers to shift to other economic sectors, the ability of investors and entrepreneurs to create rapidly profitable activities in new sectors, and the ability of the government to facilitate the transitions and support the households in difficulty.

In spite of these difficulties, this paper aims at proposing a methodological roadmap to assess sectoral and regional impacts of climate change. To highlight methodological issues, it focuses on one well-studied phenomenon – hurricanes –, on one period of time – the end of this century –, and on one well-studied region, the U.S. Atlantic and Gulf coastline. The paper proposes an assessment of the additional hurricane losses due to climate change over this region and at this time. It summarizes and combines several analyses from different disciplines, namely climatology, engineering and economy, within an interdisciplinary framework that is presented in Fig. 1. The methodology that is described could then be adapted to other regions and other climate change phenomena (e.g. winterstorms, flood, etc.). Most importantly, the present paper emphasizes the main difficulties in the assessment of the economic impacts due to climate change, and highlights issues on which additional research is needed.

The study of hurricane risk in the U.S. is a good candidate to demonstrate such a methodological roadmap because hurricanes represent a real concern in the U.S. and in the rest of the world. Indeed, many recent hurricane seasons have been particularly active, and the 2005 season remains the most active in recorded history, with 28 tropical storms, 15 hurricanes, 7 strong hurricanes (category 3 and higher); Wilma was the most intense hurricane ever observed over the North Atlantic. Some have argued that the level of hurricane activity in the North Atlantic exhibits

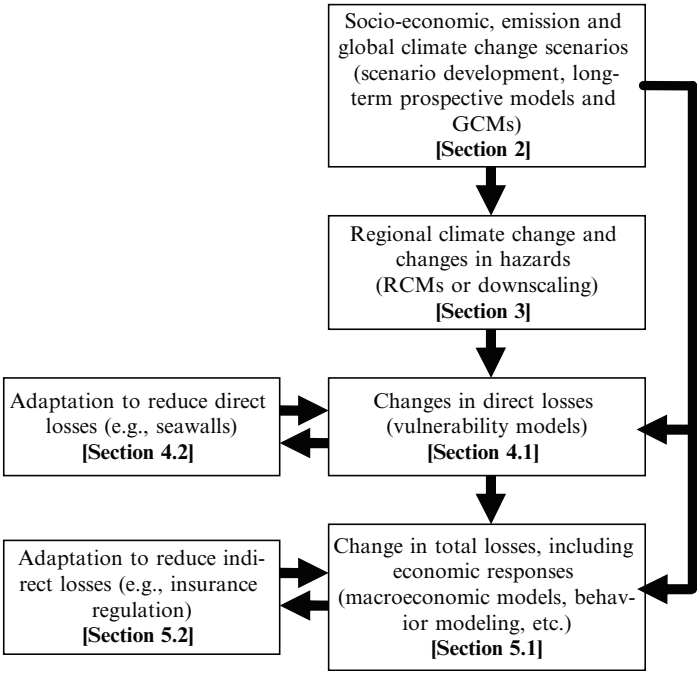

Fig. 1 The different components necessary to assess climate change impacts

inter-decadal oscillations that fully explain the present level of activity (e.g., Landsea, 2005), while others have suggested that climate change is responsible for the current situation (Emanuel, 2005; Webster et al., 2005). Regardless, the uninterrupted rise in social vulnerability (e.g., Pielke, 2005; Pielke et al., 2007), combined with the possibility that climate change may increase future hurricane intensity and frequency has raised concerns about the management of hurricane risks in the U.S. Investigating hurricane risks in relation to climate change is also important because of the high cost of coastal protection and because of the lifetime of these infrastructures. This long lifetime makes it essential to anticipate future changes in hurricane risks to avoid infrastructure ill-adaptation and sunk costs (see, e.g., Hallegatte, 2006).

In the course of this century, climate change will modify many identified drivers of hurricane activity (see, e.g., Bove et al., 1998; Murnane et al., 2000; Elsner et al., 2000; Elsner et al., 2001; Jagger et al., 2001; Emanuel, 2005): sea surface temperature, vertical wind shear, global circulation, tropopause temperature, El Niño and NAO properties, etc. The following considers only an increase in potential intensity, which summarizes not the full set of drivers but only the thermodynamical drivers of hurricanes. This paper assumes a global 10-percent increase in potential intensity, which corresponds roughly to a 2°C warming of the Atlantic Ocean

(Emanuel, 2005), all other environmental drivers being unchanged. A more detailed analysis accounting for other parameters will be published in a follow-up article.

One major drawback of the present analysis is that uncertainty is discussed but is not quantified, because only one model is used in each component of the analysis. As a consequence, this paper proposes only one estimate of the climate change influence on hurricane losses. To inform public policy and guide adaptation strategies, however, a best guess is insufficient: an uncertainty estimate, or at least an assessment of confidence level, would also be necessary (on this issue, see the IPCC guidelines, Manning et al, 2004, and a discussion in the conclusion of this article). Another drawback is that climate change will occur in many other forms than through shifts in hurricane activity. Hurricanes in the U.S. coastline represent only a part of the climate change impacts in this region and other perils need to be considered in conjunction (e.g., sea level rise). However, the narrow focus here is consistent with the aim of this paper, which is to demonstrate a methodology to estimate climate change damages rather than to provide new estimates of aggregate climate change damages.

The paper is organized following the causal chain from global climate change to economic damages, which is presented in Fig. 1. Section 2 will describe the socio-economic, emission and climate scenarios that are used in this article. Section 3 shows how to downscale simulations of global climate change, i.e. how to translate climate change information at the pertinent scale of analysis. Section 4 translates the changes in hurricane risk into changes in direct losses caused by hurricanes in the U.S. Atlantic and Gulf coastline. Section 5 translates these changes in direct losses into indirect economic impacts, taking into account macroeconomic feedbacks and limitations in reconstruction capacity, and provides a mean to estimate total macro-economic costs of the change in hurricane activity. Section 6 concludes from a methodological and substantive point of view, and highlights the need for future research.

Socio-Economic, Emission and Climate Scenarios

The first information that is needed to carry out an impact assessment is the baseline (or control) scenario, i.e. a scenario in which no climate change is included. Such scenarios have been developed by the Intergovernmental Panel on Climate Change (IPCC), in the Special Report on Emission Scenarios (SRES, Nakicenovic and Swart, 2000). The numerous SRES scenarios describe the world evolution in terms of demography, technology and economy, with different assumptions about, for instance, how the world becomes more globalized or remains regionalized or how economic development focuses on industrial production. These scenarios, however, are at a very low spatial resolution, considering only large regions.

From these socio-economic scenarios, global emission scenarios can be derived, for all greenhouse gases (GHG). From GHG emissions, carbon cycle and climate models (or General Circulation Models, GCMs) can produce climate scenarios, i.e.,

possible evolutions of all meteorological variables (temperature, precipitation, wind, pressure, etc.) at a resolution of about 200 km.

Both the socio-economic and climate scenarios, therefore, are not at a resolution that would allow a local impact analysis to be carried out. Hurricane damages, indeed, depend on population and exposure in coastal areas, on building norms, on wind speed at the scale of a neighbourhood, and other local information. This information, obviously, is not available in the scenarios developed at the global scale.

First, therefore, an impact assessment requires a *socio-economic downscaling*, i.e. the development of a local scenario that describes the socio-economic conditions at a pertinent scale. This is very difficult, because predicting social and economic trends is very difficult. An alternative, therefore, is to consider the current society and economy, and to assess the impact the future climate would have on current societies and economies. The drawback of such an approach is that vulnerability can change over time, as explained in Section 4.2. This is especially the case in developing countries where (i) the shift from the primary sector (agriculture) to other economic sectors reduces the vulnerability to climate events; (ii) the improvement in the standards of living (especially for housing quality) limits damages due to extreme weather; (iii) governments and local institutions become more able to implement mitigation policies and emergency measures. In developed countries, however, this difficulty in assessing future vulnerability is less serious, because economic changes that are expected in the next decades are less dramatic. The advantage of considering the current economy, moreover, is to control uncertainty and reduce the number of unknown parameters in the analysis.

Then, climate change also needs to be downscaled at the spatial scale that allows for impact analysis. The next section will discuss the methods to do so.

Downscaling from Global Climate Change to Local Impacts

To assess climate change impacts, one usually starts from one or several socio-economic scenarios and uses one or several GCMs to create "climate scenarios", i.e. low-resolution global simulations of climate change. Typically, GCMs will be able to provide time series for meteorological variables with a very short time sampling (up to hourly) and a medium to low resolution at the horizontal scale (so far, up to 100 km). Such a spatial resolution is sometimes good enough to carry out impact analyses, e.g. to assess the impact on agriculture or forestry.

Quite often, however, impacts are precisely localized, and a higher resolution is needed. It is the case when local characteristics play an important role and when weather conditions have a high variability. Such a situation occurs in mountain areas, where orography is essential, or in cities, where the urban heat island can play a significant role. In such situations, it is necessary to downscale GCM output, to get climate scenario at a resolution that is high enough to be used in impact models. Some sort of downscaling is also needed when the phenomena that one wants to consider are too small to be adequately reproduced by GCMs. Examples of such

phenomena are heavy precipitations that have a spatial scale of the order of a few kilometres or tropical cyclones. Tropical cyclones cannot be reproduced by GCM because their intensity depends on small-scale processes around the eye that a 100km-resolution model cannot resolve.

There are two ways of downscaling: using statistical methods or physical models. The first method uses statistical relationships, calibrated on historical data, to relate large-scale drivers – which GCMs can reproduce – to local phenomena – which GCMs cannot reproduce. Even though our knowledge of the laws of physics helps selecting potential predictors, this method is not directly based on physical laws. Example of this method applied to hurricanes is provided by Elsner and Jagger (2006), who estimate the return level of extreme hurricane wind on the U.S. coastline, as a function of global climate indices like ENSO and NAO. Statistical methods have often a good prediction skill. Statistical models, however, have two main drawbacks: first, they need long series of reliable data; second, it is difficult to know the validity domain of statistical relationships. While physical laws will not change in the future (even though we may find out that they are not what we used to think they are), a statistical relationship can be different in a different climate. For instance, the correlation between sea surface temperature and hurricane intensity is very strong in the present climate (see, e.g., Emanuel, 2005), but it does not mean that if climate gets 2°C warmer, hurricane intensity will automatically increase: the effect of a local or temporary perturbation may be different from the effect of a global or permanent change.

To avoid this validity problem, one may use physical models, which often have a lower skill than statistical models (see an example on hurricanes in Emanuel et al., 2006), but which are based on physical laws that will not change in the future. These physical models, used to downscale GCM output, can be Regional Climate Models (RCM) that take as input a large-scale forcing produced by GCM (see examples of this approach in Christensen and Christensen, 2007), or specific models like hurricane models. An example of application of this method on hurricanes is provided by Emanuel (2006), who uses a hurricane model that takes as input large-scale conditions (vertical wind shear, potential intensity, etc.), and provides hurricane tracks and intensity. Of course, physical models often require calibration, so that the distinction between physical models and statistical models is sometimes fuzzy.

As an illustration of the methodology, the present paper summarizes the main findings of Hallegatte (2007a), which investigates the changes in hurricane risk due to a 10-percent increase in potential intensity. To do so, this work uses the synthetic hurricane tracks, which were produced using a physical model described in Emanuel (2006). Two sets of tracks are used. First, a set of 3000 tracks (with 1862 landfalls), which has been produced using large-scale drivers that correspond to the present climate. This set is referred to as Present Climate (PC). Second, another set of synthetic tracks, which has been produced assuming a 10 percent increase in potential intensity, compared with the present climate conditions. Such an increase in potential intensity, together with other environmental changes and with a large uncertainty, is expected at the end of this century (Emanuel, 2005).

This set also contains 3000 tracks, with 1912 landfalls, and is hereafter referred to as Modified Climate (MC). Comprehensive description and validation of these synthetic tracks are provided in Emanuel (2006).

These tracks are used to assess how the increase in potential intensity could modify the annual probability of hurricane landfall on the U.S. Atlantic and Gulf coastline. Figure 2 shows these probabilities as derived from the HURDAT database, from the Emanuel's model in the present climate, and from the Emanuel's model in a climate where potential intensity has increased by 10 percent. It can be seen that the model is able to reproduce fairly well the historical probability of landfall, except for the weakest hurricane of category one. This discrepancy arises probably from the track model that assumes that the storm is well structured, which might not be the case of weak storms. For the strongest hurricanes, of category 2–5, the model fits well with present-day data. For these intense hurricanes, the model predicts an increase in the annual probability of landfall, and the higher the category, the larger is the probability increase. For category 5 hurricanes, the annual probability of landfall even soars from 7 percent to 21 percent, suggesting that the risk of large-scale disaster could be significantly increased by climate change.

More useful for risk analysis, the synthetic tracks can provide, see Tables 1 and 2, the annual probability of landfall for the five categories of the Saffir-Simpson scale, in 11 regions of the U.S. Atlantic and Gulf coastline (see the region definition in Hallegatte, 2007a, or in the United States Landfalling Hurricane Project website, http://www.e-transit.org/hurricane/map.asp"). These tables highlight where hurricane risk could be enhanced. In particular, one can notice (i) the 10-fold increase in the category-5 landfall probability in region 3, which includes New Orleans; (ii) the possibility of category 4 landfalls in the regions 9, 10, and 11, that lies from Virginia State to the Canadian border and include Washington D.C., New York City, Boston, and several other major American cities.

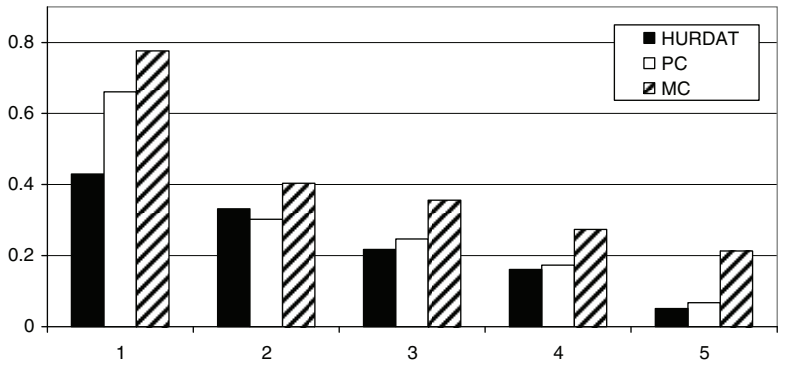

Fig. 2 Annual probability of landfall of a hurricane of a given category, according to historical data (HURDAT), and synthetic tracks in the present (PC) and modified (MC) climate

Table 1 Annual probability of landfall of a hurricane of each category, in the 11 region, for the present climate

Region	Category				
	1	2	3	4	5
1	8.9%	2.6%	1.0%	2.9%	0.0%
2	17.0%	3.2%	2.6%	3.2%	0.6%
3	11.6%	4.8%	3.6%	2.3%	0.3%
4	14.2%	5.5%	3.6%	1.0%	1.3%
5	22.1%	6.4%	7.3%	5.1%	3.6%
6	4.2%	1.9%	1.6%	0.3%	0.0%
7	6.1%	4.8%	3.9%	1.3%	0.6%
8	5.8%	1.3%	2.9%	2.3%	0.3%
9	7.0%	2.6%	0.6%	0.0%	0.0%
10	2.3%	0.6%	0.0%	0.0%	0.0%
11	1.3%	1.0%	0.3%	0.0%	0.0%

Table 2 Annual probability of landfall of a hurricane of each category, in the 11 regions, for the Modified Climate (MC)

Region	Category				
	1	2	3	4	5
1	13.9%	2.9%	2.9%	3.9%	1.9%
2	22.8%	7.3%	5.8%	3.2%	3.6%
3	15.6%	5.8%	6.7%	2.9%	2.9%
4	20.5%	7.0%	6.7%	3.2%	2.3%
5	26.9%	9.8%	10.4%	6.4%	9.5%
6	6.4%	3.6%	1.6%	1.0%	0.0%
7	7.0%	3.9%	2.9%	5.5%	2.3%
8	6.7%	3.2%	3.6%	4.2%	0.3%
9	9.8%	5.1%	1.3%	0.3%	0.0%
10	2.9%	0.3%	0.0%	0.3%	0.0%
11	2.9%	0.6%	0.3%	0.3%	0.0%

These results are useful because they describe how hurricane risks could change, which is the most important information for risk managers. They do not tell anything, however, about the economic impact of such a change. To investigate this question, it is necessary to go from hurricane risks – expressed in terms of probability – to the direct losses – expressed in terms (i) of mean annual direct losses and (ii) of probability of exceeding a given level of losses. In particular, these two variables are of the foremost importance for the insurance industry that needs to assess insurance premiums and capital requirements.

From Local Impacts to Direct Losses

This section assesses how changes in hurricane risk could translate into changes in "direct losses", i.e. in the value of the damages to property caused by the hurricane. It is important to note that this paper does not consider fatalities and injuries. This choice can be justified by the fact that, in most cases, fatalities and most injuries due to hurricanes can be avoided thanks to warning systems and evacuation schemes, as shown by the usually small number of fatalities in developed countries. Hurricane Katrina is an outlier in terms on human toll, but such a situation is exceptional and could have been avoided thanks to a more efficient warning and evacuation system. One can expect, therefore, that the human toll of hurricane will remain very low in the future and can, therefore, be disregarded in this analysis.

Assessing Direct Losses

There are two methods to assess how a change in hurricane risks, including surge and wind, would translate into destruction of buildings, equipment and infrastructure. The first one is based on physical models, while the second one is purely statistical.

In most cases, physical models have been developed by consulting companies that advise the insurance industry and help them assess their level of risk. These models are based: (i) on a comprehensive dataset of the *exposure*, i.e. the characteristics and value of the property exposed to a hazard at a fine spatial resolution; and (ii) on vulnerability models, which relate wind speed, flooding depth and any other physical description of a disaster, to a damage ratio, which is the share of the exposure that is destroyed or damaged for a given hazard level. These models describe a hurricane by its wind field and storm surge and estimate damages to properties. The drawback of these models is the amount of data they require – this information is for instance not available for developing countries – and the fact that it is particularly difficult to create scenarios to project exposure over long timescales.

Statistical models, on the other hand, can be very simple. They use past hurricanes, and data on the resulting direct economic losses to create statistical relationships able to predict future damages (Howard et al., 1972; Nordhaus, 2006; Hallegatte, 2007a; Sachs, 2007).

In Hallegatte (2007a) each coastal county is considered separately, using the normalized damages proposed by Pielke and Landsea (1998) and refined in Pielke et al. (2007). In this data set, historical hurricane losses, due to wind and surge, are normalized to remove the influence of changes in population, wealth and price level. As a consequence, for a given hurricane, the dataset estimates the amount of losses that would result if it occurred today. One can assume that the normalized losses due to a hurricane making landfall in the coastal county i depend upon the

hurricane intensity and on the vulnerability of the landfall county. This can be approximated by:

$$L = \alpha_i \cdot W^d$$

where W is the maximum wind speed of the hurricane (as provided for instance by the HURDAT database), and α_i is a vulnerability parameter, which describes the vulnerability of the entire U.S. to a hurricane making landfall in the coastal county i (even if all the losses are not only in the county i). It is interesting to note that losses are assumed here to depend on the cubed wind speed ($d = 3$), which is a proxy for the energy dissipated by the hurricane. This relationship is very conservative compared with other analyses: the statistic analysis by Sachs suggests a much larger value for d, of 6.3; Howard et al. (1972) suggest a mean value of 4.36; and Nordhaus (2006) cites values between 4 and 9. Of course, the larger this value, the larger is the sensitivity of direct losses to a change in hurricane intensity, and our analysis can be considered as conservative on this point.

In spite of data availability problems, this method provides an assessment of local vulnerability parameters, which are reproduced in Fig. 3. Most of these values are consistent with what one can expect, with large values in New York, Miami, New Orleans, Galveston and Currituck County, but an unrealistic value appears in the Lee County. As an illustration of data availability issues, negative bars show counties where no landfall occurred in the recent past and where no vulnerability information can be estimated.

Using this assessment of county vulnerability, one can estimate the mean direct losses due to a set of synthetic hurricanes. For the present climate, this method gives a value of 1578 million U.S.$ per landfall and 980 million U.S.$ per track. These

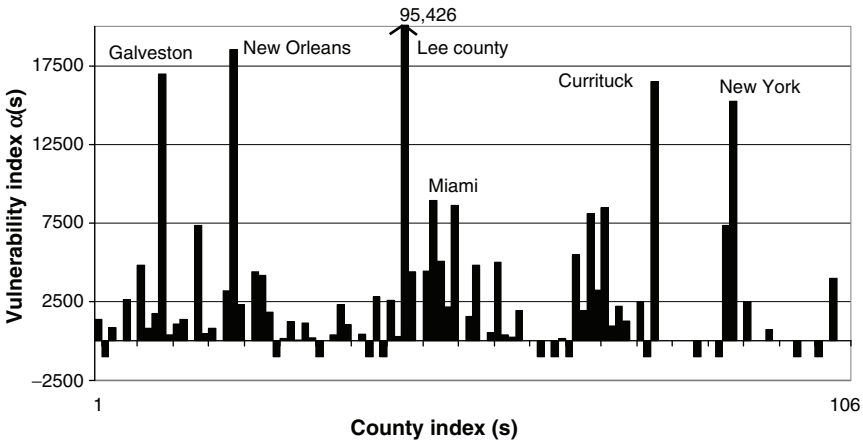

Fig. 3 Historical local vulnerability coefficients, coastal county per coastal county. The negative bars represent the counties where no data is available

values are close to historical values, which are 1833 million U.S.$ per landfall and 1005 million U.S.$ per track. Hallegatte (2007a) shows that the difference between values estimated from the model and the historical values is not statistically significant.

Using these values, and assuming that there is no change in price level, wealth and population, one can produce an estimate of how a change in hurricane intensity or frequency would translate in terms of direct losses. Here, with the Modified Climate assumption with a 10-percent increase in potential intensity, annual direct hurricane losses increase by 54 percent, from about $8 billion to about $12 billion. This cost could then be adjusted as a function of expectations about how the region will develop (how the population will change, how wealthy this population will be, where and how the population will settle). Regardless, this 54-percent increase in the mean annual normalized loss is significant, but it does not seem really threatening for this region, which is one of the richest in the world. This change, nevertheless, should cause an equivalent rise in insurance premiums that can create local issues of insurance affordability (e.g., see RMS, 2006, on the insurability of New Orleans).

Possible changes in the frequency of extreme hurricanes, however, are more worrying: among the 3000 tracks produced by the hurricane model in the present climate, only 59 cause direct losses exceeding $10 billion, and only 4 exceeding $50 billion. Among the 3000 tracks produced for a climate in which potential intensity has been increased by 10 percent, as many as 99 cause direct losses above $10 billion, and 10 cause direct losses above $50 billion. Figure 4 shows the major increase in the probability of the most intense and destructive hurricanes.

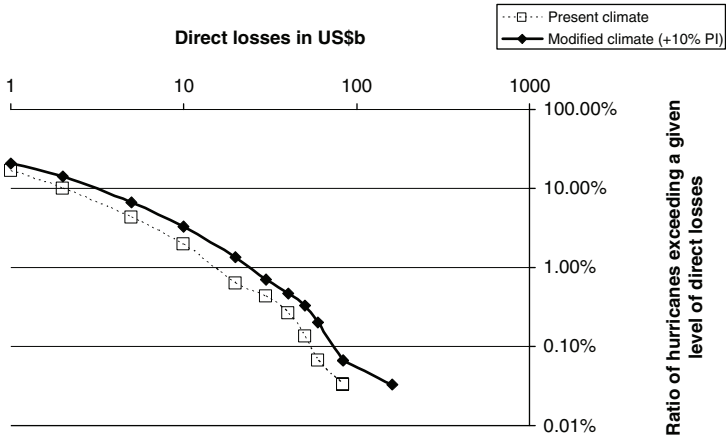

Fig. 4 Cumulative distribution of hurricane losses, including wind and surge, in the present climate and in a climate in which the potential intensity has been increased by 10 percent. For instance, this figure shows that the 0.10% probability event causes about $55 billion losses in the present climate but up to $90 billion in the modified climate

More than the change in annual losses, therefore, it is the doubling of catastrophic event frequency that seems the most problematic for society and the economy.

One important drawback of this assessment is that sea level rise is neglected, even though it is likely to cause a large increase in coastal flooding risks in the future. Nicholls et al. (2007), for instance, found that a 50 cm sea level rise would double the population exposed to the 100-yr flood event in Miami and Greater New York. A more complete analysis would have to take into account this important factor.

Adaptation, Positive and Negative Effects

Since the analysis uses normalized losses that remove the influence of inflation, population and wealth, one can then use scenarios about how these parameters will change in the future to estimate the value of future losses. But this approach cannot take into account other changes, like building norms, protection measures, etc. Only physical models can explicitly take into account how, for example, a change in building norms could reduce hurricane losses.

Numerous actions have been undertaken in the last one hundred years to reduce hurricane damages and these actions demonstrate that adaptation can be effective. First, there are investments in new protection infrastructures like flood protection systems, dams and building elevations. For example, the sea wall built in Galveston in the aftermath of the 1900 hurricane largely mitigated the consequences of Alicia's landfall in 1983. On a smaller scale, the town of Belhaven, Florida, in the aftermath of hurricane Fran (in 1996), implemented a program to elevate 379 houses. When hurricane Floyd struck in 1999, damages were reduced by 80%, thanks to this program (Williams, 2002). Hopefully, the new protection system that is currently built in New Orleans will be more efficient that the system in place before Katrina in 2005.

Second, building codes have been improved and they have limited hurricane damages. The best example is the building code implemented in Florida after Andrew's landfall, even though its effects are only starting to be visible. Also, existing norms have been enforced more rigorously, since hurricanes have shown that the lack of compliance with existing rules had significantly increased damages. The impact of building codes is far from negligible: according to Ryland (2002), "if all buildings in South Florida were either retrofitted or in compliance with the post-Andrew South Florida Building Code, or the new Florida Building Code that went into effect this year [2002], another Hurricane Andrew would cause only about half as much damage to residences and 40 percent less damage to commercial property. The combined loss reduction would be about $10.4 billion, according to the study".

Third, hurricane track forecasts have improved and better warning systems have been implemented to help people and business to prepare for hurricane landfalls and avoid damages. With early warning, people and businesses can protect houses and suspend dangerous industrial processes, which in turn will reduce direct and

indirect damages. For instance, flood damages experts quoted in Carsell (2004) estimate that a 48-hour warning can reduce flood damages by up to 50%, thanks to small-scale preparation actions inside houses. Also, protecting windows reduces wind damages by 12 to 54 percent (Williams, 2002). Preparing industrial facilities can also avoid large pollution and other ancillary damages that can be deadly and costly (e.g., RMS, 2005).

Fourth, individual responses to natural risks may have improved thanks to the direct observation of hurricane consequences or thanks to educational efforts implemented in disaster aftermaths. Nathe (2000) assess the efficacy of public education to reduce earthquake losses and this analysis has parallels with other types of natural disaster.

Most importantly for future vulnerability, much can be done to reduce risk through urban planning and land-use management (Burby and Dalton, 1994). According to the National Research Council's Board on Natural Disasters (1999), "Communities can often achieve significant reductions in losses from natural disasters by adopting land-use plans," and the Second National Assessment on Natural and Related Technological Hazards concluded that "No single approach to bringing sustainable hazard mitigation into existence shows more promise at this time than increased use of sound and equitable land-use management" (Mileti 1999). It seems, therefore, that including risk management in land-use planning could very efficiently reduce vulnerability to hurricanes and therefore reduce the direct losses from hurricane. The drawback of this method is its long timescale for implementation. A building has a long lifetime and the stock of buildings already present cannot be replaced instantaneously. Better land-use management would reduce hurricane damages only after several decades. Looking forward to assess hurricane risks by the end of this century, however, it is possible that improved land-use and urban planning could decrease vulnerability and largely compensate for almost any increase in hurricane risk.

When considering adaptation, however, one has to look at the details of how adaptation strategies can be implemented. In particular, as demonstrated in Hallegatte (2006) and Hallegatte et al. (2007a), uncertainty about future climate is a strong obstacle to the implementation of adaptation measures. Indeed, while the cost of adaptation is immediate, the benefits from adaptation measures are uncertain and delayed in the future. For instance, rejecting building permits in a zone that may become excessively vulnerable to hurricane storm surge if hurricane intensity increases in the future has an immediate political and economic cost. But the benefits of such a measure, namely limiting losses from future property expropriation because hurricane risk has become too high, are uncertain. These benefits depend on how hurricane characteristics will change in the future, which is still largely unknown. It is understandable, therefore, that costly adaptation and risk-management decisions are not always made, in spite of estimates suggesting that there will be long term benefits if climate change projections are correct. To improve this situation, innovative decision-making frameworks have to be promoted, especially those that favour decisions that can be reversed if necessary. As an example, allowing the urbanization of an area is hardly reversible: when

buildings have been built, it is economically and politically costly to retreat from the area. On the opposite, prohibiting the urbanization of an area is highly reversible, since urbanization can then be allowed at any time and at no cost. In presence of uncertainty, the latter option should, therefore, be valued higher.

Regardless, it is important to make a difference between (i) optimal adaptation measures that can be theoretically implemented if future climate and risks were known, and if decision-making processes were perfectly rational, and (ii) realistic adaptation strategies, that take into account political and economic constraints and uncertainties about future climate.

To measure the benefits from adaptation measures, it is essential to take into account also their negative side-effects. For instance, in the case of coastal infrastructure to protect against storm surge such as sea walls, these may threaten the tourism industry because they change landscape, ecosystem health and beach leisure attractions. Coastal attractiveness for leisure and tourism activities is closely linked to various parameters such as landscapes (Lothian, 2006), the quality of the environment, water availability, etc. As a consequence, in some contexts, hard protection would simply not be an option.

Also, even if successful cases do exist, geographers around the world have repeatedly demonstrated that adverse effects of dike construction are almost the norm in the past decades (see e.g. Paskoff, 1994). Beach landscape degradation, marine ecosystem damage and loss of leisure activity (e.g. diving) would surely lead to a drastic reduction in tourism flows – or at least to a decrease in the willingness to pay of tourists – leading in turn to declining local incomes. Equally important, hard protection could contribute to fish stocks depletion by further damaging coastal ecosystems (Clark, 1996). Since 90 percent of fishes depend on coastal zones at one point in their life cycle (Scialabba, 1998), such impacts could have a significant impact on economic income from fisheries.

From Direct Losses to Indirect Losses

Different actors in climate change risk management process are interested in different types of information. City planners and flood protection designers are mainly interested in landfall probabilities; insurers focus on average annual direct losses and probabilities of exceeding a given level of damages. But national and local governments, when they perform cost-benefit analyses to assess the desirability of new infrastructure, cannot consider only direct losses. The communities they represent, indeed, suffer not only from direct loss but from total losses, which include many indirect effects including production losses during the recovery and reconstruction periods (see, e.g., Tierney, 1995; Pielke and Pielke, 1997; Lindell and Prater, 2003; Hallegatte et al., 2007b).

Direct cost can be amplified (i) by spatial or sectoral propagation into the rest of the economic system over the short-term (e.g., through disruptions of lifeline services) and over the longer term (e.g., sectoral inflation due to demand surge,

energy costs, insurance company bankruptcy, larger public deficit, or housing prices that have second-order consequences on consumption); (ii) by responses to the shock (e.g., loss of confidence, change in expectations, indirect consequences of inequality deepening); (iii) by financial constraints impairing reconstruction (e.g., low-income families cannot finance rapidly the reconstruction of their home); and (iv) by technical constraints slowing down reconstruction (e.g., availability of skilled workers, difficulties in equipment and material transportation, difficulties in accommodating workers).

To measure the impact of these effects, Hallegatte et al. (2007b) introduced the *Economic Amplification Ratio* (EAR), which measures the ratio between the overall economic cost and the direct loss due to a disaster. While this ratio is less than one for small-scale disasters, EAR is found, using a simple model, to increase dramatically for large-scale disasters like the New Orleans floods. This increase arises mainly from propagation effects between sectors or regions, and from the addition to capital replacement costs of the production losses during the reconstruction phase. For example, if a $1 million plant is destroyed and immediately rebuilt, the loss is equal to $1 million; if its reconstruction is delayed by one year, the total loss is the sum of the replacement cost and of the value of one year of production. For housing, the destruction of a house with a one-year delay in reconstruction has a total cost equal to the replacement cost of the house plus the value attributed to inhabiting the house during one year. The value of such production losses, in a broad sense, can be very high in some sectors, especially when basic needs are at stake (housing, health, employment, etc.).

To carry out cost-benefit analyses in a fair way, indirect losses must be estimated in spite of the difficulties to do so. A model able to provide an assessment of a fraction of these indirect losses will now be proposed and applied, as an illustration, on the landfall of Katrina on Louisiana. This case study illustrates how indirect losses can be estimated, and how difficult this assessment is.

Assessing Indirect Losses

Case Study on Katrina and Louisiana

The assessment of the total cost of disasters is the topic of intense research (e.g., Rose et al., 1997; Brookshire et al., 1997; Gordon et al., 1998; Cochrane, 2004; Okuyama, 2004; Rose and Liao, 2005; Greenberg et al., 2007). In this literature, however, nobody pretends to reproduce all the mechanisms involved in disaster aftermaths. In the present article, only two types of indirect effects are accounted for: (i) the propagation effect between sectors; (ii) the reconstruction duration and the production loss during this period.

Many models used to assess disaster consequences are based on Input-Output (IO) models, which are powerful tools to assess how a shock, on one or several sectors, propagates into the economy through intermediate consumption and demand.

In Hallegatte (2008a), a modified IO model has been proposed: the Adaptive Regional Input-Output (ARIO) model, which is based on IO tables and a hybrid modelling methodology, in the spirit of Brookshire et al. (1997). This dynamic model takes into account changes in production capacity due to productive capital losses and adaptive behaviour in disaster aftermaths. Importantly, the model takes as an assumption that the Louisiana economy will eventually return to its pre-storm situation. Of course, the uncertainty in results is still very high and the model results must be considered only as indicators of the disaster seriousness.

As an illustration, this model is applied to the landfall of Katrina on Louisiana. Following the classification by the Bureau of Economic Analysis, the Louisiana economy is constituted of 15 sectors: (1) Agriculture, forestry, fishing, and hunting; (2) Mining; (3) Utilities; (4) Construction; (5) Manufacturing; (6) Wholesale trade; (7) Retail trade; (8) Transportation and warehousing; (9) Information; (10) Finance, insurance, real estate, rental, and leasing; (11) Professional and business services; (12) Educational services, health care, and social assistance; (13) Arts, entertainment, recreation, accommodation, and food services; (14) Other services, except government; and (15) Government. From the U.S. Input-Ouput tables, a regional one for the state of Louisiana is built. Sector losses due to Katrina have been evaluated by the Committee on the Budget U.S. House of Representatives, and are reproduced in Figure 5.

From these sectoral losses, the model simulates the reconstruction of the region, as shown in Figure 6. In its upper panel, this figure provides the evolution of the "regional economic production", i.e. the sum of the value added by all sectors of the economy. In the bottom panel, one can see that the model predicts a reconstruction period of about 10 years.

Comparisons with available data in Louisiana are proposed in Hallegatte (2008a). The orders of magnitude reproduced by this model are realistic, with an instantaneous production reduction of 8 percent after the shock, and a production

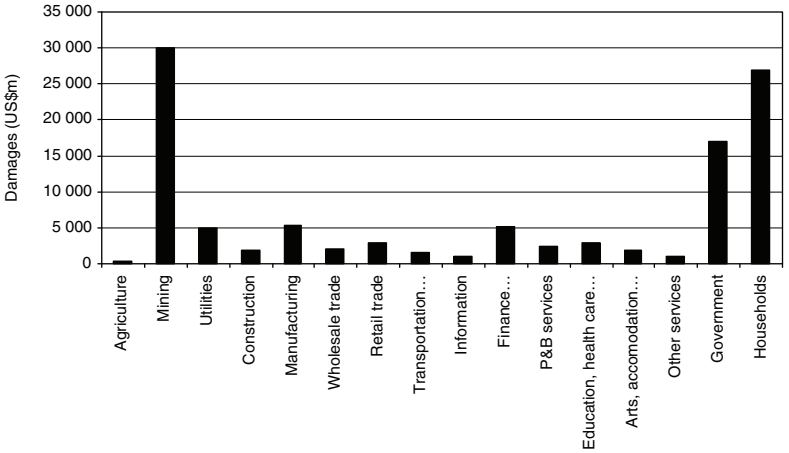

Fig. 5 Sector-per-sector estimated losses due to Katrina in Louisiana

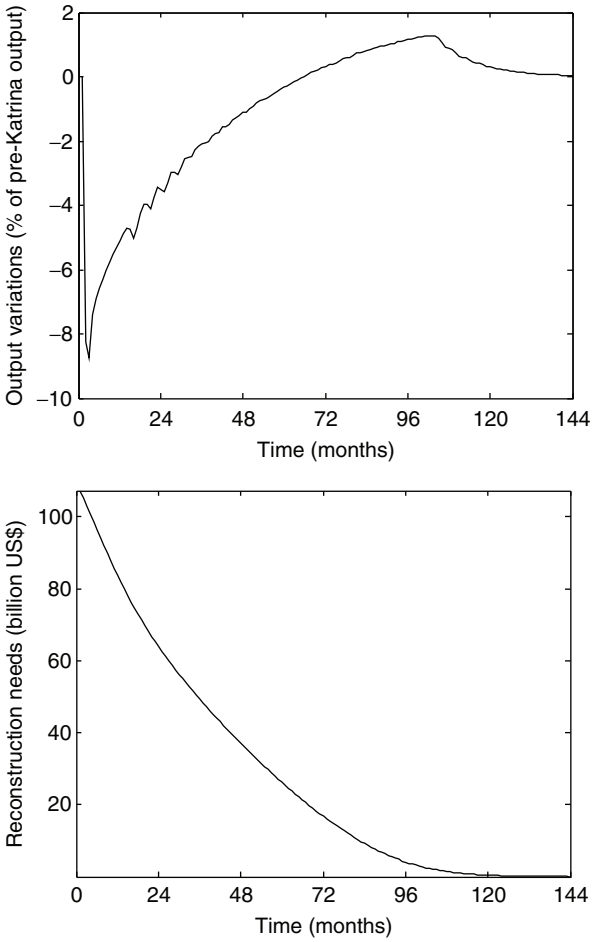

Fig. 6 Louisiana output variation, in percent of pre-Katrina output (*upper panel*); and reconstruction needs in U.S.$ billion (*bottom panel*)

loss over the four last months of 2005 of 2.8 percent of annual Gross State Product. This production loss underestimates the observed growth loss, which is close to 4.5 percent according to BEA data when exogenous growth is removed. This underestimation is likely to arise from the model inability to reproduce the New Orleans disorganization in the months following Katrina, which is caused by lifeline interruptions, bankruptcy, and supply-chain issues. Additionally, the political and practical issues linked to the reconstruction of New Orleans are not taken into account.

This model also provides the evolution of the production of each sector over time, as shown in Fig. 7. This figure shows (i) the generalized decrease in production following the event (the horizontal dark region); (ii) the large increase in

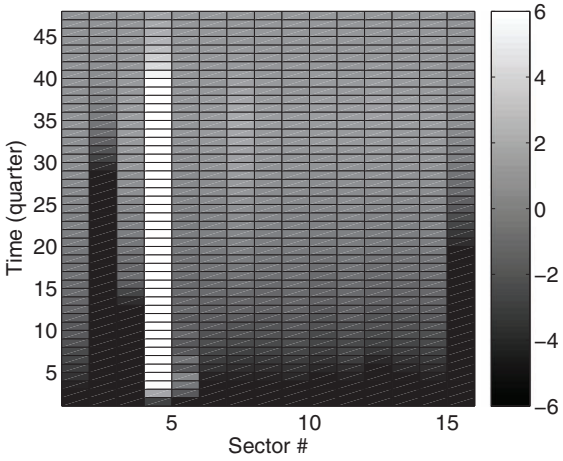

Fig. 7 Louisiana output variation, sector per sector (X-axis) as a function of time in quarter (Y-axis), in percent of pre-Katrina output. Dark colors show decrease in production; light colors show increase in production

production in the construction sector (sector #4) caused by the large demand for reconstruction, and the subsequent production increase in the sectors that are large suppliers of the construction sector (e.g., the retail trade sector, sector #7). The sum of these production losses (positive and negative) over the entire reconstruction period is estimated at $28 billion.

Also, the model provides an assessment of the "production loss" in the housing sector. Indeed, the decrease in housing services because of damaged houses and buildings has to be taken into account. The model, because it reproduces the reconstruction period and duration, can assess the total loss in housing service production. In the Katrina's case, the model estimates this loss at $19 billion. As a consequence, the total production loss (sector production plus housing services) is estimated at $47 billion, i.e. 44% of direct losses. Total losses, i.e. the total production loss plus the part of production that has to be dedicated to reconstruction instead of normal consumption, are estimated around $154 billion. The Economic Amplification Ratio, the ratio of total losses to direct losses, is, therefore, equal to 1.44.

Importantly, this model cannot capture all indirect losses. For instance, it does not assess which portion of customer demand will be satisfied and which fraction will be rationed. Such an assessment is not easy, because customers will be more or less able to turn to external producers, depending of the category of goods and services that is considered. If customers are rationed, there is an additional loss that is not included in the present analysis. Also, it is essential to repeat that the model assumes that the economy will return to its initial situation, which is not automatic. In the New Orleans case, it is even quite unlikely. It is difficult to do better, however, because the final state will depend on political choices that cannot be modelled. Finally, this model does not include losses outside the affected region

(e.g., through higher energy prices in the New Orleans case), and social and psychological costs, which are nevertheless very important (e.g., disruption of social networks, psychological trauma, loss of cultural heritage).

But the most interesting aspect of this model is the fact that it allows to relate various amount of direct losses to the corresponding total losses. Figure 8 shows that, for the same sectoral structure than Katrina (shown in Fig. 5), total losses are increasing nonlinearly with total aggregated direct losses. When direct losses are below U.S. $40b, indirect losses are negative. It means that, for most disasters, the response of the economic system damps the shock and limits the economic consequences. But when direct losses exceed U.S. $40b, the economic system is not able to react efficiently any more. Indeed, a larger disaster causes more damages and reduces production capacity in the sectors involved in reconstruction. Because of the interplay of these mechanisms, the Economic Amplification Ratio (EAR), the ratio of total losses to direct losses, increases with the size of the disaster. For a disaster like Katrina, with about $100 billion direct losses, the EAR is found equal to 1.44. For a disaster with $200 billion direct losses, this ratio reaches 2.00, with total costs twice as large as direct costs.

This relationship between direct losses and indirect losses has been estimated for the state of Louisiana in 2005, and for the consequences of Katrina. Of course, results would be different for different states, for instance because the production capacity of the construction sector would be different. Results would also be different for different disasters, for instance because affected sectors would not be the same.

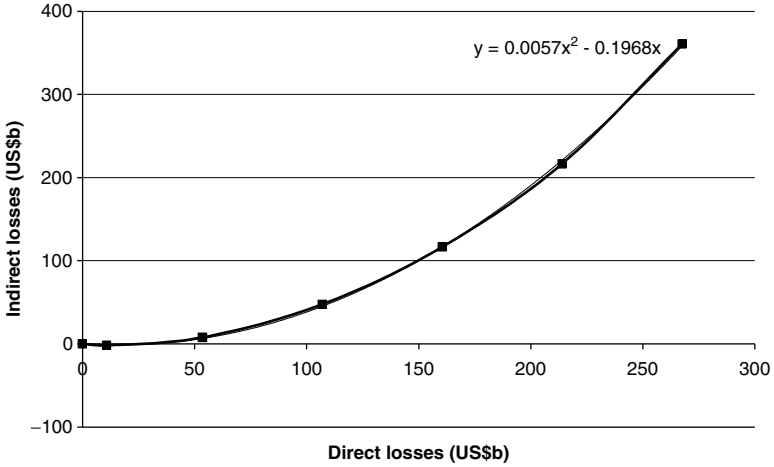

Fig. 8 Indirect losses as a function of direct losses, for a disaster with the same sectoral structure than Katrina. The equation in black is the polynomial regression of indirect losses to direct losses, for this case study

Regardless, results would be different if considering an economy in 2030 or 2080, as needed to assess climate change impacts. It seems out of reach, however, to predict how IO tables will change over several decades. Considering the huge uncertainty that would surround any attempt to do so, it seems reasonable to use the present IO table, possibly scaled to account for economic growth, assuming that all sectors will growth at the same rate. In the present analysis, however, we assess how future hurricane risks would impact the present-day economy, disregarding the impact of economic growth. This assumption corresponds to the suppression of the right-hand arrow in Fig. 1, from the top box on scenarios to the bottom box on indirect impacts. Even though this method is not satisfying, it is the only one available: one can doubt it will soon be possible to project IO tables over decades with enough accuracy to perform this type of analysis on future economies.

In the following, in spite of these large uncertainties, the nonlinearity in total losses is assumed valid for all regions and all disasters, and the Katrina's case is used as a benchmark to provide a first-order estimate of how the changes in direct losses suggested in Section 4 could translate into changes in total losses.

Assessing Indirect Losses

Using a polynomial regression on the relationship between direct and indirect losses calculated for Louisiana and Katrina, one can assess the total losses due to the 3000 synthetic tracks created by the Emanuel's model (see Section 3 and 4). In the present climate, averaged direct losses were estimated at 1578 million U.S.$ per landfall and 980 million U.S.$ per track. These values translate into averaged total losses estimated at 1426 million U.S$ per landfall and 885 million U.S$ per track. These values are lower than direct losses only, because the economic system is able to limit total losses and make them lower than direct losses for the weakest hurricanes, which constitute the large majority of hurricanes. Indeed, indirect losses are positive only for hurricane causing direct losses in excess of $40b, and only 8 landfalls cause such losses in the 3000 synthetic tracks created for the present climate. The taking into account of indirect effects leads, therefore, to a reduction in the mean annual economic losses due to hurricanes.

In the modified climate, since hurricane intensity is increased according to the Emanuel's model, total losses are larger than in the present climate: the model estimates averaged total losses at 2272 million U.S.$ per landfall and 1448 million U.S.$ per track. When considering indirect losses, the Emanuel's model suggests, therefore, that a 10-percent increase in potential intensity would translate into a 59 percent increase in total economic losses.

Like in Section 4, when were considered only direct losses, the most worrying result concerns the very rare, most intense hurricanes. According to the present analysis, with all its drawbacks including the use of a single hurricane model, a 10-percent increase in potential intensity would double the likelihood of a hurricane landfall causing more than $50 billion of damages in the U.S.

Adaptation to Reduce Indirect Losses

Adaptation options able to reduce direct losses were discussed in Section 4.2. But different adaptation options may be able to reduce indirect losses, independently of direct losses. As explained in Section 5.1, indirect losses arise mainly from propagation between sectors and from production losses during the reconstruction. Measures can be implemented to limit these two sources of indirect losses.

First, a resilient economic, i.e. an economy able to cope with a disaster in an efficient manner, is an economy where all producers are not too dependent on their suppliers. This can be the case (1) if the production of the most important production factors (especially the non-stockable goods like electricity) can be rapidly restored; (2) if each company has several redundant suppliers, implying that if one of its suppliers becomes unable to produce because of the hurricane, the company will not be forced to stop its own production; (3) if companies have inventories and can keep producing even when a supplier cannot produce. In that respect, the most recent and efficient industrial organization, with a limited number of suppliers, on-demand production, and small stocks, increases the vulnerability of the economy to disasters.

The resilience is also increased if imports from outside the affected region can replace local production. To do so, essential infrastructures have to be repaired as fast as possible, to reconnect the affected region to the rest of the economy: roads, railways, ports, airports, phone, internet, etc. Much can be done to improve this aspect of resilience: (i) making sure that utility companies and the organizations in charge of transport and communication infrastructures can mobilize enough workers to restore rapidly their services; (ii) facilitating imports in case of disasters (e.g., by simplifying administrative requirements).

Emergency services can also be improved, emergency management plans can be established and maintained, and new institutional structures can be created (see for instance, Hecker et al., 2000), to facilitate a more rapid recovery after the event.

Second, reconstruction must be done as fast as possible to restore production and housing. First, utility companies and the institutions in charge of transport infrastructure must be equipped to face large-scale disasters and reduce as much as possible the period during which their production is interrupted or unreliable. Second, the construction sector has a specific role in a disaster aftermath. There are numerous examples of cases where the reconstruction was slowed down by the lack of qualified workers in the construction sector. For instance, after the explosion of the AZF chemical plant in Toulouse in 2001, tens of thousand of windows had been damaged, and the number of glaziers was far insufficient to satisfy the demand, even though glaziers from all over France came to Toulouse. In the same way, after the particularly destructive hurricane season in 2004 in Florida, roofers were unable to satisfy the demand and reconstruction costs increased by up to 40 percent in some regions (Hallegatte et al., 2008). In most cases, reconstruction involves a few specialties (among which glaziers and roofers), and increasing the number of such specialists can reduce in a significant manner the reconstruction duration. As a

consequence, preparing for disasters by organizing a special status for foreign workers in this needed specialties can speed up the reconstruction, and therefore reduces the total cost of a disaster. Also, administrations can facilitate reconstruction, for instance by making it easier and faster to obtain building permits.

Finally, disasters can also be opportunities. For instance, when a factory has been destroyed, the reconstruction can be done using the most efficient new technology, therefore improving productivity. Examples of such improvement are: (a) for households, the reconstruction of houses with better insulation technologies and better heating systems, allowing for energy conservation and savings; (b) for companies, the replacement of old production technologies by new ones, like the replacement of paper-based management files by computer-based systems; (c) for government and public agencies, the adaptation of public infrastructure to new needs, like the reconstruction of larger or smaller schools when demographic evolutions justify it. Capital losses could, therefore, be limited by a higher productivity of the economy in the event aftermath (see also Albala-Bertrand, 1993; Stewart and Fitzgerald, 2001; Okuyama, 2003; and Benson and Clay, 2004). Several factors, however, make it doubtful that this effect is totally effective in disaster aftermaths (Hallegatte, 2008b). First, production has to be restored as fast as possible to avoid unbearable losses, especially for small businesses. Second, the productive capital is most of the time only partially destroyed, and the remaining capital creates "inheritance" constraints on the replacement capital, preventing the embodiment of new technologies or the adequacy of the capital to new needs.

Conclusions

This paper presents a methodological roadmap to assess climate change economic impacts. To go from the large-scale climate change projected by global climate models to its consequences on society, one has first to downscale this change at the spatial scale that is pertinent to investigate economic impacts. Then, one has to translate local changes into possible changes in direct losses. Of course, adaptation strategies could be undertaken to limit these losses and these possibilities have to be investigated, even though it is often out of reach to provide a quantification of their benefits. Finally, economic mechanisms enter into action to reduce or amplify direct losses: propagation from sectors to sectors, production losses during the reconstruction period, macroeconomic feedback, etc. These indirect effects have to be investigated. Again, adaptation strategies can reduce indirect losses. The quantitative effects of these adaptation strategies are often difficult to assess, but possible options have to be discussed.

Here, this roadmap is applied to one type of climate change economic impacts, namely the hurricanes, in one region, the U.S. Atlantic and Gulf coastline. Despite the difficulty of the exercise, the aim is to illustrate the usefulness of such an assessment and a methodology to do so. The complexity of this interdisciplinary analysis, the multiplicity of the models that have to be used, the uncertainty in the

results from each of these models, and the number of unknown parameters demonstrate the difficulty of climate change impact assessment.

The series of modelling exercises presented in this article can inform various stakeholders, who need specific information. City planners and flood protection designers need information about probability of landfall; insurers need projections of future average annual direct losses and of future probabilities of exceeding various loss levels; national and local governments have to take into account economic indirect effects and, therefore, need assessments of future total losses and ideas about adaptation strategies. The current analysis, in spite of its numerous limitations, tries to provide a comprehensive view of future hurricane risks, as pertinent as possible for all stakeholders.

Obviously, the tools used to assess the changes in landfall probabilities, direct losses and indirect losses are far from perfect, and their results can, and must, be questioned. Different models, based on different assumptions, would have found different results. In presence of so much uncertainty, the main shortcoming of this paper is the fact that only one model was used for each component of the analysis. In a more comprehensive analysis, several models would be used across a range of possible assumptions to bracket the uncertainty of possible results.

With respect to hurricane intensity and frequency, indeed, it seems that the Emanuel's model is particularly pessimistic, predicting a strong increase in hurricane intensity in response to global warming. There is no consensus in the scientific community about future levels of hurricane activity and other researchers (e.g., Landsea, 2005) are more optimistic. City planners and flood protection designers, nevertheless, should take into account the possibility that future hurricane risk could change by as much as is predicted by Emanuel's model. This is especially true when alternatives to be decided about involve very long timescales and are not easily reversible. Many strategies to limit hurricane damages are obviously "no-regret" strategies, meaning that they would yield significant benefit even if hurricane frequency and intensity remain unchanged. But climate change could make their benefits larger, and other strategies could also become cost-effective because of the additional risk that climate change causes.

Clearly, it is much more difficult to design a flood protection system or to manage land-use when there is such a large uncertainty about one of the main natural hazard risks. This is, however, inescapable with the reality of a future with climate change. Climate change introduces more complexity in all decisions that is related with climate conditions, but there is much to be gained by taking into account possible future changes in climate and their full economic impacts. Moreover, this uncertainty is associated with a cost, the *cost of uncertainty*, because, to avoid extensive retrofitting in the next decades, all infrastructures must be designed much more resilient than it was the case in absence of climate change.

This analysis demonstrates that the magnitude of costs associated with extreme-event changes are likely to be large and that the indirect costs are a significant portion of total costs and therefore need to be included in cost estimates. In spite of the difficulties to assess economic costs of such events, the large orders of magnitude suggest that decision-makers should not ignore these in designing responses to

climate change. Decision-makers, from land-use planners and insurers to those involved in the design and implementation of climate policies, will be better able to manage the risks of climate change if they understand the dynamic nature of climate change, the uncertainty that it creates, and the potential scope and extent of its economic impacts.

Acknowledgments The author wants to thank Kerry Emanuel, who developed the hurricane model and provided me with the sets of synthetic tracks, and Raphaël Billé, who provided information about the adverse side-effects of hard protection against hurricanes and sea level rise. François Gusdorf, Jan Corfee-Morlot and Auguste Boissonnade provided useful suggestions and comments on the manuscript. All remaining errors are the author's.

References

Albala-Bertrand, J. M., 1993: *The Political Economy of Large Natural Disasters with Special Reference to Developing Countries*. Oxford: Clarendon Press.

Benson, C., and E. Clay, 2004: *Understanding the Economic and Financial Impact of Natural Disasters*. The International Bank for Reconstruction and Development. The World Bank, Washington D. C.

Board on Natural Disasters, National Research Council, 1999: Mitigation emerges as major strategy for reducing losses caused by natural disasters. *Science*, **284**, 1943–1947.

Bove, M., J. Elsner, C. Landsea , X. Niu, and J. O'Brien , 1998: Effect of El Nino on US landfalling hurricanes, revisited. *B. Am. Meteorol. Soc*., **79**, 2477–2482.

Brookshire, D. S., S. E. Chang, H. Cochrane, R. Olson, A. Rose, and J. Steenson, 1997: Direct and indirect economic losses for earthquake damage. *Earthquake Spectra*, **13**, 683–701.

Burby, R. J., and L. C. Dalton, 1994: Plans Can Matter! The Role of Land Use Plans and State Planning Mandates in Limiting the Development of Hazardous Areas, Public Administration Review, American Society for Public Administration.

Carsell, K. M., N. D. Pingel, and D. T. Ford, 2004: Quantifying the Benefit of a Flood Warning *System. Nat. Hazards Rev*, **5**, 131–140.

Christensen, J. H., and O. B. Christensen, 2007: A summary of the PRUDENCE model projections of changes in European climate by the end of this century, *Climatic Change,* **81**, 7–30.

Cochrane, H., 2004: Economic loss: myth and measurement. *Disaster Prevention and Management*, **13**, 290–296.

Clark, J. R., 1996: *Coastal Zone Management Handbook*. Lewis Publishers, 694 p.

Emanuel, K., 2005: Increasing destructiveness of tropical cyclones over the past 30 years, *Nature*, **436**, 686–688.

Emanuel, K., 2006: Climate and tropical cyclone activity: A new model downscaling approach, *J. Climate*, **19**, 4797–4802.

Emanuel, K., S. Ravela, E. Vivant, and C. Risi, 2006: A statistical-deterministic approach to hurricane risk assessment. *Bul. Amer. Meteor. Soc*., **87**, 299–314.

Elsner, J. B., and T. H. Jagger, 2006: Prediction Models for Annual U.S. Hurricane Counts. *J. Climate*, **19**, 2935–2952.

Elsner, J. B., K. B. Liu, and B. Kocher, 2000: Spatial Variations in Major U.S. Hurricane Activity: Statistics and a Physical Mechanism. *J. Climate*, **13**, 2293–2305.

Elsner, J. B., B. H. Bossak, and X. F. Niu, 2001: Secular Changes to the ENSO-U.S. Hurricane Relationship, *Geophys. Res. Lett*., **28**, 4123–4126.

Gordon, P., H. Richardson, and B. Davis, 1998: Transport-related impacts of the Northridge earthquake. *Journal of Transportation and Statistics*, **1**, 21–36.

Greenberg, M. R., M. Lahr, and N. Mantell, 2007: Understanding the economic costs and benefits of catastrophes and their aftermath: A review and suggestions for the U.S. federal government. *Risk Analysis*, **27**, 83–96.

Hallegatte, S., 2006: A cost-benefit analysis of the New Orleans flood protection system, AEI-Brookings Joint Center. Regulatory Analysis 06–02. Mar 2006.

Hallegatte, S., 2007a: The use of synthetic hurricane tracks in risk analysis and climate change damage assessment, *J. Appl. Meteor. Clim.*, **46**, 1956–1966.

Hallegatte, S., 2007b: Do current assessments underestimate future damages from climate change? *World Economics*, **8**, 131–146.

Hallegatte, S., 2008a: An adaptive regional input-output model and its application to the assessment of the economic cost of Katrina, Risk Analysis, submitted.

Hallegatte, S., 2008b: Can natural disasters have positive consequences? Investigating the role of embodied technical change, Ecological Economics, submitted.

Hallegatte, S., J.-C. Hourcade, and P. Ambrosi, 2007a: Using climate analogues for assessing climate change economic impacts, *Climatic Change*, **82**, 47–60.

Hallegatte, S., J.-C. Hourcade, and P. Dumas, 2007b: Why economic dynamics matter in assessing climate change damages: illustration on extreme events, *Ecological Economics*, **62**, 330–340.

Hallegatte, S., A. Boissonnade, M.-E. Schlumberger, and R. Muir-Wood, 2008: Demand Surge and Worker Migrations in Disaster Aftermaths: Application to Florida in 2004 and 2005, *Journal of Regional Science*, submitted.

Hecker, E. J., W. Irwin, D. Cottrell, and A. Bruzewicz, 2000: Strategies for improving response and recovery in the future, *Nat. Hazards Rev.*, **1**, 161–170.

Howard, R.A., J.E. Matheson, and D.W. North, 1972: The decision to seed hurricanes. *Science*, **176**, 1191–1202.

IPCC, 2007: Climate Change 2007: The Physical Science Basis. Contribution of Working Group I to the Fourth Assessment Report of the Intergovernmental Panel on Climate Change [Solomon S, Qin D., Manning M, Chen Z, Marquis M, Averyt K B, Tignor M, Miller H L (eds.)]. Cambridge University Press, Cambridge, United Kingdom and New York, NY, USA, 996 pp.

Jagger, T., J.B. Elsner, and X. Niu, 2001: A dynamic probability model of hurricane winds in coastal counties of the United States, *J. Appl. Meteor.*, **40**, 853–863.

Landsea, C.W., 2005: Hurricanes and global warming. *Nature*, **438**, E11-E12.

Lindell, M.K., and C.S. Prater, 2003: Assessing Community Impacts of Natural Disasters, *Nat. Hazards Rev.*, **4**, 176–185.

Lothian, A., 2006: Coastal landscape assessment. Coast to Coast Conference, Melbourne, 23 May.

Manning, M., M. Petit, D. Easterling, J. Murphy, A. Patwardhan, H. Rogner, R. Swart, and G. Yohe, 2004: IPCC Workshop Report: Describing Scientific Uncertainties in Climate Change to Support Analysis of Risk and of Options. IPCC, Geneva.

Mileti, D.S., 1999: *Disasters by Design: A Reassessment of Natural Hazards in the United States*, Joseph Henry Press, Washington, DC.

Murnane, R.J., C. Barton, E. Collins, J. Donnelly, J. Elsner, K. Emanuel, I. Ginis, S. Howard, C. Landsea, K. Liu, D. Malmquist, M. McKay, A. Michaels, N. Nelson, J. O'Brien, D. Scott, and T. Webb, 2000: Model estimates hurricane wind speed probabilities. *Eos, Trans. Amer. Geophys. Union*, **81**, 433–438.

Nakicenovic, N., and R. Swart, 2000: Special Report on Emissions Scenarios: A Special Report of Working Group III of the Intergovernmental Panel on Climate Change, Cambridge University Press, Cambridge, U.K., 599 pp.

Nathe, S.K., 2000: Public Education for Earthquake Hazards. *Nat. Hazards Rev.*, **1**, 191–6.

Nicholls, R.J., S. Hanson, C. Herweijer, N. Patmore, S. Hallegatte, J. Corfee-Morlot, J. Chateau, and R. Muir-Wood, 2007. Screening Study: Ranking Port Cities with High Exposure and Vulnerability to Climate Extremes, *OECD Working Paper*, available on http://www.oecd.org/document/56/0,3343,en_2649_201185_39718712_1_1_1_1,00.html

Nordhaus, W.D., 2006: The economics of hurricanes in the United States, prepared for the Snowmass Workshop on Abrupt and Catastrophic Climate Change. Snowmass, CO: Annual Meetings of the American Economic Association.

Okuyama, Y., 2003: Economics of natural disasters: a critical review. Research Paper 2003-12, Regional Research Institute, West Virginia University, USA.

Okuyama, Y., 2004: Modeling spatial economic impacts of an earthquake: Input-Output approaches. *Disaster Prevention and Management*, **13**, 297–306.

Paskoff, R., 1994: *Les littoraux. Impact des aménagements sur leur évolution*. Masson, Géographie.

Pielke, R.A., 2005: Meteorology: Are there trends in hurricane destruction? *Nature*, **438**, E11.

Pielke, R.A. Jr., and R.A. Pielke Sr., 1997: *Hurricanes, their Nature and Impacts on Society*, Wiley, New-York.

Pielke, R.A., and C.W. Landsea, 1998: Normalized Hurricane Damages in the United States: 1925–95. *Weather and Forecasting*, **13**, 621–631.

Pielke, R.A. Jr., J. Gratz, C.W. Landsea, D. Collins, M.A. Saunders, and R. Musulin, 2007: Normalized Hurricane Damages in the United States: 1900-2005. *Nat. Hazards Rev.* (accepted).

RMS, 2005: *Hurricane Katrina: Profile of a Super Cat. Lessons and Implications for Catastrophe Risk Management*. https://www.rms.com.

RMS, 2006: *Flood Risk in New Orleans: Implications for Future Management and Insurability*. http://www.rms.com/NewsPress/PR_120406_NOFloodRisk.asp.

Rose, A., 2004: Economic principles, issues, and research priorities in hazard loss estimation. *Modeling Spatial and Economic Impacts of Disasters*, Okuyama, Y., Chang, S., Eds., Springer, 14–36.

Rose, A., and S.-Y. Liao, 2005: Modeling regional economic resilience to disasters: a computable general equilibrium analysis of water service disruptions. *Journal of Regional Science*, **45**, 75–112.

Ryland, H.G., 2002: Better building codes cut property loss. National Underwriter, 106.

Sachs, A., 2007: *The Influence of ENSO on Hurricane Damages: A New Methodology for Pricing Risk*, PhD Thesis.

Scialabba, N., 1998: *Integrated Coastal Management and Agriculture, Forestry and Fisheries*. FAO Guidelines, Environment and Natural Resources Service, FAO, Rome.

Stewart, F., and E. V. K. Fitzgerald, 2001: *War and Underdevelopment*. Oxford: Oxford University Press.

Tierney, K.J., 1995: Impacts of Recent U.S. Disasters On Businesses: The 1993 Midwest Floods and the 1994 Northridge Earthquake, Disaster Research Center, University of Delaware.

Webster, P.J., G.J. Holland, J.A. Curry, and H.-R. Chang, 2005: Changes in Tropical Cyclone Number, Duration, and Intensity in a Warming Environment, *Science*, **309**, 1844–1846.

Williams, B.A., 2002: Fran, Floyd and mitigation policy, Berry A. Williams and Associates, Inc.

The Science and Politics Problem: Policymaking, Climate Change and Hurricanes

Glen Sussman

Abstract In February 2007, the Intergovernmental Panel on Climate Change released its Fourth Assessment Report that discussed the progress made in our understanding of the impact of natural and anthropogenic activities involving global warming and climate change. On the basis of this report, policy makers and citizens alike now have a scientific basis upon which to assess the problem of global climate change and should be encouraged to implement appropriate national and international actions in response to the warming of the planet. Given this background, this study will: 1) examine the "science and politics problem" as it relates to the subject of this book, 2) provide an overview of the scientific understanding of global warming, climate change and hurricanes, 3) focus on the political factors that influence environmental policy making with emphasis on the United States since it is a dominant global power and major producer of greenhouse gases, and 4) offer a framework that shows the conditions when science is more or less likely to have substantive input into the policy making process as it relates to global climate change.

Between June 2005 and January 2006, twenty-seven tropical storms crossed the Atlantic Ocean and threatened coastal communities in the United States. Three of these storms became serious hurricanes that brought death and destruction to coastal and inland regions in the United States. This tropical cyclone activity that spawned Hurricane Katrina in August, Hurricane Rita in September and Hurricane Wilma in October was part of an Atlantic tropical storm season never seen before (Hayden 2006:68). The devastation unleashed by this tropical cyclone activity revealed a number of sociopolitical and economic problems including increasing populations in coastal regions with the concomitant development of housing and businesses, a lack of vision on the part of policymakers in Washington and the expense incurred when monster hurricanes make landfall. The consequences of hurricane damage also revealed the reality of the threat – namely, insurance companies that are in the business of dealing with risk have begun to refuse providing coverage to homeowners and businesses in the potential path of hurricanes. Climate change is now an important issue for Lloyds of London Swiss Re and Munich Re in Europe while

J.B. Elsner and T.H. Jagger (eds.), *Hurricanes and Climate Change,*
doi: 10.1007/978-0-387-09410-6,

major insurance companies in the United States including State Farm, Traveler's Insurance and Allstate established criteria that reduced their risk (Garreau 2006). For instance, Gulf Coast communities are no longer able to obtain insurance from American International Group, Inc. the largest insurer in the world while in Florida Allstate dropped 95,000 policies in 2005 and 120,000 in 2006 and in New York the insurer dropped 28,000 of its policyholders (Larsen 2007). Moreover, as Larsen (2007) reports, Allstate and MetLife have decided not to issue new policies on Long Island, New York, the site of a powerful hurricane in 1938.

In February 2007, the Intergovernmental Panel on Climate Change (IPCC) released its Fourth Assessment Report that discussed the progress made in our understanding of the impact of natural and human activities on climate change. While the report confirmed that "warming of the climate system is unequivocal, as is not evident from observations in global average air and ocean temperatures, widespread melting of snow and ice, and rising global mean sea level," it stressed the role played by anthropogenic actions that are now seen as a major contributor to global climate change (IPCC 2007). What was noteworthy about this Fourth Assessment Report was that it had built upon earlier studies and produced, in the words of the authors, "improvements in the quantitative estimates of radiative forcing." In short, policymakers and citizens alike now have a scientific basis upon which to assess the problem of global climate change and should be encouraged to implement appropriate national and international actions in response to the likelihood of continuing warming of the planet. As the authors of the report stress:

> Global atmospheric concentrations of carbon dioxide, methane, nitrous oxide have increased markedly as a result of human activities since 1750 and now far exceed pre-industrial values determined from ice cores spanning thousands of years. The global increases in carbon dioxide concentration are due primarily to fossil fuel use and land-use change, while those of methane and nitrous oxide are primarily due to agriculture (IPCC 2007).

The IPCC along with other scientific agencies have informed the international community that global climate change will have serious consequences. While some countries including the United States have moved slowly in response to the growing body of global climate science that demands action, other countries including Sweden, Britain and Denmark have taken the lead in efforts to reduce greenhouse gas emissions (Kennedy 2006). However, an increasing effort is needed to secure leadership by the United States and participation by developing countries to address this transnational problem.

Although the research findings of the IPCC among other sources have been distributed to policymakers and citizens, it is important to note that global warming and climate change are complex and difficult to understand contemporary global environmental policy problems. While it is unlikely that average citizens in the United States and other countries would read scientific studies about global warming, it is noteworthy that the mass media (broadcast and print) have made an important effort to inform and educate citizens. Moreover, citizens around the world have, generally, acknowledged and accepted the argument set forth by the scientific community as shown by numerous public opinion polls (Pew Global Attitudes Project 2007).

Given this background, this study will: 1) examine the "science and politics problem" as it relates to the subject of this book, 2) provide an overview of the scientific understanding of global warming, climate change and hurricanes, 3) focus on the political factors that influence environmental policymaking with emphasis on the United States since it is a dominate global power and the major producer of greenhouse gases, and 4) offer a framework that shows the conditions upon which science can be effectively integrated into the environmental policymaking process as it relates to global warming and climate change.

The "Science and Politics Problem"

Before proceeding to the issue of global warming, climate change and hurricanes, it is important to address the "science and politics problem." As Sam Earman (1996:13) has written, "although there may be such a thing as 'science policy,' science and policy are two entirely different things, and they are practiced by groups that are, for the most part, mutually exclusive." The public official and the scientist operate in two different worlds with two different cultures and two different languages. It has become increasingly apparent that the two fields work to ensure more collaboration in the field of environmental policy in order to effectively address global environmental problems. So, what role should science play in the environmental policy making arena where officials who speak for the public exhibit both shared and diverse concerns? Offering an optimistic view on this issue, Kai Lee has written, "the appropriate application of science to political decision making will provide humanity with the guides it needs to direct itself away from its current course of destruction" (Switzer 1998:307–308). Moreover, Arild Underdal (2000:184–185) sets forth the position that "Governments rarely explicitly dispute what the scientific community considers to be 'consensual knowledge'," that "faced with broad consensus among competent experts on the description and diagnosis of a (severe) environmental problem, governments do in fact most often take some kind of collective action," that in "thinking about the role of science in international environmental regimes we probably see science as a supplier of warnings serving as spurs for protective measures," and finally that "we would also expect to find a positive relationship between the demand for and the supply of scientific inputs." However, as Lynton Caldwell (1990:19–20) has lamented:

> Science alone cannot save the environment. Political choice is required to translate the findings of the environmental sciences into viable policies. Scientific information, even in its limited present state is far from being fully utilized in contemporary society. Unless political will and ecological rationality can bring about the transformations necessary to achieve a sustainable future of high environmental quality, science can do little more than to slow the pace of environmental decline and to project the consequences for a world in which all things are not possible.

Moreover, Lawrence Susskind (1994:63–64) argues that there are several reasons why the scientific community does not have the kind of impact assumed by the public. These factors include uncertainty and complexity that result in "rough

estimates at best;" political actors that use any notion of uncertainty to delay or oppose collective action; and members of the scientific community itself that enjoy promoting debates over issues that confuse the lay public and policy makers who don't understand the difference between real scientific conflict and "intramural disagreements among experts." In addition, Neil Harrison and Gary Bryner (2004:329) conclude, "Uncertain problems . . . are especially difficult to handle in the anarchic international system, because the nature of the problem must be negotiated through contending national preferences and interpretations."

Continued debate exists over the role of science in policy making and the need for an improved effort to bridge the two diverse fields. For instance, where policymakers and citizens are inclined to look at the short term, the scientific community can keep the policy process focused on the long-term. For instance, where scientists are guided by the scientific method, objectivity, the collection of data and the replication of their studies, politicians are more likely to view issues through the prism of partisanship or ideology or be influenced by interest groups. Where scientists might need time to experiment, politicians might need an answer prior to the next election. The science and politics "problem" can be viewed in the following way – scientific knowledge might be ignored or politicized by officeholders or it might be integrated effectively into the policymaking process. In short, as Desler and Parson (2006:39) argue, "In addition to the challenges that policy debates pose to science, science also poses hard challenges to policy debates, because citizens and politicians are not generally able to make independent judgments of the merits of scientific claims." Nonetheless, the discoveries of science must be used to educate the public and must be effectively mediated through the political process in order to provide policymakers with the knowledge needed to implement appropriate environmental policies both nationally and globally.

Scientific Understanding of Global Warming, Climate Change, Hurricanes

The U.S. National Academy of Sciences distinguishes between global warming and climate change in the following way: *global warming* refers to an "average increase in the temperature of the Earth's surface and in the troposphere, which can contribute to changes in global climate patterns" while *climate change* concerns "significant change in measures of climate (such as temperature, precipitation, or wind) lasting for an extended period" (U.S. EPA 2006a).

Global Warming and Climate Change

Over the years, the environmental policy domain has become diversified into a variety of issues demanding attention. As Michael Kraft (2001:15) has suggested, we are now facing a "third generation" of environmental problems that are quite

distinct from earlier concerns about "first generation" issues involving air and water pollution and "second generation" issues dealing with toxic chemicals and hazardous wastes. As Kraft (2001:15) explains, "third generation" policy problems including global climate change are "global in origin and effects," are more "politically controversial" and are more "difficult to address than the environmental issues of earlier eras"

Over the centuries, the Earth's climate has changed as a result of natural cycles alternating between periods of warmth and ice ages. Beginning with the Industrial Revolution in the mid-to-late 19th century, human activities began to have an influence on the Earth's atmosphere. During this period, several "greenhouse effect pioneers" including French mathematician Jean-Baptiste Fourier in 1827, British scientist John Tyndall in 1861 and Swedish chemist Svante Arrhenius in 1896 discovered that a buildup of greenhouse gases was associated with the warming of the Earth (Sussman et al. 2002:291). Over time, scientific knowledge about global warming expanded with new experimentation and research findings by British engineer, G. S. Callendar in 1938, Roger Revelle and Hans Suess of Scripps Institution of Oceanography in the late 1950s and Stephen Schneider of the National Center for Atmospheric Research in the late 1980's (Sussman et al. 2002:291). For instance, Revelle and Suess argued that "mankind is now engaged in a great experiment" while Stephen Schneider suggested that global warming "could well cause climate change over the next two generations as large or larger than civilization has experienced."

As described by the Energy Information Administration of the Department of Energy of the United States:

> Many chemical compounds found in the Earth's atmosphere act as "greenhouse gases." These gases allow sunlight to enter the atmosphere freely. When sunlight strikes the earth's surface, some of it is reflected back towards space as infrared radiation (heat). Greenhouse gases absorb this infrared radiation and trap the heat in the atmosphere. Over time, the amount of energy sent from the sun to the Earth's surface should be about the same as the amount of energy radiated back into space, leaving the temperature of the Earth's surface roughly constant (U.S. DoE 2004).

There are four major types of greenhouse gases – namely, carbon dioxide, methane, nitrous oxide and fluorinated gases (U.S.EPA 2006c). The main culprit is carbon dioxide that is produced primarily from the burning of fossil fuels (oil, coal, natural gas). World carbon dioxide emissions are, in most cases, increasing. As the data in Table 1 show, however, among a selected sample of countries/regions, variation in greenhouse gas emissions is evident. Where OECD (Europe) and Russia are projected to reduce their emissions by about 5% by 2010, China's contribution will increase by almost 9%. A modest decrease is expected for the United States while Japan's emissions will remain relatively stable. The problem remains that the U.S. will continue to be the major producer of greenhouse gas emissions unless fundamental changes are implemented while China's contribution is expected to surpass the U.S. very shortly.

Table 1 World Carbon Dioxide Emissions, Selected Countries (% total emissions)

Country/Region	1990	2003	2010 (projected)	Percent Change (1990–2010)*
China	10.6%	14.1%	19.3%	+8.7%
India	2.7	4.1	4.5	+1.8
Japan	4.8	4.8	4.0	-.8
OECD (Europe)	19.3	17.0	14.7	-4.6
Russia	11.0	6.4	5.9	-5.1
United States	23.5	23.2	21.0	-2.5

Adapted from the Energy Information Administration, U.S. Department of Energy, "International Energy Outlook 2006" at www.eia.gov. Accessed August 15, 2007.
*Calculations by author.

In 2001, the National Research Council stated:

> Greenhouse gases are accumulating in the Earth's atmosphere as a result of human activities, causing surface air temperatures and sub-surface ocean temperatures to rise. Temperatures are, in fact, rising. The changes observed over the last several decades are most likely due to human activities, but we cannot rule out that some significant part of these changes is also a reflection of natural variability" (U.S. DoE 2004).

Five years later, however, the U.S. Environmental Protection Agency (2006b) stated that "scientists know with virtual certainty" that the buildup of greenhouse gases in the atmosphere including the burning of fossil fuels is largely the result of human activities. Moreover, beginning in 1990, the Intergovernmental Panel on Climate Change has issued four reports on global warming and climate change. The conclusions set forth in the IPCC's Fourth Report issued in February 2007 was important and noteworthy since it stressed that scientists are ninety percent certain that human activities are the cause of the conspicuous increase in the warming of the Earth's atmosphere.

Global Warming, Climate Change and Hurricanes

The hurricane season for the Atlantic region begins on June 1 and ends on November 30. Since these "intense tropical storms" require warm ocean temperatures, the "more heat available in the surface water, the more potential there is to generate heavy rain and high wind" (Pew Center on Global Climate Change 2007). Notwithstanding natural factors that influence the development of hurricanes, the question has been raised whether and to what extent anthropogenic activities have played a role in generating an increase in frequency as well as severity of Atlantic hurricanes.

According to the U.S. National Oceanic and Atmospheric Administration (NOAA) (U.S. NOAA 2006a), our "science is not mature enough to determine what percentage of anthropogenic climate change and what percentage of natural climatic variability is driving our current hurricanes." Ironically, while NOAA

argued in favor of "improving the quality and scope of hurricane relevant data sets, a two-year study by the U.S. National Academy of Sciences revealed that the budget of the National Air and Space Administration (NASA) declined by thirty percent between 2000 and 2006 and especially since 2002 thus reducing NASA's ability to support many Earth satellite programs that provide important weather-related data (Kaufman 2007). Meanwhile, an increasing number of governmental and non-governmental organizations as well as work conducted by members of the scientific community have provided research findings that point to the increasing likelihood that human activities have had an increasing impact on climatic change in general and hurricane activity in particular. From the World Meteorological Organization to the Pew Center on Global Climate Change to the U.S. National Center for Atmospheric Research, studies show that human beings are increasingly responsible for global warming and global warming is having a direct impact on weather patterns. For instance, consequences include sea level rise, changing amounts of regional precipitation, altered agricultural patterns among others. Among these concerns raised about climate change is an increase in the frequency and intensity of hurricanes.

The cumulative impact of rising seas, a warmer planet and increased residential and commercial development in coastal zones along with the increasing likelihood of severe hurricanes suggests a future of what some scientists call a "recipe for potentially serious natural degradation" (Associated Press 2007). Mounting evidence of the consequences of global warming and climate change acts as a counter to "a Bush administration that contends global warming is an unproven theory" (Reuters 2007a). In short, while political debates over global warming, climate change and hurricanes reflect the politics in American politics, the scientific community has demonstrated that "human- induced global warming – driven by heat-trapping gases in air pollution from cars and factories – could be heating sea water, which in turn fuels stronger hurricanes" – research that contradicts those who argue that potentially severe future hurricanes will result from natural climatic cycles (Reuters 2007b, 2007c).

Recent research by Santer, et. al. has added to the debate over the extent to which human activities are linked to global warming and thus to climatic changes including more intensified hurricanes. These researchers have raised questions over policy statements made by the Bush administration in 2005 that "rising global temperatures were due entirely to natural fluctuations" and instead argue that there is a "link between warmer ocean temperatures and human use of fossil fuels" (Reuters 2007c). Consequently, the warm water that serves as fuel for hurricanes is viewed as a product of human activities rather than natural cycles. Subsequent research by the National Center for Atmospheric Research supports these results. For instance, the Center stated that its study "contradicts recent claims that natural cycles are responsible for the upturn in Atlantic hurricane activity since 1995. It also adds support to the premise that hurricane seasons will become more active as global temperatures rise" (MSNBC 2006). Moreover, the World Meteorological Organization (WMO 2007) has reported that "We know for certain that there is an intensification of the hydrological cycle, which translates into greater risk in

some areas of a rain deficit and accentuated problems of drought linked to climate change" suggesting that there is an "increasing link between global warming and natural disasters such as droughts and flooding." The policy position of the WMO was produced at its 6th International Workshop on Tropical Cyclones in November 2006 when it stated that: "The surfaces of most tropical oceans have warmed by 0.25–0.5 degree Celsius during the past several decades. The Intergovernmental Panel on Climate Change (IPCC) considers the likely primary cause of the rise in global mean surface temperature in the past 50 years is the increase in greenhouse gas concentrations" (U.S. NOAA 2006b).

Wither United States Leadership?

Environmental issues have assumed increased salience as they reflect transnational or cross-national impact. For instance, actions taken by one country can have a regional or global effect ranging from coal-fired power plants in the midwest region of the U.S. affecting eastern Canada or greenhouse gases emanating from industrialized countries thus having a global impact. As Jacqueline Vaughn Switzer (2001:67) notes, a global approach to environmental issues didn't occur until the Nixon administration and the involvement of the U.S. at the 1972 UN Conference on the Environment in Stockholm. Several years later, the Carter administration produced the first-ever examination of global environmental issues in the *Global 2000 Report to the President*. As a foundation for long-term planning, the Report emphasized the following: "Environmental problems do not stop at national boundaries. In the past decade, we and other nations have come to recognize the urgency of international efforts to protect our common environment" (U.S. CEQ and U.S. DoS 1982).

Despite research findings presented by American and international scientific bodies, the United States has become increasingly isolated from the international community for its failure to demonstrate leadership and vision on the combined global warming/climate change issue. Policymakers within the United States have argued over 1) the extent to which human activities as well as natural cycles are contributing to global warming and climate change and 2) what policy should be initiated in response to global warming. The most vocal and visible opponent of international collaborative efforts to address global warming has been President George W. Bush. He repudiated the Kyoto Protocol two months after moving into the White House. As a matter of fact, it was Vice President Dick Cheney who "pushed Bush to abandon a campaign pledge to impose mandatory reductions on carbon emissions from power plants" (Baker 2008:10). Moreover, government scientists have been required to receive clearance from the White House before they could speak with journalists.

We also know, for example, that fundamental partisan differences divide Congressional Democrats and Republicans over the issue of global warming. According to the *National Journal*'s "Insider's Poll conducted in February 2007, 95% of

House and Senate Democrats agreed that the "Earth is warming because of man-made problems" compared to "84% of House and Senate Republicans" who disagreed with this statement (National Journal 2007: 6–7). Among the dissenters in Congress who have vigorously argued against the scientific community's research findings about global warming is Senator James Inhofe, an Oklahoma Republican. In 2003, when Inhofe was chair of the Senate Environment and Public Works Committee he stated that "Kyoto . . . is an extreme approach" and he has referred to global warming as a "hoax perpetrated by environmentalists on the American public" (CBS News 2003). Moreover, as Chris Mooney informs us in a CBS News report, Senator Inhofe attacked the "hockey stick" explanatory graphic proposed by climate scientist Michael Mann where Dr. Mann depicts a spike in warming in the 20th century and Senator Inhofe also used Michael Crichton's novel, *State of Fear,* as a scholarly example of the flaws put forth by proponents of global warming and climate change (Inhofe, 2001; Mooney 2005).

In addition to Inhofe, vocal dissenters include Senators Larry Craig of Idaho, Kit Bond of Missouri and David McIntosh of Indiana who have raised concerns about efforts to curb greenhouse gas emissions. For instance, during President Bush's first year in office, the Energy Information Administration housed within the Department of Energy (DOE) prepared a report at the request of Representative McIntosh who opposed mandatory cuts in greenhouse gas emissions that, in effect, "ignored the findings of the DOE's much more thorough report, "Scenarios for a Clean Energy Future," as well as input from independent reviewers and analysts at the Environmental Protection Agency" (Hawkins 2001). Two years later, responding to the Senate's rejection of the McCain-Lieberman legislation that required industrial plants to reduce carbon dioxide emissions, Senator Craig publicly opposed a "massive new regulatory process" because he opposed the idea that carbon dioxide is a pollutant and therefore it "does not represent a direct threat to public health" while his colleague Senator Bond argued that the bill would have a deleterious impact on the U.S. economy (CBS News 2003). In short, opponents of efforts to curb greenhouse gas emissions, especially carbon dioxide, have criticized the science of global warming or have diminished the potential consequences of climate change.

The American political system is characterized by a variety of political actors that use their power resources in order to shape public policy. Among these actors are the presidency and the Congress that have important responsibilities related to public policymaking. The president has a variety of legislative and executive powers that can be employed in the policymaking process. For instance, the president can issue executive orders or proclamations as chief executive or sign or veto legislation passed by the Congress. Presidents can respond to environmental issues as an activist, in a symbolic way or as an obstructionist. Recent research on American presidents has found, for instance, that Democratic presidents including Lyndon Johnson, Jimmy Carter and Bill Clinton had a much more favorable impact on the environmental agenda compared to Republicans including Ronald Reagan, George H.W. Bush and George W. Bush (Daynes and Sussman 2007).

Located at the other end of Pennsylvania Avenue is Congress where political power has been fragmented into committees and subcommittees that can promote, delay or oppose legislation. Jurisdiction over environmental affairs can be found among several different committees in the House and the Senate. Consequently, environmental affairs can receive critical support or fall victim to fragmented government. Moreover, partisanship can play a role in legislative affairs. For instance, research over the last three decades has shown that Democratic legislators are more likely to support environmental legislation compared to their Republican counterparts (Dunlap and Michael 1973; Kamieniecki 1995:146–167; Sussman et al. 2002:96–97).

While the global warming issue caught the attention of the Carter administration and was discussed in *The Global 2000 Report to the President* (U.S. CEQ and U.S. DoS 1982) prepared by the Council on Environmental Quality and the Department of State, Congress did not take action in a substantive way until 1988. In response to Congressional hearings during the 1980s held by Al Gore, Tim Wirth and John Chaffe, "President Reagan reluctantly signed the Global Climate Protection Act . . . which obliged him to submit to the Congress a plan for stabilizing greenhouse gases in the atmosphere" (Agrawala and Andresen 1999). During the 1988 campaign for the presidency, George H.W. Bush proclaimed himself an environmentalist in the tradition of Theodore Roosevelt. After winning the presidential election, three noteworthy events illustrated his approach to the environment in general and global warming in particular. On the one hand, he used the power resources of his office in support of the 1990 Clean Air Act Amendments that were important in addressing transboundary air pollution. On the other hand, in 1992, in response to pressure from the fossil fuel industry and his concern about the state of the economy, he gave lukewarm support to the Energy Policy Act of 1992 and the United Nations Framework Convention on Climate Change. As Michael Kraft (2004) argues, although the legislation offered several items to improve U.S. energy efficiency, it "did not raise [Corporate Average Fuel Economy] CAFÉ standards for motor vehicles, which was the top priority of environmental groups, nor did it do much to reduce the use of oil." Thus, the legislation did little to address the problem of increasing levels of carbon dioxide in the atmosphere.

When Bill Clinton captured the White House in 1992, one of the first efforts he made was to push a deficit reduction plan early in 1993 that included a tax on energy production that, he believed, would result in less energy consumption thus reducing the use of fossil fuels and thereby cutting greenhouse gas emissions (Paarlberg 1997). Although the House of Representatives passed Clinton's legislative proposal, organized interests opposed to the energy tax succeeded in killing the proposal in the Senate Finance Committee.

Over a decade passed before Congress updated the energy bill. However, the 2005 Energy Policy Act "emphasized greater production and use of oil, natural gas and coal and strongly boosted federal support for nuclear power" while critics "especially faulted the act's billions of dollars of subsidies and tax breaks for the oil, gas, coal and nuclear industries" (Kraft and Furlong 2007:353). In effect, the 2005 Act actually encouraged increased production of greenhouse gases. Two years

later, while several legislative proposals were being prepared to address global warming, George W. Bush signed the Energy Independence and Security Act of 2007 that the president argued would "improve vehicle fuel economy and help reduce U.S. dependence on oil" and "could reduce projected CO2 emissions of billions of metric tons" (The White House 2007). While the new Act was notable for its effort to improve fuel efficiency it also provided billions of dollars in subsidies to the fossil fuel and nuclear industries, continued to push for oil exploration in Alaska's Arctic National Wildlife Refuge and as reported in the *Washington Post* just "hours after Bush signed the energy bill, the administration invalidated an effort by California and 17 other states to impose tougher tailpipe emission rules" (Baker 2008).

The fragmented political system in the United States promotes actions by organized interests due to multiple access points into the policymaking process. The environmental domain has been characterized by two types of organized interests. On the one hand, we find the umbrella "environmental movement" comprised of a variety of groups committed to conservation and preservation values. Yet these groups are characterized by diversity in membership, resources, strategies and tactics. On the other hand, we find groups that are committed to developmental values. While some of these groups represent business and industry (e.g., fossil fuel industry, mining, timber) other groups are concerned about property rights.

Finally, to what extent is the citizenry informed and concerned about environmental issues? Moreover, to what extent should policymakers follow public opinion? Generally, it depends on how one examines public opinion. On the one hand, when asked specifically about the environment, American citizens exhibit strong views in support of protecting the environment. On the other hand, when the environment is one among several issues, it can be characterized as a latent issue as Americans show more concern about the economy, jobs, health care, Social Security among others. Having said this, when The Gallup Poll (2006) asked Americans their opinion about the environment, this policy domain elicited serious attention among citizens who expressed concern that the "government is doing too little to protect the environment," the "quality of the environment is getting worse," that "human activities rather than natural causes explain the rise in the Earth's temperature," and that the "effects of global warming are already manifest or will happen within five years."

American public opinion data also indicates that U.S. citizens are increasingly concerned about global warming in general and its causal relationship to hurricanes in particular (Zogby International 2006). Not only do more Americans (74%) believe that global warming is occurring but this sentiment cuts across all sociodemographic characteristics including age, gender, race, religion, region of the country and partisan identification. More importantly, in terms of this study, seven out of ten Americans now believe that global warming has a "major or some influence" on hurricanes. Consequently, global warming as an important transnational public policy issue remains problematic as policymakers in the United States face pressure from organized interests as they read public opinion.

All of these political actors play a role in foreign as well as domestic policy-making – a point not missed on political commentators who point out the important role of the U.S. as the dominant global power. For instance, as Paul Harris (2001:34) argues, "Because the U.S. economy is so large, its diplomatic influence so great and its contributions to environmental problems so extensive . . . the United States must be part of international solutions to environmental change. Over the last three decades or so, the U.S. has played a relatively positive role regarding global environmental affairs. At the same time, as environmental issues become increasingly transnational in character and impact, domestic political factors have played an important role in shaping U.S. policy toward global environmental policy (Sussman 2004). It is noteworthy, therefore, as global climate change assumes increasing salience in domestic and global politics that the U.S. offer guidance and leadership. Failure to do so can have serious consequences. As Beldrich Moldan, former Minister of the Environment of the Czech Republic lamented a decade ago, "The United States is watched much more than Americans realize. As a European, you may like the United States or not like it, but you know it's the future. So when the United States refuses to reform, other countries will refuse as well" (Hertsgaard 1998:288).

The issue of global warming gained prominence during the presidential administrations of George H.W. Bush, Bill Clinton and George W. Bush. What is noteworthy is how each president addressed the issue in a different way (see Table 2).

George H.W. Bush [hereafter Bush (41)] came into office stating that he would be an "environmental" president and indeed he used the power resources of the White House to ensure passage of the 1990 Clean Air Act Amendments that had languished during the administration of Ronald Reagan. However, when he had the opportunity to demonstrate leadership at the international level he failed in this regard. Bush (41) had two opportunities to take the lead in addressing global warming – namely, the 1990 World Climate Change Conference and two years later at the Earth Summit in Rio. The impact of carbon dioxide accumulation in the atmosphere was discussed at the World Climate Change Conference where an agreement was obtained to stabilize the amount of greenhouse gases emitted into the atmosphere (Sussman 2004:362). The 1992 Earth Summit again focused on the issue of greenhouse gases and their impact on global climate. However, the president's lack of interest in addition to pressure from the fossil fuel industry, resulted in, in the words of political scientist Gary Bryner (2001:142), opposition to the "development of a global climate change agreement" because Bush (41) believed that "limits on emissions would require major changes in Americans' way of life and would threaten an already weakened economy."

The behavior of Bush (41) regarding the Earth Summit's focus on global climate change affected the success of the international gathering. First, as Lawence Susskind (1994:39–40) informs us, the president attended the conference for only three days and had waited until a month before the summit whether to attend at all. Second, the resulting global climate change agreement required that the costs and technologies be shared by the signatories and most importantly that the guidelines and timetables would be mandatory. Bush (41), therefore, used his influence to

Table 2 Comparing Presidents George H.W. Bush, Bill Clinton and George W. Bush and Global Warming

	Bush (41)	Clinton	Bush (43)
Environmental Theme	To be an environmental president	Great green hope	Eco-friendly president
Environmental Philosophy	Pro-development	Sustainable development	Pro-development
Important International Conference	Earth Summit, Rio, 1992	3rd Session of the COPS, Kyoto, 1997	3rd Session of the COPS, Kyoto, 1997; Bali Conference, 2007
Global Environmental Agreement	Convention on Global Warming	Kyoto Protocol	Kyoto Protocol
Requirements of Agreement	Voluntary	Mandatory	Mandatory
Presidential and Congressional Response	Agreement signed by President and ratified by the U.S. Senate	Agreement signed by President but not ratified by the U.S. Senate	Agreement renounced by the President and opposed by the U.S. Senate
Implications	Basis established for Kyoto Protocol albeit with voluntary measures	U.S. leadership questioned due to lack of Senate ratification	Kyoto Protocol weakened due to non- participation by the U.S; Bali effort weakened due to continued U.S. opposition to explicit emission targets

revise the agreement so that it reflected voluntary rather than mandatory requirements in reducing greenhouse gas emissions. Consequently, on the one hand, the U. S. was a signatory to the Global Climate Change Convention produced at the Earth Summit. On the other hand, the actions by Bush (41) created a problem for international cooperation and ignored the warnings of the scientific community regarding human-induced global warming.

Bush (41)'s successor, Bill Clinton, did not bring "environmental" credentials with him when he assumed the presidency of the United States. However, he did make important "green" appointments to important positions within his administration. For instance, former Senator Al Gore who published *Earth in the Balance* in 1992 was selected as his Vice Presidential running mate, Carol Browner was chosen to head the Environmental Protection Agency and former Arizona Governor, Bruce Babbit, became Secretary of the Interior.

In 1997, delegates from industrialized countries met in Kyoto, Japan to formalize agreements made in Berlin two years earlier to address the problem of greenhouse gases and global climate change. Delegates were successful in securing agreements on two important issues. First, signatories accepted mandatory cuts in

greenhouse gas emissions to 1990 levels. In doing so, different countries were given different target levels since they produced different amounts of greenhouse gases. Second, the industrialized countries were willing to excuse developing countries from the requirements of the agreement although China and India, in particular, were increasingly adding greenhouse gases into the atmosphere. On the advise of Vice President Al Gore, President Clinton signed the Kyoto Protocol thus committing the U.S. to reducing its greenhouse gas emissions.

Clinton was faced with two problems, however. First, an alliance consisting of the fossil fuel industry and organized labor opposed U.S. adherence to the agreement. Second, Clinton was confronted with two legislative obstacles – namely, a Republican-controlled U.S. Senate that was obstructionist with regard to environmental initiatives making it clear that the protocol would not receive Senate ratification and a Senate that through passage of the Byrd-Hagel Resolution made it clear that *any* international environmental agreement that did not include developing countries would be opposed.

Despite the fact that the Kyoto Protocol remained in limbo in the United States, delegates from industrialized countries continued to meet – in Buenos Aires in 1998, in Bonn in 1999 and in the Hague in 2000 – to continue the debate about human contributions to global warming. Moreover, the Intergovernmental Panel on Climate Change and the U.S. National Academy of Sciences continued to warn the global community about the effects of greenhouse gases on climate change.

George W. Bush [hereafter Bush (43)] occupied the White House in January 2001 and in a fateful decision only two months into his presidency he renounced the Kyoto Protocol. In doing so, the president argued that the international environmental agreement was flawed, it needed to include developing countries, especially China and India, and it would have a negative impact on the U.S. economy. While his rejection of the protocol had global impact since the U.S. was and remains the major emitter of greenhouse gases, President Bush (43) also refused to attend the global warming conference eight months later in Morocco (Cable News Network 2001). The following year, the American president reported to the United Nations that countries should adapt to the changes resulting from global warming (Revkin 2002).

By 2004, a sufficient number of signatories to the Kyoto Protocol had ratified the agreement to put it into effect. However, without the participation of the United States, the effort to address greenhouse gas emissions and global climate change remains problematic. Ironically, according to President Bush (43)'s own Environmental Protection Agency (U.S. EPA 2006a):

> For over the past 200 years, the burning of fossil fuels… [has] caused the concentrations of heat-trapping 'greenhouse gases' to increase significantly in our atmosphere.… Most of the warming in recent decades is likely the result of human activities.… Scientists are certain that human activities are changing the composition of the atmosphere, and that increasing the concentration of greenhouse gases will change the planet's climate.… Scientists have observed that some changes are already occurring. Observed effects include sea level rise, shrinking glaciers, changes in the range and distribution of plants and animals, trees blooming earlier, lengthening of growing seasons, ice on rivers and lakes freezing later

> and breaking up earlier, and thawing of permafrost. Another key issue being studied is how societies and the Earth's environment will adapt to or cope with climate change.… "human health can be affected directly and indirectly by climate change.…

Despite the warnings of the scientific community and poll data results of American public opinion, by 2007 the Bush (43) administration has yet to take substantive action regarding this most important global environmental problem. While some observers of the Bush (43) presidency have argued that his legacy is linked to the war in Iraq, it is clear that his legacy is also closely tied to the inaction of his administration in response to global warming and climate change.

The Global Community

While the United States has refrained from adhering to the principles of the Kyoto Protocol, other members of the global community have made efforts, some substantial, some nominal regarding the commitment to reduce greenhouse gas emissions. Among the 168 countries that have ratified the Kyoto Protocol are seven of the world's wealthiest and industrialized countries including Canada, France, Germany, Italy, Japan, Russia and the United Kingdom. In contrast, along with the United States, Australia, Croatia and Kazakhstan have failed to ratify the Kyoto agreement.

According to two observers of the global warming issue, "The [U.S.} president's 'greenless' diplomacy, challenged at home, has provoked an international response as well. Efforts to persuade the [Bush] administration and Americans to change course have been undertaken by such loyal allies as British Prime Minister Tony Blair, who began drawing up a climate change treaty at the end of 2004 that he hoped even the United States could support" (Daynes and Sussman 2005:442). Despite Blair's efforts at the meeting of the G-8 summit in July 2005, the United States, in essence, backed off any formal commitment to take substantive actions with regard to greenhouse gas emissions. As *The Observer* reported, "it was a contrast between the British approach, demanding 'immediate placing of controls on transport, factories and power suppliers,' and the 'more leisurely' American approach, asking countries to 'put faith in technology' – even in technology 'as yet undeveloped' – that could help reduce global warming by the year 2025" (Daynes and Sussman 2005:442).

Although a sufficient number of countries have ratified the Kyoto Protocol to put it into effect, problems remain. President George W. Bush continues to oppose the international agreement and the U.S. Senate through the Byrd-Hagel Resolution passed 95–0 in July 1997 requires developing countries to make formal commitments regarding targets to reduce greenhouse gases. Moreover, as Jeff Frankel (1999) of *The Brookings Institution* explained in 1999, from the "viewpoint from the north," it is essential for developing countries to offer meaningful participation because a) "a global problem requires a global solution," b) "Emissions in

developing countries are increasing the most rapidly, and will pass those from the industrialized countries early in the next century," c) "if developing countries do not participate in the international regime, their emissions might rise by even more than anticipated under a continuation of global business as usual," and d) developing country participation is crucial because it would permit relatively low-cost reductions in emissions in place of high-cost reductions in the industrialized countries." Having said this, developing countries also maintain a position that centers on economic development and improving the standard of living of their citizens. Moreover, as Frankel (1999) informs us, developing countries argue that "their priority must be raising their own economic standards of living. To do so, they must raise incomes as reflected in market transactions, while also controlling local air and water pollution. . . . Controlling local pollution must take precedence over controlling greenhouse gases, which are not visible, and which may not have serious health effects until a century into the future" and second, "the developing countries should not be required to take any step that entails economic sacrifice until the industrialized countries have done so. The industrialized countries created the problem; and they are richer and can more readily afford to make sacrifices" (Frankel 1999).

The wealthy United States and member states of the European Union have played leadership roles regarding two important global issues. As Miranda Schreurs (2004:222) points out, "The U.S. was considered an international leader in the development of the 1987 Montreal Protocol addressing stratospheric ozone depletion caused by the release of chlorofluorocarbons and other manmade substances. In contrast, it has been the EU that has been the champion of the Kyoto Protocol and international efforts to address climate change." Over a decade ago prior to the establishment of the Kyoto Protocol, James Sebenius (1995:73) of the Harvard Business School warned that the "power of the coalitions that will arise to block greenhouse action – not merely for reasons of economic interest, but also for reasons of science, ideology, or opportunism – must be taken into account in the design of an effective negotiating process." Yet a decade later, when Russia ratified the Kyoto Protocol, the international environmental agreement went into effect demonstrating that countries were formally committed to the Kyoto Protocol. At the same time, the reluctance of the United States to join its wealthy partners and the increasing contribution of greenhouse gases by China, India and other developing countries poses a continued dilemma for addressing global warming and climate change. As John Dutton (1994:101–102) reminds us, "governments must . . . provide informed leadership," "governments must seek international cooperation to address global problems," and "governments must act as catalysts of change."

In 2007, the Bush administration responded in two ways that, once again, demonstrated its commitment to oppose mandatory goals and timetables and continue support for voluntary guidelines. In preparation for the Group of Eight meeting scheduled in Germany in June, Bush announced that he would offer a "new global framework" that would show the U.S. willingness to deal with global warming. Heading into the last year of his administration, the American president wanted the international community to see an active U.S. role in shaping global

environmental policy. However, as reported in the *Washington Post*, the administration continues to oppose binding targets and instead puts forth "aspirational goals" to reduce greenhouse gas emissions (Fletcher and Eilperin 2007). Moreover, the Bush announcement would have a negative effect on the U.N.-sponsored global warming conference scheduled for December in Bali that had the goal of preparing a successor to the Kyoto Protocol. In the words of the British newspaper, *The Guardian*, the purpose of the Bali conference was "thrown in doubt by the initiative announced yesterday by President Bush" since the American president set forth a position that "killed off hopes of an agreement on basic principles for combating climate change at the G8 meeting" (Borger, Adam, Goldenberg 2007). Adding to the difficulties for the G8 and Bali conferences was a public position taken by Michael Griffin who heads NASA, the U.S. space agency. In a radio interview in the summer of 2007, while accepting the proposition that a "trend of global warming exists" he asserted that "I am not sure that it is fair to say that it is a problem we must wrestle with" (Borger, Adam, Goldenberg 2007).

In December, the U.N.-sponsored global warming conference in Bali convened to put forth a post-Kyoto Protocol mechanism to address greenhouse gas emissions. Prior to the meeting itself, internal dissension arose in the White House over who should represent the U.S. at the conference. While President Bush wanted his environmental advisor, James Connaughton, to co-head the U.S. delegation, the U.S. Department of State argued that this would be a "breach of protocol" (Baker 2008:11). Although Undersecretary of State Paula Dobrinasky was eventually sent to lead the U.S. delegation, the U. S. position remained the same – namely, opposing explicit emission targets – while delegates from other countries criticized the United States and put forth a proposal that developed and developing countries "make measurable but unspecified cuts in greenhouse gases" (Baker 2008:11). In short, without U.S. leadership, problems rather than opportunities and unilateralism rather than collaboration remained the theme and approach of the U.S. role regarding global warming and climate change.

Integrating Science and Politics

According to the Pew Climate Center, "Given future trends in population growth and increasing development in coastal areas, we know that the damage caused by severe weather will increase regardless of global warming. Climate change, namely sea level rise and increases in tropical storm activity, likely will exacerbate the damage" (Pew Center on Global Climate Change 2007). In light of the recent findings of the IPCC, United Nations Environment Program executive director Achim Steiner stated that failure to act on global warming "will one day in the history books be considered irresponsible" (Leicester 2007). Or, as former CBS New Anchor Walter Chronkite (2004) warned during the 2004 presidential election: "Global warming is at least as important as gay marriage or the cost of Social Security. And if it is not seriously debated in the general election, it will measure

the irresponsibility of the entire political class. This is an issue that cannot, and must not, be ignored any longer."

While concerned about securing collective action on an international scale to effectively address global environmental problems, researcher Lawrence Susskind (1994:76–78) has argued that scientists play five important roles in the global environmental policy process. These five roles are "trend spotters" who identify changing environmental patterns; "theory builders" who attempt to explain the changes noted by trend spotters; "theory testers" who are involved in experimentation to test hypotheses set forth by theory builders; "communicators" who function is to take complicated scientific findings and make them understandable to the lay public and policy makers; and "applied-policy analysts" who offer scientific advice to policy makers based upon the work of the other groups of scientists. As Susskind argues, in order to be effective, scientists involved in each role must interact within a public framework and confront the sources of their disagreement as a means to adequately perform their responsibilities.

Taking into consideration Susskind's view of the role of scientists in the policy making process and on the basis of the discussion set forth so for, five steps that might be considered in an effort to improve the linkage between science and politics are set forth in Table 3. The table depicts the importance of addressing the role of data gathering, communication, understanding, politicization and recalcitrance. The solutions suggested in the table represent a preliminary effort to help to improve the linkage between science and politics that will foster better decision making in the domestic and global environmental domains.

Since policy makers and citizens alike rely on the scientific community to provide warnings and potential solutions in response to environmental problems, to what extent will scientists and scientific knowledge play a role in the policy making process regarding global warming? The Montreal Protocol represents the outcome of collaboration between scientists, policy makers, and organized interests (environmentalists and business and industry) to address the global problem of

Table 3 Linking Science, Politics and Policy

Problem	Solution
Inadequate data	More research and continued replication and refinement of experimentation
Poor communication between scientists and policy makers	Clarify the issues and concepts addressed in the scientific and policy making domain
Lack of understanding between science and citizens	Improve the education system to enhance the scientific knowledge base of citizens to strengthen their understanding and decision making ability
Politicization of issues	Develop and improve methods to ensure policy makers a transparent and open decision making process
Recalcitrant skeptics	Increased efforts to ensure that consensus or majority view positions among members of the scientific community are disseminated to the citizenry

stratospheric ozone depletion (Sussman 2004:360–362). Although chlorofluorocarbons (CFC's) were discovered in the 1930s, it wasn't until 1974 when two chemists, Molina and Rowland, concluded that once in the stratosphere they contribute to the breakdown of the ozone layer (Miller 2002:466–467). Although steps were taken in the U.S. to address this problem, international cooperation was needed to take a global view about this environmental threat. A decade later, notwithstanding an American president (Ronald Reagan) who pushed an anti-environmental agenda, the chemical industry concerned about the impact on their industry resulting from the prohibition of ozone depleting substances and pressure from organized interests (e.g., The Alliance for Responsible CFC Policy) that opposed the protocol, consensus was achieved to reduce CFC's. In this case, the work of the scientific community was effectively integrated into the decision making and policy process resulting in an important international environmental agreement.

In contrast, despite the warnings of the IPCC and other national and international organizations, the case of global warming and climate change has yet to achieve this same kind of consensus among the relevant political, scientific and economic players. As Miranda Schreurs (2004:207) observed, fundamental differences separate the United States and the members of the European Union (EU): "The [European Union] and the U.S. have reluctantly agreed to disagree on their climate change strategies. The fifteen members of the EU strongly support the Kyoto Protocol. . . . The United States, in contrast, has rejected the Kyoto Protocol and instead is advocating what it calls a voluntary, science-based approach to reduction of greenhouse gas emissions."

Arild Underdal (2000) established a framework to better understand the role of science in the environmental policy making process. The study reported here employs Underdal's framework and adapts it to the issue of global warming and climate change (see Table 4). The purpose is to assess when science and scientists are more or less likely to have inputs into the policy making process regarding global warming and climate change.

It is evident that scientists and science are more likely to be employed in the environmental policy making process when there is a consensus on the issue and whether there is a feasible "cure" for the problem. Notwithstanding the arguments

Table 4 The Impact of Science on Global Warming Policymaking

Factors	Impact of Science on Policymaking More Likely	Mixed	Impact of Science on Policymaking Less Likely
Consensus	*		
Cure	*		
Effects		*	
Socio-Economic Center		*	
Development of Problem		*	
Effect on Public		*	
Political Conflict			*

put forth by some naysayers, members of the scientific community are in general agreement that human activities are a major contributor to greenhouse gas emissions that are generating global warming. There are several climatic consequences resulting from this global phenomenon and one is the increased likelihood of powerful hurricanes impacting the coastal eastern and gulf states of the United States and countries located on the Asian pacific rim. Moreover, a variety of options have been offered to address this problem from the scientific community to policy makers and most recently by former Vice President Al Gore through his recent film, *An Inconvenient Truth*. For instance, industrialized countries can slowly ween themselves off of fossil fuels, put more funding and research into alternative sources of energy and employ conservation of natural resources as a fundamental principle of their energy policy.

It is less clear whether and to what extent four factors put forth by Underdal– whether the effects are close or remote, does the problem effect the socio-economic center of society, whether the problem is developing quickly or slowly and are the effects being experienced by the public – will lead to substantive inputs by the scientific community. Unlike earlier environmental problems including air and water quality that were more easily "experienced" by the consumer, global climate change is a complex problem. As Michael Kraft (1996:14) has described it:

> Increasingly, it seems, the so-call "third generation" of environmental problems, such as global climate change and loss of biodiversity, are even more problematic than the more familiar issues of the "first generation" of environmental concerns of the early 1970s (e.g., air and water pollution) and the "second generation" that emerged later in the 1970s (toxic chemicals and hazardous wastes). The third generation of problems are less visible, their impacts are distant and uncertain, they are often not very salient to the public, and experts disagree on the magnitude, timing, and location of their effects."

For policy makers and citizens alike, it is difficult to understand whether the "effects" are close or distant in time, how quickly or slowly this is happening and the extent to which these effects are experienced by the general public. Moreover, compared to visible air pollution or an oil spill, global climate changes may seem to be occurring incrementally and slowly over time according to the lay person. While scientists can inform us that the polar caps are melting, for instance, this phenomenon is far from the social center of society. Moreover, notwithstanding recent and powerful hurricanes impacting the U.S., most recently Hurricane Katrina, coastal dwellers are accustomed to "hurricane season" and may not understand the potential impact of global warming on the intensity of hurricanes of the future. Consequently, the results appear to be mixed in terms of integrating science into the policy making process under these circumstances.

Finally, science is least likely to be part of the policy making process when political conflict is high. Despite the recent report of the IPCC, domestic forces within certain countries and international disagreements work against effective efforts to address the problem. For instance, the current U.S. President Bush along with a Republican-controlled Congress (1994–2006) supported only voluntary measures to address the problem. Democratic legislators representing automobile or energy-producing states oppose any changes unless developing countries are

included in any global warming agreements. Despite a new U.S. Congress with a Democratic majority, efforts to deal with global warming and its consequences appear to be "backbenchers" as the war in Iraq remains the primary issue of concern. At the same time, several U.S. states, including the largest state California, have undertaken initiatives to reduce greenhouse gas emissions. Moreover, hundreds of U.S. cities in 44 states have joined together in an effort to curb greenhouse gas emissions through the U.S. Mayors' Climate Protection Agreement (ICLEI 2007). These efforts include land use management, transportation planning, energy efficiency, green power among others. Furthermore, over 600 cities around the world have announced their commitment to combat global warming (Herro 2007).

Despite the fact that a sufficient number of countries including Japan, Russia and member states of the European Union have ratified the Kyoto Protocol putting it into effect, in addition to increased efforts at the subnational level in the U.S. and other countries, the effort to achieve successful international collaboration on this issue remains problematic without the leadership of the United States.

Conclusion

The global community is being confronted with new challenges of global change that involve both the scientific and political communities. As John Dutton (1994:78–79) persuasively argues, the challenge facing the scientific community involves the "task of understanding a complex and fascinating system and the responsibility of providing a reliable basis for policy decisions concerning possible modification of human activities in order to mitigate or adapt to global change." In the political arena, as Jacobson and Weiss (1998:7) put it, "the actions of other states in implementing and complying with [an international environmental agreement] can also affect a state's compliance with an agreement. To what extent have other countries' noncompliance or compliance with [an international environmental agreement] affected the willingness of countries to abide by the accord?"

Over the last three or four decades, members of the global community have demonstrated a willingness to engage in constructive efforts to establish international environmental agreements across a range of issues. Among these agreements are the Convention on International Trade in Endangered Species of Wild Fauna and Flora (1973), the International Convention on Long-Range Transboundary Air Pollution (1979), United Nations Convention on the Law of the Sea (1983), the Montreal Protocol on Substances that Deplete the Ozone Layer (1987), the Convention on Biodiversity (1992), the United Nations Framework Convention on Climate Change (1992) and the International Tropical Timber Agreement (1994). Having said this, while the U.S. has played a leading role in the international environmental domain in the past, more recently, the American president (Bush [41]) failed to sign the Convention on Biodiversity and he signed the United

Nations Framework Convention on Climate Change only after the requirements of the agreement were changed from mandatory to voluntary.

Sadly, the contemporary role of the U.S. regarding international efforts to address global warming and climate change resemble its position in 1992 on biodiversity and climate change rather than its leadership role involving the Montreal Protocol in 1987. Moreover, other major contributors to global warming including China and India remain outside an international environmental agreement. While the scientific basis for political action has been provided by the IPCC and other national and international agencies, political conflict remains within and between countries on this issue.

As far as hurricanes are concerned, what remains is a debate between scientists on the one hand who argue that "human-caused global warming is responsible for raising sea surface temperatures, making stronger hurricanes more likely" while on the other hand, a small but vocal group of critics maintain the position that "hurricane intensity goes in natural cycles, and say the record-breaking 2005 Atlantic and Caribbean season was part of a high-category hurricane cycle" (Reuters 2007d). Residents and commercial interests in coastal areas face the consequences of increasingly devastating storm surges and major flooding due to hurricanes feeding off of warmer waters resulting from global warming. As scientists continue to study the relationship between global warming, climate change and hurricanes, world governments face the challenge of finding appropriate means to respond to the global warming problem while at the same time improving emergency management procedures. Ultimately, as Steel, Clinton and Lovrich (2003:70) warn:

> Human cloning, global warming, biodiversity protection, and yet unknown issues affecting the biosphere we share with the rest of nature are all going to involve the active interaction of science, scientists, and major political institutions. . . . It seems clear that public education, scientific outreach to policy makers, active debate, and political engagement over policy options all need to occupy a high priority on the public policy agenda for the development of effective environmental policies in our country and elsewhere across the world.

It remains to be seen whether and to what extent appropriate actions will be taken to ensure that global warming will be addressed in order to reduce climate threats including severe tropical cyclone activity.

References

Agrawala, A. and S. Andresen, 1999: Indespensibility and indefensibility? the united states in the climate treaty negotiations. *Global Governance*, **5**, 457–482.

Associated Press, cited 2007: Hurricanes shape new natural order. [Available online at www.enn.com/archive.html?id=9773&cat=jtoday.]

Baker, P., 2008: A greener bush, *The Washington Post National Weekly*, January 7–13, 10–11.

Borger, J., D., Adam, S. Goldenberg, cited 2007: Bush kills off hopes for G8 climate change plan, *The Guardian* [Available online at www.guardian.co.uk/environment/2007/jun/01/usnews.climatechange.print.]

Bryner, G., 2001: *Gaia's Wager: Environmental Movements and the Challenge of Sustainability*. Rowman and Littlefield, 253 pp.

Cable News Network, cited 2001: Climate treaty set to be ratified. [Available online at www.cnn.com/2001/TECH/science/11/10climate.talks/index.html.]

Caldwell, L. K., 1990: *Between Two Worlds: Science, the Environmental Movement, and Policy Choice*. Cambridge University Press, 224 p.

CBS News, cited 2003: "Senate rejects global warming bill. [Available online at www.cbs.news.com/stories/2003/10/30/politics/printable580915.shtml.]

Chronkite, W., cited 2004: Make global warming an issue. *The Philadelphia Inquirer*. [Available online at www.philly.com/mld/philly/8187862.html?1c.]

Daynes, B. W. and G. Sussman, 2005: The 'greenless' response to global warming. *Current History*, **104**, 438–443.

Daynes, B. W., and G. Sussman, Unpublished manuscript. *White House Politics and the Environment* (approved for publication by Texas A&M University Press).

Desler, A. L., and E. A. Parson, 2006: *The Science and Politics of Global Climate Change*. Cambridge University Press, 190 p.

Dunlap, R. E., and P. A. Michael, 1973: Partisan differences on environmental issues: a congressional roll-call analysis. *Western Political Quarterly*, **29**, 384–397.

Dutton, J., 1994: The challenges of global change. *Science, Technology and the Environment*, J. R. Fleming and H. A. Genery, Eds., The University of Akron Press, 53–111.

Earman, S., 1996: The intersection of science and law: who has the right of way? *At the Nexus: Science* Policy, D. Soden, Ed., Nova Science Publishers, Inc., 13–27.

Fletcher, M. E., and J. Eilperin, cited 2007: Bush proposes talks on warming. *The Washington Post* [Available online at www.washingtonpost.com/wp-dyn/content/article/2007/05/31/AR2007053100934_pf.]

Frankel, J. A., cited 1999: Greenhouse gas emissions, policy brief #52. *The Brookings Institution*. [Available online at www.brook.edu/printme.wbs?page=/comm/policybriefs/pb52.htm.

Garreau, J., 2006: Batten down the hatches: climate change already has a chilling effect on coastal homeowners. *The Washington Post National Weekly*, **24**, 4, 6.

Harris, P., 2001: International environmental affairs and U.S. foreign policy. *The Environment, International Relations, and U.S. Foreign Policy,* P. Harris, Ed., Georgetown University Press, 276 p.

Harrison, N. E., and G. C. Bryner, 2004: Toward theory. *Science and Politic in the International* Environment. N. E. Harrison and G. C. Bryner, G. C. Eds., Rowman & Littlefield Publishers, 327–350.

Hawkins, D., NRDC, cited 2001: Bush's flawed arguments against regulating carbon pollution. [Available online at www. nrdc.org/globalWarming/abushco2.asp.]

Hayden, T., 2006: Super storms: no end in sight. *National Geographic*, **210**, 66–77.

Herro, A., cited 2007: Cities, countries make up for what bali lacked. [Available online at www.enn.com/top_stories/article/28396/print.]

Hertsgaard, M., 1998: *Earth Odyssey*. Broadway Books, 372 p.

ICLEI, cited 2007: U.S. mayors climate protection agreement. [Available online at www.iclei.org/usa.]

Inhofe, James, cited 2005: Climate change update, senate floor statement by u.s. senator james m. Inhofe (r-okla). [Available online at http://inhofe.senate.gov/pressreleases/climateupdate.htm.]

IPCC, cited 2007: Climate Change 2007: The physical science basis: summary for policymakers. [Available online at www.ipcc.ch.]

Jacobson, H. K. and E. B. Weiss, E.B., 1998: A framework for analysis. *Engaging Countries: Strengthening Compliance with International Environmental Accords*, E. B. Weiss and H. K. Jacobson, Eds., The MIT Press, 1–18.

Kamieniecki. S., 1995: Political parties and environmental policy. *Environmental Politics and Policy: Theories and Evidence*, 2nd ed. J. P. Lester, Ed., Duke University Press, 146–167.
Kaufman, M., 2007. What on earth is happening? budget cuts imperil climate studies, a science panel concludes. *The Washington Post National Weekly Edition,* **25**, 29.
Kennedy, E. A., cited 2006: Sweden tops climate change efforts, u.s. near bottom, environmentalists say. [Available online at www.enn.com/today_PF.html?id=11653].
Kraft, M. E. and S. R. Furlong, 2007: *Public Policy*. CQ Press, 459 p.
Kraft, M. E., 2004: *Environmental Policy and Politics*. 3rd ed. Longman, 310 p.
Kraft, M. E., 2001: *Environmental Policy and Politics*. 2nd ed. Longman, 286 p.
Kraft, M. E., 1996. *Environmental Policy and Politics*. HarperCollins College Publishers, 240 p.
Larsen, J., cited 2007: Hurricane dangers soar to new levels. [Available online at www.enn.com/archive.html?id=1629&cat=net.]
Leicester, J., cited 2007. Climate report spurs immediate calls for drastic, speedy change. [Available online at www.enn.com/today_PF.html?id=12151.]
Miller, Jr., G. T., 2002: *Living in the Environment*, 12th ed. Brooks/Cole, 810 p.
Mooney, C., cited 2005: Warmed over. [Available online at www.cbsnews.com/stories/2005/01/11/opinion/printable666190.shtml.]
MSNBC, cited 2006: Study: warming tied to hurricanes. [Available online at www.msnbc.msn.com/id/13477989/print/1/displaymode/1098.]
National Journal, 2007: Inside washington: congressional insiders poll. *National Journal*, 6–7.
Paarlberg, R., 1997: Earth in abeyance: explaining weak leadership in u.s. international environmental policy. *Eagle Adrift: American Foreign Policy at the End of the Century*, R. J. Lieber, Ed., Longman, 135–160.
Pew Center on Global Climate Change, cited 2007: Hurricanes and global warming: q & a. [Available online at www.pewclimate.org/hurricanes.cfm.]
Pew Global Attitudes Project, cited 2007: Rising environmental concern in 47-nation survey: global unease with major world powers. [Available online at www.pewglobal.org.]
Reuters, cited 2007a: Global warming behind record 2005 wtorms, u.s. expert says. [Available online at www.enn.com/archive.html?id=10326&cat=today.]
Reuters, cited 2007b: Global warming affects hurricane intensity, u.s. study shows. [Available online at www.enn.com/archive.html?id=11067&cat=today.]
Reuters, cited 2007c: Humans affect sea warming in hurricane zones. [Available online at www.enn.com/archive.html?id=11240&cat=today.]
Reuters, cited 2007d: Stronger hurricanes spawn bigger storm surges. [Available online at www.enn.com/archive.html?id=11033&cat=today.]
Revkin, A.C., cited 2002: U.S. sees problems in climate change. *New York Times*. [Available online at http://query.nytimes.com/gst/fullpage.html.]
Schreurs, M. A., 2004. The climate change divide: the european union, the united states, and the future of the kyoto protocol. *Green Giants? Environmental Policies of the United States and the European Union*, N. J. Vig, and M. G. Faure, Eds., The MIT Press, 207–230.
Sebenius, J. K., 1995: Overcoming obstacles to a successful climate convention. *Shaping National Responses to Climate* Change, Island Press, 41–79.
Steel, B. S., R. L. Cullen, and N. P. Lovrich, 2003: *Environmental Politics and Policy*. McGraw Hill, 317 p.
Susskind, L., 1994: *Environmental Diplomacy: Negotiating More Effective Global Agreements*. Oxford University Press, 201 p.
Sussman, G., 2004: The USA and global environmental policy: domestic constraints on effective leadership. *International Political Science Review*, **25**, 349–369.
Sussman, G., B. W. Daynes, J. P. West, J.P., 2002: *American Politics and the Environmen*. Longman, 334 p.
Switzer, J. V., 2001. *Environmental Politics: Domestic and Global* Dimensions, 3rd ed. Bedford/St. Martin's, 336 p.

Switzer, J. V. with G. C. Bryner, 1998: *Environmental Politics: Domestic and Global Dimensions,* 2nd ed. St. Martin's Press, 323 p.

The Gallup Poll, cited 2006. "The environment: gallup's pulse of democracy. [Available online at www.galluppoll.con/content/?ci=1615.]

The White House, cited 2007: Fact sheet: energy independence and security act of 2007. [Available online at www.whitehouse.gov/infocus/energy.]

Underdal, A., 2000: Science and politics: the anatomy of an uneasy partnership. *Science and Politics in International Environmental Regimes*, S. Andresen, T. Skodvin, A. Underdal, and J. Wettestad, Eds., Manchester University Press, 1–21.

U.S. CEQ and U.S. DoS, 1982. *The Global 2000 Report to the President: Entering the Twenty-First Century*. Penguin Books., 766 p.

U.S. DoE, EIA, cited 2004: Greenhouse gases, climate change, and energy. [Available online at www.eia.doe.gov/oiaf/1605/ggccebro/chapter1.html.]

U.S. EPA, cited 2006a: "Climate change: basic information," [Available online at www.epa.gov/climatechange/basicinfo.html].

U.S. EPA, cited 2006b: Climate change: state of knowledge. [Available online at www.epa.gov/climatechange/science/stateofknowledge.html.]

U.S. EPA, cited 2006c: Greenhouse gas emissions. [Available online at www.epa.gov/climatechange/emissions/index.html.]

U.S. NOAA, cited 2006a. FAQ/state of the science: atlantic hurricanes & climate. [Available online at www.noaa.gov.]

U.S. NOAA, cited 2006b: Global warming and hurricanes: new WMO/IWTC statement on tropical cyclones and climate change. [Available online at www.gfdl.noaa.gov/tk/glob_warm_hurr.html.]

WMO, cited 2007: WMO sees link between global warming and hurricanes. [Available online at www.enn.com/archive.html?id=10137&cat=today.]

Zogby International., 2006: Poll shows public linking hurricanes and heat waves to global warming. [Available online at www.zogby.com/Soundbites/ReadClips.dbm?ID=13554.]

Index